The Synthesis and Biological Characterisation of High Affinity, Selective Macrocyclic Ligands Targeting the CREBBP/p300 Bromodomains

A Thesis submitted for the degree of:

DPhil in Organic Chemistry

Alistair Montgomerie Boyd

Wadham College, University of Oxford

Supervisor: Stuart J. Conway

Abstract

Lysine acetylation of histone tails is a post-translational modification recognised by epigenetic “reader” domains, otherwise known as bromodomains. These proteins aid in regulating cellular processes and have been implicated in multiple diseases, particularly in cancer. A pair of bromodomain-containing proteins of particular interest are the paralogues CBP and p300. These large multi-domain proteins play a key role in gene expression through their recruitment of transcription factors onto DNA, both of these paralogues contain bromodomains. Recently they have emerged as a promising oncology target with efforts conducted to produce inhibitors of the bromodomain, thus preventing oncogene expression and cancer cell proliferation. The challenge of developing bromodomain inhibitors is that target selectivity often proves difficult. In order to overcome this selectivity problem, building upon previous work within the Conway group macrocyclic ligands were synthesised to gain selectivity, unfortunately these original macrolactams demonstrated significantly weaker affinity for the CREBBP bromodomain (CBP^{BRD}). The work presented herein attempts to overcome this decrease in affinity through SAR investigation, identifying compound **19** as a high-affinity and highly selective macrocyclic ligand for the CBP^{BRD}.

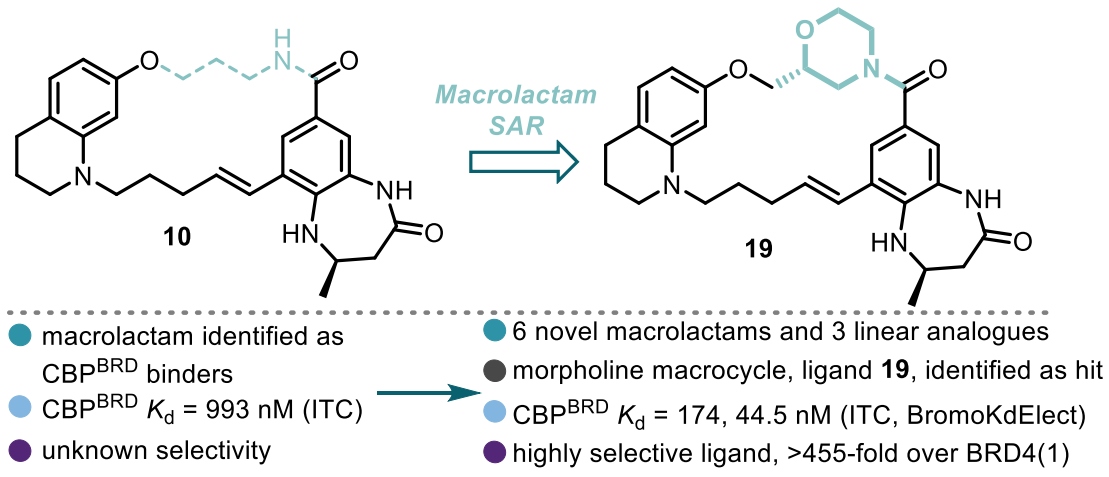

Abstract Figure: Original macrolactam ligand **10** and the hit ligand **19** identified through SAR investigation.

Table of Contents

Acknowledgements

I would like to acknowledge the entire Conway lab for putting up with me. I would like to thank Harriet Haysom for having even worse chemistry than my own and therefore adding perspective to my lab woes. She also supplied some of the best-looking Western blots I have seen, which showed absolutely nothing, most lovely to admire as if an abstract piece of artwork during group meetings. I would like to thank Dr Glen Brodie to being the other major nerd in the lab and the good chat. A special shout-out is deserved for his suggestion of reading Brandon Sanderson, much appreciated now I spend half my stipend on his book. I would like to thank Keefe Oei for my coffee addiction, without which I would probably not have worked quite as much in my DPhil. I would like to thank Michael for always being positive in the lab even if he had spent weeks purifying peptides and then AlphaScreen eating them all, the same applies to his crystal plates eating all his protein, poor Trim24… He also provided invaluable feedback on a lot of the work and thoughts presented herein. I would like to thank Maxim Mallerman for all the useful synthesis chat and having top-class banter even if your dutty playlist wasn't very good. I would like to thank Dr Antoine Wallerabregue for coming in on the weekends so I could do more synthesis, and all the publication and science chats so far and for being the lab grandpa or weird uncle whichever you would prefer. All the interesting and slightly controversial chats kept me in the lab for far too long on many occasions! I would like to thank Dr Adam Thomas for always being so full of energy (as well as banter) and playing good vibes in the lab whenever he could. I would like to thank Dr Darius McArdle for seemingly never being phased by anything and being the king of bleach and grease. I would like to thank Dr Patrick Brennan for being the music man and always being up for a pint. He also embodies the philosophy of you can never have enough, when it comes to disposable biology plasticware. I

would like to thank Dr Jennifer Carter for making me realise that everywhere is always too cold (for her) and that there is such a thing as too much exercise. I would like to thank Dr Marta Serafine for making me feel like I am never doing enough synthesis. I would like to thank Dr Bernadette (Bernie) Lee for having as many opinions as my own not putting up with rubbish from anyone and supplying excellent lab cakes and bakes. She also put up with reading some dire thesis chapters and providing valuable feedback, glad she has got the silly orange cat that she deserves. I would like to thank Ceri Foster for always being in the lab to prevent all that unsafe lone working I would have had to do, all the best with finish off your work this year! I would like to thank Ada for always smiling and being positive even when everything sucks, and chemistry is cruel. I would like to like to thank all the team CBP members past and present for all of the discussions in sub-group. I would especially like to thank Dr Katrina Andrews for being CBP lab mum and for looking after me and teaching me how everything worked when I first arrived in the group and continuing to put up with my existence and moaning about synthesis almost as much as me. Pascal Heitel for his perseverance despite receiving absolutely not help, I hope married life suits you well! Oliver (Oli) Stratton for being the best totally **not** a biologist to come out of the group and his extensive knowledge of the CBP/p300 literature (we all know p300 is the real target). Even if he has spent most of his DPhil doing biology experiments, I still think he is a better organic chemist (sorry but you should be doing synthesis or med chem), he also helped in providing feedback on some dire drafts, so I would like to thank him for his help in improving those chapters. Many thanks to Dr Niall Anderson my previous industrial supervisor for allowing me to send my compounds for physiochemical property testing and supporting my project with valuable advice. I would like to thank my current industrial supervisor Dr Mustafa Moroglu (who also doubles as the

progenitor of this project) for all the useful discussions we have had. He also was instrumental in setting up an industrial placement at GSK where I learned a lot, met some wonderful people and synthesised all the macrolactam ligands in this thesis. I would ultimately like to thank Professor Conway for putting up with my slow and erratic progress and supporting my work.

I would like to thank my collaborators for their respective contributions to this project, without which the chemistry would have gone nowhere. David Staunton for his valuable advice on biophysics and help when things have gone terribly wrong (it was my fault all along not the poor ITC machine). Disha Kashyap for performing all of the in-cell testing of my compounds, performing the experiments we both agreed on and going through all the data, even if your experiments were too good at times (those *c*-MYC qPCR errors are so very small). Marius Amann for all of the protein crystal structures presented in this thesis, which have been incredibly informative, and look (in my opinion) really quite cool, he also took it upon himself to get all of the structures ready for the PDB and dealt with uploading all of these structures for which I am incredibly grateful. I would also like to thank Dr Carole Bataille, without whom this thesis would not be what it is and for providing support and expanding my scientific discussion around my work by giving some of the only scientific feedback I have received upon my work.

I would also like to thank the doctors at the JR and Churchill hospitals along with all the staff for putting up with me for 3 months straight and also performing 2 emergency and one elected operation during the last 2 years of my DPhil. Without this, the majority of the work conducted in this thesis and all the wonderful results I have gained, would not have been possible as I would either be **dead** or unable to do work at all.

A very special thank you to my former housemates Thomas Corner, Swaraj Dash and Zhong Hui-Lim for making my two months in hospital more bearable and supporting me during the most trying time of my life (so far). Thanks to Jorin Riexinger for proving that lab is life but still having more of a life than myself, how have you managed that? I would also like to send a special thank you to Elizabeth Bateman (little pea) for all the silly chats and very useful feedback on this thesis and putting up with my nonsense and illegal purchasing of gifts, the bread gifts were a fair trade in my opinion.

I would also like to give a special thank you to my family (particularly my parents) for supporting and visiting me during my DPhil, for looking after me when I was recovering from my operations and making sure I stayed mostly sane in hospital. I very much doubt I would have bothered completing the DPhil after the hellish end of my second year, but you taught me that hard work will eventually get you there and I am glad to say it has (I hope). Thank you to my brother Frazer Boyd for allowing me to moan a lot, and having his life far too sorted for a younger brother. I would like to thank my nan, Carol Saul for (almost) always being up for a chat and taking my mind off of work and my medical woes. I would also like to thank Norrie, Dorrie, Lulu and Amber for being such good cattos and putting up with my continued existence in their house, allowing me to pet them occasionally, and sometimes being nice to me.

Abbreviations

Ac	acetyl
ADME	adsorption, distribution, metabolism, and excretion
BCL-2	β-cell lymphoma 2
BRD4(1)	human bromodomain containing protein 4, first bromodomain
BRD4(2)	human bromodomain containing protein 4, second bromodomain
Brine	refers to a saturated aqueous solution of sodium chloride
CBP^{BRD}	CREBBP bromodomain
Celite	refers to Celite® 545 filter aid, treated with sodium carbonate, flux calcined which was purchased from Alfa Aesar
c-MYC	MYC proto-oncogene, bHLH transcription factor
CREBBP	cyclic-AMP response element-binding protein binding protein also known as CBP
DEAD	Diethyl azocarboxylate
DIPEA	*N*,*N*-diisopropylethylamine
DIAD	Diisopropyl azocarboxylate
DMF	dimethyl formamide
DMSO	dimethyl sulfoxide
DPPE	1,2-bis(diphenylphosphine)ethane
DTBAD	di-*tert*-butyl azocarboxylate
Et	Ethyl
FA	formic acid
FT-IR	fourier transformed infra-red spectroscopy
HEPES	(4-(2-hydroxyethyl)-1-piperazineethanesulfonic acid)
HPLC	high pressure liquid chromatography
HRMS	high resolution mass spectrometry
IC_{50}	half maximal inhibition concentration

in vacuo	refers to the removal of solvents under reduced pressure using a BuchiTM rotary evaporator in a water bath at 40 °C, unless overwise stated.
KAc	ε-*N*-acetylated lysine
K_d	dissociation constant
LC-MS	liquid chromatography (usually HPLC) with mass spectrometry analysis
LRMS	Low resolution mass spectrometry
lyophilisation	refers to the removal of a mixture of H_2O and acetonitrile by freeze drying using a CHRIST Alpha 2-4 LSCbasic lyophiliser.
m.p.	Melting point
Me	Methyl
MilliQ water	Refers to water purified by a Merck Millipore MilliQ® water purification system, specifically Milli-Q direct 8 with a Millipak® Express 40 filter
MS	mass spectrometry
MYB	MYB proto-oncogene or transcriptional-activator MYB.
NMR	nuclear magnetic resonance spectroscopy
p300	E1A-associated protein p300 also known as EP300
$p300^{BRD}$	p300 bromodomain
PDB	protein data bank,
PEG	polyethyleneglycol
Pet ether	Unless otherwise stated refers to the fraction of light petroleum ether boiling within the range of 40-60 °C.
PTFE	Polytetrafluoroethylene
PyBOP	Benzotriazole-1-yl-oxy-tris-pyrrolidino-phosphonium hexafluorophosphate
qPCR	quantitative polymerase chain reaction
r.t.	room temperature
R_f	retention factor
SAR	structure activity relationship

SEC	size exclusion chromatography
TBAF	tetrabutyl ammonium fluoride
TBAI	tetrabutyl ammonium iodide
TFA	trifluoroacetic acid
THF	tetrahydrofuran
TIPS	triisopropylsilyl
TLC	thin layer chromatography

Chapter 1:

Introduction

1.1 Epigenetics

The term epigenetics (or “above genetics”) refers to changes in phenotype without underlying alterations to the genotype; this definition covers the modification of proteins, DNA, and RNA.[1–4] These changes can alter the accessibility of the DNA, dictating gene expression. As a result, epigenetic modifications play a key role in controlling protein levels and cellular processes, influencing fundamental cell function.[5] Thus, epigenetics is an exciting area of research as it allows for a greater understanding of biological functions, as well as providing a potential route for the treatment of diseases such as cancer.[5]

1.1.1 Chromatin structure and post-translational modifications

Histone proteins, around which DNA is supercoiled, frequently undergo post-translational modifications.[5] The wrapping of DNA around histones, makes up nucleosomes which is a single histone unit which consists of an octamer made up of two copies of each histone protein: H2A, H2B, H3, and H4.[6] The nucleosome units are joined by DNA and compressed into higher order chromatin fibres which make up chromosomes.[7] The epigenetic modifications can occur on DNA such as methylation and hydroxylation but this is not the focus of this thesis.[8] Post-translational modification of histones allows the formation of an open chromatin conformation or compact conformation.[9] The chromatin conformation and thus the accessibility of the DNA is dictated by the post-translational modifications on the histone proteins, which often occur on lysine residues on the histone tails (see Figure 1). For example, the acetylation of the lysine tails on histones weakens the interaction between DNA and chromatin, due to the loss of a strong charged interaction between the negative phosphate backbone of DNA and the positive protonated lysine residue. This results in a more open conformation and thus allows for increased expression of genes.[10] The

methylation of lysine residues on histones prompts the opposite effect of acetylation (see Figure 1). The post-translational methylation of the lysine amino acids causes an increase in the compact conformation of chromatin, decreasing DNA accessibility, and lowering gene expression. The levels of these epigenetic marks fluctuate, with the addition and removal of such marks occurring in an enzyme-dependant manner.[10,11] Another post-translational modification to histones is phosphorylation of threonine, tyrosine, and serine (Figure 1).[12] This modification plays a role in recruiting different effectors onto DNA and controlling key processes such as DNA damage repair, cell division and transcriptional regulation.[13] Other post-translational modifications which occur on histones include succinylation, malonylation, sumoylation, and ubiquitination all altering chromatin and gene expression (Figure 1). [14–17]

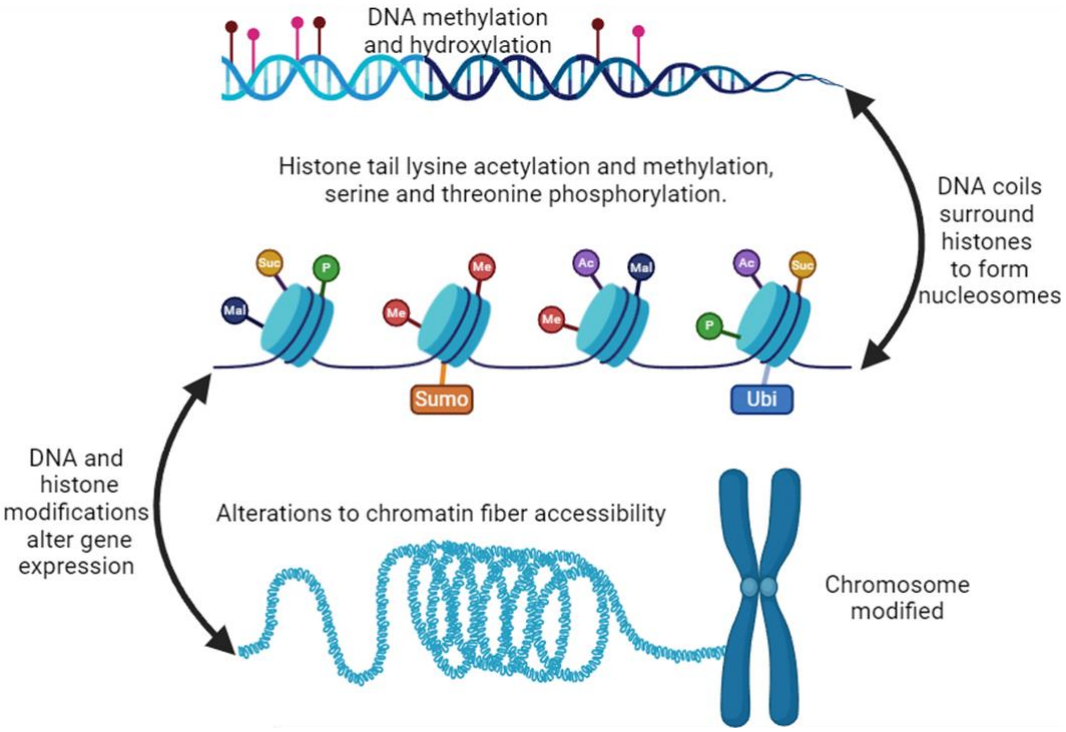

Figure 1: Epigenetic modifications to DNA and histone proteins, including methylation (brown), hydroxylation (pink), acetylation (purple), phosphorylation (green), malonylation (dark blue), succinylation (dark yellow), sumoylation (orange), and ubiquitination (light blue), displaying chromosome make up from chromatin fibres made up of histones around which DNA is coiled, figure created with biorender.com.

1.1.2 Reader, writer, and erasers of acetylated lysines

Lysine acetylation on histones is controlled by three types of proteins: reader (bromodomain), writer (histone acetyltransferases or HATs), and eraser (histone deacetylases or HDACs and sirtuins) domains (see Figure 2).[18] HAT domains act to acetylate lysines, using acetyl-CoA, increasing gene expression (see Figure 2A).[19] The HDAC domains remove acetylated lysine marks, regenerating the native lysine residues, supressing gene expression (see Figure 2B).[20] The bromodomains (or BRDs) act to read the acetylated lysines (or the epigenetic code) and regulate gene expression by either chromatin remodelling or transcription machinery recruitment (see Figure 2C).[21] The work presented in this thesis focuses on BRD containing proteins.

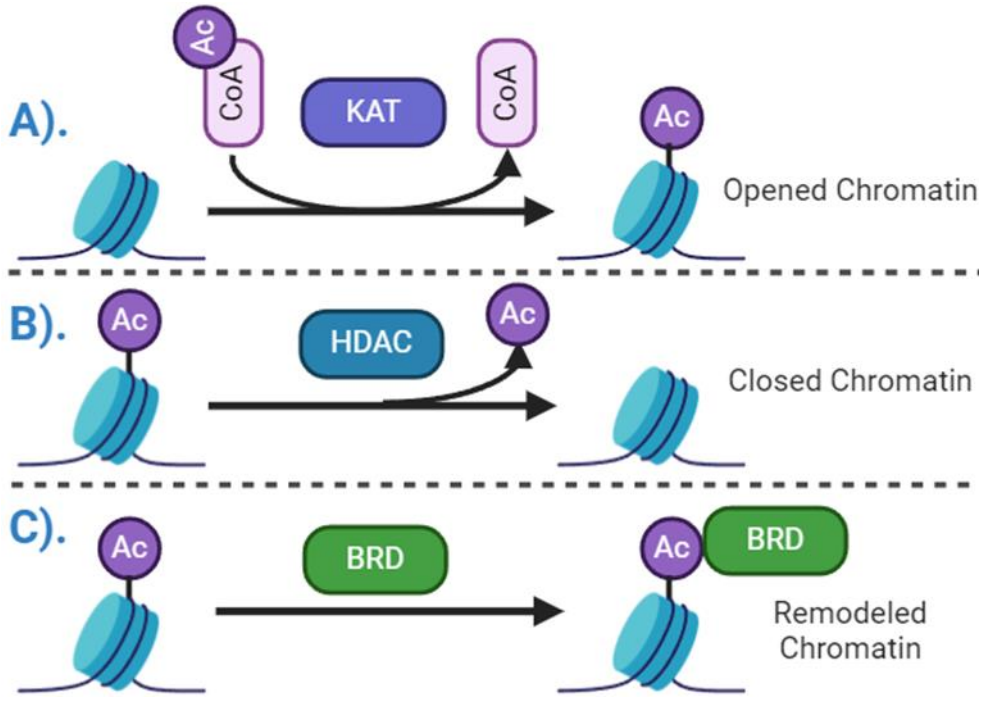

Figure 2: Epigenetic acetyl associated proteins of chromatin, A). Function of HAT domains, adding acetyl groups onto lysines of histones to form KAc moieties; B). Function of HDAC domains removing acetyl marks on lysines of histones removing Ac from KAc; C). Function of bromodomains to interact with acetyl lysines and thus induce and cause gene expression in a spatiotemporal manner, figure created with biorender.com.

1.2 Bromodomains

BRDs have emerged as a key domain in transcriptional regulation, due to their ability to recruit transcription factors and activators to chromatin, through protein-protein interactions.[21–24] This acts to direct and control the expression of particular genes in a dynamic manner, through the recognition of acetylated lysines (KAc) marks. With this in mind, bromodomain-containing proteins have been implicated across an array of diseases including cancer, multiple sclerosis, and inflammation-related diseases such as colitis.[21,25] Within the human proteome there are 61 unique bromodomains contained within 46 proteins, which illustrates how a single protein can contain multiple reader domains.[26] These bromodomains are divided into 8 families based on their respective sequences and structures.[26]

1.2.1 Bromodomain structure

BRDs have a conserved structure, made up of four alpha helices, bridged by ZA and BC loops which form the KAc binding pocket (see Figure 3A).[24,26] The KAc is often (but not exclusively) bound to an asparagine or tyrosine residue through direct and or water-mediated hydrogen bonding respectively (see Figure 3B).[24,26] Usually bromodomain KAc binding sites contain 4 or 5 water molecules at the base of the pocket, which are conserved upon KAc binding and thus are considered structured waters (as shown in Figure 3B).[24,26] In many canonical BRDs, the acetylated nitrogen forms a water-mediated hydrogen bond with a further residue (such as the proline in Figure 3B).[24] The most highly studied bromodomains are those within the BET family consisting of: BRD2, BRD3, BRD4, BRDT (the structure of BRD4 is displayed in Figure 3A), because of their disease relevance.[24,26] Due to their well-understood binding sites most BRDs present a readily targetable domain.

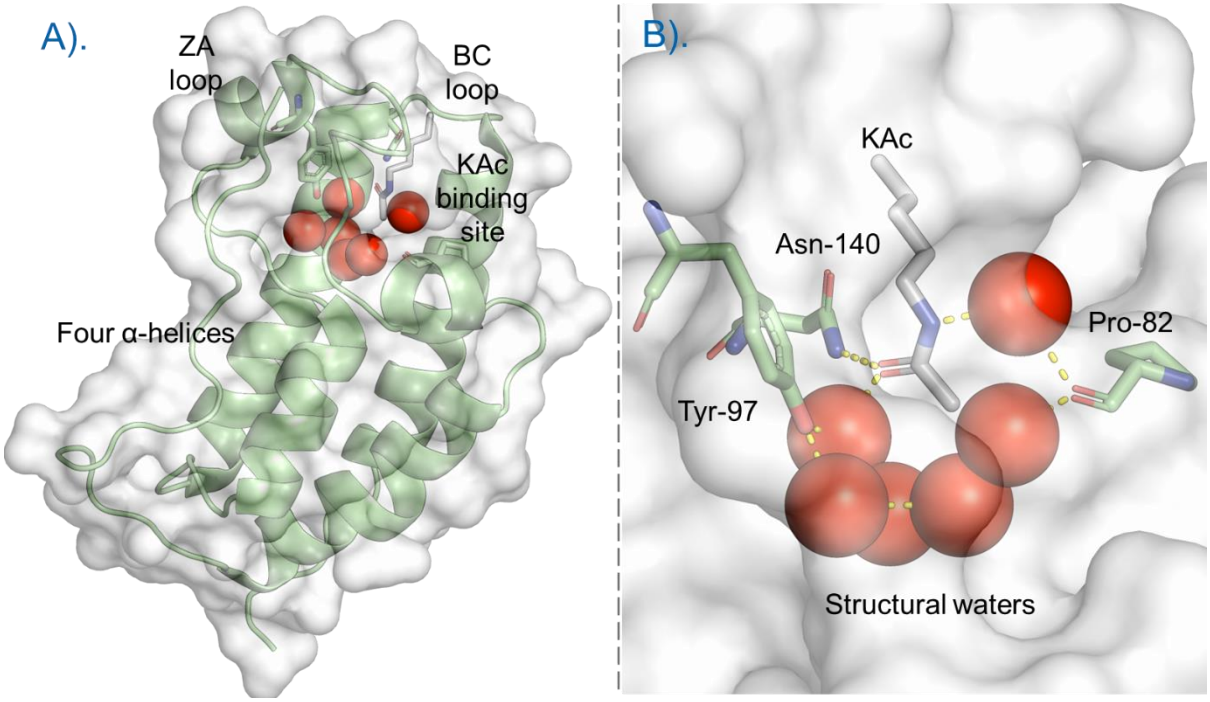

Figure 3: Co-crystal structure of KAc bound to BRD4(1) (PDB: 3UVX) at 1.9 Å resolution; A). image of the whole bromodomain bound to KAc showing the four α-helices and the ZA and BC loops; B). a focused image of the KAc binding pocket, showing the key hydrogen bonding interactions (yellow dashed lines), residues (green) with labels and water molecules as spheres (red), with the KAc chain shown (grey).[24,26]

1.2.2 Bromodomains as an emerging therapeutic target

As BRDs play a key role in DNA transcription and disease related to altered gene expression, efforts have been made to find ligands to displace the KAc from the binding site and prevent bromodomain binding to chromatin.[21,25,26] Due to similarities in the KAc-binding sites present within BRDs, there have been a number of successes in the development of high-potency bromodomain ligands.[23,27–31] These successes spread beyond just small molecule non-selective inhibitors (such as **JQ-1** in Figure 4) and includes covalent ligands (such as ZEN-3411 in Figure 4), protein degraders (such as proteolysis targeting chimeras (PROTACs) **MZ1** and **dBET1** in Figure 4), bi-valent ligands which inhibit adjacent bromodomains (such as **AZD-5153** in Figure 4) and other bivalent compounds (such as molecular glue **ML 1-50**, bivalent molecular glue **IBG1**, and triple inhibitor **SRX3177** in Figure 4).[23,29,32–36] Thus, the number of compounds targeting bromodomains has grown extensively since the discovery of the

original BRD ligand of **JQ-1** in 2010, far beyond monovalent small molecule inhibitors, with molecular weight less than 500 Da.[23]

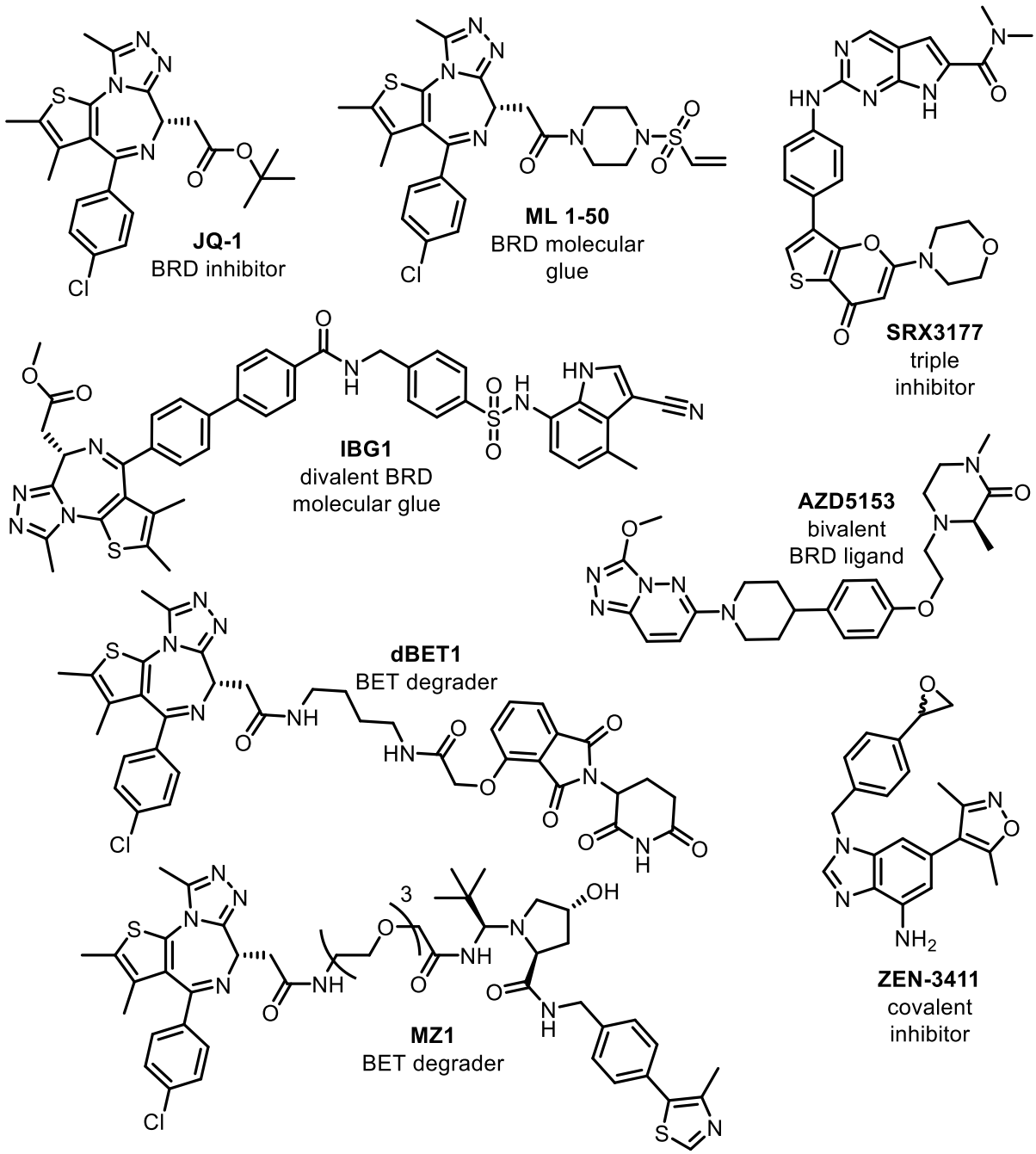

Figure 4: A selection of chemical moieties targeting BET family bromodomains including JQ-1 (the original high-affinity BET bromodomain ligand), dBET-1 and MZ-1 (the PROTACS using this ligand), ML 1-50 (a molecular glue based on this ligand), IBG-1 (a bivalent molecular glue targeting the 1st and 2nd BRDs in BRD4 and BRD2), AZD5153 (a bivalent inhibitor of the 1st and 2nd BRDs of BRD4), SR3177 (a simultaneous inhibitor of BET BRDs, PI3K and CDK), and ZEN-3411 (a covalent inhibitor BET inhibitor).

With the plethora of bromodomain ligands developed across the families of bromodomain-containing proteins, several have reached clinical trials.[31] The majority of compounds in clinical trials target the BET BRDs (such as **AZD5153**), due to their well-understood biological function, strong phenotype upon inhibition and disease relevance particularly in the field of oncology.[31,37,38] However, as BET bromodomains are important for continued cell function, inhibition of these proteins frequently causes serious off-target cytotoxicity, which is one of the main reasons behind the lack of BRD inhibitors currently approved as drugs.[38] It is, therefore, key when developing BRD inhibitors of other protein families outside of the BET family, that the lead compound demonstrates high selectivity over the BET BRDs.

1.3 CBP

1.3.1 CBP/p300 Structure

There are a number of BRD-containing proteins outside of the BET family, which could provide therapeutic value. One such set of proteins is CBP (c-AMP response element binding protein binding protein sometimes referred to as KAT3A or CREBBP) and p300 (E1A binding protein sometimes referred to as EP300), which are the targets of the only BRD inhibitor outside of the BET family that is in clinical trials.[22,39–42] CBP/p300 are paralogues which both play a key role in gene transcription, through both a BRD and HAT domain, recruiting these proteins onto chromatin. The other domains of the paralogues recruit transcription activators and thus CBP/p300 behave as transcriptional co-activators (see Figure 5).[39,43,44] CBP and p300 are involved in the expression of important oncogenes (such as *c*-MYC, MYB and BCL-2) along with tumour suppressors (such as p53), highlighting their importance as oncology targets.[39,41,42,45,46] Within the ten domains of CBP and p300, the overall sequence is

58-61% similar, with the highest sequence homology occurring within the catalytic core, containing the BRD, PHD (plant homeodomain), RING (really interesting new gene), KAT (acetyltransferase), ZZ (ZZ-type zinc finger), and TAZ2 (transcription Adaptor putative Zinc finger 2) domains, which are 86% similar across the two proteins making it challenging to achieve paralogue selectivity (see Figure 5).[39,41,43–45]

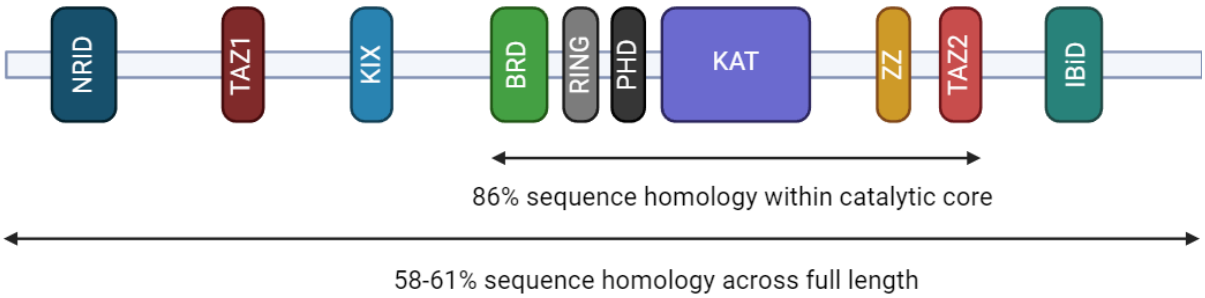

Figure 5: Protein structure of CBP and p300, showing the ten total domains as well as the sequence homology across the full length and within the catalytic core, figure created with biorender.com.[44]

CBP/p300 are involved in over 400 protein-protein interactions, mediating important responses to cellular stress.[39,41–45] This reinforces the essential function of CBP/p300, and making it an attractive target for possible therapeutics.[41,42]

1.3.2 CBP/p300 BRD Inhibitors as potential therapeutics

Efforts are ongoing to target the individual domains within CBP/p300, including the KAT, BRD, KIX, and TAZ1 domains.[47–51] Of particular interest are the BRD inhibitors developed, improving upon the affinity and selectivity of the original inhibitors published in 2014 (Figure 6A). Both ligand **1** and **SGC-CBP30** provided limited selectivity for CBP/p300 BRDs over the BET family proteins such as BRD4(1) (see Figure 6A).[40,52] Since then, many high-affinity ligands have been developed such as **CPI-637**, **GNE-781**, and **GNE-207**, including the clinical candidate Inobrodib (**CCS1477**); these ligands offer vast improvements in affinity and selectivity for the CBP^{BRD}/$p300^{BRD}$ (see Figure 6B).[28,30,42,53,54] Inobrodib demonstrated effective decreases in cancer growth/progression and was fast-tracked by the FDA for the

treatment of relapsed or refractory multiple myeloma (MM) patients, it is still undergoing clinical trials in MM, AML (acute myeloid leukaemia), non-Hodgkin lymphoma and prostate cancer.[22,30,42,48,50] The ligands displayed (in Figure 6), highlight the diverse chemotypes which the CBP/p300 BRDs bind and the KAc mimicking groups (highlighted in blue in Figure 6). In addition, novel efforts have been directed to target the full-length CBP/p300, through highly potent PROTACs, as novel therapeutics for cancer.[55–57]

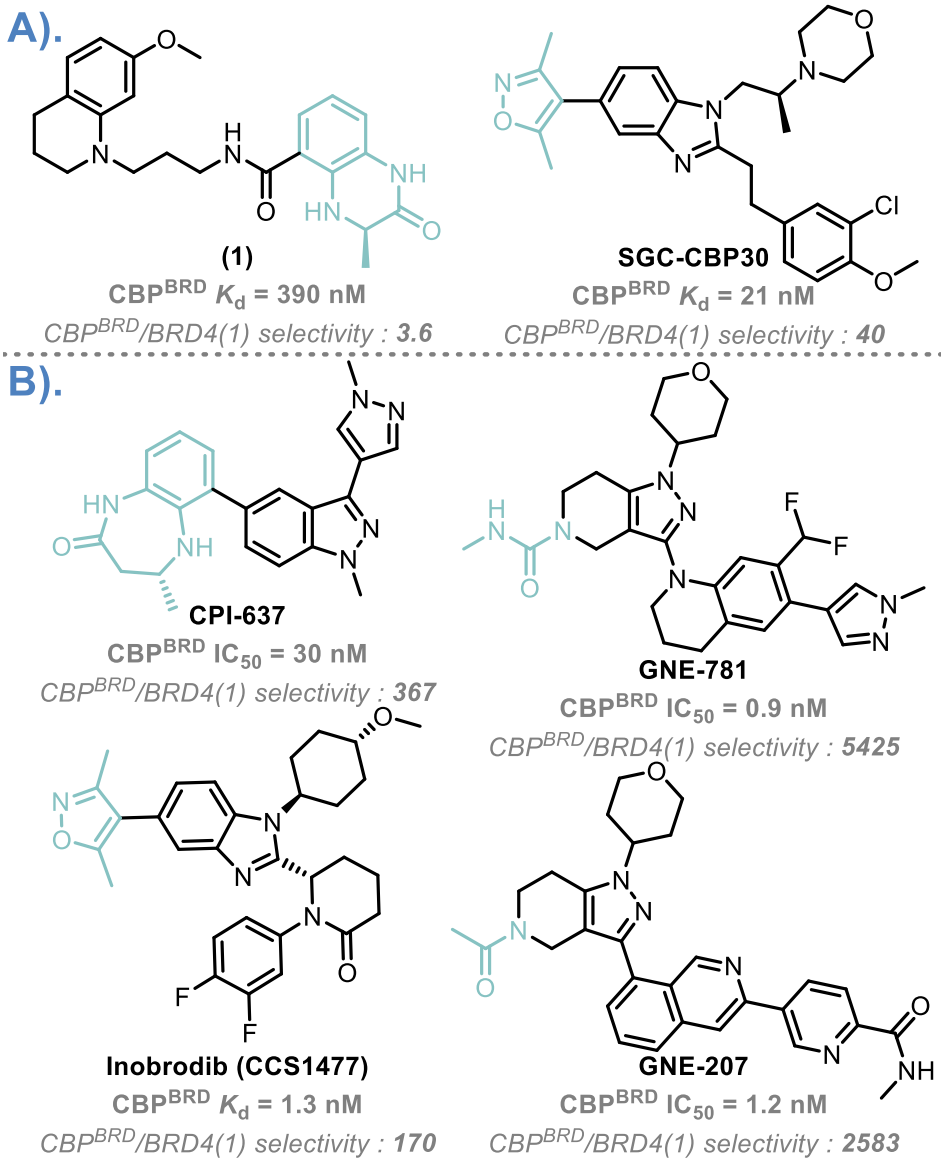

Figure 6: Chemical structures of CBP/p300 BRD ligands, with the respective K_d or IC_{50} below each compound along with the CBP^{BRD} fold selectivity over BRD4(1); A). The original CBP ligands published; B). More recent ligands published, including the clinical candidate Inobrodib.

The current clinical candidate Inobrodib, possesses very high affinity with a K_d of 1.3 nM for the CBP^{BRD} and K_d of 1.7 nM for $p300^{BRD}$.[30,42] This ligand is also a *bona fide* orally bioavailable inhibitor of tumour growth in multiple tumour models and human patients (with or without combination therapy).[30,42] As highlighted from the binding data shown and in further studies, Inobrodib does not demonstrate the most favourable selectivity profile (170-fold selective for the CBP^{BRD} over BRD4(1)). Inobrodib showed affinity for all of the first BRDs of the BET family (BRD2(1), BRD3(1), BRD4(1), and BRDT at 1 μM).[30] This provides a challenge as BET inhibition could provide synergy in the antiproliferative effects but also makes it difficult to delineate if the therapeutic effects are entirely driven by CBP/p300 BRD inhibition. But this challenge exists due to the similarities within the BRDs KAc binding sites, presenting a problem to overcome in terms of the development of a ligand which is selective for one BRD. This also offers an opportunity for more selective inhibitors to be synthesised overcoming this shortfall with respect to the selectivity of Inobrodib.

1.3.3 CBP^{BRD} and $p300^{BRD}$ structures

As previously discussed, (see section 1.2.1) the CBP and p300 BRDs are made up of four α-helices joined by ZA and BC loops. The KAc binding site contains 4 or 5 conserved water molecules, with the asparagine and tyrosine forming hydrogen bonding interactions (direct and water-mediated respectively), present along with a water-mediated hydrogen bond to a proline (Figure 7). This similarity in structure means that often KAc mimicking groups are recognised by the majority of BRDs, presenting a selectivity challenge during ligand design and implementation.[22,31,38]

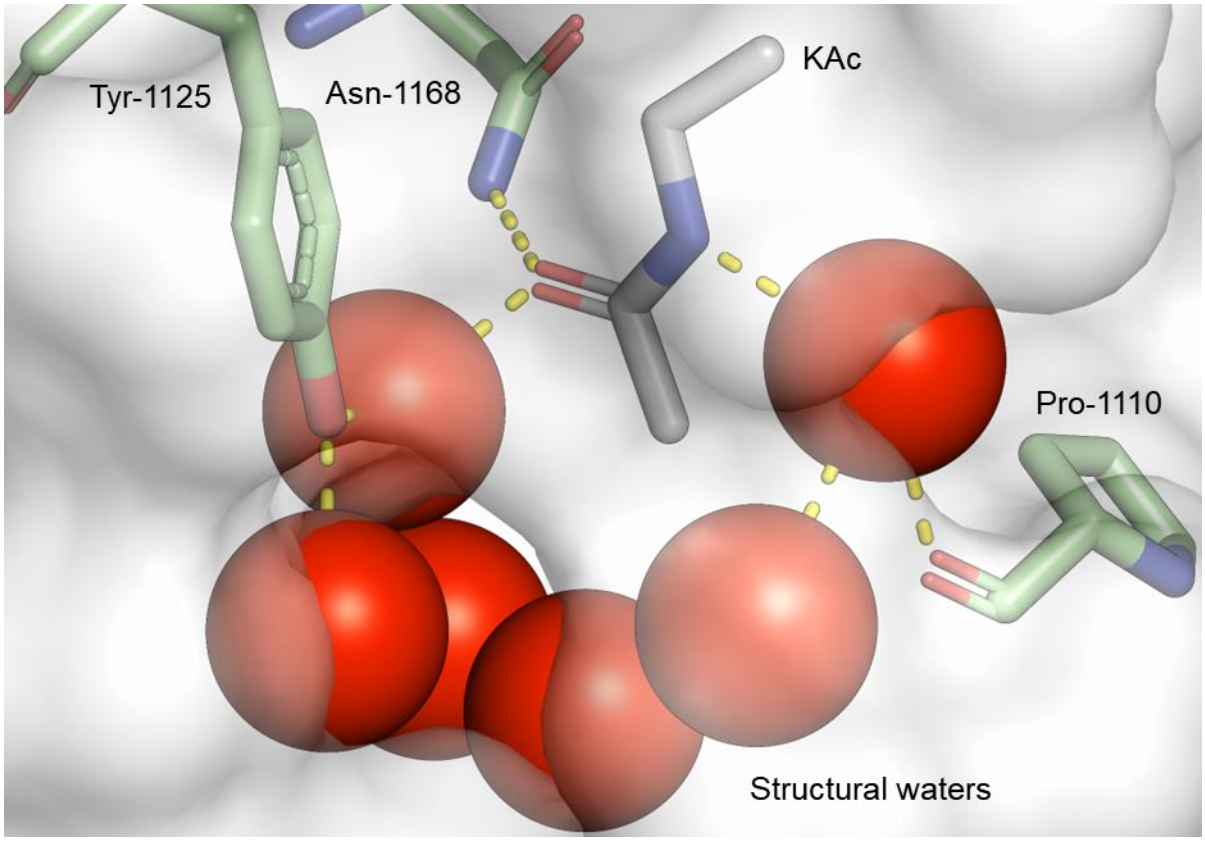

Figure 7: Co-crystal structure of KAc containing peptide bound to the CBP^{BRD} (PDB: 3P1C), a focused image of the KAc binding pocket, showing the key hydrogen bonding interactions (yellow dashed lines), residues (green) with labels and water molecules as spheres (red), with the KAc chain shown (grey).[24]

However, CBP/p300 share different amino acids near the KAc binding sites, compared to the BET BRDs, allowing selectivity to be built through the targeting of these residues, a strategy used to great effect by the ligands GNE-781 and GNE-207 to gain selectivity over BET BRDs. The difference in the binding sites is that the Trp-81 of BRD4(1) is replaced with Leu-1109 in the CBP/p300 BRDs, Leu-94 is replaced with Ile-1122, Asp-145 is replaced with Arg-1173, Ile-104 is replaced with Val-1174, and Met-149 is replaced with Phe-1177 (see Figure 8). The most important amino acid residue differences are the change of Trp-81 to Leu-1109; this opens up the leucine proline phenylalanine (LPF) shelf of the CBP/p300 BRDs and Asp-145 to Arg-1173, which is a key difference targeted by the work in this thesis (see Figure 8). These altered residues within the CBP/p300 BRDs provides a useful handle with which ligands can be designed to afford selectivity over the BET bromodomains.

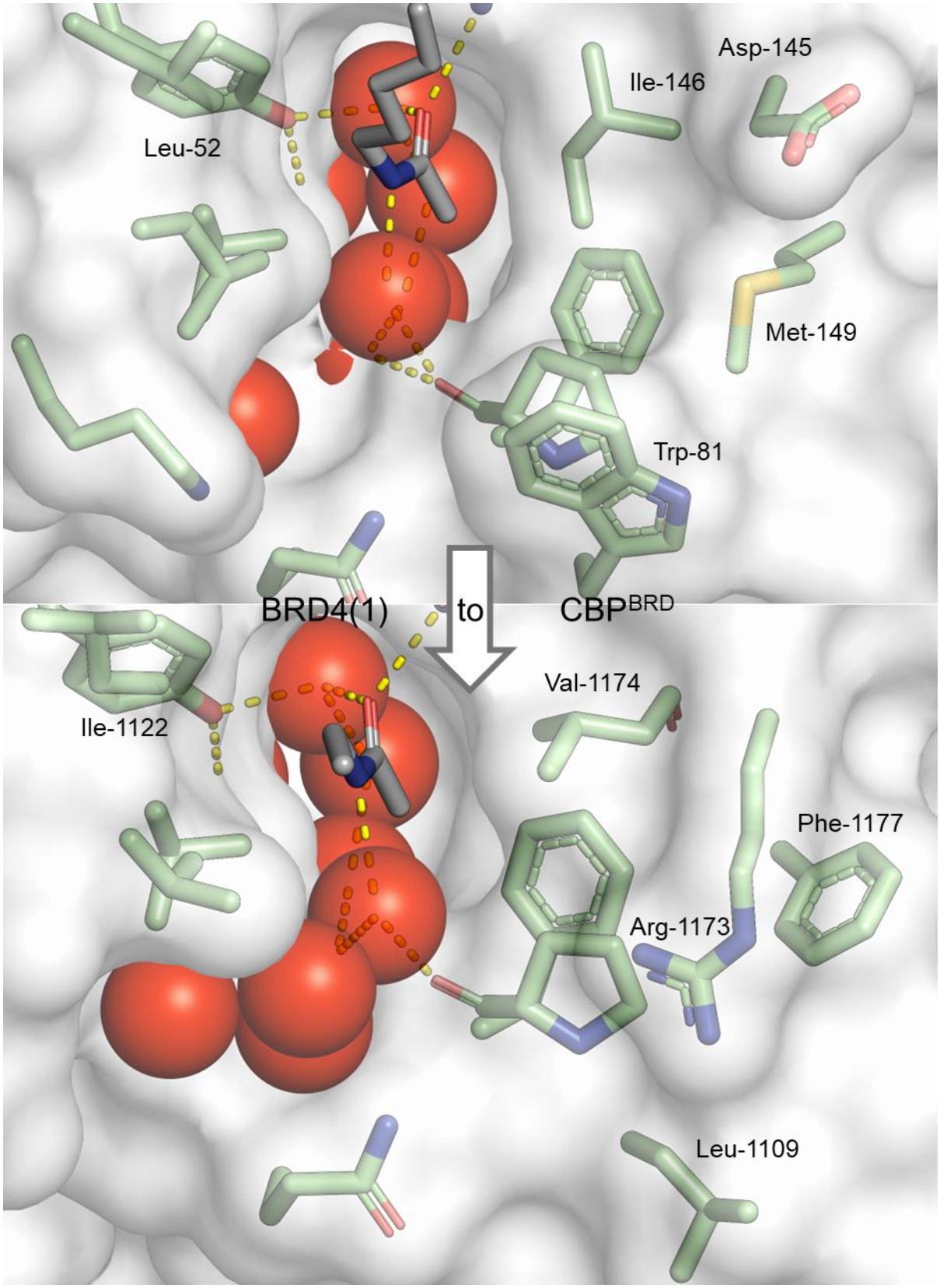

Figure 8: Co-crystal structures of KAc containing peptides (grey) in the binding sights viewed from above of BRD4(1) (top) (PDB: 3UVX) at 1.9 Å resolution and CBP^{BRD} (bottom) (PDB: 3P1C) at 1.8 Å resolution, with the residue changes highlighted by their respective three letter amino acid codes and corresponding sequence number, showing hydrogen bonding interactions (yellow dashed lines), residues (green) with amide backbone removed and water molecules as spheres (red).[24]

1.2 Macrocycles in drug discovery and their benefits

Macrocycles are defined as cyclic molecules containing 12 or more atoms in a ring, which span a broad class of compounds from supramolecular chemistry to medicinal chemistry.[58–60] Historically, most macrocyclic drugs have been natural products (Figure 9A): whereas modern drug discovery efforts aim for the rational design of macrocyclic ligands with improved properties such as increased selectivity or solvent front mutant protein inhibition in the case of kinase inhibitors (Figure 9B).[61–68] The small molecule synthetic macrocycles often exhibit improved affinity and selectivity and these properties are achieved through conformationally constraining the compound into the bioactive conformation, preventing off-target binding modes whilst also decreasing the entropy of binding to the on-target protein.[58,59,69–71]

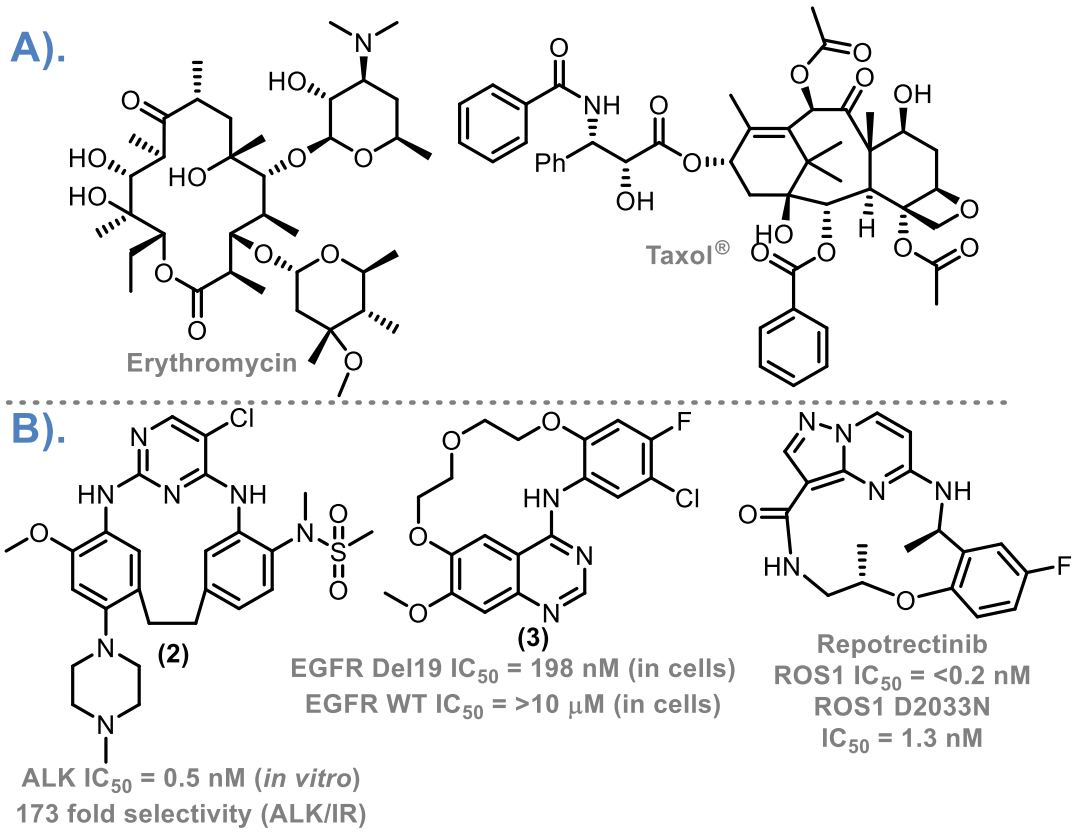

Figure 9: Chemical structures of small molecule macrocyclic drugs and inhibitors; A). natural product macrocycle drugs; B). macrocyclic inhibitors as well as drugs derived through chemical design

Macrocyclic ligands offer an opportunity to inhibit previously undruggable targets, due to the large surface area provided, such as RAS proteins and HIF1 and 2, utilising peptide-based macrocycles for these difficult to target proteins and as protein-protein interaction (PPI) inhibitors (Figure 10).[72–74] The work conducted allows these novel macrocyclic peptides to overcome previous issues with peptides as therapeutics, such as low oral bioavailability, allowing these drugs to progress into clinical trials (such as LUNA-18 in Figure 10).[72,73]

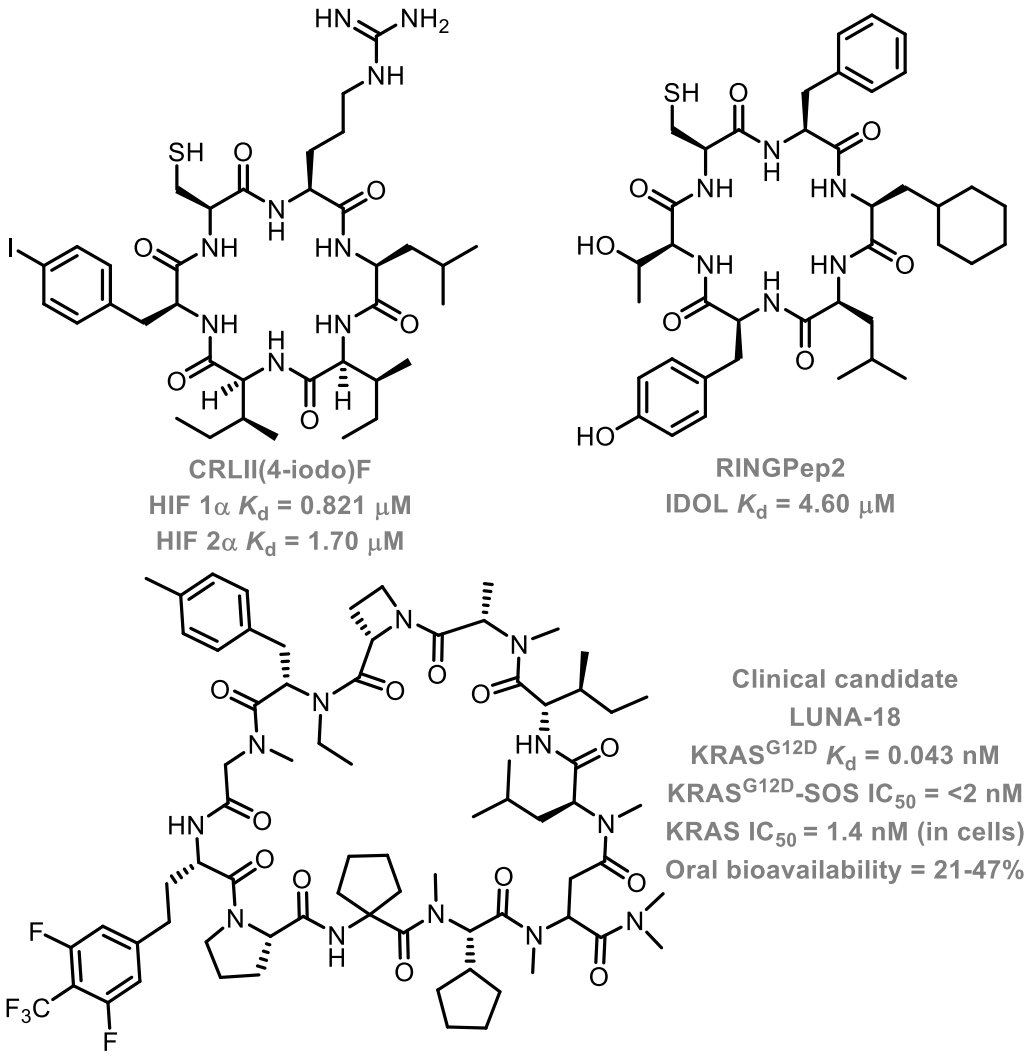

Figure 10: Novel macrocyclic peptides targeting previously undruggable proteins, including the orally bioavailable macrocyclic KRAS inhibitor LUNA-18.

However, utilising a macrocyclisation strategy is not always advantageous, as ligands can prefer extended rather than constrained conformations when protein bound, with

flexible side chains also proving potential sources of selectivity through extra on-target interactions. The work presented in this thesis focuses on the development of small molecule, non-peptide macrocyclic ligands.

1.4.2. Modulation of Physiochemical properties through macrocyclisation

Lipinski's rule of 5 for good oral bioavailability of small molecules states that a ligand needs to have no more than 5 hydrogen bond donors, 10 hydrogen bond acceptors, 500 Da molecular weight, and a LogP of 5 or less.[75] However, most macrocyclic drugs are considered beyond rule of five (bRo5, such as Erythromycin and Luna-18 in Figure 9A and 10), due to their molecular mass exceeding 500 Da, with a high number of hydrogen-bond acceptors and donors, breaking Lipinski's rule of 5 and thus are considered bRo5 drugs.[67,72,76,77] In recent years, compounds that are bRo5 have become steadily more common, particularly with the growth of novel bio-active and orally bioavailable modalities such as increased size small molecules for difficult to target proteins (such as PPI inhibitors), bivalent ligands (such as PROTACs), and macrocyclic peptides.[55,72,78–80] This is exemplified by the growing number of bRo5 compounds approved by the FDA, from 2014-2017, 12 novel chemical entities were approved across 4 different therapeutic areas, with more approved each year.[79] Due to unique properties of macrocycles, which exhibit chemical chameleonicity, meaning that in order to overcome breaking the rule of 5, these compounds change their conformations based upon the surrounding environment.[59,76,77]

As a result of chemical chameleonicity, it is often insufficient to use 2D descriptors such as total polar surface area and the number of hydrogen bond donors and acceptors. This is because in an aqueous environment, the hydrogen bond donors/acceptors would hydrogen bond to the surrounding water, adopting an open conformation.[76,77] However, in a hydrophobic environment such as the lipophilic cell

membrane, these hydrogen bonding polar groups can be shielded by the macrocycle adopting a conformation that allows for intramolecular hydrogen bond formation shielding these moieties from the hydrophobic lipid membrane (see Figure 11).[76,77] The chemical chameleonicity of compounds can now be better described by their solution state conformations using NMR spectroscopy in D_2O (mimicking an aqueous environment) and $CDCl_3$ (to mimic a hydrophobic environment) and thus gaining a solution state structure of a ligand. This is used to calculate the 3D total polar surface area of a conformation, giving a superior descriptor of these compounds behave in solution.[76,77]

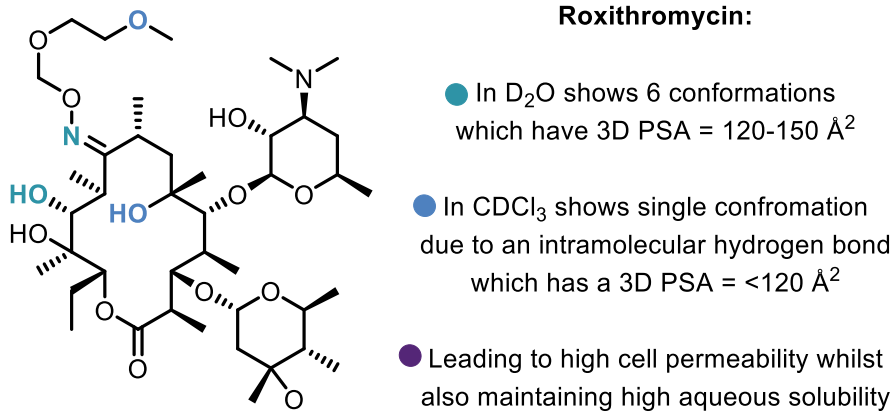

Figure 11: Chemical structure of the macrocycle Roxithromycin (an erythromycin-based antibiotic) with the atoms which form intramolecular hydrogen bonds highlighted in the corresponding shade of blue between donor/acceptor pairs, whilst also describing the behaviour of the ligand in hydrophilic/phobic environments, with its chemical chameleonic behaviour highlighted by high aqueous solubility and membrane permeability [77]

These examples show that although many macrocycles are bRo5, they can still achieve oral bioavailability, hence although it is useful to consider physiochemical properties, a more direct measure can be required to describe macrocycle PhysChem, such as the ligands synthesised in this thesis.

1.4.3 Previous Macrocyclic bromodomain Inhibitors

Within the literature exists three examples of macrocyclic compounds targeting BRDs.[71,81] Two examples utilise macrocyclic peptides to target the CBP^{BRD}, whilst the other conformationally constraints linear compound **4** to afford macrocyclic **5** with improved affinity for BRD4(1) (Figure 12).[71,81,82] The macrocyclic BRD4(1) inhibitor **5** demonstrates how macrocyclisation improves upon the affinity (6.4-fold decrease in K_i) leading to a more pronounced phenotypic effect on cancer proliferation.

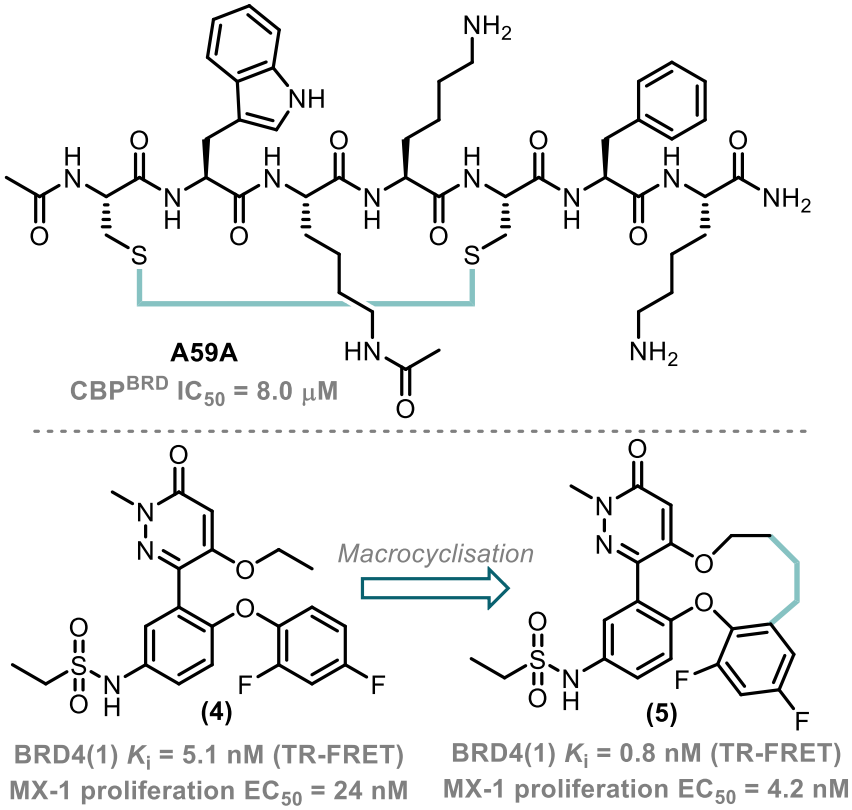

Figure 12: Prior state of the art in macrocyclic BRD inhibitors, with the macrocyclisation bonds highlighted in bold (cyan), top shows the original macrocyclic peptide targeting the CBP^{BRD} and lead small molecule macrocyclic ligand which targets BRD4(1).

To date, within the literature, no high affinity, selective small molecule macrocycles have been described which inhibit any BRDs outside the BET family, although for BRD4(1) this has proved an effective strategy. However, the most recent example of macrocyclic peptides that targets the CBP^{BRD} are the first high affinity macrocyclic inhibitors of this BRD using a stapled peptide strategy (sub μM IC_{50} by TR-FRET).[82]

1.5 Biological techniques for Evaluation of Ligands

This section of the introduction aims to provide the background of the biological techniques used during this thesis to measure compound binding. Assays for measuring the affinity (K_d) or potency (IC_{50}) are described as well as techniques for quantifying compound-based effects in cells.

1.5.1 Isothermal Titration Calorimetry Assays

Isothermal titration calorimetry (ITC) is an assay widely used for the study of macromolecule and ligand interactions in solution.[83] As the binding of a ligand to a protein is usually an exothermic process, the heat released upon sequential addition of a ligand to a protein in a titration is measured, allowing for thermodynamic data to be collected to give equilibrium constants (Figure 13).[83] The technique is considered isothermal (as experiments are conducted at a constant temperature) and isobaric (as experiments are carried out under constant pressure), and this allows for the assay to measure the enthalpy and entropy changes within a system.[83] These can then be used to calculate a dissociation constant (K_d) which is used as a thermodynamic measure of affinity as it gives the concentration at which 50% of the supramolecule is ligand bound (Figure 13).

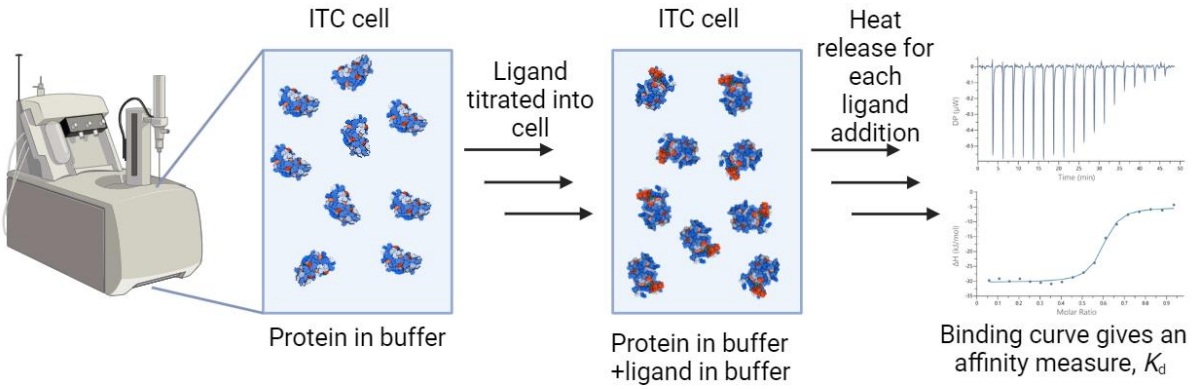

Figure 13: Illustration of ITC experiments, with protein in cell and ligand titrated into the solution figure created with biorender.com.

1.5.2 AlphaScreen® Assays

AlphaScreen® is a technique often used to measure displacement from a protein binding site and therefore gives a 50% inhibition coefficient (IC_{50}).[23,24,40,52,84,85] This assay is bead-based, and requires close proximity of the donor and acceptor beads in order to produce an emission signal.[23] The donor bead is excited at 680 nm, generating singlet oxygen, which diffuses a short distance through solution and reacts with the acceptor bead which releases light between 520 – 620 nm (Figure 14).[23] Each bead surface is coated to allow for bio-molecule binding, with the donor bead usually coated with streptavidin to allow for biotin binding, whilst the acceptor bead is usually coated with a protein tag binder (such as a nickel chelate or glutathione).[23] When an inhibitor is added, it displaces the biotinylated molecule from the protein binding site, meaning the donor and acceptor beads are no longer in close proximity, decreasing the signal measured from the emission of the acceptor bead (Figure 14).[23]

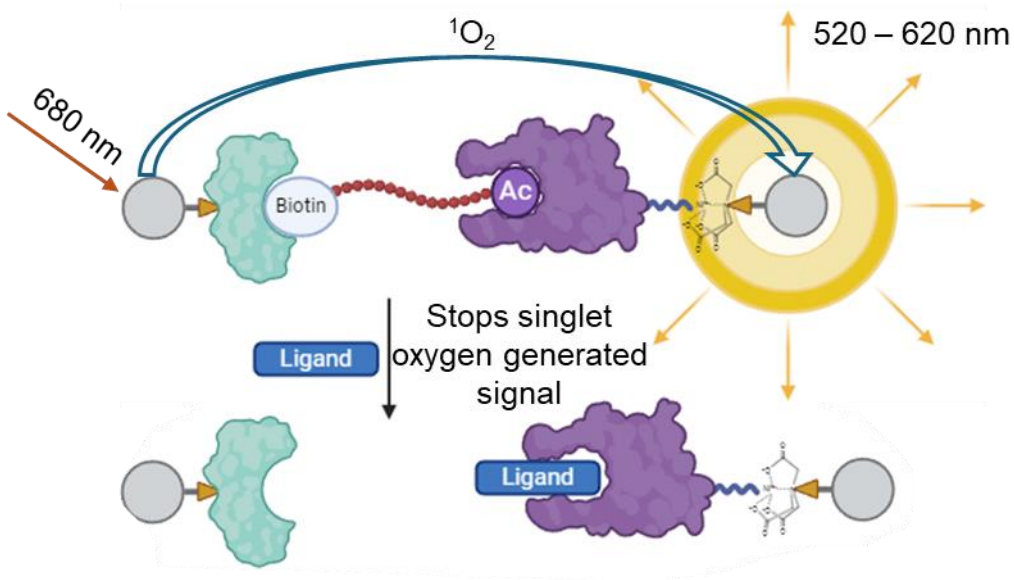

Figure 14: Illustration of the bead-based AlphaScreen® assay, to give an inhibition curve of a ligand figure created with biorender.com.

1.5.3 BROMO*scan* Assay

BROMO*scan*, BromoKdElect, and BromoMax are biophysical *in vitro* assays.[86] The BromoKdElect assay is a titration across 12 concentrations, using a 1 in 3 dilution, of which the resulting data gives K_d values against a specific target. A BromoMax assay tests a compound at a fixed concentration, giving the results as a % control (or protein) remaining, across 32-unique bromodomains from across a wide array of bromodomain containing proteins. Both of these assays are based on the same technology in order to gain binding affinity data.[86] The assays rely on ligands immobilised onto magnetic beads, which are known binders to a specific bromodomain, with a cleavable DNA tag attached (Figure 15).[86] When treated with ligands which bind, the immobilised ligand-bromodomain interaction breaks, the magnetic beads are removed with the remaining protein attached (Figure 15).[86] The DNA tag is then cleaved and amplified by qPCR to give a quantification of BRD remaining: thus, allowing for affinity of a BRD to be calculated based upon the ability of a given ligand to inhibit the immobilised ligand-BRD interaction (Figure 15).

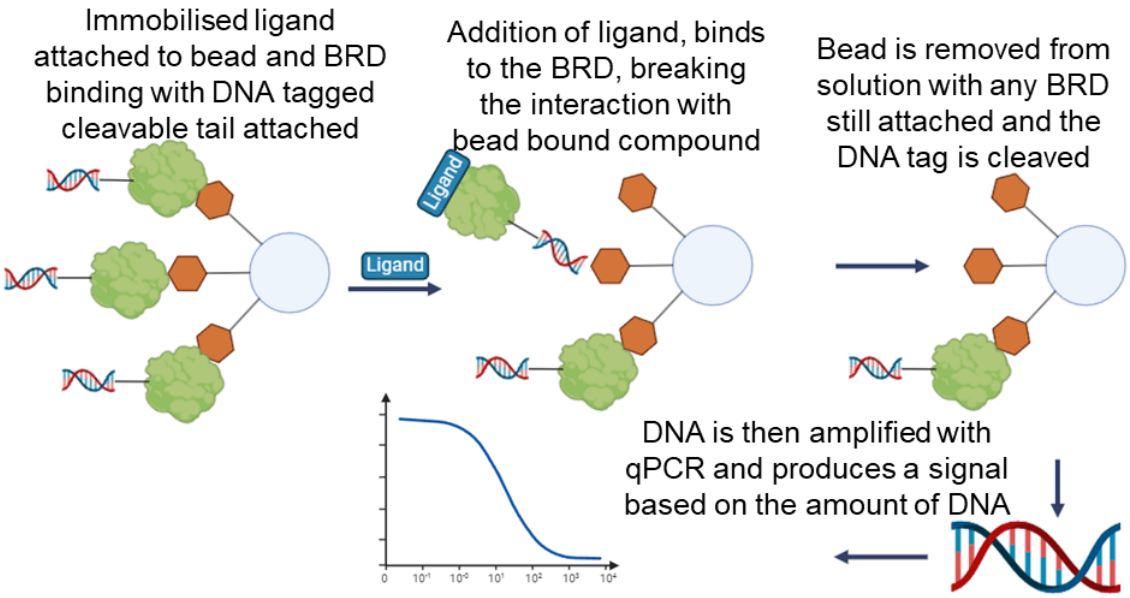

Figure 15: Schematic of how BROMO*scan* based assays function and produce *in vitro* BRD binding data, figure created with biorender.com.

1.5.4 Cell Titre Glo®

Cell viability, or cell death is often measured as a phenotypic effect as a function of protein inhibition or to ensure that ligands have not produced any undesirable cell death, interfering with potential phenotypic readouts. The Cell Titre Glo® is often used to measure cytotoxicity and proliferation, it involves treatment of seeded cells with different conditions, leaving for a set time period and then performing the assay. The cell viability is then measured by lysing the treated cells upon the addition of the assay reagents, and the resulting luminescent signal corresponding to the cell viability, which can be corrected to a vehicle control and given as a percentage. The luminescent signal produced corresponds to the level of ATP in the sample, which is only produced by living cells. The luciferase reaction used in the production of the luminescent signal from ATP involves the reaction of luciferin, using Mg^{2+} and oxygen as cofactors, with ATP to produce oxyluciferin catalysed by an engineered luciferase enzyme to produce a long-lasting luminescent signal (Figure 16). As ATP is required for the reaction of luciferin to oxyluciferin which is required to produce the signal, and only living cells produce ATP, providing a simple method to measure cell viability.

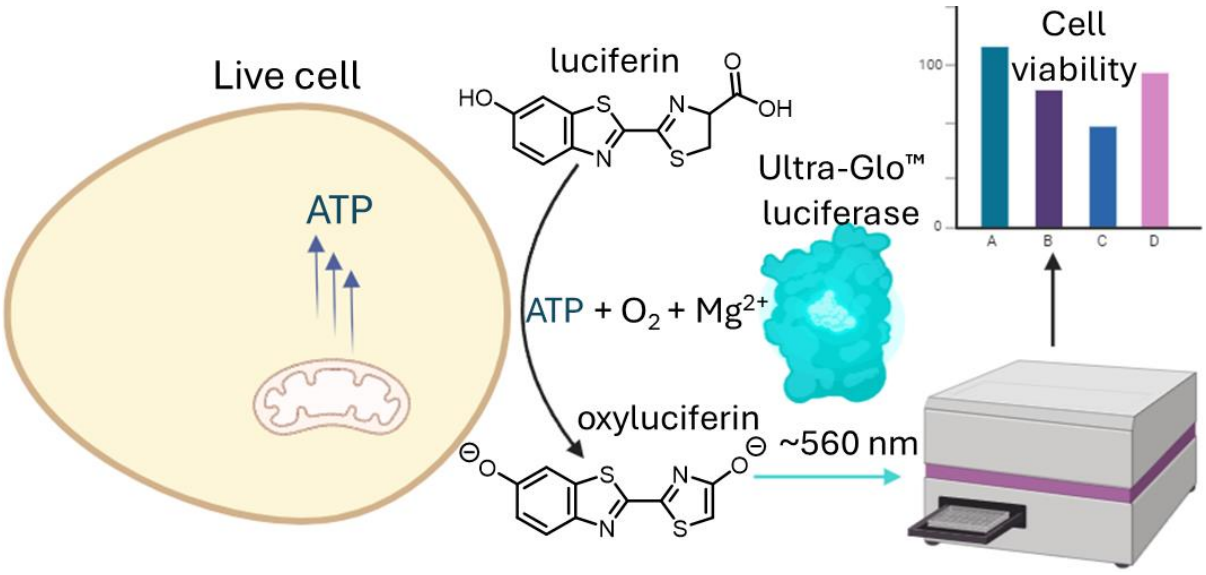

Figure 16: Cell Titre Glo® assay principles demonstrating how the measurements are taken, the source of signal and the chemistry underlying how the signal is produced, figure created with biorender.com.

1.5.5 Western Blotting

Western blotting is a technique used to qualitatively assess protein levels in cells. This is often used to monitor the disappearance of a particular protein during treatment of cells with a compound. Ligand-treated cells are aspirated after a specific time point, lysing, denatured and then loaded onto an SDS-PAGE gel (Figure 17). This allows for the proteins present within the lysate to separate based upon molecular weight, the separated proteins are then transferred onto a membrane, which is treated with a generic protein, to prevent non-specific antibody binding from occurring. A protein specific (primary) antibody is then added to the membrane, which binds to the protein of interest (Figure 17). A secondary antibody, specific to the primary antibody used is added, usually containing a fluorescent chromophore which can be visualised giving a western blot showing the effect of compound treatment in cells on that specific protein (Figure 17).

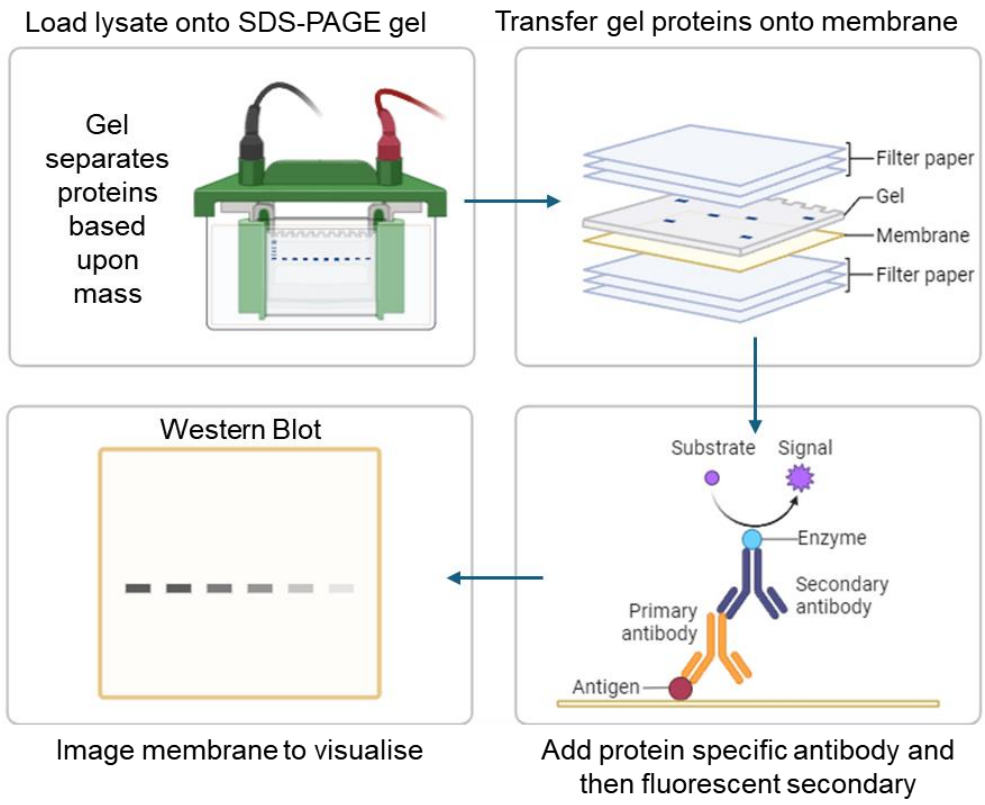

Figure 17: Illustration of the western blotting assay technique, figure created with biorender.com.

1.5.6 qPCR

A qPCR or RT-PCR is a technique which is often used to quantify the transcription of genes by quantitatively measuring the amount of mRNA present which codes for a specific protein, measuring the levels of transcription for the associated gene. Cells are treated and incubated for the appropriate time frame, after this they are lysed, and the RNA present is purified from the lysis solution by fractionation (Figure 18). To the RNA containing solution is added the complementary DNA (oligonucleotide sequence) which binds forming a double stranded complex. A compound is then added which binds to these double stranded complexes and produces a fluorescent signal (Figure 18). This allows for a real time quantification of the RNA levels in the treated cells, this means that as the complementary DNA binds to a specific RNA sequence coding a particular target protein in a quantitative manner (Figure 18). This allows the gene transcription to be measured and scaled relative to negative control, such as cells treated with DMSO. As this technique measures gene transcription, it is often complementary to techniques which quantify protein levels.

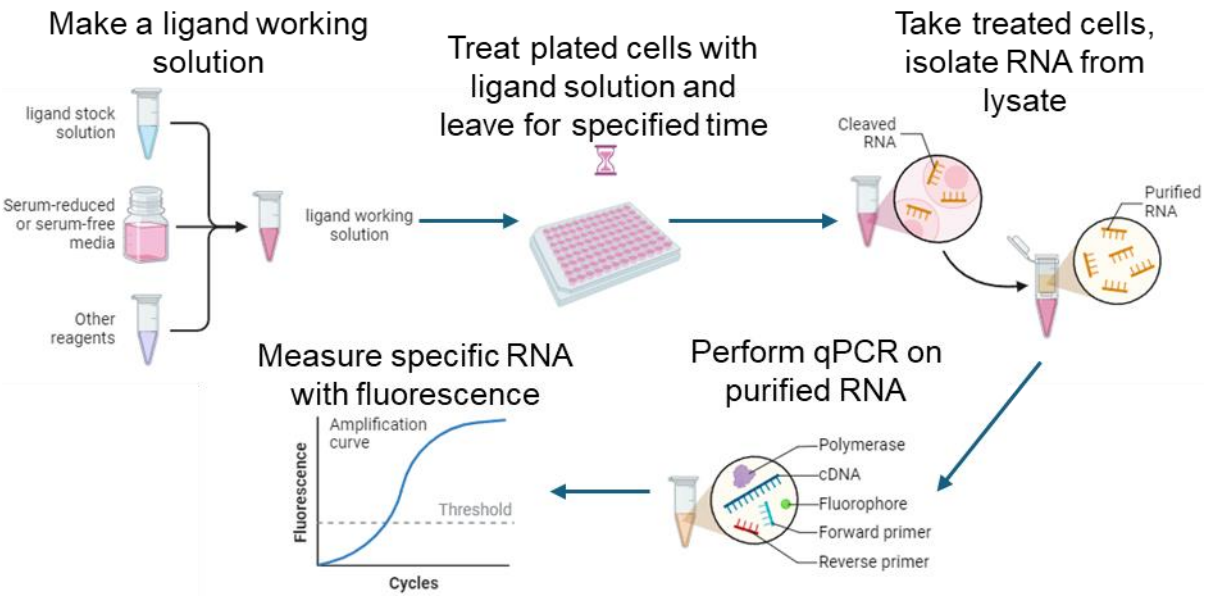

Figure 18: Schematic of a qPCR assay for measuring RNA levels, to quantify the expression of a specific gene, figure created with biorender.com.

1.6 Prior Work on CBP^{BRD} inhibitors

The Conway group is responsible for one of the original CBP^{BRD} inhibitors, ligand **1** (Figure 6 and 19), which has been further developed.[40,44]

1.6.1 Prior CBP^{BRD} ligands developed in the Conway group

Compound **1** exhibited poor selectivity for the CBP^{BRD} over BRD4(1) (3.6-fold), demonstrating the need for further improvements to the molecule. Upon co-crystallisation with the CBP^{BRD}, ligand **1** demonstrates some key ligand-BRD interactions in the KAc binding site, namely the 2 direct hydrogen bonds of the KAc mimic (cyan in Figure 19) with Asn-1168, and a water mediated hydrogen bond to Tyr-1125 (Figure 20).[40] The most significant change in the CBP^{BRD} binding site, is the induced fit pocket, created by the LPF shelf and Arg-1173 upon addition of **1** (Figure 20).[40] This is due to Pro-1110 forming hydrophobic interactions with the tetrahydroquinoline (THQ) of ligand **1** (dark blue in Figure 19), as well as Arg-1173 forming a cation-π interaction with the THQ along with a partial dipole interaction with the electronegative oxygen of the aryl methoxy (Figure 20).[40] The hydrophobic interactions between compound **1** and the CBP^{BRD} are between the KAc mimic and residues Phe-1111, Try-1125, Ile-1122, and Val-1174 as well as the THQ and residues Leu-1109 and Phe-1177.[40] The highlighted interactions afford the selectivity of **1** for the CBP^{BRD} such as Arg-1173 and the LPF shelf, which this work focusses on.

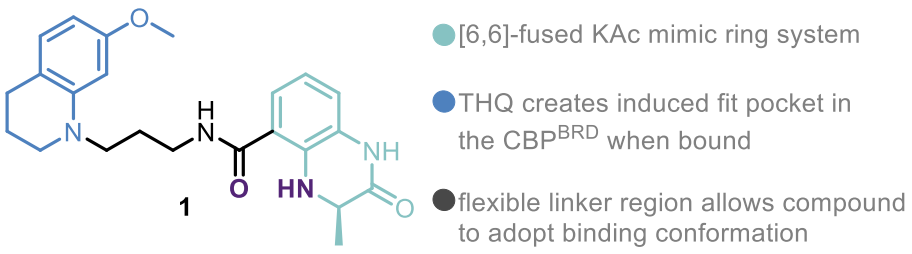

Figure 19: Chemical structure of ligand **1**, with the three sections the KAc mimic (blue), the THQ (dark blue), and the linker region (black) shown, as well as some of the key functions of each section, the intramolecular hydrogen bonding atoms are also shown in **bold** (purple).

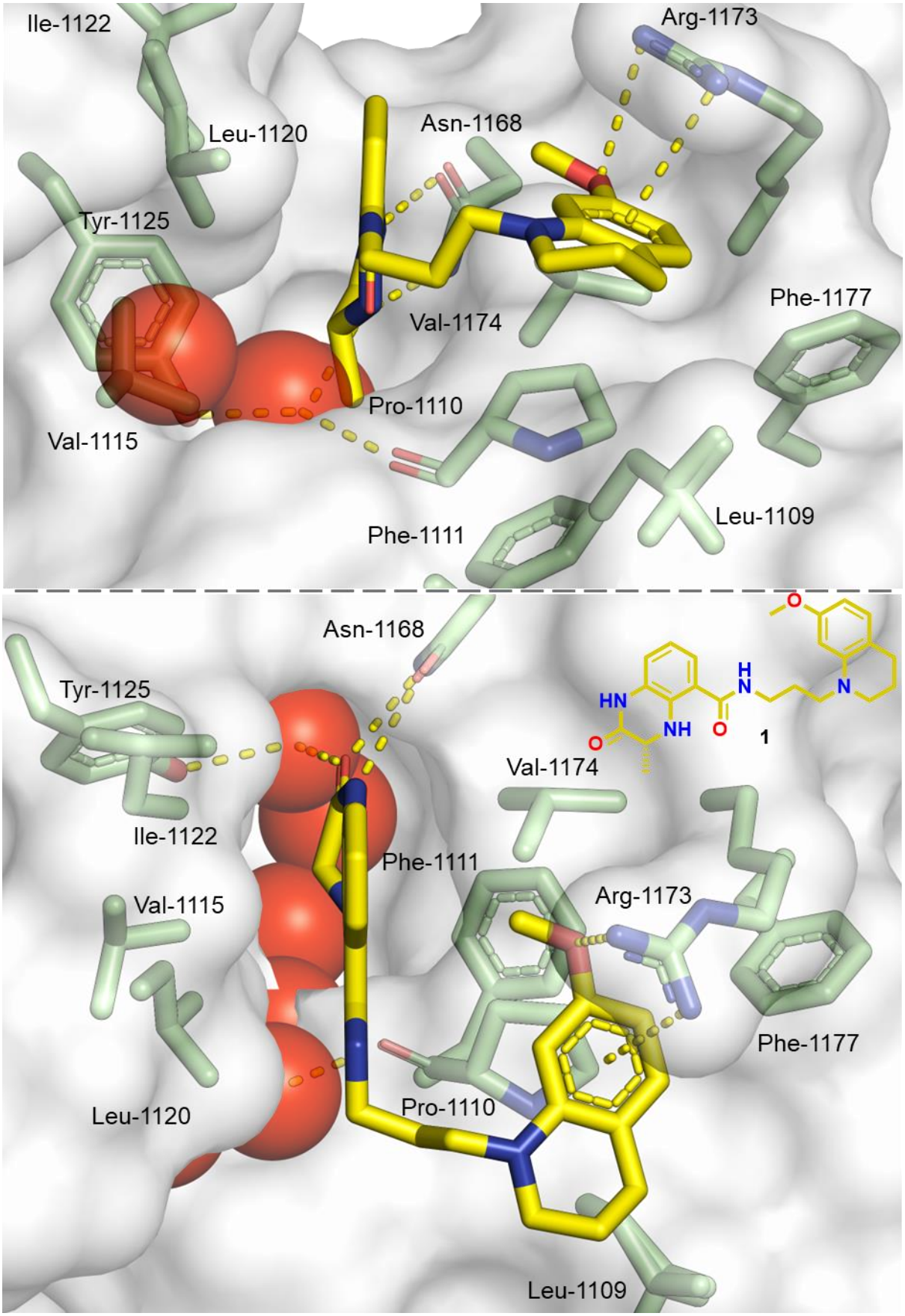

Figure 20: Co-crystal structure of **1** (yellow) bound to the CBP^{BRD} (PDB: 4NYX) at 1.10 Å resolution, with key interactions highlighted (yellow dashed line), viewed from the side (top) and the top (bottom), residues (green) and three letter code with number and water molecules as spheres (red) included.[40]

From original hit compound **1**, a change from a [6,6]-KAc mimic to a [6,7]-KAc mimic was conducted to give ligand **6**. Compound **6** afforded an improvement in selectivity for the CBP^{BRD} (6.1-fold vs 3.6-fold), but the affinity for the CBP^{BRD} had decreased (466 nM vs 390 nM) (Figure 21). To better understand this, the dynamics of the ligand were studied when bound to the CBP^{BRD} and without the presence of a protein. It was observed that compound **6**, when bound to the CBP^{BRD} adopted one conformation of the [6,7]-KAc mimic, in the absence of the BRD, the intramolecular hydrogen bond (**purple** atoms in Figure 21A) created an energy barrier to adopting the binding conformation as only the non-binding [6,7]-KAc conformation was observed.[44] This proposed energy barrier aids in the explanation of the weaker affinity for the CBP^{BRD} but does not explain why ligand **6** continues to bind to BRD4(1). In order to investigate this a co-crystal structure of **6** bound to BRD4(1) was obtained (Figure 21C).[44] This combined with the co-crystal structure of ligand **6** bound to the CBP^{BRD}, identified a conformational change undergone by **6** upon on-target binding (Figure 21B and 21C).[44] When bound to the CBP^{BRD}, **6** adopts a "curled-up" binding mode, caused by a cation-π interaction between Arg-1173 and formation of the induced fit pocket (Figure 21C). Whereas, when bound to BRD4(1), compound **6** adopts a linear conformation, which allows the compound to form hydrogen bonding interactions with Lys-91 and a π-π interaction with Trp-81 (Figure 21C).[44] In order to overcome the decreased affinity for the CBP^{BRD} caused by intramolecular hydrogen bonding, the amide moiety of **6** was replaced with a non-hydrogen bonding *E*-alkene bioisostere, to give **OXFBD05** (Figure 21A).[44] **OXFBD05** exhibited improved affinity for the CBP^{BRD}, with no detectable affinity for BRD4(1) by ITC and showed no affinity for 12 bromodomain containing proteins at 1 μM by BROMO*Scan*, unfortunately **OXFBD05** could not be co-crystallised with BRD4(1).[44]

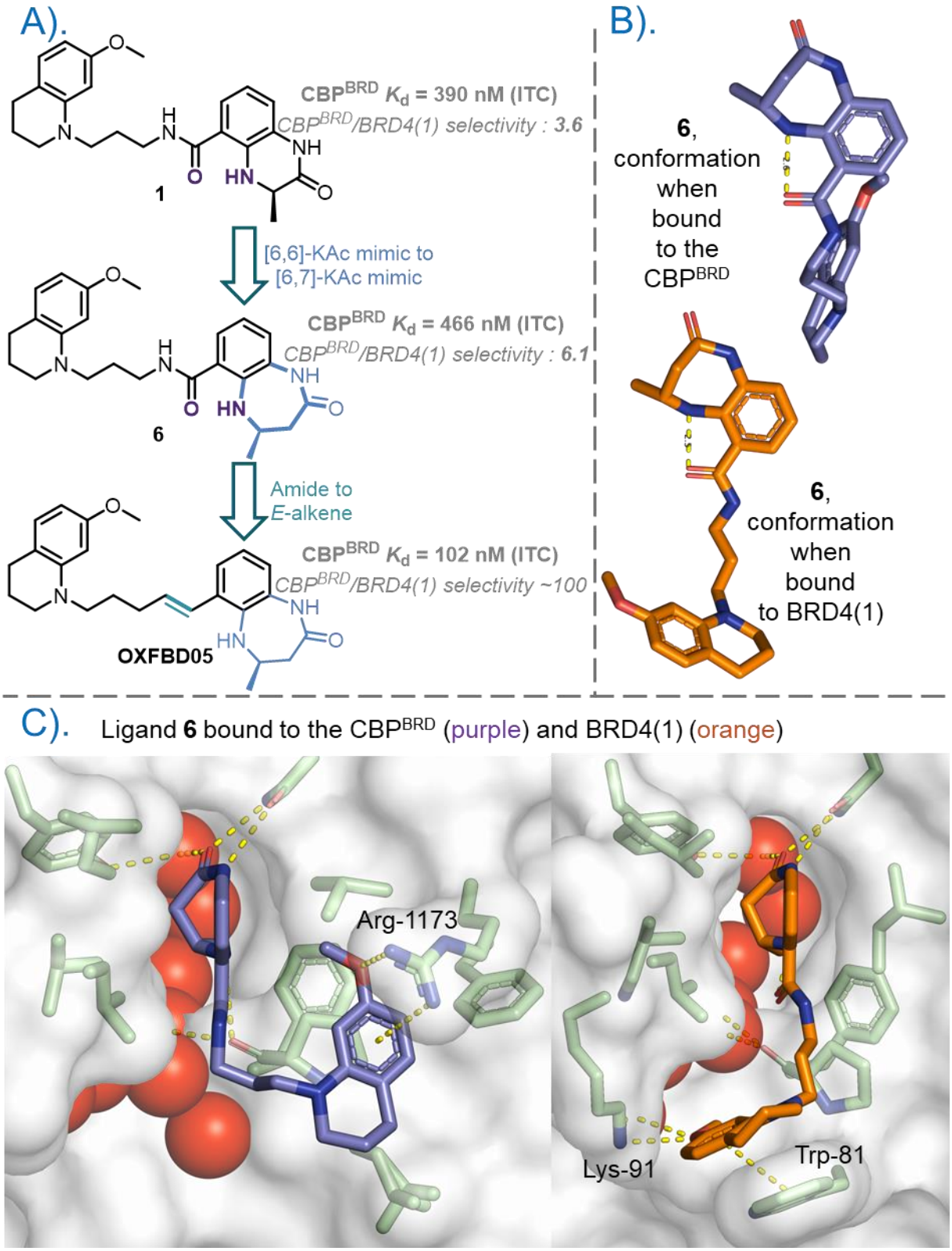

Figure 21: A). CBP^{BRD} ligands developed within the Conway group, the transformations to reach each ligand highlighted and their respective affinities and selectivities; B). Protein bound conformations of ligand **6** bound to the CBP^{BRD} (purple) and BRD4(1) (orange), demonstrating the on-target "curled up" conformation, the intramolecular hydrogen bond is shown (yellow dashed line); C). Co-crystal of **6** bound to the CBP^{BRD} (purple ligand, left, PDB: 6YIM) at 1.23 Å resolution and BRD4(1) (orange ligand, right, PDB: 6YIN) at 1.53 Å resolution, residues (green) and water molecules as spheres (red) as shown along with the three-letter code for different residues between the two BRDs which **6** interacts.

1.6.2 Prior Macrocyclic ligands targeting the CBP^{BRD}

After observing this switch in conformation of ligand **6** upon binding to the on-target CBP^{BRD}, therefore it was hypothesised that macrocyclisation offered a means to gain further affinity and selectivity for the CBP^{BRD}, which has proved an effective strategy in the literature.[58,59,69,78,87] Constraining the compound into a macrocyclic scaffold, precludes binding to the major off target of BRD4(1) as the covalent bonds generate a high energy barrier to adopting a linear conformation. The "curled-up" conformation when bound to the CBP^{BRD} is similar to the C-shaped bio-active shapes observed in co-crystal structures in many successfully implemented macrocyclisation strategies in medicinal chemistry campaigns, often leading to approved drugs.[78] Dr Mustafa Moroglu, a previous DPhil student, endeavoured to explore macrocycles in order to prove these as viable ligands for the CBP^{BRD} (Figure 22).[88] Through his work three different macrocyclic series were synthesised, based upon the linear ligand **OXFBD05**, an alkyl macrocycle (compound **7**), two triazole macrocycles (compound **8** and **9**), and three macrolactams (compound **10**, **11** and **12**) (Figure 22).[88] Macrolactams emerged as the only macrocycles which showed binding affinity to the CBP^{BRD} by ITC. However, the reason for compounds **7**, **8** and **9** demonstrating no detectable binding was not illucidated. The macrolactams exhibited 10-fold decreased affinity for target CBP^{BRD} compared to **OXFBD05**, and no detectable affinity for BRD4(1).[88] Compounds **10** and **11** appeared to offer an improvement in selectivity over a linear analogue that was synthesised which demonstrated affinity for BRD4(1).[88] However, due to time constraints on the project the reason for the decrease in on-target affinity was not investigated and no assays for quantifying off-target binding apart from ITC were conducted.[88] Therefore, no fold-selectivity could be calculated for ligands **10**-**12**.[88] Again, due to time constraints none of the

macrolactam ligands were evaluated for activity in a phenotypic assay such as, monitoring for decreased oncoproteins by Western blotting or oncogene transcription by qPCR, in an appropriate cancer cell line.[88]

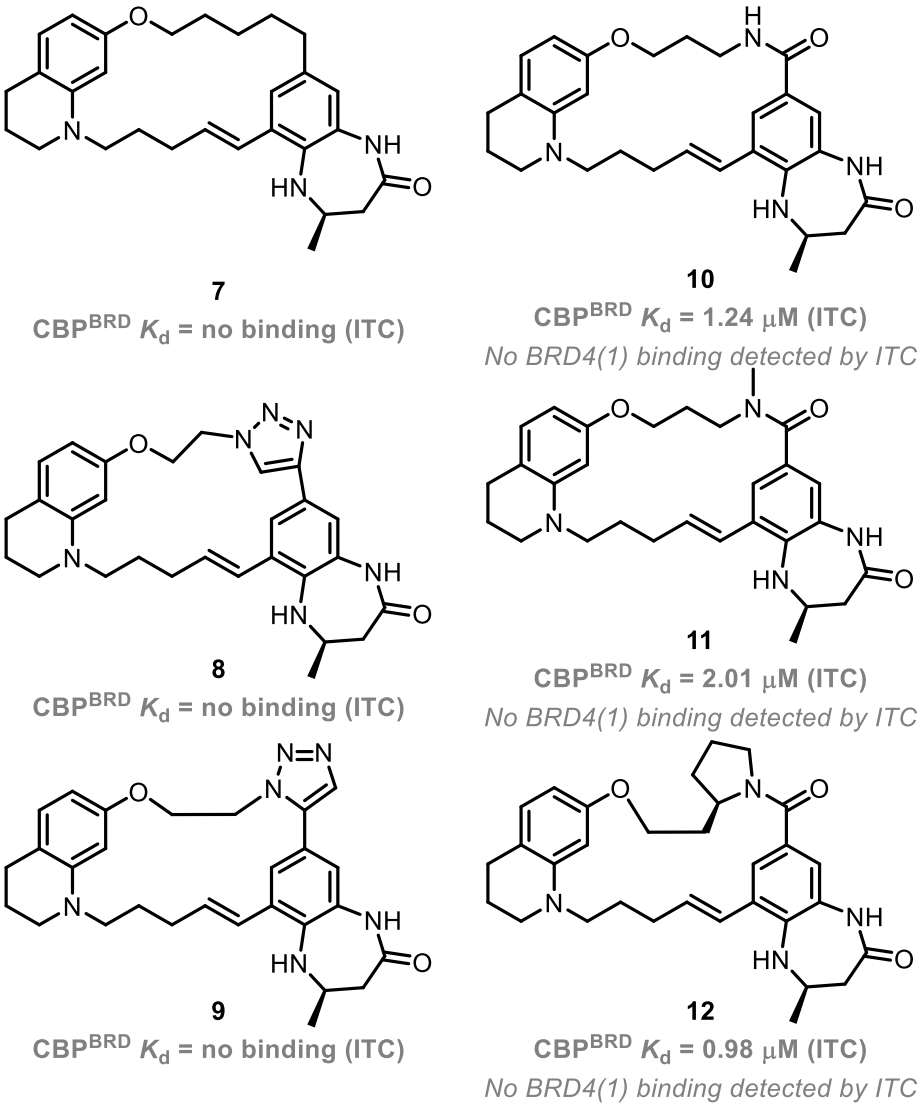

Figure 22: Previously synthesised ligands targeting the CBP^{BRD}, with their respective ITC binding properties displayed.[88]

Therefore, the hypothesis of macrocyclic ligands targeting the “curled-up” binding conformation and thus affording a high affinity, selectivity, and potent ligand for the CBP^{BRD} has yet to be fully validated. Hence, the work in this thesis aims to verify this hypothesis, through ligand synthesis, binding affinity measurement, structural investigation, and phenotypic assays.

1.7 Project Aims

The main aim of the research project which this thesis describes is a macrolactam SAR with the goal of improving affinity for the CBP^{BRD} and increasing selectivity. In order to evaluate the novel macrocycles, thorough *in vitro* characterisation will be carried out, with the goal of identifying a potent hit ligand, through a variety of biophysical techniques. The macrocyclic hit will be further screened across a panel of BRDs to compare against other published ligands. The binding mode of the macrolactams shall be characterised using X-ray crystallography and compared to an appropriate linear analogue. Furthermore, the hit compound will be assayed in an appropriate cancer cell line for the ability to down regular oncogene transcription and oncoprotein levels, with the goal of decreasing cancer cell proliferation, without effecting cell viability.

Then with a macrolactam hit ligand identified, possible improvements to the scaffold will be investigated as a means of gaining further improvements to affinity, selectivity, and ultimately phenotypic effect in cells.

Another point of investigation is into the ligands that did not bind (such as compound **7**, **8** and **9**), and what could have been the underlying cause for the lack of detectable affinity to the CBP^{BRD} which was observed.

Chapter 2:

Synthesis of Macrolactam Ligands to Selectively Target the CREBBP Bromodomain

2.1 Introduction

In order to discover higher affinity and more selective macrocyclic ligands, the previous lactam scaffolds (Figure 21 and Figure 23A) were used as a source of inspiration.[88] From these examples, a series of ligands were designed (Figure 22B) utilising the same common intermediate (Figure 23A, compound **13**) which was previously employed in the synthesis of the original macrolactam ligands (Figure 23A, **10**, **11**, and **12**). These ligands would allow for a structure activity relationship (SAR) to be built through the difference in binding affinities of target ligands (Figure 23B). The target ligands aim to provide a deeper understanding of the macrolactam SAR, building upon the structures of prior macrolactams. The chemotypes explored include decreased and increased alkyl chain lengths (Figure 23B, **14** and **15**); different β-turn mimetic diastereomers (Figure 23B, **16** and **17**); and building increased rigidity through inclusion of ring systems into the linker region (Figure 23B, **18** and **19**). These ligands aim to improve physiochemical properties of **OXFBD05** through both an increase in hydrogen bond acceptors and donors and the effect of macrocyclisation itself.[89–92] Although the previously synthesised macrolactams were the only macrocycle chemotype that achieved measurable binding to the CBP^{BRD} by ITC, their binding affinities were considerably weaker than that of **OXFBD05**.[44,88] The target ligands aim to provide a deeper understanding of the macrolactam SAR, building upon the structures of prior macrolactams.

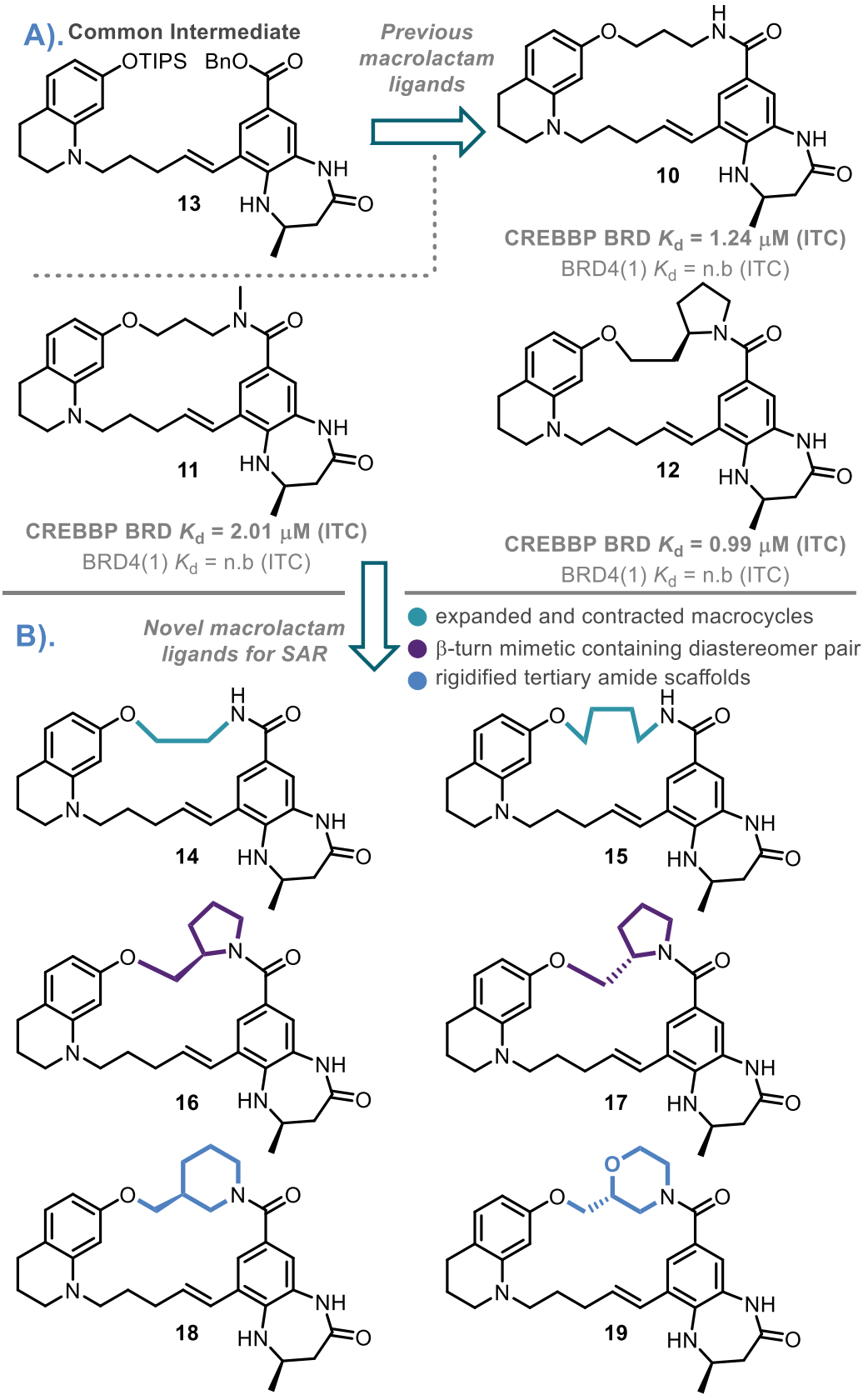

Figure 23: A). The common intermediate (**13**) and the previously synthesised lactam containing macrocyclic ligands targeting CBP^{BRD} (**10**, **11** and **12**), along with their respective binding affinities and selectivities by ITC; B). Novel macrolactam ligands in the small SAR screen, with the chemotypes highlighted in different colours (**14**, **15**, **16**, **17**, **18** and **19**).

2.2 Synthesis of the common intermediate

Firstly, in order to produce the six desired macrolactam ligands, a large quantity of the common intermediate **13** was needed. Although the synthesis of this intermediate has previously been reported, it had never been achieved on such a large scale.[88] The synthesis of this intermediate is aided by its convergent nature, as outlined in the retrosynthesis which is the same as that carried out previously (Figure 24).[88]

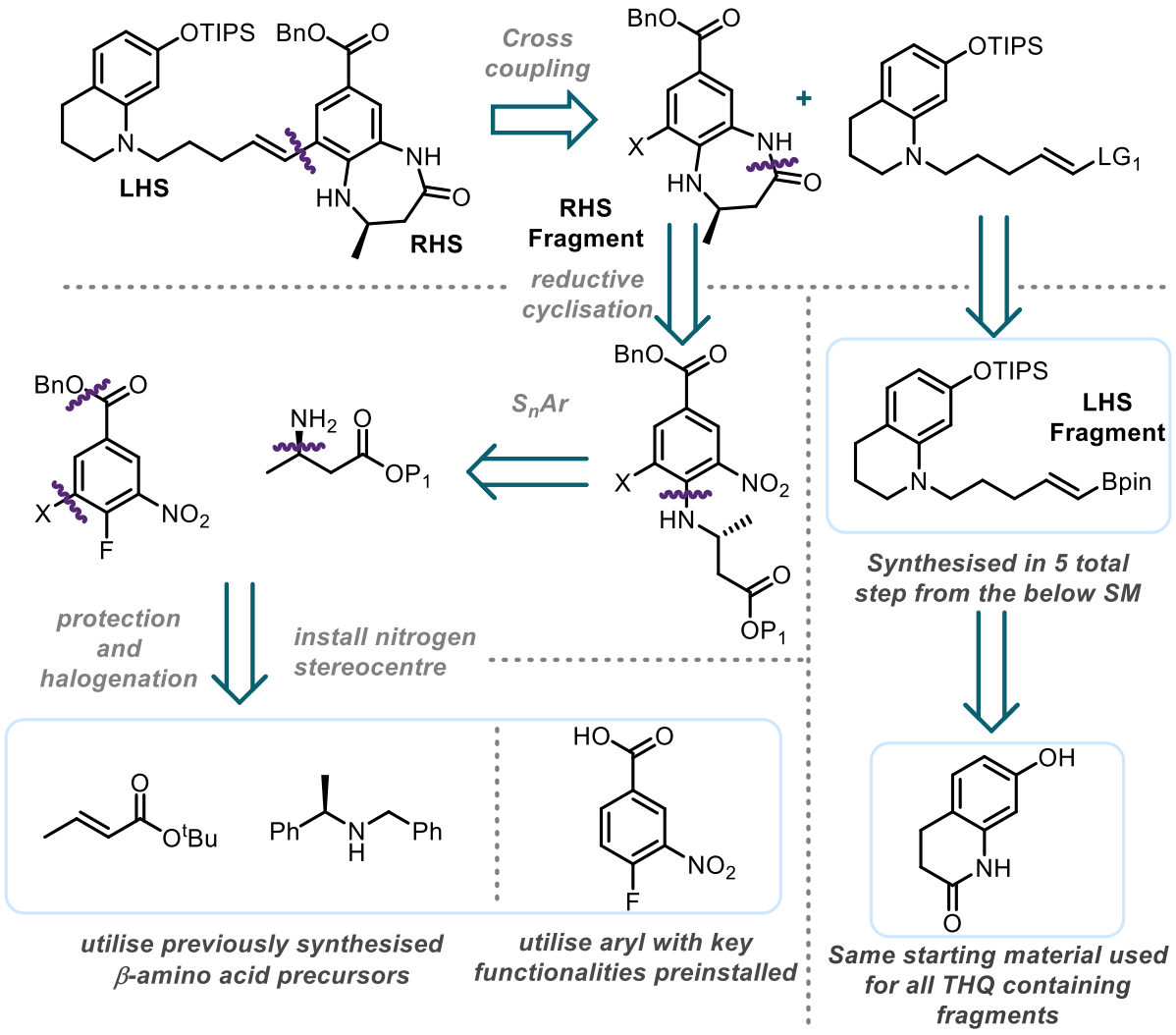

Figure 24: Retrosynthetic analysis of the common intermediate **13** from which macrolactam ligands can be derived, utilising the previously synthesised THQ fragment (compound **30**), a commercial aryl building block and using the β-amino acid building block **23**.

Due to the convergent nature of the key intermediates' synthesis, the molecule can be divided into a left-hand side (LHS) and right-hand side (RHS) fragments. The LHS

fragment contains the key tetrahydroquinoline, which participates in the cation-π interaction with Arg-1173 on the CBP^{BRD}, and the *E*-alkene is primed to undergo a Suzuki reaction during the final step of the synthesis. The RHS fragment contains the [6,7]-KAc mimetic along with the ester handle for macrolactamisation and an aryl halide bond primed to undergo the Suzuki reaction.

2.2.1 Synthesis of the fragments

The RHS fragment was afforded by combining the functionalised aryl ring and the β-amino acid, in an S_NAr reaction then the 7-membered ring is forged by a reductive amide bond formation (see Figure 24, left hand side). To form the RHS fragment iodination of the aromatic starting material was performed using iodine in fuming sulfuric acid to give compound **20** (Scheme 1, left hand side, step a). These harsh conditions are required as the ring is highly deactivated towards electrophilic aromatic substitution. Mono-iodination occurs at the meta position, due to the directing effects of both the nitro and carboxylic acid moieties. The singular spot by TLC indicated that the reaction was completed however by NMR spectroscopy residual starting material remained. This leftover starting material possessed a similar polarity to the product, therefore separation of residual un-iodinated material from **20** could not be achieved by column chromatography. As a result, the iodination reaction was left for a further 24 hours with another equivalent of iodine giving full conversion to **20** with no remaining starting material observed upon analysis. This is required as the remaining starting material can be carried forward until the Suzuki cross coupling, giving a persistent impurity in future reactions. The halogenated aryl ring then undergoes a benzyl protection in order to prevent the carboxylic acid interfering in future reactions, giving compound **21** (Scheme 1, left-hand side, step b). An S_NAr reaction is then carried out, using the enantiopure β-amino acid **23** to give intermediate **24** (Scheme 1

right hand side and left-hand side, step c). Once attached, the carboxylic acid can be obtained *via* selective cleavage of the *tert*-butyl ester under acidic conditions and the [6,7]-KAc mimic formed via a reductive cyclisation to give the RHS fragment or **25** (Scheme 1, step d, **25** in the light blue box). All steps were carried out in high yields giving the desired fragment **25** on a 6.5 g scale.

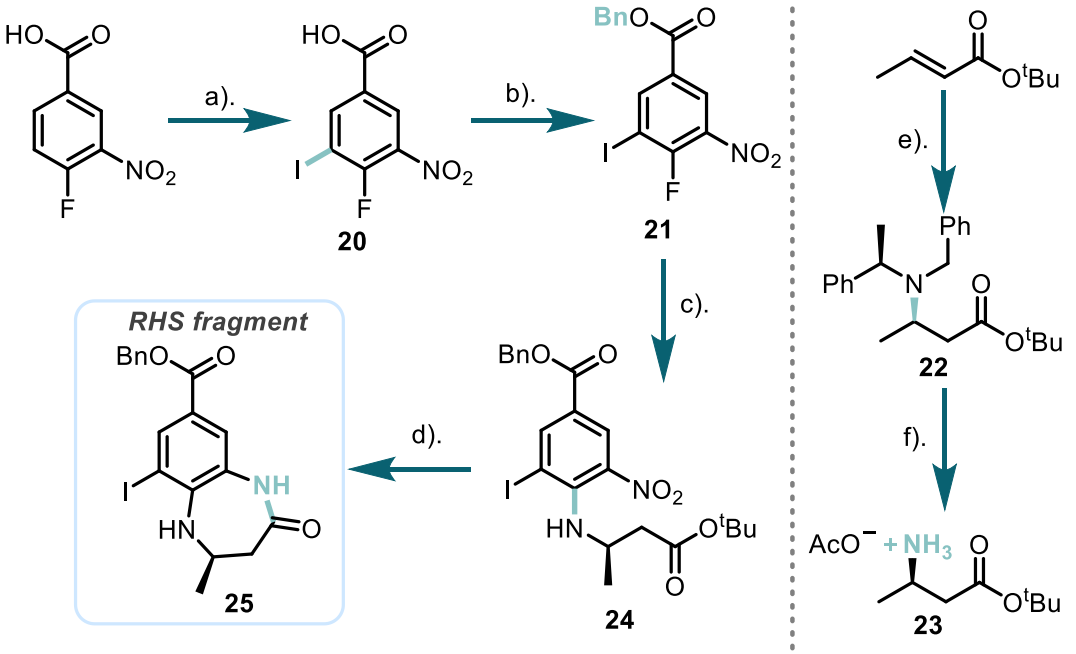

Scheme 1: Synthesis of the [6,7]-KAc containing aromatic (RHS fragment), *Reagents and conditions:* a). I_2, fuming H_2SO_4, 85 °C, 48 h, 91%; b). Benzyl bromide, K_2CO_3, DMF, 60 °C, 5 h, 72%; c). Compound **23**, Cs_2CO_3, tol, 85 °C, 48 h, 97%; d). TFA:CH_2Cl_2 (1:1 *v*/*v*), r.t., 2.5 h, followed by, Fe, AcOH, 120 °C, 4.5 h, 91%; e). (*R*)-(+)-*N*-Benzyl-α-methylbenzyl amine, *n*-BuLi, THF, −78 °C, 4.5 h, 89%; f). $H_{2\,(g)}$, 20% $Pd(OH)_2/C$, AcOH, MeOH, H_2O, r.t., 20 h, 86%.

The LHS fragment **30** was synthesised in a similar manner to previously reported (see Scheme 2).[88] This involves phenol protection, amide reduction, amine alkylation and hydroborylation to give fragment **30**. The synthesis was carried out on a large scale (>5 grams of each intermediate), maintaining high yields (>70%) for each step of the synthesis. The installation of TIPS protecting group proceeded in very high yields due to the formation of a protonated *N*-triisopropylsilylimidazole intermediate which rapidly reacted with the deprotonated phenol.[93] The reaction was performed in DMF, as this solvent acts as a catalyst and thus increased the rate of phenol silylation, giving

compound **26** in 96% yield (Scheme 2, step a).[93] In the $LiAlH_4$ reduction of compound **26** to **27**, by increasing the reaction time by 1.5 h, the reaction proceeded cleanly to completion removing the need for column chromatography (Scheme, step b). The alkylation of **27** with **28** (Scheme 2, step e), to form tertiary amine **29** was performed thermally using 5 equivalents of base at 100 °C, supplemented with TBAI (previously reports used KI) for 48 h (Scheme 2, step c). These conditions are harsher than previously reported but gave an increase in yield of 20%, the resultant increase can be attributed to the thermal heating and change of catalytic iodinated reagent.[94] The key hydroboration reaction proceeds with exquisite stereoselectivity giving only the *trans*-alkene isomer **30** (Scheme 2, step d).[95,96] In this case the reaction is carried out neat with Schwartz's reagent and the electrophile all in one pot, undergoing syn addition of the Zr-H bond, followed by attack of the C-Zr bond onto the boron atom, regenerating the catalyst and producing compound **30,** in 73% yield.

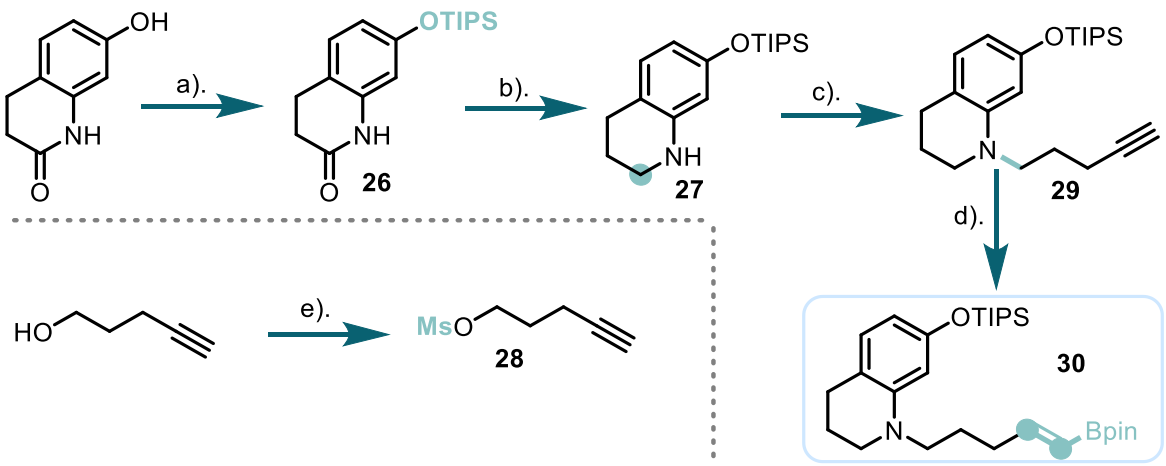

Scheme 2: Synthesis of THQ bearing fragment **30**. *Reagents and conditions*: a).TIPSCl, imidazole, DMF, r.t., 48 h, 96%; b). $LiAlH_4$, Et_2O, 0 °C – r.t., 4.5 h, 97%; c). Compound **28**, TBAI, DIPEA, DMF, 100 C, 48 h, 76%; d). HBpin, Cp^*_2ZrClH, NEt_3, 60 °C, 18 h, dark, 73% (>95% *E*-alkene by NMR); e). Mesyl chloride, NEt_3, CH_2Cl_2, 0 °C – r.t**,** 4 h, 95%.

2.2.2 Common Intermediate **13** synthesis

With both fragments now in-hand at a suitable scale, the Suzuki cross-coupling was carried out utilising a lower palladium catalyst loading (from 0.05 equiv. to 0.025 equiv.), lowering the cost and environmental impact of the reaction. It is worth noting that the reaction mixture was separated into 4 reaction flasks to avoid uneven heat distribution, a common occurrence in large reaction vessels, meaning approximately 3.5 g total mass of **30** and **25** were placed into each vessel.[97] Purification of this reaction proved challenging as the product possess a similar retention time to the unreacted starting material **30**. Nonetheless, 6.5 g of compound **13** was still obtained. With the key intermediate now in hand the target macrocycles could be afforded.

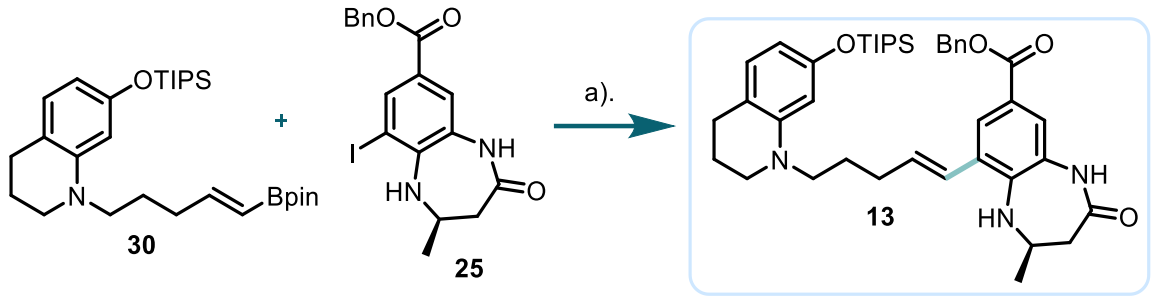

Scheme 3: Combination of the LHS and RHS fragments in a Suzuki reaction giving compound **13**, *Reagents and conditions:* a). $Pd(dppf)Cl_2$, K_2CO_3, 1,4-dioxane:H_2O (9:1 *v*/*v*), 100 °C, 18h, 65%.

2.3 Reaction Optimisation

2.3.1 Alkylation Optimisation

Reaction optimisation proved a necessary step as upon attempting the below phenol alkylations (Scheme 4) the yields proved far lower than those previously reported.[88] Previously this alkylation had given 39 – 25% yields, however, the yields achieved now ranged from 30 – <1% representing a precipitous decrease.

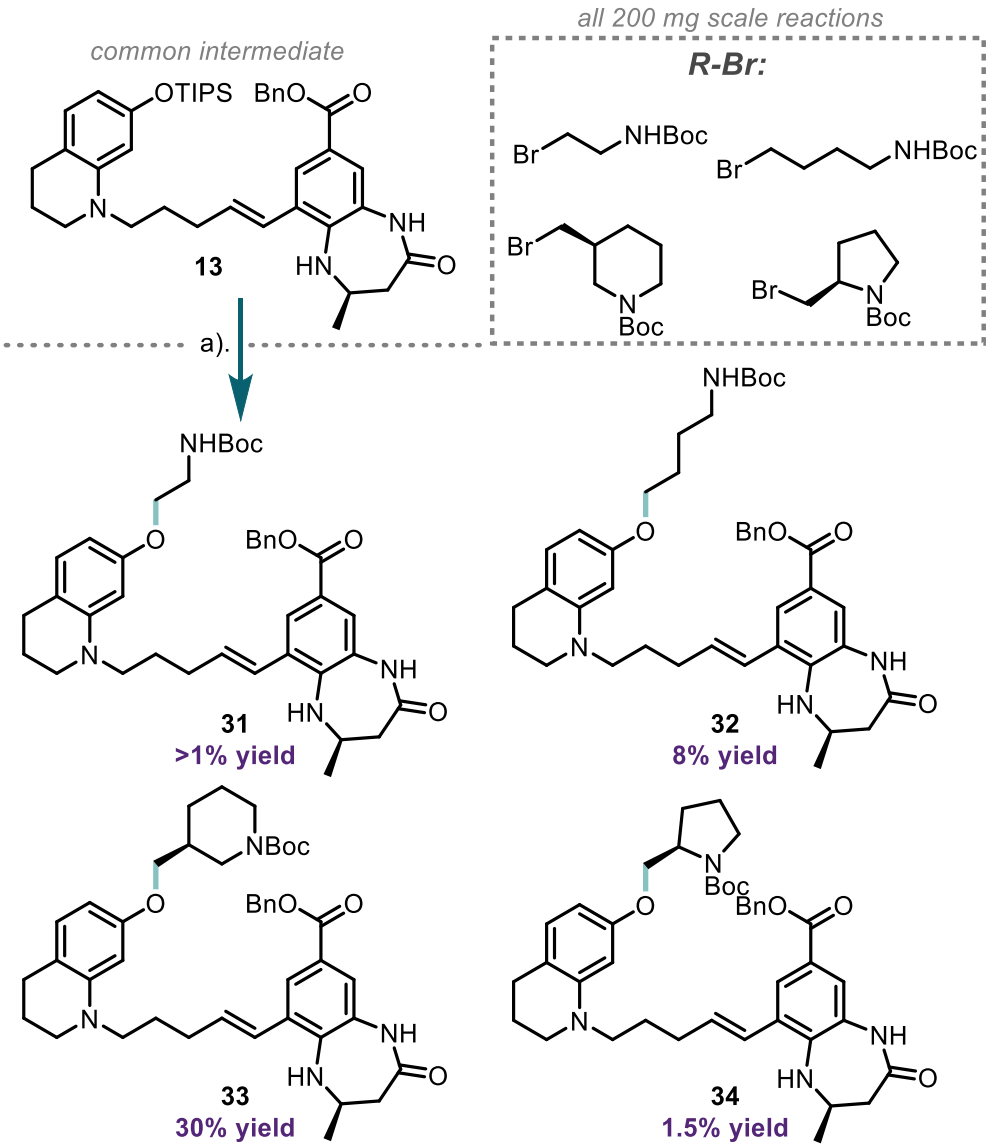

Scheme 4: Initial attempts at alkylating the deprotected phenol fragment produced from the common intermediate, with the alkylating reagents using in the grey dashed box, and the yields highlighted in purple to demonstrate the low yields, *Reagents and conditions:* a). TBAF (1M in THF), THF, r.t., 1 h followed by R-Br, K_2CO_3, 85 °C, DMF, 24 h.

Thus, in order to improve reaction with these unreactive electrophiles, a condition screen was performed. *Tert*-butyl (*S*)-2-(bromomethyl) pyrrolidine-1-carboxylate) (R-BR-1) was chosen for the screening conditions as the opposite enantiomer had proved unreactive under the previous alkylation conditions (reaction shown in Scheme 5, condition 1 of Table 1). The opposite enantiomer of R-BR-1 was no longer available on a sufficient scale to undergo the screen and hence its enantiomer was chosen. The low reactivity of the electrophile is potentially due the *tert*-butyl group sterically blocking

the electrophilic alkyl bromide from nucleophilic attack. The ratio of un-reacted phenol to desired product compound **35** for the model reaction (Scheme 5) was calculated by using the corresponding peak area in LC-MS chromatograms for the screened reaction conditions (shown in Table 1, see Appendix C Figures 1-7 for corresponding chromatograms and MS data).

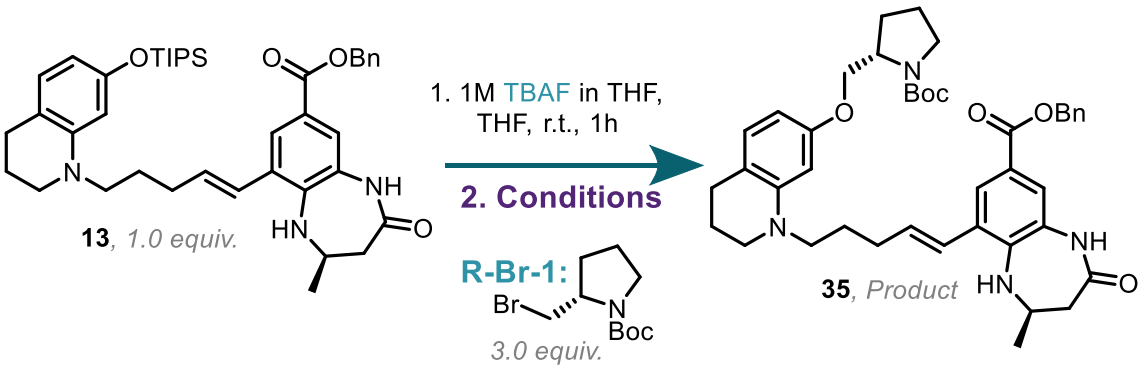

Scheme 5: Model phenol alkylation reaction on which the different conditions below were screened.

Table 1: Alkylation conditions screened for the reaction of the phenol and alkyl bromide to give **35** as shown in Scheme 5, with the improvements in product to unalkylated phenol remaining highlighted in the **bold green** text.

Number	Conditions	LC-MS ratio of phenol to product
1	K_2CO_3, DMF, 85 °C, 18 h	1 : 0.2
2	K_2CO_3, DMF, 100 °C, 18 h	1 : 0.1
3	**K_2CO_3, TBAI, DMF, 85 °C, 18 h**	**1: 0.4**
4	K_2CO_3, MeCN, 85 °C, 18 h	1: 0.2
5	**Cs_2CO_3, DMF, 85 °C, 18 h**	**1 : 0.7**
6	Cs_2CO_3, MeCN, 85 °C, 18 h	1 : 0.2
7	K_2CO_3, DMSO/MeCN (1:1), 100 °C, 1 h, μW	1 : 0.2

From the seven conditions trialled, optimum conversion was obtained with Cs_2CO_3, a stronger more soluble base (condition 5), and TBAI, a catalytic nucleophilic iodinating reagent (condition 3) (highlighted in green text Table 1).[98–101]

2.3.2 Macrolactamisation Optimisation

As the alkylation reaction had proved challenging prior to proceeding further in the ligand synthesis, the amide coupling reaction conditions used for the macrolactamisation were optimised in a small screen. This is due to the macrolactamisation providing low yields in prior syntheses ranging from 51% to as low as 12% yield. The previously synthesised propyl chain-containing macrolactam (Compound **10**) was used as a model substrate. Firstly, the di-protected intermediate **36** was synthesised on a scale which would allow for both the reaction conditions and the reaction concentration to be optimised for the macrolactamisation step (Scheme 6). The phenol alkylation was performed utilising 1 g of **13** to give more than 500 mg of intermediate **36**.

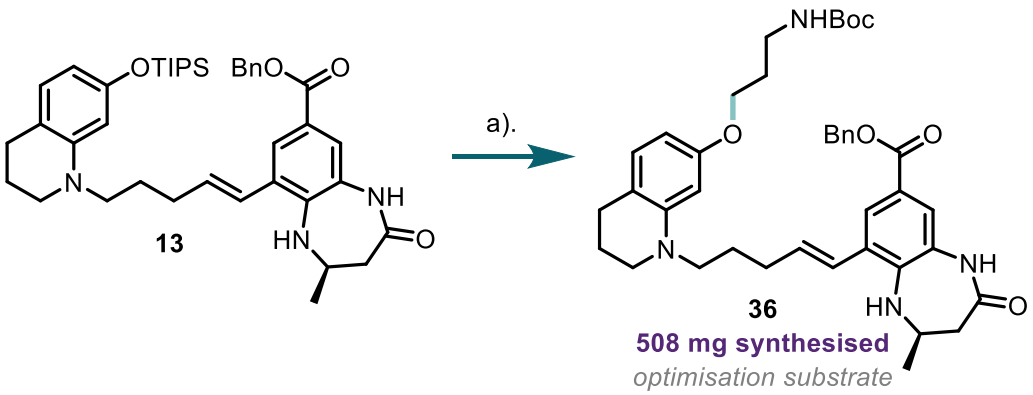

Scheme 6: Synthesis of the intermediate **36** to be utilised in the macrocyclisation reaction condition screen, *Reagents and conditions:* a). 1M TBAF (in THF), THF, r.t., 1 h, followed by, *tert*-butyl (3-bromopropyl) carbamate, K_2CO_3, DMF, 65 °C, 48 h, 51%.

PyBOP was previously utilised as the amide coupling reagent, DIPEA as the base, in DMF (0.002 M) at r.t. for 48 h.[102] With these conditions yields of <50% of the desired macrocycle were achieved, as this is the final step, an increase in yield at this late

stage of the route was highly desirable. With PyBOP as a starting point a variety of coupling reagents were chosen across different families of amide bond forming compounds, these were: HATU, COMU, TCFH and HOBt with EDC (the structure of each is shown in Figure 26).[102–106]

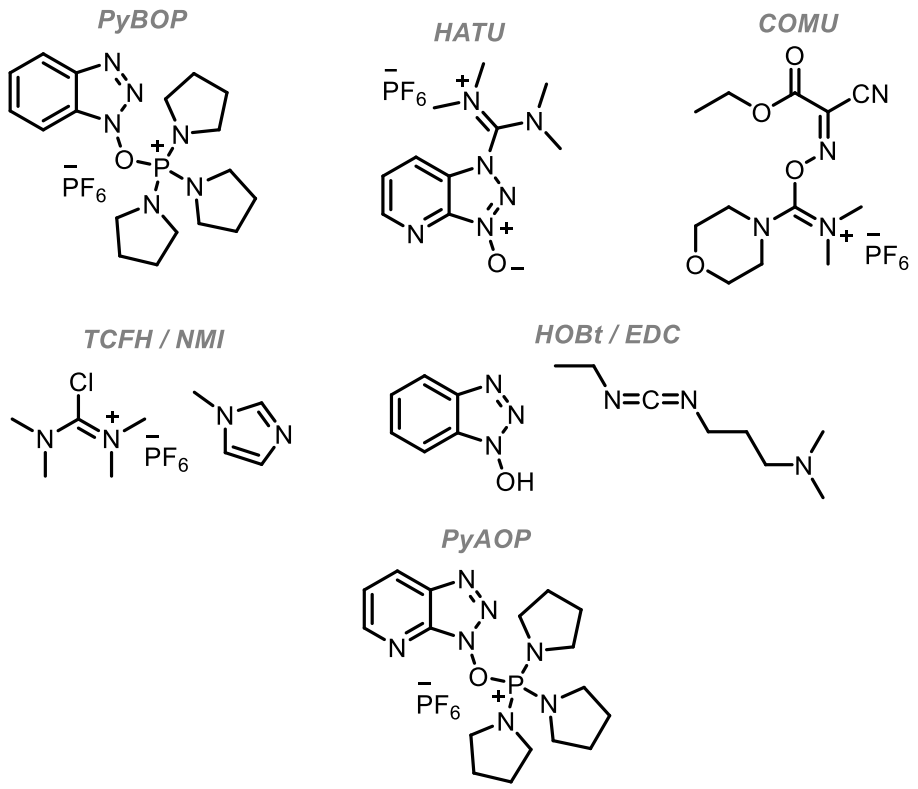

Figure 26: Amide coupling reagents chosen for reaction screening of the macrolactamisation reaction using the model substrate.[102,103,105,107–109]

These reagents (Figure 26) were utilised for the macrolactamisation final step, after unveiling the model substrate using LiOH, followed by TFA to give the desired carboxylic acid and amine containing compound **37** (Scheme 7A). The amide coupling reactions were monitored by LC-MS for the formation of desired products (Scheme 7B). Unfortunately, only the reactions with HATU and PyBOP showed product **10** formation by LC-MS, and both produced similar isolated yields after purification (Table 2).

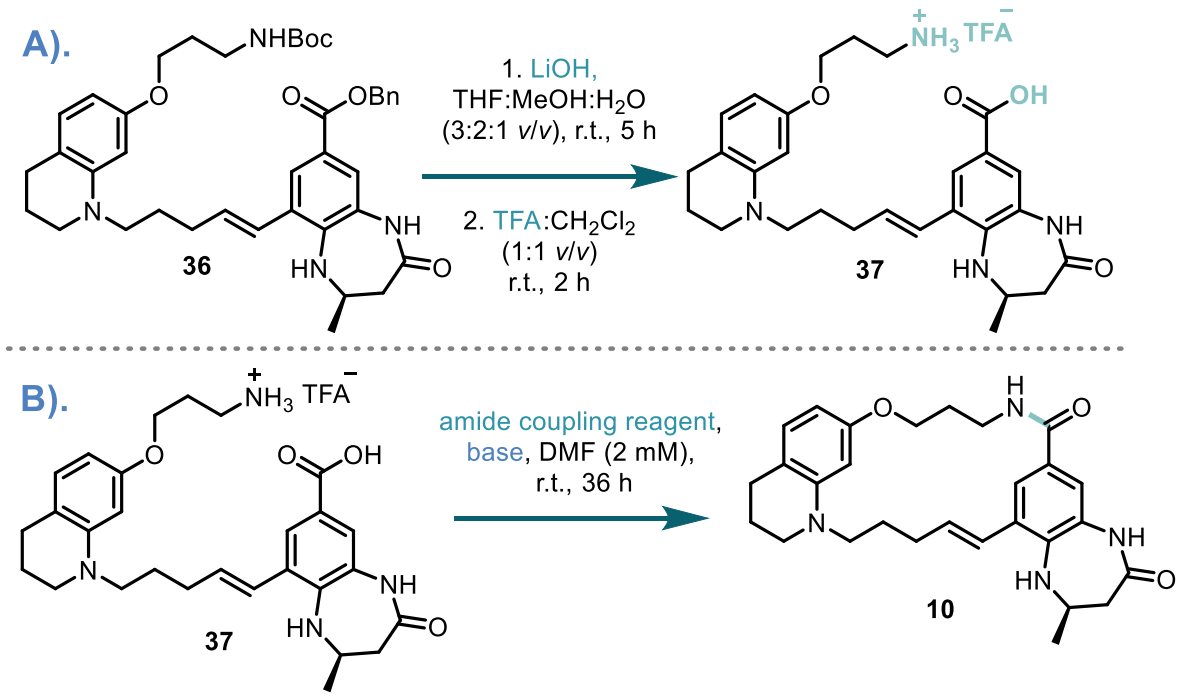

Scheme 7: Macrolactamisation condition screen; A). Double deprotection of intermediate **36** to give penultimate intermediate **37**, which is primed for amide coupling; B). Amide coupling reaction to form ligand **10**, upon which the reaction conditions in Table 2 were screened.

Table 2: Reaction conditions screened for the reaction shown in Scheme 7B, with the isolated yields displayed after purification by both reverse and normal phase chromatography, a value of 0 pertains to no detected product formation after 36 h by LC-MS, the highest yielding conditions are highlighted in **bold green** text.

Condition	Amide coupling reagent	Base	Solvent	Isolated yield, %
1	**PyBOP**	**DIPEA**	**DMF**	**41**
2	**HATU**	**DIPEA**	**DMF**	**40**
3	EDC + HOBt	DIPEA	DMF	0
4	TCFH	NMI	MeCN	0
5	COMU	DIPEA	DMF	0

Hence PyBOP was the reagent of choice in further optimisation of the macrolactamisation reaction, due to its prior success in macrolactamisation of similar scaffolds.[88] The synthesis of **10** was then performed at different concentrations (2 mM, 4 mM, and 8 mM) in order to see if the reaction would tolerate increased concentrations without compromising the yield (Scheme 8).

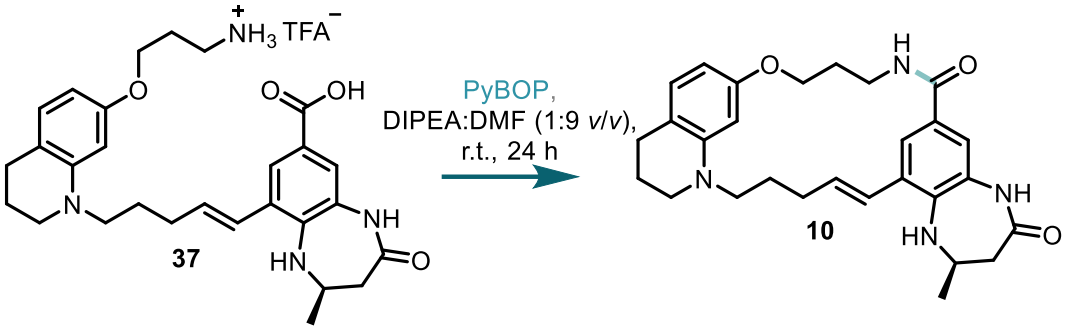

Scheme 8: Macrolactamisation reaction to form ligand 10 screened for reaction concentrations effect on yield, the results of which are shown in Table 3.

Table 3: Reaction concentrations screened for the reaction shown in Scheme 8, with the isolated yields displayed after purification by both reverse and normal phase chromatography, the highest yielding concentration are highlighted in **bold green** text.

Reaction Concentration, mM	Isolated yield, %
2	**36**
4	33
8	21

Upon screening different concentrations of macrocyclisation reaction, it became clear that increasing concentration had a deleterious effect on yield. The reaction concentration was therefore maintained at 2 mM. With the optimised alkylation and macrocyclisation conditions in hand, the next step was to synthesise the novel target macrolactam ligands.

2.4 Synthesis of ligands

2.4.1 Alkylation Reactions for Intermediate Formation

The alkylation reactions were carried out using the remaining intermediate **13** and the improved reaction conditions, to give all of the desired di-protected intermediates, improving upon the previous yields (Scheme 9).

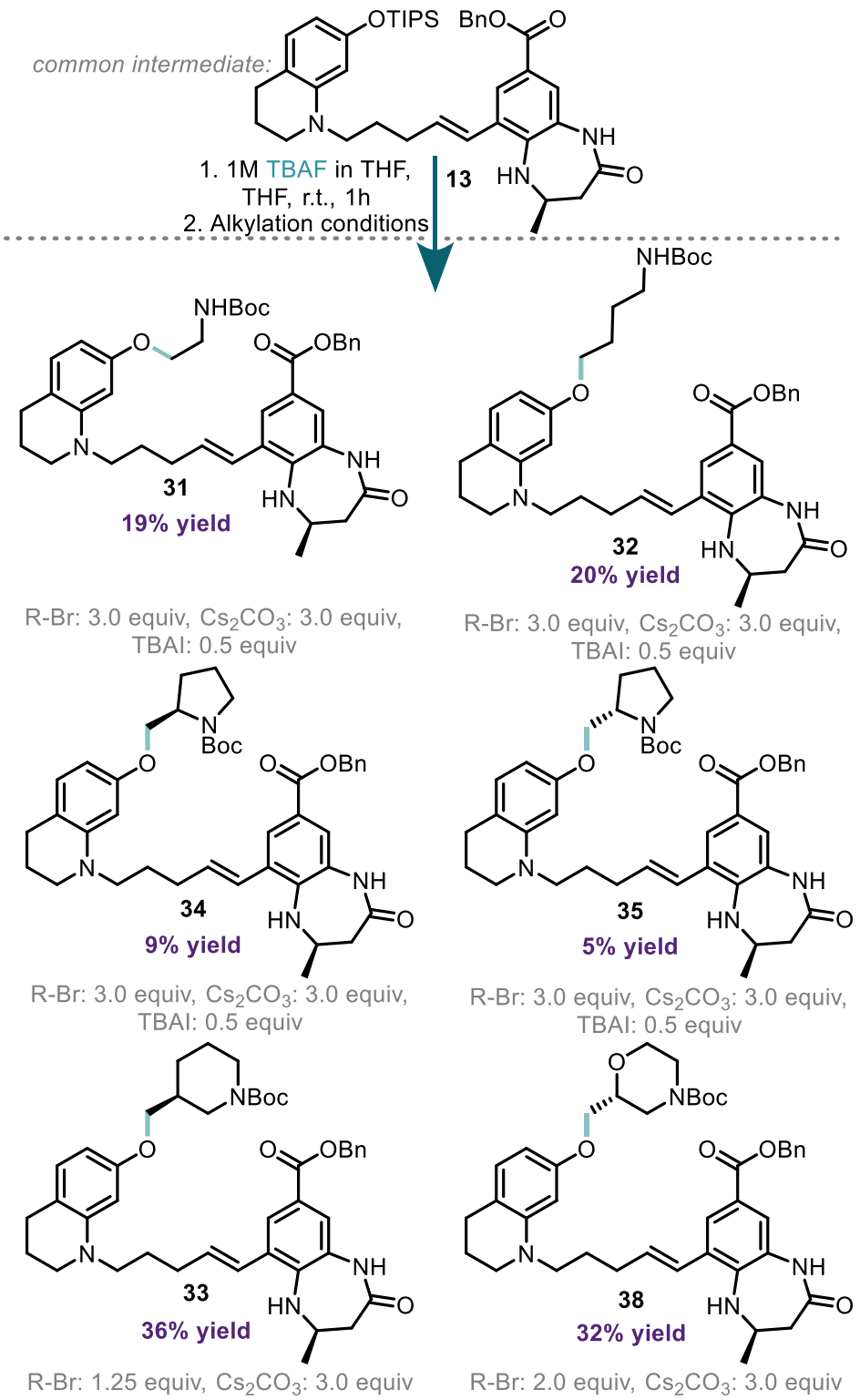

Scheme 9: Alkylation of the deprotected common intermediate **13** to form the target di-protected intermediates **31-35** and **38**, with the individual conditions in grey under the corresponding compound they were utilised in the synthesis of, with the yields highlighted in purple under each structure.

To avoid over-alkylation of compounds **33** and **38**, their syntheses were carried out with fewer equivalents of alkyl bromide and without the use of TBAI (Scheme 9). This

proved a fruitful alternation as even under the conditions shown, there was still a small amount of the di-alkylated product observed by LC-MS. The dialkylated product is likely to be the caused by the *N*-alkylation of the aniline nitrogen contained within the [6,7]-KAc mimic. The other intermediates were all furnished on a sufficient scale, and even though the yields were low, enough of these compounds were obtained to proceed to the macrocyclisation step (Scheme 9). Again, the pyrrolidine-based alkylation reagents produced the lowest yields.

2.4.2. Macrolactamisation for Final Product Formation

The intermediates were first subjected to the ester hydrolysis conditions, and post solvent removal, were then reacted with TFA to remove the *tert*-butyl carbamate amine-protecting groups. After removal of the TFA/CH_2Cl_2 solvent mixture, this gave all the products as the TFA salt, with both the amine and carboxylic acid now primed for amide coupling. All of the compounds were then subjected to the optimised macrolactamisation conditions to afford the desired products, in 51 – 15% yields with at least 5 mg of each product obtained, allowing for characterisation and biological evaluation (Scheme 10).

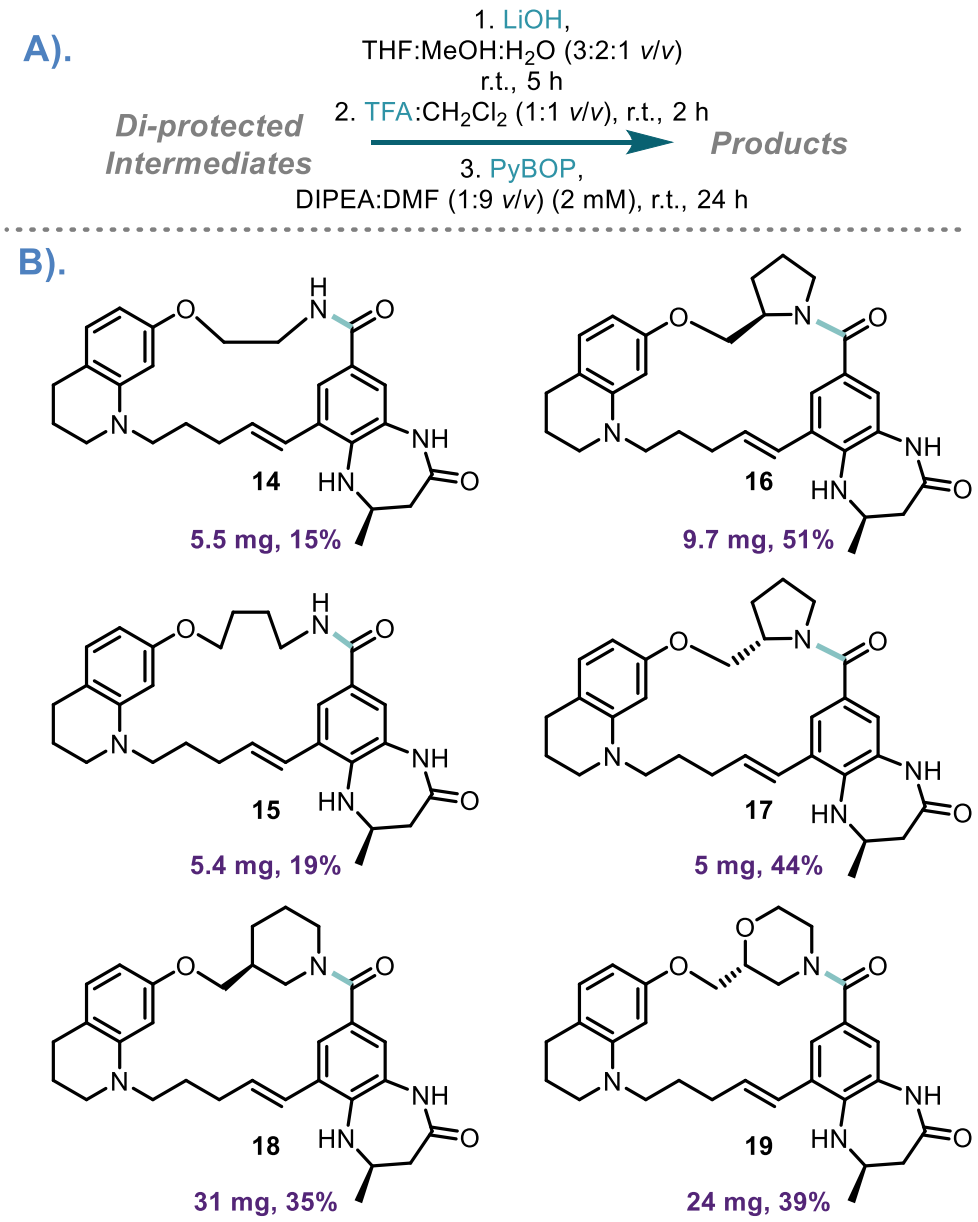

Scheme 10: Synthesis of the target macrolactams **14-19**, A). General reaction scheme of macrolactamisation conditions; B). The yields and mass (purple) of the final compounds after both the deprotections and amide coupling reaction.

In order to further improve yields of the macrolactamisation step, a more reactive coupling reagent such as PyAOP (see Figure 26) which combines HATU and PyBOP could be applied as this may improve yields but could lead to increase in deleterious side reactions. This coupling reagent was unavailable when the optimisation was performed.

To visualise the conformation of the macrolactams and assess whether they can adopt a similar shape to the bioactive conformation compound **18** was crystallised. The piperidine macrolactam (**18**) was crystallised from EtOAc with hexane as the anti-solvent, using the vapour diffusion method at room temperature, giving the small molecule X-ray crystal structure shown below (Figure 27).

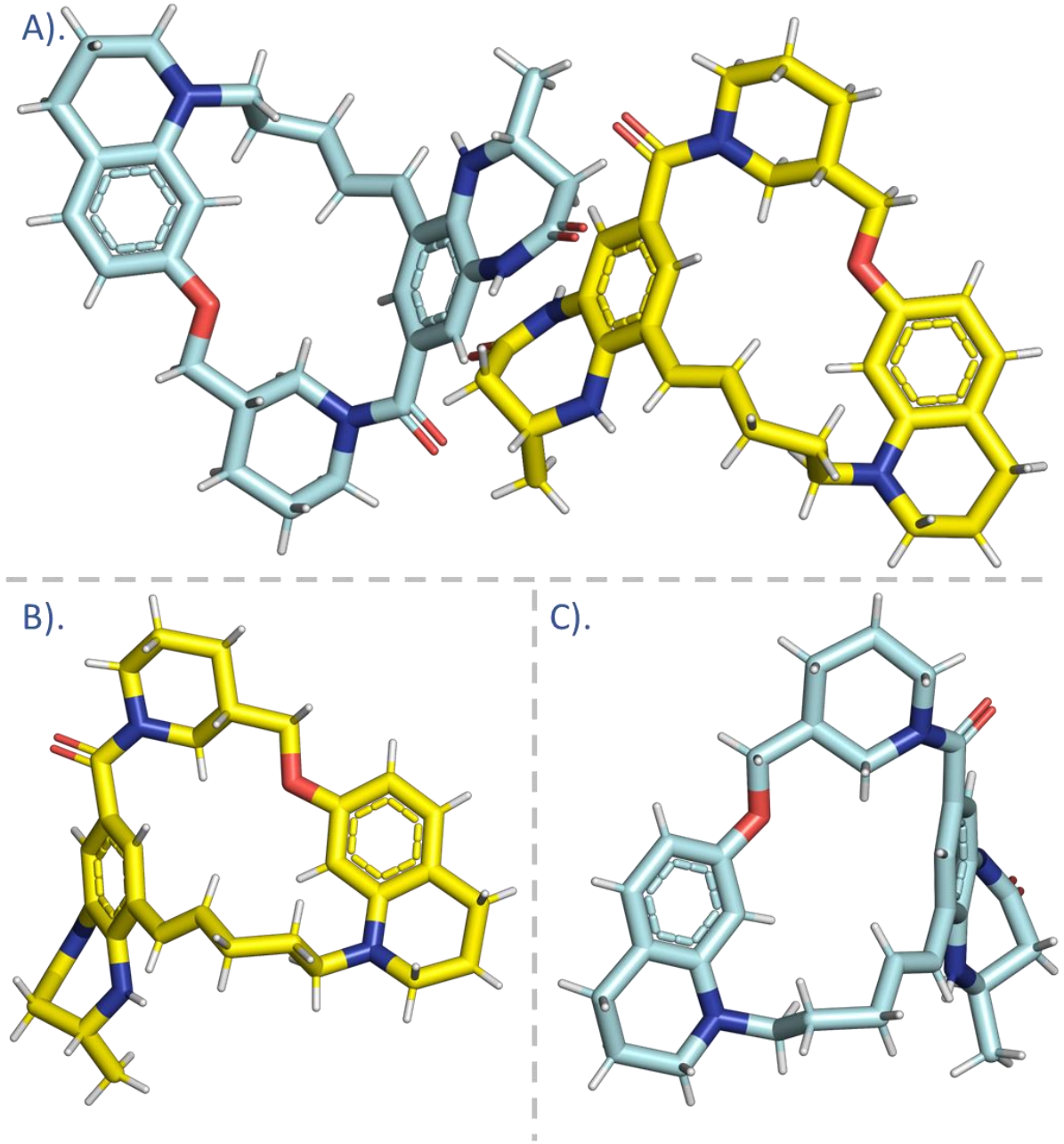

Figure 27: A). Small molecule X-ray crystal structure of the piperidine macrocycle **18** showing two different conformations in the solid state; B).one conformation of **18** (yellow); C). the other conformation of **18** (cyan).

Interestingly the one of the conformations (Figure 27, highlighted in yellow) displays a whole molecule conformation that is of a similar shape to the expected binding conformation to the CBP^{BRD}. This small molecule crystal structure confirms the structure of **18**, with both of the stereogenic centres in the correct configuration.

2.5 Synthesis of acyclic analogues

The acyclic analogues of the macrolactam containing compounds (**39** – **41**) were then afforded, to allow for the benefits of macrocyclisation to be discerned from the addition of the heterocycles to the scaffold. The synthesis of these target molecules will be described in this section (Figure 28).

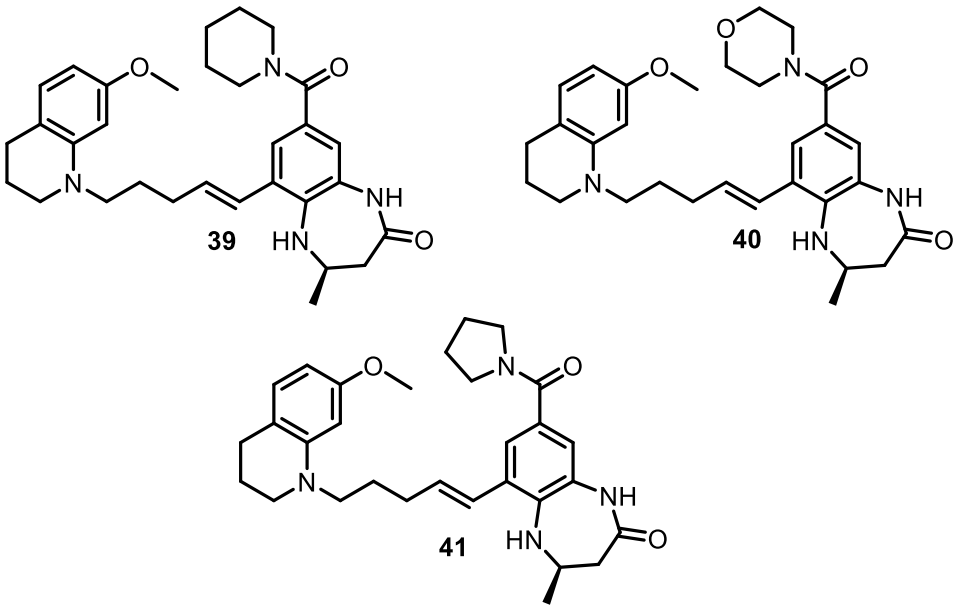

Figure 28: Target acyclic ligands to target the CBP^{BRD}: **39**, **40** and **41**.

2.5.1 Synthesis of a common intermediate

In order to synthesise the target compounds, first the common intermediate must be produced. This contains the previously furnished fragment for the macrolactam synthesis (Scheme 1, **25**) and THQ bearing fragment (compound **45**) which is synthesised in a similar manner to compound **30** (Scheme 11).

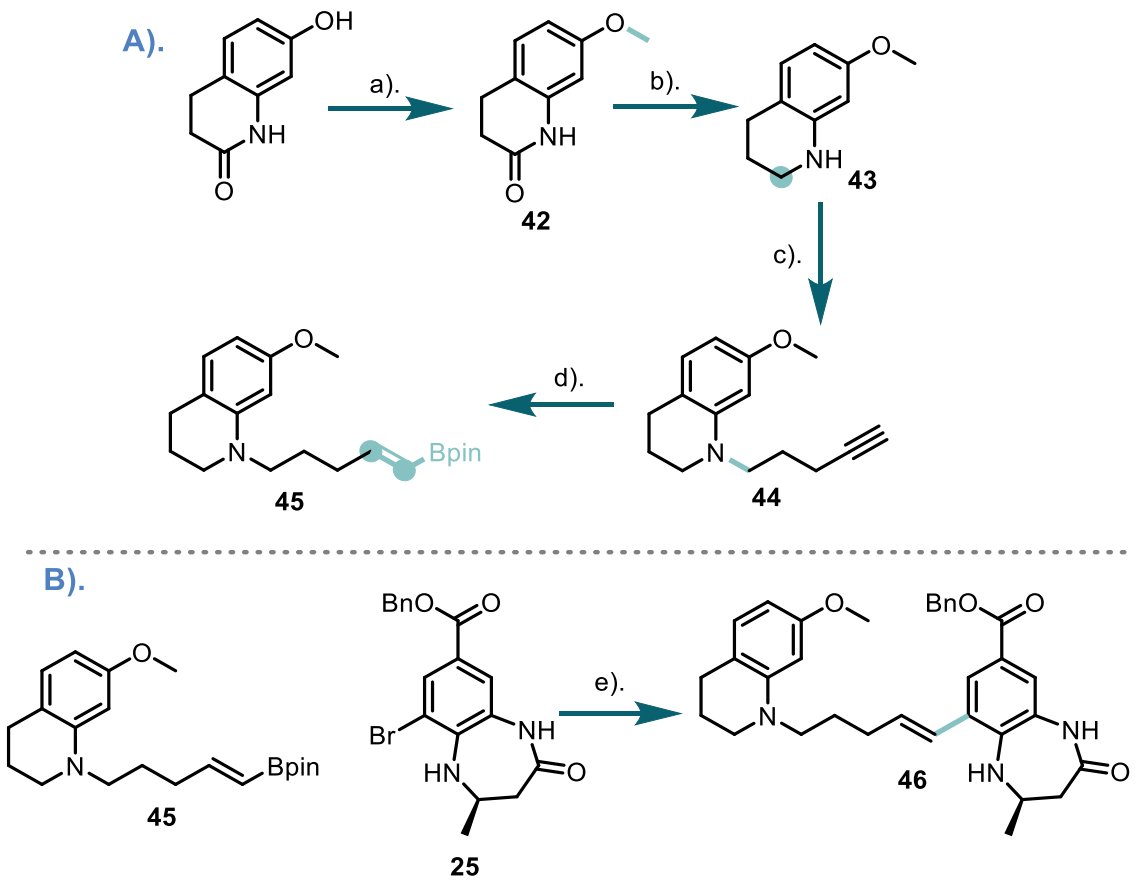

Scheme 11: A). Synthesis of THQ fragment **45**; B). Synthesis of the common intermediate **46** primed for synthesis of the target acyclic ligands, *Reagents and conditions:* a). Methyl iodide, K_2CO_3, DMF, 60 °C, 24 h, 57%; b). $LiAlH_4$, THF, 0 °C – r.t., 5 h, 98%; c). Compound **28**, DIPEA, TBAI, DMF, 100 °C, 48 h, 25%; d). HBpin, $Zr(C_5H_5)_2ClH$, NEt_3, 60 °C, dark, 18 h, 65% (>95% *E*-alkene by NMR); e). $Pd(dppf)Cl_2$, K_2CO_3, 1,4-dioxane:H_2O (5:1 *v*/*v*), 100 °C, 24 h, 74%.

With the key intermediate **46** in-hand, each of the target acyclic targets can be afforded *via* deprotection of the benzyl ester and subsequent amide coupling with the desired amine. The amide couplings were performed post ester cleavage, utilising PyBOP and the relevant amine (see Scheme 12 in the grey box).

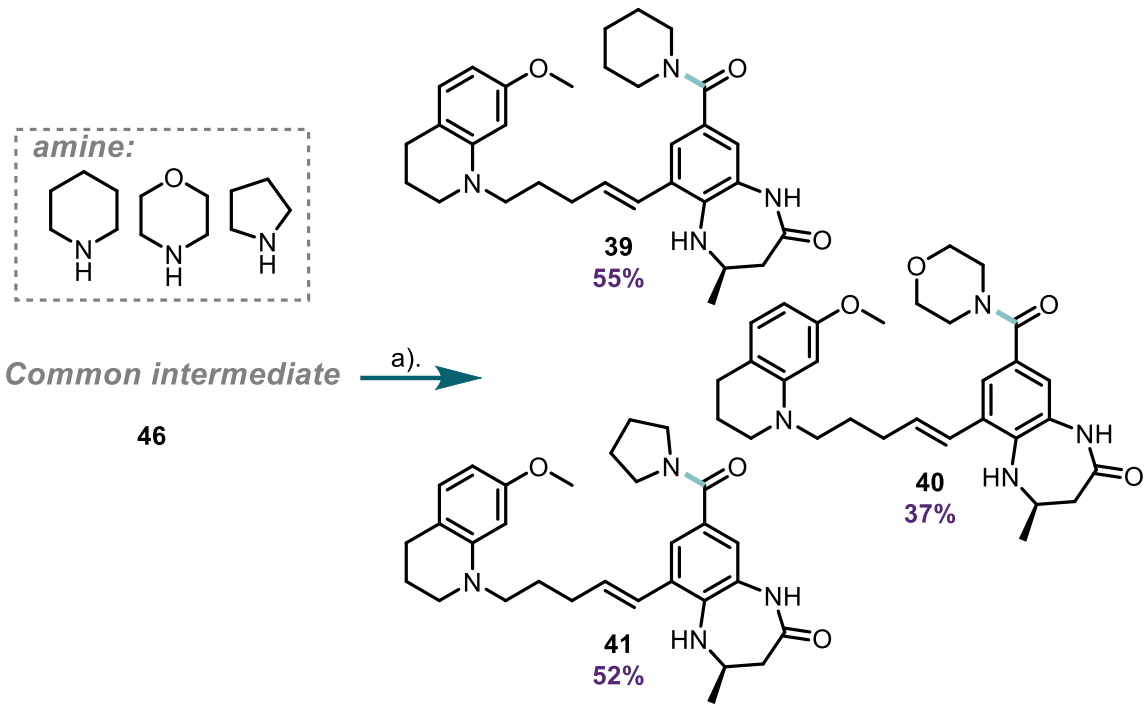

Scheme 12: Synthesis of the target acyclic lactam ligands **39**-**41**, derived from the shared common intermediate, yields are those achieved after HPLC prep purification, *Reagents and conditions:* a). LiOH, THF:MeOH:H_2O (3:2:1 *v*/*v*), r.t., 18 h, followed by, amine, PyBOP, DMF, r.t., 24 h, yields after HPLC purification highlighted under the corresponding structure in **purple**.

Unfortunately, upon the normal phase silica column purification of these compounds (**39**-**41**) a persistent impurity appeared in each ligand post-purification upon HPLC analysis. This impurity possessed a very similar retention time to each of the products upon reverse phase purification. It was found that these impurities varied between each of the products and was the results of un-reacted starting material **25** remaining after the Suzuki cross-coupling. This could not be removed from the product **46** post-Suzuki reaction. This unreacted starting material could then undergo the benzyl deprotection and amide coupling to form a reacted impurity that requires purification from the desired product (see Figure 29A). Due to the proximity of the impurities and final compounds on reverse phase, a HPLC purification was performed using a higher wavelength (≥340 nm) in order to avoid collection of the impurities (Figure 29B). This gave the desired final acyclic compounds in >95% purity making them viable for biological evaluation (Figure 29C and yields after purification shown in Scheme 12).

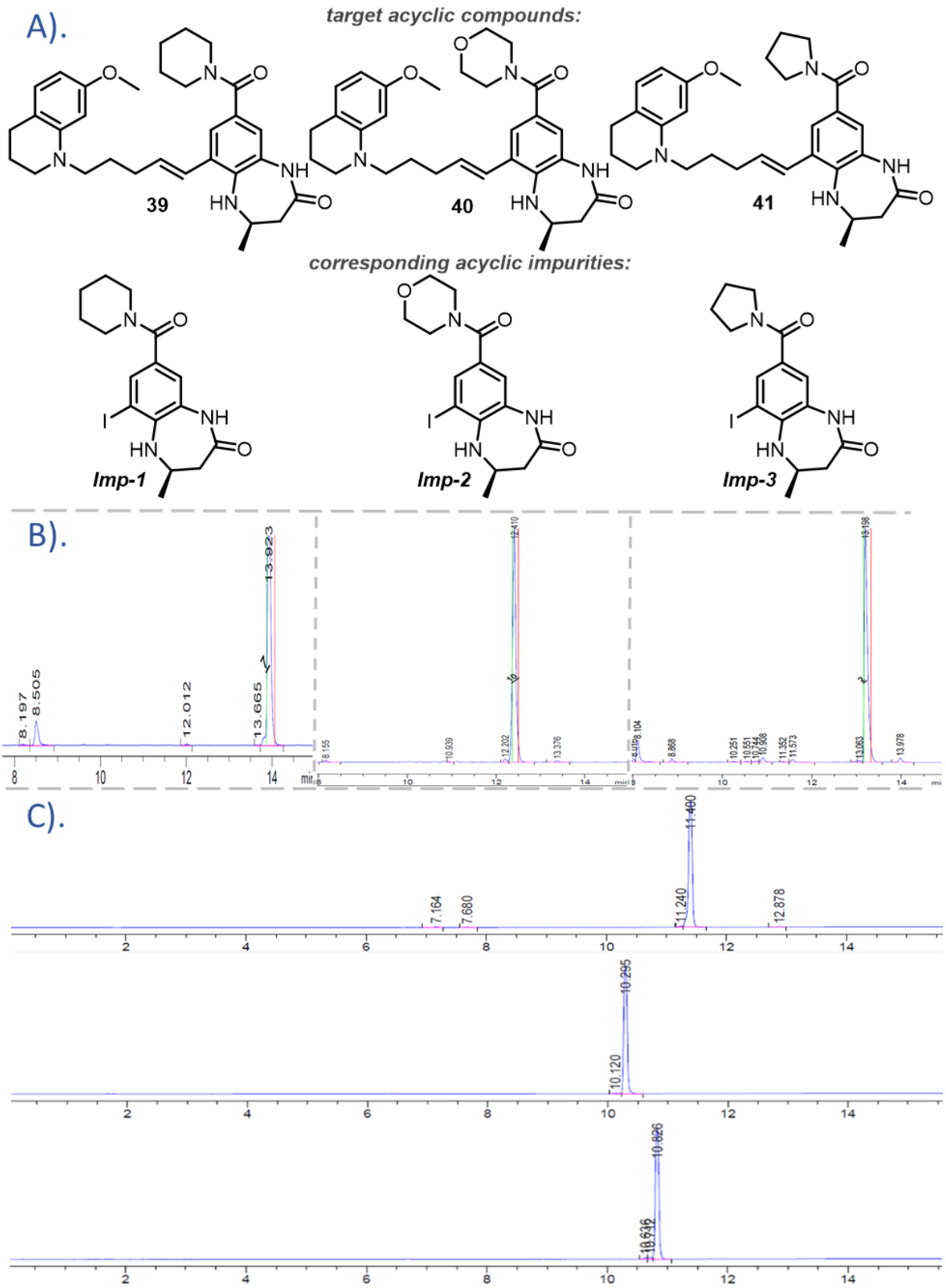

Figure 29: A). Target acyclic ligands and their corresponding impurities underneath each structure; B). the prep HPLC chromatograms, with the final compound fractions collected highlighted between the green and red lines; C). the analytical HPLC chromatograms at 254 nm of the target compounds after the prep HPLC purification, from top down, **39-41**.

2.6 Synthesis of positive control

The synthesis of the positive control for CBP^{BRD} binding (**OXFBD05**) was carried out as previously described.[44] An improvement in the purification of the [6,7]-KAc binding head group **48** was made (Scheme 13 step b), whereby the compound was purified by column chromatography (previously this was the only purification) and then crystallised using IPA to give >99% pure crystals (by HPLC). Compound **48** was then combined in a Suzuki cross-coupling with compound **45**, to afford **OXFBD05** (Scheme 13B).

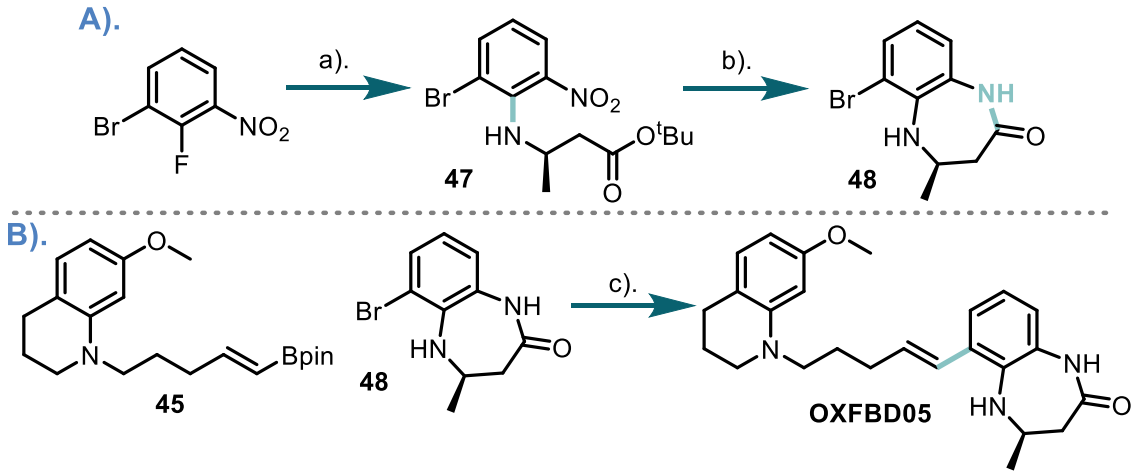

Scheme 13: C). Synthesis of [6,7]-KAc mimic **48**; D). Combination of **45** and **48** affording the **OXFBD05** ligand; *Reagents and conditions:* a). Compound **23**, Cs_2CO_3, toluene, 85 °C, 18 h, 92%; b). TFA:CH_2Cl_2 (1:1 *v/v*), r.t., 2 h, followed by, Fe, AcOH, 120 °C, 18 h, 54%; c). Pd(dppf)Cl_2, K_2CO_3, 1,4-dioxane:H_2O (4:1 *v/v*), 100 °C, 24 h, 75%.

2.7 Conclusion

With the target macrocycles **14-19** synthesised, their acyclic analogues **39-41** (see Table 2 below), along with the positive control for CBP^{BRD} inhibition ligand **OXFBD05**, the binding affinities of these compounds both against the CBP^{BRD} and BRD4(1) could be assessed. These data and further biological characterisation and binding mode investigation are described in Chapter 3, in which a hit macrolactam is identified, with both a high affinity for the CBPBRD whilst maintaining selectivity over BRD4(1).

Table 4: All final compounds synthesised in this chapter, their structures, numbers, purities, and their overall yield with step count.

Structure	Compound number	Overall yield and total step count	HPLC purity, %
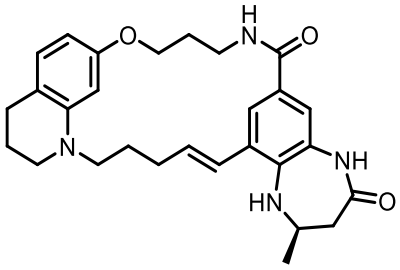	**10**	1.8% overall yield from 18 steps	98.2
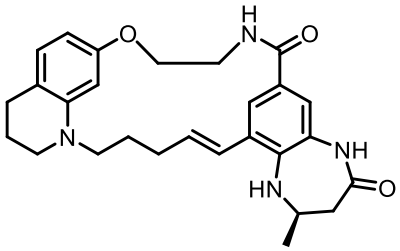	**14**	0.3% overall yield from 18 steps	99.4
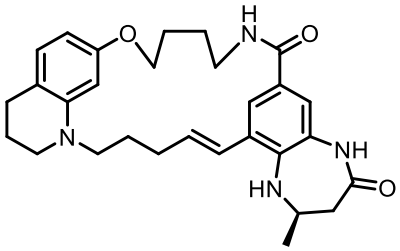	**15**	0.4% overall yield from 18 steps	96.6
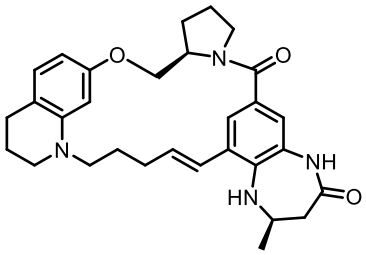	**16**	0.4% overall yield from 18 steps	95.1
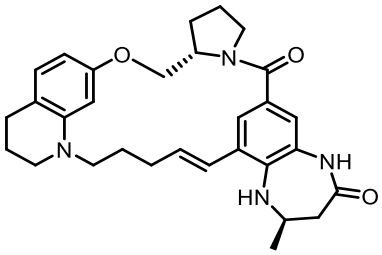	**17**	0.2% overall yield from 18 steps	95.3
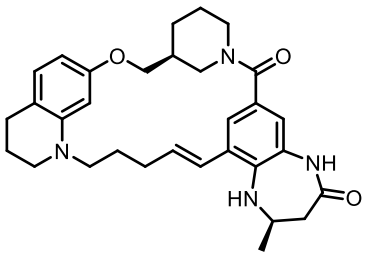	**18**	1.2% overall yield from 18 steps	95.3

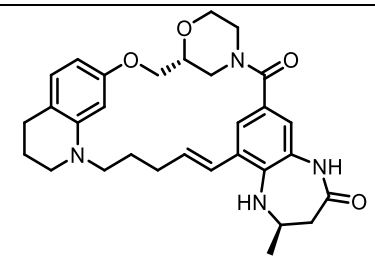	**19**	1.2% overall yield from 18 steps	98.2
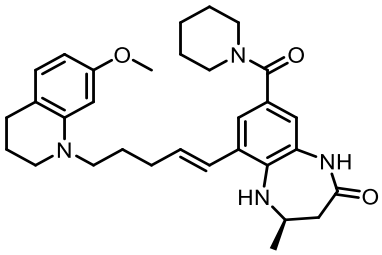	**39**	2.5% overall yield from 15 steps	98.4
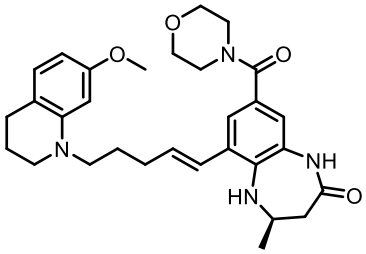	**40**	1.7% overall yield from 15 steps	98.9
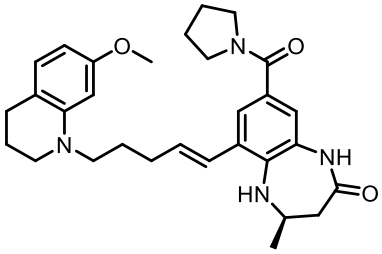	**41**	2.3% overall yield from 15 steps	98.0
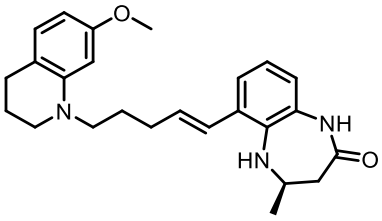	**OXFBD05**	2.6% overall yield from 10 steps	99.8

Chapter 3:

Evaluation of Macrolactams as Ligands for the CREBBP Bromodomain

3.1 Introduction

With the macrolactams (compounds **10** and **14-19**) and their linear non-macrocyclic analogues (compounds **39-41**) in hand (chemical structures shown in Figure 31), the following chapter focuses on characterising their binding affinity and interactions with the on-target protein of the CBP^{BRD} and the major off-target domain, BRD4(1). Binding affinities and selectivities for the CBP^{BRD} were first determined, with positive controls being used to ensure assay functionality (chemical structures shown in Figure 30). Ligands which possessed promising attributes were submitted for co-crystallisation and X-ray diffraction to attain insights into their binding modes. Concomitantly, the ligand which exhibited the most favourable selectivity, also referred to as the hit, was further evaluated against a wider range of BRD-containing proteins. The hit ligand was then tested in an acute myeloid leukaemia cell line, to assess the ability of the compound to elicit a phenotypic response comparing to the clinical candidate Inobrodib, as this the cancer for which clinical trials are currently underway.[30]

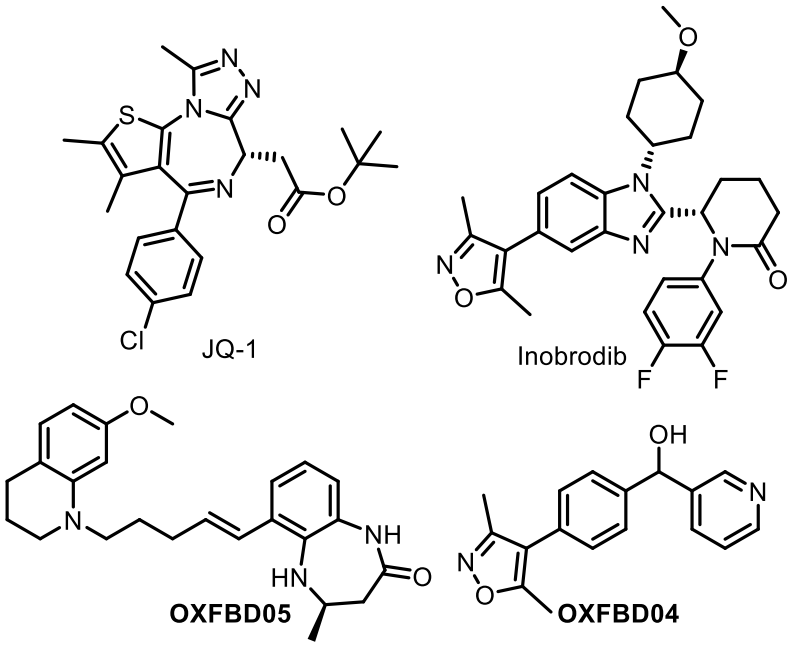

Figure 30: Positive control compounds used in this chapter for assessing assay functionality, with their respective binding affinities compared to literature values.

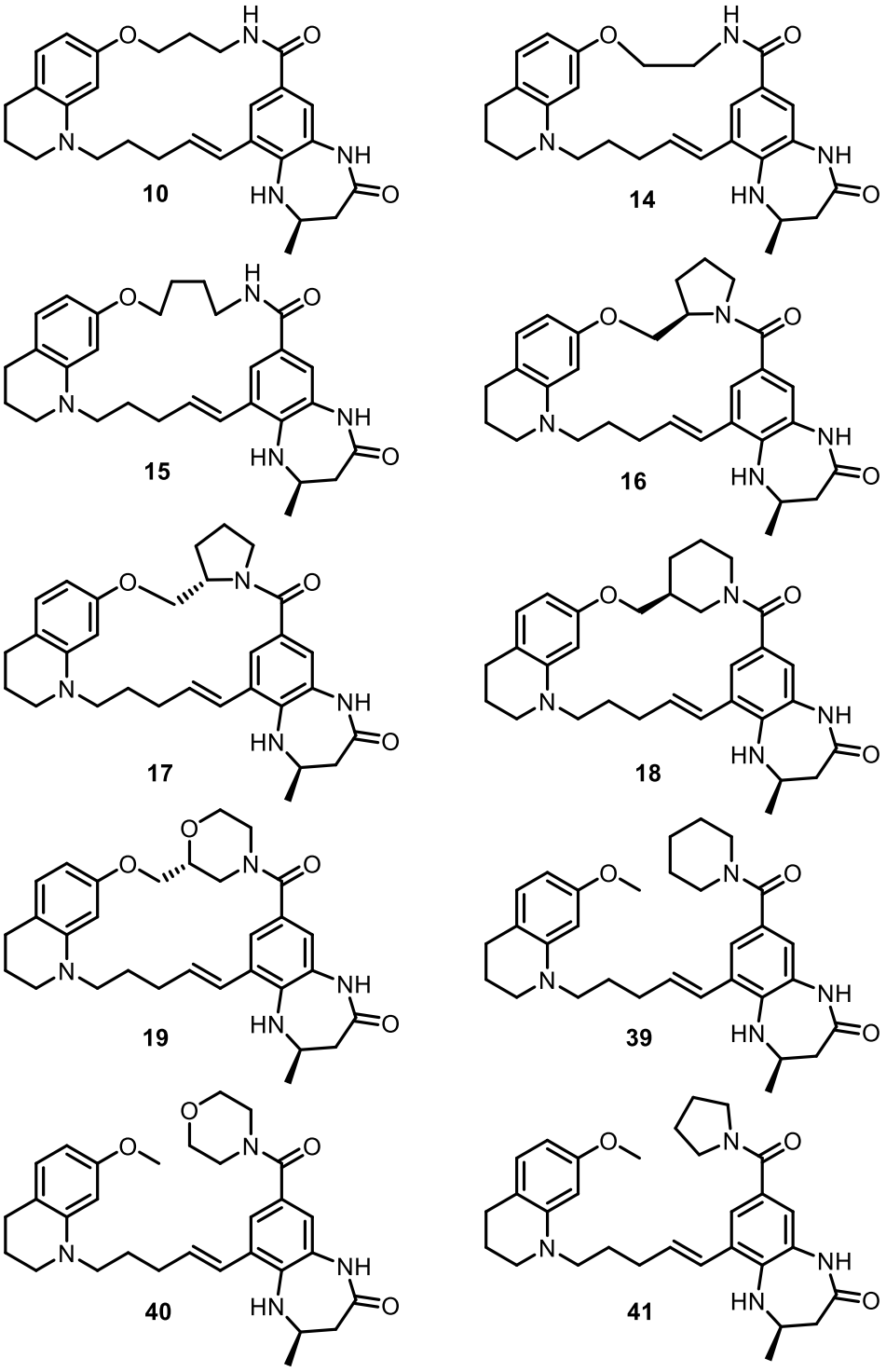

Figure 31: Chemical structures of the ligands synthesised in Chapter 3 and the positive control compounds used in this chapter; including macrolactams **10** as well as **14**-**19**, their linear analogues **39**-**41**, and the positive control compound Inobrodib.[23,110,111]

3.2 AlphaScreen®

3.2.1 BRD4(1) Inhibition using AlphaScreen® and Ligands **14-19**

The binding of macrocycles **14-19** to BRD4(1) was assessed, with **OXFBD04** used as a positive control (Figure 32, blue dots and curve) in an AlphaScreen® assay (the assay functions as described in Chapter 1) due to its high throughput nature.[85] As the BRD4(1) tracer peptide $H4_{1-20}(KAc)_4$-biotin was available, inhibition to the off-target was first assessed. The IC_{50} values for each compound are presented along with the error (Table 5) below the inhibitory curves (Figure 32).

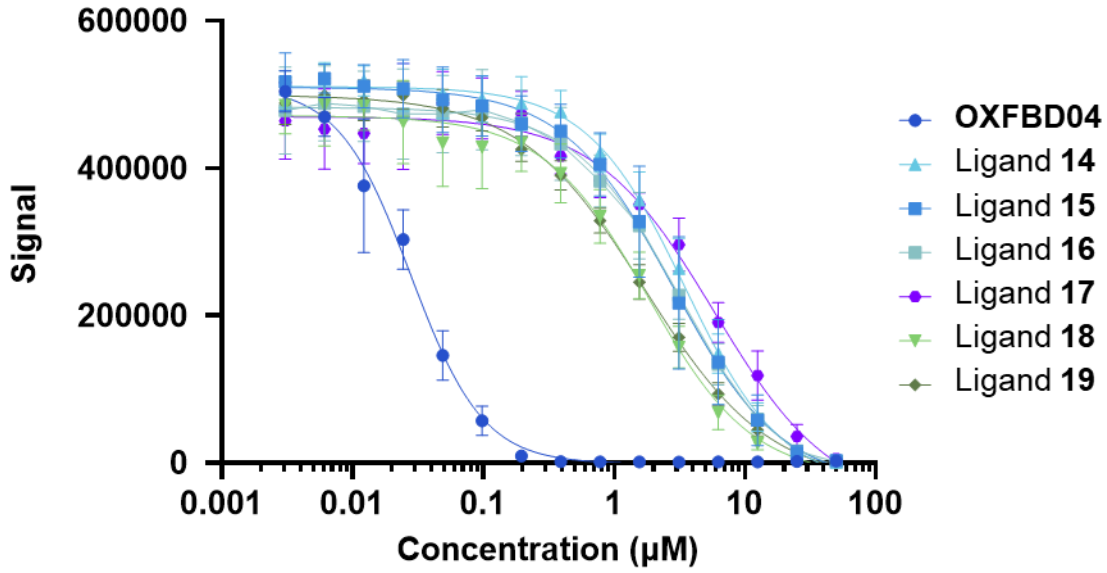

Figure 32: AlphaScreen® dose-response curves for macrocycles **14-19** along with **OXFBD04** against BRD4(1), displacing the $H4_{1-20}(KAc)_4$-biotin peptide (n = 3). Error bars indicate the standard deviation.

Table 5: IC_{50} values for macrocycles **14-19** and **OXFBD04** for BRD4(1), along with their respective errors (n = 3).

Compound name	**OXFBD04**	**14**	**15**	**16**	**17**	**18**	**19**
IC_{50} value (μM) and error (s.d.)	0.0278 ±0.0039	3.47 ±0.40	2.80 ±0.44	3.05 ±0.26	5.80 ±3.27	1.81 ±0.39	1.72 ±0.19

The AlphaScreen® IC_{50} values for ligands **14-19** produced were unexpected, as all showed inhibition of BRD4(1) at micro-molar concentrations. An investigation was

performed using TrueHits™ kit to determine whether the apparent binding to BRD4(1) was true inhibition.

3.2.2 AlphaScreen® TrueHits™ Assays

A TrueHits™ assay was performed which identifies if a ligand is a false positive in the AlphaScreen® assay. These false positives can be caused by a number of factors such as: singlet oxygen quenching, colour quenching (compound absorbance between 520-620 nm), light scattering, biotin mimicking, and nickel binding compounds. A technical negative control of just the bead mix is used to give a 100% signal response (this mix consists of streptavidin-coated donor and biotin-coated acceptor beads). Any ligands that caused signal suppression relative to this control (Figure 33, green triangles and curve), were considered as false positive in AlphaScreen®. The results of the TrueHits™ assay are summarised in Figure 33 for compounds **10** (dark blue), **16** (blue) and **41** (light blue).

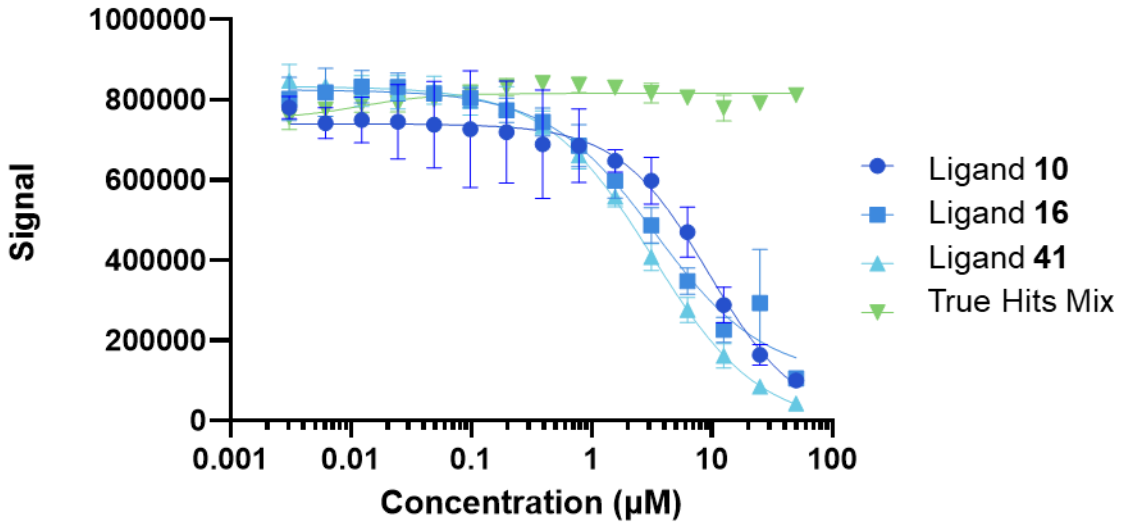

Figure 33: TrueHits™ AlphaScreen® assay performed with compounds **10** (dark blue dots), **16** (blue squares) and **41** (light blue triangles) along with the mixture of the TrueHits™ mix displayed as a negative control (green triangles) (n = 3). Error bars indicate the standard deviation.

All of the tested compounds (**10**, **16** and **41**) demonstrated inhibition of the signal response, meaning that all of the compounds would give rise to false positives in an

AlphaScreen® inhibition assay. The IC_{50} for ligand **16** in the AlphaScreen® (3.05 μM ±0.129 μM) and the TrueHits™ (3.38 μM ±1.05 μM) are insignificantly different when plotted on the same graph the trends appear parallel to each other (see Figure 34A for normalised binding and normalised TrueHits™ curves for **16**). This result from the TrueHits™ assay shows that AlphaScreen is not an appropriate assay to test the binding potential of the compounds (see Figure 31).

It is not believed that any of the ligands targeting the CBP^{BRD} synthesised in this thesis act as biotin mimetics (as they lack the required binding moieties) or nickel binders (as they lack strongly metal chelating groups) and, therefore, are not producing false positives through these mechanisms.[112–115] The ligands also do not absorb across the 520-620 nm wavelengths as they lack the required conjugated systems, and no absorption is observed in diode array detection by HPLC. It is hypothesised that the interference of these ligands (see Chapter 2), is due to the introduction of an electron-rich alkene, a feature from **OXFBD05** which the macrolactams were based upon (alkene highlighted in **blue** in Figure 34C). This alkene moiety is thought to quench the singlet oxygen produced, as this moiety is known to undergo reactions with singlet oxygen (Figure 34B for proposed mechanisms).[116–118]

A simple modification to the TrueHits™ assay to evaluate whether this functional group is to use both **OXFBD05** and **6** in the assay and compare the data, as **6** shares the scaffold of **OXFBD05** but contains an amide in place of the alkene (amide highlighted in **purple** in Figure 34C). Both **OXFBD05** and **6** were assessed in a TrueHits™ assay to test whether the alkene is the sole moiety responsible for singlet oxygen quenching (Figure 34D).

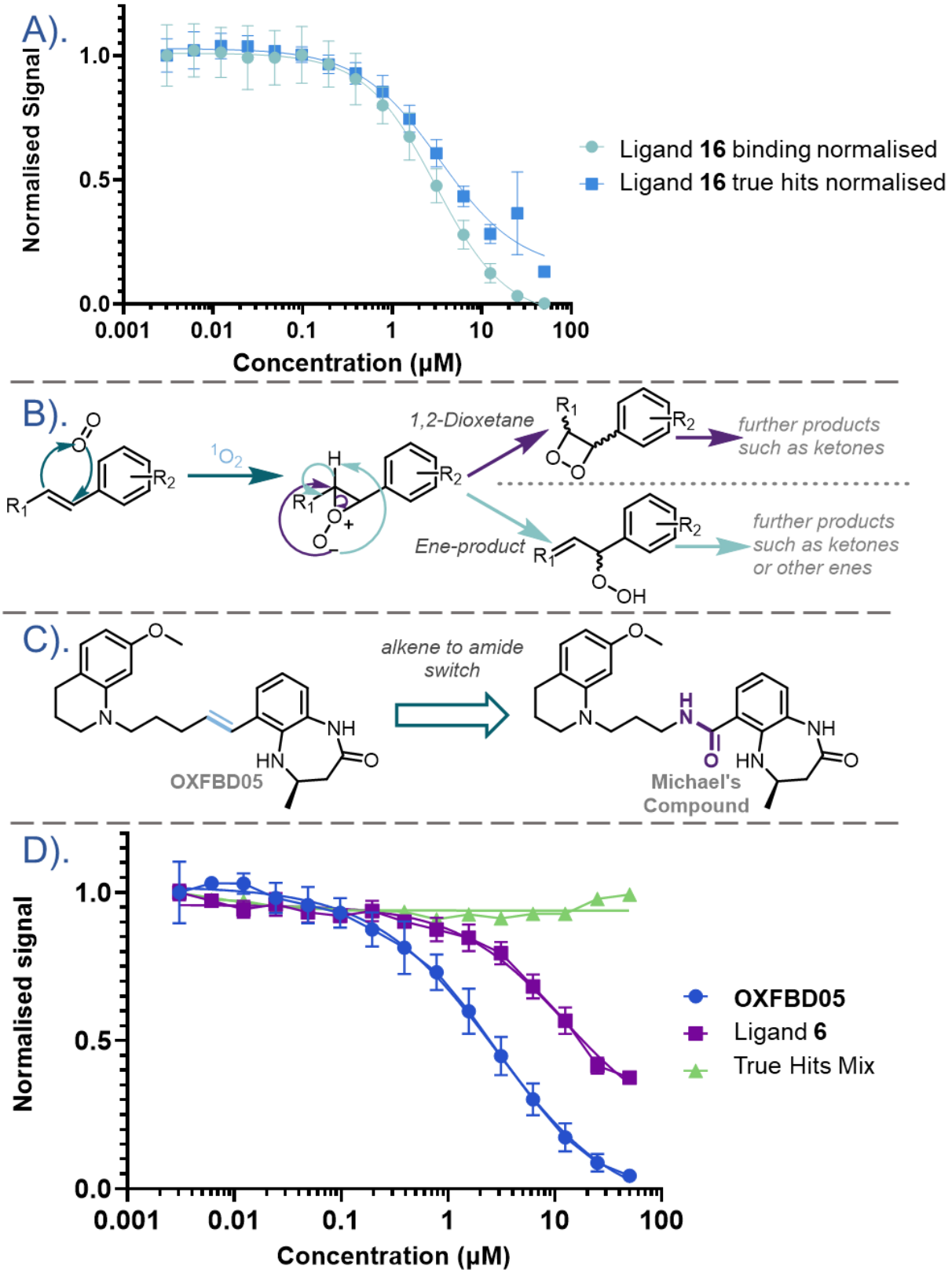

Figure 34: A). Ligand **16** normalised AlphaScreen® inhibition (light blue dots) and TrueHits™ inhibition (blue squares) data (n = 3); B). Proposed mechanisms of singlet oxygen quenching caused by the electron rich alkenes of ligands **14-19**, **39-41** and **OXFBD05**; C). Structural match of **OXFBD05** (with alkene highlighted in light blue) and **6** (amide highlighted in purple); D). TrueHits™ assay of **OXFBD05** (blue dots) and **6** (purple squares) (n = 3).

As displayed in Figure 34D, the replacement of the alkene (in **OXFBD05**) and with an amide (**6**) resulted in a decrease in the IC_{50} value in the TrueHits™ assay (2.78 μM for **OXFBD05** vs 12.3 μM for **6**). These data mean that both **OXFBD05** and **6** are inhibiting the signal in the TrueHits™ assay and therefore would interfere with an AlphaScreen® assay. This >4-fold reduction indicates that the alkene is indeed participating in singlet oxygen quenching, likely through one of the mechanisms highlighted (Figure 34B).[116,117] Additionally compounds that contain electron-rich alkenes have been previously reported to quench singlet oxygen, further supporting findings discussed (Figure 35A).[117–119] However, **6** still exhibits inhibition in the TrueHits™ assay. This moderate activity in the assay is unlikely to be caused by light scattering as the ligand appeared fully dissolved. Therefore, it is hypothesised that the electron-rich THQ could be interfering in the assay, as similar aniline and nitrogen heterocycles have been noted in the literature to perform singlet oxygen quenching (Figure 35B).[120–122] With this data in-hand and the macrolactams along with other analogues confirmed as false positives in AlphaScreen®, an alternative assay was required to assess the binding affinity of the ligands synthesised in Chapter 2.

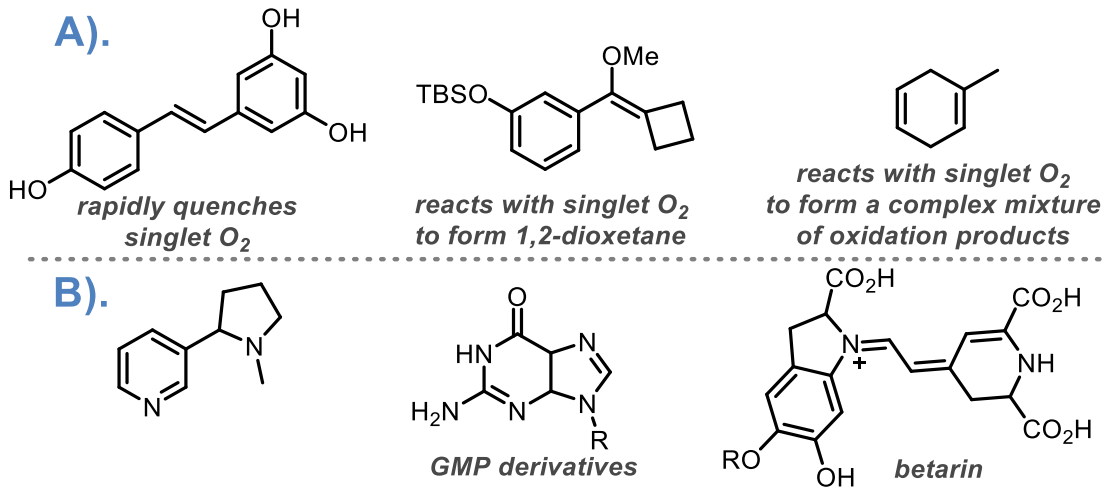

Figure 35: Chemical structures of singlet oxygen quenchers from the literature, A). Alkene-containing structures which are confirmed singlet oxygen quenchers; B). Electron-rich aniline and nitrogen heterocyclic structures confirmed to react with singlet oxygen. [117–122]

3.3 Isothermal Titration Calorimetry

With AlphaScreen® not providing the desired high-throughput assay because of ligand interference, other assays were considered as alternatives. Therefore, without a validated assay to hand TR-FRET was considered but discounted due to concerns around compound interference with the wavelengths used, such as those used to excite lanthanide complexes. Isothermal titration Calorimetry (ITC) appeared the most reliable option to assess the compounds binding affinity to both CBP^{BRD} and BRD4(1), the assay was not applied originally for the 9 novel ligands due to the low throughput nature of its execution (the assay functions as described in Chapter 1). ITC is a reliable assay for K_d = 10 nM - 10 μM binders, which rarely produces false positives and can yield total thermodynamic data for binding events, despite the drawbacks of using it to detect weak binding affinities for low-solubility ligands.

3.3.1 ITC Binding Affinity to the CBP^{BRD} and BRD4(1)

Initially, the assay and protein were assessed using the positive controls of **OXFBD05** (for the CBP^{BRD}) and JQ-1 (for BRD4(1)). Both **OXFBD05** (K_d = 132 nM for CBP^{BRD}) (see Appendix D Figure 3 for ITC traces) and JQ-1 (K_d = 52.0 nM for BRD4(1)) (see Appendix D Figure 5 for ITC traces) demonstrated binding affinities close to the published literature values for their respective protein, indicating the functionality of both proteins and the assay (see Table 6).[23,44] To further validate the assay functionality and also to assure the high binding affinity of the positive control compound which was used during the *in vitro* cell based assays (Section 3.7) Inobrodib the clinical candidate was also analysed for CBP^{BRD} binding. The Inobrodib binding affinity (K_d = 18 nM) (see Appendix D Figure 5 for ITC traces) which is in line with previous ITC data for this ligand but vastly different from the SPR data reported

upon binding to the CBP^{BRD} (K_d = 1.3 nM).[30,42,123] With the assay performing as expected, the binding affinities of **10**, **14-19** and **39-41** were evaluated against both the on-target CBP^{BRD} (see Appendix D Figure 6-14 for ITC traces) and the major off-target BRD4(1) (see Appendix D Figure 15-22 for ITC traces) using ITC to discern their affinities for each protein.

Table 6: ITC K_d values for ligands **10**, **14-19** and **39-41** against the CBP^{BRD} and BRD4(1) along with the fold selectivity which can be calculated from these binding affinities, **OXFBD05** (the CBP^{BRD} positive control), JQ-1 (the BRD4(1) positive control) and Inobrodib (CBP^{BRD} inhibitor clinical candidate) are included, a dash (–) indicates experiments not performed, n.b stands for no binding hence N/A indicates that a fold selectivity cannot be calculated, each standard error of the mean is presented (±) for each K_d value.

Compound Number	CBP^{BRD} K_d (μM) (n≥3)	BRD4(1) K_d (μM) (n≥2)	Fold selectivity (CREBBP/BRD4(1))
OXFBD05	0.132 ±0.003	-	-
JQ-1	-	0.053 ±0.001	-
Inobrodib	0.018 ±0.001	-	-
10	0.993 ±0.032	n.b	N/A
14	0.320 ±0.094	n.b	N/A
15	1.31 ± 0.21	n.b	N/A
16	0.860 ±0.082	n.b	N/A
17	0.435 ±0.085	n.b	N/A
18	0.834 ±0.026	1.49 ±0.06	1.79
19	0.174 ±0.008	n.b	N/A
39	2.95 ±0.29	1.28 ±0.07	0.43
40	0.826 ±0.040	0.964 ±0.095	1.17
41	-	-	N/A

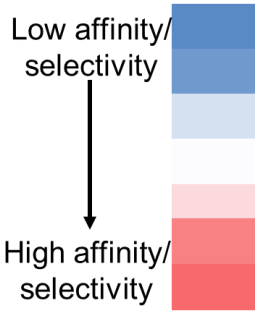

The binding affinity data illustrates that compound **19** (K_d = 174 nM), **14** (K_d = 320 nM) and **17** (K_d = 435 nM) are the highest binding affinity macrolactams within the ligand

series (see Figure 31 for chemical structures). With increasing length of the amide chain between secondary amide ligands (**14** with an ethyl, **10** with a propyl, and **15** with a butyl) the K_d increases and binding affinity decreases (see Figure 31 for structures). The longer chain length likely causes unfavourable interactions with the protein, resulting in higher hydrophobicity and also potentially perturbing the adoption of the desired curled-up binding conformation through increased ligand flexibility. For the two linear analogues with detectable binding by ITC to the CBP^{BRD}, both also demonstrated higher affinity for BRD4(1). Making these linear ligands unselective for the CBP^{BRD} over BRD4(1), due to the ability of the **39** and **40** to linearise, lacking the conformational fix provided by the macrocycle. Within the diastereomeric pair of ligands **16** and **17**, compound **17** (K_d = 435 nM) displays a higher affinity than **16** (K_d = 834 nM), which could be rationalised by how the different stereocentres of the pyrrolidine ring caused a difference in conformation. Possibly leading to increased interactions with the protein surface or through a lower energy barrier to adopting the desired curled-up binding conformation to the CBP^{BRD}. A comparison of ligands **19** and **18** shows an increased affinity in the morpholine-containing structure of **19** (K_d = 174 nM) compared to the piperidine-comprising structure of **18** (K_d = 834 nM), thus presenting a 4.8-fold increase in K_d for the CBP^{BRD}. This trend is also observed between the linear analogues of these macrolactams, as **40** (K_d = 826 nM) exhibits a marked improvement in affinity when compared to **39** (K_d = 2950 nM) possessing a 3.6-fold increase in K_d. This indicates that morpholine-based amides are better tolerated within the CBP^{BRD} binding site compared to structures bearing piperidines, potentially through addition hydrogen bonding interactions within the binding site.

With regard to the binding affinities measured for BRD4(1), ITC is limited by compound solubility for detecting weak binding (K_d > 10 μM) interactions between a ligand and a

protein. The volume of DMSO in the buffer also cannot exceed > 0.2% *v*/*v* as previously discussed, limiting the ability of the assay to detect binding affinities for poorly soluble ligand. Although the ligands are soluble at the concentrations tested (up to 40 μM in some cases), in order to obtain K_d values for all of the macrolactams against BRD4(1), the ligands would need to be assayed at double the highest concentration tested, at which point the ligands would no longer be soluble.

The macrolactam-based ligands demonstrated improved selectivity compared to their acyclic counterparts by ITC. This is illustrated by all the macrocycles having no detectable binding to BRD4(1) by ITC (except **18**) again highlighting the limitations of ITC as an assay for weak binding detection. With respect to compound **18**, this ligand displayed a ~3.9-fold increase in selectivity for the CBP^{BRD} over BRD4(1) compared to the linear version of this compound **39**. The ITC assay has highlighted ligand **19** as the highest affinity for the CBP^{BRD} making it the first small molecule macrocyclic ligand to demonstrate a K_d below 174 nM for the CBP^{BRD}. Although the all the macrolactams (ligands **10** and **14**-**19**) show weaker affinity (higher K_ds) that the positive control of **OXFBD05** (K_d = 132 nM), this is potentially due to the addition of an electron withdrawing amide onto the [6,7]-KAc mimic. This is due to the electron rich nature KAc mimics, as the increased electron density allows for strong hydrophobic and hydrogen bonding interactions. Although the ligands **14**, **17**, and **19** have higher affinity than the rest of the macrolactam series, illustrating that the addition of an electron withdrawing group can be partially overcome, conceivably through a conformational effect of their macrocyclic structures, or additional interactions with the CBP^{BRD}. However, to assess the selectivity of macrolactams ligands which did not show binding by ITC to BRD4(1), further investigation was required.

3.4 BROMO*Scan* Binding Assays

As discussed previously (section 3.3.1) ITC is limited by compound solubility for detecting weak binding (K_d > 10 μM) interactions between a ligand and a protein. Therefore, the commercially performed BROMO*Scan* (Eurofins Discovery) based assays were used for characterisation of binding affinities.[86] The BromoKdElect platform is an assay based upon BROMO*Scan* technology. Ligands **14**, **16**, **17**, **19** and **41** were chosen to perform this assay on as they demonstrated no measurable binding to BRD4(1) by ITC and K_d <1 μM for the CBP^{BRD}.

3.4.2 BromoKdElect

The binding affinity BromoKdElect assays were performed with n = 2 repeats against the BRDs of CBP, p300, BDR4(1), and BDR4(2) (Table 7 and Appendix E Figures 1-6 for a graphical representation of the data).

Table 7: BromoKdElect binding affinities (K_d) for compounds **14**, **16**, **17**, **19** and **41** against the four BRDs displayed (n = 2), along with the standard error of the mean (±) below each value.

Compound Number	CBP^{BRD} K_d (μM) (n=2)	$p300^{BRD}$ K_d (μM) (n=2)	BRD4(1) K_d (μM) (n=2)	BRD4(2) K_d (μM) (n=2)
14	0.055 ±0.014	0.057 ±0.009	2.25 ±0.15	0.72 ±0.15
16	0.190 ±0.030	0.245 ±0.025	3.60 ±1.10	3.95 ±0.95
17	0.110 ±0.000	0.130 ±0.000	3.95 ±0.45	0.48 ±0.04
19	0.045 ±0.012	0.130 ±0.010	>20.0 ±10.0	3.60 ±0.60
41	0.135 ±0.025	0.300 ±0.100	7.85 ±0.45	2.35 ±0.35

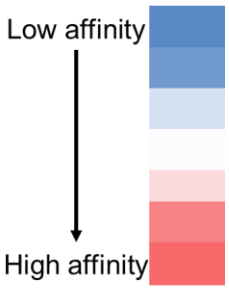

Generally, the BromoKdElect binding affinities (K_ds) obtained for all the ligands to the target proteins appear lower than those afforded by ITC. This in contrast to the positive control of **OXFBD05**, which shows a weaker affinity by BromoKdElect (K_d = 180 nM) when compared to ITC (K_d = 132 nM).[44,88] Therefore, ligands **14**, **17**, **19**, and **41** exhibit increased affinity (lower K_ds) when compared to **OXFBD05** in the BromoKdElect assay, showing that these ligands have overcome the addition of the electron withdrawing amide to the KAc mimic. The binding affinity data for the BromoKdElect assays performed highlights both compound **14** and **19** as binding to the CBP^{BRD} with K_d <100 nM. Molecule **17** demonstrates higher affinity for the CBP^{BRD} and $p300^{BRD}$ than both its diastereomer **16** and linear analogue **41**, reinforcing the ITC data. With these data in-hand, selectivities for all of the ligands can be calculated (Table 8).

Table 8: Selectivities from the BromoKdElect assays performed on ligands **14**, **16**, **17**, **19**, and **25** calculated using the K_d data previously displayed (Table 7).

Compound Number	Fold selectivity (CBP^{BRD}/$p300^{BRD}$)	Fold selectivity (CBP^{BRD}/BRD4(1))	Fold selectivity (CBP^{BRD}/BRD4(2))	Fold selectivity ($p300^{BRD}$/BRD4(1))
14	1.0	41	13	39
16	1.3	19	21	15
17	1.2	36	4.4	30
19	2.9	>455	82	>154
41	2.2	58	17	26

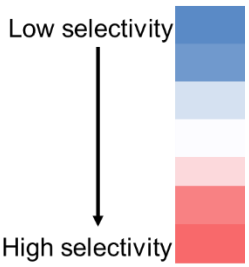

The selectivity data highlights ligand **19** as the most selective for the CBP^{BRD} and $p300^{BRD}$ over BRD4(1) and (2). Compound **19** displays >455-fold and 82-fold selectivity for the CBP^{BRD} over BRD4(1) and BRD4(2), respectively, while maintaining

high affinity for the CBP^{BRD} and $p300^{BRD}$. However, it is worth noting that according to the BromoKdElect binding affinity data **19** has a 3-fold increased affinity for the CBP^{BRD} when compared to the $p300^{BRD}$. This is hypothesised to be due to the weakened ability of $p300^{BRD}$ to form cation-π interactions with ligands, as a phenylalanine (Phe-1177) in the CBP^{BRD} is substituted for a tyrosine (Tyr-1177) in the $p300^{BRD}$.[124] This Tyr-1177, hydrogen bonds with the arginine (Arg-1173) in the $p300^{BRD}$, this residue participates in the cation-π interactions with ligands when bound to the CBP^{BRD}, forming an induced fit pocket, but is pulled away in the $p300^{BRD}$ removing the cation-π interaction and the induced fit pocket.[124] This is demonstrated by the crystal structures of SGC-CP30 with the CBP^{BRD} (PDB: 4NR7) and $p300^{BRD}$ (PDB: 5BT3).[52,124] This effect causes ligands which rely on the interaction with this arginine residue to demonstrate weaker binding to the $p300^{BRD}$ compared to the CBP^{BRD}.[124]

The selectivity data also demonstrated that for compounds **16** and **17** there are little to no benefits in selectivity gained from macrocyclisation as these macrolactams exhibit the same selectivity for CBP^{BRD} when compared to **41**. These data highlight that although ligand **14** possess high affinity to both the CBP^{BRD} and $p300^{BRD}$ (55 and 57 nM respectively) it does not enjoy the high level of selectivity that compound **19** furnishes (Table 8). Compound **19** also shows a similar affinity for the target CBP^{BRD} (K_d = 44.5 nM) compared to **14** (K_d = 55 nM) (Table 7). Compared to its linear analogue **40** (K_d = 826 nM by ITC) macrolactam **19** exhibits both increased affinity (K_d = 174 nM and 44.5 nM by ITC and BromoKdElect respectively) for the CBP^{BRD} and selectivity (>455-fold selective for the CBP^{BRD} over BRD4(1) for ligand **19** compared to <1.2-fold for ligand **40)**, highlighting the extensive benefits of macrocyclisation (Table 8). Ligand **19** distinguished itself as both the highest affinity (K_d = 44.5 nM) and most selective

ligand: >455-fold and 82-fold selectivity over BRD4(1) and BRD4(2) respectively for the CBP^{BRD}.

3.4.3 BromoMax

To better understand the selectivity of ligand **19** against other BRDs outside of the BRD4, **19** was tested for affinity against 32 BRD-containing proteins in a BromoMax assay. This assay was performed, applying the same principles of the BROMO*scan* assay (described in Chapter 1) but testing across a panel of 32 BRDs at a fixed concentration.[86] Therefore, the data are presented as a percentage of remaining control post-treatment with ligand, meaning a lower percentage remaining indicates a greater affinity. The data for compound **19** is presented for both the 1 and 10 μM concentrations assayed (Table 9, see Appendix E figures 6 and 7 for the raw data).

Table 9: BromoMax data for compound **19** at 1 μM ,10 μM, as well as Inobrodib at 1 μM for comparison with the gene symbol for each protein displayed (left column) along with the percentage of control remaining after treatment with **19**, a high number indicates weak or no inhibition (dark blue (35-100%), medium blue (25-35%), and light blue (15-25%)) whilst a lower number (dark red (0-1%), medium red (1-5%), light red (5-10%), and white (10-15%)) denotes strong inhibition of that BRD.[30]

Ligand 19 at 1 μM		Ligand 19 at 10 μM		Inobrodib at 1 μM	
Protein, gene symbol	Percentage control remaining	Protein, gene symbol	Percentage control remaining	Protein, gene symbol	Percentage control remaining
ATAD2A	98	*ATAD2A*	100	*ATAD2A*	99
ATAD2B	85	*ATAD2B*	83	*ATAD2B*	76
BAZ2A	77	*BAZ2A*	3	*BAZ2A*	100
BAZ2B	86	*BAZ2B*	60	*BAZ2B*	100
BRD1	100	*BRD1*	96	*BRD1*	99
BRD2(1)	69	*BRD2(1)*	56	*BRD2(1)*	14
BRD2(2)	96	*BRD2(2)*	29	*BRD2(2)*	71
BRD3(1)	97	*BRD3(1)*	43	*BRD3(1)*	23
BRD3(2)	91	*BRD3(2)*	16	*BRD3(2)*	80
BRD4(1)	92	*BRD4(1)*	51	*BRD4(1)*	18
BRD4(2)	88	*BRD4(2)*	28	*BRD4(2)*	79
BRD7	100	*BRD7*	48	*BRD7*	99
BRD9	100	*BRD9*	26	*BRD9*	33
BRDT(1)	96	*BRDT(1)*	48	*BRDT(1)*	43
BRDT(2)	88	*BRDT(2)*	39	*BRDT(2)*	87
BRPF1	85	*BRPF1*	22	*BRPF1*	46
BRPF3	98	*BRPF3*	76	*BRPF3*	100
CECR2	100	*CECR2*	48	*CECR2*	100
CREBBP	2.7	*CREBBP*	0	*CREBBP*	0
EP300	9	*EP300*	0.1	*EP300*	0
FALZ	99	*FALZ*	38	*FALZ*	68
GCN5L2	71	*GCN5L2*	100	*GCN5L2*	96
PBRM1(2)	82	*PBRM1(2)*	97	*PBRM1(2)*	84
PBRM1(5)	100	*PBRM1(5)*	21	*PBRM1(5)*	91
PCAF	93	*PCAF*	100	*PCAF*	99
SMARCA2	54	*SMARCA2*	3.2	*SMARCA2*	82
SMARCA4	98	*SMARCA4*	69	*SMARCA4*	69
TAF1(2)	55	*TAF1(2)*	2	*TAF1(2)*	76
TAF1L(2)	96	*TAF1L(2)*	54	*TAF1L(2)*	96
TRIM24	90	*TRIM24*	36	*TRIM24*	74
TRIM33	87	*TRIM33*	100	*TRIM33*	73
WDR9(2)	95	*WDR9(2)*	99	*WDR9(2)*	33

35-100%
25-35%
15-25%
10-15%
5-10%
1-5%
0-1%

A value of 35 percent control remaining or lower (medium blue to dark red) is classed as an affinity for that protein in this assay (as defined by Eurofins). With this in mind at

1 μM, ligand **19** is not classed as binding to any other BRDs except for the on-target CBP^{BRD} and $p300^{BRD}$. This is shown by only the CBP^{BRD} and $p300^{BRD}$ demonstrating percentage control below 35 (2.7 and 9 respectively).[124] When compound **19** was tested at an increased concentration of 10 μM the BRDs: BAZ2A, SMARCA2, and TAF1(2) exhibited strong affinity for **19** along with CBP and p300 (dark red and medium red in Table 9, rightmost column). Both TAF1(2) and BAZ2A have been previously identified as off-targets of CBP^{BRD} inhibitors.[53] Running the BromoMax for **19** at 10 μM also elucidated affinity for the second domain of the BET (BRD2, BRD3, BRD4, and BRDT) proteins over the first domains. Affinity for the second BET BRDs is expected, as **19** demonstrated increased affinity for BRD4(2) relative to BRD4(1) (BromoKdElect). With respect to the second BRDs of the BET family, compound **19** demonstrates weak (16-35% control remained in Table ZZ5 for BRD2(2), 3(2) and 4(2)) affinity at 10 μM. The assay also highlights the PBRM1(5) (21% control remaining), BRPF1 (22% control remaining) and BRD9 (26% control remaining) BRDs as exhibiting weak affinity (Table 9, medium blue) for **19**. The BromoMax data presented can be visualised using a phylogenetic tree diagram for the BRDs (32 out of 58 displayed in Figure 36A and 36B) tested at both 1 (Figure 36A) and 10 μM (Figure 36B) of ligand **19**. At 10 μM **19** exhibits selectivity over the majority of the BRDs tested in the BromoMax assay (21 out of 30) and displays no affinity (dark blue in Table 9) for the first BRD of the BET proteins. At 10 μM, the BromoMax assay identified nine off-target BRDs to which ligand **19** binds, the highest affinity of these being with BAZ2A, SMARCA2, and TAF1(2) however at 1 μM **19** shows no affinity for these proteins. These proteins which macrolactam **19** shows high affinity for at 10 μM (BAZ2A, SMARCA2, and TAF1(2)), when inhibited do not have the same phenotypic effects as CBP^{BRD} and $p300^{BRD}$ inhibition in cells.[27,125,126]

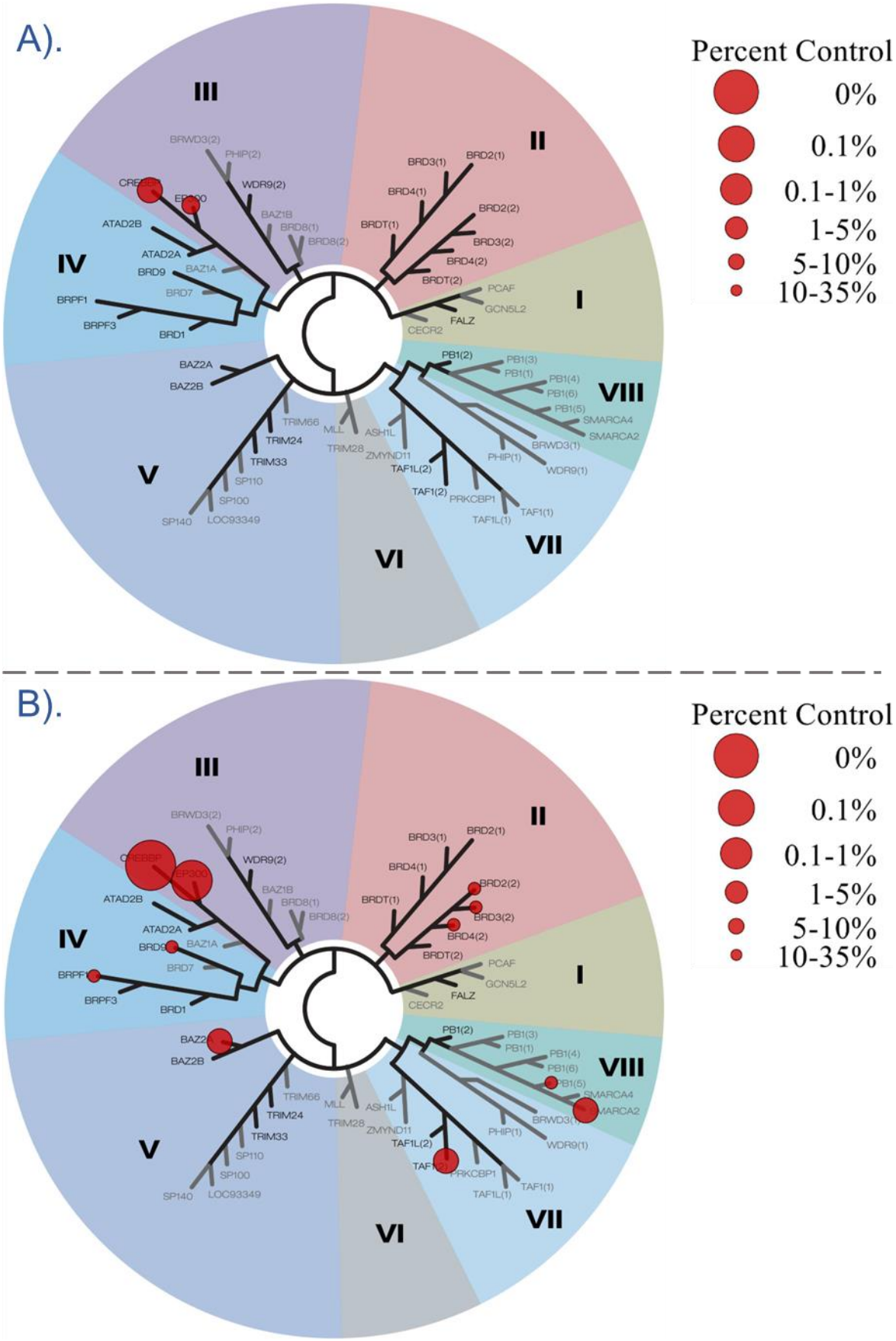

Figure 36: Phylogenetic trees of BromoMax data for compound **19** at, A). 1 μM and B). 10 μM with increasing inhibition indicated by increasing red dot size and proteins tested highlighted with dark text.

When comparing the affinity and selectivity of **19** to other CBP^{BRD} inhibitors, it appears most relevant to compare to the only $CBP^{BRD}/p300^{BRD}$ inhibitor currently in clinical trials Inobrodib (Table 9, 3rd column). The published BromoMax data for Inobrodib indicates that at 1 μM, it is less selective than compound **19** (inhibiting 7 out of 32 BRDs tested), nevertheless Inobrodib has higher affinity for both the CBP^{BRD} and $p300^{BRD}$ compared to **19** at 1 μM (0 and 0% control remaining for Inobrodib *vs* 2.7 and 9% control remaining for **19** respectively).[30] Inobrodib demonstrates a very low K_d of 1.3 and 1.7 nM for the $CBP/p300^{BRD}$ respectively (by SPR), while **19** exhibits a more modest K_d of 44.5 and 130 nM for $CBP/p300^{BRD}$ respectively (BromoKdElect), an ~10 fold increase in is observed between Inobrodib (K_d = 18 nM) and macrolactam **19** (K_d = 174 nM) using ITC (Table 6).[42] This increased on-target affinity, would no doubt, provide Inobrodib with a more pronounced phenotypic effect due to $CBP/p300^{BRD}$ inhibition *in vivo*.[30,42] It is also worth noting that at 1 μM, Inobrodib begins to inhibit the first domains of the BET family proteins, unlike ligand **19**, thereby presenting a different off-target selectivity profile.[30] The BromoMax data highlights that at 1 μM, **19** has total on-target selectivity and required testing at 10-fold increased concentration to elucidate the off-target BRDs of this ligand. This makes macrolactam **19** the first high affinity, selective ligand for the CBP^{BRD}. In order to discern why this is the case, structural studies of the macrolactam ligands and their respective linear analogues were performed to better understand the selectivity and affinities of these molecules.

3.5 Protein-Ligand X-ray Crystallographic Studies

Given that the morpholine macrolactam **19** had both the highest affinity and selectivity for the CBP^{BRD}, an investigation of the binding mode and conformation using X-ray crystal structures was performed. This was also carried out on the original macrolactam **10** from which the SAR was built. To complement the co-crystal structure

of **19**, the acyclic morpholine compound **40** was also co-crystallised with the CBP^{BRD} in order to observe any differences that could have caused the increased binding affinity of **19** relative to its linear analogue. Finally, ligand **14** was co-crystallised with the target CBP^{BRD} to see what structural information could be gained in relation to the decreased selectivity of this compound compared to **19**. The crystals grown for each compound and the solved structures, presented herein, were produced by Marius Amann (University of Freiburg, Germany) for ligands **10**, **14**, **19**, and **40**. Both 6×His tagged CBP^{BRD} along with the TEV cleaved CBP^{BRD} were used in crystallographic studies (Appendix B figure 2 for tag-less CBP^{BRD} SDS-PAGE and LC-MS data). However, only the 6×His CBP^{BRD} protein produced high resolution structures when crystallised with the ligands.

For clarity, only the KAc binding site containing the ligands for each structure is shown from along the ZA channel and from above the binding pocket to better visualise the interactions of each ligand (see Appendix F figures 1 – 4 for the full BRD crystal structure with each ligand). Each ligand bound to the CBP^{BRD} is given a different colour (**19** is yellow (PDB: 9GEJ), **40** is purple (PDB: 9GET), **10** is light blue (PDB: 9GEY), and **14** is cyan (PDB: 9GEU)), while the protein surface is transparent, structural waters (such as those present in the KAc binding pocket and down the ZA channel) are denoted by red spheres. The residues to which each ligand possess any interactions (both water-mediated, and non-water-mediated hydrogen bonds, dipole-dipole, cation-π, π-π and Van der Waals interactions) are displayed (carbon atoms are green, nitrogen atoms are blue, and oxygen atoms are red for these residues) and labelled with the residue three-letter code and number. The hydrogen bonding and cation-π interactions highlighted (by yellow dashed lines). For clarity, the backbone

amide of each amino acid is removed, unless a hydrogen bonding interaction is present between the ligand and CBP^{BRD}.

3.5.1 Co-crystal structure of Ligand **14** in complex with the CBP^{BRD}

When co-crystallised with the CBP^{BRD}, both ligands **10** and **14** demonstrated similar binding modes. Due to the higher affinity of **14** this is the ligand that is discussed in the following section with differences between the two structures discussed where relevant (see Appendix F for **10** co-crystal structure with the CBP^{BRD}). Compound **14** displays the same crystallographic artefact as **OXFBD05** (PDB: 6YIJ) when bound to the CBP^{BRD}.[44] The aforementioned artefact exhibits that the THQ moiety of **14** is likely forming an interaction with the Arg-1173 residue of an adjacent protein unit (Figure 37 and 38). The same phenomenon is also observed in the co-crystal structure of **10**. The linearisation of the ligands observed in the solid state was proven for **OXFBD05** to be a crystallographic artefact using size exclusion multi-angle light scattering (SEC-MALS) experiments.[44] Therefore, the same phenomenon is hypothesised to be a crystallographic artefact for both ligand **10** and **14**, given the similarity with the **OXFBD05** crystal structure.[44] This particular crystallographic artefact caused linearisation of the ligands, loss of the induce fit pocket caused by the cation-π interaction with Arg-1173, meaning that both **14** and **10** do not displayed the desired curled-up binding conformations to the CBP^{BRD}.

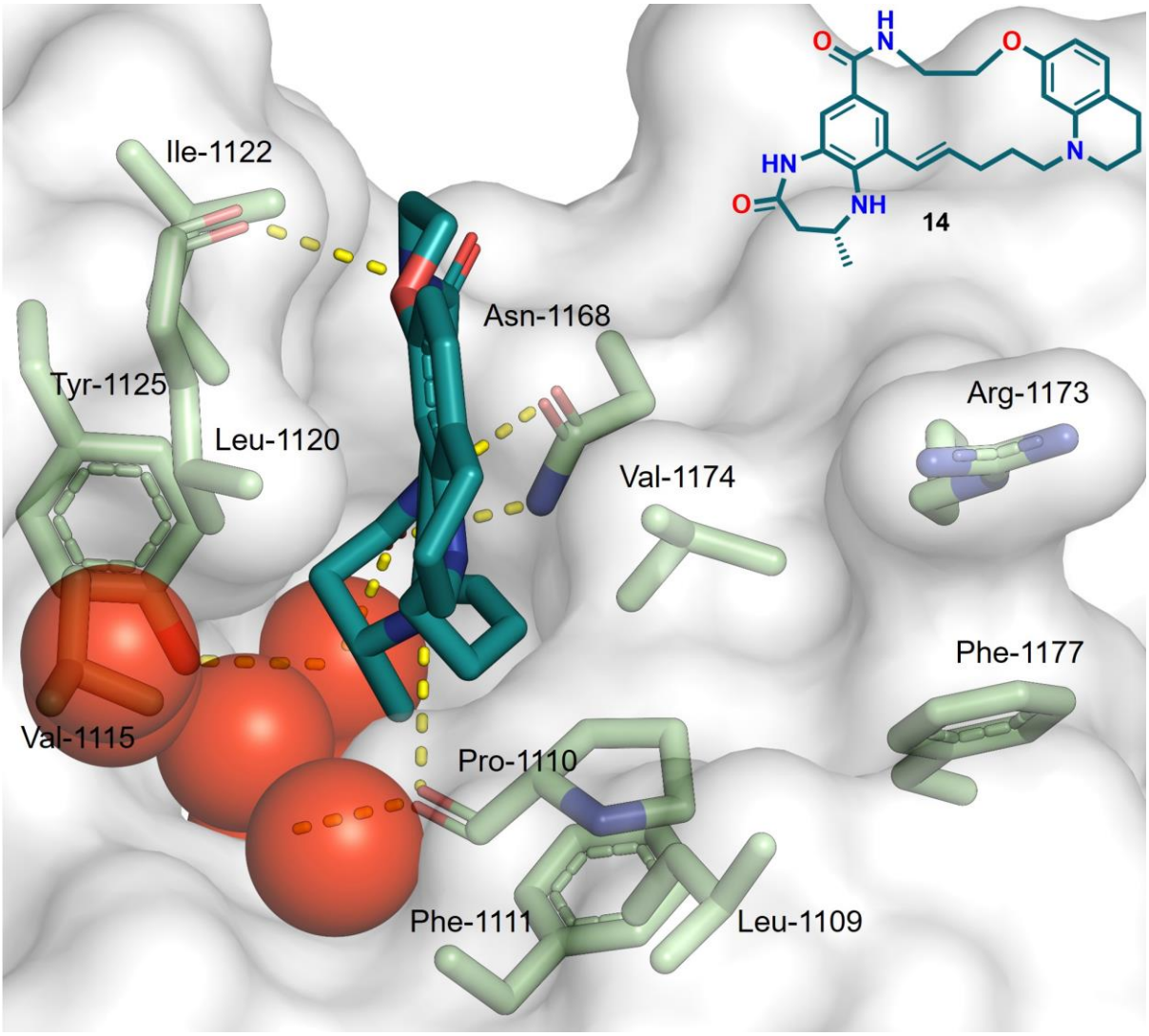

Figure 37: X-ray co-crystal structure of ligand **14** (cyan) in complex with the CBP^{BRD} (PDB: 9GEU) at 1.56 Å resolution, viewed from the side of the binding pocket along the ZA channel with water occupying the channel. All residues which the ligand interacts with are displayed (green) with labels and the backbone amide removed for clarity unless otherwise involved in hydrogen bonding and the hydrogen bonding interactions to the ligand highlighted by the dashed (yellow) lines, and with the chemical structure of **14** shown in the top right.

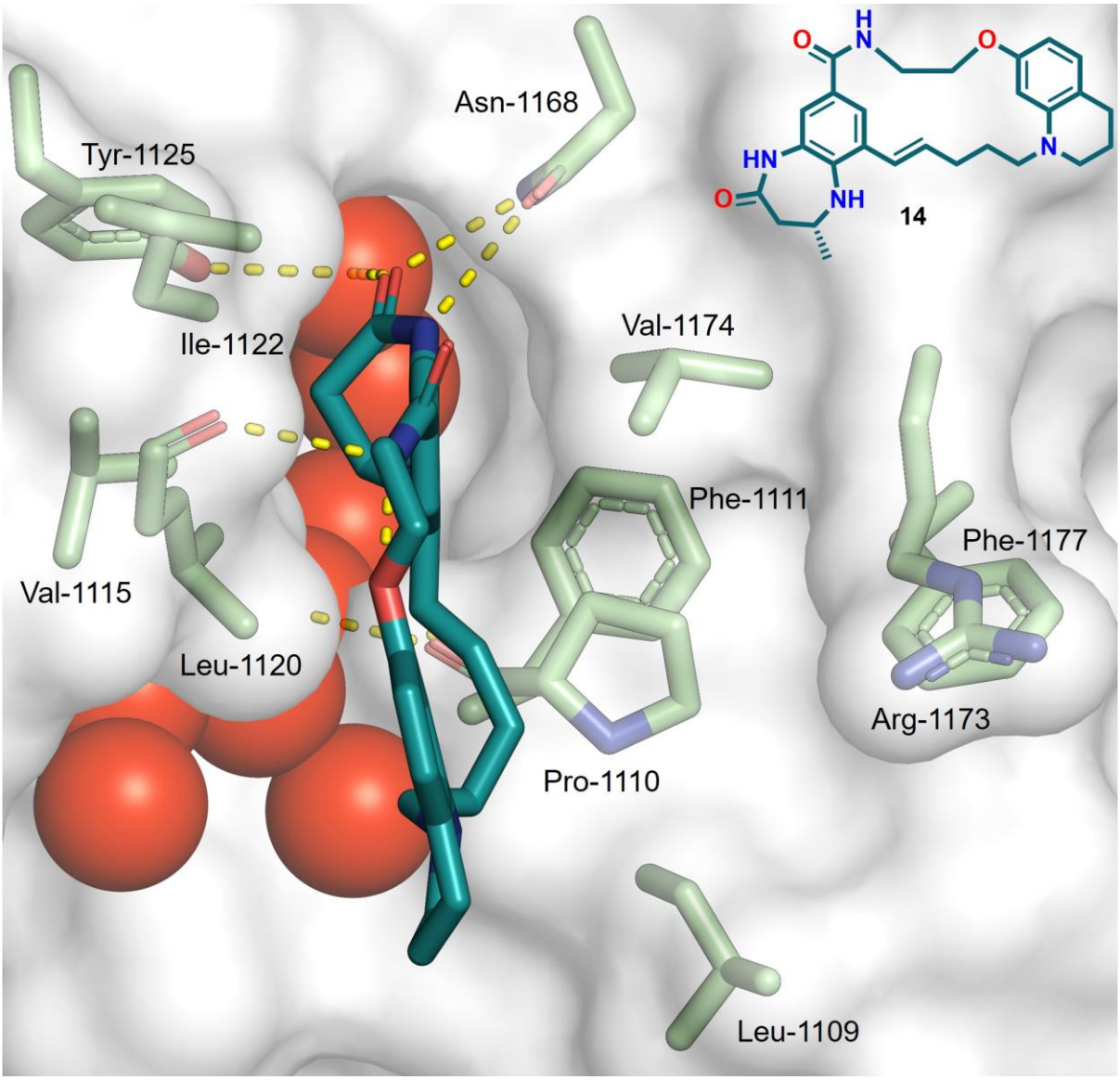

Figure 38: X-ray co-crystal structure of ligand **14** (cyan) in complex with the CBP^{BRD} (PDB: 9GEU) at 1.56 Å resolution, viewed from above the binding pocket and LPF shelf with water occupying the channel. All residues which the ligand interacts with are displayed (green) with labels and the backbone amide removed for clarity unless otherwise involved in hydrogen bonding and the hydrogen bonding interactions to the ligand highlighted by the dashed (yellow) lines, and with the chemical structure of **14** shown in the top right.

Although the co-crystal structures are heavily influenced by the crystallographic artefact, it is worth noting that the [6,7]-KAc mimic maintains the expected hydrogen bonding interactions with Asn-1168, Pro-1110 and water-mediated bond with Tyr-1125. There is also a possibility for **14** to produce a hydrogen bond donating interaction with either the backbone amide of Leu-1120 or intramolecularly with the aryl ether oxygen, however, the bond angles do not appear to be optimal for either interaction. In the

structure of **10**, only the intramolecular hydrogen bond is observed. However, due to the overwhelming effect of the crystallographic artefact, the induced fit pocket caused by the cation-π interaction, is not observed and no firm structural insight can be provided to explain the increased affinity of **14** compared to **10** for the CBP^{BRD}.

3.5.2 Co-crystal structure of Ligand **40** in complex with the CBP^{BRD}

The co-crystal structure of compound **40** when bound to the CBP^{BRD} differs from **10**, **14** and **OXFBD05**, in that the induced fit pocket is visible between the THQ and Arg-1173 mediated cation-π interaction (Figure 39 and 40, dashed yellow lines). The interactions of the induced fit pocket appear with one nitrogen of Arg-1173 above the methoxy group, participating in a dipole-dipole interaction, whilst the other nitrogen of Arg-1173 was present above the aromatic ring performing the desired cation-π interaction. This leads to ligand **40** demonstrating the desired curled-up conformation similar to that observed for **6** (PDB: 6YIM) and **1** (PDB: 4NYX). Ligand **40** forms the expected hydrogen bonding interactions in the KAc binding pocket through the [6,7]-ring system. Those hydrogen bonds are with the residues Asn-1168 and Pro-1110 as well as the water-mediated hydrogen bond to Tyr-1125. Rather unexpectedly the morpholine and attached amide do not exhibit any additional hydrogen bonds directly with the binding pocket on the CBP^{BRD}. There is also a lack of water mediated-hydrogen bonding interactions between the morpholine of **40** and the CBP^{BRD} meaning that this moiety offers no appreciable beneficial interactions with the protein which is again unexpected and highlights the hydrophobic nature of the binding pocket. The [6,7]-KAc mimic forms several hydrophobic interactions, such as those with Phe-1111, Val-1115, Ile-1122 and Tyr-1125. The alkyl chain connecting the THQ and [6,7]-ring system forms hydrophobic interactions along the ZA channel with Pro-1111 and Leu-1120. The THQ forms the induced fit pocket causing hydrophobic

interactions with the residues Leu-1109, Pro-1110 and Phe-1177 on the leucine, proline, phenylalanine (LPF) shelf.

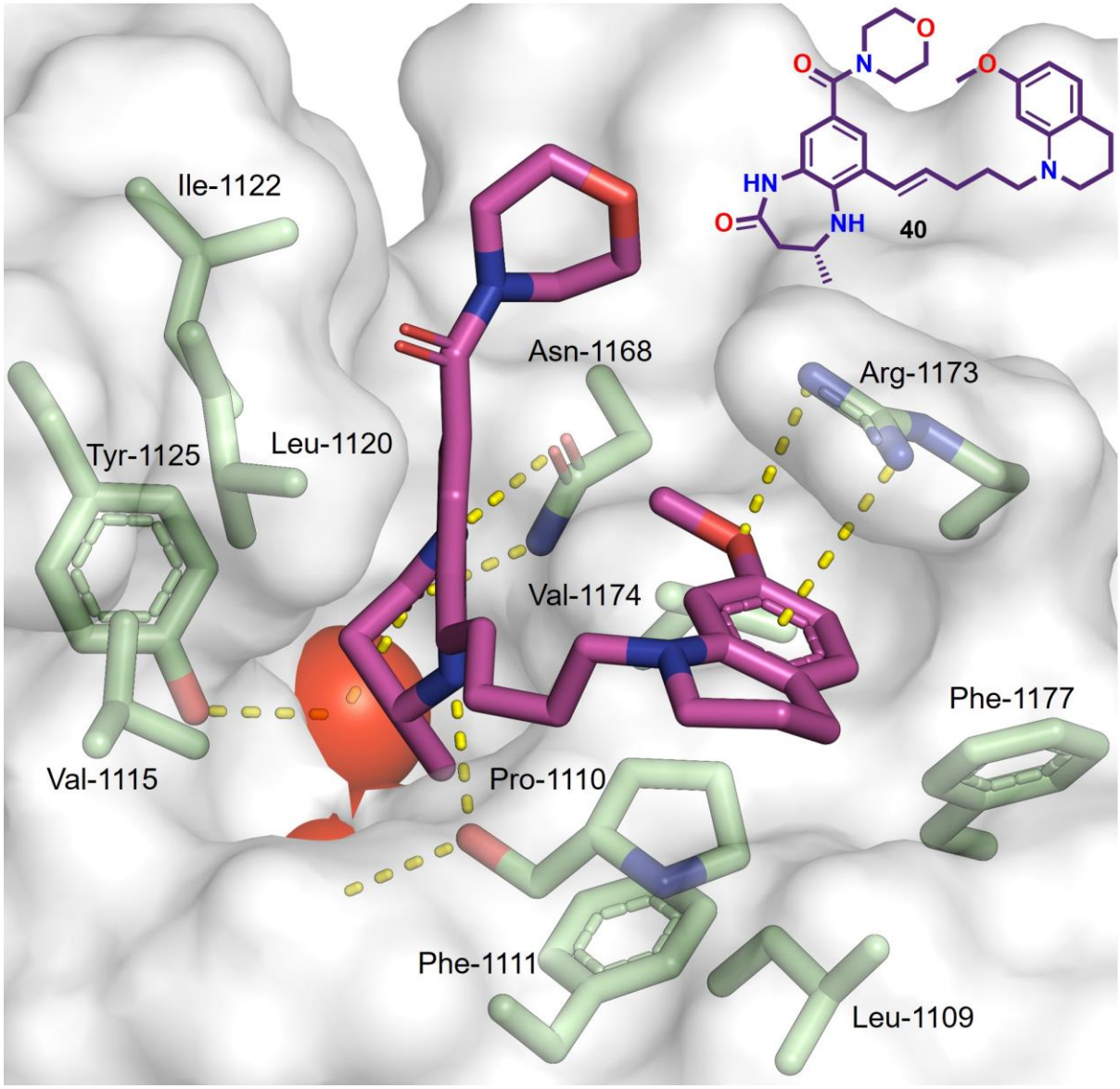

Figure 39: X-ray co-crystal structure of ligand **40** (purple) in complex with the CBP^{BRD} (PDB: 9GET) at 1.29 Å resolution, viewed from the side of the binding pocket along the ZA channel with water occupying the channel removed for clarity. All residues which the ligand interacts with are displayed (green) with labels and the backbone amide removed for clarity unless otherwise involved in hydrogen bonding and the hydrogen bonding interactions to the ligand highlighted by the dashed (yellow) lines, and with the chemical structure of **40** shown in the top right.

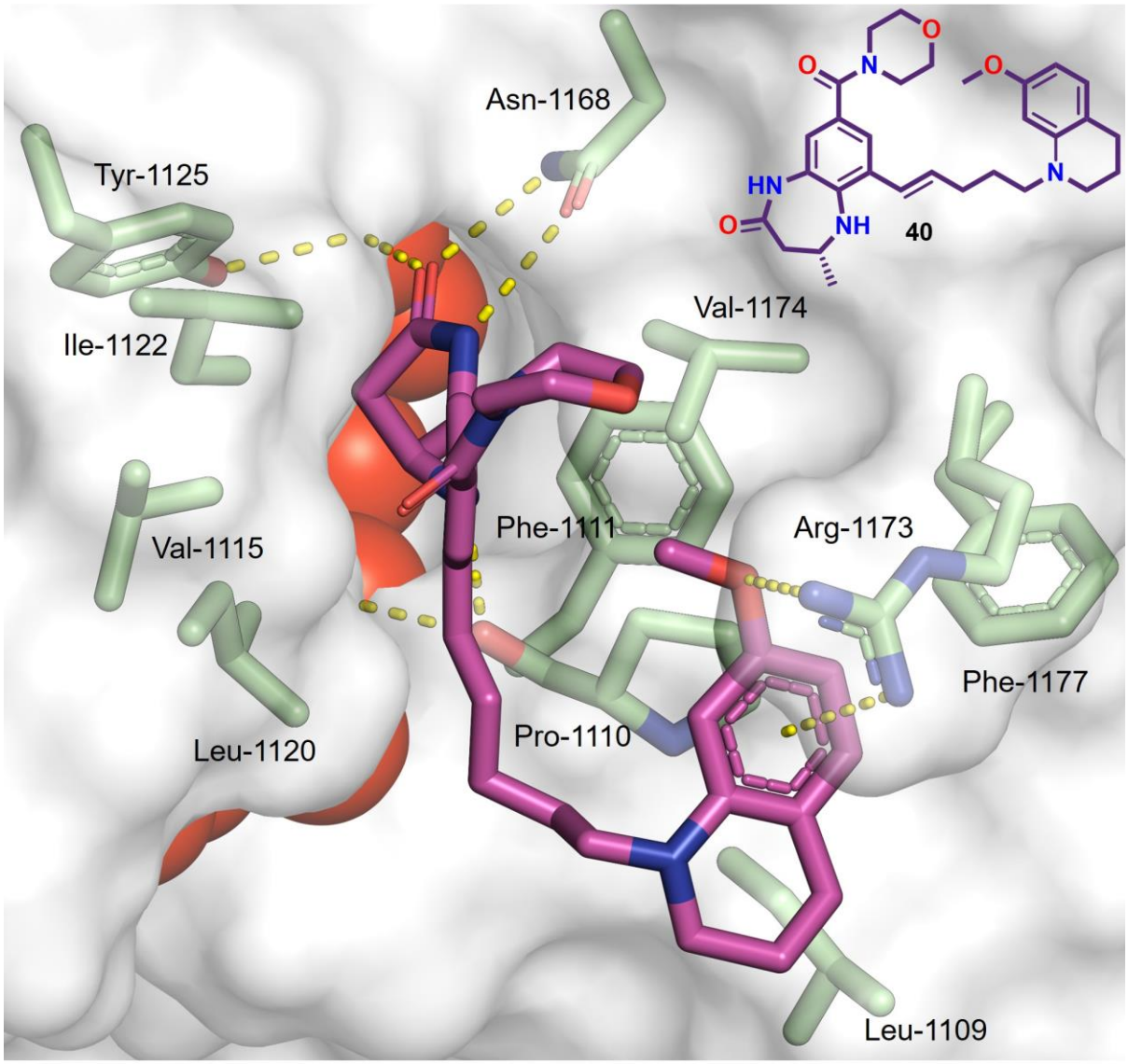

Figure 40: X-ray co-crystal structure of ligand **40** (purple) in complex with the CBP^{BRD} (PDB: 9GEU) at 1.29 Å resolution, viewed from above the binding pocket and LPF shelf and with water occupying the channel shown. All residues which the ligand interacts with are displayed (green) with labels and the backbone amide removed for clarity unless otherwise involved in hydrogen bonding and the hydrogen bonding interactions to the ligand highlighted by the dashed (yellow) lines, and with the chemical structure of **40** shown in the top right.

The co-crystal structure of **40** demonstrates the desired binding conformation caused by the presence of the induced fit pocket produced through the cation-π interaction between the THQ and Arg-1173. Even with this structural data displaying the curled-up binding conformation of the ligand, it lacks selectivity for the CBP^{BRD} over BRD4(1). This can be attributed to the flexibility of **40** resulting from the sp^3 alkyl chain within its structure. The fact that **40** lacks conformationally constraint means that the ligand has a low energy barrier to adopting the linear conformation required to bind to BRD4(1).

The weaker binding affinity when compared to the positive control compound **OXFBD05** can be rationalised by the addition of the electron withdrawing amide, weakening the hydrophobic interactions to Phe-1111, Val-1115, Ile-1122, and Val-1174. The amide and attached morpholine ring do not appear to make additional interactions with the protein to compensate for this, causing a further decrease in affinity.

3.5.3 Co-crystal structure of Ligand **19** in complex with the CBP^{BRD}

With the co-crystal structure of **40** demonstrating the desired curled-up conformation through the formation of the induced fit pocket, the structure of **19** bound to the CBP^{BRD} was next analysed (Figure 41 and 42). The structures of **40** and **19** bound to the CBP^{BRD} exhibit the desired curled-up conformation, with one marked difference, **19** did not display the induced fit pocket and lacked the cation-π interaction between the THQ and Arg-1173. This is hypothesised to be the result of a crystallographic artefact leading to the heptamer formation observed (see Appendix F). This is a homo-heptamer as all the single BRDs within the heptamer display the same shape and binding mode of **19** with structural water molecules maintained. Ligand **19** forms the two hydrogen bonding interactions in the KAc binding pocket with Asp-1168, and the water-mediated hydrogen bond to Try-1125. However, the hydrogen bond to Pro-1110 now appears to be mediated by a water molecule as opposed to the direct hydrogen bond observed in the co-crystal structure of **40** with the CBP^{BRD}. Unlike in the structure of **40** bound to the target BRD, the morpholine oxygen of **19** forms water-mediated hydrogen bonds to the backbone amides of both Arg-1173 and Val-1174. The amide attached to the morpholine also demonstrates a water-mediated hydrogen bond to the backbone amide of Leu-1120. This could be the caused of ligand **19** demonstrating high affinity even with decreased electron density on the KAc mimic. There is also potential for ligand preorganisation into the binding conformation, resulting in an

increase in affinity. The [6,7]-KAc mimic makes the weakened hydrophobic interactions with Phe-1111, Val-1115, Ile-1122, Tyr-1125 and Val-1174. The alkyl linker between the [6,7]-ring system and THQ, forms hydrophobic contacts with Pro-1110 and Leu-1120. Whilst the THQ forms hydrophobic interactions on the LPF shelf with Leu-1109, Pro-1110, and Phe-1177, without the induced fit pocket cation-π interaction.

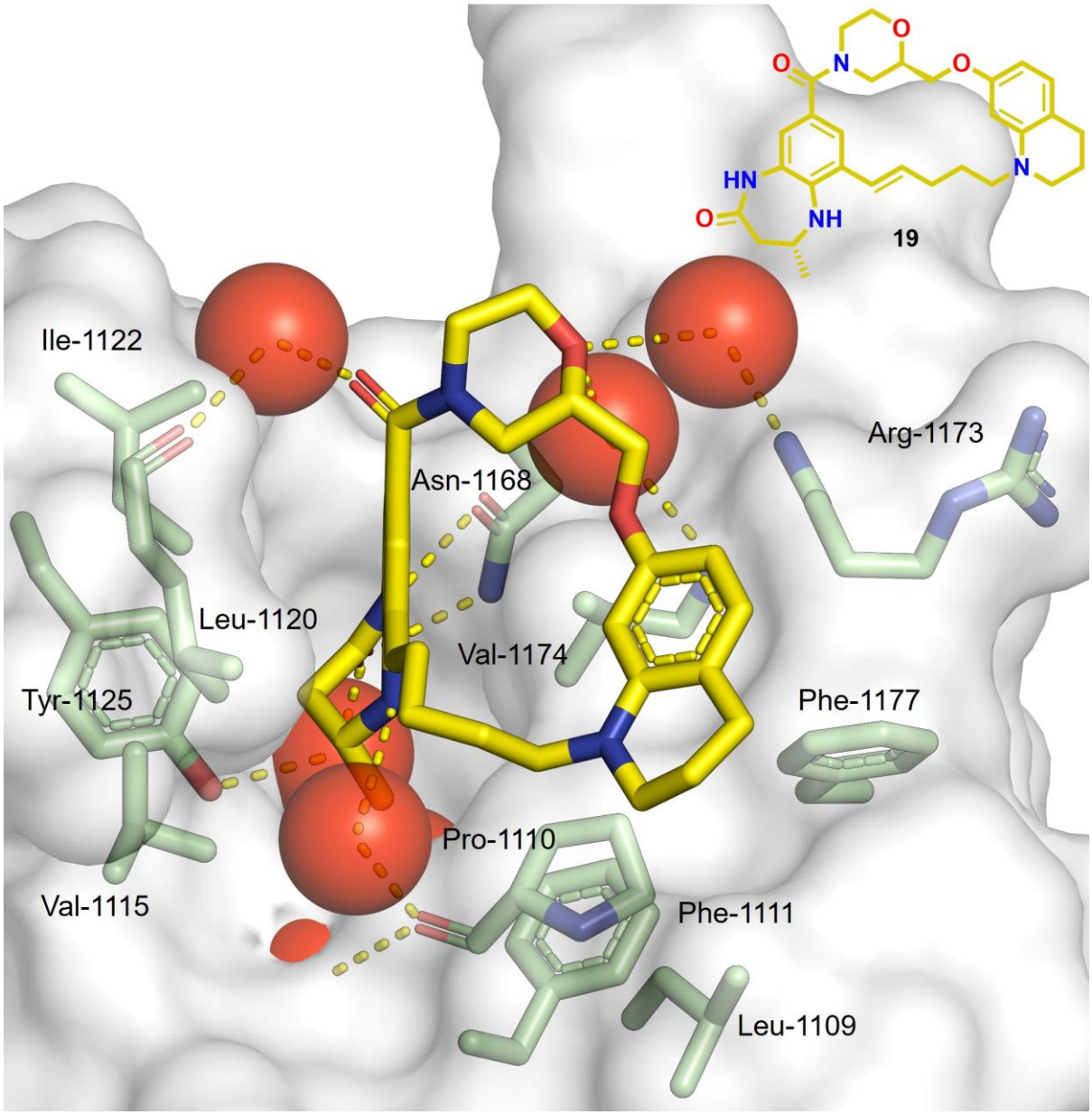

Figure 41: X-ray co-crystal structure of ligand **19** (yellow) in complex with the CBP^{BRD} (PDB: 9GEJ) at 1.84 Å resolution, viewed from the side of the binding pocket along the ZA channel with water occupying the channel removed for clarity. All residues which the ligand interacts with are displayed (green) with labels and the backbone amide removed for clarity unless otherwise involved in hydrogen bonding and the hydrogen bonding interactions to the ligand highlighted by the dashed (yellow) lines, and with the chemical structure of **19** shown in the top right.

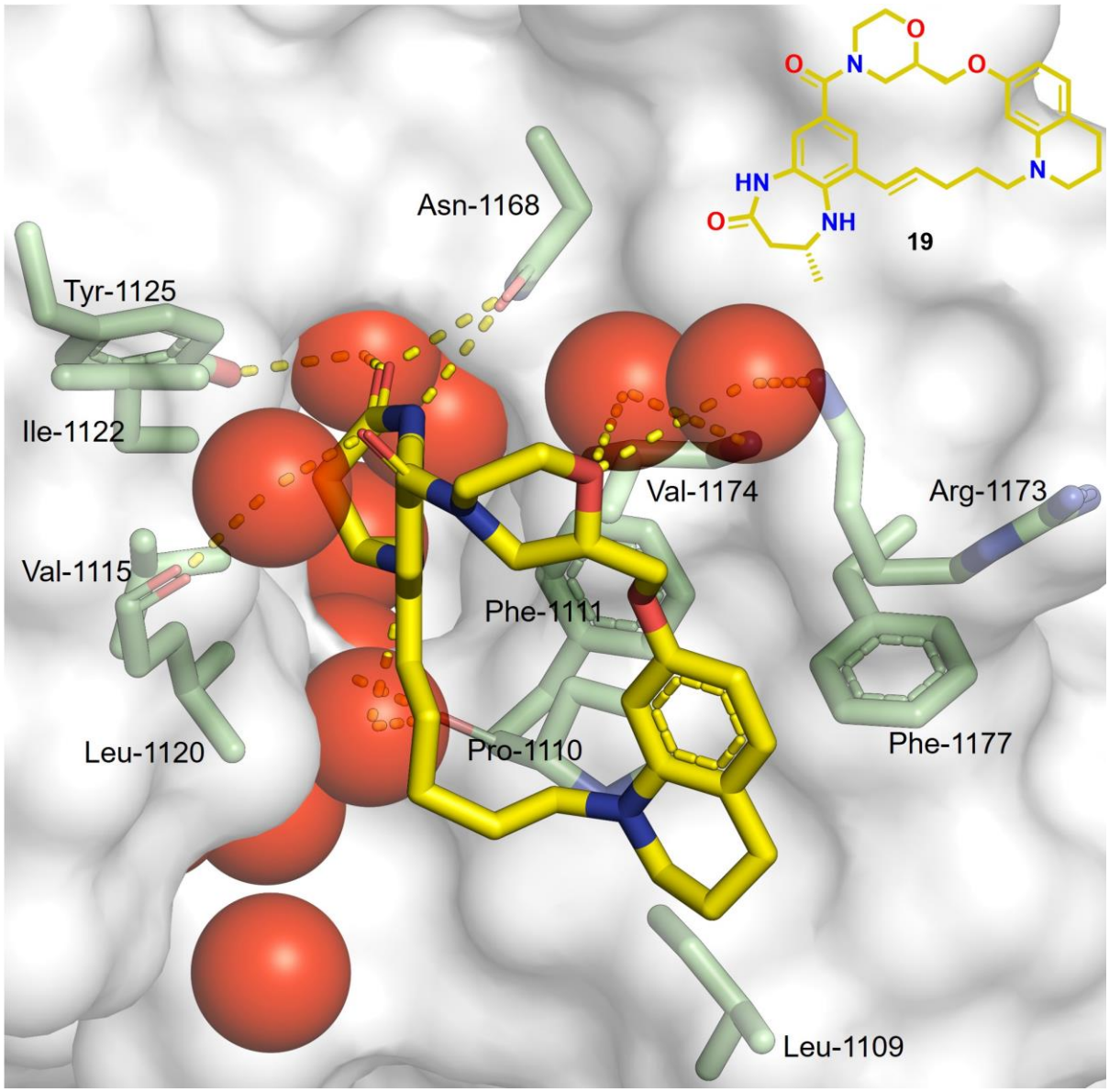

Figure 42: X-ray co-crystal structure of ligand **19** (yellow) in complex with the CBP^{BRD} (PDB: 9GEJ) at 1.84 Å resolution, viewed from above the binding pocket and LPF shelf and with water occupying the channel shown. All residues which the ligand interacts with are displayed (green) with labels and the backbone amide removed for clarity unless otherwise involved in hydrogen bonding and the hydrogen bonding interactions to the ligand highlighted by the dashed (yellow) lines, and with the chemical structure of **19** shown in the top right.

The movement of residue Arg-1173 away from the binding site, leading to a lack of induced fit pocket, is likely due to a crystallographic artefact because this residue strongly interacts with the next unit of the CBP^{BRD}. The interaction demonstrated is a strong hydrogen bonding interaction with a glutamic and aspartic acid residue, the strength of which can also be attributed to a dipole-dipole interaction between the positively charged amidine of the arginine and negatively charged carboxylic acid side

chains (see Figure 43A and B). This is a consistent interaction between each single unit of the CBP^{BRD} that make up the heptameric structure, between Arg-1173 of the first CBP^{BRD} and Asp-1155 (this interaction is consistent), and with Glu-1149 (this interaction depends on the orientation of the side chain and so is only observed across some units of the heptamer) of the second CBP^{BRD}. The interactions between the units of the CBP^{BRD} causing the formation of the heptameric unit are also likely enhanced by ligand **19** providing a hydrophobic surface through which interactions can occur. This is observed with residue Trp-1158 which stacks onto macrocycle **19** (Figure 43C).

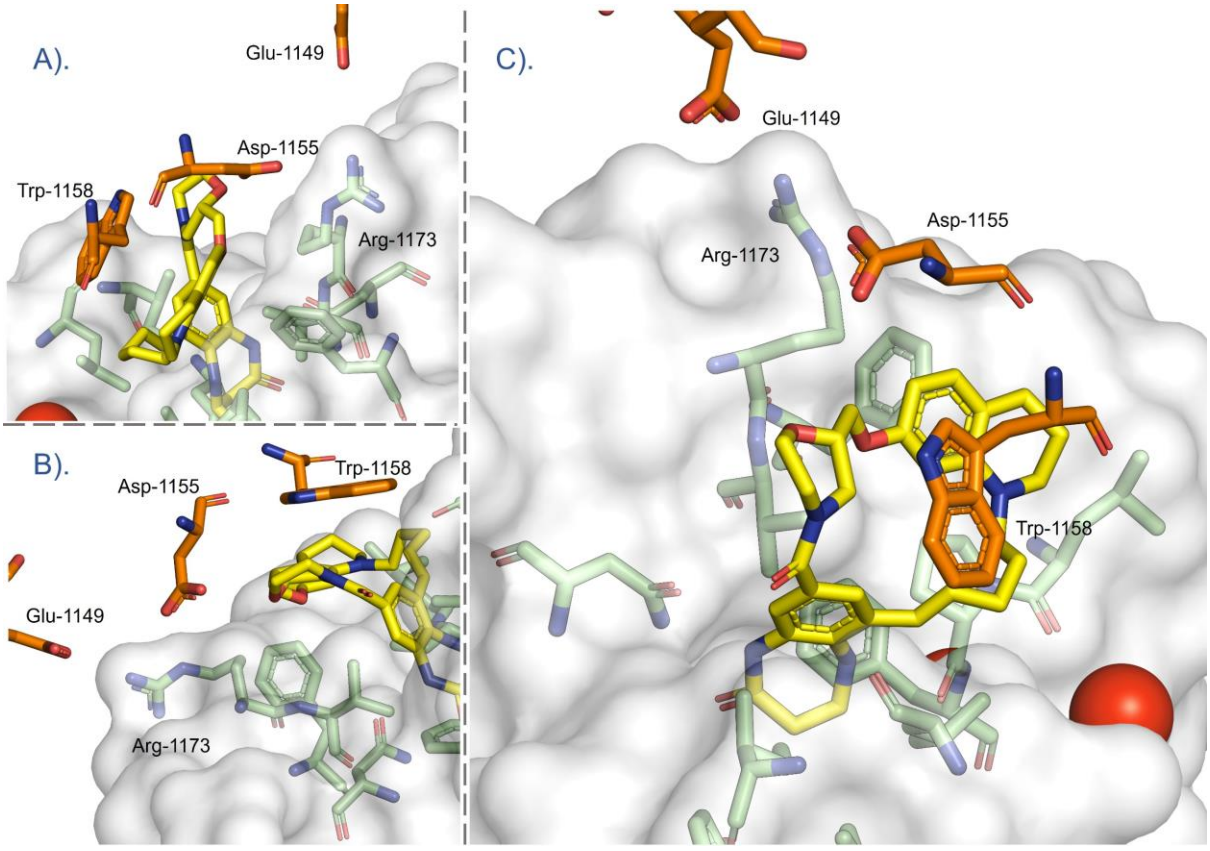

Figure 43: The co-crystal structure of **19** (yellow) and the CBP^{BRD} (PDB: 9GEJ) at 1.84 Å resolution, with the residues which interact with the ligand and Arg-1173 of the adjacent BRD unit of CBP highlighted in orange, A) and B). Two co-crystal images underlining the strong polar and hydrogen bonding interactions between the Arg-1173 which usually participates in cation-π interactions and the residue which it interacts with instead Asp-1155 and Glu-1149 of the adjacent BRD protein unit in highlighted in orange, C). Co-crystal image focussed on the hydrophobic interactions between ligand **19** and the Trp-1158 of the adjacent CBP^{BRD} highlighted in orange.

Although Arg-1173 does not form the induced fit pocket in the crystal structure, ligand **19** still demonstrates the desired binding conformation, hinting at why this ligand

shows the greatest selectivity for the CBP^{BRD} over BRD4(1). The ligand **19** is trapped and thus unable to adopt a linear conformation to BRD4(1), presenting too high of an energy barrier to overcome and straighten in order to bind to the off-target BRDs. So, it is conformationally constrained to the CBP^{BRD} binding mode. It is also likely that in solution the induced fit pocket is present and plays a key role in the binding of macrolactam **19**, as without this interaction, no difference in K_d would be observed between the CBP^{BRD} and $p300^{BRD}$. This is not the case as both the BromoKdElect and BromoMax data indicate a greater affinity for the CBP^{BRD} over the $p300^{BRD}$ as the compound possesses a CBP/p300 selectivity of 3-fold. Although this appears a small fold selectivity, consider that CBP and p300 are paralogue proteins which share a 97% sequence homology within the BRDs, with only 4 amino acids different between the two.[127] The most obvious reason for this increased affinity for the CBP^{BRD} over the $p300^{BRD}$ was the assumed formation of the cation-π interaction, giving increased affinity for CBP^{BRD}, which has been previously observed in the literature although to a lesser extent.[124] But the selectivity for the CBP^{BRD} could also be explained by the additional water-mediated hydrogen bonds between the morpholine of macrocycle **19** and Arg-1173 and Val-1174, which might not be present with the $p300^{BRD}$. Although further investigations would need to be conducted to prove this hypothesis, the co-crystal structure of **19** presented is the first structure demonstrating how conformational constraint can be used to afford a selective, high-affinity ligand for the CBP^{BRD}. In order to validate the hypothesis of the oligomer formation observed in the crystal structure of **19** and the CBP^{BRD}, experiments aimed to identify this as a crystallographic artefact were carried out.

3.5.4 Investigation of Heptamer formation upon **19** binding

To investigate the crystallographic artefacts obtained from the co-crystal structures of the macrolactam ligands bound to the CBP^{BRD}, compound **19** was chosen, as it is the most thoroughly characterised in terms of binding affinity. Unlike **10** and **14**, the artefact exhibited by **19** is unique with regard to CBP^{BRD} ligands, thus reinforcing the choice to investigate this phenomenon further. The binding of **19** to the next BRD causes a homo-heptamer observed in the solid state, if observed in solution this could undermine the extensive *in vitro* data previously obtained. In order to characterise the protein structure in solution analytical ultra centrifugation (AUC) was performed with ligand **19** and the CBP^{BRD}. This technique relies on sedimentation of higher molecular weight species occurring more rapidly from solution, so upon oligomer formation the traces should appear different if this phenomenon is driven by addition of macrolactam **19**.

Originally the CBP^{BRD} was diluted to 40 μM, to demonstrate that only monomers of the domain were observed, and no higher-order structures are present (Figure 44 and see Appendix G figure 1 for full data) in the native protein.

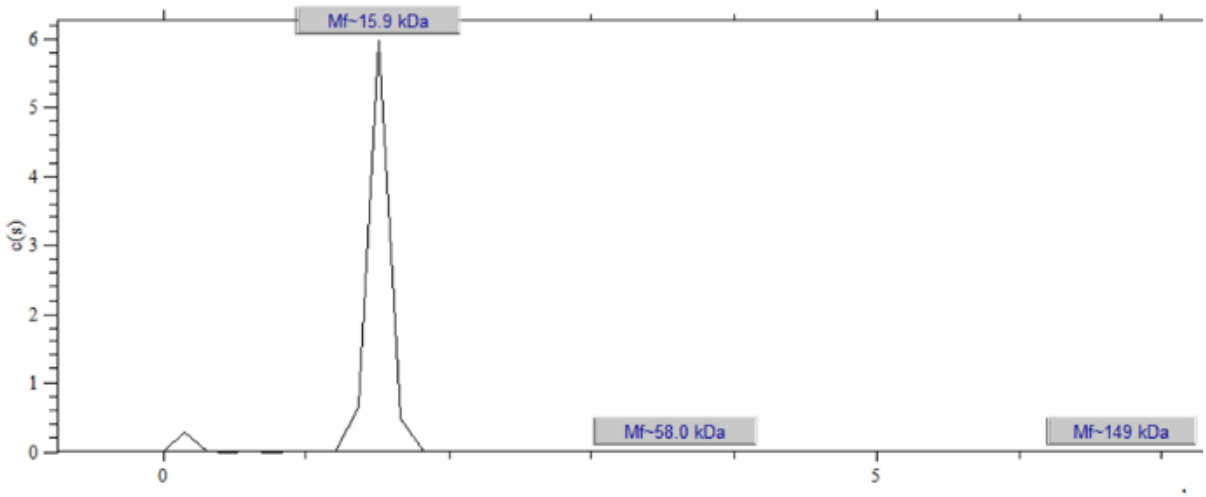

Figure 44: AUC data for the CBP^{BRD}, with molecular masses of the species observed displayed above each peak in kDa.

When the CBP^{BRD} was analysed by AUC, the molecular weight mass of the monomeric protein obtained was ~15.9 kDa which is close to the 15.7 kDa measured by mass spectrometry (see Appendix B figure 1). Compound **19** was then added at 0.5, 1 and 1.5 equivalents (20, 40, and 60 μM) to a set concentration (40 μM) of the CBP^{BRD} and analysed by AUC (Figure 45 and see Appendix G figures 2-4 for full data). Upon addition of ligand **19**, no large peaks corresponding to dimer or higher order structures such as heptamers were observed by AUC. Instead, only a minor peak corresponding to a mass of 40.1 kDa was observed upon the addition of **19** at 20 μM, indicating low-level dimer formation but the majority of the protein remained in its monomeric form (Figure 45A). There is a smaller peak at 60.4 kDa observed at equimolar concentration of **19** and the CBP^{BRD}, which could indicate minor trimer formation, again this makes up a small proportion of total protein observed (Figure 45B). All of the peaks in the AUC observed with the addition of the **19**, experience broadening, likely caused by addition of DMSO to both the control and protein containing samples.

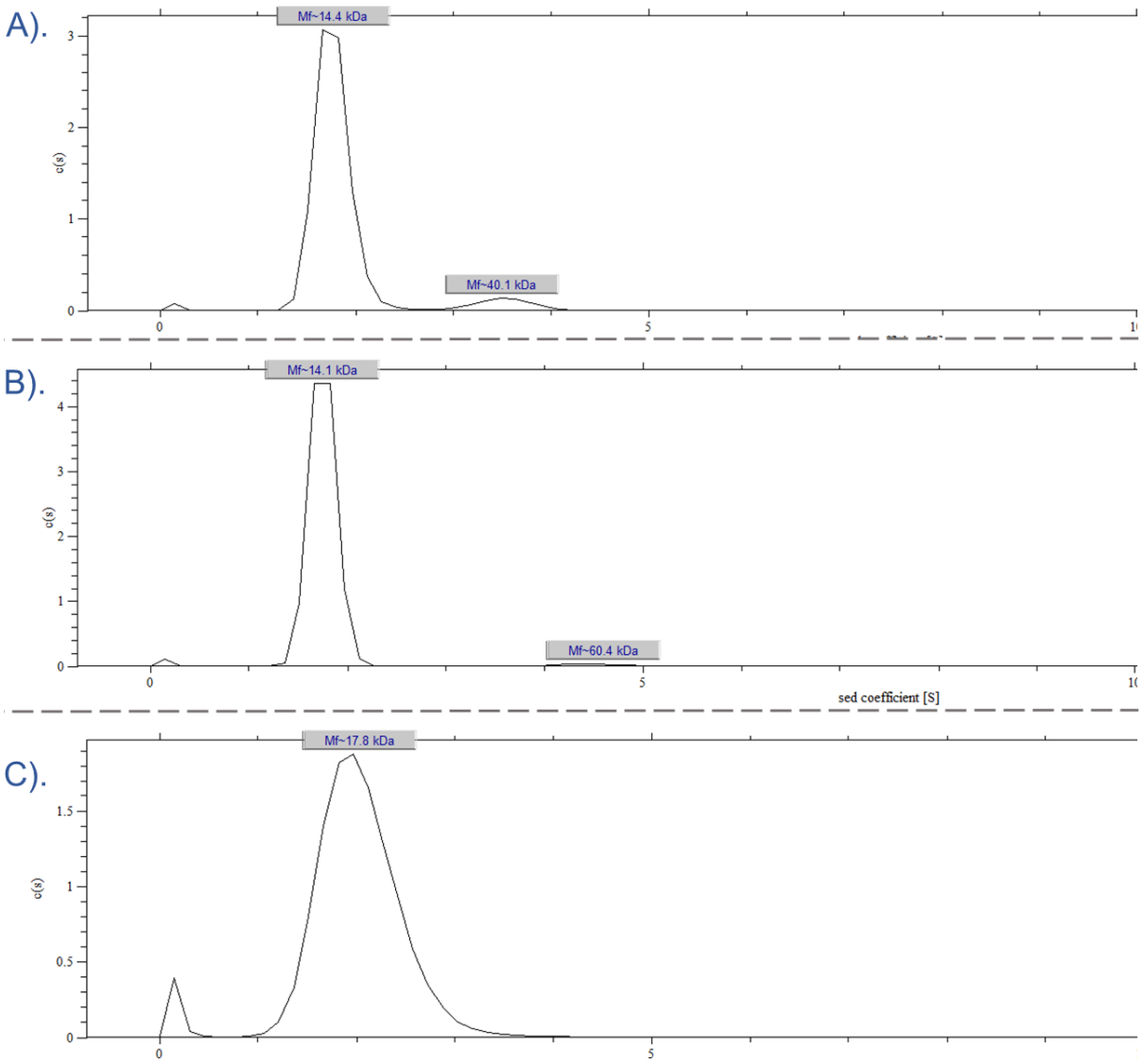

Figure 45: AUC data for the CBP^{BRD} at 40 μM, with ligand **19** at 20 (A), 40 (B), and 60 (C) μM, a blank subtraction containing 0.2% *v*/*v* DMSO was carried out, the same percentage DMSO as each sample.

In order to ensure that the addition of the ligand was not causing any assay interference through background absorbance at 280 nm, the AUC assays were repeated but this time with the corresponding concentration of ligand added to each buffer from which the results were calculated (Figure 46 and Appendix G figures 5-7 for full data).

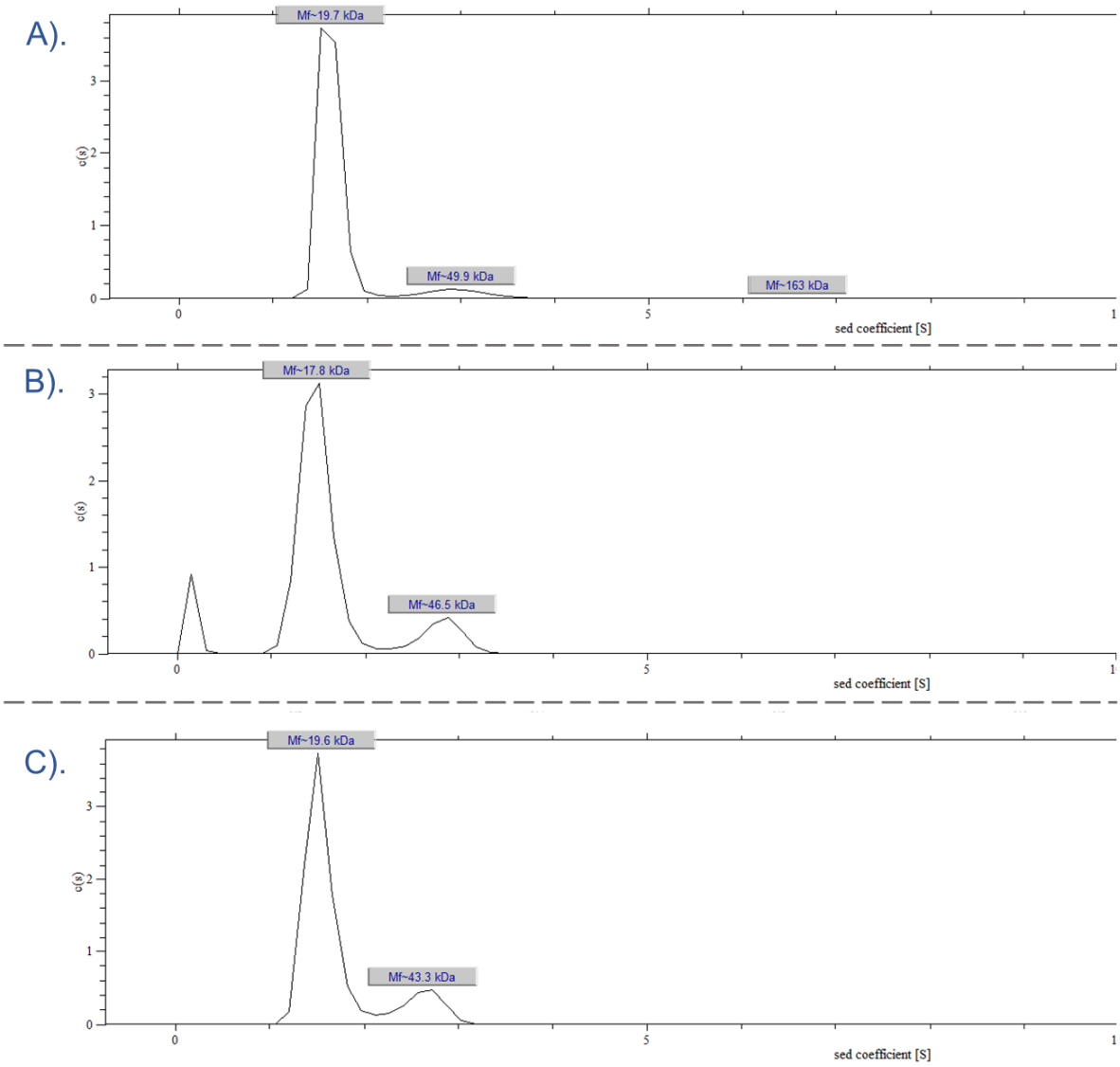

Figure 46: AUC data for the CBP^{BRD} at 40 μM, with ligand **19** at 20 (A), 40 (B), and 60 (C) μM, a blank subtraction containing 0.2% *v*/*v* DMSO and the respective concentration of **19** was carried out, the same percentage DMSO was added to each sample.

At all concentrations analysed there appears to be minor dimer formation which occurred upon the addition of the ligand, this increased from 20 to 40 μM of **19** but demonstrated no visible increase from 40 to 60 μM. Once again, this dimer still makes up a minority of the species observed by AUC. This indicates that only dimeric species can be observed in solution between **19** and the CBP^{BRD} and this is only a small proportion of the total number of species observed, with the majority remaining monomeric in nature. This provides a piece of evidence that the interactions observed between **19** and two units of the CBP^{BRD} in the co-crystal structure (Appendix F, figures

1 and 2) are likely a crystallographic artefact. Seeking further confirmation of this, native mass spectrometry was used to monitor if interactions caused between **19** and the CBP^{BRD} can cause oligomer formation (see Appendix G for Native-MS data). This technique can be utilised in the observation of non-covalent interactions between small molecules and macromolecules, the strength of these interactions and further binding data. Using native-MS there were no dimer or higher order oligomers observed upon the addition of ligand **19** to the CBP^{BRD} by native-MS. The binding of ligand **19** was observed using native-MS, illustrating how non-covalent interaction can be detected with this technique if sufficiently strong binding occurred. Both this data, along with the AUC experiments, indicate that heptamer formation observed in the co-crystal structure of **19** bound to the CBP^{BRD} was due to crystallographic artefact. This would imply that in solution the Arg-1173 residue forms the induced fit pocket through a cation-π interaction with macrolactam **19**.

3.6 Physiochemical Properties

With respect to the ITC testing of the positive control **OXFBD05** discussed previously in section 3.3.1, it became clear that the previously utilised conditions to assess binding of this ligand were not viable. This is due to the published conditions using a concentration of 40 μM, which caused visible desolvation of the ligand as white particulate matter even with 0.2% *v*/*v* DMSO at pH 7.4.[44] Due to this the assay was re-optimised to use a half the concentration of **OXFBD05** (20 μM) and this gave a binding affinity more in line with the literature value but not within error (K_d = 132 nM ±3 nM vs K_d = 102 nM ±10 nM as reported).[44] However, this highlighted the poor solubility of the positive control ligand, therefore, **OXFBD05**, the novel macrolactams **14**-**19** and respective linear analogues **39**-**41** were assay for their physiochemical properties.

3.6.1 Physiochemical data for **OXFBD05**, ligands **14-19**, and ligand **39-41**

The physiochemical properties were assessed using GSKs inhouse methods which are described in the experimental (Chapter 7). These data also help to highlight differences between the macrolactams and their linear analogues, whilst also providing a comparison to the positive control **OXFBD05** (Table 10). This also allows for ligands with poor physiochemical properties to be highlighted prior to testing in cell-based assays, with particular interest in the properties of Ligand **19**.

Table 10: Selected physiochemical properties of **OXFBD05**, compounds **14-19** and compounds **39-41**, these data were produced using the in-house GSK methods, where Chrom stands for chromatographic, SFI stands for solubility forecast index (ChromLogD+#aromatics) and HSA stands for human serum albumin, the ChromLogD was measured at pH 7.4.

Compound Number	Chrom LogD	SFI	Molecular weight, Da	H-bond donors and acceptors	Artificial membrane permeability, cm s^{-1}	HSA percentage binding
OXFBD05	6.89	8.89	405.5	2 and 5	1.61×10^{-6}	97.6
10	6.02	8.02	474.6	3 and 7	5.30×10^{-6}	96.4
14	5.16	7.16	460.6	3 and 7	4.97×10^{-6}	95.0
15	6.17	8.17	488.6	3 and 7	3.22×10^{-6}	96.3
16	5.83	7.83	500.6	2 and 7	4.33×10^{-6}	94.6
17	5.85	7.85	500.6	2 and 7	4.78×10^{-6}	95.3
18	6.51	8.51	514.7	2 and 7	3.75×10^{-6}	96.0
19	5.47	7.47	516.6	2 and 8	4.01×10^{-6}	94.0
39	6.83	8.83	516.7	2 and 7	-	93.1
40	5.53	7.53	518.7	2 and 8	-	96.1
41	6.12	8.12	502.7	2 and 7	-	95.6

Usually, a $LogD_{7.4}$ of between 0 – 5 and SFI less than 8 indicating good aqueous solubility in small molecules, with a target value for $ChromLogD_{7.4}$ of 2 – 3 and SFI of around 5.[128] The physchem data highlights the poor properties of **OXFBD05**, as it demonstrates very high hydrophobicity (Chrom $LogD_{7.4}$ of 6.89 and SFI of 8.89),

indicating that is ligand has very poor aqueous solubility even with the lowest molecular weight of the compounds tested. As indicated by the physiochemical testing, ligands 16-19 and 39-41 would be considered bRo5 compounds as they break two of Lipinski's rule based upon molecular weight and possessing a $LogD_{7.4}$>5. However, the least hydrophobic ligands by SFI are **14** (7.16), **19** (7.47), and **40** (7.53), two of which are bRo5 compounds. With the diastereomer pair of **16** and **17** demonstrating similar SFIs (7.83 and 7.85 respectively). The artificial membrane solubilities of macrolactams **14-19** are similar, ranging from 3.22×10^{-6} cm s^{-1} for **15** to 5.3×10^{-6} cm s^{-1} for **10**, meaning that all the macrocycles demonstrate improved permeability compared to **OXFBD05** (1.81×10^{-6} cm s^{-1}). The hit ligand **19** demonstrates improved physiochemical properties for all characteristics assayed relative to the positive control **OXFBD05**, decreased $ChromLogD_{7.4}$ (>1 unit), SFI (>1 unit), and HSA binding (3.6% less) along with an increase in membrane solubility (>2-fold) (Table 10). The differences exhibited by ligand **19** relative to **OXFBD05** are likely due to the inclusion of more hydrogen bond accepts (8 compared to 5) increasing the hydrophilicity of the hit macrolactam, leading to the observed improvements in physiochemistry. When **19** is compared to the equivalent linear analogue **40**, it also has improved HSA binding and slightly decreased $ChromLogD_{7.4}$ and SFI. This highlights that macrolactam **19** is unlikely to present significant issues when tested on cells due to physiochemical properties, as although the ligand is bRo5 and is hydrophobic in nature, it has an SFI<8 and possess membrane permeability. If further improvements to the physiochemistry of such a ligand were required, due to the poor characteristics of the **OXFBD05** on which the macrolactams were based, it would be prudent to change the parts of the macrocycles based upon this scaffold to aim to improve their solubility and permeability.

3.7 Cellular testing of **19** in OCI-AML3 Cells

The testing of ligand **19** was performed in an acute myeloid leukaemia cell line, OCI-AML3, which has been utilised in previous studies of CBP^{BRD} inhibitors.[30] Although all *in vitro* work has been performed on purified BRDs, the work in cells will demonstrate whether macrolactam **19** can engage the CBP^{BRD} within the full-length protein in cells. Therefore, the testing of **19** in cells will test whether the ligand can engage the target domain of the full-length protein in cells and if the macrocycle can cause the desired phenotype. The testing was performed by Disha Kashyap (Milne and Booth Labs, 2024). As the selectivity of compound **19** was highlighted at 1 μM, it was decided to test the ligand up to a maximum concentration of 10 μM in each assay. Those readouts are decreased levels of *c*-MYC, MYB, and BCL-2 which are all oncoproteins associated with CBP^{BRD} inhibition that have previously been monitored in the literature when assessing CBP/$p300^{BRD}$ inhibitors.[123] The off-target BRD-containing proteins, that **19** interacts with, (BAZ2A, SMARCA2 and TAF1(2)) are not believed to interfere with the readouts used in the cell-based assays.[27,125,126] The levels of these proteins were monitored by both Western blotting (measuring oncoprotein levels) as well as qPCR (measuring oncogene transcription through mRNA levels) giving orthogonal assays which measure both protein and mRNA levels in the treated cells. The monitoring of these proteins is a phenotype of CBP^{BRD} inhibition, as by binding to the BRD, it prevents transcription factors recruitment to chromatin in a CBP mediated manner. This lowers the level of the oncogene-associated transcription. In turn, the oncoproteins already present within the cell are short lived, hence broken down by the proteasome whilst these proteins are no longer being transcribed and produced, decreasing their overall levels overtime. This phenotype has previously been established in cancer cells as being a response to CBP^{BRD} inhibition.[28,52,123,129]

Inobrodib was used as the positive control due to its robust cellular activity and strong phenotypic effects in leukaemia cell lines.[30,42]

3.7.1 Evaluation of Cell Viability

To ensure that the desired phenotype of decreased oncoprotein levels is not due to cell death upon treatment with the ligand **19** or Inobrodib, a CellTiter-Glo® assay was performed, and the percentage of cell survival at 6, 12, and 24 hours were calculated relative to a DMSO control in triplicate (Figure 47). At both 1 (rose) and 10 (brown) μM compound **19** demonstrated <10% cell death up to the 24-hour timepoint measured: the positive control of Inobrodib (lilac) also demonstrated a decrease in cell viability but maintained <10% cell death up to 24 hours. This data gives further credence to the phenotype of decreased protein levels being due to CBP/p300^{BRD} inhibition.

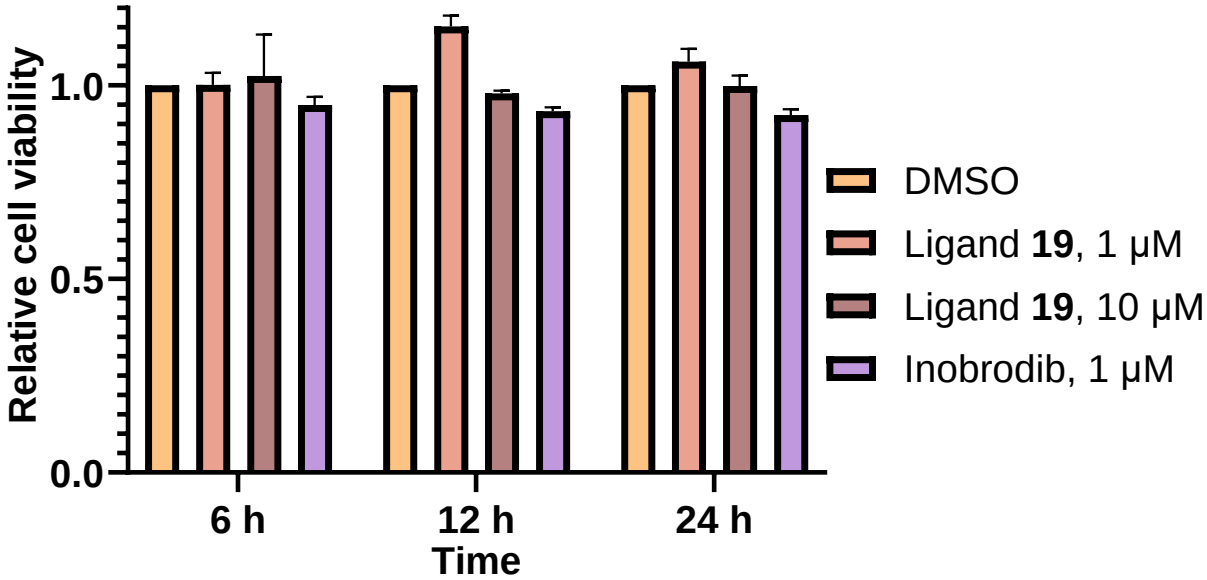

Figure 47: CellTitre-Glo® assay performed on OCI-AML3 cells to assess cell death relative to a DMSO negative control, with Ligand **19** tested at 1 and 10 μM and the positive control Inobrodib tested at 1 μM.

3.7.2 Compound Concentration *in vivo* assays

With the information in hand that neither Inobrodib nor **19** caused a loss of cell viability, the concentration of **19** and Inobrodib required to decrease levels of the target oncoproteins was evaluated. This was assayed by both Western blotting (Figure 38)

and qPCR (Figure 39) at a 24-hour timepoint. Although BCL-2 was assessed by qPCR, the antibody was unavailable to perform Western blot analysis.

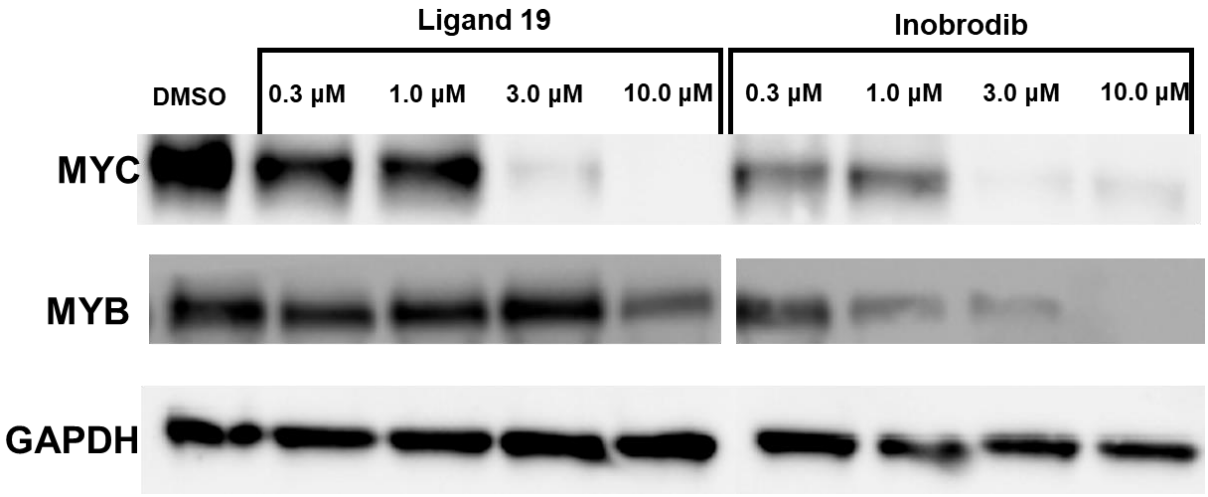

Figure 38: Representative western blots of compound **19** and Inobrodib between 0.3 – 10 μM after treatment of OCI-AML3 cells for 24 hours, with the levels of *c*-MYC and MYB monitored.

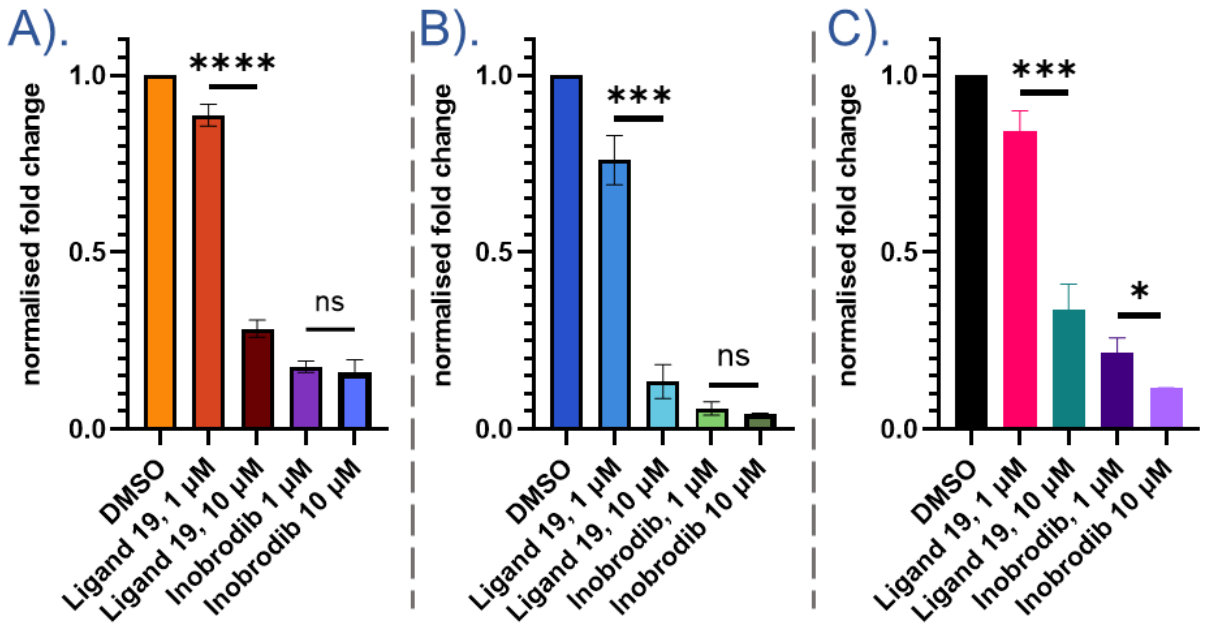

Figure 39: qPCR data for *c*-MYC (A), MYB (B), and BCL-2 (C) mRNA levels of OCI-AML3 cells after 24 hours from treatment with both **19** and Inobrodib at 1 and 10 μM, as a measure of oncogene transcription with the significance compared between the two concentrations for each compound and displayed above the corresponding data, from n = 3 repeats.

Both the Western blots indicate that Inobrodib exhibits a greater decrease across the oncoproteins analysed compared to ligand **19**, whilst the qPCR data also demonstrates a greater decrease of transcription for the associated oncogenes. This is to be expected from the increased affinity of Inobrodib for the CBP^{BRD} and the fact

that this is a clinical candidate and therefore has been optimised for not only it's *in vitro* but also its *in vivo* effects. The data also demonstrate that compound **19** only exhibited the desired phenotypic effect of decreased oncoprotein levels at ≥3 μM (as shown by Figure 38 for *c*-MYC levels). This was why 10 μM was utilised as the top concentration in the qPCR assay (Figure 39), as it begins to produce a similar response to a 1 μM dose of Inobrodib. Therefore, moving forward only 1 μM of Inobrodib is used for positive control experiments, as there is little difference (no significant difference or * significance upon data analysis) between this concentration and a 10 μM dose as a positive control (the most pronounced difference being in BCL-2 levels, but only one * significance, Figure 39C). However, testing of ligand **19** was conducted at both 1 and 10 μM in subsequent experiments as no phenotype was observed after 24 hours for 1 μM but a strong phenotype was observed at 10 μM.

3.7.3 Time Response Assays

The time required to observe the desired phenotype (lowered transcription and overall levels of oncoproteins) was next assessed. This required time point experiments where cells were treated with **19** (at 1 μM and 10 μM) and Inobrodib (1 μM) at 6, 12, and 24 hours. This would establish the time required for a strong phenotypic response from treatment with ligand **19** on oncoprotein levels. This was first assessed using Western blotting (Figure 40) and then verified by qPCR (Figure 41).

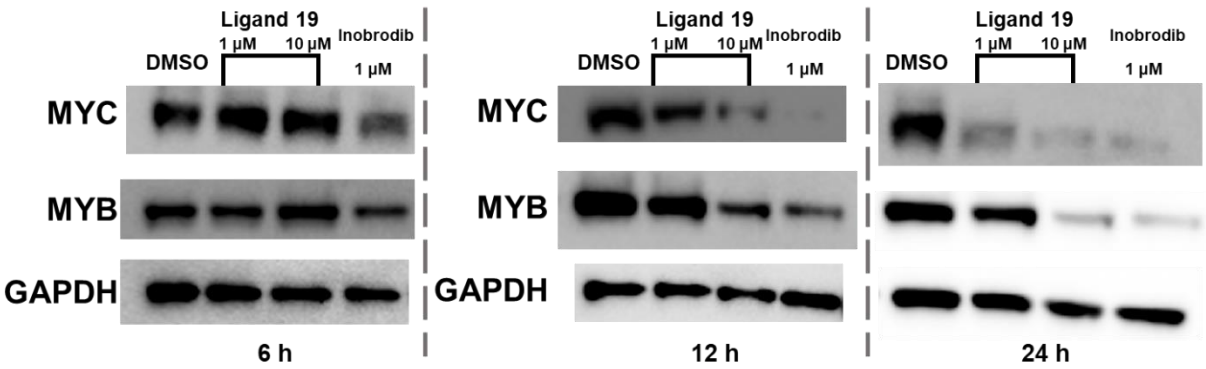

Figure 40: Western blots of *c*-MYC, MYB and GAPDH (as a negative control) at 6, 12, and 24 hours.

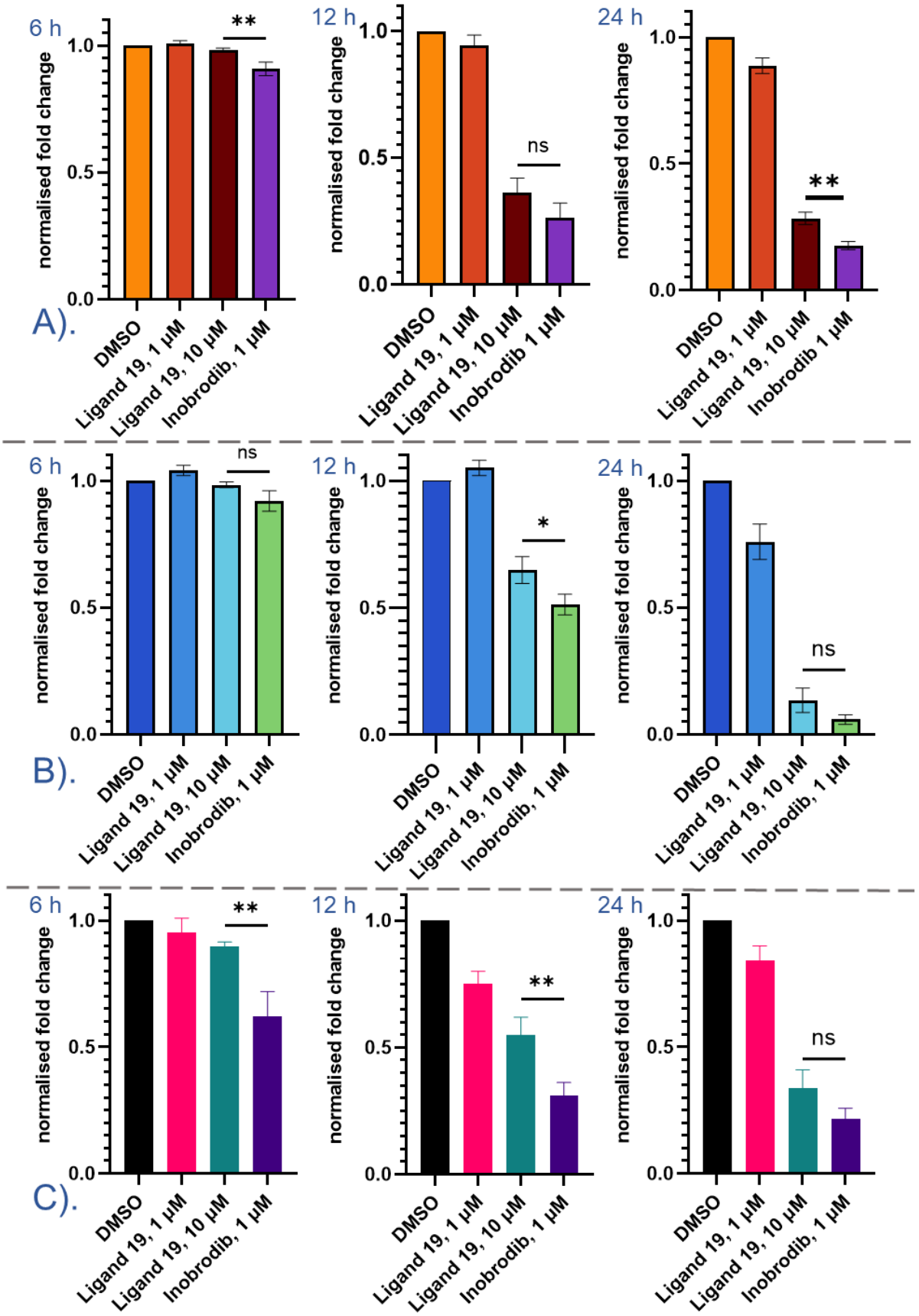

Figure 41: qPCR data normalised to DMSO mRNA transcription levels of treated OCI-AML3 cells using DMSO (negative control), **19** at 1 and 10 µM and Inobrodib at 1 µM (positive control) for oncoproteins *c*-MYC (A), MYB (B) and BCL-2 (C) at 6 h, 12 h, and 24 hours, with the significance between the **19** at 10 µM and the positive control at 1 µM displayed above the corresponding data from n = 3.

Both the Western blot and qPCR data indicate that protein levels and transcription do not present a pronounced decrease 6 hours after treatment with either **19** or Inobrodib relative to the DMSO controls. However, after 12 hours from the treatment, both **19** at 10 μM and the Inobrodib at 1 μM indicate decreased levels of *c*-MYC, MYB and BCL-2 protein and transcription relative to the DMSO control (Figure 40 and 41). Only after 24 hours did treatment at 1 μM of **19** demonstrate a small decrease in protein levels and the associated mRNA (Figure 40 and 41). It can be concluded that treatment at 1 μM of ligand **19** is insufficient to produce the desired phenotypic response in this cell line. The qPCR (Figure 41) data also demonstrates that for *c*-MYC, MYB, and BCL-2 protein transcription continue to decrease at 24 hours for both **19** at 10 μM and Inobrodib at 1 μM. The data also indicates that although the concentration of Inobrodib is 10-fold less than **19**, it affords a stronger phenotypic effect in cells (this is exemplified by the lower levels of all proteins at the three time points tested). However, the data indicate that at 10 μM, in the OCI-AML3 cells, ligand **19** produces the desired phenotype of decreased levels of oncoproteins at both 12 and 24 hour timepoints (Figure 40), at 24 hours the transcription levels of *c*-MYC, MYB, and BCL-2 have nearly reached those of Inobrodib treatment at 1 μM (28% vs 18%, 14% vs 6%, and 31% vs 22% protein transcription respectively relative to DMSO in Figure 41). For both MYB and BCL-2 transcription there is not a statistically significant difference between **19** (10 μM) and Inobrodib (1 μM), whereas for *c*-MYC transcription at 24 hours, the difference is significant (**) (Figure 41). It also appears that by Western blotting at 24 hours for *c*-MYC and MYB the level of protein remaining for both **19** at 10 μM and Inobrodib at 1 μM are similar. The difference in concentration between **19** and Inobrodib required to cause these changes (10-fold increased concentration of **19**) can be explained due to the >10-fold higher affinity of Inobrodib for the CBP/p300^{BRD} with

also potentially improved physiochemical properties of the clinical candidate.[30,42,123] However, **19** demonstrating decreased oncoprotein levels and transcription at 10 μM highlights the potential of this ligand for further improvement in phenotypic activity, through either increased affinity or improved physiochemical properties. With the decreased levels of oncoproteins upon treatment with **19**, the cells are expected to decrease their growth rate, which is the expected overall phenotypic effect of CBP^{BRD} inhibition: decreased cell proliferation. [28,30,42,52,123,129] Assays to evaluate whether **19** can cause this overall phenotype are still ongoing at this time.

3.8 Conclusion

In this chapter, the biological evaluation of the macrolactam ligands (**14-19**) and their linear analogues (**39-41**) have been described. These ligands were first assayed using a competitive AlphaScreen® assay. However, it became rapidly apparent that the ligands interfered with the assay readout through singlet oxygen quenching. Therefore, ITC was used to evaluate ligand affinity to both the CBP^{BRD} and BRD4(1). The ITC data highlighted several compounds of interest which were further assayed using the BromoKdElect platform against the CBP^{BRD}, $p300^{BRD}$, BRD4(1) and BRD4(2). As evidenced by the data obtained, **19** demonstrated the most favourable affinity (K_d = 44.5 nM) and selectivity for the CBP^{BRD} (>455-fold over BRD4(1)) and therefore this ligand was further assessed across a panel of 32 BRDs in the BromoMax assay at 1 and 10 μM concentrations. At 1 μM **19** demonstrated no off-target BRD affinities, whilst at 10 μM affinity for 7 off-target BRDs was observed. Making **19** a highly selective CBP^{BRD} inhibitor. Through the structural studies conducted the novel X-ray co-crystal structures of small molecule macrocyclic ligands (**10** (PDB: 9GEY), **14** (PDB: 9GEU), and **19** PDB: 9GEJ)) bound to the CBP^{BRD} are displayed, along with the linear compound **40**. The co-crystal structures of the

macrolactams bound to the CBP^{BRD} are the first crystal structures of small molecule macrocycles bound to the CBP^{BRD} published. The structural information elucidated from the co-crystal structure emphasised that ligand **19** demonstrated the desired, curled-up conformation, which is likely the cause of the superior selectivity of this ligand relative to the other macrolactams characterised. The conformation adopted by **19** is similar to the shape of its linear analogue **40**. However, **40** lacks the constraint of macrolactamisation, lacking selectivity for CBP^{BRD} over BRD4(1) (by ITC) in contrast to the exquisite selectivity showed by **19**. When tested in an acute myeloid leukaemia cell line (OCI-AML3 cells), previously highlighted in the literature, **19** (at 10 μM) caused decreased levels of oncoproteins (*c*-MYC, MYB and BCL-2) and their transcription (by Western blotting and qPCR), which is the desired phenotype of CBP^{BRD} inhibition in cells.[30,123] Making **19** the first high affinity, selective macrocyclic ligand for the CBP^{BRD}, with potential for further improvement to the phenotypic effects, leading to a prospective hit compound.

Chapter 4:

Improving Cation-π Interactions

4.1 Introduction

With the lead compound, **19**, identified (Figure 42), further changes were sought to improve both binding affinity and physiochemical properties which would be beneficial *in vivo*. Modifications to the THQ (tetrahydroquinoline) within the macrolactam (Figure 42 highlighted in **purple**) presented an opportunity for improving affinity and physiochemical properties without compromising flexibility and overall molecular shape. The affinity can be improved by increasing the strength of the cation-π interaction, which can be achieved by augmenting the electron density of the aromatic ring within the THQ fragment. The physiochemistry of ligands **OXFBD05** and **19** can be improved by increasing the heteroatom count in the THQ to accept or donate hydrogen bonds, improving the solubility without compromising permeability.

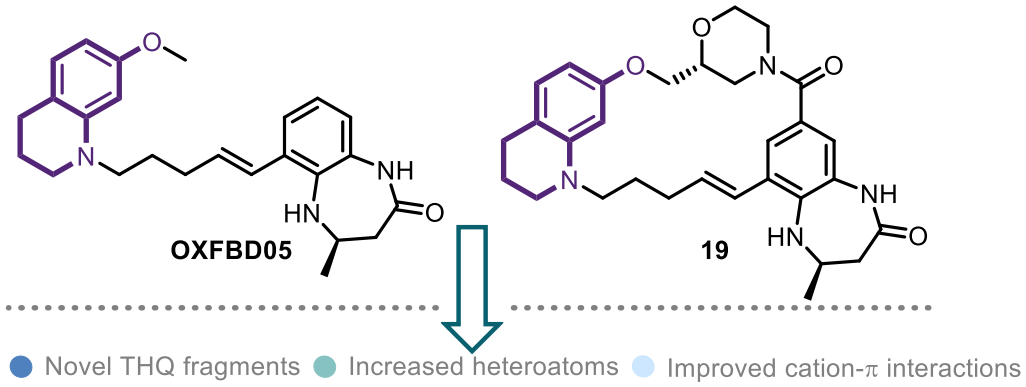

Figure 42: Ligand **19** and **OXFBD05** chemical structures with the THQ highlighted in purple, along with the goals of alterations in the scaffolds (bullet points) displayed below.

The main aim of these alterations is to increase the hydrogen bond acceptor character of the ligands and increasing the strength of the interactions between with Arg-1173. This approach of forming additional hydrogen bonding interactions has been applied in other CBP^{BRD} inhibitors such as in the lactam of **Inobrodib** (PDB: 7XH6).[110] Building these improvements to the THQ into macrolactam **19** would have proven a challenging process. Therefore, it was decided that the linear scaffold of **OXFBD05** could be used as a proxy to validate the alterations before incorporating into ligand **19**. The THQ

fragment of **OXFBD05** was altered through replacement of the methoxy moiety with a methyl sulfone and the THQ into a benzomorpholine (Figure 43 ligand **49** and **50**).

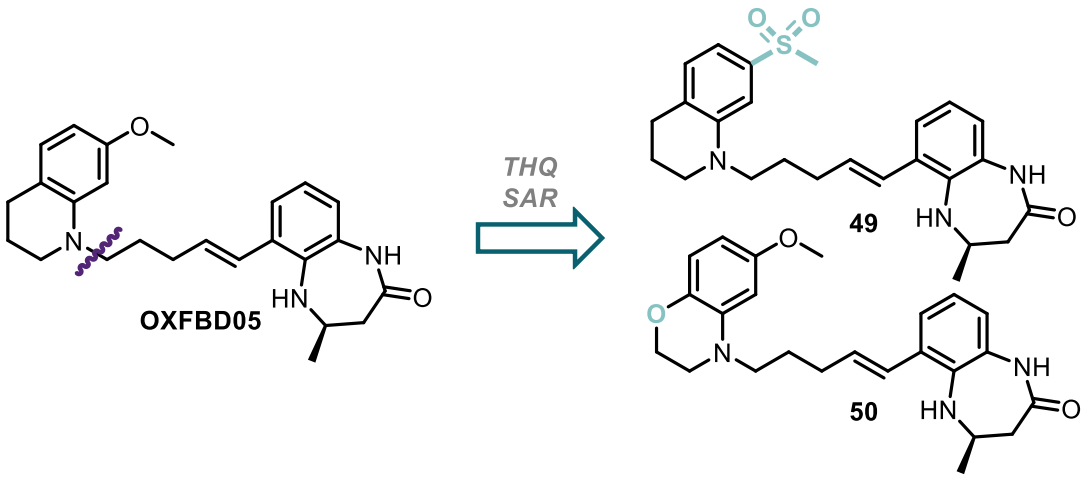

Figure 43: Target ligands containing THQ alterations to **OXFBD05** which include the conversion to a methyl sulfone (**49**) and a single atom transmutation to convert the THQ to a benzomorpholine (**50**).

The sulfone can act as a hydrogen bond acceptor to form increased interactions with the arginine whilst maintaining the cation-π interaction already present within the ligands. In the literature this type of hydrogen bonding interaction has been previously theorised to occur with aryl-sulphonamides when bound the CBP^{BRD}.[130] The benzomorpholine fragment aims to increase the electron density in the aromatic ring thus strengthening the cation-π interaction. The inclusion of an oxygen atom also improves the aqueous solubility of the ligand, through addition of another hydrogen bond acceptor. A 1.4-fold decrease in IC_{50} has been reported between ligand **51** and **52** when the THQ was replaced with a benzomorpholine (see Figure 44).[40]

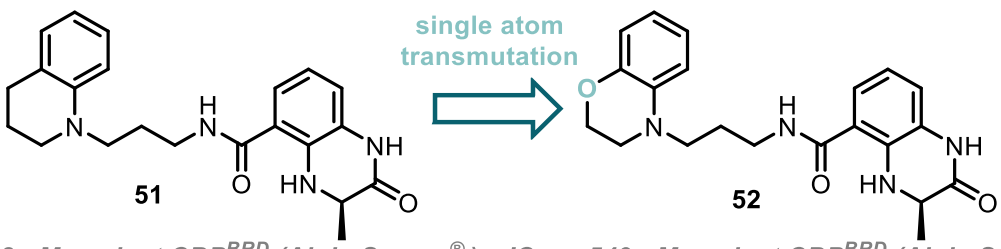

IC_{50} = 758 nM against CBP^{BRD} (AlphaScreen®) *IC_{50} = 549 nM against CBP^{BRD} (AlphaScreen®)*

Figure 44: A benzomorpholine bioisostere which demonstrates a decrease in IC_{50} compared to a THQ.[40]

4.2 Synthesis of Target Ligands **49** and **50**

Both **49** and **50** can be synthesised *via* a manner that mimics the synthesis of **OXFBD05** (see Figure 45). Both the sulfone THQ and benzomorpholine compounds (Figure 45 **FG1** and **FG2**) have been previously synthesised in the literature.[131,132]

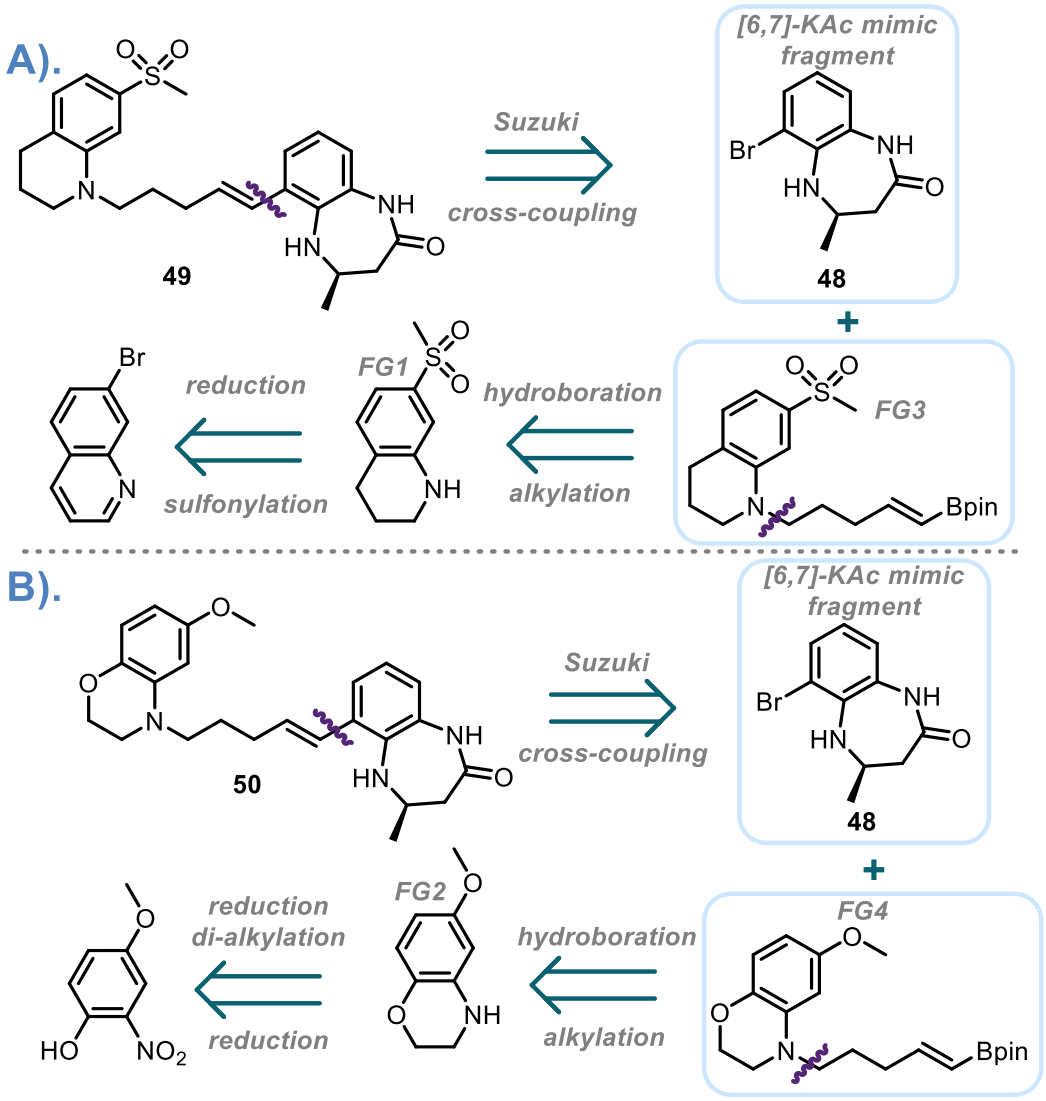

Figure 45: Retrosynthesis of target ligands and their respective starting fragments, A). The retrosynthetic strategy for compound **49** relying on a Suzuki coupling between **48** and **FG3**; B). The retrosynthetic strategy for compound **50** relying on a Suzuki coupling between **48** and **FG4**.

4.2.1 Synthesis of Ligand **49**

To form compound **51** a literature procedure which employed a copper(I) catalyst and sodium methyl-sulfinate was employed, giving **53** in 56% (Scheme 14).[132] Reduction

of **53** was reported in the same publication, using a Hantzsch ester (Scheme AA1) to form compound **54**.[132] However, this reduction did not lead to full conversion to **54** and proved difficult to purify. Alternatively, hydrogen borrowing reduction has been used on similar scaffolds in the literature.[133] Therefore the fused ring system of **53** was reduced to afford the THQ in **54** (**FG1** in Figure 45A) under these conditions (Scheme 14), with the IPA solvent acting as the source of hydrogen. This type of reduction had been performed on a similar quinoline scaffold in the literature.[133] This resulted in complete formation of **54** observed by TLC analysis. The secondary amine of **52** was alkylated with **28** in an S_N2 reaction, furnishing **55** in 58% yield. Compound **55** was subsequently hydroborylated using Swartz's reagent under the conditions previously described throughout this thesis to give the sulfone fragment **56** (**FG3** in Figure 45A) in 59% yield (Scheme 14).[44] Compound **56** was then combined with the previously compound **48** in a Suzuki-coupling to give ligand **49** in 35% yield in a total of 10 steps (Scheme 15).

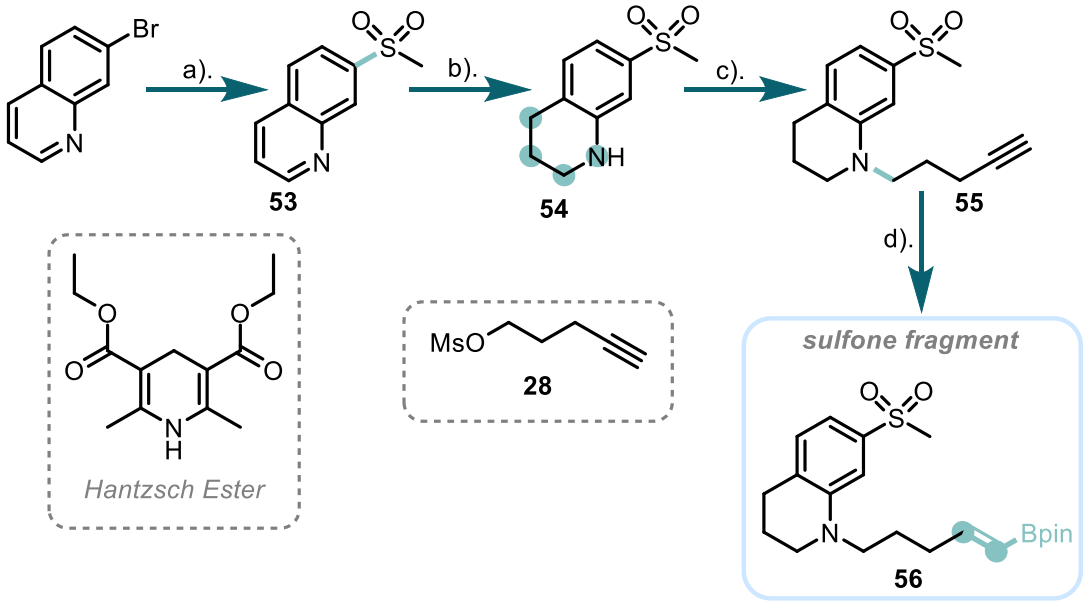

Scheme 14: Synthesis of sulfone fragment **56** and the Hantzsch ester used in the attempted reduction of **53** to **54** (grey dashed box). *Reagents and conditions:* a). Sodium methyl-sulfinate, $Cu^{(I)}$ triflate · tol complex, $(CH_3NHCH_2)_2$, DMSO, 120 °C, 4h, 56%; b). Pentamethylcyclopentadienyl iridium dichloride dimer, perchloric acid, IPA, H_2O, 100 °C, 48 h, 65%; c). Compound **28**, DIPEA, TBAI, DMF, 100 °C, 48 h, 58%; d). HBpin, Cp^*_2ZrClH, NEt_3, 60 °C, 18 h, dark, 59%.

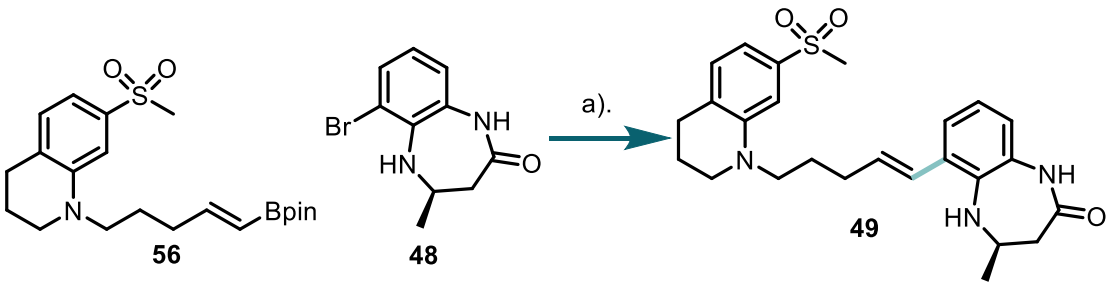

Scheme 15: Synthesis of ligand **49**. *Reagents and conditions:* a). $Pd(dppf)Cl_2$, K_2CO_3, 1,4-dioxane:H_2O (5:1 *v*/*v*), 100 °C, 24 h, 35%.

4.2.2 Synthesis of Ligand **50**

The readily available 4-methoxy-2-nitrophenol was used to access desired benzomorpholine fragment **FG2** (Figure 45B) through a series of reactions built upon literature precedent.[131] Initially, the 4-methoxy-2-nitrophenol starting material was reduced to the corresponding aniline **57** under a hydrogen atmosphere at 1 bar as described in the literature but required the reaction to be left for a day.[134,135] However, increasing the hydrogen pressure to ~4 bar, shortened the reaction time from 24 hours to 1 hour forging **57** in 91% yield. (Scheme 16A).[131] Compound **57** was then reacted with chloroacetyl chloride under basic conditions to afford **58** in 57% yield as light pink crystals (Scheme 16A).[131,135] Compound **58** was recrystallised from EtOAc and hexane to give the crystal structure shown (Scheme 16A in pink), that confirms the formation of the amide in **58**, as there were concerns that the ester was instead formed. The amide of **58** was reduced using $LiAlH_4$ to give the corresponding benzomorpholine ring of **59** in 79% yield (Scheme 16A).[131] The secondary amine of **59** was then alkylated with compound **28** in an S_N2 reaction, with 90% yield. The resulting compound **60** underwent hydroborylation of the terminal alkyne with Swartz's reagent to furnish **61** (**FG4** in Figure 16B) in 46% yield. With the benzomorpholine fragment **61** in hand, it was then coupled with compound **48** in a Suzuki-reaction to furnish ligand **50** in 61% yield, with **50** afforded in a 9-step synthesis (scheme 16B).

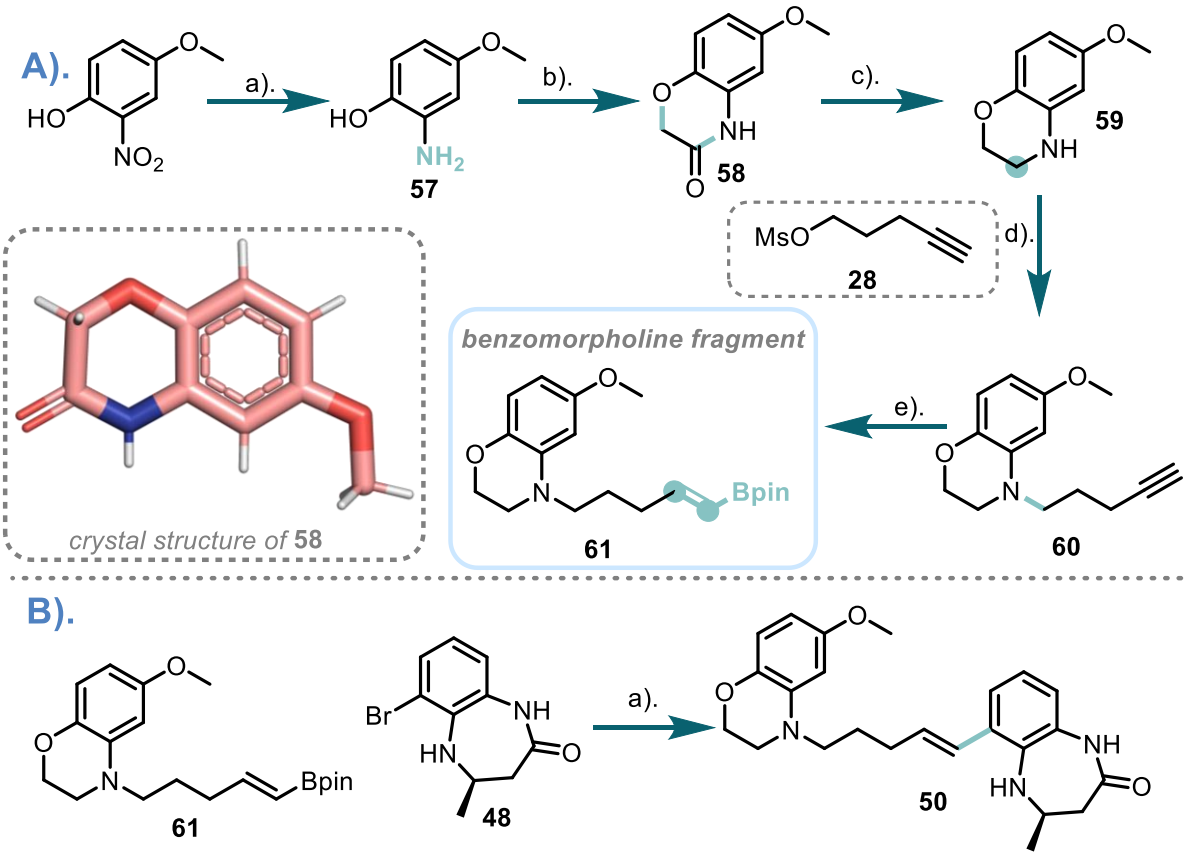

Scheme 16: A). Synthesis of benzomorpholine fragment **61** (**FG4**) and small molecule X-ray crystal structure of compound **58** (pink). *Reagents and conditions:* a). H_2 (4 bar), 10 wt% Pd/C, EtOH, r.t., 1h, 91%; b). Chloroacetyl chloride, K_2CO_3, MeCN, 80 °C, 5h, 57%; c). $LiAlH_4$, THF, 0 °C – r.t., 5h, 79%; d). Compound **28**, DIPEA, TBAI, DMF, 100 °C, 48h, 90%; e). HBpin, Cp^*_2ZrClH, NEt_3, 60 °C, 18 h, dark, 46%; B). Synthesis of ligand **50**. *Reagents and conditions:* a). $Pd(dppf)Cl_2$, K_2CO_3, 1,4-dioxane:H_2O (5:1 *v*/*v*), 100 °C, 24 h, 61%.

4.3 Biological Assessment of Ligands **49** and **50**

With the target compounds of **49** and **50** in hand, their binding affinities to the CBP^{BRD} and physiochemical properties were analysed. As previously discussed, (Chapter 3.3) the affinities of the ligands were analysed by ITC.

4.3.1 ITC Binding for Ligands **49** and **50** to the CBP^{BRD}

The binding affinity of **49** (K_d = 299 nM) is lower relative to **OXFBD05** (K_d = 132 nM), by approximately 2.3-fold for the CBP^{BRD} by ITC (Figure 46, see Appendix D Figure 23 for all ITC traces). Although, the N sites are now closer to one for **49**, indicating an improved stoichiometry between the ligand and the CBP^{BRD} (0.69 for **49** *vs* 2.66 for

OXFBD05). This likely means that the proximity of the sulfone to the cation-π interaction renders it unable to perform hydrogen bonding interactions with Arg-1173. Even though the affinity for the CBP^{BRD} decreased relative to **OXFBD05**, **49** could still possess improved physiochemical properties relative to **OXFBD05**.

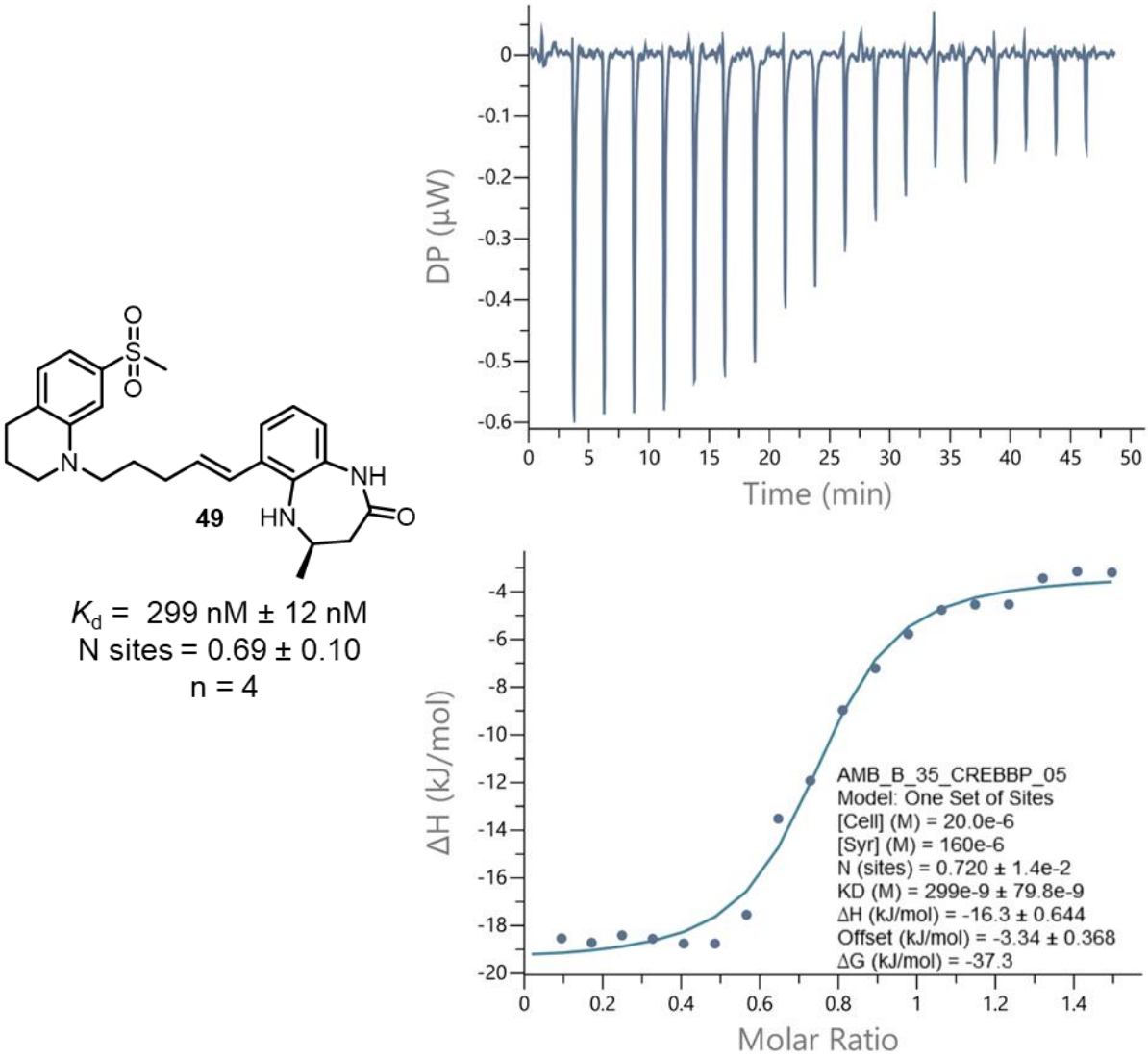

Figure 46: Example of an ITC trace between ligand **49** and the CBP^{BRD}, with the structure of ligand **49** and its binding affinity as an average along with the N sites from n = 4 technical repeats, see Appendix D for all traces.

The binding affinity of **50** (K_d = 89.6 nM) is improved relative to **OXFBD05** (K_d = 132 nM), representing an approximately 30% decrease in K_d for the CBP^{BRD} by ITC making it a 1.3-fold increase in affinity (Figure 47, see Appendix D Figure 24 for all ITC traces). The N sites of ligand **50** was also lower than **OXFBD05** (2.26 for **50** *vs*

2.66 for **OXFBD05**) meaning there is again improved stoichiometry for the novel ligand. Due to the lower K_d achieved, the bound state of **50** with the CBP^{BRD} was investigated by co-crystallography to probe the binding mode of this novel ligand.

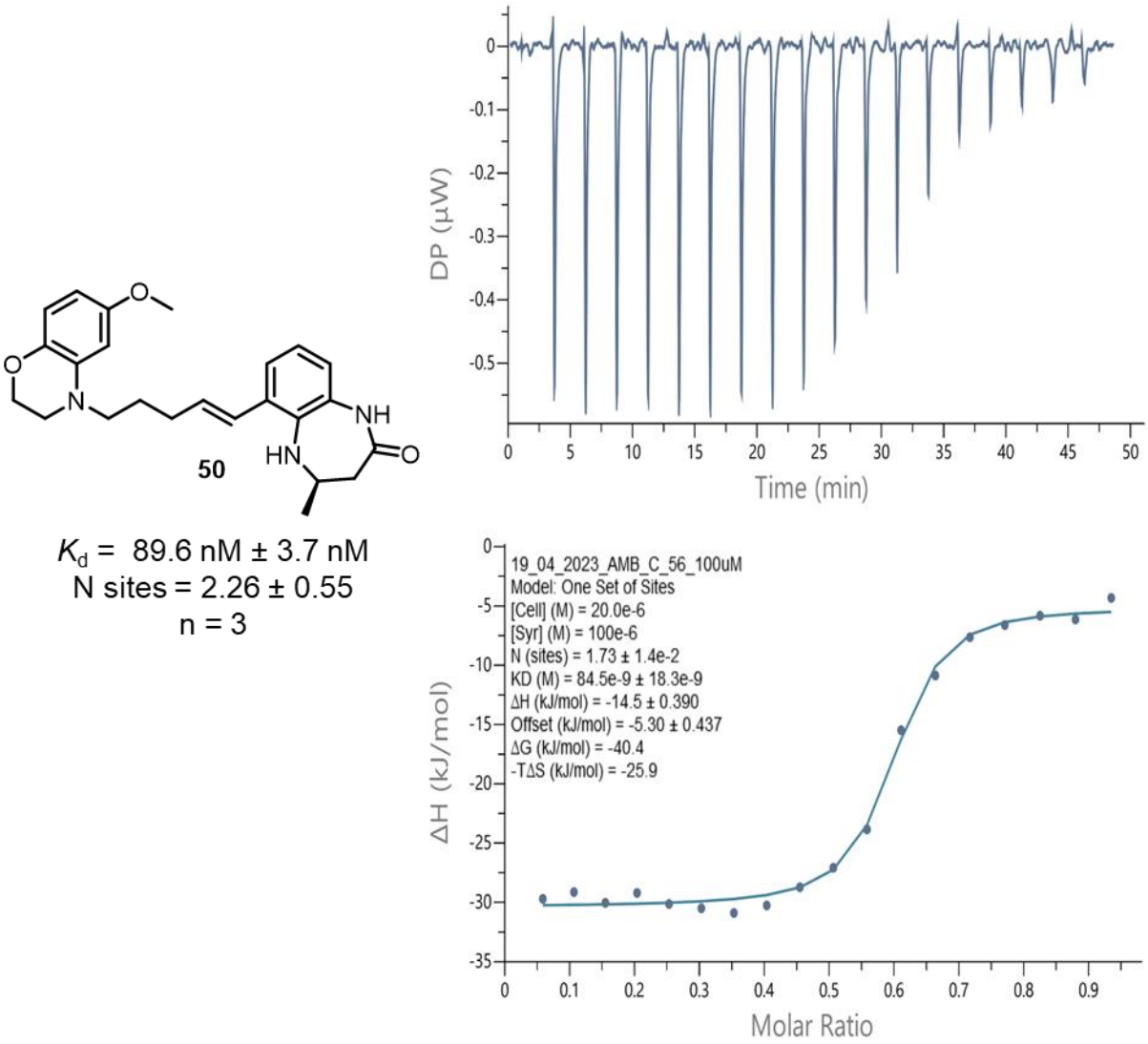

Figure 47: Example of an ITC trace between ligand **50** and the CBP^{BRD}, with the structure of ligand **50** and its binding affinity as an average along with the N sites from n = 3 technical repeats, see Appendix D for all traces.

This data highlights that there are further advances in SAR that can be performed on the **OXFBD05** scaffold with the opportunity for improved affinity and physiochemistry. According to thermodynamic and computational calculations, in order to further increase the strength of the cation-π interaction, the oxygen of the benzomorpholine can be replaced with an alkylated nitrogen.[136,137]

4.3.2 Co-crystal structure of the CBP^{BRD} and **50**

The crystal structures presented in this section were grown and solved by Marius Amman (University of Freiburg). The crystal structure of **50** in the KAc binding site of the CBP^{BRD} is displayed (Figure 48 and 49), notably lacking the crystallographic artifacts within the **OXFBD05** co-crystal structure with the CBP^{BRD} (PDB: 6YIJ).[44]

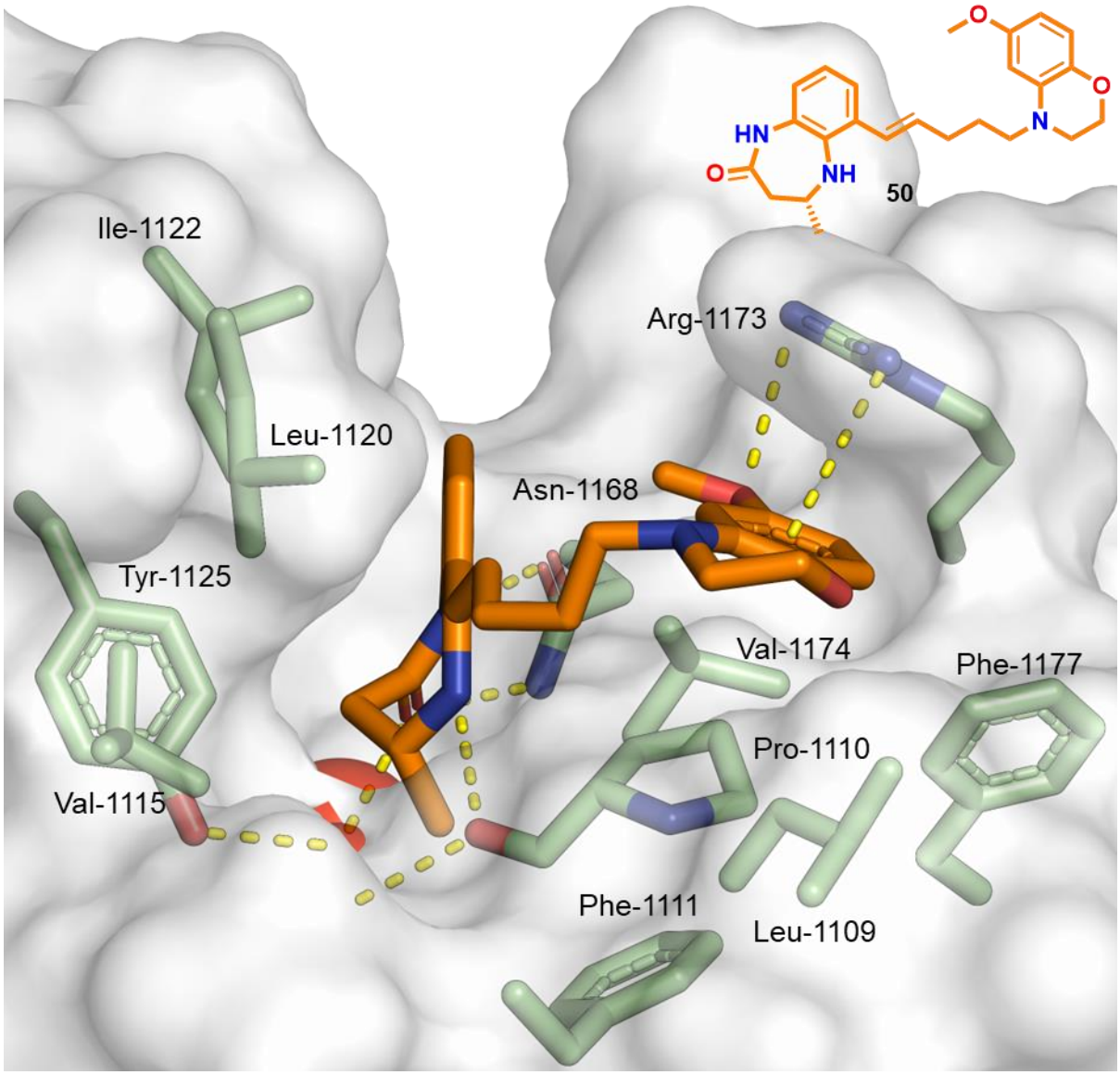

Figure 48: X-ray co-crystal structure of ligand **50** (orange) in complex with the CBP^{BRD} (PDB: 9GEW) at 1.47 Å resolution, viewed from the side of the binding pocket along the ZA channel with the water molecules occupying the channel removed for clarity. All residues which the ligand interacts with are displayed (green) with labels and the backbone amide removed for clarity unless otherwise involved in hydrogen bonding and the cation-π interaction along with hydrogen bonding interactions to the ligand highlighted by the dashed (yellow) lines, and with the chemical structure of **50** shown in the top right.

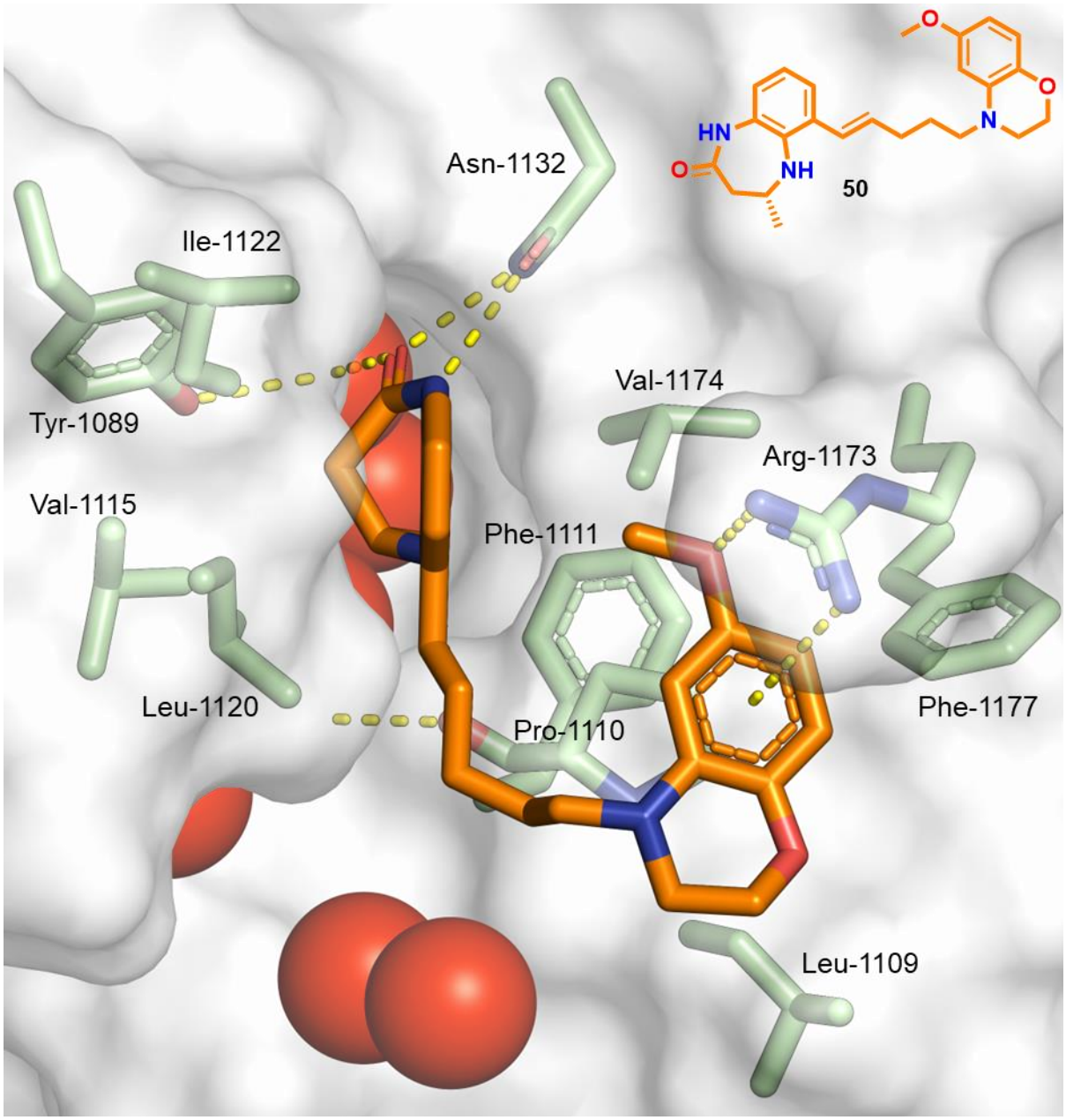

Figure 49: X-ray co-crystal structure of ligand **50** (orange) in complex with the CBP^{BRD} (PDB: 9GEW) at 1.47 Å resolution, viewed from above the binding pocket showing the LPF shelf and arginine, all residues which the ligand interacts with are displayed (green) with labels and the backbone amide removed for clarity unless otherwise involved in hydrogen bonding and the cation-π interaction along with hydrogen bonding interactions to the ligand highlighted by the dashed (yellow) lines, and with the chemical structure of **50** shown in the top right.

The incorporation of the benzomorpholine into **50** is well tolerated because the same binding mode is displayed as ligands **1** (PDB: 4NYX), **6** (PDB: 6YIM), and **40** (PDB: 9GET), with the desired curled-up conformation when bound to the CBP^{BRD} with the induced fit pocket on the LPF shelf (Figure 48 and 49).[44] The ligand **50** forms three key hydrogen bonding interactions within the KAc binding pocket; two with Asn-1132

through the amide of the seven membered ring and a water mediated interaction with Tyr-1089 through the carbonyl of the amide (Figure 48 and 49 shown by the yellow dashed lines). Another interaction highlighted in the crystal structure of a hydrogen bond between the backbone amide of Pro-1110 and the aniline nitrogen of the seven-membered ring. The KAc mimic forms the expected hydrophobic interactions with residues: Phe-1111, Val-1115, Ile-1122, and Val-1174 as displayed. The alkyl chain, connecting the [6,7]-KAc mimic and the benzomorpholine, forms hydrophobic interaction along the ZA channel with Leu-1120 and Pro-1110 (Figure 48 and 49). The benzomorpholine causes the formation of the induced fit pocket displayed by ligands such as **1**, **6**, and **40** as well as many other CBP^{BRD} inhibitors.[40,52,110,124] Hence **50** forms hydrophobic interactions on the LPF shelf as well as the cation-π interaction with Arg-1173 along with a dipole interaction between the oxygen atom of the aryl methoxy and Arg-1173 (highlighted by dashed yellow lines). All of the interactions demonstrated in the co-crystal structure of **50** and the CBP^{BRD} are expected, and no new interactions could be identified with ligand **50** which would explain the improved binding affinity compared to **OXFBD05**. This suggests that the increase in affinity indeed arises from stronger cation-π interactions between the benzomorpholine ring and Arg-1173. With this knowledge now in hand the ligands **49** and **50** were evaluated for their respective physiochemical properties.

4.3.3 Physiochemical Properties of Ligand **49** and **50**

The physiochemical properties were again submitted to GSKs ADME assays for ligands **49** and **50** for a comparison to **OXFBD05**, with the data presented below (Table AA1).[138–140]

Table 11: Physiochemical properties of ligands **49**, **50** and **OXFBD05** for comparison, with the assays carried out using the in-house methods of GSK for physchem characterisation.

Compound number	Average solubility (μM)	Chrom $logD_{7.4}$	Artificial Membrane permeability (cm s^{-1})	Polarity (total polar surface area) ($Å^2$)	HSA percentage binding (%)	BRD4(1) TR-FRET IC_{50} (μM)
OXFBD05	26	6.89	1.81×10^{-5}	53.6	97.6	6.31
49	56	5.27	8.49×10^{-5}	78.5	99.0	4.47
50	-	5.59	6.46×10^{-5}	62.8	95.4	-

These data indicate that both ligands **49** and **50** are more polar than **OXFBD05** as the polar surface areas have increased (78.5 and 62.8 compared to 53.6 $Å^2$, respectively) Compounds **49** and **50** both exhibit a decrease in Chrom $logD_{7.4}$ relative to **OXFBD05** (5.27 and 5.59 compared to 6.89 respectively), giving both ligands an SFI below 8 giving both improved properties compared to the SFI of 8.89 of **OXFB05**. Interestingly **49** and **50** both have increased polarity and membrane permeability compared to **OXFBD05**. The aqueous solubility of **OXFBD05** in phosphate buffer is highlighted by a low average aqueous solubility (26 μM), this demonstrates why the prior ITC experiments (see Chapter 3.2.1) required half of the concentration (20 μM) compared to the original literature conditions (40 μM).[44,88] This illustrates the poor solubility of the positive control, which ligand **49** improves on by more than 2-fold (56 μM aqueous solubility in phosphate buffer). This implies that both ligand **49** and **50** has improved physiochemical properties when compared to **OXFBD05**.

4.4 Conclusion

These data indicate that both ligands **49** and **50** possess improvements in physiochemical properties relative to **OXFBD05**. With compound **50** affording an increase in affinity (K_d decrease of 30 nM relative to **OXFBD05**) for the CBP^{BRD} by ITC, mediated by the increased strength of the cation-π interaction. The benzomorpholine of **50** also grants improved physiochemical properties relative to **OXFBD05**. In conclusion therefore, the benzomorpholine could be incorporated into macrocyclic ligands such as **19**, in order to improve both their affinities and physiochemical properties, which could lead to greater phenotypic effect in cells. The work in this chapter also highlights there is freedom within the scaffold in the THQ for scaffold modification to be accommodated which can grant the same binding mode whilst improving affinity.

Chapter 5:

Synthesis and biophysical evaluation of [6,6]-KAc mimic containing alkyl macrocycle

5.1. Introduction

Previous *in silico* studies performed by Dr. Mustafa Moroglu (Conway group, 2019) indicated that an alkyl-linked macrocycle ligand (Figure 50A, compound **7**) would bind with high affinity to the CBP^{BRD}.[88] However, upon its synthesis and evaluation by ITC, no detectable binding occurred (Figure 50B).[88] One hypothesis is that the seven membered ring could be perturbing binding. In order to investigate this potential The substitution of the previously utilised [6,7]-KAc mimetic with a [6,6]-fused system, which is recognised by BRDs (as shown in ligand **1**), was incorporated into a novel macrocyclic (compound **62**). This bioisostere replacement was theorised to have the ability to rescue binding if the seven membered ring of the KAc mimic was the cause of the previously synthesised ligand **7** showing not binding to the CBP^{BRD} by ITC.

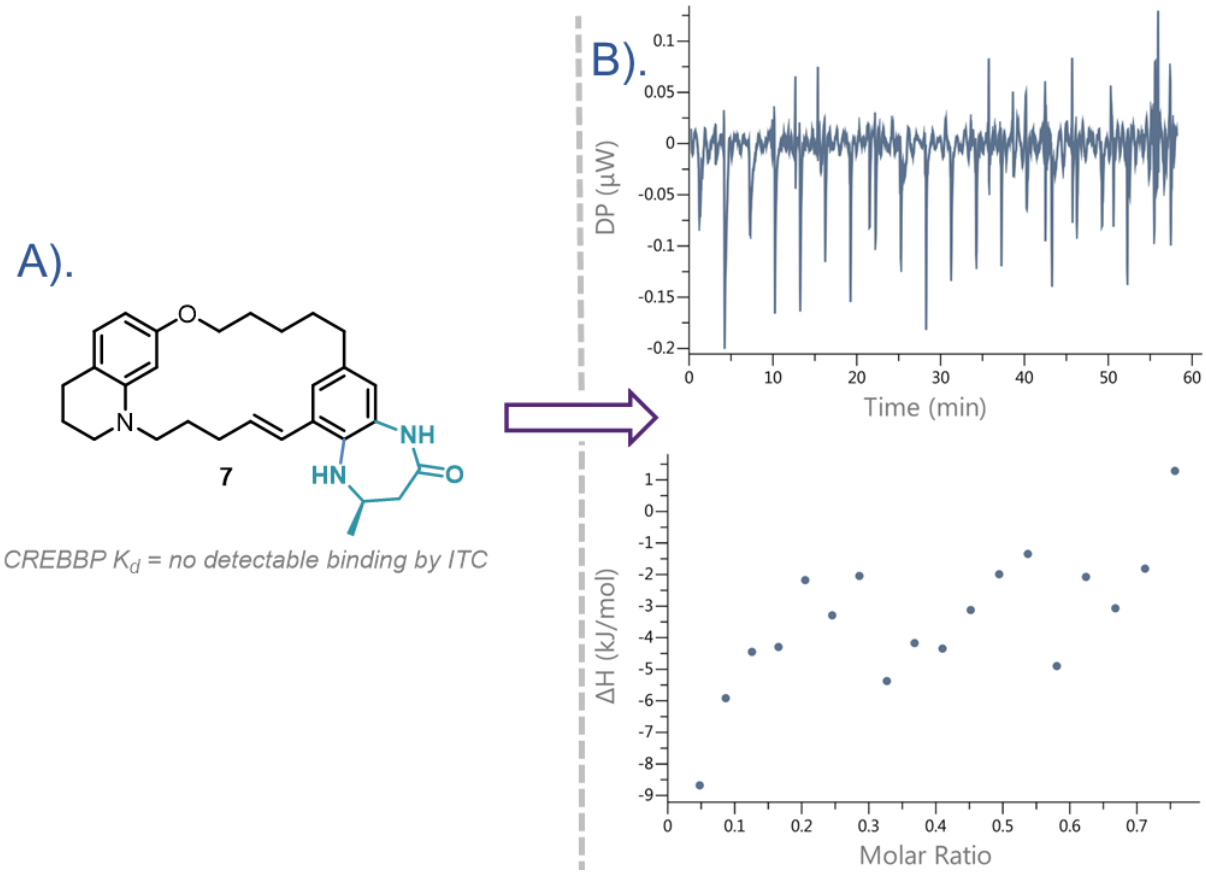

Figure 50: A). Chemical structure of the previously synthesised alkyl macrocycle **7**; B). A representative ITC trace of a binding from compound **7** and the CBP^{BRD}.

To investigate the seven membered ring as the source of no detectable binding to the CBP^{BRD}, a macrocycle containing a [6,6]-KAc mimic (compound **62** with the KAc mimic highlighted in light blue in Figure 51) was synthesised as opposed to the [6,7]-chemotype (highlighted in cyan in Figure 50A and 51) previously utilised.

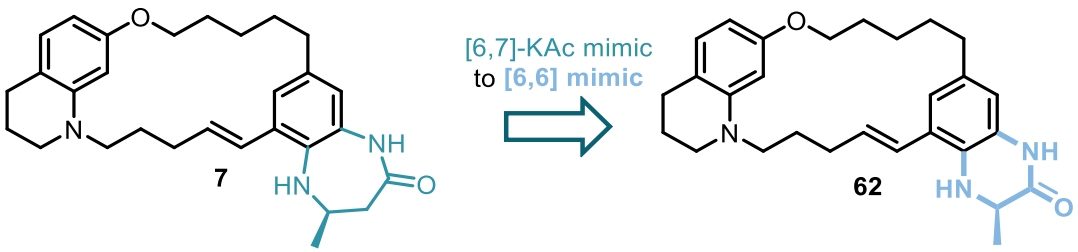

Figure 51: Previously synthesised alkyl macrocycle **7** and the novel target [6,6]-KAc mimic comprising of the alkyl macrocycle target ligand **62**, with the alternative KAc mimic highlighted in **bold light blue bonds**.

Synthesis of **62** would also allow for investigation into alternative macrocyclisation strategies centred around different chemistries, providing an opportunity to compare methods of closing the macrocyclic ring. As alkyl chains can be created in a multitude of manners, the proposed macrocycle can be synthesised *via* alternative macrocyclisation reactions (as shown in Figure 52).

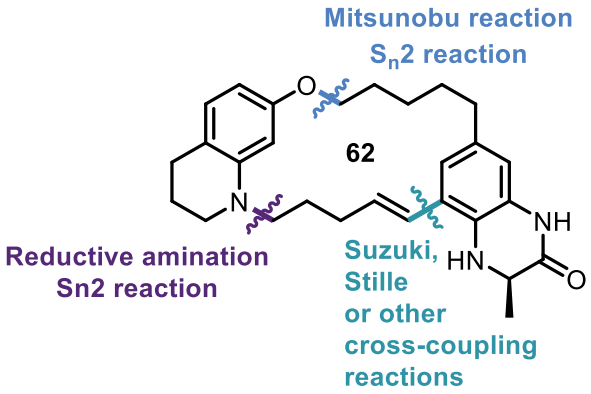

Figure 52: The potential macrocyclisation reactions which could yield the 18-membered ring of the compound **62**.

Both a Mitsunobu and S_N2 strategy would require the late-stage formation of a phenolic ether, which could prove challenging due to the flexibility of the substrate.

Macrocyclisation via reductive amination could prove a chemoselectivity issue. The cross-coupling based macrocyclisation strategy would require late-stage installation of a transmetalating functional group, providing another challenge in chemoselectivity.

5.2. Synthesis of Alkyl Macrocycle *via* S_N2 reaction Macrocyclisation

The section below covers the work undertaken to close the [6,6]-alkyl macrocycle via an S_N2 reaction, as previously described in the synthesis of the [6,7]-KAc mimic-containing macrocycle.[88]

5.2.1. Retrosynthesis

The retrosynthesis described below is based upon the synthesis of the [6,7]-alkyl macrocycle **7** previously reported by Dr Mustafa Moroglu (Conway group, 2019), which focused on a late-stage phenolic ether formation macrocyclisation strategy (Figure 53).[88]

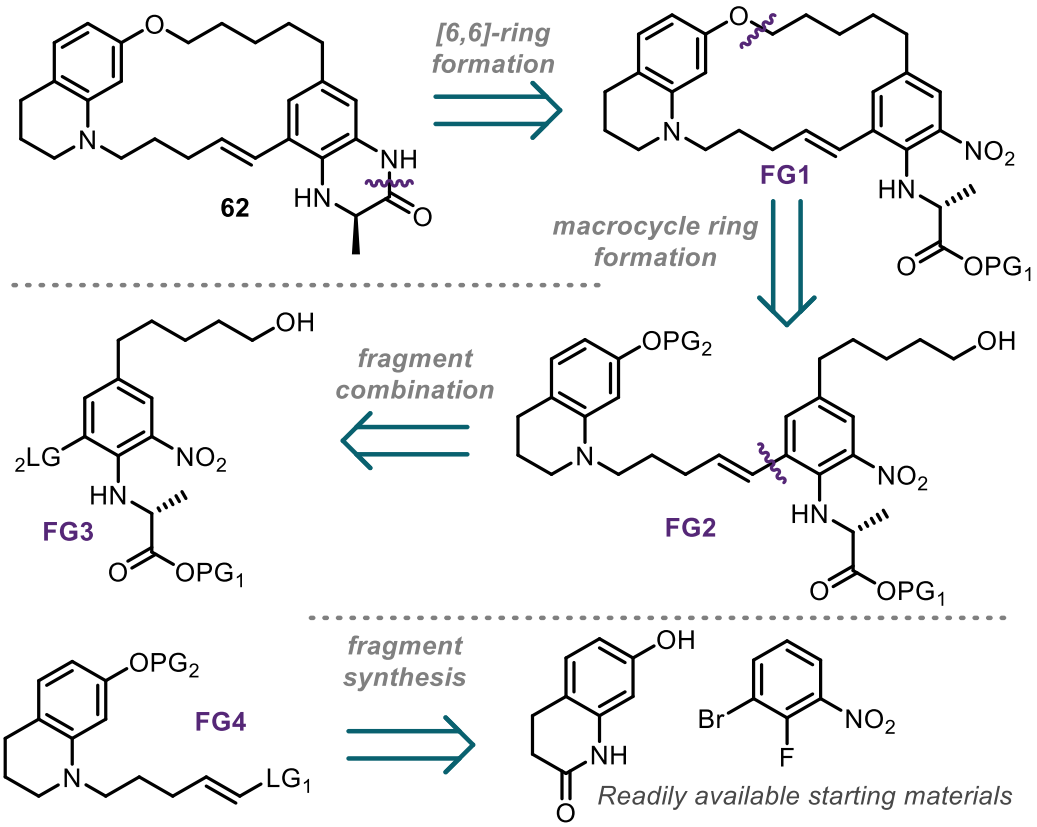

Figure 53: Retrosynthetic analysis of a nucleophilic substitution-reaction based macrocyclisation strategy to garner the desired product **62**, through late-stage etherification.

If macrocyclisation is mediated by a substitution reaction, the same fragment used for the tetrahydroquinoline (THQ) installation in the original alkyl macrocycle could be employed in the synthesis of the THQ fragment and utilised in Chapter 2 in the synthesis of the macrolactams (Figure 54A, compound **30**).[88] Doing so allowed for the reactions previously developed in the synthesis of ligand **7** to be utilised, which eliminated the need for lengthy optimisation. It also means that the **FG3** and **FG4** (Figure 53) could be readily combined *via* a Suzuki cross–coupling. The (*R*)-stereogenic centre of compound **62** is essential for binding to the CBP^{BRD}, as inversion of the stereocenter has been shown to cause a 9-fold decrease in binding affinity within a similar system (see Figure 54C, compound **67** and **68**).[40,44] Therefore to prevent racemisation the KAc mimic is only formed in the final step in the synthesis (**FG1** (see Figure 54B). It is also essential to protect the carboxylic acid as an ester to

prevent undesirable interference with the reactions taking place. By protecting the carboxylic acid, the stereochemistry is maintained during the synthesis when harsh conditions are utilised which could cause a compound such as **64** to convert to **66** (such as basic or oxidising conditions, see Figure 54B). The aniline nitrogen on compound **62** also poses a risk of racemisation due to their electron-rich nature readily undergo oxidation.[88] As outlined in the previously reported synthesis of ligands **67** and **68**, a methyl ester was used as the protecting group for the carboxylic acid, hence this is the protecting group used **FG3** to give compound **63** (see Figure 54A).[40]

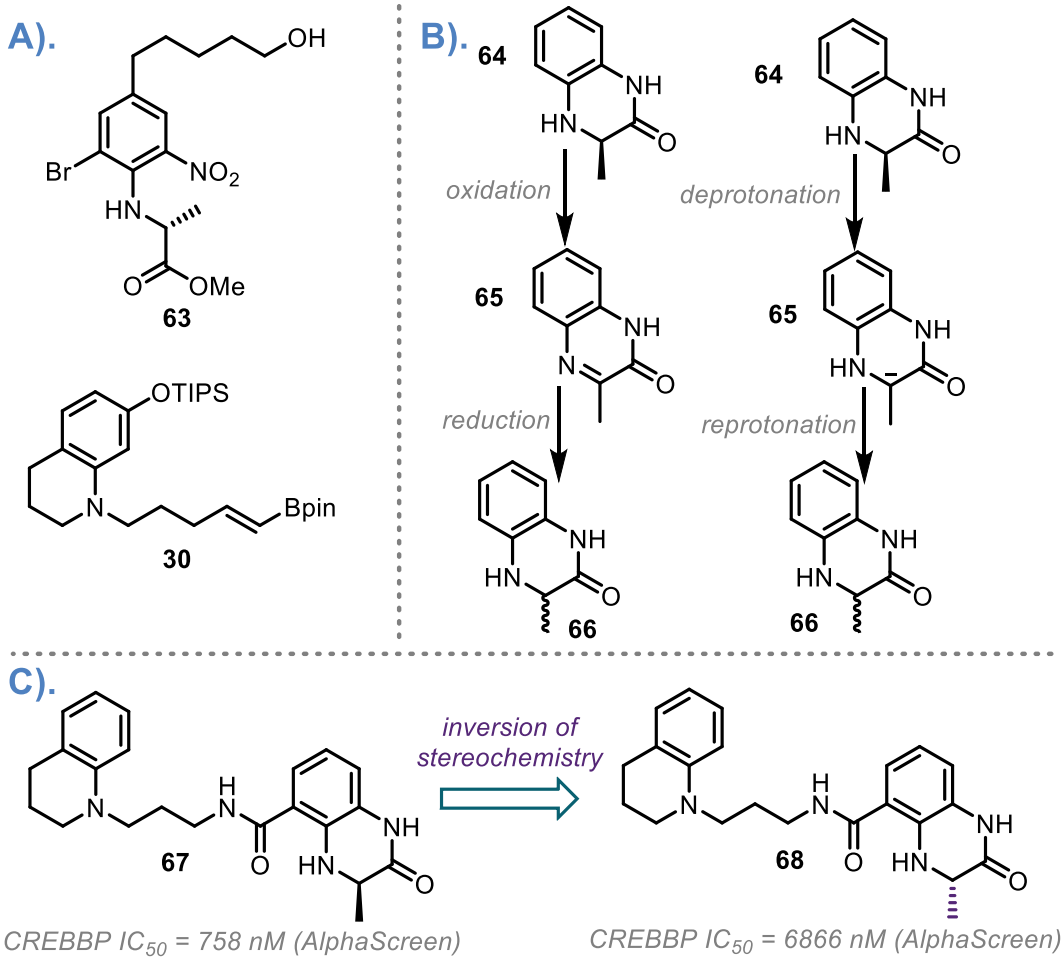

Figure 54: A). Target fragments **63** and **30** to be combined in a Suzuki reaction during the synthesis of the alkyl macrocycle **62**, B). Potential mechanisms for stereocenter racemisation from **64** to **66**, C). An example of stereochemical inversion between **67** and **68** and the resulting decrease in binding affinity observed to the CBP^{BRD}.[40]

5.2.2. Ligand Synthesis Utilising a Methyl Ester Protecting Group Strategy

The THQ containing fragment **30** was synthesised in a similar manner to that previously reported (see Scheme 2 in Chapter 2).[88] The KAc fragment compound **63** (Figure 54A) was then synthesised (see Scheme 17). 1-Bromo-2-fluoro-3-nitrobenzene was first mono-iodinated to give **69**, which then underwent an S_NAr to give **70**, a Sonogashira-coupling was performed to afford **71** which was reduced to give fragment **63**.

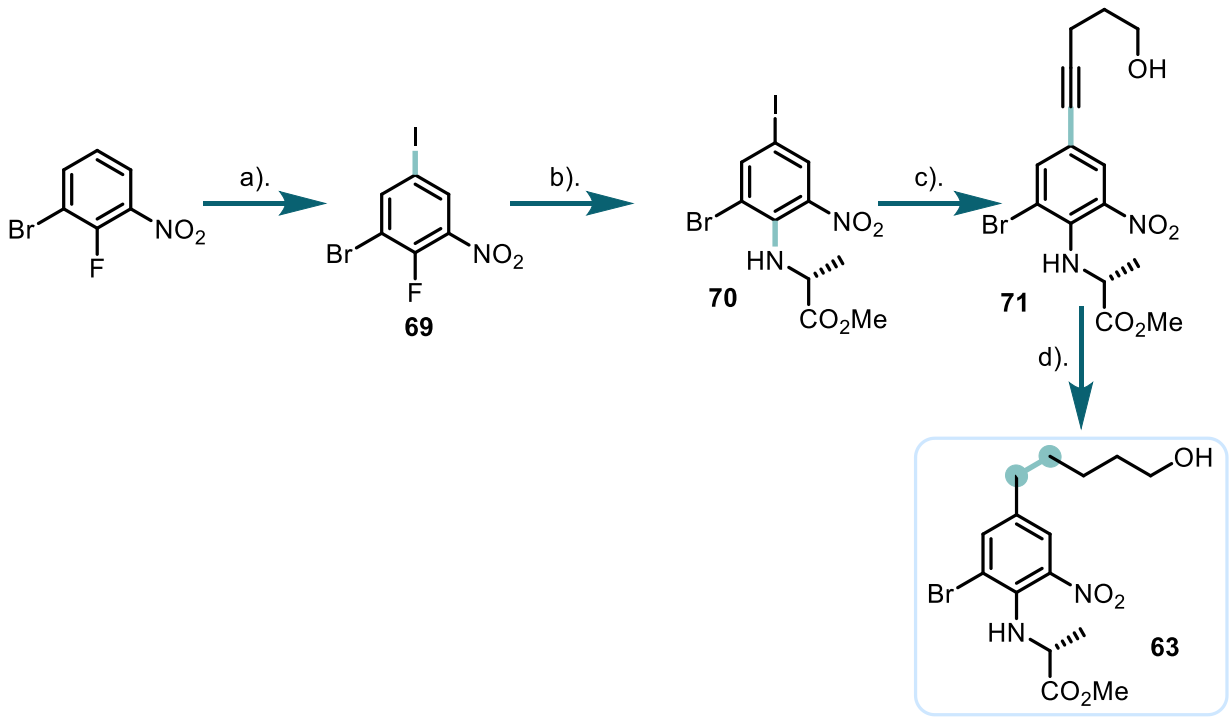

Scheme 17: Synthesis of fragment **63** primed for [6,6]-KAc mimic formation. *Reagents and conditions*: a). *N*-Iodosuccinamide, conc. $H_2SO_{4(aq)}$, r.t., 24 h, 84%; b). D-alanine methyl ester hydrochloride, Cs_2CO_3, tol, 85 °C, 24 h, 62%; c). 4-Pentyl-1-ol, $Pd(PPh_3)_2Cl_2$, CuI, THF/NEt_3 (9:1), r.t., 18 h, 98%; d). H_2, $Rh(PPh_3)_3Cl$, tol, 60 °C, 24 h, 99%.

N-Iodosuccinimide was chosen to selectively mono-iodinate 1-bromo-2-fluoro-3-nitrobenzene to furnish compound **69**, it had previously been reported that when I_2 was employed the di-iodinated product was formed.[88] The S_NAr reaction with compound **69** and Sonogashira cross-coupling with **70** proceeded smoothly to afford

71. The chemoselective reduction of the alkyne, using Wilkinson's catalyst, gave a yield of 99%, thus fragment **63** was garnered.

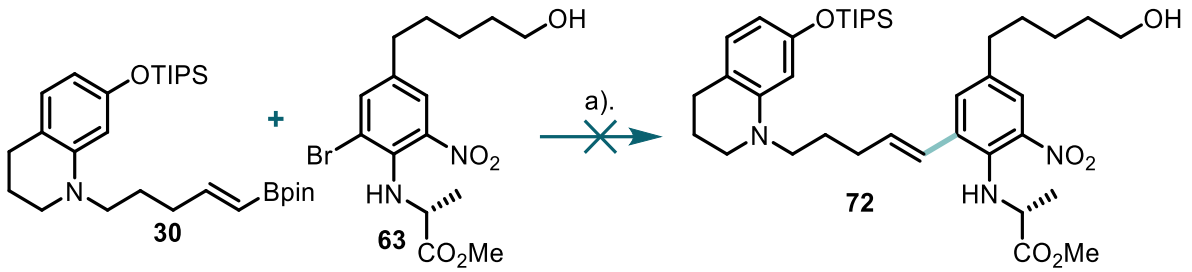

Scheme 18: Attempted suzuki-Miyaura cross-coupling between fragments **30** and **63**. *Reagents and conditions*: a). $Pd(PPh_3)_2Cl_2$, K_2CO_3, 1,4-dioxane:H_2O (4:1), 100 °C, 24 h.

Formation of product **72** was not observed when **30** and **63** were subjected to the Suzuki cross-coupling conditions (Scheme 18). The methyl ester was hypothesised to be deprotected during this reaction, affording no detectable product, as this protecting group is known to cleave under prolonged high temperatures and under aqueous basic conditions, such as K_2CO_3.[141] However, undesired formation of the carboxylic acid that would have subsequently formed was not isolated, presumably due to its high polarity.

5.2.3 *tert*-Butyl ester Protecting Group Strategy

As a result of the lability of the methyl ester under Suzuki coupling reaction conditions, the *tert*-butyl ester was therefore explored as an alternative carboxylic acid protecting group, as this was expected to be more stable under the Suzuki coupling reaction conditions.[141] A fragment containing the *tert*-butyl ester (compound **75**, Figure 54A) was synthesised. using the same steps as compound **63** with one minor alteration. For both the Suzuki and Sonogashira cross–couplings, the catalyst was changed to $Pd(dppf)Cl_2$ to avoid the potential impurities of residual triphenyl phosphine and triphenyl phosphine oxide (Scheme 19). Both impurities can be difficult to remove, as they form favourable interactions with lipophilic compounds.[142–144] Adopting the *tert*-butyl ester as a protecting group proved successful, as the desired Suzuki coupled

intermediate **76** was formed and isolated (Scheme 19). This indicated that the methyl ester protecting group was the cause of the lack of product **72**, as the change in catalyst was only for purification purposes.

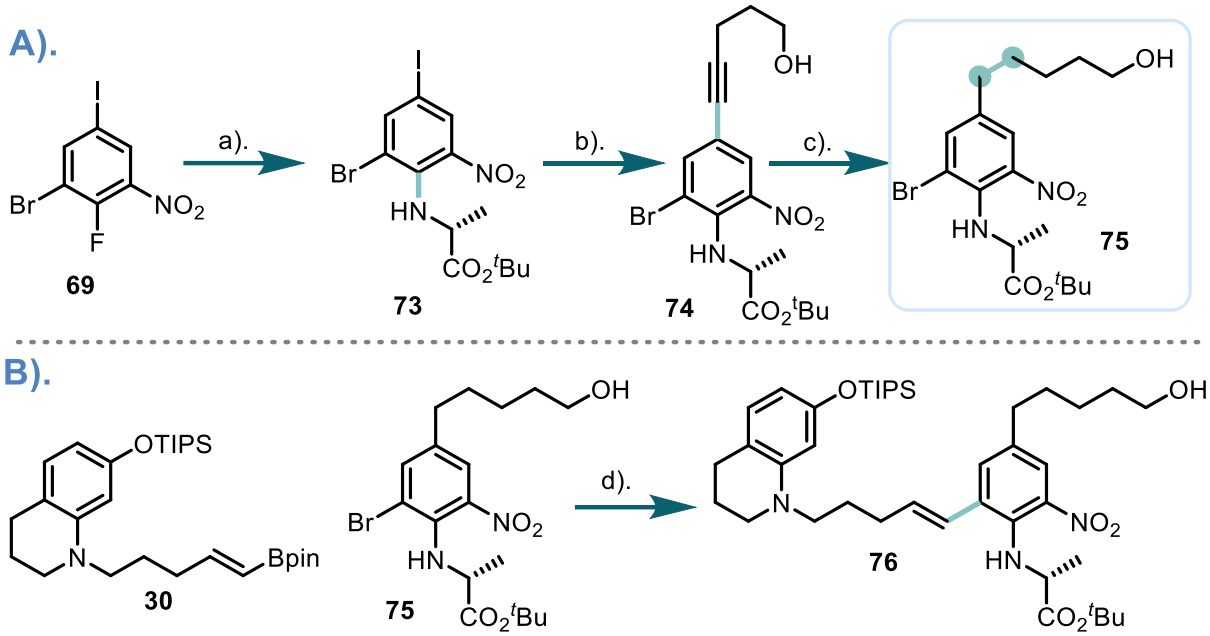

Scheme 19: A). Synthesis of *tert*-butyl protected fragment. *Reagents and conditions:* a). D-Alanine *tert*-butyl ester hydrochloride, Cs_2CO_3, toluene, 85 °C, 18 h, 91%; b). 4-Pentyn-1-ol, $Pd(dppf)Cl_2$, NEt_3, THF, r.t., 18 h, 93%; c). $H_{2(g)}$, $Rh(PPh_3)_3Cl$, toluene, 60 °C, 24 h, 86%; B). Synthesis of Suzuki cross-coupled intermediate **76**. *Reagents and conditions:* d). $Pd(dppf)Cl_2$, K_2CO_3, 1,4-dioxane:H_2O (5:1), 100 °C, 24 h, 72%.

With the Suzuki coupled intermediate **76** in hand, the TIPS group was selectivity removed using TBAF, giving the corresponding diol **77** (Scheme 20). Compound **77** was then subjected to mesylation conditions, followed by an S_N2 reaction (Scheme 20). However, this did not garner the desired macrocyclic product **78**. Even upon increased equivalents of base up to 5 equiv, and longer reaction times of up to 24 hours the S_N2 had no observable formation of **78** was observed at a concentration of 2 mM, thus this approach was abandoned.

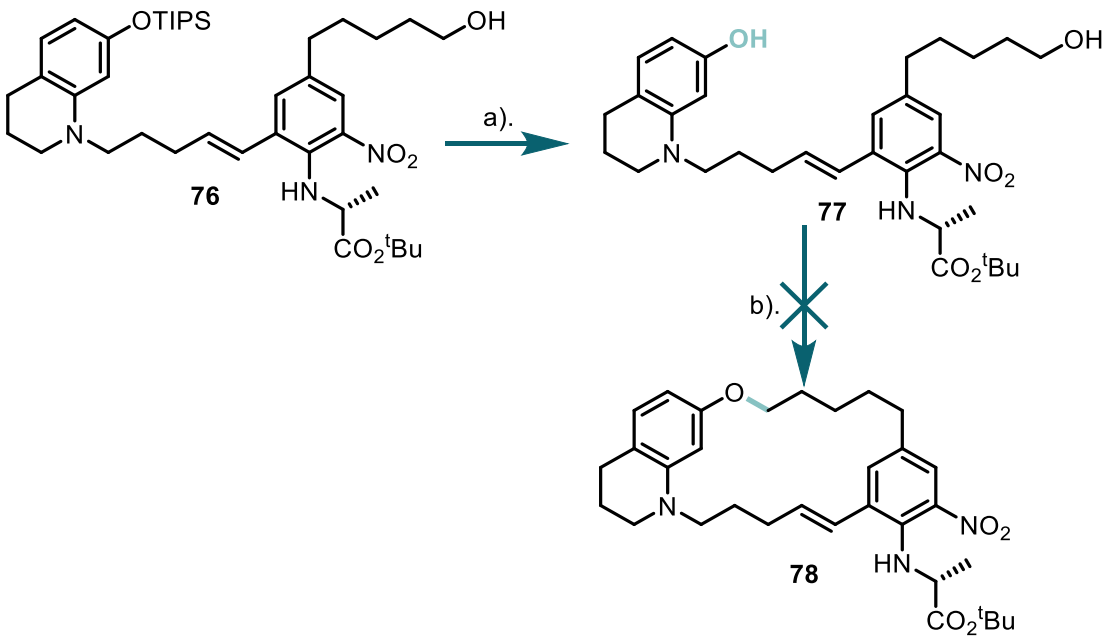

Scheme 20: Attempted synthesis of the macrocyclic ring *via* an S_N2 reaction to give **78**. *Reagents and conditions:* a). 1 M TBAF (in THF), THF, r.t., 1 h, 92%; b). MsCl, pyridine, r.t., 3 h, followed by, Cs_2CO_3, DMF (0.002 M), 80 °C, 5 h.

The lack of product **78** formation could be perpetrated by a number of factors: the phenolic oxygen could be undergoing mesylation as opposed to the desired primary alcohol; unproductive dimesylation of the diol intermediate could occur; and the highly flexible nature of the two alkyl chains contained within the **77**. The flexible nature of the macrocycle could mean that in solution it is difficult for the mesylate and phenol to react as it is entropically disfavoured. The presence of a competing nucleophile in the aniline nitrogen also presenting a potential problem. Due to these potential pitfalls, an alternative macrocyclisation reaction was sought.

5.3 Synthesis of Alkyl Macrocycle *via* Mitsunobu reaction Macrocyclisation

The Mitsunobu reaction was explored as an alternative to the S_N2-mediated macrocyclisation to form **78**, as this reaction has been applied several times previously to afford macrocyclic products in the literature.[63,145,146] The planned alteration to the

synthetic route would also enable the use of existing intermediate, and the planned ether bond formation would still be the macrocyclisation step.

It was hypothesised that the previous S_N2 macrocyclisation proved ineffective due to the increased flexibility of the pre-macrocyclisation intermediate without the [6,6]-fused ring formed. Thus, upon attempting to utilise a Mitsunobu reaction, the [6,6]-ring system was first formed, and then the macrocyclisation *via* Mitsunobu reaction was attempted.

5.3.1 Synthesis of Pre-macrocyclisation Intermediate

Utilising the previous routes to the Suzuki cross-coupled intermediate **76** (Scheme 19), the *tert*-butyl ester was deprotected and the six-membered ring closed. The formation of the [6,6]-fused ring proceeded with the nitro reduction performed under mild conditions (Zn powder, NH_4Cl, DMF, r.t.) followed by spontaneous amide bond formation to give the [6,6]-fused KAc mimetic ring system in compound **79** (Scheme 21).[147]

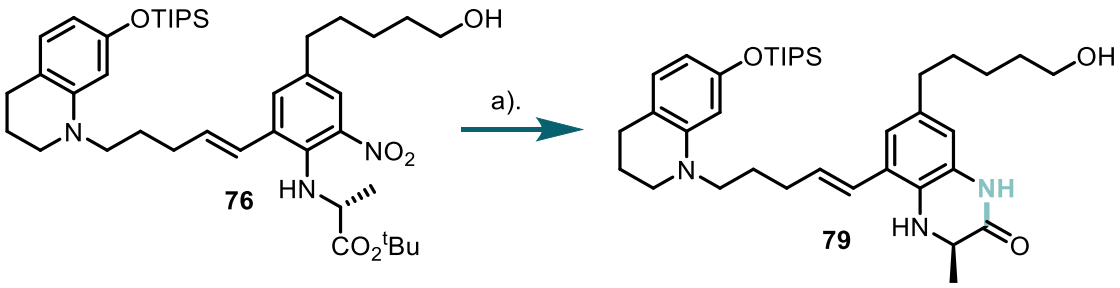

Scheme 21: Formation of the [6,6]-fused ring, KAc mimetic in compound **79**. *Reagents and conditions:* a). TFA:CH_2Cl_2 (1:3), r.t., 3.5 h, followed by, Zn, NH_4Cl, DMF, 24 h, 46%.

With intermediate **79** in hand, the TIPS group was next removed, utilising TBAF under mild conditions, to give the desired phenolic product **80** (Scheme 22), with the crude product carried forward into the next reaction.

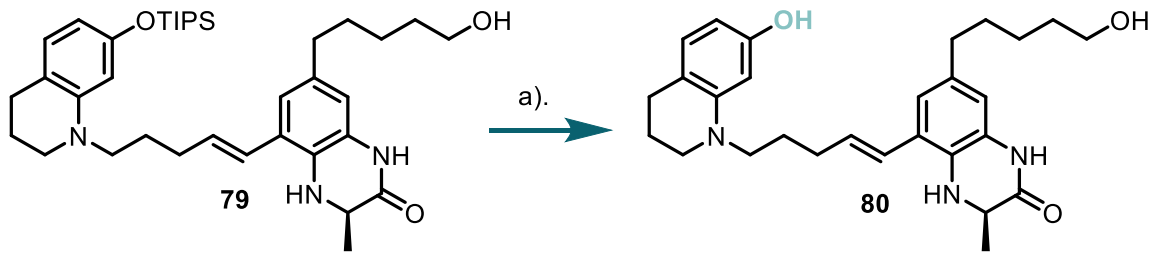

Scheme 22: TIPS deprotection of **79** under mild conditions to give **80**. *Reagents and conditions:* a). TBAF (1M in THF), THF, r.t., 4 h, no isolated yield.

5.3.2 Mitsunobu Macrocyclisation

Mitsunobu ring closure of **80** to give macrocycle **62** was then performed (Scheme 23).

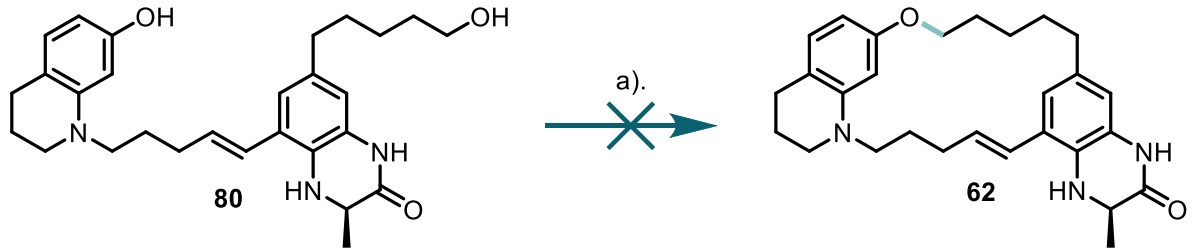

Scheme 23: Mitsunobu macrocyclisation reaction aimed to form the phenolic ether bond. *Reagents and conditions:* a). DMEAD, PPh_3, THF (0.002 M), r.t., 48 h.

Although there was product detected in the crude reaction mixture by LC-MS, it proved impossible to isolate the **62** detected from the reaction mixture. Consequently, an alternative macrocyclisation strategy and route were pursued to furnish macrocycle **62**.

5.4 Synthesis of Alkyl Macrocycle **62** *via* Suzuki Cross-Coupling Macrocyclisation

An alternative macrocyclisation strategy was investigated, avoiding the late-stage formation of the phenolic ether bond which had proved challenging, as the ether bond in this strategy is formed earlier in the route, using a Mitsunobu reaction to combine fragments (Figure 55, Compound **29** and **75**). After the phenolic ether is formed, the terminal alkyne is then selectively hydroborylated using Schwartz's reagent, garnering

the intermediate primed for use in a Suzuki cross-coupling macrocyclisation reaction. Palladium-catalysed cross-coupling reactions have been used previously to form carbon-rich macrocycles, providing confidence in this approach.[63,148]

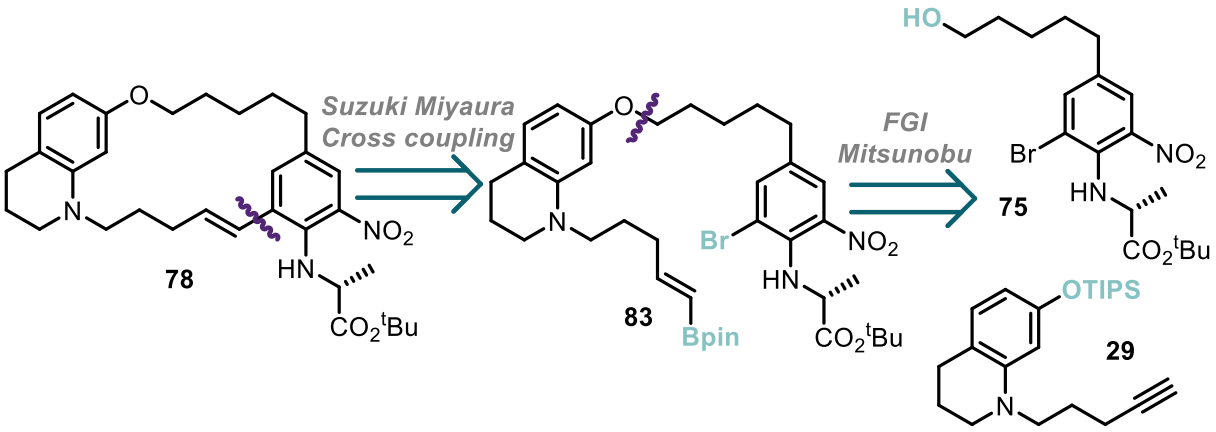

Figure 55: Retrosynthesis of a Suzuki-based macrocyclisation strategy to afford intermediate **78**, with the reactive handles which are used to form the purple target bonds highlighted in **bold**.

This macrocyclisation strategy offers several advantages: the Suzuki reaction conditions will not remove the *tert*-butyl ester protecting group; and could offer a level of preorganisation of the compound through palladium chelation bringing the carbon centres close together to encourage their reaction.

5.4.1 Mitsunobu reaction conditions screen

To enable the Suzuki cross-coupling macrocyclisation, a phenolic ether intermediate was synthesised. It was proposed that the key ether bond could be formed with a Mitsunobu reaction. As this reaction had proved difficult to achieve previously when attempting to form the macrocyclic ring (see section 5.3.2), a reaction screen was performed to optimise yield of the desired.

Three different sets of conditions were investigated to optimise the TIPS deprotection of intermediate **29** to give **81** (see Scheme 24 and Table 12) and six conditions were utilised for the Mitsunobu reaction to form **82** (see Scheme 25 and Table 13). From the deprotection conditions, hydrochloric acid (37% aqueous) over 24 hours gave 75%

conversion to the desired phenol as monitored by LC–MS, TFA only gave 50% conversion at this time whereas TBAF led to complete conversion after 30 minutes.

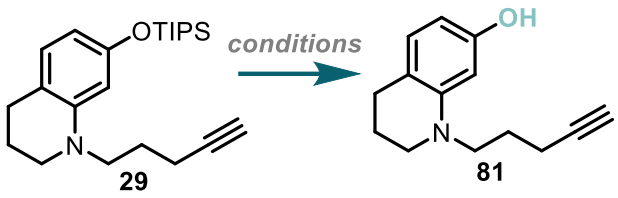

Scheme 24: TIPS deprotection reaction of **29** to give the corresponding phenol **81.**

Table 12: The reaction conditions screened for the reaction shown in Scheme 24, with the conditions carried forward highlighted in **bold green** text.

Conditions	Time (h)	Conversion, %
2 M $HCl_{(aq)}$, 1,4-dioxane, r.t.	24	75
TFA, CH_2Cl_2, r.t.	24	50
1 M TBAF (in THF), THF, r.t.	**0.5**	**>99**

The combination of fragments **75** and **81** was next explored using a Mitsunobu reaction by screening a set of 6 conditions. All the Mitsunobu reactions produced the compound **82** (see Table 13) after 48 h; the reaction profile which contained the fewest impurities and highest conversion to product **82** by both TLC and LC-MS was DIAD and triphenylphosphine in THF (see Appendix 3 figures 1-6 for LC-MS traces of each condition).

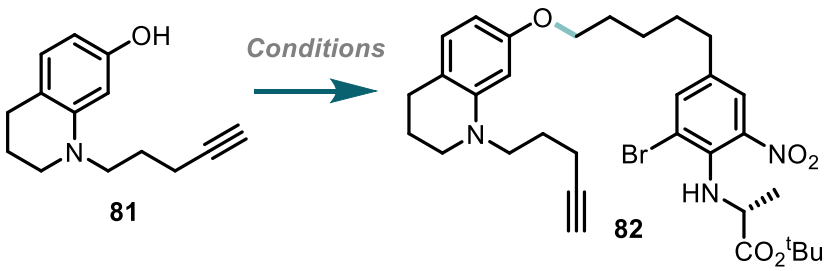

Scheme 25: Mitsunobu reaction to afford compound **82**, containing the difficult to form phenolic ether bond.

Table 13: The reaction conditions screened for the reaction shown in Scheme 25, with the conditions carried forward highlighted in **bold green** text (see Appendix C Figure 8-13 for the LC-MS data).

Conditions	Solvent	Temperature	Product peak area of crude by LC-MS, %
DIAD, PPh_3	**THF**	**0 °C – r.t.**	**38.6**
DEAD, PPh_3	THF	0 °C – r.t.	18.2
DTBAD, PPh_3	THF	0 °C – r.t.	4.5
DIAD, DPPE	THF	0 °C – r.t.	24.0
DIAD, PPh_3	Et_2O	0 °C – r.t.	25.4
DIAD, PPh_3	THF:tol	r.t.	8.5

The application of both the TBAF-mediated TIPS removal, followed by the DIAD and triphenylphosphine-mediated Mitsunobu reaction in THF gave a high yield of 72% upon reaction scale-up.

5.4.2 Suzuki Cross-Coupling Macrocyclisation

Following the Mitsunobu reaction, the substrate is primed for a selective hydroboration reaction using Schwartz's reagent (Scheme 26). This reaction chemoselectively borylated and reduced the alkyne in the presence of the aryl bromide. The *E*-alkene (highlighted in compound **83**) was formed selectively, which gave the correct stereochemistry required for the Suzuki macrocyclisation step (Scheme 26).

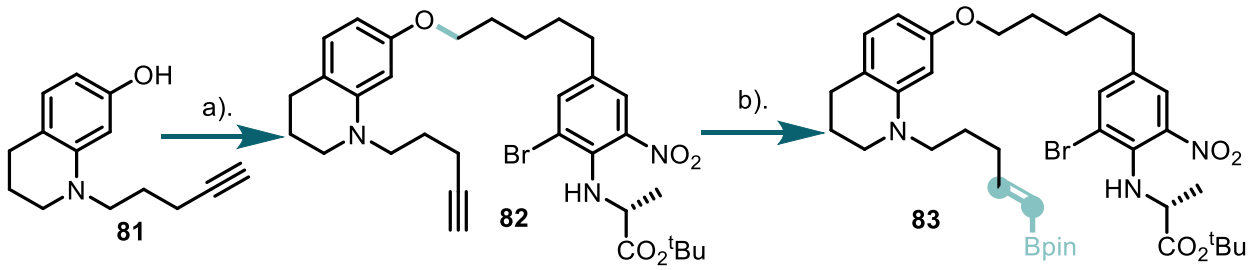

Scheme 26: Synthesis of intermediate primed for Suzuki macrocyclisation. *Reagents and conditions:*

a). Compound **75**, DIAD, PPh_3, THF, 0 °C – r.t., 48 h, 72%; HBpin, $Zr(C_5H_5)_2ClH$, NEt_3, 60 °C, dark, 18 h, 70%.

The Suzuki reaction was carried out at 2 mM solvent concentration to give product **78** which proved difficult to purify due to the appearance of a side product with very similar retention time to the product (Scheme 27). This compound was theorised to be the proto-deborolated product giving the terminal alkene.

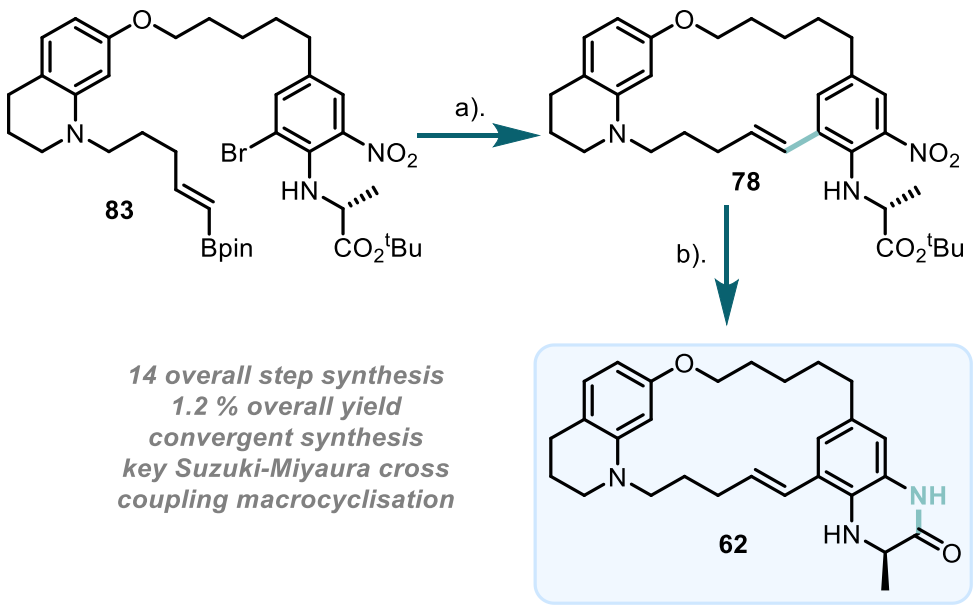

Scheme 27: Synthesis of [6,6]-KAc mimic containing macro alkyl ligand **62**. *Reagents and conditions:* a). $Pd(dppf)Cl_2$, K_2CO_3, 1,4-dioxane:H_2O (5:1) (2 mM), 100 °C, 24 h, 19%; b). TFA/CH_2Cl_2 (1:3), r.t., 3.5 h, followed by, Zn, NH_4Cl, DMF, r.t., 18 h, 52%.

With this Suzuki cross-coupling product **78** purified, the ester deprotection and reductive cyclisation were carried out to give the [6,6]-alkyl macrocycle **62** in 52% yield (Scheme 27). The final purification also proved challenging and required the use of a reverse phase semi-preparative HPLC, which had poor mass recovery of **62**. However, a 1.4% overall yield in 14 steps to give product **62** was achieved.

5.5 Synthesis of the corresponding linear equivalent compound 84

An acyclic analogue **84** (see Figure 56) was synthesised in order to compare to the binding of macrocycle **62**.

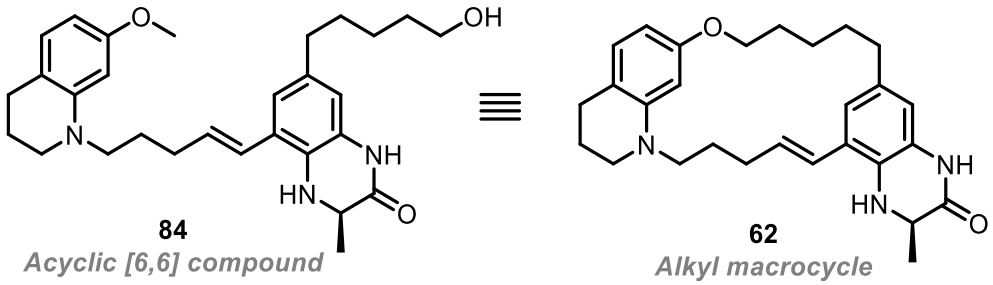

Figure 56: Chemical structure of **62** and its acyclic analogue **84**.

5.5.1 Synthesis of Acyclic [6,6]-KAc mimic compound

With the synthesis of the positive control compound completed, the synthesis of the acyclic [6,6]-KAc mimetic-containing compound was carried out. The route utilised the same THQ fragment as the **OXFBD05** ligand (compound **45**) and the pre-[6,6] membered fragment (compound **75**) used in the synthesis of the alkyl macrocycle which were combined in a Suzuki cross-coupling to give **85** (Scheme 28). Once again, the [6,6]-membered ring was formed after the Suzuki cross-coupling garnering the desired product **84** (Scheme 28).

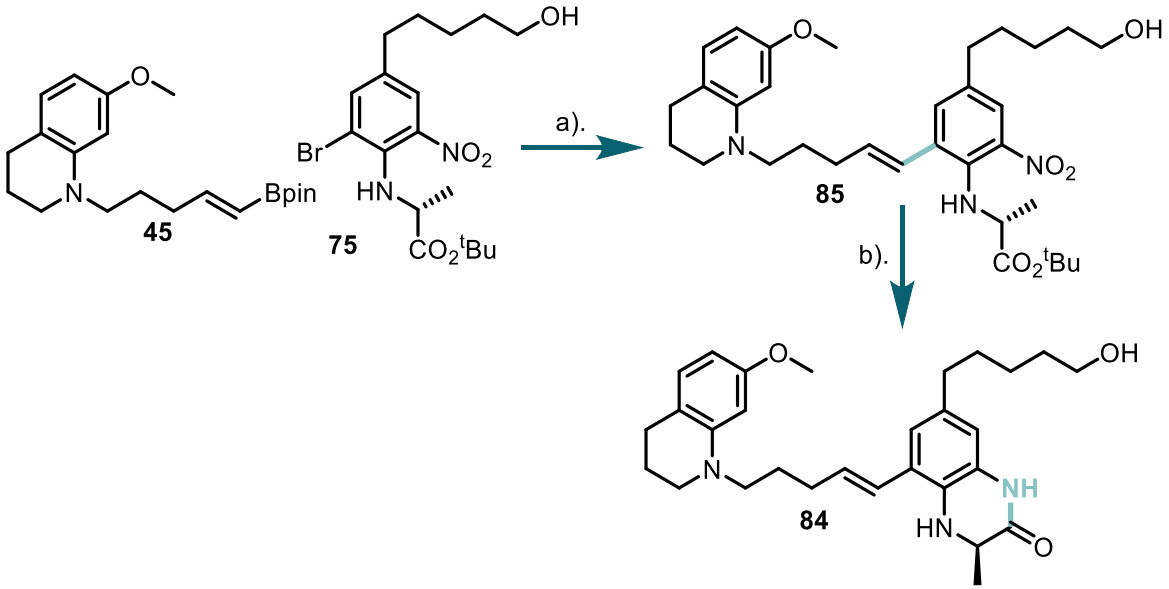

Scheme 28: Synthesis of acyclic analogue **84**. *Reagents and conditions:* a). $Pd(dppf)Cl_2$, K_2CO_3, 1,4-dioxane:H_2O (9:1), 100 °C, 24 h, 60%; b). TFA:CH_2Cl_2 (1:3), r.t., 4 h, followed by, Zn, NH_4Cl, DMF, r.t., 24 h, 65%.

5.5.2 Instability of the [6,6]-KAc mimic

The acyclic [6,6]-KAc mimic containing compound **84** was unstable when left in deuterated chloroform for an extended period. Degradation of **84** was indicated by the presence of unknown peaks in the proton and carbon NMR spectra after >24 hours (see Figure 57). This is postulated to be due to residual acid present in the solvent. As a result, the ^{1}H and ^{13}C NMR experiments for all [6,6]-KAc mimicking compounds were carried out in d_6-DMSO (see Appendix I).

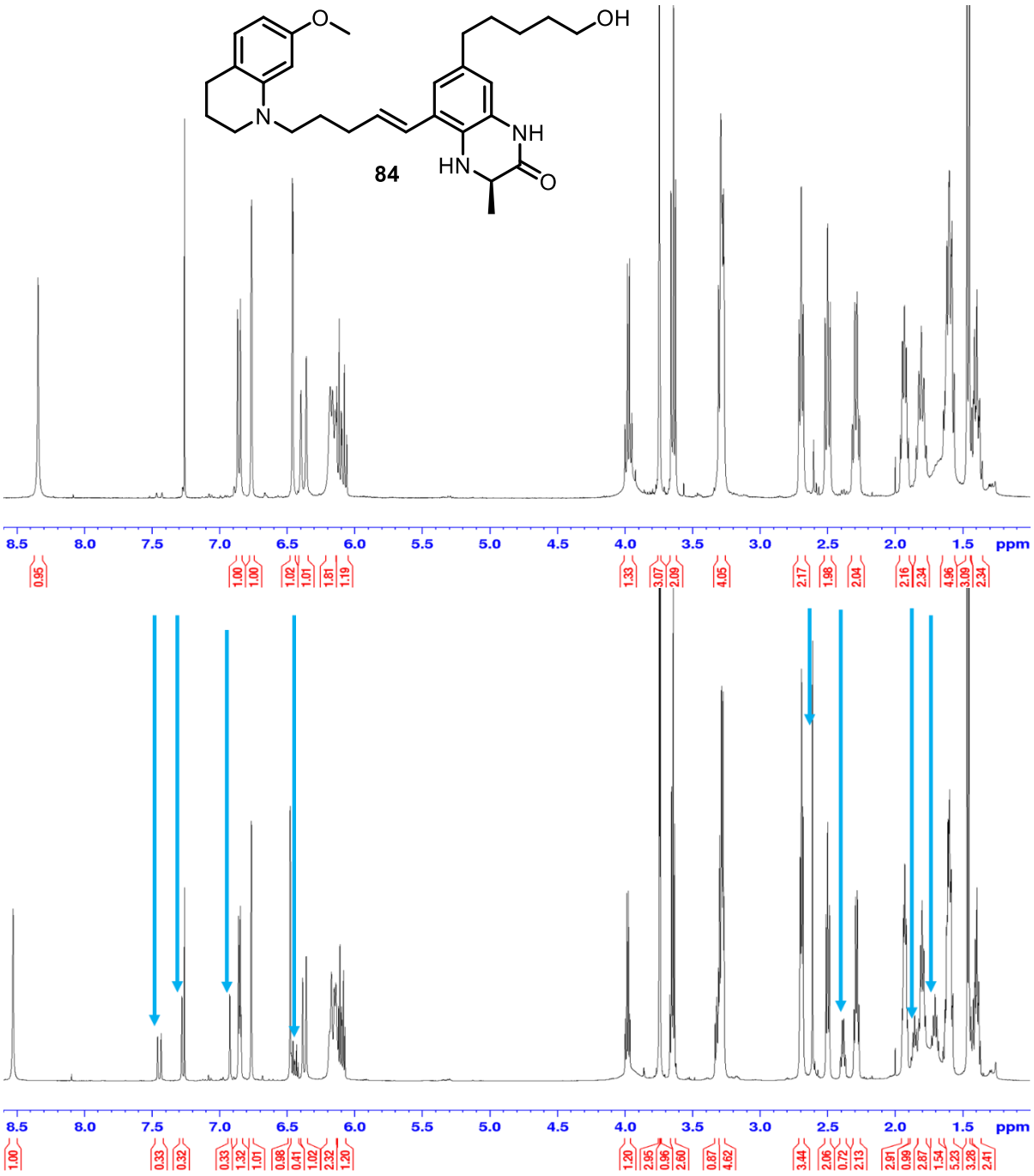

Figure 57: The ^{1}H NMR spectra of the acyclic [6,6]-KAc mimic **84**, top is the spectrum taken rapidly (<1 h) after the sample was made up; bottom is the same sample after >24 h have passed with the blue arrows represent degradation product peaks.

The acid instability of **84** also meant that the compound could be unstable when purified using formic acid to improve peak shape on reverse phase chromatography, hence, two normal phase columns were instead conducted to give the compound with high purity. With both these control compounds now in hand, the biophysical analysis was carried out.

5.6 Biophysical analysis of alkyl macrocycle and its linear equivalent

With the fully characterised linear and macrocyclic compounds **62** and **84** in hand, assessment of their respective binding was conducted through ITC with the purified CBP^{BRD} (see Appendix B figure 1).

5.6.1 Novel Compound ITC data

With the knowledge that the protein is functional, and the assay performed as expected, the novel macrocycle was next analysed for binding to the CBP^{BRD}. The ITC assays were performed with the same concentrations as those utilised for the positive control compound **OXFBD05** (20 μM of compound and 160 μM of protein) to maintain consistency. No detectable binding of the macrocycle to the CBP^{BRD} was observed using ITC. (Figure 58).

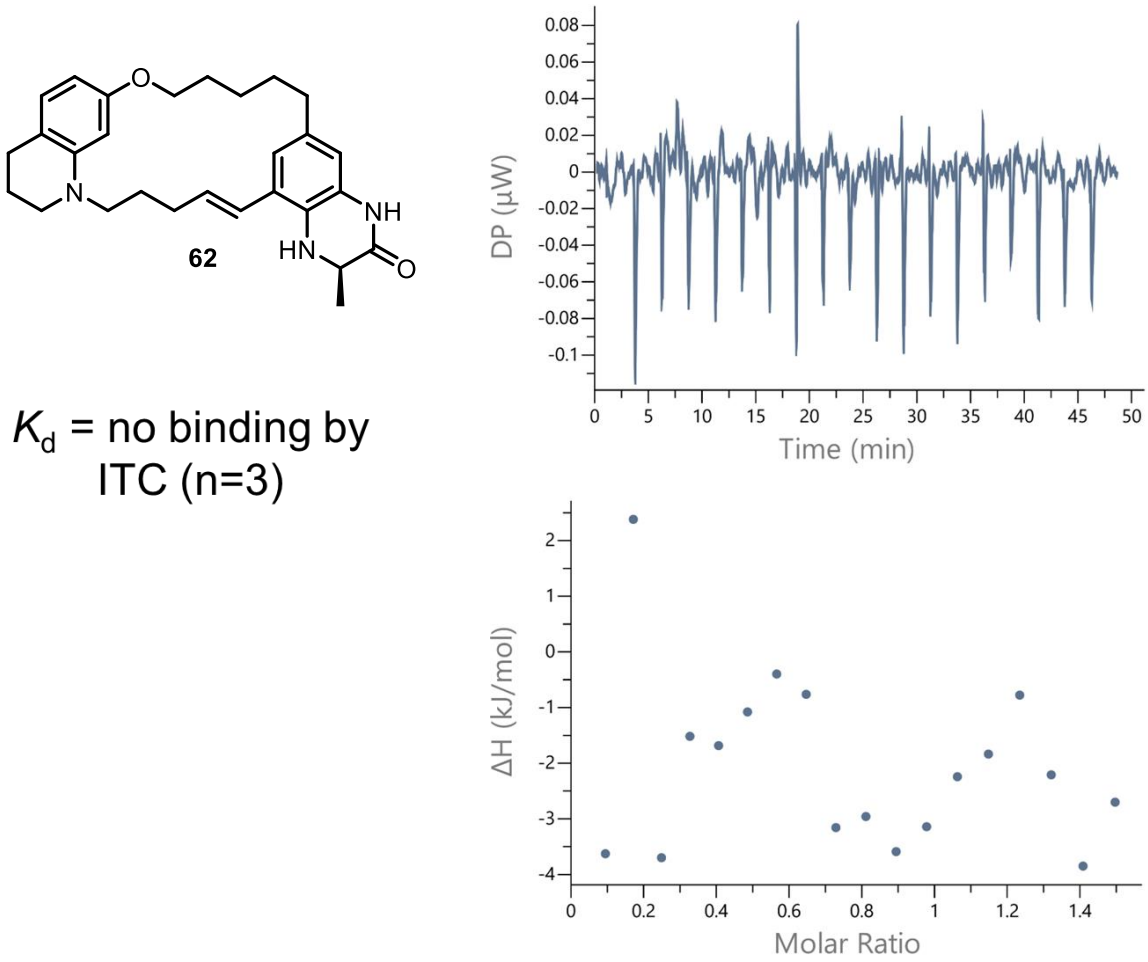

Figure 58: ITC traces of the macro alkyl ligand **62** against the CBP^{BRD}, demonstrating a lack of measurable binding with this assay, from n = 3 repeats.

The macro alkyl scaffolds used in **7** and **62** were abandoned due to their lack of detectable binding by ITC to the CBP^{BRD} (with both the [6,6] and [6,7]-KAc mimetics).[88] The lack of detectable binding for **62**, points to the seven-membered ring flip not being the root cause of a lack of binding in **7**, instead pointing to the poor solubility and lack of rigidification in these macrocycles leading to their lack of detectable binding by ITC. This is reinforced by the macrolactam ligands **14-19** synthesised in Chapter 2 and characterised in Chapter 3 still demonstrating binding to the CBPBRD, in some cases with high affinity (K_ds < 100 nM) and in some cases higher affinity (by BromoKdElect) than **OXFBD05** upon which they were based. This is why an alkyl macrocycle targeting the CBP^{BRD} was not pursued further.

5.7 Conclusion

The work presented in this chapter covers a variety of synthesis approaches for the preparation of an alkyl macrocycle (**62**) which aimed to target the CBP^{BRD}. With macrocyclisation by Suzuki cross-coupling proving a successful strategy in the synthesis of compound **62**. Unfortunately, the target molecule displayed no detectable binding to the CBP^{BRD} when assessed by ITC. The lack of detectable binding for **62** by ITC highlights that the hypothesised seven membered ring flipping was not the source of no-detectable binding by ITC in the previously synthesised macrocyclic ligand **7**. Instead, this result highlights that the poorly soluble alkyl chain is not a desirable scaffold modification in an already low solubility compound.

Chapter 6:

Conclusions and Future Work

6.1 Conclusion

The work in this thesis has focussed on the synthesis and biological evaluation of novel compounds targeting the CBP^{BRD} with emphasis on macrocyclisation as a strategy to afford selective high-affinity ligands. Through an SAR approach based upon the prior work by Dr. Mustafa Moroglu which identified macrolactams as binding to the CBP^{BRD} but with decreased affinity (K_d ~ 1 μM) compared to the linear ligand **OXFBD05** (K_d = 132 nM) from which these original macrolactams were derived. A hit ligand from the SAR was investigated using X-ray crystallography in order to observe the conformation of the small molecule when protein bound. The hit was further characterised for overall BRD selectivity and potency in cancer cells. A small SAR was explored to identify improvements to the **OXFBD05** scaffold which could be incorporated into a macrocyclic hit scaffold.

In Chapter 2 a series of macrolactam ligands were synthesised based upon a previously validated weak binding macrocycle, ligand **10**. These six novel ligands (**14**-**19**) required optimised chemical strategies to obtain the target ligands. The synthesis of the target macrocycles was enabled by an optimised amide coupling macrolactamisation reaction, along with a late-stage phenol alkylation to afford the desired final compounds. The macrolactams were synthesised from a common intermediate (**13**) over 18 total steps, with overall yields of 2 – 0.2%. It was also decided that it would be beneficial to prepare the match pair to the corresponding macrocycle, linear ligands (**39**-**41**) were synthesised in 15 steps from common intermediate (**46**) with overall yields from 2.5 – 1.7%.

In Chapter 3, the novel ligands synthesised in Chapter 2 were tested for their respective binding affinities to both the CBP^{BRD} and the major off-target bromodomain

of BRD4(1). The compounds were first assessed using AlphaScreen®, but it soon became apparent that the compounds interfered with the assay readout through singlet oxygen quenching. Therefore, ITC was used to assess compound affinities to both the CBP^{BRD} and BRD4(1), identifying several ligands of interest. The affinity and selectivity of these compounds was further probed using the BromoKdElect assay against CBP^{BRD}, $p300^{BRD}$, BRD4(1), and BRD4(2). Through this assay, two high affinity (K_d < 100 nM) macrolactams were identified, with the morpholine-containing macrocyclic ligand **19** displaying the highest selectivity for the CBP^{BRD} (>455-fold vs BRD4(1)) in this assay. This hit ligand (**19**) was further characterised against a phylogenetically diverse panel of 32 bromodomains in a BromoMax assay. Impressively, at a concentration of 1 μM, compound **19** only displayed on-target selectivity for the CBP and p300 bromodomains, whilst at 10 μM **19** demonstrated affinity for 7 off-target bromodomains. This highlights the high selectivity of **19** for the target bromodomains and the high affinity it displays for the CBP^{BRD}.

In order to further rationalise the affinity and selectivity of the macrolactam ligands, the first X-ray crystal structures of macrocycles bound to the CBP^{BRD} were produced. These structures were for macrolactams **10** (PDB: 9GEY), **14** (PDB: 9GEU), and **19** (PDB: 9GEJ) as well as for the linear analogue **40** (PDB: 9GET). The resultant data emphasised the desired “curled-up” ligand conformation for **19** which when constrained into a macrocycle precludes binding to BRD4(1), driving the selectivity displayed for the CBP^{BRD}. This assertion is exemplified by linear ligand **40**, which adopts the same binding conformation as **19**, but lacks selectivity for the CBP^{BRD}, due to the lack of sufficient conformational constraint.

An acute myeloid leukaemia cell line (OCI-AML3) was chosen to assay the potential of the hit ligand **19**, which was tested for the ability to prevent oncogene transcription

and decreasing oncoprotein levels. The oncoproteins of interest were *c*-MYC, MYB, and BCL-2, which have previously been identified to decrease upon CBP^{BRD} inhibition were used.[30,44,46,52,123,149] Ligand **19** demonstrated a concentration and time-dependent decrease in oncogene transcription and oncoprotein levels. However, the effective concentration required for this change was ≥ 3 μM of **19**, displaying that there is room for improved potency. The macrolactam SAR findings of this work are summarised in Figure 59.

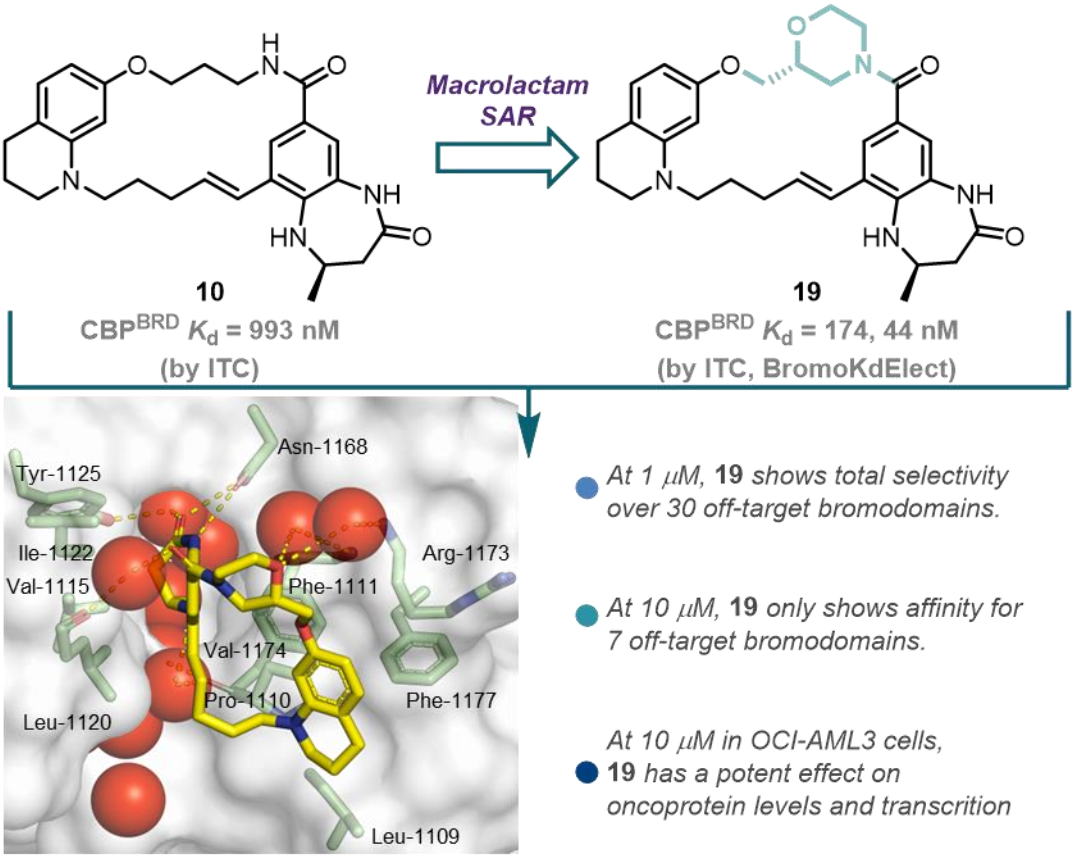

Figure 59: Summary of macrolactam work carried out in this thesis and the identification of the hit compound **19**, *in vitro* and cell-based data as well as the co-crystal structure of the compound in complex with the CBP^{BRD} (PDB: 9GEJ) at 1.85 Å resolution.

With this in mind, an exploration of the tetrahydroquinoline (THQ) was performed in Chapter 4, in order to improve the physiochemical properties of ligands whilst also aiming to improve the affinity for the CBP^{BRD} through improved interactions with Arg-1173. Due to the lengthy synthesis of the macrolactams, the THQ SAR was carried

out on the **OXFBD05** as by using this scaffold the target ligands can be more readily accessed, thus making the hypothesis easier to test. Taking inspiration from experimental and computational work surrounding the strength of cation-π interactions, along with previously published examples, compounds **49** and **50** were synthesised. This work identified that the THQ of **OXFBD05** could accommodate modifications. Pleasingly both **49** and **50** fulfilled the aim of improved physiochemical properties in terms of greater aqueous solubility and membrane permeability compared to **OXFBD05**. With ligand **50**, where a benzomorpholine substituted the THQ, improving the affinity for the CBP^{BRD} and the X-ray co-crystal structure (PDB: 9GEW) showed **50** adopting expected binding mode. The findings of the THQ SAR work are highlighted in Figure 60 below:

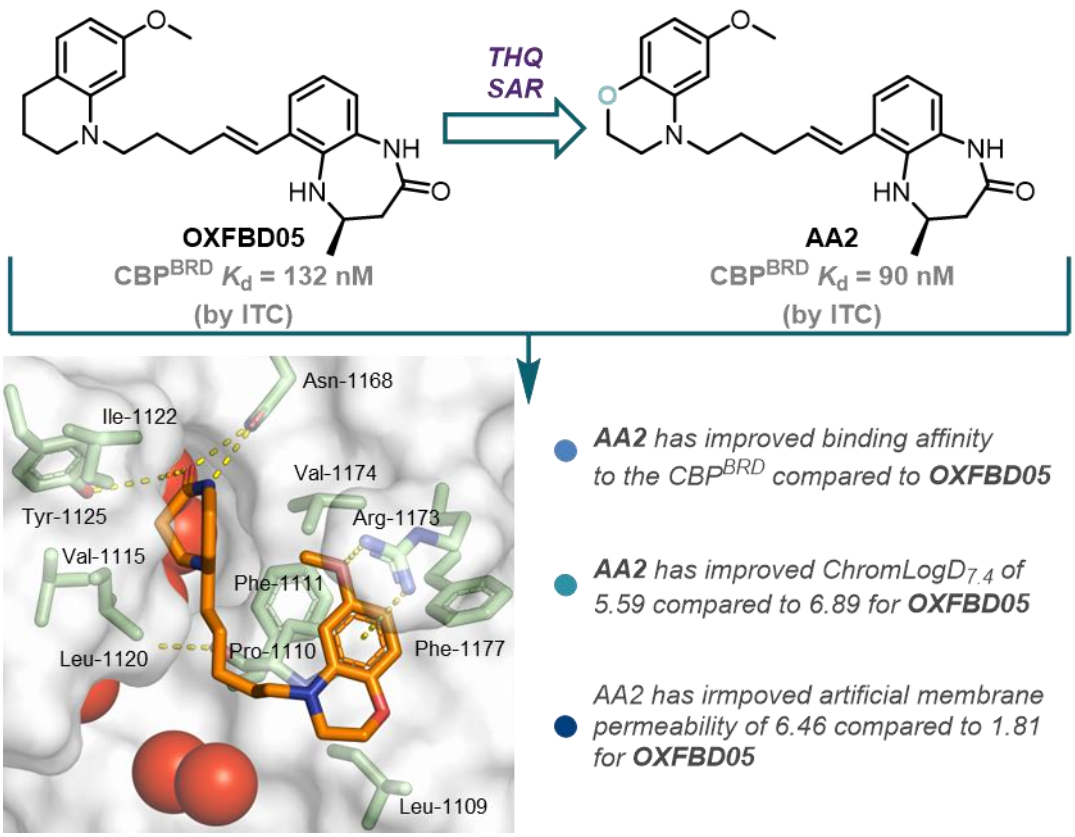

Figure 60: Summary of the THQ SAR affording ligand **50** which has improved physiochemical properties relative to **OXFBD05**, with the co-crystallised with the CBP^{BRD} (PDB: 9GEW) to illustrate the induced fit pocket and cation-π interaction and thus desired binding mode, at 1.47 Å resolution.

Chapter 5 reported on the synthesis and binding evaluation of a [6,6]-KAc mimic-containing alkyl macrocycle **62**, which is analogous to a previously synthesised [6,7]-KAc mimic compound **7** (Figure 61). This previously synthesised ligand **7** afforded no detectable affinity by ITC, therefore a change to a [6,6]-KAc mimic was hypothesised to be a potential method to rescue affinity for the CBP^{BRD}.[88] However, when the novel [6,6]-system was evaluated by ITC, no detectable binding was demonstrated. This ruled out the hypothesis for the [6,7]-alkyl macrocycle lacking binding as a result of the seven-membered and instead highlighted how this is likely a result of ligand flexibility and high hydrophobicity.

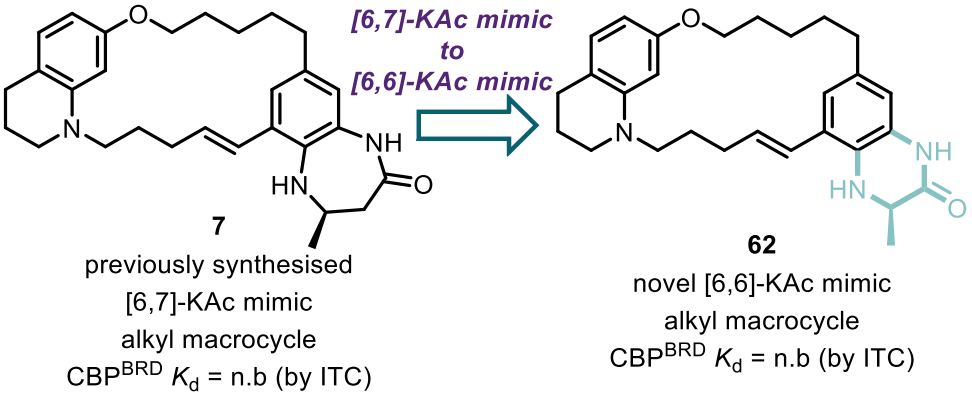

Figure 61: The previously synthesis [6,7]-alkyl macrocycle **7** and the novel [6,6]-alkyl macrocycle **62**.

6.2 Future Work

The work in this thesis proves that macrolactams can be developed into selective inhibitors of the CBP^{BRD} over other bromodomains. This validates macrocyclisation as a viable strategy to gain selectivity, which could be applied to other ligands with drastic differences between the on-target and off-target binding mode. Ligand **19** should be further tested in proliferation assays (such as colony, BrdU or Edu assays) in order to show further phenotypic effects on cancer cells. It would also be of interest to test the hit macrolactam **19** in further target tumour cell lines such as prostate cancer cells (for example LNCaP, 22Rv1 or VCaP cells) for which the clinical candidate Inobrodib is aimed at treating. The research regarding the modifications to the THQ has laid the foundation for further SAR exploration and highlighted how subtle modifications can lead to profound improvements in binding affinity and physiochemical properties. To further validate this modification, *in vitro* assays comparing the effect of **50** and **OXFBD05** on oncoproteins should be performed (such as the experiments conducted on macrocycle **19** in Chapter 3). However, to increase the potency of the macrocyclic ligands whilst maintaining high selectivity improvements in affinity must be sought, in order to accomplish this, the linear compound upon which these macrolactams would be based must first be improved further with respect to affinity and physiochemical properties. This could be accomplished through further modifications to the benzomorpholine identified in Chapter 5 (Figure 62A), such as changing the morpholine to a piperazine, or introducing additional substituents on the aromatic rings to increase the cation-π interactions. Those beneficial modifications would then need to be incorporated into the macrolactam scaffold of **19**, upon which further SAR to produce a lead ligand comparable with Inobrodib (Figure 62B). The morpholine could be changed to a piperazine, or further substitution of the morpholine ring to explore

the stereogenic centre possessing the possibility of a “magic methyl” effect. This lead compound would then maintain the high selectivity provided through macrocyclisation with improved affinity. This could lead to a strong, robust, and prolonged effect in cancer cells. This would then allow the improved macrocycle to progress into *in vivo* tumour models.

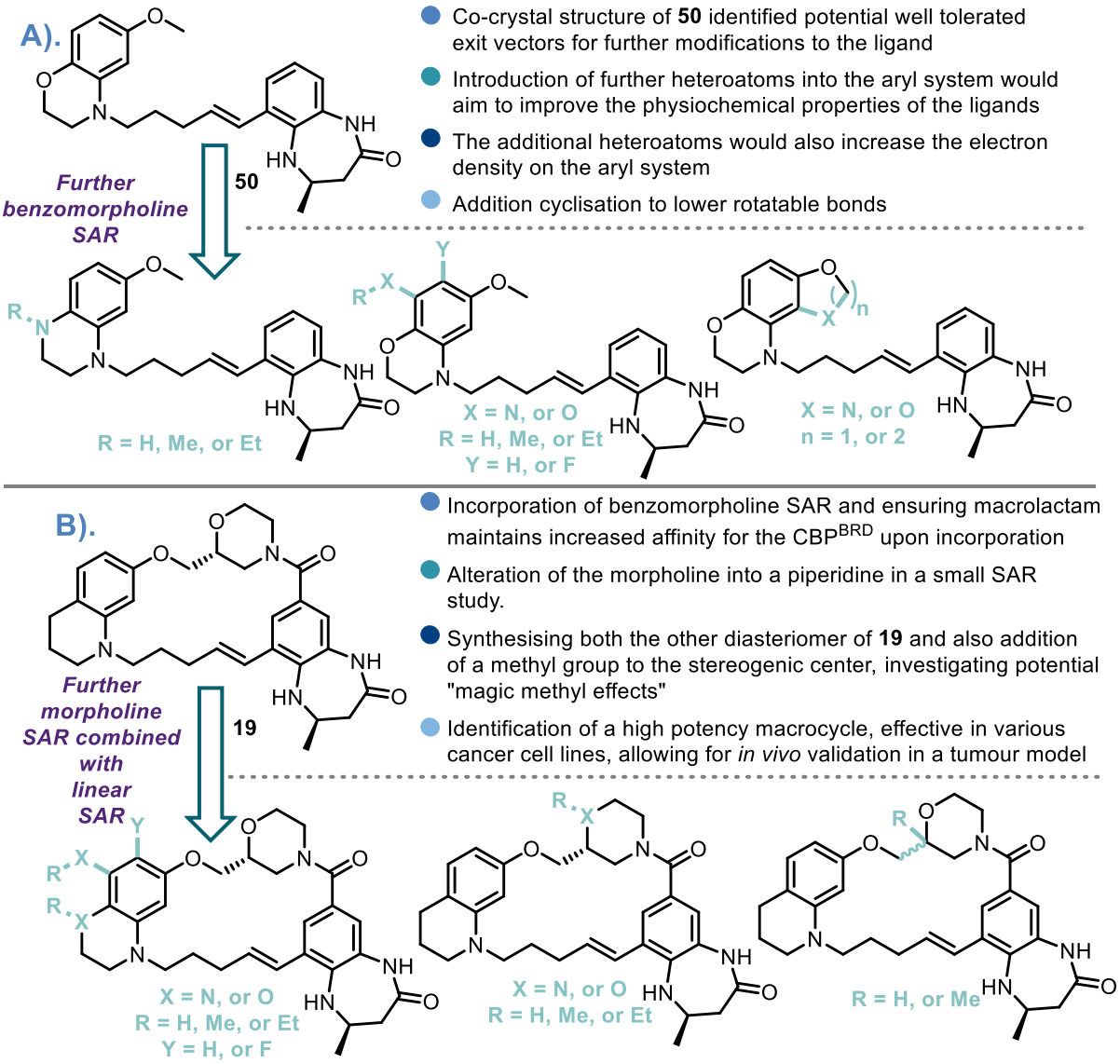

Figure 62: Potential future work; A). Further SAR work that could be conducted on ligand **50** to improve affinity and physiochemical properties; B). Further SAR work on the ligand **19** scaffold.

Chapter 7:

Experimental

7.1 Biochemical and biophysical methods

pH measurements

Measurements were performed on an Oakton PH 550 Benchtop pH Meter Kit was used to measure the pH of all buffers. Calibration was performed against standard solutions at pH 4.0 (solution of potassium acid phthalate, cetyl pyridinium chloride, and methyl red), pH 7.0 (solution of potassium phosphate, acetyl pyridinium chloride, sodium hydrogen phosphate, and methyl orange) and pH 10.0 (solution of sodium carbonate, sodium bicarbonate and thymol blue). The electrode was stored in 3 M $KCl_{(aq)}$ solution when not in use. Buffer solutions pHs were adjusted to within ±0.1 units of the desired pH adjusting with sodium $hydroxide_{(aq)}$ or $hydrochloric\ acid_{(aq)}$ (1 M or 2 M).

Protein concentration measurements

Protein concentrations were calculated using the absorbance of proteins at 280 nm which was measured using a Thermo Scientific Nanodrop Lite, with the Protein A280 Program. From this, the approximate concentration of protein samples was determined with the Beer-Lambert Law:

$$A = \varepsilon cl$$

Where A is the absorbance, ε is the molar extinction coefficient of the protein ($M^{-1}\ cm^{-1}$), c is the concentration of the protein (M), and l is the path length (set to 1.0 cm). Each measurement of concentration was taken a minimum of five times, from which the mean was used.

Protein expression and purification

The CBP^{BRD} (Addgene plasmid # 38977) and BRD4(1) bromodomain (Addgene plasmid # 38942) constructs were transformed into *E. coli* BL21 Gold (DE3) for expression. The proteins were purified using Immobilized Metal Affinity Chromatography (IMAC) with a HisTrapTM column (GE Healthcare) followed by gel filtration chromatography with Superdex 75 resin (GE Healthcare). The protein purity was assessed using SDS-PAGE and LC-MS analysis.

A general procedure was followed for both the CBP^{BRD} and BRD4(1) which is outlined in the following. All procedures for bacterial expression work were carried out in a sterile environment and all pipette tips, flasks and media were autoclave prior to use. Antibiotic stocks and other solutions (such as mobile phases for protein purification) were filtered through 0.22 μM syringe filters in order to ensure sterility.

Protein Expression

BL21 Gold (DE3) competent *E. coli* cells were thawed on ice. 2 × YT media with agar was autoclaving and after was kept at 55 °C with a water bath in order to prevent solidification. Upon removing this media from the water bath, 400 μL of kanamycin stock (50 mg/mL) was added. This media was then poured into colony plates (10 cm diameter), left to reach room temperature to solidify and the inverted. To the thawed BL21 DE3 bacteria was added 1 μL of the appropriate plasmid, which was then incubated at 4 °C for 20 mins, the cells were then placed into a water bath set to 42 °C for 1 min, the bacteria were then incubated at 4 °C for a further 5 mins, to the bacteria was added 500 μL of Super Optimal broth with Catabolite repression (S.O.C) media and the cells were again placed into a water bath at 37 °C for 1 h. After this time the bacteria were plated into the agar dishes by adding 10, 40, or 100 μL of bacteria solution. These plated bacteria were then incubated overnight at 37 °C.

Single transformed colonies were selected from the agar plates using a sterilised pipette tip and were added to 100 mL of 2 × YT media supplemented with 100 µL of kanamycin stock (50 mg/mL). This culture was then incubated overnight at 37 °C overnight with shaking at 200 rpm. From this starter culture, 1 mL was sub-cultured into 1 L of 2 × YT media with 1 mL of kanamycin stock (50 mg/mL) added prior inside of baffled flasks. This culture was incubated at 37 °C with shaking at 180 rpm until an optical density at 600 nm (OD_{600}) value of 0.8 was measured. At this stage of growth, the temperature was decreased to 18 °C and 500 µL of a 0.5 M stock of isopropyl ß-D-1-thiogalactopyranoside (IPTG) was added to induce protein expression.

After incubating overnight, the culture was centrifuged at 5000 rpm and 4 °C for 15 mins, pelleting the bacteria from the supernatant. The supernatant was removed, and the pellet left to dry in the inverted centrifuge flask, once dry the pellets were removed and combined. The combined pellet was stored at −80 °C for long term storage.

Protein Purification

The solution utilised for protein purification, the volumes are shown, all solutions were degassed, and stored at 4 °C prior. and their compositions are displayed in the table below:

Binding buffer	400 mL	50 mM HEPES, 500 mM NaCl, 10% glycerol, 10 mM β-mercaptoethanol at pH 7.4
Lysis buffer	≥100 mL	50 mM HEPES, 500 mM NaCl, 10% glycerol at pH

		7.4, one sigmafast protease tablet is added and dissolved before use
Elution buffer	500 mL	50 mM HEPES, 500 mM NaCl, 500 mM imidazole, 10% glycerol, 10 mM β-mercaptoethanol at pH 7.4
Strip buffer	1000 mL	50 mM HEPES, 500 mM NaCl, 50 mM EDTA at pH 7.4
Loading buffer	500 mL	100 mM $NiSO_4$
Gel filtration buffer	1000 mL	50 mM HEPES, 500 mM NaCl at pH 7.4
MilliQ water	2000 mL	

The bacteria pellet was placed on ice and allowed to thaw in a tall beaker, once thawed, lysis buffer is added to the pellet (at an approximate ratio of 20 g of cell pellet to 100 mL of lysis buffer) and the protease tablet was added, and the bacteria pellet solution was stirred on ice for 15 mins. After this time the cells were lysed using sonication (35% amplitude, 5s burst/5s pause cycles for 10 mins), the DNA was precipitated using a polyethyleneimine solution (5% *v*/*v* in H_2O) and incubated on ice for 30 mins. Cell debris was pelleted by centrifugation at 30000 × *g* for 30 mins at 4 °C and filtered through 0.45 μM to give the lysate as a light brown liquid. This filtrate was then loaded onto a nickel affinity column (Cytiva HisTrap™ FF column) which was equilibrated with loading buffer (3 CV), washed with MilliQ H_2O (3 CV) and elution

buffer (3 CV) attached to an AKTA FPLC system (GE Healthcare) in a cold room (~4 °C). After loading the column was washed with binding buffer (10 CV), then it was washed with elution buffer in a stepwise manner (10%, 25%, 50%, 75%, 100% each for 5 CV) with fractions being collected automatically (5 mL). Fractions which showed a clear UV peak above background were collected and analysed by SDS-PAGE (4-12% Bis-Tris in MES buffer). Those fractions that appeared pure by SDS-PAGE, were combined and concentrated, using centrifuge concentrations with a 5 kDa cut off, to a final volume of 2 mL. These concentrated fractions were then loading onto a size exclusion (SEC) column (75-120 superdex column), which was equilibrated with gel filtration buffer (1.2 CV), the column was run for until protein eluted (1.5 CV). The fractions were collected throughout and again analysed by SDS-PAGE to confirm their purity. The purified fractions of protein were concentrated to the desired concentration and then aliquoted into PCR tubes (150-100 µL) in each and were then flash frozen in liquid N_2 and place into a −80 °C freezer for long term storage.

SDS-PAGE and Coomassie Blue staining

Sodium dodecyl sulfate polyacrylamide gel was cast using Mini-PROTEAN® 3 Cell (Bio-Rad). Sodium dodecyl sulfate polyacrylamide gel electrophoresis (SDS-PAGE) was performed using Mini-PROTEAN® 3 Electrophoresis Module (Bio-Rad). The tris-glycine discontinuous buffer system was used in the SDS-PAGE experiments. Protein samples for SDS-PAGE was first prepared in 1 × Laemmli sample buffer (diluted from 4 × Laemmli sample buffer, Bio-Rad) containing 1.42 M β-mercaptoethanol$_{(aq)}$ (aliquoted from 14.2 M β-mercaptoethanol, Sigma-Aldrich), and then denatured at 100 °C for 3 mins. Chemicals for SDS-PAGE, Trizma® base, 30% acrylamide/bis-acrylamide solution, sodium dodecyl sulfate dust-free pellets, *N*,*N*,*N*′,*N*′-tetramethylethane-1,2-diamine (TEMED) and ammonium persulfate (APS),

were purchased from Sigma Aldrich. Glycine was purchased from Fisher Scientific. After SDS-PAGE, the gels were stained with Staining Solution (0.5% Brilliant Blue G (Sigma Aldrich), 50% (*v*/*v*) MeOH (Sigma Aldrich), 10% (*v*/*v*) glacial acetic acid (Fisher Scientific), 40% (*v*/*v*) Milli-Q water) for 30 mins. Destaining was performed by washing gels with 70% *v*/*v* EtOH in Milli-Q water to remove excess Staining solution and then gels were washed 3 times with Milli-Q water and left on a plate shaker (300 rpm) overnight to full destain.

Isothermal calorimetry

All calorimetric experiments were performed on either a MicroCal iTC200 or MicroCal PEAQ-ITC Automated (Malvern) or MicroCal PEAQ-ITC (Malvern) and analysed with MicroCal PEAQ-ITC Analysis software 1.1.0.1262 (Malvern) using a single binding site model. The first data point was excluded from all analyses. The purified CBP^{BRD} was dialysed into either 50 mM HEPES, 150 mM NaCl or 137 mM NaCl, 3 mM KCl, 8 mM Na_2HPO_3 1.5 mM KH_2PO_4 (Dulbecco A tablets 10 × in 1 litre) buffers containing 0.2% *v*/*v* DMSO; pH 7.4 (this was filtered through a 0.2 µM filter paper prior to use), using a Slide-A-Lyzer® MINI Dialysis Device (2000 MWCO; Thermo Scientific Life Technologies) for a minimum of 12 hours at 4 °C. The dialysed protein was then centrifuged to remove aggregates (3 min, 3000 rpm, 25 °C). Protein concentrations were then measured (CBP^{BRD}: ε_{280} = 26930 M^{-1} cm^{-1}). Small molecule ligands were dissolved in DMSO to give stock solutions (20 mM) and diluted appropriately using dialysis buffer and DMSO as necessary. The cell was stirred at 750 rpm, reference power at 5 µcal s^{-1} and temperature set to 25 °C. After an initial delay of 60 s, 20 × 2 µL injections (first injection of 0.4 µL) were performed, with 150 s intervals between injections. Heat of dilutions were measured under the same conditions and subtracter

for analysis. Small molecule solutions in the calorimeter cell (300 µL, (20 µM)) were titrated with the protein solutions in the syringe (60 µL, (160 µM)).

AlphaScreen™

Binding assay

To evaluate whether compounds binding to the purified BRD4(1) protein using the $H4_{1\text{-}20}(KAc)_4$-biotin peptide with the amino acid sequence as follows:

H_2N-YSGRGK(Ac)GGK(Ac)GLGK(Ac)GLGK(Ac)GGAK(Ac)RHRK(Biotin)-$CONH_2$

This was supplied by GenScript and was stored as 1 mM stocks in Milli-Q water at −80 °C. The assay buffer (25 mM HEPES, 100 mM NaCl, 0.05 wt% CHAPS and 0.1 wt% BSA at pH 7.6) was filtered through a 0.22 µM filter prior to use. The compounds, protein and peptides were dispensed into a ProxiPlate-384 Plus using a Thermo-Fischer electronic multi-channel pipette. Compound stocks of 40 mM in DMSO were serially diluted in a clear plate with 100 µL wells. BRD4(1) and peptide were diluted in the assay buffer and added to the assay plated wells so as to give a final assay concentration of 10 and 8 nM respectively (7 µL per well), in each assay well. This was sealed and then incubated for 30 mins at 450 rpm, then the compound dilution series were added (5 µL per well) and the plate was sealed and then incubated for 1 hour at 450 rpm. After this time assay beads (Ni^{2+} chelate acceptor and streptavidin donor) at 5 µg/mL were (8 µL per well) to give a total volume of 20 µL in each well and the plate was then sealed and incubated at 450 rpm in the absence of light for 1 hour. The plate was then moved to the Pherastar and the plate was opened and place into the machine and left for a further 30 mins after light exposure to allow for full equilibration. After this time the assay was performed using the inbuilt AlphaScreen™ 384 ProxiPlate function (excitation at 680 nm, 0.18 sec; emission at

570 nm, 0.37 s) and the results recorded. Dose response curves for each compound were obtained in triplicate.

True Hits

To evaluate whether the compounds tested by AlphaScreen™ for BRD4(1) inhibition gave false positives the below assay was carried out.

Compound dilution series were produced in the same manner as for AlphaScreen™ binding assay, containing 0.25% DMSO FAC, in the same buffer which was utilised previously. The biotinylated acceptor beads and streptavidin donor beads were added to buffer containing no DMSO (5 µL of each into 1.99 mL of buffer) to a FAC of 4.7 µg/mL. This True Hits bead mix was added to a 384 well plate and incubated in the absence of light for 30 mins at room temperature on a plate shaker at 450 rpm. After this time the desired compound dilutions were added to the assay plate in triplicate and the plate was sealed and incubated for a further 30 minutes in the absence of light. The plate was then moved to the Pherastar and the plate was opened and place into the machine and left for a further 30 minutes after light exposure to allow for full equilibration. After this time the assay was performed using the inbuilt AlphaScreen™ 384 ProxiPlate function (excitation at 680 nm, 0.18 sec; emission at 570 nm, 0.37 sec) and the results recorded.

Protein/ligand crystallography

Protein Preparation

CBP^{BRD} was purified as previously described and concentrated to 10 mg/mL. The ligand dissolved in a 100 mM DMSO was added to the protein solution and incubated on ice for 30 mins at 5 times the molar excess to ensure complete complexation. The protein-ligand solution was centrifuged 12,000 XG for 5 mins at 4 °C to remove

aggregates.

Crystallization Conditions

Crystallization trials were set up using the sitting drop vapor diffusion method in Intelli-Plate 96-3 low-profile plates. The crystallization drops were dispensed using an OryxNano (Douglas Instruments) robot. For each condition, two drops were prepared: the first drop contained 33% protein solution, and the second drop contained 50% protein solution, with a total drop size of 600 nL.

The following crystallization conditions provided diffraction quality crystals which then were used to produce the structures displayed in this thesis:

Conditions for AMB_C_62 = reservoir solution: 0.2 M ammonium acetate, 0.1 M Tris pH 8.5, 25% *w*/*v* polyethylene glycol 3,350.

Conditions for ELN123758 = reservoir solution: 0.3 M Li_2SO_4, 0.1 M Tris pH 8, 15% *w*/*v* polyethylene glycol 3,350.

Conditions for ELN122375 = reservoir solution: 0.1 M citric acid pH 3.5, 25% *w*/*v* polyethylene glycol 3,350.

Conditions for AMB_D_15 = Reservoir solution: 0.1 M HEPES pH 7.5, 25% *w*/*v* polyethylene glycol 3,350.

Conditions for AMB_C_56 = Reservoir solution: 5% Tacsimate pH 7, 0.1 M Hepes pH 7, 10% w/v Polyethylene glycol monomethyl ether 5,000.

Crystallisation

Each well of the Intelli-Plate was filled with 50 µL of the reservoir solution. A total of

600 nL of the protein-ligand solution was dispensed as a drop into wells of the plate, which were then sealed with clear tape to prevent evaporation and incubated at 8 °C. Diffractable crystals grew within 2 days to 1 week after crystallization setup. The drops were monitored periodically using a light microscope to check for the formation of crystals. Once crystals appeared, they were harvested using nylon loops and cryoprotected with the appropriate reservoir solution containing 10% (*R*,*R*)-2,3-butanediol before being flash-cooled in liquid nitrogen and then shipped to ESRF for analysis.

Data Collection and Analysis

X-ray diffraction data were collected at the ESRF at different beamlines (ID30B, ID23-2, BM07). The crystals were measured using a cryostream at 100 K. Data were processed using the ESRF autoprocessing pipeline with Autoproc. Additional software used for data processing and structure determination included:

- Aimless: For scaling and merging of diffraction data.
- Molrep: For molecular replacement (Initial model used PDB-ID: 5NU3) to determine the initial phases.
- Phaser: For molecular replacement and phase determination.
- Phenix refine: For automated refinement of the crystal structure. Coot: For manual model building and validation.

Physiochemical Property analysis

Below is a short description of the physiochemical analyses performed by GSK.

CAD solubility assay

GSK in-house kinetic solubility assay: 5 µL of 10 mM DMSO stock solution is diluted to 100 µL with pH 7.4 phosphate buffered saline, equilibrated for 1 hour at room temperature and filtered through Millipore Multiscreen$_{HTS}$-PCF filter plates (MSSL BPC). The filtrate is quantified by suitably calibrated Charged Aerosol Detector.[140] The standard error of the CAD solubility determination is ±30 µM, the upper limit of the solubility is 500 µM when working from 10 mM DMSO stock solution.

Artificial Membrane Permeability assay

Technique to measure the permeability of a compound in a phospholipid bilayer system

The lipid is egg phosphatidyl choline (1.8%) and cholesterol (1%) dissolved in *n*-decane. This is applied to the bottom of the microfiltration filter inserts in a Transwell plate. Phosphate buffer (50 mM Na_2HPO_4 with 0.5% 2-hydroxypropyl-β-cyclodextrin), pH 7.4 is added to the top and bottom of the plate. The lipids are allowed to form bilayers across the small holes in the filter. Permeation experiment is initiated by adding the compound to the bottom well and stopped at a pre-determined elapsed time. The compound permeates through the membrane to enter the acceptor well. The compound concentration in both the donor and acceptor compartments is determined by liquid chromatography after 3 h incubation at room temperature.[139,150] The permeability ($logP_{app}$) measuring how fast molecules pass through the black lipid membrane is expressed in nm/s. The average standard error of the assay is around ±30 nm/s; this can be higher at the low permeability range.

Lipophilicity: ChromlogD assay

The Chromatographic Hydrophobicity Index (CHI) values are measured using reversed phase HPLC column (50 x 2 mm 3 µM Gemini NX C_{18}, Phenomenex, UK) with fast acetonitrile gradient at starting mobile phase of pHs 2, 7.4 and 10.5.[151] CHI values are derived directly from the gradient retention times by using a calibration line obtained for standard compounds. The CHI value approximates to the volume % organic concentration when the compound elutes. CHI is linearly transformed into ChromlogD by least-square fitting of experimental CHI values to calculated ClogP values for over 20K research compounds using the following formula: ChromlogD = 0.0857CHI-2.00. The average error of the assay is ±3 CHI unit or ±0.25 ChromlogD.[138]

Protein binding assay (HSA and AGP)

Chemically bonded Human Serum Albumin (HSA) and alpha-1-acidglycoprotein (AGP) HPLC stationary phases (Chiral Technologies, France) are used for measuring compounds' binding to plasma proteins, applying linear gradient elution up to 30% *iso*-propanol. The run time is 6 minutes including the re-equilibration of the stationary phases with the 50 mM pH7.4 ammonium acetate buffer. The gradient retention times are standardised using a calibration set of mixtures as described in the reference.[152] The average standard error of the assay depends on the binding strength and kinetic of the compounds. It ranges from ±5% in the medium binding range which reduces to 0.1% at binding above 99% with fast kinetic.

Phospholipid binding assay (IAM)

The binding of compounds to immobilised artificial membrane (IAM) is measured using commercially available IAM PC DD2 100 x 4.6mm 10 µM (Regis Analytical, West Lafayette, USA) HPLC column. Gradient retention times obtained by applying

acetonitrile gradient up to 85% are converted to Chromatographic Hydrophobicity Indices (CHI IAM) using a calibration set of compounds as described by Valko *et al*.[153] The CHI IAM values are converted to the logarithmic retention factors using the following formula: log k IAM = 0.046*CHI IAM + 0.42, that was obtained from the correlation of isocratic and gradient retention time.[153]

ASSAY	ERROR
CAD Solubility	+/- 30 uM
AMP Permeability	+/- 30 nm/s
ChromLogD	+/- 0.3
HSA % binding	+/- 5%, +/- 0.1% when above 99%

ASSAY	Low	Medium	High
Kinetic Solubility	< 30uM	30-200 uM	> 200uM
AMP	< 30nm/s	30-200 nm/s	> 200nm/s

7.2 Synthetic Methods

7.2.1 Materials

Chemicals

All chemicals were purchased from the following list of suppliers: Alfa Aesar, Sigma Aldrich UK, Fluorochem, Chem Cruz, Thermo scientific, Fluka UK, Merck Millipore and Fisher Chemical. All small reagents were of ≥95% purity, solvents were of at least reagent grade when performing reactions, HPLC grade or higher purity solvents were utilised for semi-preparative LC, HPLC and LC-MS. Zinc and iron metal powders were activated by either washing with concentrated $HCl_{(aq)}$ (37%) three times, followed by water, ethanol and then Et_2O three times and then dried or *via* reaction/entrainment with TMSCl, 1,2-dibromoethane, iodine or bromine.[154–156] All reactions with non-aqueous solvents were performed in a flask under an argon atmosphere unless otherwise stated.

Anhydrous solvents

These include DMF, THF, Et_2O, CH_2Cl_2, toluene and NEt_3 were dried by passing through a column of activated basic alumina according to Grubbs' procedure.[157] These solvents were then left overnight on activated molecular sieves under an argon atmosphere. In the case of anhydrous DMSO, MeOH and MeCN, these were purchased from Sigma Aldrich UK in SureSeal™ bottles and were used without further purification. Some solvents (particularly for cross coupling reactions) were degassed using argon for 15 minutes prior to use.

7.2.2 Methods

NMR Spectroscopy

All solvents used for NMR spectroscopy were ≥99.8% deuterated and were purchased from Eurisotope, VWR chemicals, and Sigma Aldrich UK. NMR data were processed using MestReNova 14.2.0, ACD Spectrus Version 2022 or Bruker Topspin 4.0.5 software.

^{1}H NMR

Spectra were recorded on a Bruker AVIIIHD 400 nanobay (400 MHz) spectrometer, Bruker AVII500 (500 MHz) spectrometer with dual ^{13}C(^{1}H) cryoprobe, Bruker AVIIHD 500 (500MHz) spectrometer in the stated solvents as a reference for the internal deuterium lock or Bruker NEO 600 (600 MHz) spectrometer with broadband helium cryoprobe. The chemical shift for each signal is given as δ_H in units of parts per million (ppm) relative to tetramethylsilane (δ_c = 0.00 ppm) and the spectra were calibrated using the solvent peak(s) and the known chemical shifts.[158] The coupling constants are determined by analysis using picked peaks on MestReNova version 14.3.0 software or ACD Spectrus Version 2022. ^{1}H NMR spectra are reported as follows: chemical shift (number of protons, multiplicity (s (singlet); br s (broad singlet); d (doublet); t (triplet); q (quartet); m (multiplet) or combinations thereof), coupling constants *J* (to the nearest 0.1 Hz, with identical coupling constants averaged), assignment). The ^{1}H are assigned using COSY, HSQC and NOESY experiments as appropriate.

^{13}C NMR

Spectra were recorded on a Bruker AVIIIHD 400 nanobay (101 MHz) spectrometer, Bruker AVII500 (500 MHz) spectrometer with dual ^{13}C(^{1}H) cryoprobe in the stated

solvent with broadband proton decoupling and an internal deuterium lock, or Bruker NEO 600 (151 MHz) spectrometer with broadband proton decoupling. All ^{13}C NMR spectra were run as proton decoupled and so no multiplicities, or coupling constants are given. Chemical shifts for each signal are given as δ_C in units of parts per million (ppm) relative to tetramethylsilane (δ_C = 0.00 ppm) and the spectra were calibrated using the solvent peak(s) and the known chemical shifts.[158] Peaks were picked using the MestReNova 14.2.0 software or ACD Spectrus Version 2022. The carbon nuclei were assigned using HSQC and HMBC experiments as appropriate.

^{19}F NMR

Spectra were recorded on a Bruker AVIIHD 400 nanobay (376 MHz) spectrometer using a deuterium internal lock. The chemical shift for each signal is given as δ_F in units of parts per million (ppm). The multiplicity of each signal is indicated by: s (singlet); d (doublet); t (triplet); q (quartet) or m (multiplet). Coupling constants (*J*) are quoted in Hz and reported to the nearest 0.1 Hz. The coupling constants are determined by analysis using picked peaks on MestReNova version 14.3.0 software.

^{11}B NMR

Spectra were recorded on a Bruker AVIIIHD 400 nanobay (128 MHz) Bruker or a NEO 600 (193 MHz) spectrometer using boron trifluoride diethyl etherate as an external reference standard. The chemical shift for each signal is given as δ_B in units of parts per million (ppm). Due to the broad nature of spin 3/2 nuclei multiplicities are not given. The chemical shifts were determined using the MestReNova 14.2.0 software. Due to the NMR tubes being made of borosilicate glass all spectra appear with a large chemical shift at ~ -30 ppm.

Chromatography and mass spectrometry

Below are the methods carried out for chromatographic and mass spectrometry analysis. HPLC and Semi-preparative LC were analysed using Agilent OpenLab Chemstation software While LC-MS and low-resolution MS were analysed using MestReNova 14.2.0 software and Mass Lynx version 4.2.

TLC

TLC analysis was carried out on normal phase Merck Silica gel 60 F_{254} aluminium-supported chromatographic sheets or POLYGRAM® SIL G/UV_{254} plates with a 0.2 mm silica gel layer with fluorescent indicator produced by machery-nagel. Visualisation was by: UV light absorption (λ_{max} 254 or 365 nm) using a UVItec lamp inside of a black box or by chemical staining using iodine vapour, or thermal development after dipping into ethanolic ninhydrin or aqueous potassium permanganate.

Normal phase silica gel flash column chromatography

This technique was performed either by manual column chromatography using Geduran® (Merck Millipore) silica gel 60 (40-63 μM) or on a Biotage SP1 automated column chromatography system using KP-Sil® SNAP Flash silica cartridges. The system used during the synthesis of macrolactams YY5-10 was the Teledyne ISCO CombiFlash® Rf^+ purification system using RediSep® silver columns between 5-12 g of silica system.

Semi-preparative liquid chromatography

Compounds that were purified using semi-preparative liquid chromatography (Semi-prep LC) were dissolved in the minimum amount of MeCN with some samples containing 20% *v*/*v* IPA or DMSO to aid in dissolving of compounds. The solution was then filtered through a Fisherbrand PTFE syringe filter (30 mm, 0.2 μM) into an Agilent

5 mL semi prep vial with a pre-slit cap. Then the samples were purified using an Agilent 1260 Infinity II Semi Prep system with an Agilent prep C_{18} [5 μM, 50 × 21.2 mm] column, the flow rate was kept constant at 20 mL min^{-1}, the column was at room temperature and UV detection was carried out at 254 nm. The mobile phases used unless otherwise stated were MilliQ water (mobile phase A) and HPLC grade MeCN (mobile phase B). The gradient utilised was as follows: 0-1 min hold at 5% mobile phase B, 1-10 mins 5-95% mobile phase B, then a varied length of hold at 95% mobile phase B up to 20 mins. After purification the fractions were collected and lyophilised to give the products as colourless solid powders. The injection volume was varied between purifications ranging from 50-1000 μL depending upon the level of resolution of the chromatograms. The macrolactam compounds **14-19** and their intermediates **31-35** and **38** were purified using an ACCQPrep purification was performed on Teledyne ACCQPrep HP150 purification system with an attached AS 2×2 Autosampler. For the same series of macrocycles and intermediates and in-house mass directed purification system (MDAP) was used at GSK. ACCQPrep methods and MDAP methods are tabulated below with extended and normal methods listed consecutively where appropriate. The flow rate for all MDAP and ACCQPrep methods is maintained at 40 mL/min, each method below has a separate table with a caption describing the solvents utilised.

High pH (HpH) Method C: constant flow rate of 40 mL/min, with solvent A: 10 mM *aq*. ammonium bicarbonate at pH 10; solvent B: MeCN.

Time	Percentage solvent A, %	Percentage solvent B, %
0.0	70	30
3.0	70	30

12.0	15	85
12.5	15	85
13.0	1	99
17.0	1	99

High pH (HpH) Method C extended: constant flow rate of 40 mL/min, with solvent A: 10 mM *aq*. ammonium bicarbonate at pH 10; solvent B: MeCN.

Time	Percentage solvent A, %	Percentage solvent B, %
0.0	70	30
3.0	70	30
22.0	15	85
22.5	15	85
23.0	1	99
27.0	1	99

High pH (HpH) Method D: constant flow rate of 40 mL/min, with solvent A: 10 mM *aq*. ammonium bicarbonate at pH 10; solvent B: MeCN.

Time	Percentage solvent A, %	Percentage solvent B, %
0.0	50	50
3.0	50	50
9.0	1	99
17.0	1	99

High pH (HpH) Method E: constant flow rate of 40 mL/min, with solvent A: 10 mM *aq*. ammonium bicarbonate at pH 10; solvent B: MeCN.

Time	Percentage solvent A, %	Percentage solvent B, %
0.0	20	80
3.0	20	80
9.0	1	99
17.0	1	99

High pH (HpH) Method E extended: constant flow rate of 40 mL/min, with solvent A: 10 mM *aq*. ammonium bicarbonate at pH 10; solvent B: MeCN.

Time	Percentage solvent A, %	Percentage solvent B, %
0.0	20	80
3.0	20	80
16.0	1	99
27.0	1	99

Formic acid (FA) Method C: constant flow rate of 40 mL/min, with solvent A: *aq*. 0.1% *v*/*v* formic acid; solvent B: 0.1% *v*/*v* formic acid in MeCN

Time	Percentage solvent A, %	Percentage solvent B, %
0.0	70	30
3.0	70	30
12.0	15	85
12.5	15	85

13.0	1	99
17.0	1	99

Formic acid (FA) Method D: constant flow rate of 40 mL/min, with solvent A: *aq*. 0.1% *v*/*v* formic acid; solvent B: 0.1% *v*/*v* formic acid in MeCN.

Time	Percentage solvent A, %	Percentage solvent B, %
0.0	50	50
3.0	50	50
9.0	1	99
17.0	1	99

The ACCQPrep methods copy the same gradients and solvent systems as those indicated for MDAP purifications.

HPLC purification chromatography

Compounds that were purified by HPLC were first dissolved in either pure MeCN or a mixture of MeCN and DMSO (4:1) and then filtered through either a Gilson PTFE syringe filter (13 mm, 0.22 µM) or Fisherbrand PTFE filter (13mm, 0.2µM) into an insert vial (300 µL total volume). Compounds were purified using an Agilent 1260 Infinity II system with a Quaternary LC Pump, DADWR and Agilent Infinity Fraction Collector. An Agilent Zorbax SB-C_{18} [5 µm, 9.4 mm × 250 mm] column heated to 40 °C with a constant flow rate of 4 mL min^{-1}, injecting volume of 25 µL and UV detection at a wavelength at or above 340 nm. The mobile phases were MilliQ water containing 0.1% *v*/*v* formic acid or MilliQ water (mobile phase A) and HPLC grade MeCN containing 0.1% *v*/*v* formic acid or MeCN without modifier (mobile phase B). The gradients utilised

were as follows: 0-2 min hold at 5% mobile phase B, 2-12 mins 5-95% mobile phase B, then a 5 mins of hold at 95% mobile phase B. After this hold a 5-minute post run was conducted of 95-5% mobile phase B in order to switch back to the starting conditions. Fractions of purified compound were either collected based upon retention time of threshold at a specified wavelength.

HPLC for purity and retention time

Compounds that were analysed for purity by HPLC were first dissolved in 1 mL of MeCN and were then filtered through either a Gilson PTFE syringe filter (13 mm, 0.22 μM) or Fisherbrand PTFE filter (13 mm, 0.2 μM) into a pre-slit Restek 1.5 mL vial. Compounds were analysed for purity on an Agilent 1260 Infinity II system with a Quaternary LC Pump, DADWR and Agilent Infinity Fraction Collector. An Agilent InfinityLab Poroshell 120 EC-C_{18} [4 μm, 4.6 mm × 150 mm] column heated to 40 °C was used along with constant flow rate of 1 mL min^{-1}, injection volume of 5 μL and UV detection at 220, 254 and 280 nm. The mobile phases used unless otherwise stated were MilliQ water containing 0.1% *v*/*v* formic acid (mobile phase A) and HPLC grade MeCN containing 0.1% *v*/*v* formic acid (mobile phase B). The gradients utilised were as follows: 0-1 min hold at 5% mobile phase B, 1-10 mins 5-95% mobile phase B, then a varied length of hold at 95% mobile phase B until 16 mins or 25 mins as required. After this hold a 3 min post run was conducted of 95-5% mobile phase B in order to switch back to the starting conditions. The purities of compounds are calculated based upon percentage peak area as an average of at least two wavelengths, with final compounds purities calculated from all three wavelengths, with all purities given to the nearest whole number.

Normal phase chiral HPLC

Final compounds were analysed by normal phase chiral HPLC to determine percentage enantiomeric excess (%ee). These analyses were performed using a PerkinElmer Flexar system with a Binary LC Pump and UV/Vis LC detector set at 254 nm. These analyses were performed using a ChiralPAK AD_H [5 μM, 4.6 mm × 250 mm] column with a constant flow rate of 1.0 mL min^{-1} and an isocratic method of IPA:hexane (50:50) for 30 mins. HPLC data were processed using Chromera 3.4.4 software.

Liquid Chromatography-Mass Spectrometry

For low resolution analysis when other methods of ionisation proved too harsh a Waters LCT Premier XE bench-top orthogonal acceleration TOF LC-MS was used, with the sample being dissolved in MeCN at ~1 mg mL^{-1}. Or a Waters Acquity I class plus UPLC® with a Water acquity QDA mass detector system was utilised as both a means of checking compound purity and getting LRMS data concurrently.

Low resolution electrospray ionisation (ESI) MS

Direct injection of a sample dissolved in MeCN at ~1 mg mL^{-1} into an Agilent 6120 quadrupole or aspectrometer was used in either positive or negative mode (as specified) to give low resolution mass spectra.

High resolution Mass Spectrometry

Either of the following instruments was used for high resolution MS: Bruker microToF (high resolution), or Waters BioAccord LC-MS (high resolution) spectrometer using ESI or electron ionisation (EI). Samples were dissolved in 1 mL of MeCN, filtered through a Gilson PTFE syringe filter (13 mm, 0.22 μM) or Fisherbrand PTFE filter (13

mm, 0.2 μM) and were then diluted to the appropriate concentration. *m/z* values are reported in Daltons and followed by their percentage abundance in parentheses.

Other Spectroscopic and miscellaneous techniques

FT-IR Spectroscopy

Were obtained from either neat samples (liquid or solid) or a concentrated solution in a low boiling point solvent which was then evaporated to give a thin film. The spectra were recorded using a Bruker Tensor 27 spectrometer or a PerkinElmer Spectrum 2 Spectrometer with the UATR TWO attached. Absorption maxima are reported in wavenumbers (cm^{-1}) and are reported as s (strong), m (medium), w (weak) or br (broad). Only the main relevant peaks are reported for each compound.

Specific optical rotations

Were determined using a Schmidt Haensch Unipol polarimeter or a JASCO p-1030 polarimeter, using a sodium lamp at 589 nm and a path length of 1.0 dm. The concentration (*c*) is expressed in g/100 mL (equivalent to g/0.1 dm^3). Specific rotations are quoted as an average of 10 measurements. They are denoted $[\alpha]_D^T$ and are given in implied units of 10^{-1} ° cm^2 g^{-1} (where T = ambient temperature in °C).

Melting points

Were determined using a Griffin capillary tube melting point apparatus and are uncorrected. The melting point range is given from first apparent phase change to fully melted. The crystallisation solvent is given in parentheses.

7.3 Synthetic Procedures

7.3.1 Chapter 2: Compounds **13 - 48**

4-Fluoro-3-iodo-5-nitrobenzoic acid (compound **20**)

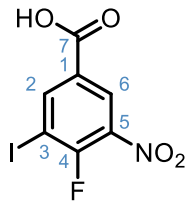

4-fluoro-3-nitro-benzoic acid (4.00 g, 21.6 mmol, 1.0 equiv.) was added to a solution of iodine (10.96 g, 43.2 mmol, 2.0 equiv.) in fuming sulfuric acid (40 mL) and the reaction mixture was stirred at 85 °C for 20 h. The cooled reaction mixture was slowly added portion wise to ice (500 g) and the resultant precipitate was extracted with CH_2Cl_2 (3 × 250 mL). The combined organic layers were washed with sat. $Na_2S_2O_{3(aq)}$ (3 × 250 mL), brine (250 mL), dried (Na_2SO_4), filtered and concentrated *in vacuo* to give 4-fluoro-3-iodo-5-nitrobenzoic acid as a colourless solid (6.116 g, 91%); R_f 0.15 (9:1, CH_2Cl_2/MeOH); m.p 172 – 175 °C (CH_2Cl_2); ^{1}H NMR (400 MHz, $CDCl_3$) δ_H 8.75 (1H, dd, *J* 5.0, 2.1 Hz, H-2), 8.73 (1H, dd, *J* 6.5, 2.1 Hz, H-6); ^{19}F{^{1}H} NMR (377 MHz, $CDCl_3$) δ_F −87.67; LRMS *m/z* (ESI$^-$) 310 ([M−H]$^-$, 100%). These data are in accordance with the literature.[88]

Benzyl 4-fluoro-3-iodo-5-nitrobenzoate (compound **21**)

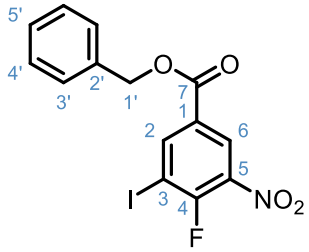

To a solution of 4-fluoro-3-iodo-5-nitrobenzoic acid (4.70 g, 15.1 mmol, 1.0 equiv.) in DMF (40 mL) was added K_2CO_3 (3.14 g, 22.7 mmol, 1.5 equiv.) and the reaction mixture was stirred at r.t. for 5 mins. Benzyl bromide (2.7 mL, 22.7 mmol, 1.5 equiv.) was added and the reaction mixture was stirred at 60 °C for 4 h. Once cooled the reaction mixture was diluted with EtOAc (500 mL) and was washed with 1M $K_2CO_{3(aq)}$ (3 × 500 mL), 0.5 M $LiCl_{(aq)}$ (3 × 500 mL), brine (500 mL), dried ($MgSO_4$), filtered and concentrated *in vacuo* to light orange oil. The crude product was purified by flash silica column chromatography (elution with 0-20% EtOAc in pet ether) to yield benzyl 4-fluoro-3-iodo-5-nitrobenzoate as an off-white solid (4.272 g, 70%); R_f 0.39 (4:1, pet ether/EtOAC); m.p 67 – 70 °C (EtOAc); ^{1}H NMR (400 MHz, $CDCl_3$) δ_H 8.69 (1H, dd, *J* 5.0, 2.1 Hz, H-2), 8.66 (1H, dd, *J* 6.6, 2.1 Hz, H-6), 7.48 – 7.34 (5H, m, H3', H-4', H-5'), 5.40 (2H, s, H-1'); ^{19}F{^{1}H} NMR (377 MHz, $CDCl_3$) δ_F −89.30; LRMS *m/z* (ESI^-) 400 ($[M-H]^-$, 100%). These data are in accordance with the literature.[88]

(*R*)-*tert*-Butyl 3-(benzyl((*R*)-1-phenylethyl)amino)butanoate (compound **22**)

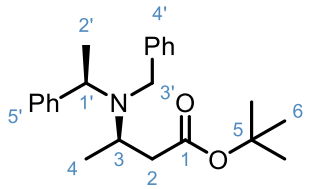

To a stirred solution of (*R*)-*N*-benzyl-1-phenylenthan-1-amine (4.46 g, 21.1 mmol, 1.5 equiv.) in THF (25 mL) at −78 °C was added *n*-BuLi in hexanes (2.5 M, 9.02 mL, 22.5 mmol, 1.6 equiv.), dropwise over 20 mins and the resultant dark pink solution was stirred at −78 °C for 30 mins. *tert*-Butyl crononate (2.26 mL, 2.00 g, 14.1 mmol, 1.0 equiv.) in THF (20 mL) was added dropwise over a period of 1 h and the reaction mixture was then stirred for a further 4 h. The reaction mixture was quenched with sat. $NH_4Cl_{(aq)}$ (20 mL) and was subsequently warmed to r.t. The reaction mixture was

evaporated *in vacuo* then 0.5 M citric acid$_{(aq)}$ (75 mL) was added, and the resultant mixture was extracted with CH_2Cl_2 (3 × 100 mL). The combined organic components were washed with sat. $NaHCO_{3(aq)}$ (150 mL), brine (150 mL), dried (Na_2SO_4), filtered and concentrated *in vacuo* to give a colourless oil. The crude oil was purified by flash silica column chromatography (elution with 0-5% Et_2O in pet ether) to give (*R*)-*tert*-Butyl 3-(benzyl((*R*)-1-phenylethyl)amino)butanoate as a colourless oil (4.42 g, 89%); R_f 0.56 (1:9, Et_2O/hexane); $[\alpha]_D^{25.9}$ = −10.6 (*c* 2.1, $CHCl_3$); ^{1}H NMR (400 MHz, $CDCl_3$) δ_H 7.44 – 7.18 (10H, m, H-5', H-4'), 3.90 (1H, q, *J* 6.9 Hz, H-1'), 3.77 (1H, d, *J* 15.0 Hz, H_AH_B-3'), 3.62 (1H, d, *J* 15.0 Hz, H_AH_B-3'), 3.44 (1H, dqd, *J* 9.1, 6.7, 4.7 Hz, H-3), 2.26 (1H, dd, *J* 14.1, 4.7 Hz, H_AH_B-2), 2.03 (1H, dd, *J* 14.1, 9.1 Hz, H_AH_B-2), 1.40 (9H, s, H-6), 1.34 (3H, d, *J* 6.9 Hz, H-2'), 1.12 (3H, d, *J* 6.7 Hz, H-4); LRMS *m/z* (ESI$^+$) 354 ([M+H]$^+$, 100%). These data are in accordance with the literature.[44,88,159]

(*R*)-*tert*-Butyl 3-aminobutanoate (compound **23**)

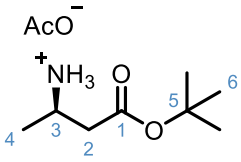

20 % $Pd(OH)_2$/C (1.74g, 2.49 mmol, 0.2 equiv.) was added to a stirred solution of (*R*)-*tert*-butyl 3-(benzyl((*R*)-1-phenylethyl)amino)butanoate (4.40 g, 12.4 mmol, 1.0 equiv.) in H_2O (7.1 mL), glacial acetic acid (4.46 mL) and MeOH (176 mL), which was purged under an argon atmosphere. The atmosphere was then replaced with hydrogen gas and the suspension was stirred at r.t. for 20 h. The reaction mixture was filtered through a pad of Celite® (eluent MeOH) and evaporated *in vacuo* to give a yellow oil. The oil was azeotroped with toluene (3 × 50 mL) to give (*R*)-*tert*-butyl 3-aminobutanoate containing 1.39 equiv. acetic acid as a colourless solid (2.334 g, 86%); R_f 0.04 (9:1, CH_2Cl_2/MeOH); $[\alpha]_D^{25}$ = −11.5 (*c* 1.0, $CHCl_3$); ^{1}H NMR (400 MHz, $CDCl_3$) δ_H 3.55 – 3.42

(1H, m, H-3), 2.55 (1H dd, *J* 16.6, 7.3 Hz, H_AH_B-2), 2.45 (1H, dd, *J* 16.5, 5.7 Hz, H_AH_B-2), 1.44 (9H, s, H-6), 1.27 (3H, d, *J* 6.6 Hz, H-4); LRMS *m/z* (ESI^+) 160 ($[M+H]^+$, 100%). These data are in accordance with the literature.[44,88,159]

Benzyl (*R*)-4-((4-(*tert*-butoxy)-4-oxobutan-2-yl)amino)-3-iodo-5-nitrobenzoate (compound **24**)

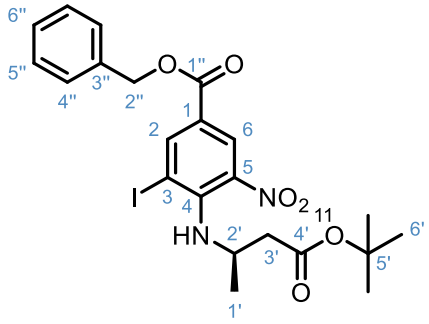

To a stirred solution of 4-fluoro-3-iodo-5-nitro-benzoate (3.05 g, 7.60 mmol, 1.0 equiv.) and Cs_2CO_3 (7.40 g, 22.8 mmol, 3.0 equiv.) in toluene (70 mL) at r.t. was added *tert*-butyl (*R*)-aminobutanoate (2.33 g, 10.6 mmol, 1.4 equiv.) and the reaction was stirred at 85 °C for 20 h. Once cooled the reaction mixture was added to 1M $K_2CO_{3(aq)}$ (500 mL) and the resulting mixture was extracted with EtOAc (3 × 250 mL). The combined organic layers were washed with brine (250 mL), dried ($MgSO_4$), filtered and evaporated *in vacuo* to give an orange oil. The crude product was purified by flash silica column chromatography (10% Et_2O in n-hexane) to yield (*R*)-4-((4-(*tert*-butoxy)-4-oxobutan-2-yl)amino)-3-iodo-5-nitrobenzoate as a dark orange oil (3.99 g, 97%); R_f 0.2 (1:4, Et_2O/hexane); $[\alpha]_D^{25}$ = −29.3 (*c* 0.8, $CHCl_3$); ^{1}H NMR (400 MHz, $CDCl_3$) δ_H 8.59 (1H, d, *J* 2.1 Hz, H-6), 8.55 (1H, d, *J* 2.1 Hz, H-2), 7.46 – 7.31 (5H, m, H-4'', H-5'', H-6''), 6.39 (1H, d, *J* 10.0 Hz, NH-4), 5.34 (2H. s, H-2''), 4.16 (1H, m, H-2'), 2.52 (1H, dd, *J* 15.5, 5.7 Hz, H_AH_B-3'), 2.45 (1H, dd, *J* 15.5, 5.9 Hz, H_AH_B-3'), 1.39 (9H, s, H-6'), 1.31 (3H, d, *J* 6.4 Hz, H-1'); LRMS *m/z* (ESI^-) 539 ($[M-H]^-$, 100%). These data are in accordance with the literature.[88]

(*R*)-9-Iodo-2-methyl-4-oxo-2,3,4,5-tetrahydro-1*H*-benzo[*b*][1,4]diazepine-7-carboxylate (compound **25**)

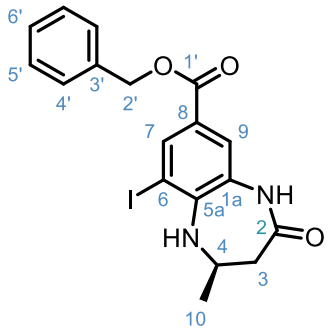

To a solution of (*R*)-4-((4-(*tert*-butoxy)-4-oxobutan-2-yl)amino)-3-iodo-5-nitrobenzoate (3.77 g, 6.98 mmol, 1.0 equiv.) in CH_2Cl_2 (18 mL) was added TFA (18 mL) and the reaction stirred at r.t. for 2 h. The solvents were then removed *in vacuo* and the resulting dark orange oil was dissolved in glacial acetic acid (42 mL). To this was added iron powder (1.95 g, 34.9 mmol, 5.0 equiv.) and the reaction was heated to reflux (120 °C) for 4 h. To the cooled reaction mixture was added 1 M K_2CO_3 (500 mL) and the resulting mixture was extracted with EtOAc (3 × 500 mL). The combined organic components were washed with brine (500 mL), dried ($MgSO_4$), filtered and evaporated *in vacuo* to yield (*R*)-9-iodo-2-methyl-4-oxo-2,3,4,5-tetrahydro-1*H*-benzo[*b*][1,4]diazepine-7-carboxylate as a colourless solid (3.04 g, 91%); R_f 0.55 (EtOAc); $[\alpha]_D^{25}$ = −20.4 (*c* 1.0, $CHCl_3$); m.p; 166 – 168 °C; ^{1}H NMR (400 MHz, DMSO) δ_H 9.73 (1H, s, NH-9a), 8.03 (1H, d, *J* 2.0 Hz, H-7), 7.58 (1H, d, *J* 2.0 Hz, H-9), 7.46 – 7.32 (5H, m, H-4', H-5', H-6'), 5.28 (2H, s, H-2'), 5.15 (1H, d, *J* 3.1 Hz, NH-5a), 4.07 (1H, m, H-4), 2.50 (1H, dd, *J* 13.9, 8.1 Hz, H_AH_B-3), 2.39 (1H, dd, *J* 13.9, 8.1 Hz, H_AH_B-3), 1.29 (3H, d, *J* 6.3 Hz, H-10); LRMS *m/z* (ESI$^-$) 435 ([M−H]$^-$, 100%). These data are in accordance with the literature.[88]

7-((Triisopropylsilyl)oxy)-3,4-dihydroquinolin-2(1*H*)-one (compound **26**)

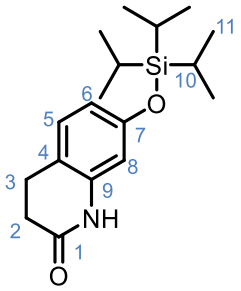

Triisopropylsilyl chloride (6.81 mL, 31.8 mmol, 1.3 equiv.) was added to a solution of 7-hydroxy-3,4-dihydroquinolin-2(1H)-one (4.00 g, 24.6 mmol, 1.0 equiv.) and imidazole (3.34 g, 49.2 mmol, 2.0 equiv.) in DMF (30 mL) and the reaction mixture was stirred at r.t. for 24 h. The reaction mixture was dissolved in Et_2O (150 mL) and washed with H_2O (3 × 100 mL). The organic component was washed with brine (100 mL), dried ($MgSO_4$), filtered and evaporated *in vacuo* to afford a colourless oil. The crude oil was purified by silica gel chromatography (elution with 0-50% EtOAc in pet ether) to yield 7-((triisopropylsilyl)oxy)-3,4-dihydroquinolin-2(1*H*)-one as a colourless solid (6.52 g, 96%); R_f 0.50 (1:1, EtOAc/pet ether); mp 65 − 67 °C (EtOAc); $\bar{\nu}_{max}$ (neat)/cm^{-1} 3918 (N-H, w), 2960 (C-H, w), 1673 (C=O, s), 1174 (C-O, s); ^{1}H NMR (500 MHz; $CDCl_3$) δ_H 8.09 (1H, s, NH-9), 6.96 (1H, d, *J* 8.4, H-5), 6.49 (1H, dd, *J* 8.4, 2.4, H-6), 6.32 (1H, d, *J* 2.4, H-8), 2.88 (2H, dd, *J* 8.4, 6.6, H-3), 2.61 (2H, dd, *J* 8.4, 6.6, H-2), 1.28-1.20 (3H, m, H-10), 1.10 (18H, d, *J* 7.4, H-11); ^{13}C NMR (101 MHz; CDCl3) δ_C 171.78 (C-1), 155.7 (C-7), 138.1 (C-9), 128.7 (C-5), 116.2 (C-4), 114.3 (C-6), 107.3 (C-8), 31.2 (C-2), 24.8 (C-3), 18.1 (C-10), 12.8 (C-11); HRMS *m/z* (ESI^+) [Found: 320.2040 $C_{18}H_{29}NO_2{}^{28}Si$ requires $[M+H]^+$ 320.2040)]; LRMS *m/z* (ESI^+) 320 ($[M+H]^+$, 100%); HPLC: retention time 12.51 mins, purity >99.9 %. These data are in accordance with the literature.[88]

7-((Triisopropylsilyl)oxy)-1,2,3,4-tetrahydroquinoline (compound **27**)

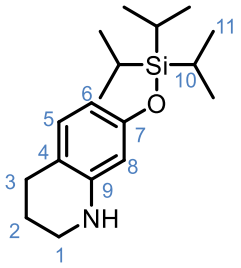

7-((triisopropylsilyl)oxy)-3,4-dihydrodroquinolin-2(1*H*)-one (6.50 g, 18.5 mmol, 1.0 equiv.) was dissolved in Et_2O (50 mL) and added portion wise to $LiAlH_4$ (1.05 g, 27.7 mmol, 1.5 equiv.) in Et_2O (50 mL) at 0 °C and the suspension was stirred at 0 °C for 10 mins. The suspension was then warmed to room temperature and was left to stir for 4 h. The reaction was then returned to 0 °C and H_2O (1.5 mL), followed by 15 wt% $NaOH_{(aq)}$ (1.5 mL) and H_2O (4 mL) were added dropwise. $MgSO_4$ was added, and the suspension was stirred at room temperature for 30 minutes. The reaction was filtered and was diluted with ethyl acetate (200 mL). This was evaporated in *vacuo* to afford a colourless oil. This was then purified by flash silica column chromatography (elution with 0-10% EtOAc in pet ether) to yield 7-((triisopropylsilyl)oxy)-1,2,3,4-tetrahydroquinoline as a colourless oil (4.17 g, 97%). R_f 0.50 (1:9, EtOAc/pet ether); $\bar{\nu}_{max}$ (neat)/cm^{-1} 3410 (N-H, w), 2943 (C-H, w), 1183 (C-O, s); ^1H NMR (400 MHz; $CDCl_3$) δ_H 6.75 (1H, dt, *J* 8.1, 1.0 Hz, H-5), 6.16 (1H, dd, *J* 8.1, 2.4 Hz, H-6), 6.03 (1H, d, *J* 2.4 Hz, H-8), 3.82 (1H, br s, NH-9) 3.29 – 3.22 (2H, m, H-1), 2.72 – 2.64 (2H, m, H-3), 1.96 – 1.86 (2H, m, H-2), 1.31 – 1.15 (3H, m, H-10), 1.13 – 1.02 (18H, d, *J* 7.4, H-11); LRMS *m/z* (ESI^+) 306 ($[M+H]^+$, 100%); HPLC: retention time 13.64 mins, purity 96.5%. These data are in accordance with the literature.[88]

Pent-4-yn-1-yl methanesulfonate (compound **28**)

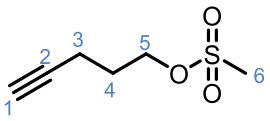

To 4-pentyn-1-ol (2.20 mL, 23.8 mmol, 1.0 equiv.), trimethylamine (6.64 mL, 47.8 mmol, 2.0 equiv.) in dichloromethane (20 mL) at 0 °C was added mesyl chloride (2.76 mL, 35.6 mmol, 1.5 equiv.) dropwise and stirred for 10 mins. The reaction was warmed to room temperature and stirred for 3.5 h. The reaction was diluted with dichloromethane (100 mL), was washed with water (3 × 100 mL), sat. $NaHCO_{3(aq)}$ (100 mL), brine (100 mL) and dried ($MgSO_4$), filtered, and then concentrated. This gave pent-4-yn-1-yl methanesulfonate as a brown oil (4.45 g, 95%). R_f 0.40 (2:3, EtOAc/pet ether); ^{1}H NMR (400 MHz, $CDCl_3$) δ_H 4.34 (2H, t, *J* 6.1 Hz, H-5), 3.01 (3H, s, H-6), 2.35 (2H, td, *J* 6.8, 2.7 Hz, H-3), 2.00 (1H, t, *J* 2.7 Hz, H-1), 1.95 (2H, tt, *J* 6.8, 6.1, H-4); LRMS *m/z* (ESI^-) 163 ($[M+H]^-$, 100%). These data are in accordance with the literature.[88]

1-(Pent-4-yn-1-yl)-7-((triisopropylsilyl)oxy)-1,2,3,4-tetrahydroquinoline (compound **29**)

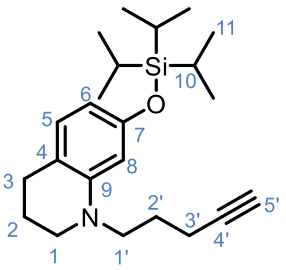

Pent-4-yn-1-yl methanesulfonate (3.90 g, 21.0 mmol, 1.5 equiv.), was added to a solution of 7-((triisopropylsilyl)oxy)-1,2,3,4-tetrahydroquinoline (5.20 g, 14.0 mmol, 1.0 equiv.), TBAI (3.23 g, 8.75 mmol, 0.6 equiv.), and DIPEA (5.94 mL, 28.0 mmol, 2.00 equiv.) in dry DMF (80 mL) under an argon atmosphere. The reaction mixture was then heated to 100 °C for 48 h. The cooled solution was diluted in diethyl ether (500 mL),

which was then washed with water (3 × 300 mL). The organic layer was then washed with brine (300 mL), dried over $MgSO_4$, filtered, and concentrated in *vacuo*. This gave a crude orange oil which was then purified using flash silica gel column chromatography (100% toluene) to give 1-(pent-4-yn-1-yl)-7-((triisopropylsilyl)oxy)-1,2,3,4-tetrahydroquinoline as a light orange oil (4.786 g, 76%); R_f 0.71 (tol); $\bar{\nu}_{max}$ (neat)/cm^{-1} 2943 (C-H, w), 1506 (s); ^1H NMR (400 MHz; $CDCl_3$) δ_H 6.75 (1H, dt, *J* 8.0, 1.0 Hz, H-5), 6.17 (1H, d, *J* 2.3 Hz, H-8), 6.12 (1H, dd, *J* 8.0, 2.3 Hz, H-6), 3.37 – 3.30 (2H, m, H-1'), 3.29 – 3.22 (2H, m, H-1), 2.68 (2H, t, *J* 6.3 Hz, H-3), 2.26 (2H, td, *J* 7.0, 2.7 Hz, H-3'), 1.99 (1H, t, *J* 2.7 Hz, H-5'), 1.95 -1.89 (2H, m, H-2), 1.81 (2H, p, *J* 7.0 Hz, H-2'), 1.32 – 1.19 (3H, m, H-10), 1.12 (18H, d, *J* 7.2 Hz, H-11); LRMS *m/z* (ESI+) 372 ($[M+H]^+$, 100%); HPLC: retention time 16.15 mins, purity 97.2 %. These data are in accordance with the literature.[88]

(*E*)-1-(5-(4,4,5,5-Tetramethyl-1,3,2-dioxaborolan-2-yl)pent-4-en-1-yl)-7-((triisopropylsilyl)oxy)-1,2,3,4-tetrahydroquinoline (compound **30**)

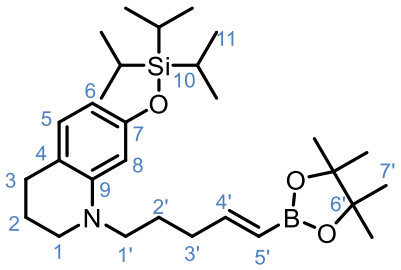

1-(Pent-4-yn-1-yl)-7-((triisopropylsilyl)oxy)-1,2,3,4-tetrahydroquinoline (310 mg, 1.04 mmol, 1.00 equiv.) and bis(cyclopentadienyl)zirconium$^{(IV)}$ chloride hydride (22 mg, 0.104 mmol, 0.1 equiv.) were added to a microwave vial (in the absence of light) and sealed under an argon atmosphere. Triethylamine (25.0 µL, 0.104 mmol, 0.1 equiv.) and 4,4,5,5-tetramethyl-1,3,2-dioxaborolane (134 µL, 1.14 mmol, 1.10 equiv.) were added and the reaction mixture was stirred at 60 °C for 18 h. The reaction mixture was

purified by flash silica gel column chromatography (elution with 0-100% CH_2Cl_2 in pet ether) to yield (*E*)-1-(5-(4,4,5,5-tetramethyl-1,3,2-dioxaborolan-2-yl)pent-4-en-1-yl)-7-((triisopropylsilyl)oxy)-1,2,3,4-tetrahydroquinoline as a brown oil (363 mg, 87 %); R_f 0.41 (1:9, EtOAc/pet ether); $\bar{\nu}_{max}$ (neat)/cm^{-1} 2942 (C-H, w), 1506 (s); ^{1}H NMR (400 MHz; $CDCl_3$) δ_H 6.73 (1H, dt, *J* 8.8, 1.3 Hz, H-5), 6.65 (1H, dt, *J* 18.0, 6.4 Hz, H-4'), 6.13 – 6.06 (2H, m, H-6, H-8), 5.47 (1H, d, *J* 18.0 Hz, H-5'), 3.26 – 3.14 (4H, m, H-1', H-1), 2.65 (2H, t, *J* 6.4 Hz, H-3), 2.24 – 2.16 (2H, m, H-3'), 1.92 – 1.89 (2H, m, H-2), 1.71 (2H, tt, *J* 8.5, 6.4 Hz, H-2'), 1.27 (12H s, H-7'), 1.26 – 1.20 (3H, m, H-10), 1.15 – 1.09 (18H, d, *J* 7.3 Hz, H-11); ^{11}B NMR (128 MHz, $CDCl_3$) δ_B 29.7 (B-5'); LRMS *m/z* (ESI$^+$) 500 ([M+H]$^+$, 100%). These data are in accordance with the literature.[88]

(*R*,*E*)-2-Methyl-4-oxo-9-(5-(7-((triisopropylsilyl)oxy)-3,4-dihydroquinolin-1(2*H*)-yl)pent-1-en-1-yl)-2,3,4,5-tetrahydro-1*H*-benzo[*b*][1,4]diazepine-7-carboxylate (compound **13**)

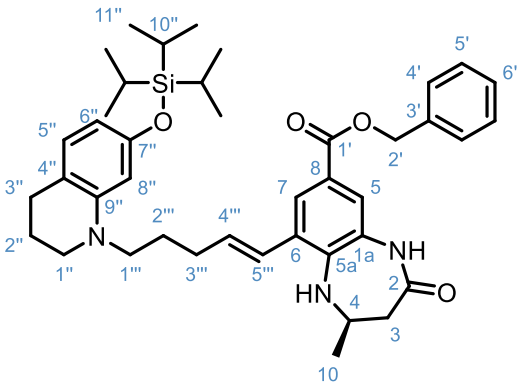

(*R*)-9-iodo-2-methyl-4-oxo-2,3,4,5-tetrahydro-1*H*-benzo[*b*][1,4]diazepine-7-carboxylate (1.38 g, 3.16 mmol, 1.0 equiv.), (*E*)-1-(5-(4,4,5,5-tetramethyl-1,3,2-dioxaborolan-2-yl)pent-4-en-1-yl)-7-((triisopropylsilyl)oxy)-1,2,3,4-tetrahydroquinoline (2.22 g, 4.74 mmol, 1.5 equiv.), K_2CO_3 (1.22 g, 9.50 mmol, 3.0 equiv.) and [1,1′-Bis(diphenylphosphino)ferrocene]dichloropalladium$^{(II)}$ (149 mg, 0.0791 mmol, 0.025 equiv.) were added to reaction vessel under an argon atmosphere. To this was added

1,4-dioxane (40 mL) and H_2O (10 mL), the reaction was then heated to 100 °C for 24 h. Once cooled the reaction mixture was evaporated and then diluted with EtOAc (250 mL), which was then filtered through a Celite® pad. The filtrate was then washed with H_2O (3 × 250 mL) and brine (250 mL), then dried ($MgSO_4$), filtered and concentrated *in vacuo* to yield a brown oil. The crude product was purified by flash silica column chromatography (elution with 20-75 % EtOAc in pet ether) to give (*R*,*E*)-2-methyl-4-oxo-9-(5-(7-((triisopropylsilyl)oxy)-3,4-dihydroquinolin-1(2*H*)-yl)pent-1-en-1-yl)-2,3,4,5-tetrahydro-1*H*-benzo[*b*][1,4]diazepine-7-carboxylate as a dark brown oil (1.403 g, 65%); R_f 0.30 (1:1, EtOAc/pet ether); $[\alpha]_D^{25}$ = −2.2 (*c* 1.0, $CHCl_3$); ^{1}H NMR (400 MHz, $CDCl_3$) δ_H 7.97 (1H, s, NH-9a), 7.74 (1H, d, *J* 2.0 Hz, H-9), 7.53 (1H, d, *J* 2.0 Hz, H-7), 7.45 – 7.30 (5H, m, H-4', H-5', H-6'), 6.75 (1H, d, *J* 7.7 Hz, H-5''), 6.34 (1H, d, *J* 15.6 Hz, H-5'''), 6.19 – 6.06 (3H, m, H-6'', H-8'', H-4'''), 5.33 (2H, s, H-2'), 4.15 – 4.06 (1H, m, H-4), 4.02 (1H, s, NH-5a), 3.35 – 3.14 (4H, m, H-1'', H-1'''), 2.71 – 2.60 (3H, m, H_AH_B-3, H-3''), 2.51 (dd, *J* 13.9, 8.1 Hz, H_AH_B-3), 2.34 – 2.24 (2H, m, H-3'''), 1.97 – 1.85 (2H, m, H-2''), 1.84 – 1.70 (2H, m, H-2'''), 1.37 (3H, d, *J* 6.3 Hz, H-10), 1.25-1.18 (3H, m, H-10''), 1.08 (18H, d, *J* 7.4 Hz, H-11''); LRMS *m/z* ;(ESI$^+$) 682 ($[M+H]^+$, 100%). These data are in accordance with the literature.[88]

Benzyl (*R*,*E*)-9-(5-(7-(3-((*tert*-butoxycarbonyl)amino)propoxy)-3,4-dihydroquinolin-1(2*H*)-yl)pent-1-en-1-yl)-2-methyl-4-oxo-2,3,4,5-tetrahydro-1*H*-benzo[*b*][1,4]diazepine-7-carboxylate (compound **36**)

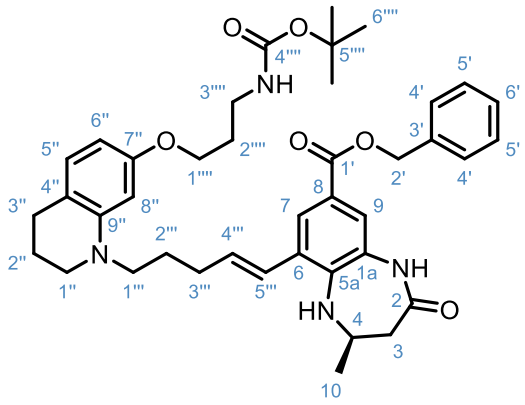

To a solution of benzyl (*R*,*E*)-2-methyl-4-oxo-9-(5-(7-((triisopropylsilyl)oxy)-3,4-dihydroquinolin-1(2*H*)-yl)pent-1-en-1-yl)-2,3,4,5-tetrahydro-1*H*-benzo[*b*][1,4]diazepine-7-carboxylate (1.00 mg, 1.47 mmol, 1.0 equiv.) in THF (30 mL) was added 1 M TBAF in THF (3.00 mL, 2.94 mmol, 2.0 equiv.) and the reaction mixture was stirred at r.t. for 1 h. The reaction mixture was evaporated *in vacuo* to afford an orange residue. The crude oil was purified by silica gel chromatography (elution with 50-100% EtOAc in pet ether) to yield a brown solid. The brown solid was dissolved in anhydrous DMF (7.5 mL). K_2CO_3 (300 mg, 4.94 mmol, 1.5 equiv.) and *tert*-butyl (3-bromopropyl)carbamate (434 mg, 1.77 mmol, 1.5 equiv.) were added to the solution and the reaction mixture was stirred at 65 °C for 48 h. The reaction mixture was diluted with 1 M $K_2CO_{3(aq)}$ (250 mL) and was extracted with EtOAc (3 × 100 mL). The combined organic components were washed with 0.5 M $LiCl_{(aq)}$ (3 × 200 mL), brine (200 mL), dried (Na_2SO_4), filtered and evaporated *in vacuo* to afford a brown oil. The crude oil was purified by silica gel chromatography (elution with 10-20% acetone in toluene) to yield benzyl (*R*,*E*)-9-(5-(7-(3-((*tert*-butoxycarbonyl)amino)propoxy)-3,4-dihydroquinolin-1(2*H*)-yl)pent-1-en-1-yl)-2-methyl-4-oxo-2,3,4,5-tetrahydro-1*H*-

benzo[*b*][1,4]diazepine-7-carboxylate as a yellow oil (508 mg, 50%); R_f 0.30 (1:4, acetone/toluene); $[\alpha]_D^{20}$ = −8.14 (*c* 0.5, $CHCl_3$); $\bar{\nu}_{max}$ (thin film)/cm-1 3371 (N-H, br w), 2931 (C-H, w), 1692 (C=O, s), 1674 (C=O, s); ^{1}H NMR (400 MHz; $CDCl_3$) δ_H 7.75 (1H, d, *J* 1.9, H-9), 7.53 (1H, s, NH-1a), 7.48 (1H, d, *J* 1.9, H-7), 7.45–7.30 (5H, m, H-4', H-5', H-6'), 6.83 (1H, d, *J* 7.8, H-5''), 6.36 (1H, d, *J* 15.4, H-14''), 6.19–6.06 (3H, m, H-6'', H-8'', H-13''), 5.33 (2H, s, H-2'), 4.78 (1H, s, NH-3''''), 4.12 –4.05 (1H, m, H-4), 3.93 (2H, t, *J* 6.0, H-3''''), 3.31 – 3.20 (6H, m, H-1'', H-1''', H-1''''), 2.69 (2H, t, *J* 6.4, H-3''), 2.63 (1H, dd, *J* 13.8, 3.3, H_AH_B-3), 2.50 (1H, dd, *J* 13.8, 8.3, H_AH_B-3), 2.31 (2H, q, *J* 6.9, H-3'''), 1.95 – 1.86 (4H, m, H-2'''', H-2''), 1.83 – 1.76 (2H, m, H-2'''), 1.43 (9H, s, H-6''''), 1.35 (3H, d, *J* 6.4, H-10); HRMS *m/z* (ESI+) [Found: 683.3796, $C_{40}H_{51}N_6O_4$ requires M+ 683.3803)]; LRMS *m/z* (ESI+) 583 ([M-Boc]+, 100%); HPLC: Retention time 12.7 min, purity 98.3%. These data are in accordance with the literature.[88]

(2*R*,24*E*)-2-Methyl-1,2,3,9,10,11,12,18,19,21,22,23-dodecahydro-8*H*,17*H*-14,16-etheno-26,7-(metheno)[1,4]diazepino[2,3-*l*]pyrido[2,1-*d*][1,5,17]oxadiazacycloicosine-4,8(5*H*)-dione (compound **10**)

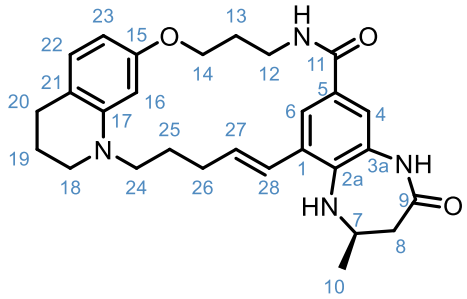

(*R*,*E*)-9-(5-(7-(3-((*tert*-Butoxycarbonyl)amino)propoxy)-3,4-dihydroquinolin-1(2*H*)-yl)pent-1-en-1-yl)-2-methyl-4-oxo-2,3,4,5-tetrahydro-1*H*-benzo[*b*][1,4]diazepine-7-carboxylate (55.3 mg, 0.081 mmol, 1.0 equiv.) was dissolved in a mixture of THF/MeOH/H_2O (3:2:1, 0.8 mL) was added LiOH (27 mg, 1.13 mmol, 14.0 equiv.) and the reaction mixture was stirred at r.t. for 5 h. The reaction mixture was evaporated *in*

vacuo to afford a yellow residue. The residue was dissolved in CH_2Cl_2 (0.5 mL) was added trifluoroacetic acid (0.5 mL) and the brown solution was stirred at r.t. for 2 h. The reaction mixture was evaporated *in vacuo* to afford a brown residue. The residue was dissolved in DMF (29 mL) and was adjusted to pH 9 with DIPEA (2.0 mL). PyBOP (46 mg, 0.089 mmol, 1.1 equiv.) was added to the solution and the reaction mixture was stirred at r.t. for 36 h. The reaction mixture was concentrated under a constant stream of nitrogen to afford a brown oil. The crude oil was diluted with 1 M $K_2CO_{3(aq)}$ (50 mL) and extracted with $CHCl_3$/IPA (9:1, 3 × 20 mL). The combined organic components were washed with 0.5 M $LiCl_{(aq)}$ (3 × 20 mL), brine (10 mL), dried ($MgSO_4$), filtered, and evaporated *in vacuo* to afford a brown oil. The crude oil was purified by silica gel chromatography (elution with 0-100% IPA in Et_2O) and then further purified by semi-preperative HPLC (retention time, 7.77 mins), the solvent was then removed *via* lyophilisation to yield (2*R*,24*Z*)-2,9-dimethyl-1,2,3,9,10,11,12,18,19,21,22,23-dodecahydro-8*H*,17*H*-14,16-etheno-26,7-(metheno)[1,4]diazepino[2,3-*l*]pyrido[2,1-*d*][1,5,17]oxadiazacycloicosine-4,8(5*H*)-dione as a white lysophilate (11.36 mg, 41%); Rf 0.52 (9:1, acetone/Et_2O); $[\alpha]_D^{25}$ = −51.1 (*c* 0.4, DMSO); mp 290 °C decomposed (acetone); $\bar{\nu}_{max}$ (thin film)/cm^{-1} 3448 (N-H, br w), 3248 (N-H, br w), 2928 (C-H, w), 1671 (C=O, s); 1H NMR (400 MHz; d_6-DMSO) δ_H 9.56 (1H, s, NH-3a/9), 7.92 (1H, t, *J* 5.3 Hz, NH-11/12), 7.52 (1H, d, *J* 2.0 Hz, H-6), 7.33 (1H, d, *J* 2.0 Hz, H-4), 6.77 (1H, d, *J* 8.1 Hz, H-22), 6.71 (1H, d, *J* 15.2 Hz, H-28), 6.28 (1H, dt, *J* 15.2, 7.3 Hz, H-27), 6.12 (1H, d, *J* 2.3 Hz, H-16), 6.09 (1H, dd, *J* 8.1, 2.3 Hz, H-23), 5.08 (1H, d, *J* 3.1 Hz, NH-2a/7), 4.07 – 3.93 (3H, m, H-7, H-14), 3.47 (2H, q, *J* 5.3 Hz, H-12), 3.30 – 3.15 (4H, m, H-18, H-24), 2.60 (2H, t, *J* 6.3 Hz, H-20), 2.49 – 2.42 (1H, m, H_AH_B-8), 2.35 – 2.23 (2H, m, H-26), 2.21 (1H, dd, *J* 13.3, 7.2 Hz, H_AH_B-8), 1.93 (2H, p, *J* 5.3 Hz, H-13), 1.86 – 1.76 (2H, m, H-19), 1.73 –

1.64 (2H, m, H-25), 1.24 (3H, d, *J* 6.3 Hz, H-10); LRMS *m/z* (ESI+) 475 ([M+H]+, 100%); HPLC: retention time 9.4 min, purity 98.2%. These data are in accordance with the literature.[88]

Benzyl (*R*,*E*)-9-(5-(7-(2-((*tert*-butoxycarbonyl)amino)ethoxy)-3,4-dihydroquinolin-1(2*H*)-yl)pent-1-en-1-yl)-2-methyl-4-oxo-2,3,4,5-tetrahydro-1*H*-benzo[*b*][1,4]diazepine-7-carboxylate (compound **31**)

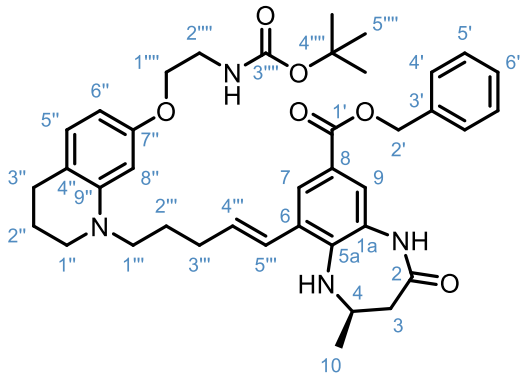

To a solution of benzyl (*R*,*E*)-2-methyl-4-oxo-9-(5-(7-((triisopropylsilyl)oxy)-3,4-dihydroquinolin-1(2*H*)-yl)pent-1-en-1-yl)-2,3,4,5-tetrahydro-1*H*-benzo[*b*][1,4]diazepine-7-carboxylate of (300 mg, 0.440 mmol, 1.0 equiv.) in THF (5.00 mL) was added 1M TBAF in THF (230 mg, 880 µL, 0.974 mmol, 2.0 equiv.) and the reaction mixture was stirred at r.t. for 1 h. Upon this time the reaction was observed to be complete so the solvent was removed under a stream of nitrogen to give a dark brown oil, the crude reaction mixture was then redissolved in CH_2Cl_2 and purified by normal phase silica gel flash column chromatography (0-100% EtOAc in cyclohexane) to yield benzyl (*R*,*E*)-9-(5-(7-hydroxy-3,4-dihydroquinolin-1(2*H*)-yl)pent-1-en-1-yl)-2-methyl-4-oxo-2,3,4,5-tetrahydro-1*H*-benzo[*b*][1,4]diazepine-7-carboxylate as a light brown oil that was utilised without further characterisation. To the crude product was added caesium carbonate (430 mg, 1.32 mmol, 3.0 equiv.), TBAI (81 mg, 0.220 mmol, 0.5 equiv.) and *tert*-butyl (2-bromoethyl)carbamate (296 mg, 1.32 mmol, 3.0 equiv.) in

a microwave vial which was sealed and placed under an inert atmosphere and then anhydrous DMF (1.00 mL) was added and the reaction mixture was stirred at 85 °C for 18 h. After this time the reaction was observed to be complete, and the reaction mixture was then diluted with 1M $K_2CO_{3(aq)}$ (100 mL) which was then washed with EtOAC (3 × 50 mL), the combined organic layers were then washed with 5 wt% $LiCl_{(aq)}$ (3 × 50 mL), brine (100 mL), dried ($MgSO_4$), filtered and concentrated in *vacuo* to give the crude product as a transparent brown oil. The crude product was then purified using ACCQPrep HpH method E using 80-99% acetonitrile(B)/10mM ammonium bicarbonate in water adjusted to pH 10 with ammonia solution(A) gradient over 17 mins, the resultant solution was concentrated under a stream of nitrogen at 40 °C to yield benzyl (*R*,*E*)-9-(5-(7-(2-((*tert*-butoxycarbonyl)amino)ethoxy)-3,4-dihydroquinolin-1(2*H*)-yl)pent-1-en-1-yl)-2-methyl-4-oxo-2,3,4,5-tetrahydro-1*H*-benzo[*b*][1,4]diazepine-7-carboxylate as a colourless oil (55 mg, 19% yield); R_f 0.46 (EtOAc); $[\alpha]_D^{20}$ = +28.13 (*c* 1.3, MeCN); $\bar{\nu}_{max}$ (thin film MeCN)/ cm^{-1} 2932 (C-H, br, m), 1694 and 1673 (C=O, s), 1507 (C=C, s), 1167 (C-O, s); ^{1}H NMR (400 MHz, $CDCl_3$) δ_H 7.77 (1H, d, *J* 1.8 Hz, H-7), 7.48 (1H, d, *J* 1.8 Hz, H-9), 7.46 – 7.34 (5 H, m, H-4', H-5', H-6'), 6.84 (1H, d, *J* 7.9 Hz, H-5''), 6.38 (1H, d, *J* 15.8 Hz, H-5'''), 6.20 – 6.10 (3H, m, H-6'', H-8'', H-4'''), 5.34 (2H, s, H-2'), 5.04 – 4.94 (1H, m, NH-2''''/3''''), 4.15 – 4.05 (1H, m, H-4), 4.02 (1H, br s, NH-4/5a), 3.96 (2H, t, *J* 5.2 Hz, H-1''''), 3.47 (2H, q, *J* 4.9 Hz, H-2''''), 3.33 – 3.26 (4H, m, H-1'', H-1'''), 2.73 – 2.63 (3H, m, H-3'', H_AH_B-7), 2.50 (1H, dd, *J* 13.8, 8.2 Hz, H_AH_B-7), 2.33 (2H, q, *J* 6.9 Hz, H-3'''), 1.99 - 1.88 (2H, m, H-2''), 1.81 (2H, p, *J* 7.4 Hz, H-2'''), 1.44 (9H, s, H-5''''), 1.38 (3H, d, *J* 6.4 Hz, H-10); ^{13}C NMR (101 MHz, $CDCl_3$) δ_C 171.8 (C-2), 165.8 (C-1'), 158.3 (C-7''), 155.9 (C-3'''), 146.2 (C-9''), 139.8 (C-5a), 136.5 (C-4''''), 136.2 (C-3'), 129.6 (C-5''), 128.9 (C-6), 128.6 (C-5'), 128.2 (C-4'), 126.2 (C-6'), 126.0 (C-7), 124.9 (C-5'''), 122.6 (C-9), 121.1 (C-1a),

115.6 (C-4''), 100.5 (C-6''), 97.7 (C-8''), 79.6 (C-4''''), 67.1 (C-1''''), 66.5 (C-1'), 52.9 (C-4), 50.9 (C-1'''), 49.4 (C-1''), 41.5 (C-4), 40.28 (C-2''''), 31.0 (C-3'''), 28.4 (C-5''''), 27.4 (C-3''), 26.0 (C-2'''), 24.3 (C-10), 22.4 (C-2''); HRMS *m/z* (ESI^+) [Found 669.3637 $C_{39}H_{48}N_4O_6$ requires 669.3633 $[M+H]^+$]; LRMS *m/z* (ESI^+) 669.3 ($[M+H^+]$, 100%); LC-MS, HpH method: retention time 1.51 mins, 98.8% purity.

Benzyl (*R*,*E*)-9-(5-(7-(4-((*tert*-butoxycarbonyl)amino)butoxy)-3,4-dihydroquinolin-1(2*H*)-yl)pent-1-en-1-yl)-2-methyl-4-oxo-2,3,4,5-tetrahydro-1*H*-benzo[*b*][1,4]diazepine-7-carboxylate (compound **32**)

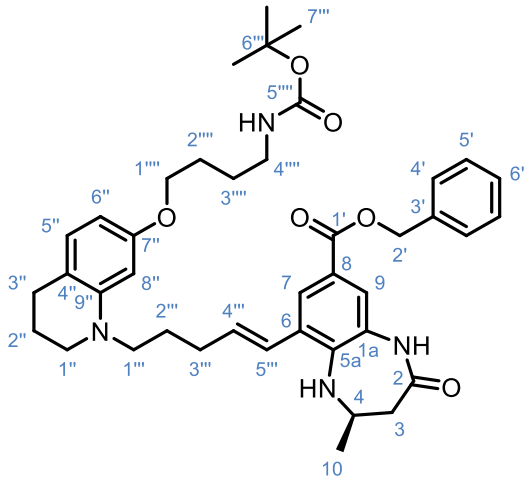

To a solution of benzyl (*R,E*)-2-methyl-4-oxo-9-(5-(7-((triisopropylsilyl)oxy)-3,4-dihydroquinolin-1(2*H*)-yl)pent-1-en-1-yl)-2,3,4,5-tetrahydro-1*H*-benzo[*b*][1,4]diazepine-7-carboxylate (200 mg, 0.293 mmol, 1.0 equiv.) in THF (5.00 mL) was added 1 M TBAF in THF (153 mg, 650 µL, 0.587 mmol, 2.0 equiv.) and the reaction mixture was stirred at r.t. for 1 h. After this time the reaction mixture was concentrated *in vacuo* to afford a brown residue. The crude oil was purified by silica gel flash column chromatography (0-100% EtOAc in cyclohexane) to yield benzyl (*R*,*E*)-9-(5-(7-hydroxy-3,4-dihydroquinolin-1(2*H*)-yl)pent-1-en-1-yl)-2-methyl-4-oxo-2,3,4,5-tetrahydro-1*H*-benzo[*b*][1,4]diazepine-7-carboxylate as a viscous brown oil

which was used without further purification. To this was added caesium carbonate (287 mg, 0.880 mmol, 3.0 equiv.), TBAI (54.2 mg, 0.147 mmol, 0.5 equiv.) and *tert*-butyl (4-bromobutyl)carbamate (222 mg, 0.880 mmol, 3.0 equiv.) in a microwave vial which was sealed and placed under an inert atmosphere and then anhydrous DMF (1.00 mL) was added and the reaction mixture was stirred at 85 °C for 18 h. The crude reaction mixture was then diluted with 1M $K_2CO_{3(aq)}$ (100 mL) which was then washed with EtOAc (3 × 50 mL), the combined organic layers were then washed with 5 wt% $LiCl_{(aq)}$ (3 × 50 mL), brine (100 mL), dried ($MgSO_4$), filtered and concentrated in *vacuo* to give the crude product as a dark brown oil. The crude oil was taken up in DMSO (1 mL) and then purified by ACCQPrep method E using 80-99% acetonitrile(B)/10mM ammonium bicarbonate in water adjusted to pH 10 with ammonia solution(A) gradient over 17 mins the resultant solution was concentrated under a stream of nitrogen at 40 °C to give benzyl (*R*,*E*)-9-(5-(7-(4-((*tert*-butoxycarbonyl)amino)butoxy)-3,4-dihydroquinolin-1(2*H*)-yl)pent-1-en-1-yl)-2-methyl-4-oxo-2,3,4,5-tetrahydro-1*H*-benzo[*b*][1,4]diazepine-7-carboxylate as a colourless oil (41 mg, 20% yield); R_f 0.48 (EtOAc); $[\alpha]_D^{20}$ = +19.05 (*c* 1.0, MeCN); $\bar{\nu}_{max}$ (thin film MeCN)/ cm^{-1} 2932 (C-H, br, m), 1689 and 1674 (C=O, s), 1508 (C=C, s), 1170 (C-O, s); ^{1}H NMR (600 MHz, d_6-DMSO) δ_H 9.56 (1H, s, NH-1a/2), 7.65 (1H, d, *J* 2.2 Hz, H-7), 7.47 (1H, d, *J* 2.2 Hz, H-9), 7.44 – 7.32 (5H, m, H-4', H-5', H-6'), 6.78 (1H, br t, *J* 5.5 Hz, NH-4''''/5''''), 6.72 (1H, d, *J* 8.1 Hz, H-5''), 6.64 (1H, d, *J* 15.4 Hz, H-5'''), 6.14 (1H, dt, *J* 15.3, 6.8 Hz, H-4'''), 6.06 (1H, d, *J* 2.6 Hz, H-8''), 6.02 (1H, dd, *J* 8.1, 2.6 Hz, H-6''), 5.44 (1H, d, *J* 3.3 Hz, NH-4/5a), 5.29 (2H, s, H-2'), 4.04 – 3.96 (1H, m, H-4), 3.81 (2H, t, *J* 6.4 Hz, H-1''''), 3.28 – 3.24 (2H, m, H-1'''), 3.24 – 3.21 (2H, m, H-1''), 2.92 (2H, q, *J* 6.9 Hz, H-4''''), 2.60 – 2.56 (2H, m, H-3''), 2.53 – 2.51 (1H, m, H_AH_B-7), 2.29 – 2.24 (3H, m, H_AH_B-7, H-3'''), 1.83 – 1.78 (2H, m, H-2''), 1.75 – 1.70 (2H, m, H-2'''), 1.61 – 1.55 (2H, m, H-2''''), 1.48 –

1.43 (2H, m, H-3’’’’), 1.36 (9H, s, H-7’’’’), 1.24 (3H, d, *J* 6.2 Hz, H-10); HRMS *m/z* (ESI^+) [Found 697.3961 $C_{41}H_{52}N_4O_6$ requires 697.3957 $[M+H]^+$]; LRMS *m/z* (ESI^+) 697.4 ($[M+H^+]$, 100%), 597.3 ($[M\text{-}Boc^+]$, 100%); LC-MS, HpH method (retention time 1.56 mins) 100% purity.

Benzyl (*R*)-9-((*E*)-5-(7-(((*S*)-1-(*tert*-butoxycarbonyl)piperidin-3-yl)methoxy)-3,4-dihydroquinolin-1(2*H*)-yl)pent-1-en-1-yl)-2-methyl-4-oxo-2,3,4,5-tetrahydro-1*H*-benzo[*b*][1,4]diazepine-7-carboxylate (compound **33**)

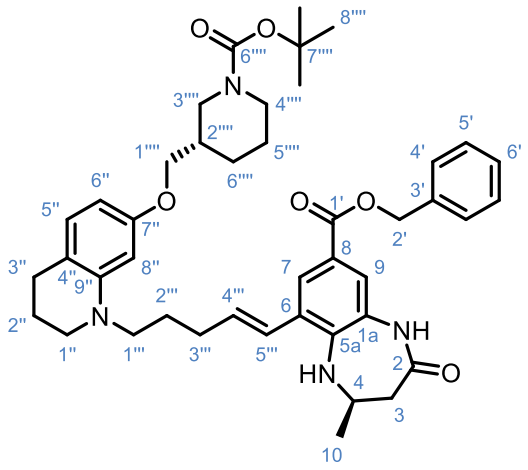

To a solution of benzyl (*R,E*)-2-methyl-4-oxo-9-(5-(7-((triisopropylsilyl)oxy)-3,4-dihydroquinolin-1(2*H*)-yl)pent-1-en-1-yl)-2,3,4,5-tetrahydro-1*H*-benzo[*b*][1,4]diazepine-7-carboxylate (335 mg, 0.491 mmol, 1.0 equiv.) in THF (7.00 mL) was added 1M TBAF in THF (257 mg, 1.08 mL, 0.982 mmol, 2.0 equiv.) and the reaction mixture was stirred at r.t. for 1 h. After this time the reaction mixture was concentrated *in vacuo* to afford a brown residue. The crude oil was purified by silica gel flash column chromatography (0-100% EtOAc in cyclohexane) to yield benzyl (*R*,*E*)-9-(5-(7-hydroxy-3,4-dihydroquinolin-1(2*H*)-yl)pent-1-en-1-yl)-2-methyl-4-oxo-2,3,4,5-tetrahydro-1*H*-benzo[*b*][1,4]diazepine-7-carboxylate as a viscous brown oil which was used without further purification. To this oil was added caesium carbonate (480 mg, 1.47 mmol, 3.0 equiv.) and *tert*-butyl (*S*)-3-(bromomethyl)piperidine-1-

carboxylate (171 mg, 0.614 mmol, 1.3 equiv.) in a microwave vial which was sealed and placed under an inert atmosphere and then anhydrous DMF (1.25 mL) was added, and the reaction mixture was stirred at 85 °C for 18 h. The reaction mixture was then diluted with 1M $K_2CO_{3(aq)}$ (100 mL) and this was washed with EtOAc (3 × 50 mL), the combined organic layers were then washed with 5 wt% $LiCl_{(aq)}$ (3 × 50 mL), brine (100 mL), dried ($MgSO_4$), filtered and concentrated *in vacuo* to give a light brown oil. The crude oil was then taken up in DMSO (1 mL) and purified by ACCQprep using method E using 80-99% acetonitrile(B)/10mM ammonium bicarbonate in water adjusted to pH 10 with ammonia solution(A) gradient over 17 mins. The residual compound was purified by MDAP using 100 mg HpH method E and was loaded onto the High pH Xselect CSH C_{18} column (150mm x 30mm i.d. 5µm packing diameter) column. The product was then eluted using 80-99% acetonitrile(B)/10mM ammonium bicarbonate in water adjusted to pH 10 with ammonia solution(A) gradient over 17 mins and the resultant solution was concentrated under a stream of nitrogen at 40 °C to give the benzyl (*R*)-9-((*E*)-5-(7-(((*S*)-1-(*tert*-butoxycarbonyl)piperidin-3-yl)methoxy)-3,4-dihydroquinolin-1(2*H*)-yl)pent-1-en-1-yl)-2-methyl-4-oxo-2,3,4,5-tetrahydro-1*H*-benzo[*b*][1,4]diazepine-7-carboxylate as a colourless oil (127 mg, 36% yield); R_f 0.48 (EtOAc); $[\alpha]_D^{18}$ = +31.6 (*c* 1.1, MeCN); $\bar{\nu}_{max}$ (thin film MeCN)/ cm^{-1} 2932 (C-H, br, m), 1675 (C=O, s), 1508 (C=C, s), 1264 and 1150 (C-O, s); ^{1}H NMR (600 MHz, d_6-DMSO) δ_H 9.57 (1H, s, NH-1a/2), 7.65 (1H, d, *J* 2.0 Hz, H-7), 7.48 (1H, d *J* 2.0 Hz, H-9), 7.44 – 7.32 (5H, m, H-4', H-5', H-6'), 6.73 (1H, d, *J* 8.1 Hz, H-5''), 6.64 (1H, d, *J* 15.5 Hz, H-5'''), 6.13 (1H, dt, *J* 15.3, 6.8 Hz, H-4'''), 6.07 (1H, d, *J* 2.4 Hz, H-8''), 6.03 (1H, dd, *J* 8.1, 2.4 Hz, H-6''), 5.44 (1H, d, *J* 3.4 Hz, NH-4/5a), 5.29 (2H, s, H-2'), 4.05 – 3.95 (1H, m, H-4), 3.85 – 3.60 (4H, m, H-1'''', H-3''''), 3.26 (2H, t, *J* 7.4 Hz, H-1'''), 3.23 (2H, t, *J* 5.6 Hz, H-1''), 2.76 (2H, m, H-4''''), 2.59 (2H, t, *J* 6.3 Hz, H-3''), 2.52 (1H, m,

H_AH_B-3), 2.30 – 2.23 (3H, m, H_AH_B-3, H-3’’’), 1.85 – 1.78 (2H, m, H-2’’), 1.75 – 1.68 (3H, m, H-2’’’, H-2’’’’), 1.62 – 1.48 (1H, m, H-6’’’’), 1.35 (9H, s, H-8’’’’), 1.28 – 1.27 (2H, m, H-6’’’’), 1.24 (3H, d, *J* 6.3 Hz, H-10), 1.23 – 1.09 (2H, m, H-5’’’’); ^{13}C NMR (151 MHz, d_6-DMSO) δ_C 171.1 (C-2), 165.3 (C-1’), 158.1 (C-7’’), 153.9 (C-6’’’’), 145.8 (C-9’’), 140.8 (C-5a), 136.5 (C-3’), 133.4 (C-4’’’), 129.2 (C-8’’), 128.4 (C-5’), 128.1 (C-4’), 127.9 (C-6’), 127.8 (C-6), 127.6 (C-1a), 125.6 (C-5’’’), 123.7 (C-7), 122.0 (C-9), 119.0 (C-8), 114.4 (C-4’’), 100.6 (C-6’’), 97.2 (C-5’’), 78.4 (C-7’’’’), 69.0 (C-1’’’’) 65.5 (C-2’), 52.8 (C-4), 50.2 (C-1’’’), 48.6 (C-1’’), 40.9 (C-3), 35.5 (C-2’’’’), 30.3 (C-3’’’), 28.0 (C-8’’’’), 26.9 (C-3’’), 26.5 (C-5’’’’, C-2), 25.2 (C-2’’’), 24.0 (C-5’’’), 23.4 (C-10), 22.0 (C-2’’ and C-4’’’’); HRMS *m/z* (ESI$^+$) [Found 723.4105 Chemical Formula: $C_{43}H_{55}N_4O_6$ requires 723.4122 [M+H]$^+$]; LRMS *m/z* (ESI$^+$) 723.4 ([M+H$^+$], 40%), 623.4 ([M-Boc$^+$], 100%); LC-MS, HpH method (retention time 1.66 mins) 97.2% purity.

Benzyl (*R*)-9-((*E*)-5-(7-(((*R*)-1-(*tert*-butoxycarbonyl)pyrrolidin-2-yl)methoxy)-3,4-dihydroquinolin-1(2*H*)-yl)pent-1-en-1-yl)-2-methyl-4-oxo-2,3,4,5-tetrahydro-1*H*-benzo[*b*][1,4]diazepine-7-carboxylate (compound **34**)

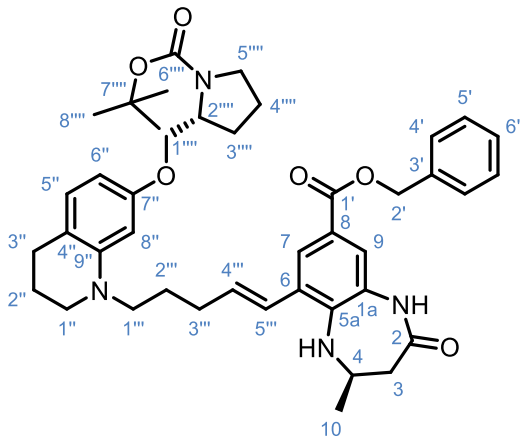

To a solution of benzyl (*R,E*)-2-methyl-4-oxo-9-(5-(7-((triisopropylsilyl)oxy)-3,4-dihydroquinolin-1(2*H*)-yl)pent-1-en-1-yl)-2,3,4,5-tetrahydro-1*H*-benzo[*b*][1,4]diazepine-7-carboxylate (300 mg, 0.440 mmol, 1.0 equiv.) in THF (5.00

mL) was added 1 M TBAF in THF (230 mg, 880 µL, 0.880 mmol, 2.0 equiv.)and the reaction mixture was stirred at r.t. for 1 h. After this time the reaction mixture was concentrated *in vacuo* to afford a brown residue. The crude oil was purified by silica gel flash column chromatography (0-100% EtOAc in cyclohexane) to yield benzyl (*R*,*E*)-9-(5-(7-hydroxy-3,4-dihydroquinolin-1(2*H*)-yl)pent-1-en-1-yl)-2-methyl-4-oxo-2,3,4,5-tetrahydro-1*H*-benzo[*b*][1,4]diazepine-7-carboxylate as a viscous brown oil which was used without further purification. To this was added caesium carbonate (430 mg, 1.32 mmol, 3.0 equiv.), TBAI (81.2 mg, 0.220 mmol, 0.5 equiv.) and *tert*-butyl (*R*)-2-(bromomethyl)pyrrolidine-1-carboxylate (349 mg, 1.32 mmol, 3.0 equiv.) in a microwave vial which was sealed and placed under an inert atmosphere and then anhydrous DMF (1.50 mL) was added and the reaction mixture was stirred at 85 °C for 18 h. Reaction mixture was diluted with 1M $K_2CO_{3(aq)}$ (100 mL) which was washed with EtOAc (3 × 50 mL), the combined organic layers were then washed with 5 wt% $LiCl_{(aq)}$ (3 × 50 mL), brine (100 mL), dried ($MgSO_4$), filtered and concentrated *in vacuo* to yield a dark brown oil. The crude oil was taken up in DMSO (1 mL) and then purified using ACCQPrep method E, the product was loaded onto the High pH Xselect CSH C_{18} column (150mm x 30mm i.d. 5µm packing diameter) column and was eluted using 80-99% acetonitrile(B)/10mM ammonium bicarbonate in water adjusted to pH 10 with ammonia solution(A) gradient over 17 mins and the resultant product was concentrated under a stream of nitrogen at 40 °C to give (*R*)-9-((*E*)-5-(7-(((*R*)-1-(*tert*-butoxycarbonyl)pyrrolidin-2-yl)methoxy)-3,4-dihydroquinolin-1(2*H*)-yl)pent-1-en-1-yl)-2-methyl-4-oxo-2,3,4,5-tetrahydro-1*H*-benzo[*b*][1,4]diazepine-7-carboxylate as a colourless oil (27 mg, 9% yield); R_f 0.45 (EtOAc); $[\alpha]_D^{21}$ = +21.13 (*c* 0.5, MeCN); $\bar{\nu}_{max}$ (thin film MeCN)/ cm^{-1} 2931 (C-H, br, m), 1676 (C=O, s), 1509 (C=C, s), 1209 (C-O, s); ^{1}H NMR (600 MHz, d_6-DMSO) δ_H 9.57 (1H, s, NH-1a/2), 7.65 (2H, d, *J* 2.2 Hz, H-7),

7.48 (1H, d, *J* 2.2 Hz, H-9), 7.45 – 7.38 (4H, m, H-4', H-5'), 7.37 – 7.33 (1H, m, H-6'), 6.73 (1H, d, *J* 8.4 Hz, H-5''), 6.64 (1H, br d, *J* 15.4 Hz, H-5'''), 6.15 – 6.12 (1H, m, H-8''), 6.14 (1H, dt, *J* 15.4, 7.0 Hz, H-4'''), 6.07 (1H, br s, H-6''), 5.43 (1H, br s), 5.30 (2H, s, H-1'), 4.04 – 3.96 (1H, m, H-4), 3.96 – 3.89 (2H, m, H_AH_B-1'''', H-2''''), 3.73 (1H, dd, *J* 9.2, 7.3 Hz, H_AH_B-1''''), 3.29 (2H, br d, *J* 5.5 Hz, H-5''''), 3.25 – 3.21 (4H, m, H-1'', H-1'''), 2.59 (2H, br t, *J* 6.2 Hz, H-3''), 2.53 – 2.52 (1H, m, H_AH_B-3), 2.32 – 2.25 (3H, m, H_AH_B-3, H-3'''), 1.85 – 1.79 (4H, m, H-2'', H-3''''), 1.76 - 1.70 (4H, m, H-2''', H-4''''), 1.38 (9H, br s, H-8''''), 1.25 (3H, d, *J* 6.2 Hz, C-10); ^{13}C NMR (151 MHz, d_6-DMSO) δ_C 171.1 (C-2), 165.3 (C-1'), 158.0 (C-7''), 154.0 (C-6''''), 145.8 (C-9''), 140.8 (C-5a), 136.5 (C-4'''), 128.4 (C-5''), 127.9 (C-4'), 127.8 (C-6), 127.6 (C-5', C-6'), 127.4 (C-1a) 126.3 (C-8), 123.7 (C-5'''), 122.0 (C-7), 119.0 (C-9), 115.1 (C-4''), 100.3 (C-6''), 97.4 (C-8''), 78.5 (C-7''''), 65.5 (C-1''''), 63.5 (C-2'), 55.6 (C-2''''), 52.8 (C-4), 50.2 (C-5''''), 48.6 (C-1'''), 46.4 (C-1''), 40.9 (C-4), 30.3 (C-3'''), 28.1 (C-8'''', C-3''''), 26.9 (C-3''), 25.0 (C-2''') 23.4 (C-10, C-4''''), 21.9 (C-2''); HRMS *m/z* (ESI$^+$) [found 709.3959 $C_{42}H_{53}N_2O_4$ requires 709.3965 $[M+H]^+$]; LRMS *m/z* (ESI$^+$) 709.3 ([M+H$^+$], 25%), 609.4 ([M-Boc$^+$], 100%); LC-MS, HpH method (retention time 1.64 mins) 100% purity.

Benzyl (*R*)-9-((*E*)-5-(7-(((*S*)-1-(*tert*-butoxycarbonyl)pyrrolidin-2-yl)methoxy)-3,4-dihydroquinolin-1(2*H*)-yl)pent-1-en-1-yl)-2-methyl-4-oxo-2,3,4,5-tetrahydro-1*H*-benzo[*b*][1,4]diazepine-7-carboxylate (compound **35**)

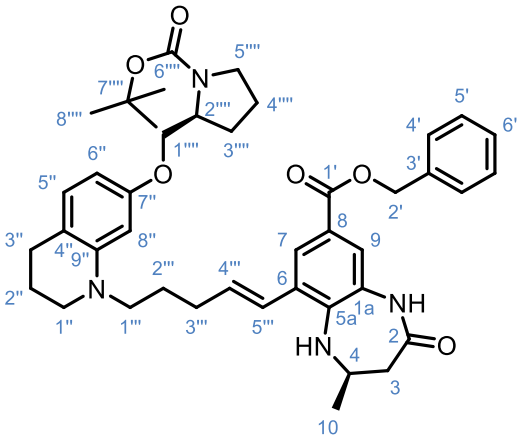

To a solution of benzyl (*R,E*)-2-methyl-4-oxo-9-(5-(7-((triisopropylsilyl)oxy)-3,4-dihydroquinolin-1(2*H*)-yl)pent-1-en-1-yl)-2,3,4,5-tetrahydro-1*H*-benzo[*b*][1,4]diazepine-7-carboxylate (335 mg, 0.491 mmol, 1.0 equiv.) in THF (7.00 mL) was added 1M TBAF in THF (257 mg, 982 µL, 0.982 mmol, 2.0 equiv.) and the reaction mixture was stirred at r.t. for 1 h. After this time the reaction mixture was concentrated *in vacuo* to afford a brown residue. The crude oil was purified by silica gel flash column chromatography (0-100% EtOAc in cyclohexane) to yield benzyl (*R*,*E*)-9-(5-(7-hydroxy-3,4-dihydroquinolin-1(2*H*)-yl)pent-1-en-1-yl)-2-methyl-4-oxo-2,3,4,5-tetrahydro-1*H*-benzo[*b*][1,4]diazepine-7-carboxylate as a viscous brown oil which was used without further purification. To this was added caesium carbonate (480.1 mg, 1.474 mmol, 3.0 equiv.), TBAI (181.4 mg, 0.491 mmol, 1.0 equiv.) and *tert*-butyl (*S*)-2-(bromomethyl)pyrrolidine-1-carboxylate (259.5 mg, 0.982 mmol, 2.0 equiv.) in a microwave vial which was sealed and placed under an inert atmosphere and then anhydrous DMF (1.25 mL) was added and the reaction mixture was stirred at 85 °C for 18 h. The reaction mixture was then diluted with 1M $K_2CO_{3(aq)}$ (100 mL) and this

was washed with EtOAc (3 × 50 mL), the combined organic layers were then washed with 5 wt% $LiCl_{(aq)}$ (3 × 50 mL), brine (100 mL), dried ($MgSO_4$), filtered and concentrated *in vacuo* to give a dark brown oil. The crude oil was then taken up in DMSO (1 mL) and purified by ACCQPrep method E, the product was loaded onto the High pH Xselect CSH C_{18} column (150mm x 30mm i.d. 5µm packing diameter) column and was eluted using 80-99% acetonitrile(B)/10mM ammonium bicarbonate in water adjusted to pH 10 with ammonia solution(A) gradient over 17 mins and the resultant product was concentrated under a stream of nitrogen at 40 °C to give benzyl (*R*)-9-((*E*)-5-(7-(((*S*)-1-(*tert*-butoxycarbonyl)pyrrolidin-2-yl)methoxy)-3,4-dihydroquinolin-1(2*H*)-yl)pent-1-en-1-yl)-2-methyl-4-oxo-2,3,4,5-tetrahydro-1*H*-benzo[*b*][1,4]diazepine-7-carboxylate as a colourless oil (17 mg, 5% yield); R_f 0.50 (EtOAc); $[\alpha]_D^{20}$ = −2.24 (*c* 0.5, MeCN); $\bar{\nu}_{max}$ (thin film MeCN)/ cm^{-1} 2932 (C-H, br, m), 1675 (C=O, s), 1508 (C=C, s), 1206 (C-O, s); ^{1}H NMR (600 MHz, d_6-DMSO) δ_H 9.57 (1H, s, NH-1a/2), 7.65 (2H, d, *J* 2.2 Hz, H-7), 7.48 (1H, d, *J* 2.2 Hz, H-9), 7.45 – 7.38 (4H, m, H-4', H-5'), 7.37 – 7.33 (1H, m, H-6'), 6.73 (1H, d, *J* 8.4 Hz, H-5''), 6.64 (1H, d, *J* 15.4 Hz, H-5'''), 6.15 – 6.12 (1H, m, H-8''), 6.14 (1H, dt, *J* 15.4, 7.0 Hz, H-4'''), 6.07 (1H, br s, H-6''), 5.43 (1H, br s), 5.30 (2H, s, H-1'), 4.05 – 3.96 (1H, m, H-4), 3.96 – 3.89 (2H, m, H_AH_B-1'''', H-2''''), 3.73 (1H, dd, *J* 9.2, 7.3 Hz, H_AH_B-1''''), 3.31 – 3.25 (2H, m, H-5''''), 3.21 – 3.20 (4H, m, H-1'', H-1'''), 2.59 (2H, br t, *J* 6.2 Hz, H-3''), 2.53 – 2.52 (1H, m, H_AH_B-3), 2.28 (3H, br dd, *J* 13.6, 7.3 Hz, H_AH_B-3, H-3'''), 1.85 – 1.79 (4H, m, H-2'', H-3''''), 1.76 – 1.70 (4H, m, H-2''', H-4''''), 1.38 (9H, br s, H-8''''), 1.25 (3H, d, *J* 6.24 Hz, C-10); ^{13}C NMR (151 MHz, d_6-DMSO) δ_C 171.1 (C-2), 165.3 (C-1'), 158.0 (C-7''), 153.7 (C-6''''), 145.8 (C-9''), 140.8 (C-5a), 136.5 (C-3'), 133.5 (C-4'''), 129.2 (C-5''), 128.4 (C-5'), 128.1 (C-6'), 127.9 (C-6), 127.8 (C-4'), 127.6 (C-8), 125.6 (C-5''), 123.7 (C-7), 122.0 (C-9), 119.0 (C-), 114.5 (C-4''), 100.6 (C-6'') 97.5 (C-8'') 78.5

(C-7’’’’), 67.9 (C-1’’’’), 65.5 (C-2’), 55.6 (C-2’’’’), 52.8 (C-4), 50.2 (C-5’’’’), 48.6 (C-1’’’), 46.4 (C-1’’), 40.8 (C-3), 30.3 (C-2’’’), 28.1 (C-3’’’’, C-8’’’’) 26.9 (C-3’’), 25.2 (C-2’’’), 23.4 (C-10), 22.0 (C-2’’, C-4’’’’); HRMS *m/z* (ESI^+) [found 709.3956 $C_{42}H_{53}N_2O_4$ requires 709.3965 $[M+H]^+$]; LRMS *m/z* (ESI^+) 709.3 ($[M+H^+]$, 30%), 609.3 ($[M\text{-}Boc^+]$, 100%); LC-MS, HpH method (retention time 1.63 mins) 95.9% purity.

tert-Butyl (*R*)-2-(((1-((*E*)-5-((*R*)-8-((benzyloxy)carbonyl)-4-methyl-2-oxo-2,3,4,5-tetrahydro-1*H*-benzo[*b*][1,4]diazepin-6-yl)pent-4-en-1-yl)-1,2,3,4-tetrahydroquinolin-7-yl)oxy)methyl)morpholine-4-carboxylate (compound **38**)

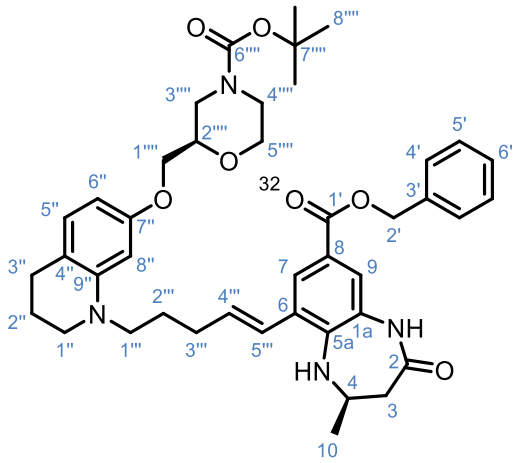

To a solution of benzyl (*R,E*)-2-methyl-4-oxo-9-(5-(7-((triisopropylsilyl)oxy)-3,4-dihydroquinolin-1(2*H*)-yl)pent-1-en-1-yl)-2,3,4,5-tetrahydro-1*H*-benzo[*b*][1,4]diazepine-7-carboxylate (250.0 mg, 0.367 mmol, 1.0 equiv.) in THF (5.00 mL) was added 1M TBAF in THF (191.7 mg, 733.2 µL, 0.733 mmol, 2.0 equiv.)and the reaction mixture was stirred at r.t. for 1 h. After this time the reaction mixture was concentrated *in vacuo* to afford a brown residue. The crude oil was purified by silica gel flash column chromatography (0-100% EtOAc in cyclohexane) to yield benzyl (*R*,*E*)-9-(5-(7-hydroxy-3,4-dihydroquinolin-1(2*H*)-yl)pent-1-en-1-yl)-2-methyl-4-oxo-2,3,4,5-tetrahydro-1*H*-benzo[*b*][1,4]diazepine-7-carboxylate as a viscous brown oil which was used without further purification. To this was added caesium carbonate

(358.0 mg, 1.10 mmol, 3.0 equiv.) and *tert*-butyl (*R*)-2-(bromomethyl)morpholine-4-carboxylate (205.4 mg, 0.733 mmol, 2.0 equiv.) in a microwave vial which was sealed and placed under an inert atmosphere and then anhydrous DMF (1.00 mL) was added, and the reaction mixture was stirred at 85 °C for 18 h. The reaction mixture was diluted 1M $K_2CO_{3(aq)}$ (100 mL), this wash washed with EtOAC (3 × 50 mL), the combined organic layers were then washed with 5 wt% $LiCl_{(aq)}$ (3 × 50 mL), brine (100 mL), dried ($MgSO_4$), filtered and then dried *in vacuo* to give a light brown oil. The crude oil was then taken up in DMSO (1 mL) and purified by ACCQPrep method E using 80-99% acetonitrile(B)/10mM ammonium bicarbonate in water adjusted to pH 10 with ammonia solution(A) gradient over 17 mins followed by further purification using MDAP purified using 100mg HpH extended method E and was loaded onto the High pH Xselect CSH C_{18} column (150mm x 30mm i.d. 5µm packing diameter) column. The product was then eluted using 80-99% acetonitrile(B)/10mM ammonium bicarbonate in water adjusted to pH 10 with ammonia solution(A) gradient over 32 mins and the resultant solution was concentrated under a stream of nitrogen at 40 °C give the *tert*-butyl (*R*)-2-(((1-((*E*)-5-((*R*)-8-((benzyloxy)carbonyl)-4-methyl-2-oxo-2,3,4,5-tetrahydro-1*H*-benzo[*b*][1,4]diazepin-6-yl)pent-4-en-1-yl)-1,2,3,4-tetrahydroquinolin-7-yl)oxy)methyl)morpholine-4-carboxylate as a colourless oil (87 mg, 32% yield); R_f 0.46 (EtOAc); $[\alpha]_D^{19}$ = +3.91 (*c* 0.6, MeCN); $\bar{\nu}_{max}$ (thin film MeCN)/ cm^{-1} 2930 (C-H, br, m), 1679 (C=O, s), 1508 (C=C, s), 1209 and 1170 (C-O, s); ^{1}H NMR (600 MHz, d_6-DMSO) δ_H 9.56 (1H, s, NH-1a/2), 7.64 (1H, d, *J* 2.1 Hz, H-7), 7.47 (1H, d, *J* 2.1 Hz, H-9), 7.44 – 7.42 (2H, m, H-4'), 7.40 – 7.37 (2H, m, H-5'), 7.35 – 7.32 (1H, m, H-6'), 6.74 (1H, d, *J* 8.1 Hz, H-5''), 6.64 (1H, d, *J* 15.5 Hz, H-5'''), 6.13 (1H, dt, *J* 15.3, 6.8 Hz, H-4'''), 6.09 (1H, d, *J* 2.4 Hz, H-8''), 6.04 (1H, dd, *J* 8.1, 2.4 Hz, H-6''), 5.44 (1H, d, *J* 3.4 Hz, NH-4/5a), 5.29 (2H, s, H-2'), 4.04 – 3.98 (1H, m, H-4), 3.90 – 3.83 (2H, m, H-1''''), 3.82

– 3.79 (1H, m, H_AH_B-5''''), 3.73 – 3.68 (1H, m, H_AH_B-4''''), 3.62 – 3.56 (1H, m, H-2''''), 3.39 (1H, td, *J* 11.6, 2.8 Hz, H_AH_B-5''''), 3.27 (2H, t, *J* 7.4 Hz, H-1'''), 3.23 (2H, t, *J* 5.6 Hz, H-1''), 2.93 – 2.79 (1H, m, H_AH_B-4''''), 2.79 – 2.69 (2H, m, H-3''''), 2.59 (2H, q, *J* 7.0 Hz, H-3''), 2.52 (1H, m, H_AH_B-3), 2.31 – 2.24 (3H, m, H_AH_B-3, H-3'''), 1.85 – 1.78 (2H, m, H-2''), 1.72 (2H, p, *J* 7.5 Hz, H-2'''), 1.39 (9H, s, H-8''''), 1.24 (3H, d, *J* 6.3 Hz, H-10); ^{13}C NMR (151 MHz, d_6-DMSO) δ_C 171.15 (C-2), 165.28 (C-1'), 157.8 (C-7''), 153.9 (C-6''''), 145.8 (C-9'') , 140.8 (C-5a), 136.5 (C-3'), 133.5 (C-4'''), 129.2 (C-5''), 128.4 (C-5'), 128.1 (C-6), 127.9 (C-6'), 127.8 (C-4'), 127.6 (C-1a), 125.6 (C-5'''), 123.7 (C-7), 122.0 (C-9), 119.0 (C-8), 114.7 (C-4''), 100.4 (C-6''), 97.2 (C-8''), 79.1 (C-7''''), 73.4 (C-2''''), 67.9 (C-1''''), 65.5 (C-2', C-5''''), 52.8 (C-4), 50.2 (C-1'''), 48.6 (C-1''), 43.8 (C-4'''') 40.9 (C-3), 30.3 (C-3'''), 28.0 (C-8''''), 26.9 (C-3''), 25.2 (C-2'''), 23.4 (C-10), 21.9 (C-2''); HRMS *m/z* (ESI$^+$) [Found 725.3904 Chemical Formula: $C_{42}H_{55}N_4O_7$ requires 725.3914 $[M+H]^+$]; LRMS *m/z* (ESI$^+$) 725.3 ([M+H$^+$], 100%), 625.3 ([M-Boc$^+$], 100%); LC-MS, HpH method (retention time 1.57 mins) 100% purity.

(*R*,*E*)-2-Methyl-1,2,3,10,11,17,18,20,21,22-decahydro-16*H*-13,15-(epiethane[1,2]diylidene)-7,25-(metheno)[1,4]diazepino[2,3-*h*]pyrido[1,2-*p*][1]oxa[4,16]diazacyclononadecine-4,8(5*H*,9*H*)-dione (compound or ligand **14**)

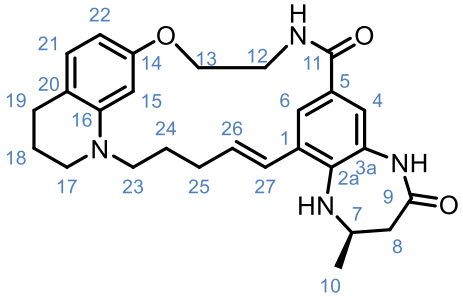

Benzyl (*R,E*)-9-(5-(7-(2-((*tert*-butoxycarbonyl)amino)ethoxy)-3,4-dihydroquinolin-1(2*H*)-yl)pent-1-en-1-yl)-2-methyl-4-oxo-2,3,4,5-tetrahydro-1*H*-benzo[*b*][1,4]diazepine-7-carboxylate (55.0 mg, 0.0822 mmol, 1.0 equiv.) was

dissolved in a mixture of THF/MeOH/H_2O (3:2:1, 3 mL) to this is added lithium hydroxide (27.6 mg, 1.15 mmol, 14.0 equiv.) and this reaction mixture was then stirred at room temperature for 5 h. Upon the completion of this reaction, the solvents mixture was removed *in vacuo* to give a yellow residue. To this was added CH_2Cl_2 (1.70 mL) followed by careful addition of TFA (1.70 mL) and the reaction mixture was then stirred at room temperature overnight. After this time the reaction mixture was concentrated under a stream of nitrogen to give a dark brown oil. The resultant oil was placed under a nitrogen atmosphere and was then taken up in DMF (2 mL) and the resultant dark red solution was then added to PyBOP (47.1 mg, 0.0905 mmol, 1.1 equiv.), DIPEA (4.40 mL) and the remaining volume of DMF (34.7 mL). Upon complete addition the reaction mixture was then stirred at room temperature for 20 h. After this time the reaction mixture was concentrated under a stream of nitrogen at 50 °C to give a dark brown oil. This was diluted with 1.0 M $K_2CO_{3(aq)}$ (50 mL), this was washed with $CHCl_3$/IPA (9:1) mixture (3 × 25 mL) with the combined organic layers then washed with 5 wt% $LiCl_{(aq)}$ (3 × 25 mL), brine (25 mL), dried ($MgSO_4$), filtered and concentrated to give a light brown oil. The crude oil was then taken up in DMSO (1 mL) and was then purified by ACCQPrep Formic acid method C using 30-99% 0.1% *v*/*v* formic acid in acetonitrile(B)/0.1% *v*/*v* formic acid in water solution(A) gradient over 17 mins. Any residual unpurified compound in DMSO was further diluted until the total volume was again 1 mL in DMSO and this residual compound was purified by MDAP Formic acid method C and was loaded onto the High pH Xselect CSH C_{18} column (150mm x 30mm i.d. 5µm packing diameter) column. The product was then eluted using 30-99% 0.1% *v*/*v* formic acid in acetonitrile(B)/0.1% *v*/*v* formic acid in water solution(A) gradient over 17 minutes. The pure fractions from both the ACCQPrep and MDAP were combined and concentrated under a stream of nitrogen at 40 °C overnight to give (*R,E*)-2-methyl-

1,2,3,10,11,17,18,20,21,22-decahydro-16*H*-13,15-(epiethane[1,2]diylidene)-7,25-(metheno)[1,4]diazepino[2,3-*h*]pyrido[1,2-*p*][1]oxa[4,16]diazacyclononadecine-4,8(5*H*,9*H*)-dione (5.5 mg, 15% yield) as a colourless solid; R_f 0.55 (acetone); $[\alpha]_D^{18}$ = −2.46 (*c* 0.5 ,$CHCl_3$); $\bar{\nu}_{max}$ (thin film in MeCN)/ cm^{-1} 3339 (N-H, br), 2931 (C-H, m), 1668 (C=O, s), 1507 (C=C, s); ^1H NMR (600 MHz, d_6-DMSO) δ_H 9.52 (1H, s, NH-3a/9), 8.21 (1H, t, *J* 5.5 Hz, NH-11/12), 7.57 (1H, d, *J* 2.0 Hz, H-6), 7.13 (1H, d, *J* 2.0 Hz, H-4), 6.77 (1H, d, *J* 8.0 Hz, H-21), 6.69 (1H, d, *J* 15.2 Hz, H-27), 6.43 – 6.34 (2H, m, H-15, H-26), 6.18 (1H, dd, *J* 8.0, 2.2 Hz, H-22), 5.03 (1H, d, *J* 3.1 Hz, NH-2a/7), 4.02 – 3.94 (3H, m, H-7, H-13), 3.57 – 3.50 (2H, m, H-12), 3.26 – 3.18 (4H, m, H-17, H-23), 2.59 (2H, t, *J* 6.3 Hz, H-19), 2.45 (1H, dd, *J* 13.3, 4.2 Hz, H_AH_B-7), 2.32 – 2.24 (2H, m, H-25), 2.20 (dd, *J* 13.3, 7.4 Hz, H_AH_B-7), 1.85 – 1.77 (2H, m, H-18), 1.74 – 1.67 (2H, m, H-24), 1.23 (3H, d, *J* 6.2 Hz, H-10); ^{13}C NMR (151 MHz, d_6-DMSO) δ_C 171.3 (C-9), 167.4 (C-11), 158.8 (C-14), 145.9 (C-16), 138.5 (C-2a), 133.7 (C-26), 129.2 (C-5, C-21), 128.3 (C-1), 127.2 (C-27), 123.8 (C-), 120.0 (C-3a), 116.1 (C-20), 101.9 (C-22), 100.6 (C-15), 68.1 (C-13), 53.9 (C-7), 49.1 (C-23), 47.8 (C-17), 40.7 (C-8), 38.7 (C-12), 29.1 (C-25), 27.0 (C-19), 25.0 (C-24), 23.5 (C-10), 21.9 (C-18); HRMS *m/z* (ESI^+) [Found 461.2559 $C_{27}H_{32}N_4O_3$ requires 461.2565 $[M+H]^+$]; LRMS *m/z* (ESI^+) 461.27 ($[M+H^+]$, 100%); LC-MS, Formic method: retention time 1.10 mins, 100% purity; HPLC: retention time 10.09 mins, 99.4% purity.

(*R*,*E*)-2-Methyl-1,2,3,10,11,12,13,19,20,22,23,24-dodecahydro-18*H*-15,17-(epiethane[1,2]diylidene)-7,27-(metheno)[1,4]diazepino[2,3-*l*]pyrido[2,1-*d*][1]oxa[5,17]diazacyclohenicosine-4,8(5*H*,9*H*)-dione (compound or ligand **15**)

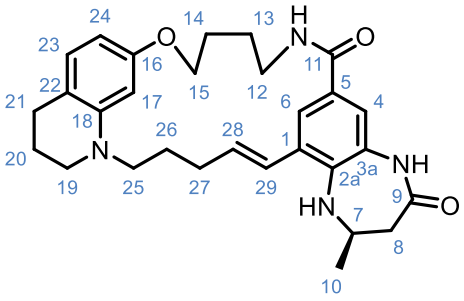

Benzyl (*R,E*)-9-(5-(7-(4-((*tert*-butoxycarbonyl)amino)butoxy)-3,4-dihydroquinolin-1(2*H*)-yl)pent-1-en-1-yl)-2-methyl-4-oxo-2,3,4,5-tetrahydro-1*H*-benzo[*b*][1,4]diazepine-7-carboxylate (41.0 mg, 0.0588 mmol, 1.0 equiv.) was dissolved in a mixture of THF/MeOH/H_2O (3:2:1, 3.0 mL) to this is added lithium hydroxide (19.7 mg, 0.827 mmol, 14.0 equiv.) and this reaction mixture was then stirred at room temperature for 5 h. Upon the completion of this reaction, the solvents mixture was removed *in vacuo* to give a brown residue. To this was added CH_2Cl_2 (1.50 mL) followed by careful addition of TFA (1.50 mL) and the reaction mixture was then stirred at room temperature overnight. After this time the reaction mixture was concentrated under a constant stream of nitrogen to give a brown oil. The resultant oil was taken up in 2 mL of DMF and was then added PyBOP (33.7 mg, 0.0647 mmol, 1.1 equiv.), DIPEA (2.94 mL) and the remaining volume of DMF (24.5 mL) the reaction mixture was then stirred at room temperature for 20 h. After this time the reaction mixture was concentrated under a stream of nitrogen at 50 °C to give a dark brown oil. This was diluted with 1.0 M $K_2CO_{3(aq)}$ (50 mL), which was then washed with $CHCl_3$/IPA (9:1) mixture (3 × 25 mL) with the combined organic layers then washed with 5 wt% $LiCl_{(aq)}$ (3 × 25 mL), brine (25 mL), dried ($MgSO_4$), filtered and concentrated to give a

light brown oil. The crude oil was then taken up in DMSO (1 mL) and purified using ACCQPrep Formic acid, method D using 50-99% 0.1% *v*/*v* formic acid in acetonitrile(B)/0.1% *v*/*v* formic acid in water solution(A) gradient over 17 mins followed the resultant fractions containing product (assessed by LC-MS) were concentrated under a stream of nitrogen at 40 °C overnight. Any residual unpurified compound in DMSO was further diluted until the total volume was again 1 mL in DMSO and this residual compound was purified by MDAP Formic acid method C and was loaded onto the High pH Xselect CSH C_{18} column (150mm x 30mm i.d. 5µm packing diameter) column. The product was then eluted using 35-99% 0.1% *v*/*v* formic acid in acetonitrile(B)/0.1% *v*/*v* formic acid in water solution(A) gradient over 17 minutes. The pure fractions from both the ACCQPrep and MDAP were combined and concentrated under a stream of nitrogen at 40 °C overnight to give (*R,E*)-2-methyl-1,2,3,10,11,12,13,19,20,22,23,24-dodecahydro-18*H*-15,17-(epiethane[1,2]diylidene)-7,27-(metheno)[1,4]diazepino[2,3-*l*]pyrido[2,1-*d*][1]oxa[5,17]diazacyclohenicosine-4,8(5*H*,9*H*)-dione (5.4 mg, 19% yield) as a colourless solid; R_f 0.4 (acetone); $[\alpha]_D^{18}$ = +10.28 (*c* 0.5, $CHCl_3$); $\bar{\nu}_{max}$ (thin film in MeCN)/ cm^{-1} 3339 (N-H, br), 2932 (C-H, m), 1669 (C=O, s), 1509 (C=C, s); ^{1}H NMR (600 MHz, $CDCl_3$); δ_H 7.60 (1H, d, *J* 2.0 Hz, H-4), 7.43 (1H, d, *J* 2.0 Hz, H-6), 7.40 (1H, s, NH-3a/9), 7.01 (1H, t, *J* 6.0 Hz, NH-11/12), 6.87 (1H, d, *J* 8.0 Hz, H-23), 6.49 (1H, d, *J* 15.3 Hz, H-29), 6.21 – 6.16 (2H, m, H-17, H-28), 6.14 (1H, dd, *J* 8.0, 2.4 Hz, H-24), 4.16 – 4.08 (1H, m, H-7), 4.04 (2H, dd, *J* 5.5, 4.2 Hz, H-15), 3.83 (1H, s, NH-2a/7), 3.54 (2H, p, *J* 5.4 Hz, H-12), 3.35 – 3.23 (4H, m, H-19, H-25), 2.70 (2H, t, *J* 6.3 Hz, H-21), 2.67 (1H, dd, *J* 13.8, 3.5 Hz, H_AH_B-7), 2.51 (1H, dd, *J* 13.8, 8.2 Hz, H_AH_B-7), 2.39 – 2.28 (2H, m, H-27), 1.98 – 1.89 (4H, m, H-14, H-20), 1.85 – 1.75 (4H, m, H-13, H-26), 1.40 (3H, d, *J* 6.3 Hz, H-10); ^{13}C NMR (151 MHz, $CDCl_3$) δ_C 171.85 (C-9), 165.57 (C-11), 158.3 (C-16), 145.7 (C-18),

138.2 (C-2a), 136.6 (C-28), 129.7 (C-23), 129.2 (C-1), 127.1 (C-29), 127.06 (C-5), 125.9 (C-3a), 122.0 (C-4), 121.9 (C-6), 116.0 (C-22), 98.5 (C-24), 98.3 (C-17), 68.0 (C-15), 53.3 (C-7), 49.2 (C-25), 48.8 (C-19), 41.5 (C-8), 38.1 (C-12), 29.9 (C-26), 27.5 (C-21), 26.6 (C-20), 25.4 (C-14), 24.4 (C-10), 23.8 (C-13), 22.4 (C-20); HRMS *m/z* (ESI^+) [Found 489.2869 $C_{29}H_{37}N_4O_3$ requires 489.2866 $[M+H]^+$]; LRMS *m/z* (ESI^+) 489.29 ($[M+H^+]$, 100%); LC-MS, Formic method: retention time 1.22 mins, 100% purity; HPLC: retention time 11.11 mins, 96.6% purity.

(2*R*,12a*R*,*E*)-2-Methyl-1,2,3,11,12,12a,13,19,20,22,23,24-dodecahydro-8*H*,10*H*,18*H*-15,17-(epiethane[1,2]diylidene)-7,27-(metheno)[1,4]diazepino[2,3-*h*]pyrido[1,2-*p*]pyrrolo[2,1-*c*][1]oxa[4,16]diazacyclononadecine-4,8(5*H*)-dione (compound or ligand **16**)

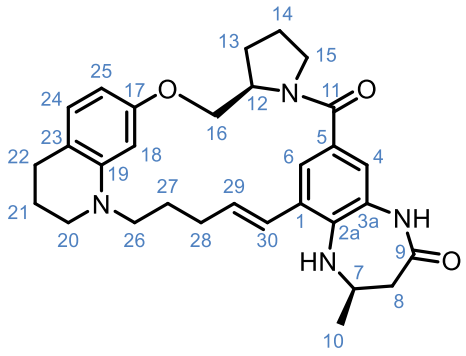

Benzyl (*R*)-9-((*E*)-5-(7-(((*R*)-1-(*tert*-butoxycarbonyl)pyrrolidin-2-yl)methoxy)-3,4-dihydroquinolin-1(2*H*)-yl)pent-1-en-1-yl)-2-methyl-4-oxo-2,3,4,5-tetrahydro-1*H*-benzo[*b*][1,4]diazepine-7-carboxylate (27.0 mg, 0.0381 mmo, 1.0 equiv.) was dissolved in a mixture of THF/MeOH/H_2O (3:2:1, 3 mL) to this is added lithium hydroxide lithium hydroxide (12.8 mg, 0.533 mmol, 14.0 equiv.) and this reaction mixture was then stirred at room temperature for 5 h. Upon the completion of this reaction, the solvents mixture was removed *in vacuo* to give a brown residue. To this was added CH_2Cl_2 (1.5 mL) followed by careful addition of TFA (1.5 mL) and the

reaction mixture was then stirred at room temperature overnight. After this time the reaction mixture was concentrated under a constant stream of nitrogen to give a brown oil. The resultant oil was taken up in DMF (4.0 mL) and was then loaded into to an appropriately sized reaction vessel under a nitrogen atmosphere containing PyBOP (21.8 mg, 0.0419 mmol, 1.1 equiv.), DIPEA (1.9 mL) and the remaining volume of DMF (13.1 mL) the reaction mixture was then stirred at room temperature for 20 h. After this time the reaction mixture was concentrated under a stream of nitrogen at 50 °C to give a dark brown oil. This was diluted with 1.0 M $K_2CO_{3(aq)}$ (50 mL), which was then washed with $CHCl_3$/IPA (9:1) mixture (3 × 25 mL) with the combined organic layers then washed with 5% wt% $LiCl_{(aq)}$ (3 × 25 mL), brine (25 mL), dried ($MgSO_4$), filtered and concentrated to give a light brown oil. The crude product was then taken up in DMSO and purified using ACCQPrep and purified utilising the ACCQPrep HpH method C using 30-99% acetonitrile(B)/10mM ammonium bicarbonate in water adjusted to pH 10 with ammonia solution(A) gradient over 17 mins. Any residual unpurified compound in DMSO from the ACCQPrep purification was further diluted until the total volume was 1 mL in DMSO and this residual compound was purified by MDAP (HpH method C) and was loaded onto the High pH Xselect CSH C_{18} column (150mm x 30mm i.d. 5µm packing diameter) column. The product was then eluted using 30-99% acetonitrile(B)/10mM ammonium bicarbonate in water adjusted to pH 10 with ammonia solution(A) gradient over 17 mins. The pure fractions from both the ACCQPrep and MDAP were combined and concentrated under a stream of nitrogen at 40 °C overnight to give (2*R*,12a*R*,*E*)-2-methyl-1,2,3,11,12,12a,13,19,20,22,23,24-dodecahydro-8*H*,10*H*,18*H*-15,17-(epiethane[1,2]diylidene)-7,27-(metheno)[1,4]diazepino[2,3-*h*]pyrido[1,2-*p*]pyrrolo[2,1-*c*][1]oxa[4,16]diazacyclononadecine-4,8(5*H*)-dione as an off-white solid (9.7, 51% yield); R_f 0.29 (acetone); $[\alpha]_D^{19}$ = +127.93 (*c* 1.0, $CHCl_3$); $\bar{\nu}_{max}$

(thin film in)/ cm^{-1} 2929 (C-H, m) 1671 and 1611 (C=O, s), 1507 (C=C, m) and 1431 (C-H, s); ^{1}H NMR (600 MHz,d_6-DMSO) δ_H 9.13 (1H, s, NH-3a/9), 7.39 (1H, d, *J* 1.9 Hz, H-6), 6.86 (1H, d, *J* 1.9 Hz, H-4), 6.76 – 6.68 (2H, m, H-24, H-30), 6.27 (1H, ddd, *J* 15.1, 9.1, 5.5 Hz, H-29), 6.16 (1H, d, *J* 2.3 Hz, H-18), 6.05 (1H, dd, *J* 8.1, 2.3 Hz, H-25), 4.65 (1H, d, *J* 3.4 Hz, NH-2a/7), 4.17 (1H, s, H-12), 4.04 – 3.92 (2H, m, H-7, H_AH_B-16), 3.85 – 3.79 (1H, m, H_AH_B-16), 3.71 – 3.65 (1H, m, H_AH_B-15), 3.40 (1H, m, H_AH_B-15), 3.34 – 3.17 (4H, m, H-20, H-26), 2.60 (2H, td, *J* 6.4, 2.7 Hz, H-22), 2.55 (1H, dd, *J* 13.5, 4.5 Hz, H_AH_B-8), 2.36 – 2.26 (1H, m, H_AH_B-28), 2.25 – 2.16 (2H, m, H_AH_B-8, H_AH_B-28), 2.08 – 1.94 (1H, m, H_AH_B-27), 1.92 – 1.79 (3H, m, H-21, H_AH_B-27), 1.79 – 1.64 (2H, m, H-14), 1.28 (3H, d, *J* 6.2 Hz, H-10); ^{13}C NMR (151 MHz, d_6-DMSO) δ_C 170.7 (C-9), 168.8 (C-11), 157.7 (C-17), 145.4 (C-19), 136.4 (C-2a), 132.6 (C-29), 129.3 (C-3a), 128.5 (C-24), 128.2 (C-30), 126.5 (C-1), 121.8 (C-6), 118.0 (C-4), 115.1 (C-23), 100.0 (C-25), 98.4 (C-18), 66.1 (C-16), 56.5 (C-12), 53.0 (C-7), 48.0 (C-26), 47.5 (C-20), 45.7 (C-15), 40.2 (C-7), 28.1 (C-28), 27.3 (C-27), 26.4 (C-22), 24.8 (C-14), 22.5 (C-7), 22.4 (C-13), 21.6 (C-21); HRMS *m/z* (ESI^+) [Found 501.2868 $C_{30}H_{37}N_4O_3$ requires 501.2866 $[M+H]^+$]; LRMS *m/z* (ESI^+) 501.4 ($[M+H^+]$, 100%); LC-MS, Formic method (retention time 1.18 mins) 98% purity; HPLC: retention time 10.74 mins, 95.1% purity.

(2*R*,12*aS*,*E*)-2-Methyl-1,2,3,11,12,12a,13,19,20,22,23,24-dodecahydro-8*H*,10*H*,18*H*-15,17-(epiethane[1,2]diylidene)-7,27-(metheno)[1,4]diazepino[2,3-*h*]pyrido[1,2-*p*]pyrrolo[2,1-*c*][1]oxa[4,16]diazacyclononadecine-4,8(5*H*)-dione (compound or ligand **17**)

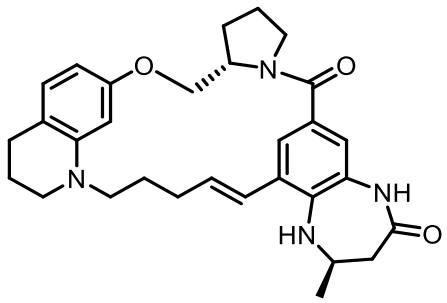

Benzyl (*R*)-9-((*E*)-5-(7-(((*S*)-1-(*tert*-butoxycarbonyl)pyrrolidin-2-yl)methoxy)-3,4-dihydroquinolin-1(2*H*)-yl)pent-1-en-1-yl)-2-methyl-4-oxo-2,3,4,5-tetrahydro-1*H*-benzo[*b*][1,4]diazepine-7-carboxylate (16.0 mg, 0.0226 mmol, 1.0 equiv.) was dissolved in a mixture of THF/MeOH/H_2O (3:2:1, 3 mL) to this is added lithium hydroxide lithium hydroxide (7.57 mg, 0.316 mmol, 14.0 equiv.) and this reaction mixture was then stirred at room temperature for 5 h. Upon the completion of this reaction, the solvents mixture was removed *in vacuo* to give a brown residue. To this was added CH_2Cl_2 (1.5 mL) followed by careful addition of TFA (1.5 mL) and the reaction mixture was then stirred at room temperature overnight. After this time the reaction mixture was concentrated under a constant stream of nitrogen to give a brown oil. The resultant oil was taken up in DMF (4.0 mL) and was then added to an appropriately sized reaction vessel under a nitrogen atmosphere containing PyBOP (12.9 mg, 0.0248 mmol, 1.1 equiv.), DIPEA (1.12 mL) and the remaining volume of DMF (6.2 mL) the reaction mixture was then stirred at room temperature for 20 h. After this time the reaction mixture was concentrated under a stream of nitrogen at 50 °C to give a dark brown oil. This was diluted with 1.0 M $K_2CO_{3(aq)}$ (50 mL), which was then

washed with $CHCl_3$/IPA (9:1) mixture (3 × 25 mL) with the combined organic layers then washed with 5 wt% $LiCl_{(aq)}$ (3 × 25 mL), brine (25 mL), dried ($MgSO_4$), filtered and concentrated to give a light brown oil. The crude product was then taken up in DMSO and purified using ACCQPrep and purified utilising the ACCQPrep HpH method C using 30-99% acetonitrile(B)/10mM ammonium bicarbonate in water adjusted to pH 10 with ammonia solution(A) gradient over 17 mins. Any residual unpurified compound in DMSO from the ACCQPrep purification was further diluted until the total volume was 1 mL in DMSO and this residual compound was purified by MDAP (HpH method C) and was loaded onto the High pH Xselect CSH C_{18} column (150mm x 30mm i.d. 5µm packing diameter) column. The product was then eluted using 30-99% acetonitrile(B)/10mM ammonium bicarbonate in water adjusted to pH 10 with ammonia solution(A) gradient over 17 mins. The pure fractions from both the ACCQPrep and MDAP were combined and concentrated under a stream of nitrogen at 40 °C overnight to give (2*R*,12a*S*,*E*)-2-methyl-1,2,3,11,12,12a,13,19,20,22,23,24-dodecahydro-8*H*,10*H*,18*H*-15,17-(epiethane[1,2]diylidene)-7,27-(metheno)[1,4]diazepino[2,3-*h*]pyrido[1,2-*p*]pyrrolo[2,1-*c*][1]oxa[4,16]diazacyclononadecine-4,8(5*H*)-dione as an off-white solid (5.0 mg, 44% yield); R_f 0.31 (acetone); $[\alpha]_D^{19}$ = −53.43 (*c* 0.5, $CHCl_3$); $\bar{\nu}_{max}$ (thin film in $CHCl_3$)/ cm^{-1} 2929 (C-H, m) 1671 and 1611 (C=O, s), 1508 (C=C, m) and 1431 (C-H, s); ^1H NMR (600 MHz, d_3-MeCN) δ_H 7.80 (1H, br s), 7.49 (1H, br s), 6.77 – 6.84 (2H, m), 6.76 (1H, d, *J* 8.1 Hz), 6.63 (1H, br d, *J* 15.4 Hz), 6.35 (1H, br d, *J* 11.4 Hz), 6.13 (3H, br s), 5.99 – 6.08 (3 H, m), 3.98 – 4.12 (8H, m), 3.89 – 3.98 (5H, m), 3.49 - 3.66 (1H, m), 3.31 – 3.46 (1H, m), 3.20 - 3.30 (10H, m), 2.62 (2H, td, *J* 6.2, 2.6 Hz), 2.40 – 2.48 (1H, m), 2.28 – 2.38 (2H, m), 2.15 – 2.20 (1H, m), 1.96 – 2.05 (2H, m), 1.80 – 1.91 (4H, m), 1.70 – 1.80 (3H, m), 1.62 – 1.70 (2H, m), 1.28 (3H, d, *J* 6.2 Hz); ^{13}C NMR (151 MHz, d_3-MeCN) δ_C 171.8, 136.7, 134.4, 130.9, 129.7, 129.3,

126.7, 118.6, 99.5, 55.1, 48.2, 40.5, 28.9, 27.7, 27.0, 25.1, 23.4, 22.2; HRMS *m/z* (ESI^+) [Found 501.2859 $C_{30}H_{37}N_4O_3$ requires 501.2866 $[M+H]^+$]; LRMS *m/z* (ESI^+) 501.43 ($[M+H^+]$, 100%); LC-MS, Formic method (retention time 1.18 mins) 94% purity; HPLC: retention time 10.79 mins, 95.3% purity.

(2*R*,13*S*,*E*)-2-Methyl-1,2,3,11,12,13,14,20,21,23,24,25-dodecahydro-8*H*,10*H*,19*H*-16,18-(epiethane[1,2]diylidene)-9,13-methano-7,28-(metheno)[1,4]diazepino[2,3-*l*]pyrido[2,1-*d*][1]oxa[5,17]diazacyclodocosine-4,8(5*H*)-dione (compound or ligand **18**)

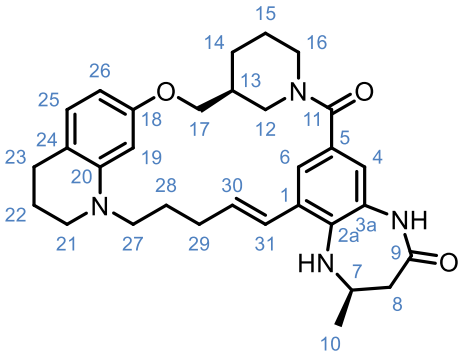

Benzyl (*R*)-9-((*E*)-5-(7-(((*S*)-1-(*tert*-butoxycarbonyl)piperidin-3-yl)methoxy)-3,4-dihydroquinolin-1(2*H*)-yl)pent-1-en-1-yl)-2-methyl-4-oxo-2,3,4,5-tetrahydro-1*H*-benzo[*b*][1,4]diazepine-7-carboxylate (127.0 mg, 0.176 mmol, 1 equiv.) was dissolved in a mixture of THF/MeOH/H_2O (3:2:1, 4.0 mL) to this is added LiOH (58.9 mg, 2.46 mmol, 14.0 equiv.) and this reaction mixture was then stirred at room temperature for 5 hour. Upon the completion of this reaction, the solvents mixture was removed under a constant stream of nitrogen at 40 °C to give a light brown residue. To this was added CH_2Cl_2 (2.0 mL) followed by careful addition of TFA (2.00 mL) and the reaction mixture was then stirred at room temperature overnight. After this time the reaction mixture was concentrated under a constant stream of nitrogen at 40 °C to give a brown oil. The resultant oil was taken up in 4 mL of DMF and was then added to an appropriately sized reaction vessel under a nitrogen atmosphere containing PyBOP (101 mg, 0.193

mmol, 1.1 equiv.), DIPEA (8.70 mL) and the remaining volume of DMF (75.2 mL) the reaction mixture was then stirred at room temperature for 20 h. After this time the reaction mixture was concentrated under a stream of nitrogen at 50 °C to give a dark brown oil. This was diluted with 1.0 M $K_2CO_{3(aq)}$ (50 mL), which was then washed with $CHCl_3$/IPA (9:1) mixture (3 × 25 mL) with the combined organic layers then washed with 5 wt% $LiCl_{(aq)}$ (3 × 25 mL), brine (25 mL), dried ($MgSO_4$), filtered and concentrated to give a brown oil. The crude product was then taken up in DMSO (1 mL) and purified using ACCQPrep HpH method D using 50-99% acetonitrile(B)/10mM ammonium bicarbonate in water adjusted to pH 10 with ammonia solution(A) gradient over 17 mins. followed by further purification using MDAP purified HpH method C and was loaded onto the High pH Xselect CSH C_{18} column (150mm x 30mm i.d. 5µm packing diameter) column. The product was then eluted using 50-99% acetonitrile(B)/10mM ammonium bicarbonate in water adjusted to pH 10 with ammonia solution(A) gradient over 17 mins. The pure fractions from both the ACCQPrep and MDAP were combined and concentrated under a stream of nitrogen at 40 °C overnight to give (2*R*,13*S*,*E*)-2-methyl-1,2,3,11,12,13,14,20,21,23,24,25-dodecahydro-8*H*,10*H*,19*H*-16,18-(epiethane[1,2]diylidene)-9,13-methano-7,28-(metheno)[1,4]diazepino[2,3-*l*]pyrido[2,1-*d*][1]oxa[5,17]diazacyclodocosine-4,8(5*H*)-dione as an off white solid (31.4 mg, 35% yield); R_f 0.58 (aceteone); $[\alpha]_D^{18}$ = +29.54 (*c* 0.5 , $CHCl_3$); $\bar{\nu}_{max}$ (thin film in)/ cm^{-1} 2926 (C-H), 1672 and 1610 (C=O), 1434 (C-H, s) and 1240 (C-O, m); ^{1}H NMR (600 MHz, d_6-DMSO); δ_H 9.53 (1H, s, NH-3a/9), 7.28 (1H, d, *J* 2.0 Hz, H-6), 6.88 (1H, d, *J* 2.0 Hz, H-4), 6.80 (1H, d, *J* 15.4 Hz, H-31), 6.72 (1H, d, *J* 8.7 Hz, H-25), 6.29 (1H, dt, *J* 15.4, 7.1 Hz, H-30), 6.02 – 5.98 (2H, m, H-19, H-26), 4.98 (1H, d, *J* 2.8 Hz, NH-2a/7), 4.04 – 3.94 (2H, m, H-7, H_AH_B-17), 3.93 – 3.82 (2H, m, H_AH_B-12, H_AH_B-16), 3.63 (1H, dd, *J* 9.3, 8.1 Hz, H_AH_B-17), 3.44 – 3.35 (1H, m, H_AH_B-27), 3.26 – 3.18 (3H,

m, H-21, H_AH_B-16), 3.16 – 3.06 (2H, m, H_AH_B-12, H_AH_B-27), 2.58 (2H, t, *J* 6.4 Hz, H-23), 2.46 (1H, dd, *J* 13.1, 4.6 Hz, H_AH_B-7), 2.33 – 2.21 (2H, m, H-29), 2.18 (1H, dd, *J* 13.1, 7.3 Hz, H_AH_B-7), 2.05 – 1.96 (1H, m, H-13), 1.82 (2H, p, *J* 6.0 Hz, H-22), 1.74 – 1.63 (4H, m, H_AH_B-14, H_AH_B-15, H-28), 1.50 (2H, t, *J* 8.8 Hz, H_AH_B-14, H_AH_B-15), 1.24 (3H, d, *J* 6.2 Hz, H-10); ^{13}C NMR (151 MHz, d_6-DMSO) δ_C 171.5 (C-9), 169.0 (C-11), 158.1 (C-18), 145.3 (C-20), 137.2 (C-2a), 132.0 (C-30), 131.3 (C-3a), 129.3 (C-25), 128.0 (C-1), 127.5 (C-5), 126.7 (C-31), 120.6 (C-4), 119.7 (C-6), 114.4 (C-24), 101.4 (C-26), 97.6 (C-19), 68.9 (C-17), 54.6 (C-7), 50.2 (C-12), 48.4 (C-27), 48.0 (C-21), 42.5 (C-16), 40.5 (C-8), 35.8 (C-13), 29.2 (C-29), 26.8 (C-23), 25.6 (C-14), 23.2 (C-28), 22.9 (C-10), 22.7 (C-15), 22.0 (C-22); HRMS *m/z* (ESI^+) [Found 515.3017 $C_{31}H_{39}N_4O_3$ requires 515.3022 $[M+H]^+$]; LRMS *m/z* (ESI^+) 515.34 ($[M+H^+]$, 100%); LC-MS, Formic method: retention time 1.26 mins, 100% purity; HPLC: retention time 11.45 mins, 95.3% purity.

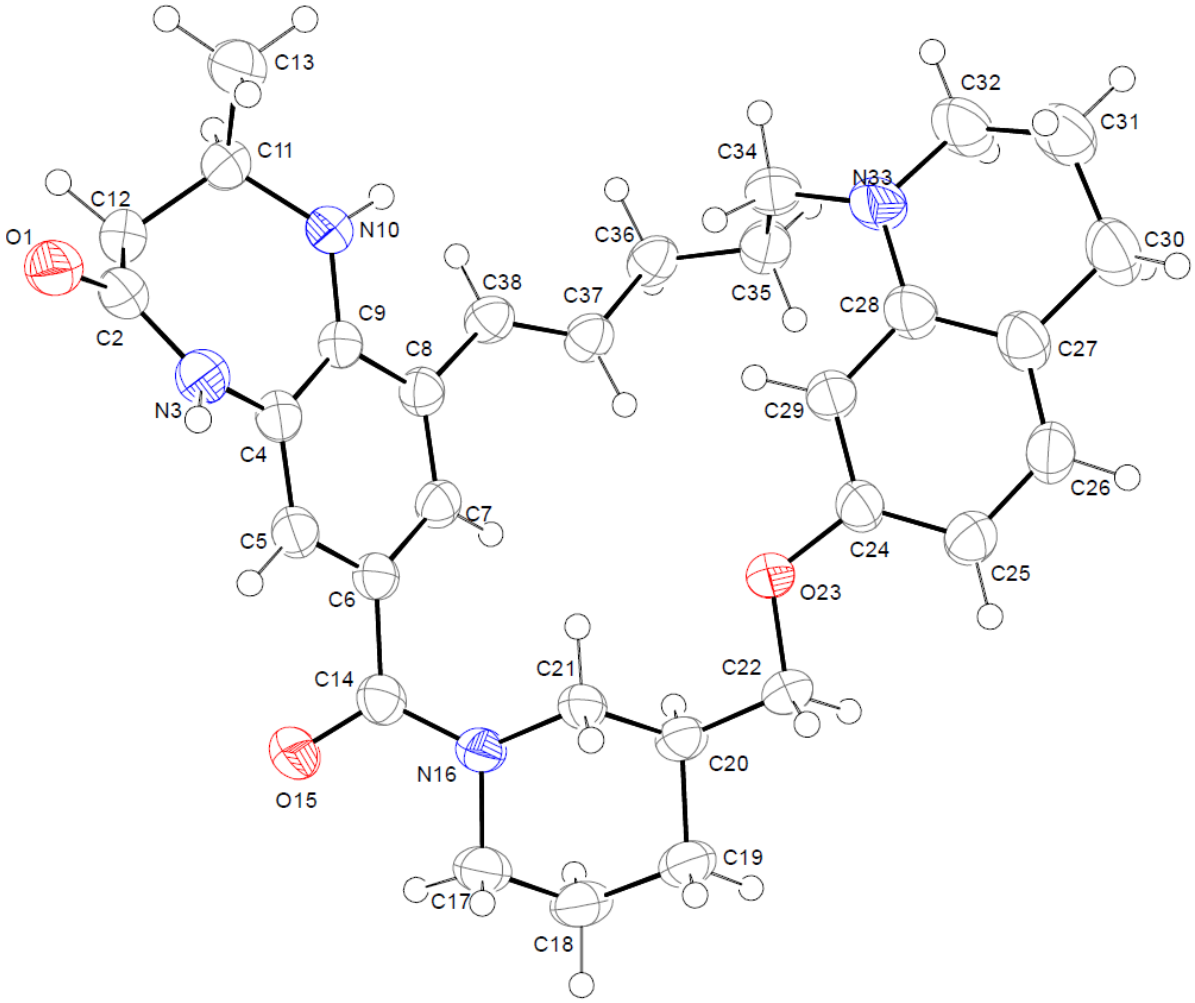
C13
C11
C12
O1
N10
C2
C9
C8
C38
C37
C36
C34
N33
C32
C31
C30
C35
C28
C27
N3
C4
C29
C26
C7
C5
C24
C25
C6
O23
C14
C21
C22
O15
N16
C20
C19
C17
C18

(2*R*,13*R*,*E*)-2-Methyl-1,2,3,10,11,13,14,20,21,23,24,25-dodecahydro-8*H*,19*H*-16,18-(epiethane[1,2]diylidene)-9,13-methano-7,28-(metheno)[1,4]diazepino[2,3-*k*]pyrido[1,2-*s*][1,4]dioxa[7,19]diazacyclodocosine-4,8(5*H*)-dione (compound or ligand **19**)

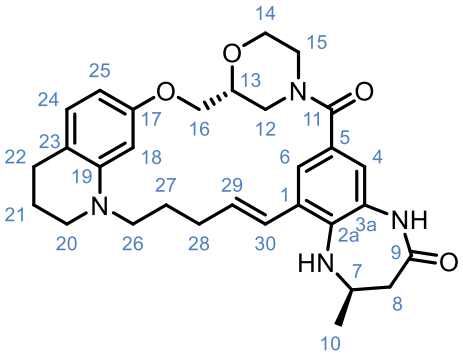

Tert-butyl (*R*)-2-(((1-((*E*)-5-((*R*)-8-((benzyloxy)carbonyl)-4-methyl-2-oxo-2,3,4,5-tetrahydro-1*H*-benzo[*b*][1,4]diazepin-6-yl)pent-4-en-1-yl)-1,2,3,4-tetrahydroquinolin-7-yl)oxy)methyl)morpholine-4-carboxylate (86.0 mg, 0.119 mmol, 1.0 equiv.) was dissolved in a mixture of THF/MeOH/H_2O (3:2:1, 6.0 mL) to this is added lithium hydroxide LiOH (40.0 mg, 1.66 mmol, 14.0 equiv.) and this reaction mixture was then stirred at room temperature for 5 h. Upon the completion of this reaction, the solvents mixture was removed *in vacuo* to give a light brown residue. To this was added CH_2Cl_2 (3.0 mL) followed by careful addition of TFA (3.0 mL), and the reaction mixture was then stirred at room temperature overnight. After this time the reaction mixture was concentrated under a constant stream of nitrogen to give a brown oil. The resultant oil was taken up in 4 mL of DMF and was then added to an appropriately sized reaction vessel under a nitrogen atmosphere containing PyBOP (68 mg, 0.131 mmol, 1.1 equiv.), DIPEA (5.9 mL) and the remaining volume of DMF (49.4 mL) the reaction mixture was then stirred at room temperature for 20 h. After this time the reaction mixture was concentrated under a stream of nitrogen at 50 °C to give a dark brown oil. This was diluted with 1.0 M $K_2CO_{3(aq)}$ (50 mL), which was then washed with $CHCl_3$/IPA

(9:1) mixture (3 × 25 mL) with the combined organic layers then washed with 5 wt% $LiCl_{(aq)}$ (3 × 25 mL), brine (25 mL), dried ($MgSO_4$), filtered and concentrated to give a brown oil. The crude oil was then taken up in DMSO (1 mL) and was then purified by ACCQPrep HpH method C using 30-99% acetonitrile(B)/10mM ammonium bicarbonate in water adjusted to pH 10 with ammonia solution(A) gradient over 17 mins. Any residual unpurified compound in DMSO from the ACCQPrep purification was further diluted until the total volume was 1 mL in DMSO and this residual compound was purified by MDAP (HpH method C) and was loaded onto the High pH Xselect CSH C_{18} column (150mm x 30mm i.d. 5µm packing diameter) column. The product was then eluted using 30-99% acetonitrile(B)/10mM ammonium bicarbonate in water adjusted to pH 10 with ammonia solution(A) gradient over 17 mins. The pure fractions from both the ACCQPrep and MDAP were combined and concentrated under a stream of nitrogen at 40 °C overnight to give (2*R*,13*R*,*E*)-2-methyl-1,2,3,10,11,13,14,20,21,23,24,25-dodecahydro-8*H*,19*H*-16,18-(epiethane[1,2]diylidene)-9,13-methano-7,28-(metheno)[1,4]diazepino[2,3-*k*]pyrido[1,2-*s*][1,4]dioxa[7,19]diazacyclodocosine-4,8(5*H*)-dione as off white fluffy crystals (23.8 mg, 39% yield); R_f 0.64 (acetone); $[\alpha]_D^{17}$ = −7.17 (*c* 0.6, $CHCl_3$); $\bar{\nu}_{max}$ (thin film in)/ cm^{-1} 2927 (C-H, m) 1673 and 1614 (C=O, s), 1508 (C=C, m) and 1433 (C-H, s); ^{1}H NMR (600 MHz, d_6-DMSO); δ_H 9.55 (1H, s, NH-3a/9), 7.34 (1H, d, *J* 2.0 Hz, H-6), 6.95 (1H, d, *J* 2.0 Hz, H-4), 6.79 (1H, d, *J* 15.5 Hz, H-30), 6.74 (1H, d, *J* 8.1 Hz, H-24), 6.31 (1H, dt, *J* 15.5, 7.0 Hz, H-29), 6.06 (1H, dd, *J* 8.1, 2.3 Hz, H-25), 6.01 (1H, d, *J* 2.3 Hz, H-18), 5.07 (1H, d, *J* 2.9 Hz, NH-2a/7), 4.19 (1H, dd, *J* 9.8, 6.4 Hz, H_AH_B-16), 4.06 – 3.96 (3H, m, 3H, H-7, H_AH_B-12, H_AH_B-15), 3.92 (1H, dt, *J* 11.6, 3.5 Hz, H_AH_B-14), 3.88 – 3.83 (1H, m, H-13), 3.72 (1H, dd, *J* 9.7, 7.3 Hz, H_AH_B-16), 3.62 – 3.55 (1H, m, H_AH_B-14), 3.37 – 3.32 (1H, m, H_AH_B-26), 3.26 – 3.11 (5H, m, H-20, H_AH_B-26,

H_AH_B-12, H_AH_B-15), 2.59 (2H, t, *J* 6.3 Hz, H-22), 2.49 – 2.45 (1H, m, H_AH_B-7), 2.27 (2H, p, *J* 6.5 Hz, H-28), 2.20 (1H, dd, *J* 13.2, 7.2 Hz, H_AH_B-7), 1.82 (2H, p, *J* 6.0 Hz, H-21), 1.68 (2H, p, *J* 8.0 Hz, H-27), 1.24 (3H, d, *J* 6.3 Hz, H-10); ^{13}C NMR (151 MHz, d_6-DMSO) δ_C 171.4 (C-8), 168.9 (C-11), 157.9 (C-17), 145.3 (C-19), 137.6 (C-2a), 132.1 (C-29), 131.1 (C-3a), 129.4 (C-24), 127.7 (C-30), 126.5 (C-5), 126.0 (C-1) 121.1 (C-4), 120.3 (C-6), 115.0 (C-23), 101.6 (C-25), 98.2 (C-18), 72.3 (C-13), 67.6 (C-16), 64.2 (C-14), 54.4 (C-7), 49.7 (C-12), 48.4 (C-26), 47.9 (C-20), 42.1 (C-15), 40.5 (C-8), 29.2 (C-28), 26.8 (C-22), 23.3 (C-10), 23.0 (C-27), 21.9 (C-21); HRMS *m/z* (ESI^+) [Found 517.2802 $C_{30}H_{37}N_4O_4$ requires 517.2815 $[M+H]^+$]; LRMS *m/z* (ESI^+) 517.28 ($[M+H^+]$, 100%); LC-MS, Formic method (retention time 1.14 mins) 100% purity; HPLC: retention time 10.46 mins, 98.2% purity.

7-Methoxy-3,4-dihydroquinolin-2(1*H*)-one (compound **42**)

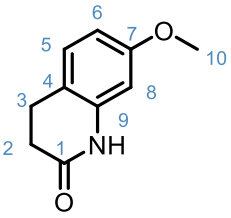

7-hydroquinolin-2(1H)-one (10.0 g, 61.2 mmol, 1.0 equiv.), K_2CO_3 (17.0 g, 122 mmol, 2.0 equiv.) and DMF (100 mL) were stirred at r.t., to this was added iodomethane (4.20 mL, 67.4 mmol, 1.1 equiv.) and then the reaction mixture was heated to 60 °C for 18 h. The reaction mixture was then cooled to rt, diluted with EtOAc (500 mL), washed with sat $K_2CO_{3(aq)}$ (3 × 300 mL), 10 wt% $LiCl_{(aq)}$ (3 × 300 mL) and brine (300 mL), dried ($MgSO_4$), filtered and concentrated to give the crude product as an off-white solid. The crude compound was then crystalised from the minimum amount of EtOH to give the pure product as colourless needles (5.121 g, 47%); R_f 0.19 (1:1, EtOAc/pet ether); m.p 123 – 126 °C (EtOH); ^{1}H NMR (400 MHz, $CDCl_3$) δ_H 7.62 (1H, br s, NH-9), 7.06 (1H,

dt, J 8.3, 0.9 Hz, H-5), 6.53 (1H, dd, J 8.3, 2.5 Hz, H-6), 6.29 (1H, d, J 2.5 Hz, H-8), 3.78 (3H, s, H-10), 2.94 – 2.86 (2H, m, H-3), 2.66 – 2.58 (2H, m, H-2); LRMS m/z (ESI$^+$) 178 ([M+H]$^+$, 100%). These data are in accordance with the literature.[40,44]

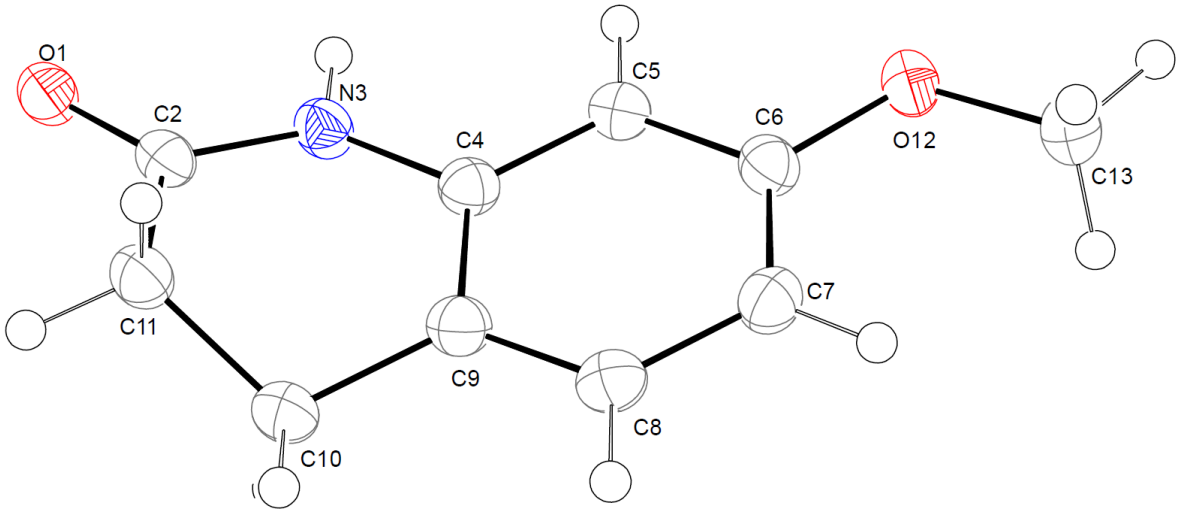

7-Methoxy-1,2,3,4-tetrahydroquinoline (compound **43**)

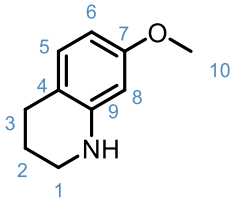

7-methoxy-3,4-dihydroquinolin-2(1*H*)-one (2.47g, 13.9 mmol, 1.0 equiv.) was dissolved in anhydrous THF (60 mL) and added portion wise to $LiAlH_4$ (0.79 g, 20.9 mmol, 1.5 equiv.) in THF (50 mL) at 0 °C and the suspension was stirred at 0 °C for 10 mins. The suspension was then warmed to room temperature and was left to stir for 4 h. The reaction was then returned to 0 °C and water (1.5 mL), followed by 15 wt% $NaOH_{(aq)}$ (1.5 mL) and water (4 mL) were added dropwise. $MgSO_4$ was added, and the suspension was stirred at room temperature for 30 minutes. The reaction was filtered, and filtrate was washed with ethyl acetate (200 mL). This was evaporated *in vacuo* to afford 7-methoxy-1,2,3,4-tetrahydroquinoline as colourless oil (2.22 g, 98%);

R_f 0.54 (1:1, EtOAc/pet ether); ^{1}H NMR (400 MHz, $CDCl_3$) δ_H 6.86 (1H, dt, J 8.2, 1.0 Hz, H-5), 6.22 (1H, dd, J 8.2, 2.5 Hz, H-6), 6.05 (d, J 2.5 Hz, H-8), 3.75 (s, 3H, H-10), 3.32 – 3.25 (2H, m, H-3), 2.72 (2H, t, J 6.2 Hz, H-1), 1.99 – 1.88 (2H, m, H-2); LRMS m/z (ESI$^+$) 164 ([M+H]$^+$, 100%). These data are in accordance with the literature.[40,44]

7-Methoxy-1-(pent-4-yn-1-yl)-1,2,3,4-tetrahydroquinoline (compound **44**)

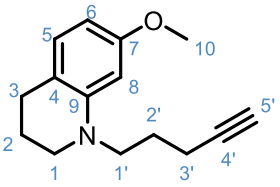

Pent-4-yn-1-yl methane sulfonate (5.31 g, 33.1 mmol, 1.5 equiv.) was added to a solution of 7-methoxy-1,2,3,4-tetrahydroquinoline (3.60 g, 22.1 mmol, 1.0 equiv.), TBAI (3.85 g, 6.74 mmol, 0.5 equiv.), DIPEA (5.29 mL, 44.1 mmol, 2.0 equiv) and DMF (20 mL). The reaction mixture was heated to 100 °C for 48 h. The cooled reaction mixture was diluted with Et_2O (500 mL), washed with H_2O (3 × 500 mL) and brine (400 mL), then dried ($MgSO_4$), filtered and evaporated *in vacuo* to give a dark brown oil. The crude product was purified by flash silica column chromatography (elution with 0-10% EtOAc in pet ether) to afford 7-methoxy-1-(pent-4-yn-1-yl)-1,2,3,4-tetrahydroquinoline as a light brown oil (2.80 g, 55%); R_f 0.20 (1:9, EtOAc/pet ether); ^{1}H NMR (400 MHz, $CDCl_3$) δ_H 6.87 (1H, dt, *J* 8.0, 1.0 Hz, H-5), 6.22 (1H, d, *J* 2.5 Hz, H-8), 6.17 (1H, dd, *J* 8.1, 2.4 Hz, H-6), 3.79 (3H, s, H-10), 3.44 – 3.33 (2H, m, H-1'), 3.32-3.28 (2H, m, H-1), 2.72 (2H, t, *J* 6.2 Hz, H-3), 2.29 (2H, td, *J* 6.9, 2.7 Hz, H-3'), 2.04 (1H, t, *J* 2.7 Hz, H-5'), 1.98 – 1.92 (2H, m, H-2), 1.85 (2H, p, *J* 7.0 Hz, H-2'); LRMS m/z (ESI$^+$) 230 ([M+H]$^+$, 100%). These data are in accordance with the literature.[44]

(*E*)-7-Methoxy-1-(5(4,4,5,5-tetramethyl-1,3,2-dioxaborolan-2-yl)pent-4-en-1-yl)-1,2,3,4-tetrahydroquinoline (compound **45**)

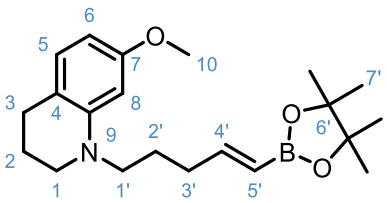

7-methoxy-1-(pent-4-yn-1-yl)-1,2,3,4-tetrahydroquinoline (30) (750 mg, 3.27 mmol, 1.0 equiv.) and bis(cyclopentadienyl)zirconium$^{(VI)}$ chloride hydride (84 mg, 0.327 mmol, 0.1 equiv.) were added to a tapered microwave vial and sealed under an argon atmosphere in the absence of light. Triethylamine (45.5 µL, 0.327 mmol, 0.1 equiv.) and 4,4,5,5-tetramethyl-1,3,2-dioxaborolane (522 µL, 3.60 mmol, 1.1 equiv.) were added and the reaction mixture was stirred at 60 °C under argon for 20 h in the dark. The reaction mixture was purified by flash silica column chromatography (elution with 0-100% CH_2Cl_2 in pet ether) to give (*E*)-7-Methoxy-1-(5(4,4,5,5-tetramethyl-1,3,2-dioxaborolan-2-yl)pent-4-en-1-yl)-1,2,3,4-tetrahydroquinoline as a light brown oil (662 mg, 57%); R_f 0.2 (CH_2Cl_2); ^{1}H NMR (400 MHz, $CDCl_3$) δ_H 6.86 – 6.79 (1H, m, H-5), 6.65 (1H, dt, *J* 17.9, 6.4 Hz, H-4'), 6.15 – 6.09 (2H, m, H-8, H-6), 5.47 (1H, dt, *J* 17.9, 1.6 Hz, H-5'), 3.75 (3H, s, H-10), 3.27 – 3.16 (4H, m, H-1', H-1), 2.67 (2H, t, *J* 6.3 Hz, H3), 2.20 (2H, tdd, *J* 7.7, 6.4, 1.6 Hz, H-3'), 1.95 – 1.85 (2H, m, H-2), 1.73 (2H, p, *J* 7.5 Hz, H-2'), 1.26 (12H, s, H-7'); ^{11}B NMR (160 MHz; $CDCl_3$) δ_B 29.7 (B-5'); LRMS m/z (ESI$^+$) 358 ([M+H]$^+$, 100%). These data are in accordance with the literature.[44]

Benzyl (*R*,*E*)-9-(5-(7-methoxy-3,4-dihydroquinolin-1(2*H*)-yl)pent-1-en-1-yl)-2-methyl-4-oxo-2,3,4,5-tetrahydro-1*H*-benzo[*b*][1,4]diazepine-7-carboxylate (compound **46**)

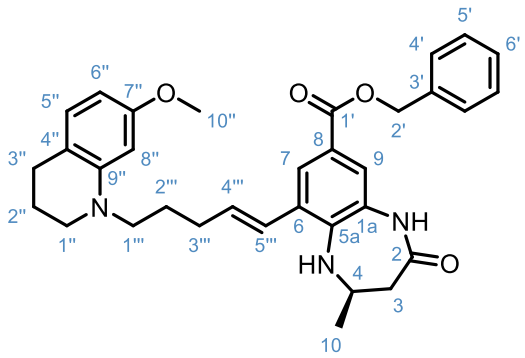

Benzyl (*R*)-9-iodo-2-methyl-4-oxo-2,3,4,5-tetrahydro-1*H*-benzo[*b*][1,4]diazepine-7-carboxylate (1.63 g, 1.0 equiv.), [1,1′-bis(diphenylphosphino)ferrocene]dichloropalladium$^{(II)}$ (137 mg, 0.05 equiv.), K_2CO_3 (1.55 g, 3.0 equiv.), were loaded into a reaction flask and placed under an argon atmosphere. (7-methoxyl-1-(5-(4,4,5,5-tetramethyl-1,3,2-dioxaboral-2-yl)pent-4-en-1-yl)-1,2,3,4-tetrahydroquinoline (2.00 g, 2.0 equiv.) in 1,4-dioxane (25 mL) was added, followed by H_2O (5 mL) and the reaction mixture was heated to 100 °C for 18 h. The reaction mixture was then cooled, and solvent removed *in vacuo*, the dark residue was then diluted with EtOAc (500 mL). The organic component was washed with water (3 × 400mL), followed by brine (400 mL), dried ($MgSO_4$), filtered and evaporated *in vacuo* to afford a brown oil. The crude oil was purified by silica gel chromatography (elution with 0-80% EtOAc in pet ether) to yield benzyl (*R*,*E*)-9-(5-(7-methoxy-3,4-dihydroquinolin-1(2*H*)-yl)pent-1-en-1-yl)-2-methyl-4-oxo-2,3,4,5-tetrahydro-1*H*-benzo[*b*][1,4]diazepine-7-carboxylate as a yellow oil (1.50 g, 74%); R_f 0.40 (1:1, EtOAc/pet ether); $[\alpha]_D^{25}$ = −40.9 (*c* 1.0, $CHCl_3$); $\bar{\nu}_{max}$ (thin film in $CHCl_3$)/ cm^{-1} 2935 (C-H, s), 1705 (C=O, m), 1671 (C=O, s), 1141 (C-O, m); ^1H NMR (400 MHz, $CDCl_3$) δ_H 7.74 (1H, d, *J* 2.0 Hz, H-9), 7.48 – 7.31 (7H, m, H-7, NH-1a/2, H-4', H-5', H-6'), 6.85 (1H, d, *J* 7.8 Hz, H-5''), 6.35 (1H, d, *J* 15.5 Hz, H-5'''), 6.17 – 6.08 (3H, m, H-6'', H-8'',

H-13''), 5.33 (2H, s, H-2'), 4.16-4.05 (1H, m, H-4), 4.02 (1H, s, NH-5a/4), 3.74 (3H, s, H-10''), 3.33 – 3.23 (4H, m, H-1'', H-1'''), 2.72 – 2.64 (3H, m, H_AH_B-3 H-3''), 2.51 (1H, dd, *J* 13.9, 8.2 Hz, H_AH_B-3), 2.34 – 2.25 (2H, m, H-3'''), 1.95 – 1.89 (2H, m, H-2''), 1.80 (2H, p, *J* 7.5 Hz, H-2'''), 1.37 (3H, d, *J* 6.3 Hz, H-10); HRMS *m/z* (ESI^+) [Found 540.2860, $C_{33}H_{38}N_3O_4$ requires $(M+H)^+$ 540.2857]; LRMS *m/z* (ESI+) 540 ($[M+H]^+$, 100%); HPLC: retention time 10.5 mins, purity 83.7%.

(*R*,*E*)-6-(5-(7-Methoxy-3,4-dihydroquinolin-1(2*H*)-yl)pent-1-en-1-yl)-4-methyl-8-(piperidine-1-carbonyl)-1,3,4,5-tetrahydro-2*H*-benzo[*b*][1,4]diazepin-2-one (compound or ligand **39**)

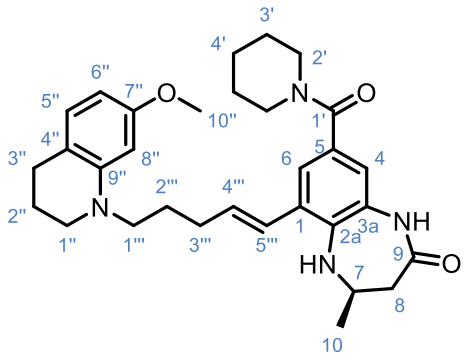

Benzyl (*R*,*E*)-9-(5-(7-methoxy-3,4-dihydroquinolin-1(2*H*)-yl)pent-1-en-1-yl)-2-methyl-4-oxo-2,3,4,5-tetrahydro-1*H*-benzo[*b*][1,4]diazepine-7-carboxylate (200 mg, 1 equiv.) was dissolved in a mixture of THF/MeOH/H_2O (3:2:1, 10 mL), once dissolved lithium hydroxide (90 mg, 10 equiv.) was added to the reaction mixture and stirred at room temperature for 5 h. After this time the reaction mixture was passed through a short silica pad which was then washed with methanol (200 mL), the filtrate was then evaporated *in vacuo* to give a brown residue. After this time the brown oil was washed with water (100 mL) and then extracted with EtOAc (100 mL), and the organic solvent evaporated *in vacuo*. This brown oil was then placed under an argon atmosphere and dissolved in DMF (13 mL). This was added to a reaction vessel containing PyBOP

(212 mg, 1.1 equiv.) under an argon atmosphere and left to stir at room temperature for 15 mins. After this time piperidine (109 µL, 3 equiv.) was added to the reaction mixture and stirred at room temperature for 20 h. After this time the reaction mixture was diluted with EtOAc (100 mL) and then washed with sat. $NH_4Cl_{(aq)}$ (3 × 50 mL), 10 wt% $LiCl_{(aq)}$ (3 × 25 mL), brine (25 mL), dried ($MgSO_4$), filtered and concentrated *in vacuo* to afford a light brown oil. The crude oil was purified by silica gel chromatography (elution with 10% MeOH in CH_2Cl_2) to give a light brown oil which was further purified by preparative HPLC (retention time, 13.9 mins and λ collection 340 nm) and the solvent removed *via* lyophilisation to give (*R*,*E*)-6-(5-(7-methoxy-3,4-dihydroquinolin-1(2*H*)-yl)pent-1-en-1-yl)-4-methyl-8-(piperidine-1-carbonyl)-1,3,4,5-tetrahydro-2*H*-benzo[*b*][1,4]diazepin-2-one as a white lysophilate (35 mg, 55%), R_f 0.27 (EtOAc); $[\alpha]_D^{25}$ = −2.76 (*c* 0.75, $CHCl_3$); $\bar{\nu}_{max}$ (thin film in $CHCl_3$)/ cm^{-1} 3391 (C-H, s), 1676 (C=O, m), 1510 (C-C), 1165 (C-O); ^{1}H NMR (500 MHz, CD_2Cl_2); δ_H 7.50 (1H, s, NH-3a/9), 7.14 (1H, d, *J* 1.9 Hz, H-6), 6.84 (1H, d, *J* 1.9 Hz, H-4), 6.80 (d, *J* 8.1 Hz, H-5''), 6.47 (1H, dt, *J* 15.4, 1.6 Hz, H-5'''), 6.18 – 6.11 (2H, m, H-8'', H-4'''), 6.08 (1H, dd, *J* 8.1, 2.5 Hz, H-6''), 4.12 – 4.03 (1H, m, H-7), 3.70 (3H, s, H-10''), 3.50 (4H, s br, H-2'), 3.34 – 3.21 (4H, m, H-1'', H-1'''), 2.66 (2H, t, *J* 6.4 Hz, H-3''), 2.59 (1H, dd, *J* 13.4, 4.3, Hz, H_AH_B-8) 2.40 (1H, dd, *J* 13.4, 7.7 Hz, H_AH_B-8), 2.35 – 2.27 (2H, m, H-3'''), 1.95 – 1.87 (2H, m, H-2''), 1.84 – 1.73 (2H, m, H-2'''), 1.66 (2H, q, *J* 6.4 Hz, H-4'), 1.56 (4H, d, *J* 8.3 Hz, H-3'), 1.33 (3H, d, *J* 6.3 Hz, H-10); ^{13}C NMR (126 MHz; CD_2Cl_2) δ_C 172.4 (C-9), 169.7 (C-1'), 159.7 (C-7''), 146.6 (C-9''), 137.3 (C-2a), 136.1 (C-4'''), 130.5 (C-1), 129.8 (C-5''), 129.4 (C-5), 129.2 (C-3a), 125.5 (C-5'''), 123.3 (C-6), 120.1 (C-4), 115.7 (C-4''), 99.9 (C-6''), 97.7 (C-8''), 55.4 (C-10''), 55.1 (C-7), 51.3 (C-1'''), 49.8 (C-1''), 41.3 (C-7), 31.4 (C-3'''), 27.8 (C-3''), 26.3 (C-2'''), 25.1 (C-), 24.3 (C-10), 23.0 (C-2''); HRMS *m/z* (ESI$^+$) [Found 517.3181, $C_{31}H_{41}N_4O_3$ requires $(M+H)^+$

517.3173]; LRMS *m/z* (ESI+) 517 ([M+H]$^+$, 97%); HPLC: retention time 11.4 mins, purity 98.4%.

(*R*,*E*)-6-(5-(7-Methoxy-3,4-dihydroquinolin-1(2H)-yl)pent-1-en-1-yl)-4-methyl-8-(morpholine-4-carbonyl)-1,3,4,5-tetrahydro-2H-benzo[b][1,4]diazepin-2-one (compound or ligand **40**)

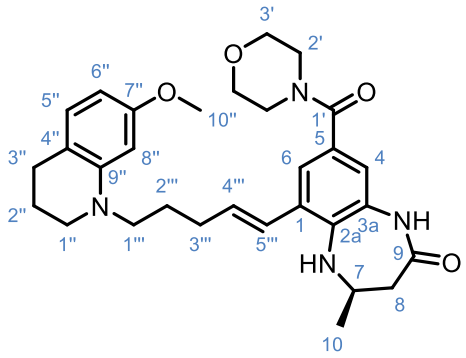

Benzyl (*R*,*E*)-9-(5-(7-methoxy-3,4-dihydroquinolin-1(2*H*)-yl)pent-1-en-1-yl)-2-methyl-4-oxo-2,3,4,5-tetrahydro-1*H*-benzo[*b*][1,4]diazepine-7-carboxylate (200 mg, 1 equiv.) was dissolved in a mixture of THF/MeOH/H_2O (3:2:1, 10 mL), once dissolved lithium hydroxide (90 mg, 10 equiv.) was added to the reaction mixture and stirred at room temperature for 5 h. After this time the reaction mixture was passed through a short silica pad which was then washed with methanol (200 mL), the filtrate was then evaporated *in vacuo* to give a brown residue. After this time the brown oil was washed with water (100 mL) and then extracted with EtOAc (100 mL), and the organic solvent evaporated *in vacuo*. This brown oil was then placed under an argon atmosphere and dissolved in DMF (13 mL). This was added to a reaction vessel containing PyBOP (212 mg, 1.1 equiv.) under an argon atmosphere and left to stir at room temperature for 15 mins. After this time morpholine (110 µL, 3 equiv.) was added to the reaction mixture and stirred at room temperature for 20 h. After this time the reaction mixture was diluted with EtOAc (100 mL) and then washed with sat. $NH_4Cl_{(aq)}$ (3 × 50 mL),

10 wt% $LiCl_{(aq)}$ (3 × 25 mL), brine (25 mL), dried ($MgSO_4$), filtered and concentrated *in vacuo* to afford a light brown oil. The crude oil was purified by silica gel chromatography (elution 0-10% MeOH in CH_2Cl_2) to give a light brown oil which was further purified by preparative HPLC (retention time, 12.37 mins and λ collection 360 nm) and the solvent removed *via* lyophilisation to give (*R*,*E*)-6-(5-(7-methoxy-3,4-dihydroquinolin-1(2*H*)-yl)pent-1-en-1-yl)-4-methyl-8-(morpholine-4-carbonyl)-1,3,4,5-tetrahydro-2*H*-benzo[*b*][1,4]diazepin-2-one (24 mg, 37%) as an off-white lysophilate, R_f 0.22 (EtOAc); ^{1}H NMR (600 MHz, *d*$_6$-DMSO); δ_H 9.50 (1H, s, NH-3a/9), 7.16 (1H, d, *J* 2.0 Hz, H-6), 6.86 (1H, d, *J* 2.0 Hz, H-4), 6.74 (1H, d, *J* 8.1 Hz, H-5''), 6.69 (1H, d, *J* 15.5 Hz, H-5'''), 6.17 (1H, dt, *J* 15.5, 6.9 Hz, H-4'''), 6.07 (1H, d, *J* 2.4 Hz, H-8''), 6.04 (1H, dd, *J* 8.1, 2.4 Hz, H-6''), 4.96 (1H, d, *J* 2.9 Hz, NH-2a/7), 4.02 – 3.94 (1H, m, H-7), 3.62 (3H, s, H-10''), 3.58 (4H, m, H-3'), 3.50 (4H, m, H-2'), 3.28 – 3.22 (4H, m, H-1'', H-1'''), 2.59 (2H, t, *J* 6.3 Hz, H-3''), 2.45 (1H, dd, *J* 13.3, 4.4 Hz, H_AH_B-8), 2.26 (2H, q, *J* 6.9 Hz, H-3'''), 2.19 (dd, *J* 13.3, 7.4 Hz, H_AH_B-8), 1.85 – 1.78 (2H, m, H-2''), 1.71 (2H, p, *J* 6.9 Hz, H-2'''), 1.22 (3H, d, *J* 6.2 Hz, H-10); ^{13}C NMR (151 MHz; *d*$_6$-DMSO); δ_C 171.5 (C-9), 168.9 (C-1'), 158.8 (C-7''), 145.7 (C-9''), 137.5 (C-2a), 133.0 (C-4'''), 129.8 (C-5), 129.2 (C-5''), 128.9 (C-1), 126.3 (C-3a), 125.6 (C-5'''), 121.5 (C-6), 119.8 (C-4), 114.4 (C-4''), 99.7 (C-6''), 96.8 (C-8''), 69.8 (C-2'), 66.1 (C-3'), 54.6 (C-10''), 54.3 (C-7), 50.2 (C-1'''), 48.7 (C-1''), 40.6 (C-8), 30.4 (C-3'''), 26.9 (C-3''), 25.2 (C-2'''), 23.4 (C-10), 22.0 (C-2''); HRMS *m/z* (ESI$^+$) [Found 519.2978, $C_{30}H_{39}N_4O_4$ requires $(M+H)^+$ 519.2966]; LRMS *m/z* (ESI+) 519 ($[M+H]^+$, 100%); HPLC: retention time 10.30 mins, purity 98.9%.

(*R*,*E*)-6-(5-(7-Methoxy-3,4-dihydroquinolin-1(2*H*)-yl)pent-1-en-1-yl)-4-methyl-8-(pyrrolidine-1-carbonyl)-1,3,4,5-tetrahydro-2*H*-benzo[*b*][1,4]diazepin-2-one (compound or ligand **41**)

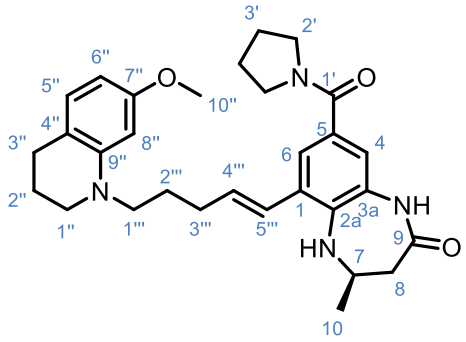

Benzyl (*R*,*E*)-9-(5-(7-methoxy-3,4-dihydroquinolin-1(2*H*)-yl)pent-1-en-1-yl)-2-methyl-4-oxo-2,3,4,5-tetrahydro-1*H*-benzo[*b*][1,4]diazepine-7-carboxylate (200 mg, 1 equiv.) was dissolved in a mixture of THF/MeOH/H_2O (3:2:1, 10 mL), once dissolved lithium hydroxide (90 mg, 10 equiv.) was added to the reaction mixture and stirred at room temperature for 5 h. After this time the reaction mixture was passed through a short silica pad which was then washed with methanol (200 mL), the filtrate was then evaporated *in vacuo* to give a brown residue. After this time the brown oil was washed with water (100 mL) and then extracted with EtOAc (100 mL), and the organic solvent evaporated *in vacuo*. This brown oil was then placed under an argon atmosphere and dissolved in DMF (13 mL). This was added to a reaction vessel containing PyBOP (212 mg, 1.1 equiv.) under an argon atmosphere and left to stir at room temperature for 15 mins. After this time pyrrolidine (100 µL, 3 equiv.) was added to the reaction mixture and stirred at room temperature for 20 h. After this time the reaction mixture was diluted with EtOAc (100 mL) and then washed with sat. $NH_4Cl_{(aq)}$ (3 × 50 mL), 10 wt% $LiCl_{(aq)}$ (3 × 25 mL), brine (25 mL), dried ($MgSO_4$), filtered and concentrated *in vacuo* to afford a light brown oil. The crude oil was purified by silica gel chromatography (elution with 10% MeOH in CH_2Cl_2) to give a light brown oil which

was further purified by preparative HPLC (retention time, 13.21 mins and λ collection 350 nm) and the solvent removed *via* lyophilisation to give (*R*,*E*)-6-(5-(7-methoxy-3,4-dihydroquinolin-1(2*H*)-yl)pent-1-en-1-yl)-4-methyl-8-(pyrrolidine-1-carbonyl)-1,3,4,5-tetrahydro-2*H*-benzo[*b*][1,4]diazepin-2-one (24 mg, 52%) as an off-white lysophilate, R_f 0.18 (EtOAc);); $[\alpha]_D^{25}$ = +0.3 (*c* 0.55, $CHCl_3$); $\bar{\nu}_{max}$ (thin film in $CHCl_3$)/ cm^{-1} 3372 (C-H, s), 1674 (C=O, s), 1612 (c=O, s), 1433 (C-C); ^1H NMR (600 MHz, d_6-DMSO); δ_H 9.50 (1H, s, NH-3a/9), 7.29 (1H, d, *J* 2.0 Hz, H-4), 6.98 (1H, d, *J* 2.0 Hz, H-6), 6.74 (1H, d, *J* 8.1 Hz H-5''), 6.69 (1H, d, *J* 15.4 Hz, H-5'''), 6.17 (1H, dt, *J* 15.4, 6.9 Hz, H-4'''), 6.07 (1H, d, *J* 2.4 Hz, H-8''), 6.04 (1H, dd, *J* 8.1, 2.4 Hz, H-6''), 4.95 (1H, d, *J* 2.9 Hz, NH-2a/7), 4.02 – 3.94 (1H, m , H-7), 3.61 (3H, s, H-10'), 3.43 (4H, d, *J* 6.0 Hz, H-2'), 3.29 – 3.21 (4H, m, H-1'', H-1'''), 2.59 (2H, t, *J* 6.3 Hz, H-3''), 2.45 (1H, dd, *J* 13.2, 4.4 Hz, H_AH_B-8), 2.29 – 2.23 (2H, m, H-3'''), 2.19 (1H, dd, *J* 13.2, 7.3 Hz, H_AH_B-8), 1.87 – 1.78 (6H, m, H-3', H-2''), 1.71 (2H, p, *J* 7.4 Hz, H-2'''), 1.22 (3H, d, *J* 6.2 Hz, H-10); ^{13}C NMR (151 MHz; d_6-DMSO); δ_C 171.5 (C-9), 167.7 (C-1'), 158.8 (C-7''), 145.8 (C-9''), 137.6 (C-2a), 132.8 (C-4'''), 129.6 (C-5), 129.2 (C-5''), 128.5 (C-1), 128.1 (C-2a), 125.7 (C-5'''), 121.4 (C-6), 119.9 (C-4), 114.4 (C-4''), 99.7 (C-6''), 96.8 (C-8''), 54.6 (C-10''), 54.2 (C-7), 50.2 (C-1'''), 49.1 (C-2'), 48.6 (C-1''), 46.0 (C-2'), 40.6 (C-8), 30.4 (C-3'''), 26.9 (C-3''), 26.1 (C-3'), 25.2 (C-2'''), 23.9 (C-3'), 23.4 (C-10), 22.0 (C-2''); HRMS *m/z* (ESI$^+$) [Found 503.3026, $C_{30}H_{39}N_4O_3$ requires $(M+H)^+$ 503.3017]; LRMS *m/z* (ESI+) 503 ($[M+H]^+$, 86% and 1027 ($[2M+Na]^+$, 100%); HPLC: retention time 10.83 mins, purity 98.0%.

tert-Butyl (*R*)-3-((2-Bromo-6-nitrophenyl)amino)butanoate (compound **47**)

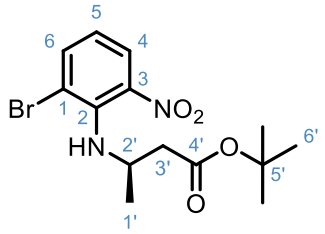

3-Bromo-2-fluoro-3-nitrobenzene (1.00 g, 4.55 mmol, 1.0 equiv.), *tert*-butyl (*R*)-aminobutanoate (1.50 g, 6.82 mmol, 1.5 equiv.) and Cs_2CO_3 (4.44g, 13.6 mmol, 3.0 equiv.) were dissolved in toluene (30 mL) and stirred at 85 °C for 20 h. After cooling the reaction mixture was diluted with sat. $NaHCO_{3(aq)}$ (150 mL), this mixture was extracted with EtOAc (3 × 100 mL). The combined organic components were washed with brine (100 mL), dried (Na_2SO_4), filtered and concentrated *in vacuo* to give an orange oil. The crude product was purified by flash silica column chromatography (elution with 0-20% EtOAc in pet ether) to give *tert*-butyl (*R*)-3-((2-Bromo-6-nitrophenyl)amino)butanoate as a light orange oil (1.502g, 92%); R_f 0.45 (4:1, hexane/Et_2O); $[\alpha]_D^{25}$ = −71.1 (*c* 1.0, $CHCl_3$); ^{1}H NMR (400 MHz, $CDCl_3$) δ_H 7.93 (1H, dd, *J* 8.4, 1.6 Hz, H-4), 7.72 (1H, dd, *J* 7.8, 1.6 Hz, H-6), 6.78 (1H, dd, *J* 8.4, 7.8 Hz, H-5), 6.36 (1H, s, NH-2/2'), 4.24 (1H, p, *J* 6.3 Hz, H-2'), 2.45 (2H, d, *J* 6.3 Hz, H-3'), 1.39 (9H, s, H-6'), 1.27 (3H, d, *J* 6.3 Hz, H-1'); LRMS *m/z* (ESI$^+$) 359 ([M+H]$^+$, 100%), 361 ([M+H]$^+$, 97%). These data are in accordance with the literature.[44]

(*R*)-6-Bromo-4-methyl-1,3,4,5-tetrahydro-2*H*-benzo[*b*][1,4]diazepin-2-one

(compound **48**)

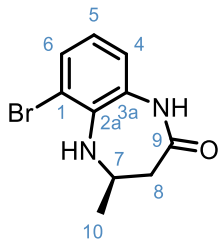

To a solution of (*R*)-3-((2-Bromo-6-nitrophenyl)amino)butanoate (1.50 g, 4.17 mmol, 1.0 equiv.) in CH_2Cl_2 (5 mL) was added TFA (5 mL) and the reaction stirred at r.t. for 2 h. The solvents were then removed *in vacuo* and the resulting dark orange oil was dissolved in glacial acetic acid (15 mL). To this was added iron powder (1.17 g, 20.9 mmol, 5.0 equiv.) and the reaction was heated to reflux (120 °C) for 6 h. After this time the cooled reaction mixture was added to 1M $K_2CO_{3(aq)}$ (100 mL) which was extracted with EtOAc (3 × 50 mL). The combined organic components were washed with brine (100 mL), dried ($MgSO_4$), filtered and concentrated *in vacuo* to give a yellow oil. The crude product was purified by flash silica column chromatography (elution with 0-100% EtOAc in pet ether) to give an off white colourless solid which was crystalised from IPA to give (*R*)-6-Bromo-4-methyl-1,3,4,5-tetrahydro-2*H*-benzo[*b*][1,4]diazepin-2-one as colourless needles (575 mg, 54%); R_f 0.15 (1:2, EtOAc/pet ether); $[\alpha]_D^{25}$ = −4.6 (*c* 1.0, $CHCl_3$); m.p 139 – 143 °C (IPA); ^{1}H NMR (400 MHz, $CDCl_3$) δ_H 7.88 (1H, br s, NH-3a), 7.33 (1H, dd, *J* 7.9, 1.5 Hz, H-6), 6.86 (1H, dd, *J* 7.9, 1.5 Hz, H-4), 6.73 (1H, t, *J* 7.9 Hz, H-5), 4.13 (1H, dqd, *J* 8.2, 6.3, 4.1 Hz, H-7), 3.57 (1H, br s, NH-2a), 2.62 (1H, dd, *J* 13.7, 4.1 Hz, H_AH_B-8), 2.45 (1H, dd, *J* 13.7, 8.2 Hz, H_AH_B-8), 1.39 (3H, d, *J* 6.3 Hz, H-10); LRMS *m/z* (ESI^+) 255 ($[M+H]^+$, 100%), 257 ($[M+H]^+$, 97%). These data are in accordance with the literature.[44]

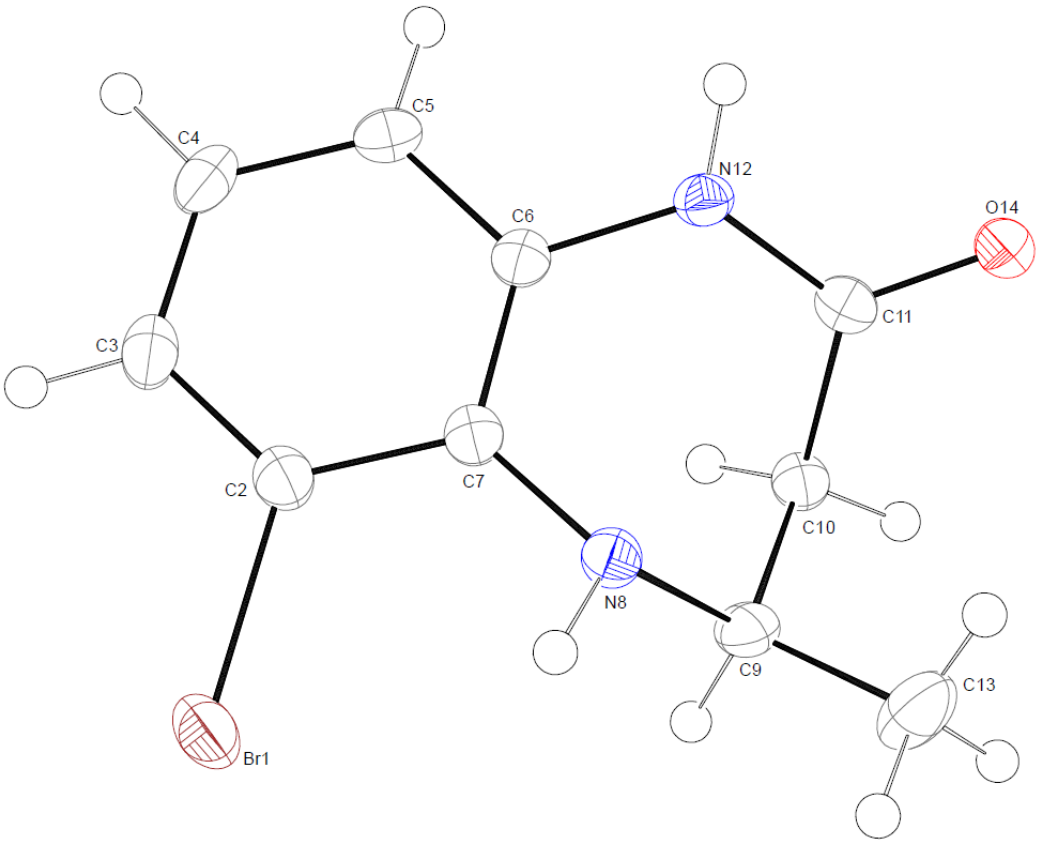

(*R*,*E*)-6-(5-(7-Methoxy-3,4-dihydroquinolin-1(2*H*)-yl)pent-1-en-1-yl)-4-methyl-1,3,4,5-tetrahydro-2*H*-benzo[*b*][1,4]diazepin-2-one (ligand **OXFBD05**)

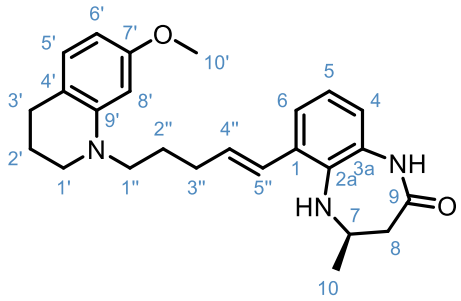

(*R*)-6-Bromo-4-methyl-1,3,4,5-tetrahydro-2*H*-benzo[*b*][1,4]diazepin-2-one (510 mg, 2.00 mmol, 1.0 equiv.), (*E*)-7-Methoxy-1-(5(4,4,5,5-tetramethyl-1,3,2-dioxaborolan-2-yl)pent-4-en-1-yl)-1,2,3,4-tetrahydroquinoline (714 mg, 2.50 mmol, 1.25 equiv.), K_2CO_3 (830 mg, 7.50 mmol, 3.75 equiv.) and [1,1′-Bis(diphenylphosphino)ferrocene]dichloropalladium$^{(II)}$ (73 mg, 0.125 mmol, 0.0625 equiv.) were added to reaction vessel under an argon atmosphere. To this was

added 1,4-dioxane (20 mL) and H_2O (4 mL), the reaction was then heated to 100 °C for 24 h. Once cooled the reaction mixture was evaporated and then diluted with EtOAc (125 mL), which was then filtered through a Celite® pad. The filtrate was then washed with brine (3 × 100 mL), dried ($MgSO_4$), filtered and concentrated *in vacuo* to give a brown oil. The crude product was then purified by flash silica column chromatography (elution with 0-100 % EtOAc in pet ether) and then further purified by semi preparative HPLC (retention time 8.58 mins) from which the fractions containing product were lyophilised to give (*R*,*E*)-6-(5-(7-Methoxy-3,4-dihydroquinolin-1(2*H*)-yl)pent-1-en-1-yl)-4-methyl-1,3,4,5-tetrahydro-2*H*-benzo[*b*][1,4]diazepin-2-one as a white lysophilate (607 mg, 75%); R_f 0.13 (1:1, EtOAc/pet ether); $[\alpha]_D^{25}$ = −4.2 (*c* 1.1, $CHCl_3$); ^{1}H NMR (400 MHz, $CDCl_3$) δ_H 7.78 (1H, br s, NH-3a), 7.12 (1H, dd, *J* 7.5, 1.7 Hz, H-6), 6.87 (2H, m, H-5, H-5', H-8'), 6.82 (dd, *J* 8.1, 1.7 Hz, H-4), 6.48 (1H, d, *J* 15.5 Hz, H-5''), 6.20 – 6.15 (1H, m, H-6'), 6.09 (1H, dt, *J* 15.5, 6.9 Hz, H-4''), 4.17 – 4.05 (1H, m, H-7), 3.75 (3H, s, H-10'), 3.28 (4H, m, H-1', H-1''), 2.70 (2H, t, *J* 6.4 Hz, H-3'), 2.61 (1H, dd, *J* 13.3, 4.7 Hz, H_AH_B-8), 2.39 (1H, dd, *J* 13.3, 7.5 Hz, H_AH_B-8), 2.33 – 2.25 (2H, m, H-3''), 1.98 – 1.88 (2H, m, H-2'), 1.80 (2H, p, *J* 7.5 Hz, H-2''), 1.36 (3H, d, *J* 6.2 Hz, H-10); LRMS *m/z* (ESI$^+$) 406 ([M+H]$^+$, 100%); HPLC: retention time 10.67 mins, purity >99.9. These data are in accordance with the literature.[44]

7.3.3. Chapter 4: Compounds **49** - **61**

7-(Methylsulfonyl)quinoline (compound **53**)

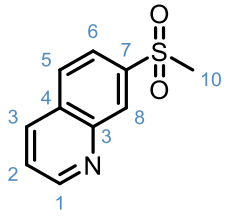

7-bromoquinoline (1.00 g, 4.81 mmol, 1.0 equiv.), dimethylethane 1,2-diamine (170 mg, 1.95 mmol, 0.4 equiv.) and copper$^{(I)}$ trifluoromethanesulfonate toluene complex (600 mg, 1.15 mmol, 0.2 equiv.) were dissolved in DMSO (10 mL) and to this was added sodium methyl sulfate (2.50 g, 24.1 mmol, 5.0 equiv.). The reaction mixture was heated to 120 °C for 4 h under an argon atmosphere. After this time the reaction mixture was diluted with EtOAc (100 mL) and was then filtered through a Celite® pad. The solvent was then removed *in vacuo* from the filtrate using an increased temperature water bath (60 °C) and azeotroping with toluene, the brown residue was then diluted with H_2O (100 mL). This was then washed with EtOAc (3 × 100 mL) The combined organic layers were then washed with brine (100 mL), dried ($MgSO_4$), filtered and concentrated *in vacuo* to give a yellow oil. The crude product was then purified by flash silica column chromatography (elution with 50-100% EtOAc in pet ether) to give 7-(methylsulfonyl)quinoline as a colourless solid (709 mg, 71%); R_f 0.09 (1:1, EtOAc/pet ether); m.p 109 – 111 °C (EtOAc); ^{1}H NMR (600 MHz, $CDCl_3$) δ 9.05 (1H, dd, *J* 4.2, 1.8 Hz, H-1), 8.73 (1H, dt, *J* 1.8, 0.8 Hz, H-8), 8.25 (1H, ddd, *J* 8.3, 1.8, 0.8 Hz, H-3), 8.04 – 7.97 (2H, m, H-6, H-7), 7.57 (1H, dd, *J* 8.3, 4.2 Hz, H-2), 3.14 (3H, s, H-10); ^{13}C NMR (151 MHz, $CDCl_3$) δ_C 152.5 (C-1), 147.4 (C-3), 141.2 (C-7), 136.1 (C-3), 130.8 (C-4), 130.4 (C-8), 129.9 (C-5), 123.8 (C-2), 123.1 (C-6), 44.5 (C-10);

HRMS *m/z* (ESI$^+$) [Found: 208.0428 $C_{10}H_{10}NO_2S$ requires 208.0427 $[M+H]^+$]; LRMS *m/z* (ESI$^+$) 423 ($[2M+H]^+$, 100%). These data are in accordance with the literature.[149]

7-(Methylsulfonyl)-1,2,3,4-tetrahydroquinoline (compound **54**)

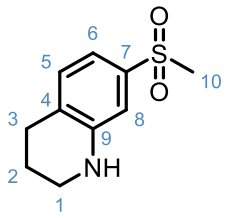

7-(methylsulfonyl)quinoline (364 mg, 1.76 mmol, 1.0 equiv.) and pentamethylcyclopentadienyliridium$^{(III)}$ chloride,dimer (28 mg, 0.0351 mmol, 0.02 equiv.) were added to a microwave vial and placed under an argon atmosphere. To this was added IPA (4.00 mL), H_2O (0.21 mL) and 70% perchloric acid (109 µL, 0.176 mmol, 0.1 equiv.) were added and the reaction mix was heated to 100 °C for 48 h. After the reaction mixture was cooled it was diluted with sat. $NaHCO_{3(aq)}$ (100 mL) and was washed with 1:9 IPA/$CHCl_3$ (3 × 50 mL), the combined organic layers were washed with brine (3 × 50 mL), dried ($MgSO_4$), filtered and concentrated *in vacuo* to give a brown oil. This was then purified by flash silica column chromatography (elution with 0-100% EtOAc in pet ether) to give 7-(methylsulfonyl)-1,2,3,4-tetrahydroquinoline as a colourless oil (240 mg, 65%); R_f 0.27 (1:1, EtOAc/pet ether); ^{1}H NMR (400 MHz, $CDCl_3$) δ_H 7.06 (2H, d, *J* 1.2 Hz, H-6, H-5), 6.97 (1H, t, *J* 1.2 Hz, H-8), 3.98 (1H, br s, NH-1/9), 3.37 – 3.30 (2H, m, H-1), 2.99 (3H, s, H-10), 2.79 (2H, t, *J* 6.4 Hz, H-3), 1.98 – 1.88 (2H, m, H-2); ^{13}C NMR (101 MHz, $CDCl_3$) δ_C 145.5, 138.9, 130.3, 127.0, 114.7, 111.8, 44.7, 41.8, 27.3, 21.3; HRMS *m/z* (ESI$^+$) [Found: 212.0741 $C_{10}H_{14}NO_2S$ requires $[M+H]^+$ 212.0740]; LRMS *m/z* (ESI$^+$) 423 ($[2M+H]^+$, 100%). These data are in accordance with the literature.[149]

7-(Methylsulfonyl)-1-(pent-4-yn-1-yl)-1,2,3,4-tetrahydroquinoline (compound **55**)

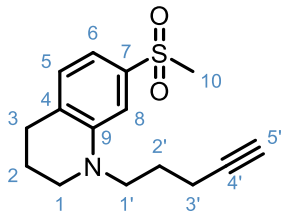

7-(methylsulfonyl)-1,2,3,4-tetrahydroquinoline (240 mg, 1.14 mmol, 1.0 equiv.), pent-4-yn-1-yl methanesulfonate (278 mg, 1.70 mmol, 1.5 equiv.) and TBAI (420 mg, 1.14 mmol, 1.0 equiv.) were added to a microwave vial sealed and placed under an argon atmosphere. To this was added DMF (700 µL) and DIPEA (394 µL, 2.27 mmol, 2.0 equiv.) and the reaction was heated to 90 °C for 72 h. Once cooled the reaction mixture was diluted with EtOAc (100 mL) and was washed with H_2O (3 × 50 mL) and brine (50 mL), dried ($MgSO_4$), filtered and concentrated *in vacuo* to give a brown oil. The crude product was purified by flash silica column chromatography (elution with 0-100% EtOAc in pet ether) to give 7-(methylsulfonyl)-1-(pent-4-yn-1-yl)-1,2,3,4-tetrahydroquinoline as light brown oil (182 mg, 58%); R_f 0.43 (1:1, EtOAc/pet ether); ^{1}H NMR (400 MHz, $CDCl_3$) δ_H 7.09 (3H, m, H-5, H-6, H-8), 3.50 – 3.41 (2H, m, H-1'), 3.39 – 3.24 (2H, m, H-1), 3.02 (3H, s, H-10), 2.80 (2H, t, *J* 6.3 Hz, H-3), 2.27 (2H, td, *J* 6.8, 2.6 Hz, H-3'), 2.07 (1H, t, *J* 2.6 Hz, H-5'), 2.04 – 1.91 (2H, m, H-2), 1.89 – 1.78 (2H, m, H-2'); ^{13}C NMR (101 MHz, $CDCl_3$) δ_C 145.9 (C-9), 139.4 (C-7), 129.9 (C-5), 128.2 (C-4), 113.9 (C-8), 108.2 (C-6), 83.6 (C-4'), 69.6 (C-5'), 50.0 (C-1'), 49.6 (C-1), 44.8 (C-10), 28.5 (C-3), 25.1 (C-2'), 21.6 (C-2), 16.2 (C-3'); LRMS *m/z* (ESI$^+$) 555 ([2M+H]$^+$, 100%), 278 ([M+H]$^+$, 40%).

(*E*)-7-(Methylsulfonyl)-1-(5-(4,4,5,5-tetramethyl-1,3,2-dioxaborolan-2-yl)pent-4-en-1-yl)-1,2,3,4-tetrahydroquinoline (compound **56**)

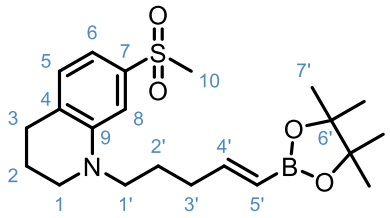

7-(methylsulfonyl)-1-(pent-4-yn-1-yl)-1,2,3,4-tetrahydroquinoline (180 mg, 0.650 mmol, 1.0 equiv.) and bis(cyclopentadienyl)zirconium(VI) chloride hydride (8.3 mg, 0.032 mmol, 0.05 equiv.) were added to a tapered microwave vial and sealed under an argon atmosphere in the absence of light. Triethylamine (10 µL, 0.065 mmol, 0.1 equiv.) and 4,4,5,5-tetramethyl-1,3,2-dioxaborolane (113 µL, 0.714 mmol, 1.1 equiv.) were added and the reaction mixture was stirred at 60 °C under argon for 20 h in the dark. After cooling to r.t. the reaction mixture was diluted with pet ether (5 mL) and purified by flash silica column chromatography (elution with 0-100% EtOAc in pet ether) to give (*E*)-7-(methylsulfonyl)-1-(5-(4,4,5,5-tetramethyl-1,3,2-dioxaborolan-2-yl)pent-4-en-1-yl)-1,2,3,4-tetrahydroquinoline as a colourless oil (155 mg, 59%); R_f 0.35 (1:1, EtOAc/pet ether); ^{1}H NMR (600 MHz, $CDCl_3$) δ_H 7.12 – 6.97 (3H, m, H-5, H-6, H-8), 6.63 (1H, dt, *J* 17.8, 6.4 Hz, H-4'), 5.47 (1H, dt, *J* 17.8, 1.6 Hz, H-5'), 3.31 (4H, m, H-1, H-1'), 3.01 (3H, s, H-10), 2.79 (2H, dt, *J* 12.9, 6.3 Hz, H-3), 2.22 (2H, tdd, *J* 7.8, 6.4, 1.6 Hz, H-3'), 1.97 – 1.91 (2H, m, H-2), 1.75 (2H, *J* 7.8 Hz, H-2'), 1.24 (12H, s, H-3''); ^{11}B NMR (128 MHz, $CDCl_3$) δ_B 29.72 (B-5'); ^{13}C NMR (151 MHz, $CDCl_3$) δ_C 153.2 (C-4'), 147.2 (C-7) 145.9 (C-9), 139.3 (C-5'), 129.8 (C-5), 128.1 (C-4), 113.7 (C-8), 108.1 (C-6), 83.3 (d, *J* 5.1 Hz, C-2''), 50.8 (C-1), 49.4 (C-1'), 44.7 (C-10), 33.3 (C-3') 25.0 (C-2'), 24.7 (C-3''), 21.5 (C-2); LRMS *m/z* (ESI$^+$) 810 ([2M+H]$^+$, 100%), 406 ([M+H]$^+$, 8%).

(*R*,*E*)-4-Methyl-6-(5-(7-(methylsulfonyl)-3,4-dihydroquinolin-1(2*H*)-yl)pent-1-en-1-yl)-1,3,4,5-tetrahydro-2*H*-benzo[*b*][1,4]diazepin-2-one (compound **49**)

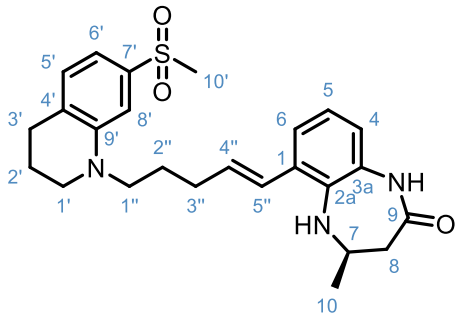

(*R*)-6-Bromo-4-methyl-1,3,4,5-tetrahydro-2H-benzo[*b*][1,4]diazepin-2-one (65 mg, 0.255 mmol, 1.0 equiv.), (*E*)-7-(methylsulfonyl)-1-(5-(4,4,5,5-tetramethyl-1,3,2-dioxaborolan-2-yl)pent-4-en-1-yl)-1,2,3,4-tetrahydroquinoline (155 mg, 0.382 mmol, 1.5 equiv.), K_2CO_3 (106 mg, 0.765 mmol, 3.0 equiv.) and [1,1′-Bis(diphenylphosphino)ferrocene]dichloropalladium$^{(II)}$ (21 mg, 0.0255 mmol, 0.1 equiv.) were added to a microwave vial which was sealed and placed under an argon atmosphere. To this was added 1,4-dioxane (1.2 mL) and H_2O (0.4 mL), and then the reaction was heated to 100 °C for 48 h. After cooling the reaction mix was diluted with EtOAc (100 mL) and passed through a pad of Celite®. The filtrate was then washed with H_2O (3 × 100 mL), brine (100 mL), the organic layer was then dried (Na_2SO_4), filtered and concentrated *in vacuo* to give brown oil. The crude product was purified by flash silica column chromatography (elution with 50-100% EtOAc in pet ether) to give (*R*,*E*)-4-methyl-6-(5-(7-(methylsulfonyl)-3,4-dihydroquinolin-1(2*H*)-yl)pent-1-en-1-yl)-1,3,4,5-tetrahydro-2*H*-benzo[*b*][1,4]diazepin-2-one as an off white solid (41 mg, 35%); R_f 0.33 (EtOAc); m.p 159 – 161 °C (EtOAc); $[\alpha]_D^{25}$ = −3.47 (*c* 1.0, $CHCl_3$); $\bar{\nu}_{max}$ (thin film $CHCl_3$)/ cm^{-1} 2934 (C-H, s), 1670 (C=O, s), 1596 (C=C, m) 1299 (S=O, s); ^{1}H NMR (600 MHz, CD_3CN) δ_H 7.73 (1H, s, NH-3a/9), 7.19 (1H, dd, *J* 7.8, 1.7 Hz, H-6), 7.09 (1H, dt, *J* 7.8, 1.0 Hz, H-5'), 7.00 (1H, d, *J* 1.7 Hz, H-8'), 6.97 (1H, dd, *J* 7.8,

1.7 Hz, H-4), 6.86 (t, *J* 7.8, Hz, H-5), 6.81 (1H, dd, *J* 7.8, 1.7 Hz, H-6'), 6.63 (1H, dd, *J* 15.5, 1.5 Hz, H-5''), 6.16 (1H, dt, *J* 15.5, 7.0 Hz, H-4''), 4.02 (1H, m, H-7), 3.40 – 3.37 (2H, m, H-1''), 3.35 (2H, t, *J* 5.7 Hz, H-1'), 2.97 (3H, s, H-10), 2.78 (2H, td, *J* 6.3, 1.0 Hz, H-3'), 2.47 (1H, dd, *J* 13.1, 5.2 Hz, H_AH_B-8), 2.32 (2H, qd, *J* 7.0, 1.5 Hz, H-3''), 2.18 (1H, dd, *J* 13.1, 7.0 Hz, H_AH_B-8), 1.94 – 1.89 (2H, m, H-2'), 1.80 (2H, p, *J* 7.0 Hz, H-2''), 1.25 (3H, d, *J* 6.2 Hz, H-10); ^{13}C NMR (151 MHz, CD_3CN) δ_C 172.9 (C-9), 146.8 (C-9'), 140.7 (C-7'), 137.4 (C-2a), 134.5 (C-4''), 132.5 (C-1), 132.0 (C-3a), 130.5 (C-5'), 129.1 (C-4'), 127.1 (C-5''), 124.3 (C-6), 122.3 (C-5), 121.6, 114.0 (C-4), 108.6 (C-8'), 56.8 (C-7), 51.2 (H-1''), 49.8 (H-1'), 44.6 (C-10'), 41.1 (C-8), 31.4 (C-3''), 28.9 (C-3'), 26.2 (C-2''), 23.9 (C-10), 22.2 (C-2'); HRMS *m/z* (ESI$^+$) [Found: 454.2164 $C_{25}H_{32}SN_3O_3$ requires 454.2159 $[M+H]^+$]; LRMS *m/z* (ESI$^+$) 454 ($[M+H]^+$, 100%) 907 ($[2M+H]^+$, 94%); HPLC (retention time 9.1 mins) 95.0% purity.

2-Amino-4-methoxyphenol (compound **57**)

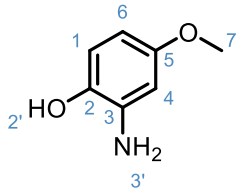

4-Methoxy-2-nitro phenol (0.5 g, 2.96 mmol, 1.0 equiv.) was dissolved in EtOH (25 mL) and then 10 wt% Pd on carbon 55-65% wet (300 mg, 0.132 mmol of Pd, 0.044 equiv. of Pd) which was placed under an argon atmosphere in a Büchi glass miniclave steel type 200mL reaction vessel. The argon atmosphere was then replaced with hydrogen and the pressure increased to 2400 mbar. After 30 mins the pressure was observed to have decreased to below 2000 mbar and so the vessel was repressurised to 3000 mbar. After 1 h the reaction was observed to be complete, and the resultant mixture was filtered through celite and washed with ethanol (200 mL). The filtrate was

then concentrated *in vacuo* to give the desired product as a dark brown solid. Due to the instability of electron rich anilines this compound was used without further purification to give 2-amino-4-methoxyphenol (410 mg, quantitative yield >99%); R_f 0.16 (1:2, EtOAc/pet ether); ^{1}H NMR (400 MHz, $CDCl_3$) δ_H 6.66 (1H, d, *J* 8.6 Hz, H-1), 6.34 (1H, d, *J* 2.8 Hz, H-4), 6.20 (1H, dd, *J* 8.6, 2.8 Hz, H-6), 3.95 (2H, br s, NH-3'), 3.72 (3H, s, H-7); LRMS *m/z* (ESI$^+$) 140 ([M+H]$^+$, 87%) These data are in accordance with the literature.[131]

6-Methoxy-2*H*-benzo[*b*][1,4]oxazin-3(4*H*)-one (compound **58**)

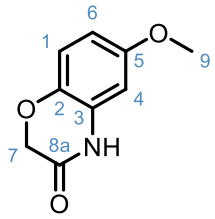

2-amino-4-methoxyphenol (0.75 g, 5.39 mmol, 1.0 equiv.) was dissolved in MeCN (45 mL) under an argon atmosphere. To this was added chloroacetyl chloride (0.47 mL, 5.93 mmol, 1.1 equiv.) dropwise and then K_2CO_3 (1.95 g, 14.0 mmol, 2.6 equiv.) was added and the reaction mixture was heated to reflux for 3 h. Once cooled the reaction mixture was filtered and then concentrated *in vacuo*. The resultant residue was dissolved in water (100 mL) and washed with CH_2Cl_2 (3 × 50 mL). The combined organic layers were then dried (Na_2SO_4), filtered and concentrated to give a purple solid which was the recrystallized from MeOH to give 6-methoxy-2*H*-benzo[*b*][1,4]oxazin-3(4*H*)-one as dark pink crystals (0.55 g, 57%); R_f 0.05 (1:2, EtOAc/pet ether); m.p 137 – 140 °C (MeOH); $\bar{\nu}_{max}$ (solid)/ cm^{-1} 2932 (C-H, s), 1706 (C=O, s), 1611 (C=C, s) 1214 (C-O, s) ^{1}H NMR (400 MHz, $CDCl_3$) δ_H 8.91 (1H, s, NH-3/8a), 6.89 (1H, d, *J* 8.8 Hz, H-1), 6.51 (1H, dd, *J* 8.8, 2.8 Hz, H-6), 6.40 (1H, d, *J* 2.8 Hz, H-4), 4.56 (2H, s, H-7), 3.72 (3H, s, H-9); ^{13}C NMR (151 MHz, $CDCl_3$) δ_C 166.7

(C-8a), 155.5 (C-5), 137.8 (C-2), 127.0 (C-3), 117.4 (C-1), 109.0 (C-6), 102.3 (C-4), 67.6 (C-7), 56.0 (C-9); HRMS *m/z* (ESI$^+$) [Found: 180.0649 $C_9H_9NO_3$ requires 180.0655 $[M+H]^+$]; LRMS *m/z* (ESI$^+$) 381 ($[2M+Na]^+$, 100%) 180 ($[M+H]^+$, 39%); HPLC: retention time 6.37 mins, purity 97.0%. These data are in accordance with the literature.[131]

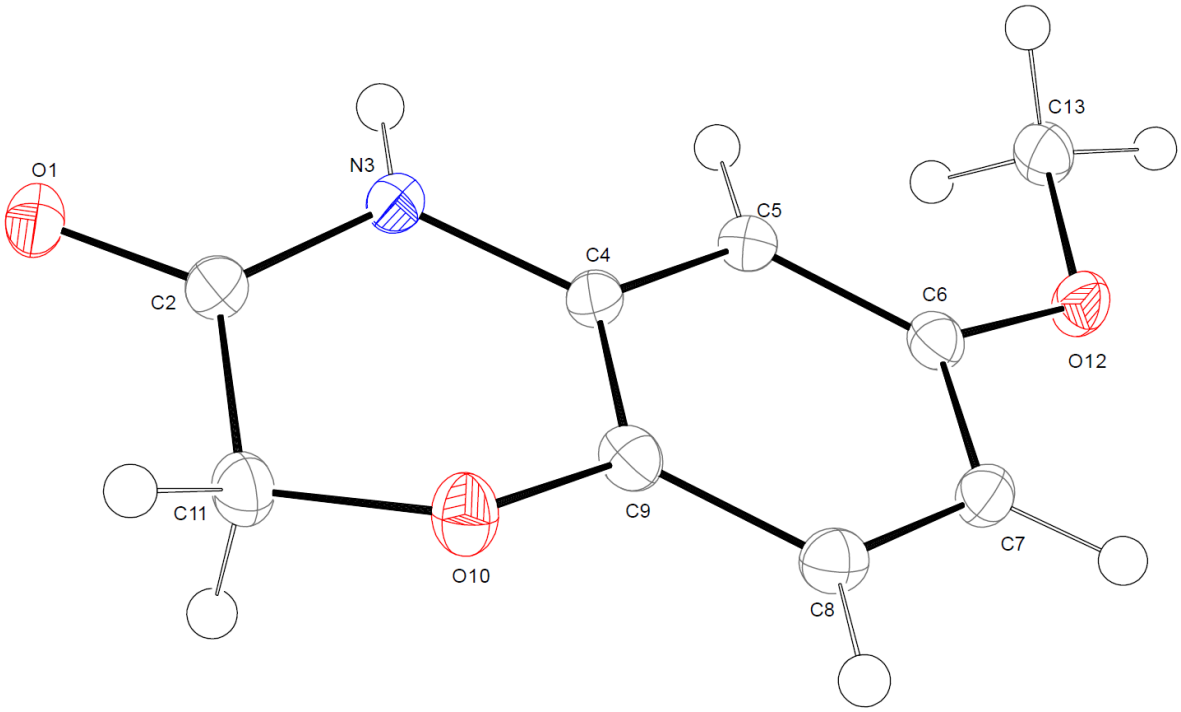

6-Methoxy-3,4-dihydro-2*H*-benzo[*b*][1,4]oxazine (compound **59**)

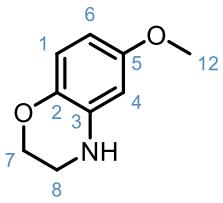

6-methoxy-2*H*-benzo[*b*][1,4]oxazin-3(4*H*)-one (550 mg, 3.07 mmol, 1.0 equiv.) was dissolved in THF (25 mL) and in a separate flask $LiAlH_4$ (300 mg, 6.14 mmol, 2.0 equiv.) was suspended in THF (50 mL) and cooled to 0 °C. The solution of 6-methoxy-2*H*-benzo[*b*][1,4]oxazin-3(4*H*)-one was added dropwise to the flask containing $LiAlH_4$, upon complete addition the reaction mixture was warmed to room temperature for 18

h. The reaction was then returned to 0 °C and water (0.5 mL), followed by 15 wt% $NaOH_{(aq)}$ (0.5 mL) and water (1.5 mL) were added dropwise. $MgSO_4$ was added, and the suspension was stirred at room temperature for 30 mins. After this time the solids were removed by filtration and the filtrate was concentrated *in vacuo* to give the crude product as a brown oil. This was then purified by flash silica column chromatography (elution with 0-50 % EtOAc in pet ether) to give 6-methoxy-3,4-dihydro-2*H*-benzo[*b*][1,4]oxazine as a light pink crystalline solid (400 mg, 79%); R_f 0.25 (1:2, EtOAc/pet ether); m.p 42 – 47 °C (EtOAc); $\bar{\nu}_{max}$ (solid)/ cm^{-1} 3388 (N-H, m), 1552 (C=C, s), 1193 (C-O, s) 1046 (C-N, s); ^{1}H NMR (600 MHz, $CDCl_3$) δ_H 6.69 (1H, d, *J* 8.7 Hz, H-1), 6.22 (1H, dd, *J* 8.7, 2.9 Hz, H-6), 6.17 (1H, d, *J* 2.9 Hz, H-4), 4.21-4.18 (2H, m, H-7), 3.72 (3H, s, H-9), 3.42-3.38 (2H, m, H-8); ^{13}C NMR (151 MHz, $CDCl_3$) δ_C 154.5 (C-5), 138.4 (C-2), 134.2 (C-3), 117.0 (C-1), 103.7 (C-6), 101.5 (C-4), 65.1 (C-7), 55.7 (C-9), 41.2 (C-8); HRMS *m/z* (ESI^+) [Found: 166.0854 $C_9H_{11}NO_2$ requires 166.0863 $[M+H]^+$]; LRMS *m/z* (ESI^+) 166 ($[M+H]^+$, 100%); HPLC method1: retention time 6.39 mins, purity 99.4%. These data are in accordance with the literature.[131]

6-Methoxy-4-(pent-4-yn-1-yl)-3,4-dihydro-2*H*-benzo[*b*][1,4]oxazine (compound **60**)

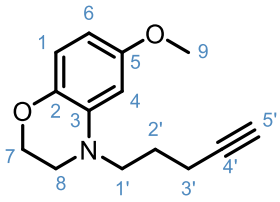

6-methoxy-3,4-dihydro-2*H*-benzo[*b*][1,4]oxazine (200 mg, 1.21 mmol, 1.0 equiv.) and TBAI (224 mg, 0.61 mmol, 0.5 equiv.) were added to a flame dried flask attached to a condenser under an argon atmosphere. To this was added DIPEA (422 µL, 2.42 mmol, 2.0 equiv.), pent-4-yn-1-yl methanesulfonate (300 mg, 1.82 mmol, 1.5 equiv.) and DMF (1.2 mL) and the reaction mixture was heated to 85 °C for 24 h. After this the resultant

brown solution was diluted with diethyl ether (50 mL) which was washed with water (3 × 50 mL), 10 wt% $LiCl_{(aq)}$ (25 mL), brine (25 mL), dried ($MgSO_4$), filtered and then concentrated *in vacuo* to give the crude product as a dark brown oil. This was then purified by flash silica column chromatography (elution with 0-50 % EtOAc in hexane) to give 6-methoxy-4-(pent-4-yn-1-yl)-3,4-dihydro-2*H*-benzo[*b*][1,4]oxazine as a light brown oil (252 mg, 90%); R_f 0.74 (1:1, EtOAc/pet ether); $\bar{\nu}_{max}$ (thin film, $CHCl_3$)/ cm^{-1} 2934 (C-H, m), 2361 (C≡C, m), 1511 (C=C, s), 1207 (C-O, s); ^1H NMR (600 MHz, $CDCl_3$) δ_H 6.69 (1H, d, *J* 8.6 Hz, H-1), 6.29 (1H, d, *J* 2.8 Hz, H-4), 6.15 (1H, dd, *J* 8.6, 2.8 Hz, H-6), 4.19 – 4.16 (2H, m, H-7), 3.75 (3H, s, H-9), 3.39 – 3.34 (4H, m, H-8, H-1'), 2.28 (2H, td, *J* 6.8, 2.7 Hz, H-3'), 2.01 (1H, t, *J* 2.7 Hz, H-5'), 1.83 (2H, p, *J* 6.8 Hz, H-2'); ^{13}C NMR (151 MHz, $CDCl_3$) δ_C 154.9 (C-5), 138.4 (C-2), 135.8 (C-3), 116.3 (C-1), 101.0 (C-6), 99.2 (C-4), 83.7 (C-4'), 69.3 (C-5'), 64.4 (C-7), 55.7 (C-9), 49.9 (C-1'), 47.6 (C-8), 25.1 (C-2'), 16.1 (C-3'); HRMS *m/z* (ESI^+) [Found: 232.1334 $C_{14}H_{17}NO_2$ requires 232.1332 $[M+H]^+$]; LRMS *m/z* (ESI^+) 460 ($[2M+H]^+$, 100%), 232 ($[M+H]^+$, 78%); HPLC: retention time 9.70 mins, purity 98.4%.

(*E*)-6-Methoxy-4-(5-(4,4,5,5-tetramethyl-1,3,2-dioxaborolan-2-yl)pent-4-en-1-yl)-3,4-dihydro-2*H*-benzo[*b*][1,4]oxazine (compound **61**)

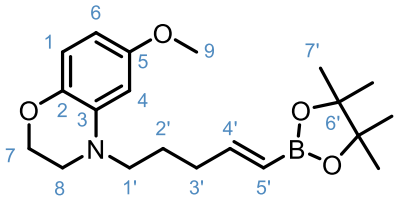

6-methoxy-4-(pent-4-yn-1-yl)-3,4-dihydro-2*H*-benzo[*b*][1,4]oxazine (220 mg, 0.951 mmol, 1.0 equiv.), bis(cyclopentadienyl)zirconium(VI) chloride hydride (25 mg, 0.0951 mmol, 0.1 equiv.) were added to a tapered microwave vial and sealed under an argon atmosphere in the absence of light. NEt_3 (13 µL, 0.0951 mmol, 0.1 equiv.) and 4,4,5,5-

tetramethyl-1,3,2-dioxaborolane (152 µL, 1.046 mmol, 1.1 equiv.) were added and the reaction mixture was stirred at 60 °C under argon for 20 h in the dark. After cooling to r.t. the reaction mixture was diluted with pet ether (5 mL) and purified by flash silica column chromatography (elution with 0-100% CH_2Cl_2 in pet ether) to give (*E*)-6-methoxy-4-(5-(4,4,5,5-tetramethyl-1,3,2-dioxaborolan-2-yl)pent-4-en-1-yl)-3,4-dihydro-2*H*-benzo[*b*][1,4]oxazine as a yellow oil (259 mg, 76%); R_f 0.55 (CH_2Cl_2); $\bar{\nu}_{max}$ (thin film, $CHCl_3$)/ cm^{-1} 2977 (C-H, m), 1638 (C=C, m), 1511 (C=C, s), 1209 (C-O, s); ^1H NMR (600 MHz, $CDCl_3$) δ_H 6.67 (1H, d, *J* 8.6 Hz, H-1), 6.64 (1H, dt, *J* 17.9, 6.4 Hz H-4'), 6.21 (1H, d, *J* 2.8 Hz, H-4), 6.13 (1H, dd, *J* 8.6, 2.8 Hz, H-6), 5.48 (1H, dt, *J* 17.9, 1.6 Hz, H-5'), 4.19 – 4.14 (2H, m, H-7), 3.74 (3H, s, H-9), 3.33 – 3.28 (2H, m, H-8), 3.25 – 3.19 (2H, m, H-1'), 2.21 (2H, tdd, *J* 7.5, 6.4, 1.6 Hz, H-3'), 1.74 (2H, p, *J* 7.5 Hz, H-2'), 1.26 (12H, s, H-7'); ^{11}B NMR (128 MHz, $CDCl_3$) δ_B 29.93 (B-5'); ^{13}C NMR (151 MHz, $CDCl_3$) δ_C 154.9 (C-5), 153.3 (C-4'), 138.4 (C-2), 136.0 (C-3), 116.2 (C-1), 100.8 (C-6), 99.1 (C-4), 83.3 (C-6'), 64.5 (C-7), 55.7 (C-9), 50.6 (C-1'), 47.3 (C-8), 33.3 (C-3'), 24.9 (C-7'), 24.8 (C-2'); HRMS *m/z* (ESI^+) [Found: 360.2373 $C_{20}H_{31}{}^{11}BNO_4$ requires 360.2341 $[M+H]^+$]; LRMS *m/z* (ESI^+) 741.2 ($[2M+2H]^+$, 99%), 360.1 ($[M+H]^+$, 100%); HPLC: retention time 11.70 mins, purity 93.5%.

(*R*,*E*)-6-(5-(6-Methoxy-2,3-dihydro-4*H*-benzo[*b*][1,4]oxazin-4-yl)pent-1-en-1-yl)-4-methyl-1,3,4,5-tetrahydro-2*H*-benzo[*b*][1,4]diazepin-2-one (compound **50**)

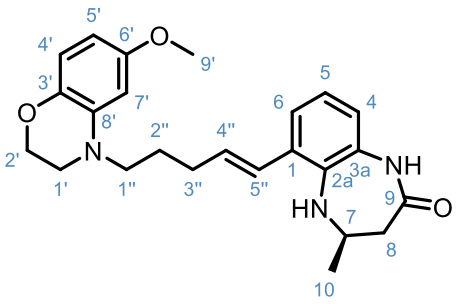

(*R*)-6-Bromo-4-methyl-1,3,4,5-tetrahydro-2*H*-benzo[*b*][1,4]diazepin-2-one (86 mg, 0.337 mmol, 1.0 equiv.), (*E*)-6-methoxy-4-(5-(4,4,5,5-tetramethyl-1,3,2-dioxaborolan-2-yl)pent-4-en-1-yl)-3,4-dihydro-2*H*-benzo[*b*][1,4]oxazine (181 mg, 0.506 mmol, 1.5 equiv.), K_2CO_3 (139 mg, 1.01 mmol, 3.0 equiv.) and [1,1′-Bis(diphenylphosphino)ferrocene]dichloropalladium$^{(II)}$ (25 mg, 0.034 mmol, 0.1 equiv.) were loaded into the reaction vessel which was placed under an argon atmosphere and then to this was added 1,4-dioxane (4 mL) and H_2O (1 mL), the reaction mixture was then heated to 100 °C for 24 h. After cooling to room temperature, the reaction mixture was diluted with EtOAc (50 mL) and was then filtered through celite and washed with EtOAc (50 mL). The combined organic layers were then washed with sat. $K_2CO_{3(aq)}$ (50 mL), brine (2 × 50 mL), dried ($MgSO_4$), filtered and concentrated *in vacuo*. The crude product was then purified by flash silica column chromatography (elution with 0-100% EtOAc in pet ether) to give a light brown oil which was then further purified by semi preparative HPLC (retention time 7.45 mins) from which the fractions containing product were lyophilised to give (*R*,*E*)-6-(5-(6-methoxy-2,3-dihydro-4*H*-benzo[*b*][1,4]oxazin-4-yl)pent-1-en-1-yl)-4-methyl-1,3,4,5-tetrahydro-2*H*-benzo[*b*][1,4]diazepin-2-one as a white lysophilate (83 mg, 60%); R_f 0.43 (EtOAc); $[\alpha]_D^{25}$ = −2.1 (*c* 0.5, $CHCl_3$); $\bar{\nu}_{max}$ (thin film, $CHCl_3$)/ cm^{-1} 2943 (C-H, m), 1673 (C=O, s),

1512 (C=C, s), 1208 (C-O, s); ^{1}H NMR (600 MHz, d_6-DMSO) δ_H 9.40 (1H, s, NH-3a/9), 7.16 (1H, dd, *J* 6.1, 3.2 Hz, H-5), 6.81 – 6.77 (2H, m, H-4, H-6), 6.72 (1H, d, *J* 15.5 Hz, H-5''), 6.55 (1H, d, *J* 8.6 Hz, H-4'), 6.22 (1H, d, *J* 2.8 Hz, H-7'), 6.14 (1H, dt, *J* 15.5, 6.9 Hz, H-4''), 6.05 (1H, dd, *J* 8.6, 2.8 Hz, H-5'), 4.55 (d, *J* 2.5 Hz, NH-2a/7), 4.10 – 4.06 (2H, m, H-2'), 3.99 – 3.91 (1H, m, H-7), 3.61 (3H, s, H-9'), 3.31 – 3.24 (4H, m, H-1', H-1''), 2.37 (1H, dd, *J* 12.9, 5.0 Hz, H_AH_B-8), 2.30 – 2.23 (2H, m, H-3''), 2.09 (1H, dd, *J* 12.9, 7.3 Hz, H_AH_B-8), 1.72 (2H, p, *J* 7.4 Hz, H-2''), 1.19 (3H, d, *J* 6.2 Hz, H-10); ^{13}C NMR (151 MHz, d_6-DMSO) δ_C 171.6 (C-9), 154.3 (C-6'), 137.7 (C-3'), 136.2 (C-3a), 135.7 (C-8'), 131.94 (C-2a), 131.9 (C-4''), 130.1 (C-1), 126.1 (C-5''), 122.1 (C-5), 120.6 (C-4, C-6), 115.7 (C-4'), 100.3 (C-5'), 98.4 (C-7'), 63.7 (C-2'), 55.4 (C-7), 55.04 (C-9'), 49.5 (C-1''), 46.4 (C-1'), 40.4 (C-8), 30.3 (C-3''), 25.1 (C-2''), 23.2 (C-10); HRMS *m/z* (ESI$^+$) [Found: 430.2104 $C_{24}H_{29}N_3O_3Na$ requires 430.2101 $[M+Na]^+$] and [Found 408.2277 $C_{24}H_{30}N_3O_3$ requires 408.2282 $[M+H]^+$]; LRMS *m/z* (ESI$^+$) 815.3 ($[2M+H]^+$, 81%), 408.1 ($[M+H]^+$, 100%); HPLC: retention time 9.66 mins, purity 99.8%.

7.3.5 Chapter 5: Compounds **62** - **85**

1-Bromo-2-fluoro-5-iodo-3-nitrobenzene (compound **69**)

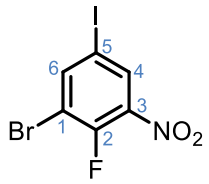

N-Iodosuccinimide (4.32g, 19.0 mmol, 1.4 equiv.) was added to a solution of 1-bromo-2-fluoro-3-nitrobenzene (3.00 g, 13.6 mmol, 1.0 equiv.) in concentrated sulphuric acid (15 mL) and the reaction mixture was stirred at r.t. for 19 h. The reaction mixture was then cooled to 0 °C and added to ice (200 g) with the resulting precipitate being extracted with dichloromethane (3 × 140 mL). The combined organic layers were

washed with 10 wt% $Na_2S_2O_{3(aq)}$ (150 mL), brine (100 mL) and dried ($Na_2S_2O_4$), filtered and concentrated *in vacuo* give a dark brown oil. The crude product was then purified *via* flash silica column chromatography (elution with 5-10% EtOAc in pet ether) to give 1-bromo-2-fluoro-5-iodo-3-nitrobenzene as a yellow solid (3.97 g, 84%). R_f 0.6 (1:9, EtOAc/pet ether); ^{1}H NMR (400 MHz; $CDCl_3$) δ_H 8.27 (1H, dd, *J* 6.2, 2.2, H-4), 8.16 (1H, dd, *J* 5.5, 2.2, H-6); $^{19}F\{^1H\}$ NMR (377 MHz; $CDCl_3$) δ_F −110.8; LRMS *m/z* (ES-API$^+$) 345.3 $[M+H]^+$, (ES-API$^-$) 343.8 ($[M-H]^-$, 100%); HPLC: retention time 11.00 mins, 93.1% purity. These data are in accordance with the literature.[88]

Methyl (2-bromo-4-iodo-6-nitrophenyl)-D-alaninate (compound **70**)

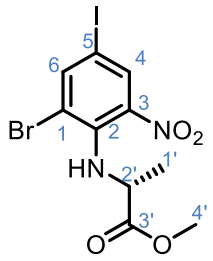

To a stirred solution of 1-bromo-2-fluoro-5-iodo-3-nitrobenzene (4.26 g, 12.3 mmol, 1.0 equiv.) and Cs_2CO_3 (12.0 g, 36.7 mmol, 3.0 equiv.) in toluene (200 mL) was added methyl (*R*)-3-aminoethanoate hydrochloride (4.50 g, 19.2 mmol, 1.4 equiv.) and the suspension was stirred at 90 °C for 24 h. After this DIPEA (0.5 mL) was added, and the reaction was left to stir for a further 12 h at 90 °C. After this time the reaction mixture was cooled to r.t. and added to 1M $K_2CO_{3(aq)}$ (400 mL). The resultant mixture was extracted with EtOAc (3 × 300 mL). The combined organic layers were washed with brine (200 mL), dried ($MgSO_4$), filtered and evaporated in *vacuo* to afford an orange oil. The crude oil was purified *via* flash silica column chromatography (elution with 0-20 % EtOAc in pet ether) to give methyl (2-bromo-4-iodo-6-nitrophenyl)-D-alaninate as an orange solid (3.230 g, 62%). R_f 0.43 (1:9, EtOAc/pet ether); m.p. 48 – 52 °C (EtOAc); $[\alpha]_D^{25}$ = −302 (*c* 1.0, $CHCl_3$); $\bar{\nu}_{max}$ (neat solid)/ cm^{-1} 3369 (N-H, m), 2949

(C-H, w), 1718 (C=O, s), 1527 (N-O, s); ^{1}H NMR (400 MHz, $CDCl_3$) δ_H 8.20 (1H, d, *J* 2.1 Hz, H-4), 8.00 (1H, d, *J* 2.1 Hz, H-6), 6.61 (1H, d, *J* 10.3 Hz, NH-2/2'), 4.56 (1H, dq, *J* 10.3, 7.1 Hz, H-2'), 3.66 (3H, s, H-4'), 1.50 (3H, d, *J* 7.1 Hz, H-1'); ^{13}C NMR (101 MHz, $CDCl_3$) δ_C 173.8 (C-3'), 146.8 (C-6), 142.7 (C-2), 141.7 (C-3), 133.9 (C-4), 117.4 (C-1), 80.7 (C-5), 54.7 (C-4'), 52.7 (C-2'), 19.3 (C-1'); HRMS *m/z* (ESI^-) [Found 426.8747 $C_{10}H_{10}{}^{79}BrIN_2O_4$ requires 426.8796 $[M-H]^-$]; LRMS (ESI^-) *m/z* 427 ($[M-H]^-$, 100%), 429 ($[M-H]^-$, 97%); HPLC: retention time 11.28 mins, 96.7% purity.

Methyl (2-bromo-4-(5-hydroxypent-1-yn-1-yl)-6-nitrophenyl)-D-alaninate (compound **71**)

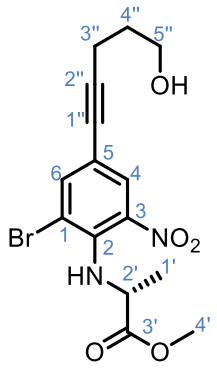

A solution of methyl (2-bromo-4-iodo-6-nitrophenyl)-D-alaninate (300 mg, 0.666 mmol, 1.00 equiv.) in THF (3 mL) was added NEt_3 (1 mL) followed by 4-penty-1-ol (0.078 mL, 0.84 mmol, 1.2 equiv.). To this mixture bis(triphenylphosphine)palladium dichloride (10 mg, 0.014 mmol, 0.02 equiv.) and copper iodide (5 mg, 0.021 mmol, 0.03 equiv.) were added. The suspension was place under an argon atmosphere and then stirred at r.t. for 15 h. The completed reaction was filtered through a Celite® pad, the filtrated was concentrated *in vacuo* to afford a brown solid. The crude solid was then dissolved in EtOAc (150 mL), and organic layer was washed with sat. $NaHCO_{3(aq)}$ (3 × 75 mL), brine (50 mL), dried ($MgSO_4$), filtered and concentrated *in vacuo* to give an orange oil. This crude product was purified *via* flash silica column chromatography (elution with

0-50% EtOAc in pet ether) to give methyl (2-bromo-4-(5-hydroxypent-1-yn-1-yl)-6-nitrophenyl)-D-alaninate as an orange oil (0.264 g, 98%). R_f 0.45 (1:1, EtOAc:pet ether); $[\alpha]_D^{25}$ = −264 (*c* 1.0, $CHCl_3$); $\bar{\nu}_{max}$ ($CHCl_3$ thin film)/ cm-1 3356 (N-H, w), 2926 (C-H, w), 2229 (C≡C, w), 1743 (C=O, s), 1535 (N-O, s); ^{1}H NMR (400 MHz, $CDCl_3$) δ_H 7.92 (1H, d, *J* 2.0 Hz, H-4), 7.71 (1H, d, *J* 2.0 Hz, H-6), 6.67 (1H, br s, NH-2/2'), 4.57 (1H, q, *J* 7.1 Hz, H-2'), 3.77 (2H, t, *J* 6.2 Hz, H-5''), 3.64 (3H, s, H-4'), 2.51 (2H, t, *J* 7.0 Hz, H-3''), 1.88 – 1.77 (2H, m, H-4''), 1.48 (3H, d, *J* 7.0 Hz, H-1'); ^{13}C NMR (101 MHz, $CDCl_3$) δ_C 173.8 (C-3'), 141.8 (C-6), 141.6 (C-2), 141.1 (C-3), 128.4 (C-4), 117.3 (C-5), 115.9 (C-5), 91.7 (C-2''), 77.7 (C-1''), 61.6 (C-5''), 54.7 (C-4'), 52.7 (C-2'), 31.3 (C-3''), 19.3 (C-1'), 16.0 (C-4''); HRMS *m/z* (ESI+) [Found: 383.0248 $C_{15}H_{16}{}^{79}BrN_2O_5$ requires 383.0415 $[M-H]^-$]; LRMS (ESI^-) *m/z* 383 ($[M-H]^-$, 100%), 385 ($[M-H]^-$, 97%); HPLC: retention time 9.65 mins, 92.7% purity.

Methyl (2-bromo-4-(5-hydroxypentyl)-6-nitrophenyl)-D-alaninate (compound **63**)

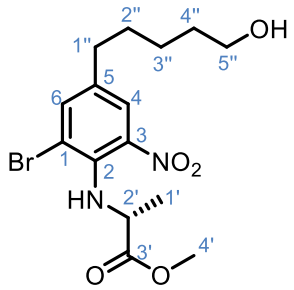

Methyl (2-bromo-4-(5-hydroxypent-1-yn-1-yl)-6-nitrophenyl)-D-alaninate (203 mg, 0.527 mmol, 1.00 equiv.) and tris(triphenylphosphine)rhodium chloride (30 mg, 0.040 mmol, 0.075 equiv.) were placed under an argon atmosphere. To the solids, dry toluene (6 mL) was added, and the atmosphere was replaced with hydrogen. Once the reaction flask was completely under a hydrogen atmosphere, the reaction mixture was heated to 65 °C for 12 h. The solvents were then removed *in vacuo* to afford a brown solid. This crude product was purified *via* flash silica column chromatography

(elution with 0-50% EtOAc in pet ether) to give methyl (2-bromo-4-(5-hydroxypentyl)-6-nitrophenyl)-D-alaninate as a brown oil (202.6 mg, 99%). R_f 0.45 (1:1, EtOAc/pet ether); $[\alpha]_D^{25}$ = −264 (*c* 1.0, $CHCl_3$); ^1H NMR (400 MHz, $CDCl_3$) δ_H 7.72 (1H, d, *J* 2.1 Hz, H-4), 7.56 (1H, d, *J* 2.1 Hz, H-6), 6.43 (1H, s, NH-2/2'), 4.52 (1H, q, *J* 7.1 Hz, H-2'), 3.66 (2H t, *J* 6.5 Hz, H-5''), 3.63 (3H, s, H-4'), 2.63 – 2.53 (2H, t, *J* 7.6 Hz, H-1''), 1.70 – 1.54 (4H, m, H-2'', H-4''), 1.50 (3H, d, *J* 7.1 Hz, H-1'), 1.44 – 1.34 (2H, m, H-3'').^{13}C NMR (101 MHz; $CDCl_3$) δ_c 174.2 (C-3'), 144.4 (C-3), 140.3 (C-2), 139.6 (C-6), 137.2 (C-5), 124.8 (C-4), 117.9 (C-1), 62.8 (C-5''), 55.1 (C-2'), 52.5 (C-4'), 34.5 (C-1''), 32.5 (C-4''), 30.8 (C-2''), 25.4 (C-3''), 19.3 (C-1'); LRMS (ESI^-) *m/z* 389 ($[M-H]^-$, 100%), 391 ($[M-H]^-$, 97%).

tert-Butyl (2-bromo-4-iodo-6-nitrophenyl)-D-alaninate (compound **73**)

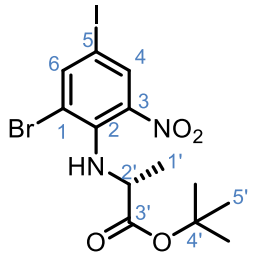

To a stirred solution of 1-bromo-2-fluoro-5-iodo-3-nitrobenzene (3.97 g, 12.1 mmol, 1.00 equiv.) and Cs_2CO_3 (11.9 g, 36.4 mmol, 3.00 equiv.) in toluene (200 mL) was added *tert*-butyl (*R*)-3-aminoethanoate hydrochloride (4.31 g, 17.0 mmol, 1.40 equiv.) and the suspension was stirred at 85 °C for 24 h. To the cooled reaction mixture was added sat. $K_2CO_{3(aq)}$ (400 mL) and the resultant mixture was extracted with EtOAc (3 × 400 mL). The combined organic layers were washed with brine (300 mL) and dried ($MgSO_4$), filtered and concentrated *in vacuo* to afford the crude product as an orange oil. The crude product was purified by flash silica column chromatography (elution with 0-100% toluene in pet ether) to give *tert*-butyl (2-bromo-4-iodo-6-nitrophenyl)-D-alaninate as a light orange solid (5.228 g, 91%). R_f 0.70 (1:8, tol/pet

ether); m.p. 75 –78 °C; $[\alpha]_D^{25}$ = −225 (*c* 1.0, $CHCl_3$); $\bar{\nu}_{max}$ ($CHCl_3$ thin film)/ cm^{-1} 3077 (N-H, w), 2947 (C-H, w), 1718 (C=O, s), 1528 (N-O, s), 1347 (C-H); ^1H NMR (400 MHz, $CDCl_3$) δ_H 8.21 (1H, d, *J* 2.1 Hz, H-4), 7.98 (1H, d, *J* 2.1 Hz, H-6), 6.81 (1H, d, *J* 9.4 Hz, NH-2/2'), 4.46 (1H, dq, *J* 9.4, 7.0 Hz, H-2'), 1.42 (3H, d, *J* 7.0 Hz, H-1'), 1.39 (9H, s, H-5'); ^{13}C NMR (101 MHz, $CDCl_3$) δ_C 172.1 (C-3'), 146.6 (C-4), 141.6 (C-2) 141. 1 (C-3), 133.9 (C-6), 128.2 (C-1), 88.2 (C-5), 79.1 (C-4'), 54.8 (C-2'), 27.8 (C-5'), 19.2 (C-1'); HRMS *m/z* (ESI^-) [Found: 468.9253 $C_{13}H_{16}{}^{79}BrIN_2O_4$ requires $[M-H]^-$ 468.9265]; LRMS *m/z* (ESI^+) 471 ($[M+H]^+$, 100%), 473 ($[M+H]^+$, 97%); HPLC: retention time 12.67 mins, 95.3% purity.

tert-Butyl (2-bromo-4-(5-hydroxypent-1-yn-1-yl)-6-nitrophenyl)-D-alaninate (compound **74**)

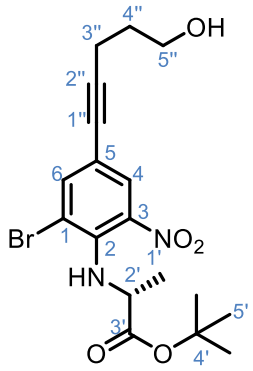

To a solution of *tert*-butyl (2-bromo-4-iodo-6-nitrophenyl)-*D*-alaninate (2.00 g, 4.25 mmol, 1.0 equiv.) in THF (20 mL) was added Bis(diphenylphosphino)ferrocene]dichloropalladium$^{(II)}$ (173 mg, 0.212 mmol, 0.05 equiv.) and CuI (81 mg, 0.425 mmol, 0.1 equiv.) at r.t. under an argon atmosphere. To this was added triethylamine (5 mL) followed by 4-pentyn-1-ol (396 µL, 4.25 mmol, 1.0 equiv.). The reaction mixture was stirred at r.t. for 18 h. After this time the reaction mixture was concentrated *in vacuo* to produce a dark orange residue. This was dissolved in EtOAc (500 mL) and passed through a Celite® pad. The filtrate was then

transferred to a separating funnel where it was washed with sat. $NaHCO_{3(aq)}$ (3 × 500 mL) and brine (250 mL). The organic layer was then dried (Na_2SO_4) and then concentrated *in vacuo* giving the crude product as a bright orange oil. This was further purified by flash silica column chromatography (elution with 0-50 % EtOAc in pet ether) to give of *tert*-butyl (2-bromo-4-(5-hydroxypent-1-yn-1-yl)-6-nitrophenyl)-D-alaninate as bright orange oil (1.683 g, 93%). R_f 0.44 (1:1, EtOAc/pet ether); $[\alpha]_D^{25}$ = −207 (*c* 1.0, $CHCl_3$); $\bar{\nu}_{max}$ ($CHCl_3$ thin film)/ cm^{-1} 3020 (N-H, w), 2927 (C-H, w), 1669 (C=O, s), 1529 (N-O, s); ^1H NMR (600 MHz, $CDCl_3$) δ_H 7.96 (1H, d, *J* 2.0 Hz, H-4), 7.72 (1H, d, *J* 2.0 Hz, H-6), 6.87 (1H, d, *J* 9.5 Hz, NH-2/2'), 4.50 (1H, dq, *J* 9.5, 7.0 Hz, H-2'), 3.80 (2H, t, *J* 6.1 Hz, H-5''), 2.52 (2H, t, *J* 7.0 Hz, H-3''), 1.91 – 1.79 (2H, m, H-4''), 1.42 (3H, d, *J* 7.0 Hz, H-1'), 1.38 (9H, s, H-5'); ^{13}C NMR (151 MHz, $CDCl_3$) δ_C 172.3 (C-3'), 141.8 (C-6), 141.3 (C-3), 128.7 (C-4), 116.2 (C-3), 115.0 (C-1), 91.2 (C-5), 82.4 (C-4'), 77.9 (C-1''), 77.4 (C-2''), 61.8 (C-5''), 55.0 (C-2'), 31.3 (C-3''), 28.0 (C-5'), 19.4 (C-1'), 16.0 (C-4''); HRMS *m/z* (ESI^+) [Found: 427.0859 $C_{18}H_{23}{}^{79}BrN_2O_5$ requires $[M+H]^+$ 427.0863]; LRMS *m/z* (ESI^+) 427 ($[M+H]^+$, 80%), 429 ($[M+H]^+$, 81%), 875 ($[2M+Na]^+$, 90%), 877 ($[2M+Na]^+$, 100%), 879 ($[2M+Na]^+$, 90%); HPLC: retention time 11.1 mins, 99.8% purity.

tert-Butyl (2-bromo-4-(5-hydroxypentyl)-6-nitrophenyl)-D-alaninate (compound **75**)

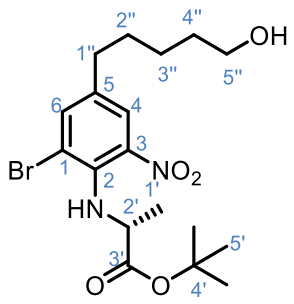

tert-Butyl (2-bromo-4-(5-hydroxypent-1-yn-1-yl)-6-nitrophenyl)-D-alaninate (1.40 g, 3.276 mmol, 1.0 equiv.) along with $Rh(PPh_3)_3Cl$ (171 mg, 0.164 mmol, 0.05 equiv.)

were charged into reaction vessel and placed under an argon atmosphere. To this dry toluene was added (20 mL), then the atmosphere was replaced with hydrogen gas and heated to 60 °C for 18 h. After this time the solvent was removed *in vacuo* to give a black oil, this was then purified by flash silica column chromatography (elution with 0-50% EtOAc in pet ether) to give *tert*-butyl (2-bromo-4-(5-hydroxypentyl)-6-nitrophenyl)-D-alaninate as a dark brown oil (1.13 g, 80%). R_f 0.46 (1:1, EtOAc/pet ether) $[\alpha]_D^{25}$ = −151 (*c* 1.0, $CHCl_3$); $\bar{\nu}_{max}$ (neat)/ cm^{-1} 3350 (N-H, w), 2950 (C-H, s), 1718 (C=O, s), 1540 (N-O, s); ^1H NMR (600 MHz, $CDCl_3$) δ_H 7.74 (1H, d, *J* 2.1 Hz, H-4), 7.56 (1H, d, *J* 2.1 Hz, H-6), 6.61 (1H, d, *J* 10.0 Hz, NH-2/2'), 4.44 (1H, dq, *J* 10.0, 7.0 Hz, H-2'), 3.65 (2H, t, *J* 6.5 Hz, H-5''), 2.61 – 2.53 (2H, t, *J* 7.8 Hz, H-1''), 1.69 – 1.50 (4H, m, H-2'', H-4''), 1.42 (3H, d, *J* 7.0 Hz, H-1'), 1.44 – 1.34 (2H, m, H-3''), 1.36 (9H, s, H-5'); ^{13}C NMR (151 MHz, $CDCl_3$) δ_C 172.5 (C-3'), 141.5 (C-2), 139.9 (C-3), 139.5 (C-6), 135.6 (C-5), 124.9 (C-4), 116.3 (C-1), 81.8 (C-4'), 62.8 (C-5''), 55.3 (C-2'), 34.4 (C-1''), 32.5(C-4''), 30.7 (C-2''), 27.8 (C-5'), 25.3 (C-3''), 19.2 (C-1'); HRMS *m/z* (ESI^+) [Found: 431.1171 $C_{18}H_{27}{}^{79}BrN_2O_5$ requires $[M+H]^+$ 431.1176]; LRMS *m/z* (ESI^+) 431 ($[M+H]^+$, 100%), 433 ($[M+H]^+$, 97%); HPLC: retention time 11.1 mins, 98.7% purity.

tert-Butyl (*E*)-(4-(5-hydroxypentyl)-2-nitro-6-(5-(7-((triisopropylsilyl)oxy)-3,4-dihydroquinolin-1(2*H*)-yl)pent-1-en-1-yl)phenyl)-D-alaninate (compound **76**)

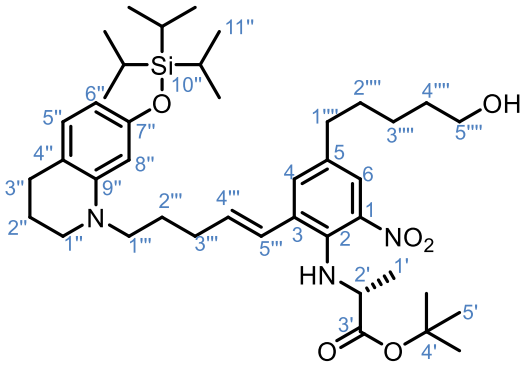

tert-Butyl (2-bromo-4-(5-hydroxypentyl)-6-nitrophenyl)-D-alaninate (397 mg, 0.920 mmol, 1.0 equiv.), (*E*)-1-(5-(4,4,5,5-tetramethyl-1,3,2-dioxaborolan-2-yl)pent-4-en-1-yl)-7-((triisopropylsilyl)oxy)-1,2,3,4-tetrahydroquinoline (689 mg, 1.38 mmol, 1.5 equiv.), K_2CO_3 (400 mg, 2.76 mmol, 3.0 equiv.) and [1,1′-Bis(diphenylphosphino)ferrocene]dichloropalladium$^{(II)}$ (83 mg, 0.0460 mmol, 0.05 equiv.) were added to reaction vessel under an argon atmosphere. To this was added 1,4-dioxane (7.5 mL) and H_2O (1.5 mL), the reaction was then heated to 100 °C for 24 h. Once cooled the reaction mixture was evaporated and then diluted with EtOAc (150 mL), which was then filtered through a Celite® pad. The filtrate was then washed with H_2O (3 × 100 mL) and brine (100 mL), then dried (Na_2SO_4), filtered and concentrated *in vacuo* to yield the crude product as brown oil. The crude oil was purified by flash silica column chromatography (elution with 0-40% EtOAc in pet ether) to yield (*E*)-(4-(5-hydroxypentyl)-2-nitro-6-(5-(7-((triisopropylsilyl)oxy)-3,4-dihydroquinolin-1(2*H*)-yl)pent-1-en-1-yl)phenyl)-D-alaninate as a bright orange oil (480 mg, 72%); R_f 0.53 (1:1, EtOAc/pet ether); $[\alpha]_D^{25}$ = −95.7 (*c* 0.7, $CHCl_3$); $\bar{\nu}_{max}$ (neat)/ cm^{-1} 3359 (N-H, w), 2934 (C-H, s), 1732 (C=O, s), 1506 (N-O, s); ^1H NMR (400 MHz, $CDCl_3$) δ_H 7.74 (1H, d, *J* 2.1 Hz, H-6), 7.29 (1H, d, *J* 2.1 Hz, H-4), 6.88 (1H, d, *J* 10.6 Hz, NH-2/2'), 6.76 (1H, d, *J* 8.0 Hz, H-5''), 6.46 (1H, dd, *J* 15.9 Hz, H-14'') 6.14 (3H,

dt, *J* 15.9, 6.8 Hz, H-13'', H-6'', H-8''), 4.05 (1H, dq, *J* 10.6, 7.0 Hz, H-2'), 3.64 (2H, t, *J* 6.5 Hz, H-5''), 3.27 (4H, t, *J* 7.5 Hz, H-1'', H-1'''), 2.68 (2H, t, *J* 6.4 Hz, H-3''), 2.57 (2H, t, *J* 6.4 Hz, H-1''''), 2.24 (2H, q, *J* 6.0 Hz, H-3'''), 1.97 – 1.89 (2H, m, H-2''), 1.82 (2H, m, H-11''), 1.70 – 1.53 (4H, m, H-2'''. H-4''''), 1.39 (3H, d, *J* 7.0 Hz, H-2'), 1.27 – 1.21 (2H, m, H-3''''), 1.31 (9H, s, H-5'), 1.28 – 1.19 (3H, m, H-10''), 1.10 (18H, d, *J* 7.2 Hz, H-11''); ^{13}C NMR (101 MHz, $CDCl_3$) δ_C 172.76 (C-3'), 155.4 (C-7''), 141 (C-2), 140.4 (C-1), 134.8 (C-3), 134.5 (C-4), 132.6 (C-5'''), 132.4 (C-9'') 129.6 (C-5''), 127.7 (C-4'''), 123.8 (C-6), 115.24, 107.07, 102.61, 81.59 (C-4'), 77.36, 62.9 (C-5''''), 57.2 (C-2'), 51.4 (C-1''), 49.5 (C-10''), 34.9 (C-1'''), 32.6 (C-2''''), 31.0 (C-1'', C-4''''), 27.8 (C-3''), 27.48, 25.91, 25.4 (C-11''), 22.5 (C-2''), 19.5 (C-1'), 18.1 (C-11''), 12.9 (C-10''); HRMS *m/z* (ESI$^+$) [Found: 724.4702 $C_{41}H_{65}N_3O_6Si$ requires $[M+H]^+$ 724.4715]; LRMS *m/z* (ESI$^+$) 724 ($[M+H]^+$, 100%); HPLC: retention time 20.7 mins, 98.8% purity.

(*R*,*E*)-7-(5-Hydroxypentyl)-3-methyl-5-(5-(7-((triisopropylsilyl)oxy)-3,4-dihydroquinolin-1(2*H*)-yl)pent-1-en-1-yl)-3,4-dihydroquinoxalin-2(1*H*)-one (compound **79**)

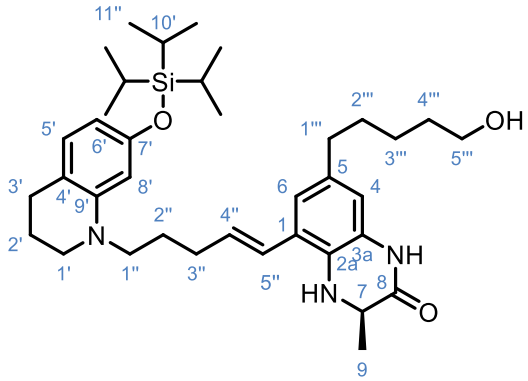

(*E*)-(4-(5-Hydroxypentyl)-2-nitro-6-(5-(7-((triisopropylsilyl)oxy)-3,4-dihydroquinolin-1(2*H*)-yl)pent-1-en-1-yl)phenyl)-D-alaninate (479 mg, 0.662 mmol, 1.0 equiv.) had TFA (2.5 mL) and CH_2Cl_2 (2.5 mL) added forming an orange solution which was stirred for 3 h at r.t. The crude reaction mixture was evaporated *in vacuo* to afford a dark orange

oil. To this was added zinc powder (1.88 g, 16.5 mmol, 25 equiv.) and ammonium chloride (1.55 g, 16.5 mmol, 25 equiv.), this mixture was then placed under an argon atmosphere and DMF (7 mL) was added. The reaction mixture was then stirred at r.t. for 24 h. The crude reaction mixture was diluted with EtOAc (100 mL) and filtered through a Celite® pad. The filtrate was then washed with 10 wt% $LiCl_{(aq)}$ (3 × 50 mL), sat $NaHCO_{3(aq)}$ (3 × 100 mL), brine (50 mL), dried (Na_2SO_4), filtered and then concentrated *in vacuo* to give a brown oil. The crude oil was then purified by flash silica column chromatography (elution with 0-100% EtOAc in pet ether) to give (*R*,*E*)-7-(5-hydroxypentyl)-3-methyl-5-(5-(7-((triisopropylsilyl)oxy)-3,4-dihydroquinolin-1(2*H*)-yl)pent-1-en-1-yl)-3,4-dihydroquinoxalin-2(1*H*)-one as a colourless oil (191 mg, 46%); R_f 0.25 (1:1, EtOAc/pet ether); $[\alpha]_D^{25}$ = −21.9 (*c* 1.0, $CHCl_3$); 3345 (N-H, w), 2936 (C-H, m), 1679 (C=O, s), 1507 (C-O, s); ^{1}H NMR (600 MHz, $CDCl_3$) δ_H 7.71 (s, NH-3a/8), 6.77 – 6.72 (2H, m, H-5', H-6'), 6.42 (1H, d, *J* 1.7 Hz, H-8'), 6.38 – 6.32 (1H, m, H-5''), 6.15 – 6.05 (3H, m, H-4, H-6, H-4''), 3.96 (1H, q, *J* 6.7 Hz, H-7), 3.90 (1H, s, NH-2a/7), 3.64 (2H, t, *J* 6.6 Hz, H-5'''), 3.29 – 3.23 (4H, m, H-1', H-1''), 2.67 (2H, t, *J* 6.3 Hz, H-3'), 2.50 (2H, t, *J* 7.7 Hz, H-1'''), 2.32 – 2.25 (2H, m, H-3''), 1.95 – 1.88 (2H, m, H-2'), 1.78 (2H, p, *J* 7.5 Hz, H-2'''), 1.64 – 1.55 (4H, m, H-2''', H-4'''), 1.46 (3H, d, *J* 6.7 Hz, H-9), 1.40 – 1.32 (2H, m, H-3'''), 1.29 – 1.18 (3H, m, H-10'), 1.10 (18H, d, *J* 7.4 Hz, H-11''); ^{13}C NMR (151 MHz, $CDCl_3$) δ_C 169.1 (C-8), 155.2 (C-7''), 145.8 (C-9'), 133.7, 133.4 (C-4''), 129.4 (C-5'), 128.3, 125.8, 124.5 (C-5''), 124.0, 122.0, 115.1, 114.0, 107.0, 102.5, 62.9 (C-5'''), 51.9 (C-7), 51.3 (C-1'), 49.5 (C-1''), 35.1 (C-1'''), 32.6 (C-4'''), 31.3 (C-2'''), 31.1 (C-3''), 27.3 (C-3'), 25.9 (C-2''), 25.3 (C-3'''), 22.5 (C-2'), 18.0 (C-11''), 17.8 (C-9), 12.7 (C-10'); HRMS m/z (ESI+) [Found: 620.4238 $C_{37}H_{58}N_3O_3Si$ requires 620.4242 [M+H]+]; LRMS m/z (ESI+) 620 ([M+H]+, 100%).

(R,E)-5-(5-(7-Hydroxy-3,4-dihydroquinolin-1(2H)-yl)pent-1-en-1-yl)-7-(5-hydroxypentyl)-3-methyl-3,4-dihydroquinoxalin-2(1H)-one (compound **80**)

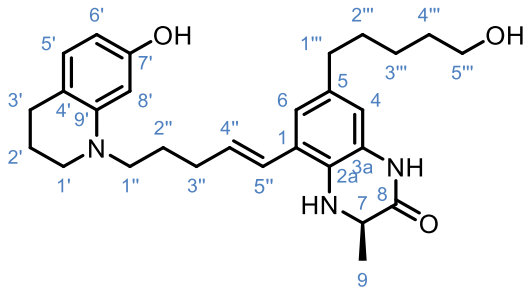

(*R*,*E*)-7-(5-Hydroxypentyl)-3-methyl-5-(5-(7-((triisopropylsilyl)oxy)-3,4-dihydroquinolin-1(2*H*)-yl)pent-1-en-1-yl)-3,4-dihydroquinoxalin-2(1*H*)-one (240 mg, 0.387 mmol, 1.0 equiv.), was dissolved in THF (4 mL), to this was added 1M TBAF in THF (774 µL, 0.774 mmol, 2.0 equiv.) and the reaction mixture was stirred at r.t. for 1 h. The reaction mixture was diluted with sat $NH_4Cl_{(aq)}$ (100 mL) which was washed with $CHCl_3$/IPA (9:1) solution (2 × 100 mL), the combined organic layer was washed with brine (2 × 50 mL), dried ($MgSO_4$), filtered and then concentrated to give the crude product as a brown oil. This crude oil was then purified by flash silica column chromatography (elution with 0-5% EtOH in EtOAc) to give (*R*,*E*)-5-(5-(7-hydroxy-3,4-dihydroquinolin-1(2*H*)-yl)pent-1-en-1-yl)-7-(5-hydroxypentyl)-3-methyl-3,4-dihydroquinoxalin-2(1*H*)-one as a light brown oil (179 mg, 99%); $[\alpha]_D^{25}$ = −21.3 (*c* 1.0, $CHCl_3$); 3447 (N-H, w), 2929 (C-H, m), 1676(C=O, s), 1509 (C=C, s); HRMS *m/z* (ESI^+) [Found: 464.2904 $C_{28}H_{38}N_3O_3$ requires 464.2908 $[M+H]^+$]; LRMS *m/z* (ESI^+) 464 ($[M+H]^+$, 100%).

1-(Pent-4-yn-1-yl)-1,2,3,4-tetrahydroquinolin-7-ol (compound **81**)

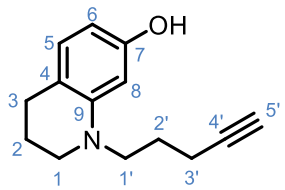

1-(pent-4-yn-1-yl)-7-((triisopropylsilyl)oxy)-1,2,3,4-tetrahydroquinoline (5.60 g, 15.1 mmol, 1.0 equiv.) was dissolved in THF (30 mL), to this was added 1M TBAF in THF (26.6 mL, 30.2 mmol, 2.0 equiv.) dropwise and then the reaction mixture was stirred at r.t. for 1 h. The reaction mixture was then diluted with EtOAc (500 mL) then washed with sat $NH_4Cl_{(aq)}$ (3 × 300 mL), brine (300 mL), dried ($MgSO_4$), filtered and concentrated *in vacuo* to give the crude product as a dark brown oil. The crude oil was then purified by flash silica column chromatography (elution with 0-15 % EtOAc in pet ether) to give 1-(pent-4-yn-1-yl)-1,2,3,4-tetrahydroquinolin-7-ol as a light brown oil (3.22 g, 99%); R_f 0.06 (1:9, EtOAc/pet ether); $\bar{\nu}_{max}$ (thin film $CHCl_3$)/ cm^{-1} 3290 (N-H, w), 2936 (C-H, m), 2120 (C≡C, w), 1509 (C-O); ^1H NMR (400 MHz, $CDCl_3$) δ_H 6.78 (1H, dt, *J* 8.0, 1.0 Hz, H-5), 6.12 (1H, d, *J* 2.4 Hz, H-8), 6.04 (1H, dd, *J* 8.0, 2.4 Hz, H-6), 4.80 (1H, s br, OH-7), 3.38 – 3.30 (2H, m, H-1'), 3.30 – 3.23 (2H, m, H-1), 2.71 – 2.63 (2H, m, H-3), 2.25 (2H, td, *J* 6.9, 2.7 Hz, H-3'), 2.02 (1H, t, *J* 2.7 Hz, H-5'), 1.97 – 1.88 (2H, m, H-2), 1.81 (p, *J* 6.9 Hz, H-2'); LRMS *m/z* (ESI^+) 216 ($[M+H]^+$, 100%); HPLC: retention time 8.7 mins, 99.0% purity. Due to the instability of the compound, carbon NMR was not collected.

tert-Butyl (2-bromo-6-nitro-4-(5-((1-(pent-4-yn-1-yl)-1,2,3,4-tetrahydroquinolin-7-yl)oxy)pentyl)phenyl)-D-alaninate (compound **82**)

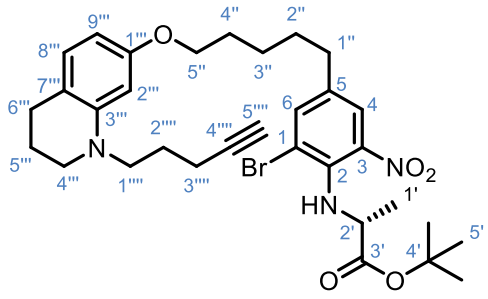

Triphenylphosphine (2.21 g, 8.44 mmol, 1.3 equiv.) and diisopropyl azodicarboxylate (1.71 g, 8.44 mmol, 1.3 equiv.) were added to a flame dried flask under argon and to

this was added THF (30 mL) and this mixture was stirred for 30 mins at 0 °C. *Tert*-butyl (2-bromo-4-(5-hydroxypentyl)-6-nitrophenyl)-D-alaninate (2.80 g, 6.49 mmol, 1.0 equiv.) was dissolved in THF (10 mL) under an argon atmosphere and then added to the flask at 0 °C and then this mixture was stirred for a further 15 mins at 0 °C. To this mixture was then added 1-(pent-4-yn-1-yl)-1,2,3,4-tetrahydroquinolin-7-ol (2.21 g, 8.44 mmol, 1.3 equiv.) in THF (5 mL) and the reaction mixture was allowed to warm to r.t. and was stirred for 48 h. The reaction mixture was evaporated *in vacuo* and to this EtOAc (500 mL) was added, this was washed with H_2O (3 × 400 mL), brine (400 mL), dried ($MgSO_4$), filtered and then concentrated *in vacuo* to give the crude product as a brown oil. The crude oil was purified by flash silica column chromatography (elution with 0-50% Et_2O in pet ether) to give *tert*-butyl (2-bromo-6-nitro-4-(5-((1-(pent-4-yn-1-yl)-1,2,3,4-tetrahydroquinolin-7-yl)oxy)pentyl)phenyl)-D-alaninate as a bright orange oil (2.93 g, 72%); R_f 0.26 (1:9, EtOAc/pet ether); $[\alpha]_D^{25}$ = −154 (*c* 1.2, $CHCl_3$); $\bar{\nu}_{max}$ (thin film $CHCl_3$)/ cm^{-1} 3230 (N-H, br w), 2935 (C-H, m), 1731 (C=O, s), 1534 (N-O, s); ^1H NMR (600 MHz, $CDCl_3$) δ_H 7.75 (1H, d, *J* 2.1 Hz, H-4), 7.57 (1H, d, *J* 2.1 Hz, H-6), 6.82 (dt, *J* 8.1, 1.0 Hz, 1H, H-8’’’), 6.62 (1H, d, *J* 10.0 Hz, NH-2/2’), 6.16 (1H, d, *J* 2.4 Hz, H-2’’’), 6.11 (dd, *J* 8.1, 2.4 Hz, 1H, H-9’’’), 4.44 (1H, dq, *J* 10.0, 7.0 Hz, H-2’), 3.92 (2H, t, *J* 6.4 Hz, H-5’’), 3.35 (2H, t, *J* 7.2 Hz, H-1’’’’), 3.30 – 3.23 (2H, m, H-4’’’), 2.68 (2H, t, *J* 6.3 Hz, H-6’’’), 2.64 – 2.54 (2H, m, H-1’’), 2.26 (2H, td, *J* 6.9, 2.7 Hz, H-3’’’’), 1.98 (1H, t, *J* 2.7 Hz, H-5’’’’), 1.95 – 1.88 (2H, m, H-5’’’), 1.87 – 1.74 (4H, m, H-2’’, H-2’’’’), 1.72 – 1.63 (2H, m, H-4’’), 1.55 – 1.46 (2H, m, H-3’’), 1.43 (3H, d, *J* 7.0 Hz, H-1’), 1.36 (9H, s, H-5’); ^{13}C NMR (151 MHz, $CDCl_3$) δ_C 172.6 (C-3’), 158.8(C-1’’’), 146.2 (C-3’’’), 141.6 (C-2), 140.0 (C-1), 139.6 (C-6), 135.8 (C-5), 129.6 (C-8’’’), 125.0 (C-4), 116.4 (C-3), 115.3 (C-7’’), 100.9 (C-9’’’), 98.0 (C-2’’’), 84.1 (C-4’’’’), 81.9 (C-4’), 68.9 (C-5’’’’), 67.7 (C-5’’), 55.4 (C-2’), 50.4 (C-1’’’’), 49.8 (C-4’’’), 34.5 (C-1’’), 30.9 (C-2’’),

29.3 (C-4''), 27.9 (C-5'), 27.5 (C-6''), 25.8 (C-3''), 25.4 (C-2''''), 22.6 (C-5'''), 19.3 (C-1'), 16.2 (C-3''''); HRMS *m/z* (ESI^+) [Found: 628.2378 $C_{32}H_{43}{}^{79}BrN_3O_5$ requires 628.2381 $[M+H]^+$]; LRMS *m/z* (ESI^+) 628 ($[M+H]^+$, 100%), 630 ($[M+H]^+$, 97%); HPLC: retention time 14.8 mins, 97.0% purity.

tert-Butyl (*E*)-(2-bromo-6-nitro-4-(5-((1-(5-(4,4,5,5-tetramethyl-1,3,2-dioxaborolan-2-yl)pent-4-en-1-yl)-1,2,3,4-tetrahydroquinolin-7-yl)oxy)pentyl)phenyl)-D-alaninate (compound **83**)

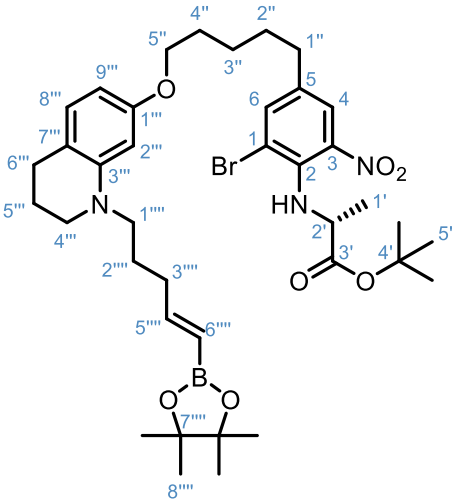

tert-Butyl (2-bromo-6-nitro-4-(5-((1-(pent-4-yn-1-yl)-1,2,3,4-tetrahydroquinolin-7-yl)oxy)pentyl)phenyl)-D-alaninate (1.385 g, 2.20 mmol, 1.0 equiv.) and bis(cyclopentadienyl)zirconium$^{(VI)}$ chloride hydride (57 mg, 0.221 mmol, 0.1 equiv.) were added to a tapered microwave vial and sealed under an argon atmosphere in the absence of light. NEt_3 (0.02 µL, 0.221 mmol, 0.1 equiv.) and 4,4,5,5-tetramethyl-1,3,2-dioxaborolane (350 µL, 2.42 mmol, 1.1 equiv.) were added and the reaction mixture was stirred at 60 °C under argon for 20 h in the dark. The reaction mixture was purified by flash silica column chromatography (elution with 0-100% CH_2Cl_2 in pet ether) to give *tert*-butyl (*E*)-(2-bromo-6-nitro-4-(5-((1-(5-(4,4,5,5-tetramethyl-1,3,2-dioxaborolan-2-yl)pent-4-en-1-yl)-1,2,3,4-tetrahydroquinolin-7-yl)oxy)pentyl)phenyl)-

D-alaninate as an orange oil (1.166 g, 70%); R_f 0.17 (1:9, EtOAc/pet ether); $[\alpha]_D^{25}$ = −156 (*c* 1.0, $CHCl_3$); $\bar{\nu}_{max}$ (thin film $CHCl_3$)/ cm^{-1} 3230 (N-H, br w), 2935 (C-H, m), 1731 (C=O, s), 1534 (N-O, s), 1365 (C=C, m), 1087 (C-O, s); ^1H NMR (600 MHz, $CDCl_3$) δ_H 7.75 (1H, d, *J* 2.1 Hz, H-4), 7.57 (1H, d, *J* 2.1 Hz, H-6), 6.83 – 6.78 (1H, m, H-8’’’), 6.65 (1H, dt, *J* 18.0, 6.3 Hz, H-5’’’’), 6.64 – 6.59 (1H, d, *J* 10.0 Hz, NH-2/2’), 6.12 – 6.06 (2H, m, H2’’’, H-9’’’), 5.47 (1H, dt, *J* 18.0, 1.6 Hz, H-6’’’’), 4.44 (1H, dq, *J* 10.0, 7.0 Hz, H-2’), 3.91 (2H, t, *J* 6.4 Hz, H-5’’), 3.25 – 3.19 (4H, m, H-4’’’, H-1’’’’), 2.66 (2H, t, *J* 6.3 Hz, H-6’’’), 2.59 (2H, t, *J* 7.8 Hz, H-1’’), 2.24 – 2.17 (2H, m, H-3’’’), 1.93 – 1.86 (2H, m, H-5’’’), 1.82 – 1.76 (2H, m, H-4’’), 1.76 – 1.70 (2H, m, H-2’’), 1.69 – 1.63 (2H, m, H-2’’’’), 1.53 – 1.48 (2H, m, H-3’’), 1.43 (3H, d, *J* 7.0 Hz, H-1’), 1.36 (9H, s, H-5’), 1.26 (12H, s, H-8’’’’); ^{11}B NMR (128 MHz, $CDCl_3$) δ_B 29.7 (B-6’’’’); ^{13}C NMR (151 MHz, $CDCl_3$) δ_C 172.6 (C-3’), 158.7 (C-1’’’), 153.7 (C-6’’’’), 146.3 (C-3’’’), 141.6 (C-2), 140.0 (C-1), 139.6 (C-6), 135.8 (C-5), 129.5 (C-8’’’), 125.0 (C-4), 116.4 (C-3), 115.3 (C-7’’’), 100.5 (C-9’’’), 98.0 (C-2’’’), 83.2 (C-7’’’’), 81.9 (C-4’), 67.6 (C-5’’), 55.4 (C-2’), 51.2 (C-1’’’’), 49.6 (C-4’’’), 34.5 (C-1’’), 33.4 (C-3’’’’), 30.9 (C-2’’), 29.3 (C-4’’), 27.9 (C-5’), 27.6 (C-6’’’), 25.8 (C-3’’), 25.0 (C-8’’’’), 24.9 (C-2’’’’), 22.6 (C-5’’’), 19.3 (C-1’); HRMS *m/z* (ESI^+) [Found: 756.3390 $C_{38}H_{46}{}^{79}Br^{11}BN_3O_7$ requires 756.3395 $[M+H]^+$]; LRMS *m/z* (ESI^+) 756 ($[M+H]^+$, 100%), 758 ($[M+H]^+$, 97%); HPLC: retention time 13.2 mins, 79.6% purity.

tert-Butyl (*E*)-(7^5-nitro-1^1,1^2,1^3,1^4-tetrahydro-13-oxa-1(1,7)-quinolina-7(1,3)-benzenacyclotridecaphan-5-en-7^6-yl)-D-alaninate (compound **78**)

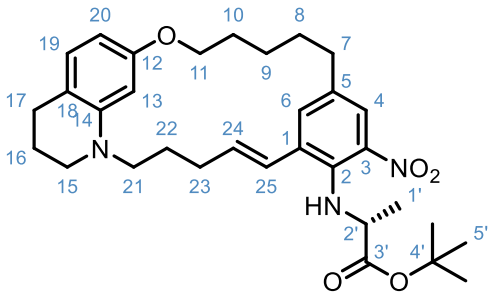

(*E*)-(2-Bromo-6-nitro-4-(5-((1-(5-(4,4,5,5-tetramethyl-1,3,2-dioxaborolan-2-yl)pent-4-en-1-yl)-1,2,3,4-tetrahydroquinolin-7-yl)oxy)pentyl)phenyl)-D-alaninate (414 mg, 0.547 mmol, 1.0 equiv.), K_2CO_3 (453 mg, 3.28 mmol, 6.0 equiv.) and [1,1′-bis(diphenylphosphino)ferrocene]dichloropalladium$^{(II)}$ (40 mg, 0.0547 mmol, 0.1 equiv.) were placed under an argon atmosphere and to this was added 1,4-dioxane (219 mL) and H_2O (54.7 mL) and the reaction mixture was heated to 100 °C for 48 h. After this time the solvent was removed *in vacuo* from the reaction mixture. The resulting residue was then dissolved in EtOAc (500 mL), which was washed with H_2O (3 × 500 mL), brine (500 mL), dried ($MgSO_4$), filtered and concentrated *in vacuo* to give the crude product as a brown oil. This was then purified by flash silica column chromatography (elution with 0-30% EtOAc in pet ether) to give *tert*-butyl (*E*)-(7^5-nitro-1^1,1^2,1^3,1^4-tetrahydro-13-oxa-1(1,7)-quinolina-7(1,3)-benzenacyclotridecaphan-5-en-7^6-yl)-D-alaninate as a bright orange oil (57 mg, 19%); R_f 0.27 (1:9, EtOAc/pet ether); $[\alpha]_D^{25}$ = −33.0 (*c* 0.2, $CHCl_3$); $\bar{\nu}_{max}$ (thin film $CHCl_3$)/ cm^{-1} 3230 (N-H, br w), 2935 (C-H, m), 1731 (C=O, s), 1534 (N-O, s), 1365 (C=C, m), 1087 (C-O, s); ^{1}H NMR (600 MHz, CD_2Cl_2) δ_H 7.75 (1H, d, *J* 2.1 Hz, H-4), 7.59 (1H, d, *J* 2.1 Hz, H-6), 6.82 – 6.76 (2H, m, NH-2/2', H-19), 6.58 (1H, dt, *J* 15.7, 1.5 Hz, H-25), 6.30 (1H, ddd, *J* 15.7, 7.9, 6.5 Hz, H-24), 6.09 (1H, d, *J* 2.4 Hz, H-13), 6.05 (1H, dd, *J* 8.1, 2.4 Hz, H-20), 4.07 (1H, m,

H-2'), 3.93 (1H,ddd, *J* 8.9, 6.4, 4.0 Hz, H_AH_B-11), 3.87 (1H, ddd, *J* 8.9, 7.6, 4.0 Hz, H_AH_B-11), 3.36 – 3.16 (4H, m, H-15, H-21), 2.72 – 2.58 (4H, m, H-7, H-17), 2.44 – 2.35 (1H, m, H_AH_B-23), 2.32 – 2.26 (1H, m, H_AH_B-23), 1.94 – 1.86 (2H, m, H-16), 1.86 – 1.71 (6H, m, H-8, H-10, H-22,), 1.53 (2H, h, *J* 6.9 Hz, H-9), 1.41 (3H, d, *J* 7.0 Hz, H-1'), 1.31 (9H, s, H-5'); ^{13}C NMR (151 MHz, CD_2Cl_2) δ_C 173.2 (C-4'), 159.4 (C-12), 146.4 (C-14), 141.8 (C-3), 140.5 (C-2), 135.7 (C-5), 134.7 (C-6), 132.9 (C-1), 132.7 (C-24), 129.7 (C-19), 128.9 (C-25), 124.6 (C-4), 115.8 (C-19), 99.5 (C-13), 98.9 (C-20), 81.7 (C-4'), 68.7 (C-11), 57.6 (C-2'), 49.7 (C-21), 49.0 (C-15), 34.0 (C-7), 30.5 (C-8), 29.9 (C-23), 28.4 (C-10), 27.9 (C-5'), 25.9 (C-9), 24.4 (C-22), 22.9 (C-16), 19.6 (C-1'); HRMS *m/z* (ESI$^+$) [Found: 550.3271 $C_{32}H_{44}N_3O_5$ requires 550.3275 $[M+H]^+$]; LRMS *m/z* (ESI$^+$) 550 ($[M+H]^+$, 100%); HPLC: retention time 16.0 mins, 94.3% purity.

(*R*,*E*)-2-Methyl-1,7,8,9,10,11,17,18,21,22-decahydro-2*H*,16*H*,20*H*-13,15-etheno-6,25-(metheno)pyrazino[2,3-*l*]pyrido[2,1-*d*][1]oxa[5]azacycloicosin-3(4*H*)-one (compound **62**)

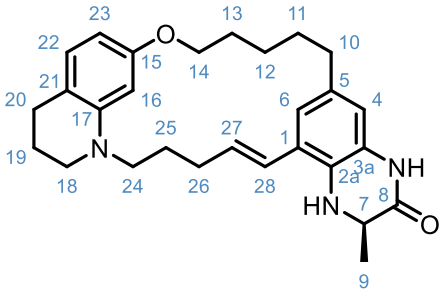

tert-Butyl (*E*)-(7^5-nitro-1^1,1^2,1^3,1^4-tetrahydro-13-oxa-1(1,7)-quinolina-7(1,3)-benzenacyclotridecaphan-5-en-7^6-yl)-D-alaninate (57 mg, 0.104 mmol, 1.0 equiv.) was dissolved in TFA (1.0 mL) and CH_2Cl_2 (1.0 mL) and stirred at r.t. for 2.5h. The reaction was then concentrated under a flow of N_2 to give a dark orange oil. To this was added zinc powder (171 mg, 2.59 mmol, 25 equiv.) and NH_4Cl (140 mg, 2.59 mmol, 25 equiv.) and the reaction vessel was placed under an argon atmosphere to which was added

DMF (3.5 mL) and the reaction mixture was stirred at r.t. for 18 h. The reaction mixture was diluted with EtOAc (50 mL) and filtered through a Celite® pad, this was then washed with 10 wt% $LiCl_{(aq)}$ (2 × 25 mL), sat. $NH_4Cl_{(aq)}$ (25 mL), sat. $NaHCO_{3(aq)}$ (25 mL) and then brine (25 mL). The organic layer was then dried ($MgSO_4$), filtered and evaporated *in vacuo* to afford an off white solid. This crude solid was then purified by flash silica column chromatography (elution with 0-100% EtOAc in pet ether) giving a colourless solid which was then further purified by semi-preparative HPLC (retention time of 10.10 mins) and the fractions containing compound were then lyophilised to give (*R*,*E*)-2-methyl-1,7,8,9,10,11,17,18,21,22-decahydro-2*H*,16*H*,20*H*-13,15-etheno-6,25-(metheno)pyrazino[2,3-*l*]pyrido[2,1-*d*][1]oxa[5]azacycloicosin-3(4*H*)-one as a white lysophilate (24 mg, 52%); R_f 0.19 (Et_2O); $[\alpha]_D^{25}$ = −12.3 (*c* 0.15, $CHCl_3$); $\bar{\nu}_{max}$ ($CHCl_3$ thin film)/ cm^{-1} 2934 (C-H, s), 1663 (C=O, s), 1576 (N-H, s), 1506 (C=C, s); ^1H NMR (600 MHz, d_6-DMSO) δ_H 10.12 (1H, s, NH-3a/8), 6.95 (1H, d, *J* 1.8 Hz, H-6), 6.75 (1H, d, *J* 15.5 Hz, H-28), 6.72 (1H, d, *J* 8.1 Hz, H-22), 6.48 (1H, d, *J* 1.8 Hz, H-4), 6.18 (1H, dt, *J* 15.5, 7.0 Hz, H-27), 6.01 (1H, dd, *J* 8.1, 2.3 Hz, H-23), 5.97 (1H, d, *J* 2.3 Hz, H-16), 5.57 (1H, d, *J* 2.2 Hz, NH-2a/7), 3.81 (2H, t, *J* 5.7 Hz, H-14), 3.75 (1H, qd, *J* 6.7, 2.2 Hz, H-7), 3.20 (4H, m, H-18, H-24), 2.58 (2H, t, *J* 6.4 Hz, H-20), 2.46 (2H, t, *J* 6.4 Hz, H-10), 2.24 (2H, p, *J* 7.0 Hz, H-26), 1.85 – 1.78 (2H, m, H-19), 1.72 – 1.57 (6H, m, H-11, H-13 ,H-25), 1.40 (2H, p, *J* 7.2 Hz, H-12), 1.27 (3H, d, *J* 6.7 Hz, H-9); ^{13}C NMR (151 MHz,d_6-DMSO) δ_C 168.5 (C-8), 158.3 (C-15), 145.3 (C-17), 131.32 (C-5), 129.6 (C-27), 129.2 (C-3a), 129.0 (C-22), 127.0 (C-2a), 125.9 (C-28), 121.8 (C-1), 119.5 (C-6), 114.5 (C-21), 114.1 (C-4), 99.4 (C-23), 97.8 (C-16), 67.2 (C-14), 51.0 (C-7), 48.6 (C-24), 48.0 (C-18), 33.0 (C-10), 29.4 (C-11), 29.1 (C-26), 27.8 (C-13), 26.8 (C-20), 23.6 (C-12), 23.4 (C-12, 22.0 (C-19), 17.4 (C-9); HRMS *m/z* (ESI^+)

[Found: 446.2791 $C_{28}H_{35}N_3O_2$ requires 446.2802 $[M+H]^+$]; LRMS *m/z* (ESI^+) 446 ($[M+H]^+$, 100%); HPLC: retention time 12.5 mins, 98.5% purity.

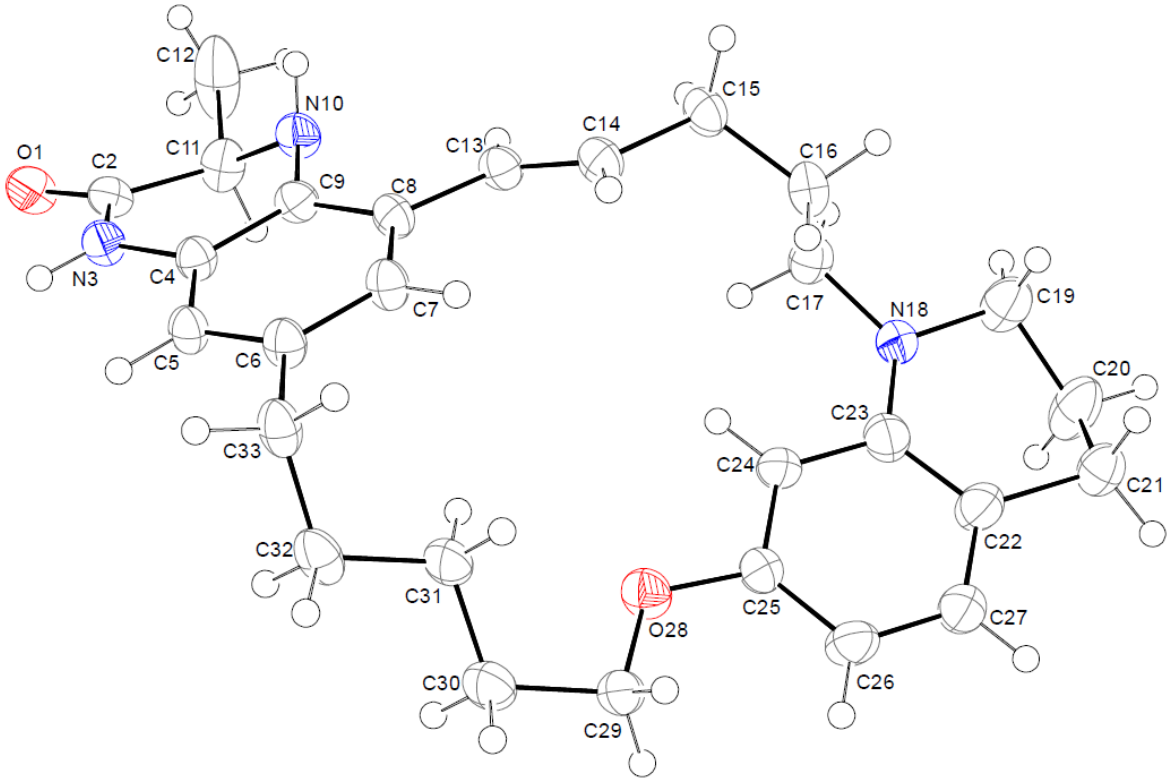

tert-Butyl (*E*)-(4-(5-hydroxypentyl)-2-(5-(7-methoxy-3,4-dihydroquinolin-1(2*H*)-yl)pent-1-en-1-yl)-6-nitrophenyl)-D-alaninate (compound **85**)

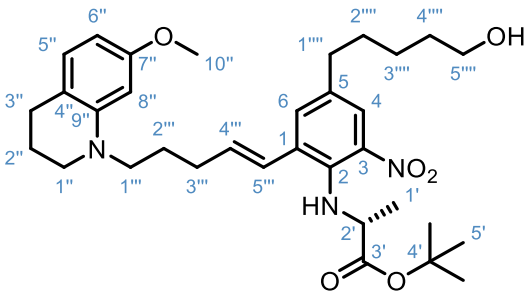

tert-Butyl (2-bromo-4-(5-hydroxypentyl)-6-nitrophenyl)-D-alaninate (165 mg, 0.383 mmol, 1.0 equiv.), (*E*)-7-Methoxy-1-(5(4,4,5,5-tetramethyl-1,3,2-dioxaborolan-2-yl)pent-4-en-1-yl)-1,2,3,4-tetrahydroquinoline (205 mg, 0.574 mmol, 1.5 equiv.), [1,1′-

Bis(diphenylphosphino)ferrocene]dichloropalladium$^{(II)}$ (30 mg, 0.0383, 0.1 equiv.)and K_2CO_3 (100 mg, 0.574 mmol, 1.5 equiv.) were added to a flame dried flask under an argon atmosphere. To this was added 1,4-dioxane (3.0 mL) and H_2O (1.0 mL) and the reaction was then heated to 100 °C for 24 h. After the reaction was cooled to r.t., the solvents were removed *in vacuo* and then the resultant residue was dissolved in EtOAc (100mL) and filtered through a pad of Celite®. The filtrate was washed with sat. $NaHCO_{3(aq)}$ (3 × 100 mL) followed by brine (50 mL), the organic layer was dried ($MgSO_4$), filtered and then the solvent was removed *in vacuo* to give a brown oil. The crude product was purified by flash silica column chromatography (elution with 0-100% EtOAc in pet ether) to give *tert*-butyl (*E*)-(4-(5-hydroxypentyl)-2-(5-(7-methoxy-3,4-dihydroquinolin-1(2*H*)-yl)pent-1-en-1-yl)-6-nitrophenyl)-D-alaninate as a bright orange oil (143 mg, 64 %); R_f 0.27 (1:1, EtOAc/pet ether); $[\alpha]_D^{25}$ = −161 (*c* 0.9, $CHCl_3$); $\bar{\nu}_{max}$ ($CHCl_3$ thin film)/ cm^{-1} 3355 (N-H, w), 2934 (C-H, s), 1731 (C=O, s), 1508 (N-O, s); ^1H NMR (600 MHz, $CDCl_3$) δ_H δ 7.74 (1H, d, *J* 2.1 Hz, H-4), 7.30 (1H, d, *J* 2.1 Hz, H-6), 6.90 – 6.83 (2H, m, NH-2/2', H-5''), 6.50 – 6.44 (1H, m, H-5'''), 6.20 – 6.11 (3H, m, H-6'', H-8'', H-4'''), 4.05 (1H, dq, *J* 10.7, 7.0 Hz, H-2'), 3.75 (3H, s, H-10''), 3.64 (2H, t, *J* 6.5 Hz, H-5''''), 3.33 – 3.26 (4H, m, H-1'', H-1'''), 2.69 (2H, t, *J* 6.3 Hz, H-3''), 2.60 – 2.56 (2H, m, H-1''''), 2.35 – 2.28 (2H, m, H-3'''), 1.96 – 1.89 (2H, m, H-2''), 1.82 (2H, h, *J* 6.5 Hz, H-2'''), 1.68 – 1.54 (4H, m, H-2'''', H-4''''), 1.43-1.37 (2H, m, H-3''''), 1.39 (3H, d, *J* 7.0 Hz, H-1'), 1.31 (9H, s, H-5'); ^{13}C NMR (151 MHz, $CDCl_3$) δ_C 172.8 (C-3'), 159.4 (C-7''), 146.2 (C-9''), 141.0 (C-2a), 140.5 (C-1), 134.9 (C-3), 134.6 (C-6), 132.7 (C-5), 132.5 (C-4'''), 129.6 (C-5''), 127.7 (C-5'''), 123.9 (C-4), 115.5 (C-4''), 99.6 (C-6''), 97.7 (C-8''), 81.6 (C-4'), 63.0 (C-5''''), 57.2 (C-2'), 55.3 (C-10''), 51.3 (C-1'''), 49.7 (C-1''), 34.9 (C-1''''), 32.7 (C-2''''), 31.0 (C-4''''), 30.85 (C-3''), 27.8 (C-5'), 27.6 (C-3''), 26.0 (C-2'''), 25.5 (C-3''''), 22.6 (C-2''), 19.5 (C-1'); HRMS *m/z* (ESI^+) [Found: 582.3527

$C_{33}H_{48}N_3O_6$ requires 582.3538 [M+H]$^+$]; LRMS *m/z* (ESI$^+$) 582 ([M+H]$^+$, 100%); HPLC (retention time 13.1 mins) 96.5% purity.

(*R*,*E*)-7-(5-Hydroxypentyl)-5-(5-(7-methoxy-3,4-dihydroquinolin-1(2*H*)-yl)pent-1-en-1-yl)-3-methyl-3,4-dihydroquinoxalin-2(1*H*)-one (compound **84**)

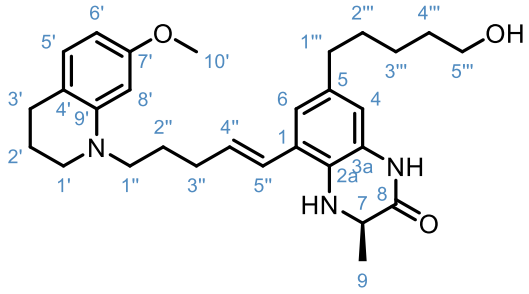

tert-Butyl (*E*)-(4-(5-hydroxypentyl)-2-(5-(7-methoxy-3,4-dihydroquinolin-1(2*H*)-yl)pent-1-en-1-yl)-6-nitrophenyl)-D-alaninate (250 mg, 0.430 mmol, 1.0 equiv.) was dissolved in CH_2Cl_2 (3 mL) and TFA (3 mL) and then stirred at r.t. for 3.5 h. After this time the solvents were removed *in vacuo* to give a dark orange oil. To this was added zinc powder (985 mg, 15.1 mmol, 35 equiv.) and ammonium chloride (808 mg, 15.1 mmol, 35 equiv.) and the flask was placed under an argon atmosphere and DMF (7 mL) was added, and the reaction mixture stirred at r.t. for 24h. After this time the reaction was diluted with EtOAc (100 mL) and filtered through a Celite® pad. The filtrate was then washed with sat. $NH_4Cl_{(aq)}$ (100 mL), 10 wt% $LiCl_{(aq)}$ (50 mL) and brine (3 × 50 mL), dried ($MgSO_4$), filtered and concentrated *in vacuo* to give a light brown oil. The crude product was then purified by flash silica column chromatography (elution with 0-100% EtOAc in pet ether) to give an off white solid which was further purified by semi-preparative HPLC (retention time of 7.97 mins) and then lyophilised to give (*R*,*E*)-7-(5-hydroxypentyl)-5-(5-(7-methoxy-3,4-dihydroquinolin-1(2*H*)-yl)pent-1-en-1-yl)-3-methyl-3,4-dihydroquinoxalin-2(1*H*)-one as an off white solid (134 mg, 65 %); R_f 0.41 (EtOAc); m.p 156 –158 °C (H_2O/MeCN); $[\alpha]_D^{25}$ = −8.9 (*c* 1.0, $CHCl_3$); $\bar{\nu}_{max}$ ($CHCl_3$ thin

film)/ cm^{-1} 2933 (C-H, s), 1668 (C=O, s), 1508 (C=C, s), 1049 (C-O, s); ^{1}H NMR (600 MHz, DMSO) δ_H 10.09 (1H, s, NH-3a/8), 6.78 (1H, d, *J* 1.8 Hz, H-4), 6.74 (1H, d, *J* 8.1 Hz, H-5'), 6.64 (1H, dt, *J* 15.5, 1.5 Hz, H-5''), 6.47 (1H, d, *J* 1.8 Hz, H-6), 6.12 (1H, dt, *J* 15.5, 6.9 Hz, H-4''), 6.07 (1H, d, *J* 2.4 Hz, H-8'), 6.04 (1H, dd, *J* 8.1, 2.4 Hz, H-6'), 5.50 (1H, d, *J* 2.3 Hz, NH-2a/7), 4.31 (1H, t, *J* 5.1 Hz, OH-5'''), 3.73 (1H, qd, *J* 6.7, 2.3 Hz, H-7), 3.62 (3H, s, H-10'), 3.37 (2H, td, *J* 6.5, 5.0 Hz, H-5'''), 3.25 (4H, dt, *J* 11.8, 6.5 Hz, H-1', H-1''), 2.59 (2H, t, *J* 6.3 Hz, H-3'), 2.39 (2H, t, *J* 7.7 Hz, H-1'''), 2.27 – 2.20 (2H, m, H-3''), 1.85 – 1.78 (2H, m, H-2'), 1.70 (2H, p, *J* 7.5 Hz, H-2''), 1.52 – 1.46 (m, 2H, H-2'''), 1.43 (2H, dt, *J* 14.3, 6.7 Hz, H-4'''), 1.33 – 1.26 (2H, m, H-3'''), 1.25 (3H, d, *J* 6.7 Hz, H-9); ^{13}C NMR (151 MHz, d_6-DMSO) δ_C 168.5 (C-8), 158.9 (C-7'), 145.7 (C-9'), 131.8 (C-5), 130.4 (C-4''), 129.2 (C-5'), 128.8 (C-2a), 126.7 (C-3a), 124.9 (C-5''), 122.5 (C-1), 119.5 (C-4), 114.4 (C-4'), 113.5 (C-6), 99.7 (C-6'), 96.7 (C-8'), 60.7 (C-5'''), 54.6 (C-10'), 51.1 (C-7), 50.2 (C-1''), 48.7 (C-1'), 34.7 (C-1'''), 32.4 (C-4'''), 31.2 (C-2'''), 30.4 (C-3''), 26.9 (C-3'), 25.4 (C-2''), 25.2 (C-3'''), 22.0 (C-2'), 17.4 (C-9); HRMS *m/z* (ESI^+) [Found: 478.3056 $C_{29}H_{40}N_3O_3$ requires 478.3064 $[M+H]^+$]; LRMS *m/z* (ESI^+) 628 ($[M+H]^+$, 100%), 630 ($[M+H]^+$, 97%); HPLC (retention time 10.4 mins) 98.4% purity.

References

(1) Pfaffeneder, T.; Spada, F.; Wagner, M.; Brandmayr, C.; Laube, S. K.; Eisen, D.; Truss, M.; Steinbacher, J.; Hackner, B.; Kotljarova, O.; Schuermann, D.; Michalakis, S.; Kosmatchev, O.; Schiesser, S.; Steigenberger, B.; Raddaoui, N.; Kashiwazaki, G.; Müller, U.; Spruijt, C. G.; Vermeulen, M.; Leonhardt, H.; Schär, P.; Müller, M.; Carell, T. Tet Oxidizes Thymine to 5-Hydroxymethyluracil in Mouse Embryonic Stem Cell DNA. *Nat Chem Biol* **2014**, *10* (7), 574–581. https://doi.org/10.1038/nchembio.1532.

(2) Fleming, A. M.; Burrows, C. J. DNA Modifications Walk a Fine Line between Epigenetics and Mutagenesis. *Nature Reviews Molecular Cell Biology*. Nature Research July 1, 2023, pp 449–450. https://doi.org/10.1038/s41580-023-00590-2.

(3) Zhao, B. S.; Roundtree, I. A.; He, C. Post-Transcriptional Gene Regulation by MRNA Modifications. *Nature Reviews Molecular Cell Biology*. Nature Publishing Group December 19, 2016, pp 31–42. https://doi.org/10.1038/nrm.2016.132.

(4) Zhong, Q.; Xiao, X.; Qiu, Y.; Xu, Z.; Chen, C.; Chong, B.; Zhao, X.; Hai, S.; Li, S.; An, Z.; Dai, L. Protein Posttranslational Modifications in Health and Diseases: Functions, Regulatory Mechanisms, and Therapeutic Implications. *MedComm*. John Wiley and Sons Inc June 1, 2023. https://doi.org/10.1002/mco2.261.

(5) Dupont, C.; Armant, D. R.; Brenner, C. A. Epigenetics: Definition, Mechanisms and Clinical Perspective. *Semin Reprod Med* **2009**, *27* (5), 351–357. https://doi.org/10.1055/s-0029-1237423.

(6) McGinty, R. K.; Tan, S. Nucleosome Structure and Function. *Chem Rev* **2015**, *115* (6), 2255–2273. https://doi.org/10.1021/cr500373h.

(7) Luger, K.; Dechassa, M. L.; Tremethick, D. J. New Insights into Nucleosome and Chromatin Structure: An Ordered State or a Disordered Affair? *Nat Rev Mol Cell Biol* **2012**, *13* (7), 436–447. https://doi.org/10.1038/nrm3382.

(8) Bai, M.; Ti, D.; Mei, Q.; Liu, J.; Yan, X.; Chen, D.; Li, X.; Wu, Z.; Han, W. The Role of Posttranslational Modifications in DNA Repair. *Biomed Res Int* **2020**, *2020*. https://doi.org/10.1155/2020/7493902.

(9) Akgol Oksuz, B.; Yang, L.; Abraham, S.; Venev, S. V.; Krietenstein, N.; Parsi, K. M.; Ozadam, H.; Oomen, M. E.; Nand, A.; Mao, H.; Genga, R. M. J.; Maehr, R.; Rando, O. J.; Mirny, L. A.; Gibcus, J. H.; Dekker, J. Systematic Evaluation of Chromosome Conformation Capture Assays. *Nat Methods* **2021**, *18* (9), 1046–1055. https://doi.org/10.1038/s41592-021-01248-7.

(10) Eberharter, A.; Becker, P. B. Histone Acetylation: A Switch between Repressive and Permissive Chromatin Second in Review Series on Chromatin Dynamics. *224 EMBO reports* **2002**, *3* (3), 224–229.

(11) Greer, E. L.; Shi, Y. Histone Methylation: A Dynamic Mark in Health, Disease and Inheritance. *Nature Reviews Genetics*. May 2012, pp 343–357. https://doi.org/10.1038/nrg3173.

(12) Bannister, A. J.; Kouzarides, T. Regulation of Chromatin by Histone Modifications. *Cell Res* **2011**, *21* (3), 381–395. https://doi.org/10.1038/cr.2011.22.

(13) Banerjee, T.; Chakravarti, D. A Peek into the Complex Realm of Histone Phosphorylation. *Mol Cell Biol* **2011**, *31* (24), 4858–4873. https://doi.org/10.1128/MCB.05631-11.

(14) Li, J.; Lu, L.; Liu, L.; Ren, X.; Chen, J.; Yin, X.; Xiao, Y.; Li, J.; Wei, G.; Huang, H.; Wei, W.; Wong, J. HDAC1/2/3 Are Major Histone Desuccinylases Critical for Promoter Desuccinylation. *Cell Discov* **2023**, *9* (1). https://doi.org/10.1038/s41421-023-00573-9.

(15) Ryu, H. Y.; Hochstrasser, M. Histone Sumoylation and Chromatin Dynamics. *Nucleic Acids Res* **2021**, *49* (11), 6043–6052. https://doi.org/10.1093/nar/gkab280.

(16) Ishiguro, T.; Tanabe, K.; Kobayashi, Y.; Mizumoto, S.; Kanai, M.; Kawashima, S. A. Malonylation of Histone H2A at Lysine 119 Inhibits Bub1-Dependent H2A Phosphorylation and Chromosomal Localization of Shugoshin Proteins. *Sci Rep* **2018**, *8* (1). https://doi.org/10.1038/s41598-018-26114-z.

(17) Cao, J.; Yan, Q. Histone Ubiquitination and Deubiquitination in Transcription, DNA Damage Response, and Cancer. *Front Oncol* **2012**, *2* (MAR). https://doi.org/10.3389/fonc.2012.00026.

(18) Ali, I.; Conrad, R. J.; Verdin, E.; Ott, M. Lysine Acetylation Goes Global: From Epigenetics to Metabolism and Therapeutics. *Chemical Reviews*. American Chemical Society February 14, 2018, pp 1216–1252. https://doi.org/10.1021/acs.chemrev.7b00181.

(19) McCullough, C. E.; Marmorstein, R. Molecular Basis for Histone Acetyltransferase Regulation by Binding Partners, Associated Domains, and

Autoacetylation. *ACS Chem Biol* **2016**, *11* (3), 632–642. https://doi.org/10.1021/acschembio.5b00841.

(20) Park, S. Y.; Kim, J. S. A Short Guide to Histone Deacetylases Including Recent Progress on Class II Enzymes. *Exp Mol Med* **2020**, *52* (2), 204–212. https://doi.org/10.1038/s12276-020-0382-4.

(21) Fujisawa, T.; Filippakopoulos, P. Functions of Bromodomain-Containing Proteins and Their Roles in Homeostasis and Cancer. *Nat Rev Mol Cell Biol* **2017**, *18* (4), 246–262. https://doi.org/10.1038/nrm.2016.143.

(22) Pan, Z.; Zhao, Y.; Wang, X.; Xie, X.; Liu, M.; Zhang, K.; Wang, L.; Bai, D.; Foster, L. J.; Shu, R.; He, G. Targeting Bromodomain-Containing Proteins: Research Advances of Drug Discovery. *Molecular Biomedicine* **2023**, *4* (1). https://doi.org/10.1186/s43556-023-00127-1.

(23) Filippakopoulos, P.; Qi, J.; Picaud, S.; Shen, Y.; Smith, W. B.; Fedorov, O.; Morse, E. M.; Keates, T.; Hickman, T. T.; Felletar, I.; Philpott, M.; Munro, S.; McKeown, M. R.; Wang, Y.; Christie, A. L.; West, N.; Cameron, M. J.; Schwartz, B.; Heightman, T. D.; La Thangue, N.; French, C. A.; Wiest, O.; Kung, A. L.; Knapp, S.; Bradner, J. E. Selective Inhibition of BET Bromodomains. *Nature* **2010**, *468* (7327), 1067–1073. https://doi.org/10.1038/nature09504.

(24) Filippakopoulos, P.; Picaud, S.; Mangos, M.; Keates, T.; Lambert, J. P.; Barsyte-Lovejoy, D.; Felletar, I.; Volkmer, R.; Müller, S.; Pawson, T.; Gingras, A. C.; Arrowsmith, C. H.; Knapp, S. Histone Recognition and Large-Scale Structural Analysis of the Human Bromodomain Family. *Cell* **2012**, *149* (1), 214–231. https://doi.org/10.1016/j.cell.2012.02.013.

(25) Wang, N.; Wu, R.; Tang, D.; Kang, R. The BET Family in Immunity and Disease. *Signal Transduct Target Ther* **2021**, *6* (1). https://doi.org/10.1038/s41392-020-00384-4.

(26) Ferri, E.; Petosa, C.; McKenna, C. E. Bromodomains: Structure, Function and Pharmacology of Inhibition. *Biochem Pharmacol* **2016**, *106*, 1–18. https://doi.org/10.1016/j.bcp.2015.12.005.

(27) Wang, S.; Tsui, V.; Crawford, T. D.; Audia, J. E.; Burdick, D. J.; Beresini, M. H.; Côté, A.; Cummings, R.; Duplessis, M.; Flynn, E. M.; Hewitt, M. C.; Huang, H. R.; Jayaram, H.; Jiang, Y.; Joshi, S.; Murray, J.; Nasveschuk, C. G.; Pardo, E.; Poy, F.; Romero, F. A.; Tang, Y.; Taylor, A. M.; Wang, J.; Xu, Z.; Zawadzke, L. E.; Zhu, X.; Albrecht, B. K.; Magnuson, S. R.; Bellon, S.; Cochran, A. G. GNE-371, a Potent and Selective Chemical Probe for the Second Bromodomains of Human Transcription-Initiation-Factor TFIID Subunit 1 and Transcription-Initiation-Factor TFIID Subunit 1-Like. *J Med Chem* **2018**, *61* (20), 9301–9315. https://doi.org/10.1021/acs.jmedchem.8b01225.

(28) Romero, F. A.; Murray, J.; Lai, K. W.; Tsui, V.; Albrecht, B. K.; An, L.; Beresini, M. H.; De Leon Boenig, G.; Bronner, S. M.; Chan, E. W.; Chen, K. X.; Chen, Z.; Choo, E. F.; Clagg, K.; Clark, K.; Crawford, T. D.; Cyr, P.; De Almeida Nagata, D.; Gascoigne, K. E.; Grogan, J. L.; Hatzivassiliou, G.; Huang, W.; Hunsaker, T. L.; Kaufman, S.; Koenig, S. G.; Li, R.; Li, Y.; Liang, X.; Liao, J.; Liu, W.; Ly, J.; Maher, J.; Masui, C.; Merchant, M.; Ran, Y.; Taylor, A. M.; Wai, J.; Wang, F.; Wei, X.; Yu, D.; Zhu, B. Y.; Zhu, X.; Magnuson, S. GNE-781, A Highly Advanced Potent and Selective Bromodomain Inhibitor of Cyclic Adenosine Monophosphate Response Element Binding Protein, Binding Protein (CBP). *J*

Med Chem **2017**, *60* (22), 9162–9183. https://doi.org/10.1021/acs.jmedchem.7b00796.

(29) Rhyasen, G. W.; Hattersley, M. M.; Yao, Y.; Dulak, A.; Wang, W.; Petteruti, P.; Dale, I. L.; Boiko, S.; Cheung, T.; Zhang, J.; Wen, S.; Castriotta, L.; Lawson, D.; Collins, M.; Bao, L.; Ahdesmaki, M. J.; Walker, G.; O'Connor, G.; Yeh, T. C.; Rabow, A. A.; Dry, J. R.; Reimer, C.; Lyne, P.; Mills, G. B.; Fawell, S. E.; Waring, M. J.; Zinda, M.; Clark, E.; Chen, H. AZD5153: A Novel Bivalent BET Bromodomain Inhibitor Highly Active against Hematologic Malignancies. *Mol Cancer Ther* **2016**, *15* (11), 2563–2574. https://doi.org/10.1158/1535-7163.MCT-16-0141.

(30) Nicosia, L.; Spencer, G. J.; Brooks, N.; Amaral, F. M. R.; Basma, N. J.; Chadwick, J. A.; Revell, B.; Wingelhofer, B.; Maiques-Diaz, A.; Sinclair, O.; Camera, F.; Ciceri, F.; Wiseman, D. H.; Pegg, N.; West, W.; Knurowski, T.; Frese, K.; Clegg, K.; Campbell, V. L.; Cavet, J.; Copland, M.; Searle, E.; Somervaille, T. C. P. Therapeutic Targeting of EP300/CBP by Bromodomain Inhibition in Hematologic Malignancies. *Cancer Cell* **2023**, *41* (12), 2136-2153.e13. https://doi.org/10.1016/j.ccell.2023.11.001.

(31) To, K. K. W.; Xing, E.; Larue, R. C.; Li, P. K. BET Bromodomain Inhibitors: Novel Design Strategies and Therapeutic Applications. *Molecules* **2023**, *28* (7). https://doi.org/10.3390/molecules28073043.

(32) Hsia, O.; Hinterndorfer, M.; Cowan, A. D.; Iso, K.; Ishida, T.; Sundaramoorthy, R.; Nakasone, M. A.; Imrichova, H.; Schätz, C.; Rukavina, A.; Husnjak, K.; Wegner, M.; Correa-Sáez, A.; Craigon, C.; Casement, R.; Maniaci, C.; Testa, A.; Kaulich, M.; Dikic, I.; Winter, G. E.; Ciulli, A. Targeted Protein Degradation via

Intramolecular Bivalent Glues. *Nature* **2024**, *627* (8002), 204–211. https://doi.org/10.1038/s41586-024-07089-6.

(33) Winter, G. E.; Paulk, J.; Roberts, J. M.; Souza, A.; Dhe-Pagano, S.; Bradner, J. E. Phthalimide Conjugation as a strategy for in Vivo Target Protein Degradation. *Science (1979)* **2015**, *348* (6241), 1376–1381. https://doi.org/10.1126/science.aab1223.

(34) Zengerle, M.; Chan, K. H.; Ciulli, A. Selective Small Molecule Induced Degradation of the BET Bromodomain Protein BRD4. *ACS Chem Biol* **2015**, *10* (8), 1770–1777. https://doi.org/10.1021/acschembio.5b00216.

(35) Burgoyne, A. M.; Vann, K. R.; Joshi, S.; Morales, G. A.; Vega, F. M.; Singh, A.; Pal, D.; Merati, A. B.; Kutateladze, T. G.; Durden, D. L. A Triple Action CDK4/6-PI3K-BET Inhibitor with Augmented Cancer Cell Cytotoxicity. *Cell Discov* **2020**, *6* (1). https://doi.org/10.1038/s41421-020-0181-z.

(36) Lim, M.; Cong, T. Do; Orr, L. M.; Toriki, E. S.; Kile, A. C.; Papatzimas, J. W.; Lee, E.; Lin, Y.; Nomura, D. K. DCAF16-Based Covalent Handle for the Rational Design of Monovalent Degraders. *ACS Cent Sci* **2024**. https://doi.org/10.1021/acscentsci.4c00286.

(37) Wang, Z. Q.; Zhang, Z. C.; Wu, Y. Y.; Pi, Y. N.; Lou, S. H.; Liu, T. B.; Lou, G.; Yang, C. Bromodomain and Extraterminal (BET) Proteins: Biological Functions, Diseases, and Targeted Therapy. *Signal Transduct Target Ther* **2023**, *8* (1). https://doi.org/10.1038/s41392-023-01647-6.

(38) Shorstova, T.; Foulkes, W. D.; Witcher, M. Achieving Clinical Success with BET Inhibitors as Anti-Cancer Agents. *Br J Cancer* **2021**, *124* (9), 1478–1490. https://doi.org/10.1038/s41416-021-01321-0.

(39) Dutto, I.; Scalera, C.; Prosperi, E. CREBBP and P300 Lysine Acetyl Transferases in the DNA Damage Response. *Cellular and Molecular Life Sciences* **2018**, *75* (8), 1325–1338. https://doi.org/10.1007/s00018-017-2717-4.

(40) Rooney, T. P. C.; Filippakopoulos, P.; Fedorov, O.; Picaud, S.; Cortopassi, W. A.; Hay, D. A.; Martin, S.; Tumber, A.; Rogers, C. M.; Philpott, M.; Wang, M.; Thompson, A. L.; Heightman, T. D.; Pryde, D. C.; Cook, A.; Paton, R. S.; Müller, S.; Knapp, S.; Brennan, P. E.; Conway, S. J. A Series of Potent Crebbp Bromodomain Ligands Reveals an Induced-Fit Pocket Stabilized by a Cation-π Interaction. *Angewandte Chemie - International Edition* **2014**, *53* (24), 6126–6130. https://doi.org/10.1002/anie.201402750.

(41) Iyer, N. G.; Özdag, H.; Caldas, C. P300/CBP and Cancer. *Oncogene* **2004**, *23* (24), 4225–4231. https://doi.org/10.1038/sj.onc.1207118.

(42) Welti, J.; Sharp, A.; Brooks, N.; Yuan, W.; McNair, C.; Chand, S. N.; Pal, A.; Figueiredo, I.; Riisnaes, R.; Gurel, B.; Rekowski, J.; Bogdan, D.; West, W.; Young, B.; Raja, M.; Prosser, A.; Lane, J.; Thomson, S.; Worthington, J.; Onions, S.; Shannon, J.; Paoletta, S.; Brown, R.; Smyth, D.; Harbottle, G. W.; Gil, V. S.; Miranda, S.; Crespo, M.; Ferreira, A.; Pereira, R.; Tunariu, N.; Carreira, S.; Neeb, A. J.; Ning, J.; Swain, A.; Taddei, D.; Schiewer, M. J.; Knudsen, K. E.; Pegg, N.; de Bono, J. S. Targeting the P300/Cbp Axis in Lethal Prostate Cancer. *Cancer Discov* **2021**, *11* (5), 1118–1137. https://doi.org/10.1158/2159-8290.CD-20-0751.

(43) Ibrahim, Z.; Wang, T.; Destaing, O.; Salvi, N.; Hoghoughi, N.; Chabert, C.; Rusu, A.; Gao, J.; Feletto, L.; Reynoird, N.; Schalch, T.; Zhao, Y.; Blackledge, M.; Khochbin, S.; Panne, D. Structural Insights into P300 Regulation and

Acetylation-Dependent Genome Organisation. *Nat Commun* **2022**, *13* (1). https://doi.org/10.1038/s41467-022-35375-2.

(44) Brand, M.; Clayton, J.; Moroglu, M.; Schiedel, M.; Picaud, S.; Bluck, J. P.; Skwarska, A.; Bolland, H.; Chan, A. K. N.; Laurin, C. M. C.; Scorah, A. R.; See, L.; Rooney, T. P. C.; Andrews, K. H.; Fedorov, O.; Perell, G.; Kalra, P.; Vinh, K. B.; Cortopassi, W. A.; Heitel, P.; Christensen, K. E.; Cooper, R. I.; Paton, R. S.; Pomerantz, W. C. K.; Biggin, P. C.; Hammond, E. M.; Filippakopoulos, P.; Conway, S. J. Controlling Intramolecular Interactions in the Design of Selective, High-Affinity Ligands for the CREBBP Bromodomain. *J Med Chem* **2021**, *64* (14), 10102–10123. https://doi.org/10.1021/acs.jmedchem.1c00348.

(45) Liu, X.; Wang, L.; Zhao, K.; Thompson, P. R.; Hwang, Y.; Marmorstein, R.; Cole, P. A. The Structural Basis of Protein Acetylation by the P300/CBP Transcriptional Coactivator. *Nature* **2008**, *451* (7180), 846–850. https://doi.org/10.1038/nature06546.

(46) Ogiwara, H.; Sasaki, M.; Mitachi, T.; Oike, T.; Higuchi, S.; Tominaga, Y.; Kohno, T. Targeting P300 Addiction in CBP-Deficient Cancers Causes Synthetic Lethality by Apoptotic Cell Death Due to Abrogation of MYC Expression. *Cancer Discov* **2016**, *6* (4), 430–445. https://doi.org/10.1158/2159-8290.CD-15-0754.

(47) Liu, M.; Zhang, K.; Li, Q.; Pang, H.; Pan, Z.; Huang, X.; Wang, L.; Wu, F.; He, G. Recent Advances on Small-Molecule Bromodomain-Containing Histone Acetyltransferase Inhibitors. *J Med Chem* **2023**, *66* (3), 1678–1699. https://doi.org/10.1021/acs.jmedchem.2c01638.

(48) Gou, P.; Zhang, W. Protein Lysine Acetyltransferase CBP/P300: A Promising Target for Small Molecules in Cancer Treatment. *Biomedicine and Pharmacotherapy* **2024**, *171*. https://doi.org/10.1016/j.biopha.2024.116130.

(49) Joy, S. T.; Henley, M. J.; De Salle, S. N.; Beyersdorf, M. S.; Vock, I. W.; Huldin, A. J. L.; Mapp, A. K. A Dual-Site Inhibitor of CBP/P300 KIX Is a Selective and Effective Modulator of Myb. *J Am Chem Soc* **2021**, *143* (37), 15056–15062. https://doi.org/10.1021/jacs.1c04432.

(50) Crawford, M. C.; Tripu, D. R.; Barritt, S. A.; Jing, Y.; Gallimore, D.; Kales, S. C.; Bhanu, N. V.; Xiong, Y.; Fang, Y.; Butler, K. A. T.; LeClair, C. A.; Coussens, N. P.; Simeonov, A.; Garcia, B. A.; Dibble, C. C.; Meier, J. L. Comparative Analysis of Drug-like EP300/CREBBP Acetyltransferase Inhibitors. *ACS Chem Biol* **2023**, *18* (10), 2249–2258. https://doi.org/10.1021/acschembio.3c00293.

(51) Jones, M.; Grosche, P.; Floersheimer, A.; André, J.; Gattlen, R.; Oser, D.; Tinchant, J.; Wille, R.; Chie-Leon, B.; Gerspacher, M.; Ertl, P.; Ostermann, N.; Altmann, E.; Manchado, E.; Vorherr, T.; Chène, P. Design and Biochemical Characterization of Peptidic Inhibitors of the Myb/P300 Interaction. *Biochemistry* **2023**, *62* (7), 1321–1329. https://doi.org/10.1021/acs.biochem.2c00690.

(52) Hay, D. A.; Fedorov, O.; Martin, S.; Singleton, D. C.; Tallant, C.; Wells, C.; Picaud, S.; Philpott, M.; Monteiro, O. P.; Rogers, C. M.; Conway, S. J.; Rooney, T. P. C.; Tumber, A.; Yapp, C.; Filippakopoulos, P.; Bunnage, M. E.; Müller, S.; Knapp, S.; Schofield, C. J.; Brennan, P. E. Discovery and Optimization of Small-Molecule Ligands for the CBP/P300 Bromodomains. *J Am Chem Soc* **2014**, *136* (26), 9308–9319. https://doi.org/10.1021/ja412434f.

(53) Lai, K. W.; Romero, F. A.; Tsui, V.; Beresini, M. H.; de Leon Boenig, G.; Bronner, S. M.; Chen, K.; Chen, Z.; Choo, E. F.; Crawford, T. D.; Cyr, P.; Kaufman, S.; Li, Y.; Liao, J.; Liu, W.; Ly, J.; Murray, J.; Shen, W.; Wai, J.; Wang, F.; Zhu, C.; Zhu, X.; Magnuson, S. Design and Synthesis of a Biaryl Series as Inhibitors for the Bromodomains of CBP/P300. *Bioorg Med Chem Lett* **2018**, *28* (1), 15–23. https://doi.org/10.1016/j.bmcl.2017.11.025.

(54) Taylor, A. M.; Côté, A.; Hewitt, M. C.; Pastor, R.; Leblanc, Y.; Nasveschuk, C. G.; Romero, F. A.; Crawford, T. D.; Cantone, N.; Jayaram, H.; Setser, J.; Murray, J.; Beresini, M. H.; De Leon Boenig, G.; Chen, Z.; Conery, A. R.; Cummings, R. T.; Dakin, L. A.; Flynn, E. M.; Huang, O. W.; Kaufman, S.; Keller, P. J.; Kiefer, J. R.; Lai, T.; Li, Y.; Liao, J.; Liu, W.; Lu, H.; Pardo, E.; Tsui, V.; Wang, J.; Wang, Y.; Xu, Z.; Yan, F.; Yu, D.; Zawadzke, L.; Zhu, X.; Zhu, X.; Sims, R. J.; Cochran, A. G.; Bellon, S.; Audia, J. E.; Magnuson, S.; Albrecht, B. K. Fragment-Based Discovery of a Selective and Cell-Active Benzodiazepinone CBP/EP300 Bromodomain Inhibitor (CPI-637). *ACS Med Chem Lett* **2016**, *7* (5), 531–536. https://doi.org/10.1021/acsmedchemlett.6b00075.

(55) Chen, Z.; Wang, M.; Wu, D.; Bai, L.; Xu, T.; Metwally, H.; Wang, Y.; McEachern, D.; Zhao, L.; Li, R.; Takyi-Williams, J.; Wang, M.; Wang, L.; Li, Q.; Wen, B.; Sun, D.; Wang, S. Discovery of CBPD-268 as an Exceptionally Potent and Orally Efficacious CBP/P300 PROTAC Degrader Capable of Achieving Tumor Regression. *J Med Chem* **2024**, *67* (7), 5275–5304. https://doi.org/10.1021/acs.jmedchem.3c02124.

(56) Hu, J.; Xu, Y. CBP/P300 Degrader: A Promising Therapeutic Strategy for Treatment of Prostate Cancer and Beyond. *J Med Chem* **2024**, *67* (7), 5272–5274. https://doi.org/10.1021/acs.jmedchem.4c00502.

(57) Chen, X.; Crawford, M. C.; Xiong, Y.; Shaik, A. B.; Suazo, K. F.; Bauer, L. G.; Penikalapati, M. S.; Williams, J. H.; Huber, K. V. M.; Andressen, T.; Swenson, R. E.; Meier, J. L. Paralogue-Selective Degradation of the Lysine Acetyltransferase EP300. *JACS Au* **2024**. https://doi.org/10.1021/jacsau.4c00442.

(58) Yudin, A. K. Macrocycles: Lessons from the Distant Past, Recent Developments, and Future Directions. *Chem Sci* **2015**, *6* (1), 30–49. https://doi.org/10.1039/c4sc03089c.

(59) Garcia Jimenez, D.; Poongavanam, V.; Kihlberg, J. Macrocycles in Drug Discovery—Learning from the Past for the Future. *J Med Chem* **2023**, *66* (8), 5377–5396. https://doi.org/10.1021/acs.jmedchem.3c00134.

(60) Yu, J.; Qi, D.; Li, J. Design, Synthesis and Applications of Responsive Macrocycles. *Commun Chem* **2020**, *3* (1). https://doi.org/10.1038/s42004-020-00438-2.

(61) Drilon, A.; Ou, S. H. I.; Cho, B. C.; Kim, D. W.; Lee, J.; Lin, J. J.; Zhu, V. W.; Ahn, M. J.; Camidge, D. R.; Nguyen, J.; Zhai, D.; Deng, W.; Huang, Z.; Rogers, E.; Liu, J.; Whitten, J.; Lim, J. K.; Stopatschinskaja, S.; Hyman, D. M.; Doebele, R. C.; Cui, J. J.; Shaw, A. T. Repotrectinib (Tpx-0005) Is a next-Generation Ros1/Trk/Alk Inhibitor That Potently Inhibits Ros1/Trk/Alk Solvent-Front Mutations. *Cancer Discov* **2018**, *8* (10). https://doi.org/10.1158/2159-8290.CD-18-0484.

(62) Amrhein, J. A.; Beyett, T. S.; Feng, W. W.; Krämer, A.; Weckesser, J.; Schaeffner, I. K.; Rana, J. K.; Jänne, P. A.; Eck, M. J.; Knapp, S.; Hanke, T. Macrocyclization of Quinazoline-Based EGFR Inhibitors Leads to Exclusive Mutant Selectivity for EGFR L858R and Del19. *J Med Chem* **2022**, *65* (23), 15679–15697. https://doi.org/10.1021/acs.jmedchem.2c01041.

(63) Amrhein, J. A.; Knapp, S.; Hanke, T. Synthetic Opportunities and Challenges for Macrocyclic Kinase Inhibitors. *J Med Chem* **2021**, *64* (12), 7991–8009. https://doi.org/10.1021/acs.jmedchem.1c00217.

(64) Breslin, H. J.; Lane, B. M.; Ott, G. R.; Ghose, A. K.; Angeles, T. S.; Albom, M. S.; Cheng, M.; Wan, W.; Haltiwanger, R. C.; Wells-Knecht, K. J.; Dorsey, B. D. Design, Synthesis, and Anaplastic Lymphoma Kinase (ALK) Inhibitory Activity for a Novel Series of 2,4,8,22-Tetraazatetracyclo[14.3.1.1 3,7.1 9,13]Docosa-1(20),3(22),4,6,9(21),10,12,16,18-Nonaene Macrocycles. *J Med Chem* **2012**, *55* (1), 449–464. https://doi.org/10.1021/jm201333e.

(65) Zhou, Y.; Kang, J.; Lu, X. Targeting Solvent-Front Mutations for Kinase Drug Discovery: From Structural Basis to Design Strategies. *J Med Chem* **2024**. https://doi.org/10.1021/acs.jmedchem.4c00361.

(66) Woodward, R. B.; Logusch, E.; Nambiar, K. P.; Sakan, K.; Ward, D. E.; Au-Yeung, B. W.; Balaram, P.; Browne, L. J.; Card, P. J.; Chen, C. H.; Chenevert, R. B.; Fliri, A.; Frobel, K.; Gais, H. J.; Garratt, D. G.; Hayakawa, K.; Heggie, W.; Hesson, D. P.; Hoppe, D.; Hoppe, I.; Hyatt, J. A.; Ikeda, D.; Jacobi, P. A.; Kim, K. S.; Kobuke, Y.; Kojima, K.; Krowicki, K.; Lee, V. J.; Leutert, T.; Malchenko, S.; Martens, J.; Matthews, R. S.; Ong, B. S.; Press, J. B.; Rajan Babu, T. V.; Rousseau, G.; Sauter, H. M.; Suzuki, M.; Tatsuta, K.; Tolbert, L. M.; Truesdale,

E. A.; Uchida, I.; Ueda, Y.; Uyehara, T.; Vasella, A. T.; Vladuchick, W. C.; Wade, P. A.; Williams, R. M.; Wong, H. N. C. Asymmetric Total Synthesis of Erythromycin. 2. Synthesis of an Erythronolide A Lactone System. *J Am Chem Soc* **1981**, *103* (11), 3213–3215. https://doi.org/10.1021/ja00401a050.

(67) Grimm, I. H.; Albertson, L.; Francisco, S. Oral Medicine CLINICAL INVESTIGATION IN THE USE OF ERYTHROMYCIN FOR INFECTION OF TEE ORAL CAVITY. *Oral Medicine* **1954**, *7* (8), 858–864.

(68) Nicolaou K C; Yang Z; Liu J J; Ueno H; Nantermet P G; Guy R K; Clalborne C F; Renaud J; Couladouros E A; Paulvannan K; Sorensen E J. Original Taxol Synthesis. *Nature* **1994**, *367*, 630–634.

(69) Marsault, E.; Peterson, M. L. Macrocycles Are Great Cycles: Applications, Opportunities, and Challenges of Synthetic Macrocycles in Drug Discovery. *J Med Chem* **2011**, *54* (7), 1961–2004. https://doi.org/10.1021/jm1012374.

(70) Yu, X.; Sun, D. Macrocyclic Drugs and Synthetic Methodologies toward Macrocycles. *Molecules* **2013**, *18* (6), 6230–6268. https://doi.org/10.3390/molecules18066230.

(71) Wang, L.; Pratt, J. K.; Soltwedel, T.; Sheppard, G. S.; Fidanze, S. D.; Liu, D.; Hasvold, L. A.; Mantei, R. A.; Holms, J. H.; McClellan, W. J.; Wendt, M. D.; Wada, C.; Frey, R.; Hansen, T. M.; Hubbard, R.; Park, C. H.; Li, L.; Magoc, T. J.; Albert, D. H.; Lin, X.; Warder, S. E.; Kovar, P.; Huang, X.; Wilcox, D.; Wang, R.; Rajaraman, G.; Petros, A. M.; Hutchins, C. W.; Panchal, S. C.; Sun, C.; Elmore, S. W.; Shen, Y.; Kati, W. M.; McDaniel, K. F. Fragment-Based, Structure-Enabled Discovery of Novel Pyridones and Pyridone Macrocycles as Potent Bromodomain and Extra-Terminal Domain (BET) Family Bromodomain

Inhibitors. *J Med Chem* **2017**, *60* (9), 3828–3850. https://doi.org/10.1021/acs.jmedchem.7b00017.

(72) Tanada, M.; Tamiya, M.; Matsuo, A.; Chiyoda, A.; Takano, K.; Ito, T.; Irie, M.; Kotake, T.; Takeyama, R.; Kawada, H.; Hayashi, R.; Ishikawa, S.; Nomura, K.; Furuichi, N.; Morita, Y.; Kage, M.; Hashimoto, S.; Nii, K.; Sase, H.; Ohara, K.; Ohta, A.; Kuramoto, S.; Nishimura, Y.; Iikura, H.; Shiraishi, T. Development of Orally Bioavailable Peptides Targeting an Intracellular Protein: From a Hit to a Clinical KRAS Inhibitor. *J Am Chem Soc* **2023**, *145* (30), 16610–16620. https://doi.org/10.1021/jacs.3c03886.

(73) Ball, A. T.; Mohammed, S.; Doigneaux, C.; Gardner, R. M.; Easton, J. W.; Turner, S.; Essex, J. W.; Pairaudeau, G.; Tavassoli, A. Identification and Development of Cyclic Peptide Inhibitors of Hypoxia Inducible Factors 1 and 2 That Disrupt Hypoxia-Response Signaling in Cancer Cells. *J Am Chem Soc* **2024**, *146* (13), 8877–8886. https://doi.org/10.1021/jacs.3c10508.

(74) Leitch, E. K.; Elumalai, N.; Fridén-Saxin, M.; Dahl, G.; Wan, P.; Clarkson, P.; Valeur, E.; Pairaudeau, G.; Boyd, H.; Tavassoli, A. Inhibition of Low-Density Lipoprotein Receptor Degradation with a Cyclic Peptide That Disrupts the Homodimerization of IDOL E3 Ubiquitin Ligase. *Chem Sci* **2018**, *9* (27), 5957–5966. https://doi.org/10.1039/c8sc01186a.

(75) Roskoski, R. Properties of FDA-Approved Small Molecule Protein Kinase Inhibitors. *Pharmacol Res* **2019**, *144*, 19–50. https://doi.org/10.1016/j.phrs.2019.03.006.

(76) Wieske, L. H. E.; Atilaw, Y.; Poongavanam, V.; Erdélyi, M.; Kihlberg, J. Going Viral: An Investigation into the Chameleonic Behaviour of Antiviral Compounds.

Chemistry - A European Journal **2023**, *29* (8). https://doi.org/10.1002/chem.202202798.

(77) Danelius, E.; Poongavanam, V.; Peintner, S.; Wieske, L. H. E.; Erdélyi, M.; Kihlberg, J. Solution Conformations Explain the Chameleonic Behaviour of Macrocyclic Drugs. *Chemistry - A European Journal* **2020**, *26* (23), 5231–5244. https://doi.org/10.1002/chem.201905599.

(78) Brudy, C.; Walz, C.; Spiske, M.; Dreizler, J. K.; Hausch, F. The Missing Link(Er): A Roadmap to Macrocyclization in Drug Discovery. *J Med Chem* **2024**. https://doi.org/10.1021/acs.jmedchem.4c01163.

(79) Degoey, D. A.; Chen, H. J.; Cox, P. B.; Wendt, M. D. Beyond the Rule of 5: Lessons Learned from AbbVie's Drugs and Compound Collection. *J Med Chem* **2018**, *61* (7), 2636–2651. https://doi.org/10.1021/acs.jmedchem.7b00717.

(80) Ohta, A.; Tanada, M.; Shinohara, S.; Morita, Y.; Nakano, K.; Yamagishi, Y.; Takano, R.; Kariyuki, S.; Iida, T.; Matsuo, A.; Ozeki, K.; Emura, T.; Sakurai, Y.; Takano, K.; Higashida, A.; Kojima, M.; Muraoka, T.; Takeyama, R.; Kato, T.; Kimura, K.; Ogawa, K.; Ohara, K.; Tanaka, S.; Kikuchi, Y.; Hisada, N.; Hayashi, R.; Nishimura, Y.; Nomura, K.; Tachibana, T.; Irie, M.; Kawada, H.; Torizawa, T.; Murao, N.; Kotake, T.; Tanaka, M.; Ishikawa, S.; Miyake, T.; Tamiya, M.; Arai, M.; Chiyoda, A.; Akai, S.; Sase, H.; Kuramoto, S.; Ito, T.; Shiraishi, T.; Kojima, T.; Iikura, H. Validation of a New Methodology to Create Oral Drugs beyond the Rule of 5 for Intracellular Tough Targets. *J Am Chem Soc* **2023**, *145* (44), 24035–24051. https://doi.org/10.1021/jacs.3c07145.

(81) Gerona-Navarro, G.; Yoel-Rodríguez; Mujtaba, S.; Frasca, A.; Patel, J.; Zeng, L.; Plotnikov, A. N.; Osman, R.; Zhou, M. M. Rational Design of Cyclic Peptide

Modulators of the Transcriptional Coactivator CBP: A New Class of P53 Inhibitors. *J Am Chem Soc* **2011**, *133* (7), 2040–2043. https://doi.org/10.1021/ja107761h.

(82) Wang, X.; Chen, X.; Chen, Z.; Xu, W.; Lai, R.; Qiu, X.; Zeng, Z.; Wang, C.; Wang, Z.; Wang, J. Integrated Anchored Stapling and Hierarchical Dynamics: MSICDA-Driven CREBBP Bromodomain Inhibition. *J Chem Inf Model* **2024**, *64* (12), 4739–4758. https://doi.org/10.1021/acs.jcim.4c00381.

(83) Bastos, M.; Abian, O.; Johnson, C. M.; Ferreira-da-Silva, F.; Vega, S.; Jimenez-Alesanco, A.; Ortega-Alarcon, D.; Velazquez-Campoy, A. Isothermal Titration Calorimetry. *Nature Reviews Methods Primers* **2023**, *3* (1). https://doi.org/10.1038/s43586-023-00199-x.

(84) Thomas, A. M.; Serafini, M.; Grant, E. K.; Coombs, E. A. J.; Bluck, J. P.; Schiedel, M.; McDonough, M. A.; Reynolds, J. K.; Lee, B.; Platt, M.; Sharlandjieva, V.; Biggin, P. C.; Duarte, F.; Milne, T. A.; Bush, J. T.; Conway, S. J. Mutate and Conjugate: A Method to Enable Rapid In-Cell Target Validation. *ACS Chem Biol* **2023**, *18* (11), 2405–2417. https://doi.org/10.1021/acschembio.3c00437.

(85) Jennings, L. E.; Schiedel, M.; Hewings, D. S.; Picaud, S.; Laurin, C. M. C.; Bruno, P. A.; Bluck, J. P.; Scorah, A. R.; See, L.; Reynolds, J. K.; Moroglu, M.; Mistry, I. N.; Hicks, A.; Guzanov, P.; Clayton, J.; Evans, C. N. G.; Stazi, G.; Biggin, P. C.; Mapp, A. K.; Hammond, E. M.; Humphreys, P. G.; Filippakopoulos, P.; Conway, S. J. BET Bromodomain Ligands: Probing the WPF Shelf to Improve BRD4 Bromodomain Affinity and Metabolic Stability. *Bioorg Med Chem* **2018**, *26* (11), 2937–2957. https://doi.org/10.1016/j.bmc.2018.05.003.

(86) Fabian, M. A.; Biggs, W. H.; Treiber, D. K.; Atteridge, C. E.; Azimioara, M. D.; Benedetti, M. G.; Carter, T. A.; Ciceri, P.; Edeen, P. T.; Floyd, M.; Ford, J. M.; Galvin, M.; Gerlach, J. L.; Grotzfeld, R. M.; Herrgard, S.; Insko, D. E.; Insko, M. A.; Lai, A. G.; Lélias, J. M.; Mehta, S. A.; Milanov, Z. V.; Velasco, A. M.; Wodicka, L. M.; Patel, H. K.; Zarrinkar, P. P.; Lockhart, D. J. A Small Molecule-Kinase Interaction Map for Clinical Kinase Inhibitors. *Nat Biotechnol* **2005**, *23* (3), 329–336. https://doi.org/10.1038/nbt1068.

(87) Driggers, E. M.; Hale, S. P.; Lee, J.; Terrett, N. K. The Exploration of Macrocycles for Drug Discovery - An Underexploited Structural Class. *Nature Reviews Drug Discovery*. July 2008, pp 608–624. https://doi.org/10.1038/nrd2590.

(88) Moroglu, M. Development of Small Molecule CREBBP Bromodomain Ligands Using Medicinal Chemistry-Based Approaches. DPhil in Organic Chemistry , University of Oxford , Oxford, 2019.

(89) Usanov, D. L.; Chan, A. I.; Maianti, J. P.; Liu, D. R. Second-Generation DNA-Templated Macrocycle Libraries for the Discovery of Bioactive Small Molecules. *Nat Chem* **2018**, *10* (7), 704–714. https://doi.org/10.1038/s41557-018-0033-8.

(90) Cummings, M. D.; Sekharan, S. Structure-Based Macrocycle Design in Small-Molecule Drug Discovery and Simple Metrics to Identify Opportunities for Macrocyclization of Small-Molecule Ligands. *Journal of Medicinal Chemistry*. American Chemical Society August 8, 2019, pp 6843–6853. https://doi.org/10.1021/acs.jmedchem.8b01985.

(91) Diao, Y.; Liu, D.; Ge, H.; Zhang, R.; Jiang, K.; Bao, R.; Zhu, X.; Bi, H.; Liao, W.; Chen, Z.; Zhang, K.; Wang, R.; Zhu, L.; Zhao, Z.; Hu, Q.; Li, H. Macrocyclization of Linear Molecules by Deep Learning to Facilitate Macrocyclic Drug Candidates

Discovery. *Nat Commun* **2023**, *14* (1). https://doi.org/10.1038/s41467-023-40219-8.

(92) Darlami, O.; Pun, R.; Ahn, S. H.; Kim, S. H.; Shin, D. Macrocyclization Strategy for Improving Candidate Profiles in Medicinal Chemistry. *European Journal of Medicinal Chemistry*. Elsevier Masson s.r.l. June 5, 2024. https://doi.org/10.1016/j.ejmech.2024.116501.

(93) Patschinski, P.; Zhang, C.; Zipse, H. The Lewis Base-Catalyzed Silylation of Alcohols-a Mechanistic Analysis. *Journal of Organic Chemistry* **2014**, *79* (17), 8348–8357. https://doi.org/10.1021/jo5016568.

(94) Cunico, R. F.; Bedell, L. The Triisopropylsilyl Group as a Hydroxyl-Protecting Function. *Journal of Organic Chemistry*. 1980, pp 4797–4798. https://doi.org/10.1021/jo01311a058.

(95) Zhao, Y.; Snieckus, V. A Practical in Situ Generation of the Schwartz Reagent. Reduction of Tertiary Amides to Aldehydes and Hydrozirconation. *Org Lett* **2014**, *16* (2), 390–393. https://doi.org/10.1021/ol403183a.

(96) Trost, B. M.; Hung, C. I.; Koester, D. C.; Miller, Y. Development of Non-C2-Symmetric ProPhenol Ligands. the Asymmetric Vinylation of N-Boc Imines. *Org Lett* **2015**, *17* (15), 3778–3781. https://doi.org/10.1021/acs.orglett.5b01755.

(97) Luyben, W. L. Temperature Setpoint-Ramp Control Structure for Batch Reactors. *Chem Eng Sci* **2019**, *208*. https://doi.org/10.1016/j.ces.2019.07.042.

(98) Dueno, E. E. Cesium Promoted O-Alkylation of Alcohols for the Efficient Ether Synthesis. *Tetrahedron Lett* **1999**, *40*, 1843–1846.

(99) Parrish, J. P.; Sudaresan, B.; Jung, K. W. Improved Cs2CO3 Promoted O-Alkylation of Phenols. *Synth Commun* **1999**, *29* (24), 4423–4431. https://doi.org/10.1080/00397919908086606.

(100) Salvatore, R. N.; Seung Il Shin; Nagle, A. S.; Kyung Woon Jung. Efficient Carbamate Synthesis via a Three-Component Coupling of an Amine, CO2, and Alkyl Halides in the Presence of Cs2CO3 and Tetrabutylammonium Iodide. *Journal of Organic Chemistry* **2001**, *66* (3), 1035–1037. https://doi.org/10.1021/jo001140u.

(101) Zhu, Z.; Colbry, N. L.; Lovdahl, M.; Mennen, K. E.; Acciacca, A.; Beylin, V. G.; Clark, J. D.; Belmont, D. T. Practical Alternative Synthesis of 1-(8-Fluoro-Naphthalen-1-Yl)Piperazine. *Org Process Res Dev* **2007**, *11* (5), 907–909. https://doi.org/10.1021/op7001535.

(102) Coste, J.; Lenguyen, D.; Castro, B. PyBOP@: A NEW PEPTIDE COUPLING REAGENT DEVOID OF TOXIC BY-PRODUCT. *Tetrahedron Lett* **1999**, *31* (2), 205–208.

(103) El-Faham, A.; Albericio, F. COMU: A Third Generation of Uronium-Type Coupling Reagents. *Journal of Peptide Science* **2010**, *16* (1), 6–9. https://doi.org/10.1002/psc.1204.

(104) Leas, D. A.; Wu, J.; Ezell, E. L.; Garrison, J. C.; Vennerstrom, J. L.; Dong, Y. Formation of 2-Imino Benzo[e]-1,3-Oxazin-4-Ones from Reactions of Salicylic Acids and Anilines with HATU: Mechanistic and Synthetic Studies. *ACS Omega* **2018**, *3* (1), 781–787. https://doi.org/10.1021/acsomega.7b01824.

(105) Beutner, G. L.; Young, I. S.; Davies, M. L.; Hickey, M. R.; Park, H.; Stevens, J. M.; Ye, Q. TCFH-NMI: Direct Access to N-Acyl Imidazoliums for Challenging

Amide Bond Formations. *Org Lett* **2018**, *20* (14), 4218–4222. https://doi.org/10.1021/acs.orglett.8b01591.

(106) Luis, N. R.; Chung, K. K.; Hickey, M. R.; Lin, Z.; Beutner, G. L.; Vosburg, D. A. Beyond Amide Bond Formation: TCFH as a Reagent for Esterification. *Org Lett* **2024**, *26* (14), 2745–2750. https://doi.org/10.1021/acs.orglett.3c01611.

(107) Shome, A.; Jha, K. T.; Chawla, P. A. Hexafluorophosphate Azabenzotriazole Tetramethyl Uronium (HATU): A Unique Cross-Coupling Reagent. *SynOpen* **2023**, *7* (4), 566–569. https://doi.org/10.1055/s-0042-1751499.

(108) König, W.; Geiger, R. Eine Neue Methode Zur Synthese von Peptiden: Aktivierung Der Carboxylgruppe Mit Dicyclohexylcarbodiimid Unter Zusatz von 1-Hydroxy-benzotriazolen. *Chem Ber* **1970**, *103* (3), 788–798. https://doi.org/10.1002/cber.19701030319.

(109) Pottorf, R. S.; Szeto, P. 1-Ethyl-3-(3′-Dimethylaminopropyl)Carbodiimide Hydrochloride. In *Encyclopedia of Reagents for Organic Synthesis*; John Wiley & Sons, Ltd, 2001. https://doi.org/10.1002/047084289x.re062.

(110) Xu, H.; Luo, G.; Wu, T.; Hu, J.; Wang, C.; Wu, X.; Zhang, Y.; Xu, Y.; Xiang, Q. Structural Insights Revealed by the Cocrystal Structure of CCS1477 in Complex with CBP Bromodomain. *Biochem Biophys Res Commun* **2022**, *623*, 17–22. https://doi.org/10.1016/j.bbrc.2022.07.021.

(111) Nicosia, L.; Spencer, G. J.; Brooks, N.; Amaral, F. M. R.; Basma, N. J.; Chadwick, J. A.; Revell, B.; Wingelhofer, B.; Maiques-Diaz, A.; Sinclair, O.; Camera, F.; Ciceri, F.; Wiseman, D. H.; Pegg, N.; West, W.; Knurowski, T.; Frese, K.; Clegg, K.; Campbell, V. L.; Cavet, J.; Copland, M.; Searle, E.; Somervaille, T. C. P. Therapeutic Targeting of EP300/CBP by Bromodomain Inhibition in Hematologic

Malignancies. *Cancer Cell* **2023**, *41* (12), 2136-2153.e13. https://doi.org/10.1016/j.ccell.2023.11.001.

(112) Liu, C.-Y. *HISTIDINE AS THE FUNCTIONAL GROUP FOR A CHELATING ION EXCHANGER*; Elsevier Science Publishers B.V, 1987; Vol. 192.

(113) Repo, E.; Kurniawan, T. A.; Warchol, J. K.; Sillanpää, M. E. T. Removal of Co(II) and Ni(II) Ions from Contaminated Water Using Silica Gel Functionalized with EDTA and/or DTPA as Chelating Agents. *J Hazard Mater* **2009**, *171* (1–3), 1071–1080. https://doi.org/10.1016/j.jhazmat.2009.06.111.

(114) Weber, P. C.; Wendoloski, J. J.; Pantoliano, M. W.; Salemme1, F. R. *Crystallographic and Thermodynamic Comparison of Natural and Synthetic Ligands Bound to Streptavidin*; 1992; Vol. 114. https://pubs.acs.org/sharingguidelines.

(115) Khake, S. M.; Chatani, N. Chelation-Assisted Nickel-Catalyzed C−H Functionalizations. *Trends in Chemistry*. Cell Press August 1, 2019, pp 524–539. https://doi.org/10.1016/j.trechm.2019.06.002.

(116) Singleton, D. A.; Hang, C.; Szymanski, M. J.; Meyer, M. P.; Leach, A. G.; Kuwata, K. T.; Chen, J. S.; Greer, A.; Foote, C. S.; Houk, K. N. Mechanism of Ene Reactions of Singlet Oxygen. A Two-Step No-Intermediate Mechanism. *J Am Chem Soc* **2003**, *125* (5), 1319–1328. https://doi.org/10.1021/ja027225p.

(117) Tannous, R.; Shelef, O.; Gutkin, S.; David, M.; Leirikh, T.; Ge, L.; Jaber, Q.; Zhou, Q.; Ma, P.; Fridman, M.; Spitz, U.; Houk, K. N.; Shabat, D. Spirostrain-Accelerated Chemiexcitation of Dioxetanes Yields Unprecedented Detection Sensitivity in Chemiluminescence Bioassays. *ACS Cent Sci* **2024**, *10* (1), 28–42. https://doi.org/10.1021/acscentsci.3c01141.

(118) Yardimci, Ş. D.; Kaya, N.; Balci, M. Regioselectivity in the Ene-Reaction of Singlet Oxygen with Cyclic Alkenes: Photooxygenation of Methyl-Substituted 1,4-Cyclohexadiene Derivatives. *Tetrahedron* **2006**, *62* (46), 10633–10638. https://doi.org/10.1016/j.tet.2006.07.103.

(119) Monsour, C. G.; Tadle, A. C.; Tafolla-Aguirre, B. J.; Lakshmanan, N.; Yoon, J. H.; Sabio, R. B.; Selke, M. Singlet Oxygen Quenching by Resveratrol Derivatives†. *Photochem Photobiol* **2023**, *99* (2), 672–679. https://doi.org/10.1111/php.13704.

(120) Smith-2002-Kinetic-Evidence-for-Both-Quenching-and-Reaction-of-Singlet-Oxygen-with-Triethylamine-in-Pyridine-Solution.

(121) Peres, P. S.; Valerio, A.; Cadena, S. M. S. C.; Winnischofer, S. M. B.; Scalfo, A. C.; Di Mascio, P.; Martinez, G. R. Glutathione Modifies the Oxidation Products of 2′-Deoxyguanosine by Singlet Molecular Oxygen. *Arch Biochem Biophys* **2015**, *586*, 33–44. https://doi.org/10.1016/j.abb.2015.09.020.

(122) Wendel, M.; Nizinski, S.; Gierszewski, M.; Prukala, D.; Sikorski, M.; Starzak, K.; Wybraniec, S.; Burdzinski, G. Chemical Quenching of Singlet Oxygen by Betanin. *Photochemical and Photobiological Sciences* **2016**, *15* (7), 872–878. https://doi.org/10.1039/c6pp00037a.

(123) Xiang, Q.; Wang, C.; Wu, T.; Zhang, C.; Hu, Q.; Luo, G.; Hu, J.; Zhuang, X.; Zou, L.; Shen, H.; Wu, X.; Zhang, Y.; Kong, X.; Liu, J.; Xu, Y. Design, Synthesis, and Biological Evaluation of 1-(Indolizin-3-Yl)Ethan-1-Ones as CBP Bromodomain Inhibitors for the Treatment of Prostate Cancer. *J Med Chem* **2022**, *65* (1), 785–810. https://doi.org/10.1021/acs.jmedchem.1c01864.

(124) Hammitzsch, A.; Tallant, C.; Fedorov, O.; O'Mahony, A.; Brennan, P. E.; Hay, D. A.; Martinez, F. O.; Al-Mossawi, M. H.; De Wit, J.; Vecellio, M.; Wells, C.;

Wordsworth, P.; Müller, S.; Knapp, S.; Bowness, P. CBP30, a Selective CBP/P300 Bromodomain Inhibitor, Suppresses Human Th17 Responses. *Proc Natl Acad Sci U S A* **2015**, *112* (34), 10768–10773. https://doi.org/10.1073/pnas.1501956112.

(125) Chen, P.; Chaikuad, A.; Bamborough, P.; Bantscheff, M.; Bountra, C.; Chung, C. W.; Fedorov, O.; Grandi, P.; Jung, D.; Lesniak, R.; Lindon, M.; Müller, S.; Philpott, M.; Prinjha, R.; Rogers, C.; Selenski, C.; Tallant, C.; Werner, T.; Willson, T. M.; Knapp, S.; Drewry, D. H. Discovery and Characterization of GSK2801, a Selective Chemical Probe for the Bromodomains BAZ2A and BAZ2B. *J Med Chem* **2016**, *59* (4), 1410–1424. https://doi.org/10.1021/acs.jmedchem.5b00209.

(126) Taylor, A. M.; Bailey, C.; Belmont, L. D.; Campbell, R.; Cantone, N.; Côté, A.; Crawford, T. D.; Cummings, R.; Dement, K.; Duplessis, M.; Flynn, M.; Good, A. C.; Huang, H. R.; Joshi, S.; Leblanc, Y.; Murray, J.; Nasveschuk, C. G.; Neiss, A.; Poy, F.; Romero, F. A.; Sandy, P.; Tang, Y.; Tsui, V.; Zawadzke, L.; Sims, R. J.; Audia, J. E.; Bellon, S. F.; Magnuson, S. R.; Albrecht, B. K.; Cochran, A. G. GNE-064: A Potent, Selective, and Orally Bioavailable Chemical Probe for the Bromodomains of SMARCA2 and SMARCA4 and the Fifth Bromodomain of PBRM1. *J Med Chem* **2022**, *65* (16), 11177–11186. https://doi.org/10.1021/acs.jmedchem.2c00662.

(127) Meslamani, J.; Smith, S. G.; Sanchez, R.; Zhou, M. M. Structural Features and Inhibitors of Bromodomains. *Drug Discovery Today: Technologies*. Elsevier Ltd March 1, 2016, pp 3–15. https://doi.org/10.1016/j.ddtec.2016.09.001.

(128) Hill, A. P.; Young, R. J. Getting Physical in Drug Discovery: A Contemporary Perspective on Solubility and Hydrophobicity. *Drug Discov Today* **2010**, *15* (15–16), 648–655. https://doi.org/10.1016/j.drudis.2010.05.016.

(129) Bronner, S. M.; Murray, J.; Romero, F. A.; Lai, K. W.; Tsui, V.; Cyr, P.; Beresini, M. H.; De Leon Boenig, G.; Chen, Z.; Choo, E. F.; Clark, K. R.; Crawford, T. D.; Jayaram, H.; Kaufman, S.; Li, R.; Li, Y.; Liao, J.; Liang, X.; Liu, W.; Ly, J.; Maher, J.; Wai, J.; Wang, F.; Zheng, A.; Zhu, X.; Magnuson, S. A Unique Approach to Design Potent and Selective Cyclic Adenosine Monophosphate Response Element Binding Protein, Binding Protein (CBP) Inhibitors. *J Med Chem* **2017**, *60* (24), 10151–10171. https://doi.org/10.1021/acs.jmedchem.7b01372.

(130) Fedorov, O.; Lingard, H.; Wells, C.; Monteiro, O. P.; Picaud, S.; Keates, T.; Yapp, C.; Philpott, M.; Martin, S. J.; Felletar, I.; Marsden, B. D.; Filippakopoulos, P.; Müller, S.; Knapp, S.; Brennan, P. E. [1,2,4]Triazolo[4,3-a]Phthalazines: Inhibitors of Diverse Bromodomains. *J Med Chem* **2014**, *57* (2), 462–476. https://doi.org/10.1021/jm401568s.

(131) Vermeulen, E. S.; Van Smeden, M.; Schmidt, A. W.; Sprouse, J. S.; Wikström, H. V.; Grol, C. J. Novel 5-HT7 Receptor Inverse Agonists. Synthesis and Molecular Modeling of Arylpiperazine- and 1,2,3,4-Tetrahydroisoquinoline-Based Arylsulfonamides. *J Med Chem* **2004**, *47* (22), 5451–5466. https://doi.org/10.1021/jm049743b.

(132) Romero, A. F.; Magnuson, S.; Pastor, R.; Tsui, V. H.-W.; Murray, J.; Crawford, T.; Albrecht, B. K.; Cote, A.; Taylor, A. M.; Lai, K. W.; Chen, K. X.; Bronner, S.; Alder, M.; Egen, J.; Liao, J.; Wang, F.; Cyr, P.; Zhu, B.-Y.; Kauder, S. WO2016086200A1_Original_document_20240717115413. WO 2016/086200

A1, June 2, 2016. https://worldwide.espacenet.com/patent/search/family/055024234/publication/WO2016086200A1?q=pn%3DWO2016086200 (accessed 2024-07-17).

(133) Fujita, K. I.; Kitatsuji, C.; Furukawa, S.; Yamaguchi, R. Regio- and Chemoselective Transfer Hydrogenation of Quinolines Catalyzed by a Cp*Ir Complex. *Tetrahedron Lett* **2004**, *45* (16), 3215–3217. https://doi.org/10.1016/j.tetlet.2004.02.123.

(134) Cui, M.; Wang, X.; Yu, P.; Zhang, J.; Li, Z.; Zhang, X.; Yang, Y.; Ono, M.; Jia, H.; Saji, H.; Liu, B. Synthesis and Evaluation of Novel 18f Labeled 2-Pyridinylbenzoxazole and 2-Pyridinylbenzothiazole Derivatives as Ligands for Positron Emission Tomography (PET) Imaging of β-Amyloid Plaques. *J Med Chem* **2012**, *55* (21), 9283–9296. https://doi.org/10.1021/jm300973k.

(135) Xia, Y.; Yu, M.; Zhao, Y.; Xia, L.; Huang, Y.; Sun, N.; Song, M.; Guo, H.; Zhang, Y.; Zhu, D.; Xie, Q.; Wang, Y. Discovery of Tetrahydroquinolines and Benzomorpholines as Novel Potent RORγt Agonists. *Eur J Med Chem* **2021**, *211*. https://doi.org/10.1016/j.ejmech.2020.113013.

(136) Mecozzi, S.; West, A. P.; Dougherty, D. A.; Beckman, M. ComprehensiVe Supramolecular Chemistry; Lehn. *J. Am. Chem. Soc* **1996**, *118* (3), 2307–2308.

(137) Wheeler, S. E.; Houk, K. N. Substituent Effects in Cation/π Interactions and Electrostatic Potentials above the Centers of Substituted Benzenes Are Due Primarily to through-Space Effects of the Substituents. *J Am Chem Soc* **2009**, *131* (9), 3126–3127. https://doi.org/10.1021/ja809097r.

(138) Young, R. J.; Green, D. V. S.; Luscombe, C. N.; Hill, A. P. Getting Physical in Drug Discovery II: The Impact of Chromatographic Hydrophobicity

Measurements and Aromaticity. *Drug Discov Today* **2011**, *16* (17–18), 822–830. https://doi.org/10.1016/j.drudis.2011.06.001.

(139) Kansy, M.; Senner, F.; Gubernator, K. Communications to the Editor Physicochemical High Throughput Screening: Parallel Artificial Membrane Permeation Assay in the Description of Passive Absorption Processes. *Journal of Medicinal Chemistry* **1998**, *41*, 1007–1010.

(140) Robinson, M. W.; Hill, A. P.; Readshaw, S. A.; Hollerton, J. C.; Upton, R. J.; Lynn, S. M.; Besley, S. C.; Boughtflower, B. J. Use of Calculated Physicochemical Properties to Enhance Quantitative Response When Using Charged Aerosol Detection. *Anal Chem* **2017**, *89* (3), 1772–1777. https://doi.org/10.1021/acs.analchem.6b04060.

(141) Wuts, P. G. M.; Greene, T. W. *Greene's Protective Groups in Organic Synthesis*; Wiley: New York, 2006. https://doi.org/10.1002/0470053488.

(142) Tamboli, Y.; Kashid, B. B.; Yadav, R. P.; Rafeeq, M.; Yeole, R.; Merwade, A. Y. Triphenylphosphine Oxide Removal from Reactions: The Role of Solvent and Temperature. *ACS Omega* **2021**, *6* (21), 13940–13945. https://doi.org/10.1021/acsomega.1c01996.

(143) Hergueta, A. R. Easy Removal of Triphenylphosphine Oxide from Reaction Mixtures by Precipitation with CaBr2. *Organic Process Research and Development*. American Chemical Society June 17, 2022, pp 1845–1853. https://doi.org/10.1021/acs.oprd.2c00104.

(144) Batesky, D. C.; Goldfogel, M. J.; Weix, D. J. Removal of Triphenylphosphine Oxide by Precipitation with Zinc Chloride in Polar Solvents. *Journal of Organic Chemistry* **2017**, *82* (19), 9931–9936. https://doi.org/10.1021/acs.joc.7b00459.

(145) Paterson, I.; De Savi, C.; Tudge, M. Total Synthesis of the Microtubule-Stabilizing Agent (-)-Laulimalide. *Org Lett* **2001**, *3* (20), 3149–3152. https://doi.org/10.1021/ol010150u.

(146) Hansen, J. G.; Feeder, N.; Hamilton, D. G.; Gunter, M. J.; Becher, J.; Sanders, J. K. M. Macrocyclization and Molecular Interlocking via Mitsunobu Alkylation: Highlighting the Role of C-H···O Interactions in Templating. *Org Lett* **2000**, *2* (4), 449–452. https://doi.org/10.1021/ol991289w.

(147) Hagiya, K.; Muramoto, N.; Misaki, T.; Sugimura, T. DMEAD: A New Dialkyl Azodicarboxylate for the Mitsunobu Reaction. *Tetrahedron* **2009**, *65* (31), 6109–6114. https://doi.org/10.1016/j.tet.2009.05.048.

(148) Saridakis, I.; Kaiser, D.; Maulide, N. Unconventional Macrocyclizations in Natural Product Synthesis. *ACS Cent Sci* **2020**, *6* (11), 1869–1889. https://doi.org/10.1021/acscentsci.0c00599.

(149) ROMERO, A. F.; MAGNUSON, S.; PASTOR, R.; TSUI, V. H.-W.; MURRAY, J.; CRAWFORD, T.; ALBRECHT, B. K.; COTE, A.; TAYLOR, A. M.; LAI, K. W.; CHEN, K. X.; BRONNER, S.; ADLER, M.; EGEN, J.; LIAO, J.; WANG, F.; CYR, P.; ZHU, B.-Y.; KAUDER, S. 4,5,6,7-TETRAHYDRO-1 H-PYRAZOLO[4,3-C]PYRIDIN-3-AMINE COMPOUNDS AS CBP AND/OR EP300 INHIBITORS. WO2016086200A1, June 2, 2016.

(150) Veber, D. F.; Johnson, S. R.; Cheng, H. Y.; Smith, B. R.; Ward, K. W.; Kopple, K. D. Molecular Properties That Influence the Oral Bioavailability of Drug Candidates. *J Med Chem* **2002**, *45* (12), 2615–2623. https://doi.org/10.1021/jm020017n.

(151) ra Valkó, K.; Bevan, C.; Reynolds, D. VCH: Weinheim, 1996. (8) Hansch, C.; Leo, A. MedChem Database; Medicinal Chemistry Project. *Anal Chem* **1997**, *69*, 2022–2029.

(152) Valko, K.; Nunhuck, S.; Bevan, C.; Abraham, M. H.; Reynolds, D. P. Fast Gradient HPLC Method to Determine Compounds Binding to Human Serum Albumin. Relationships with Octanol/Water and Immobilized Artificial Membrane Lipophilicity. *J Pharm Sci* **2003**, *92* (11), 2236–2248. https://doi.org/10.1002/jps.10494.

(153) Valko, K.; Du, C. M.; Bevan, C. D.; Reynolds, D. P.; Abraham, M. H. Rapid-Gradient HPLC Method for Measuring Drug Interactions with Immobilized Artificial Membrane: Comparison with Other Lipophilicity Measures. *J Pharm Sci* **2000**, *89* (8), 1085–1096. https://doi.org/10.1002/1520-6017(200008)89:8<1085::AID-JPS13>3.0.CO;2-N.

(154) Cao, Q.; Howard, J. L.; Wheatley, E.; Browne, D. L. Mechanochemical Activation of Zinc and Application to Negishi Cross-Coupling. *Angewandte Chemie* **2018**, *130* (35), 11509–11513. https://doi.org/10.1002/ange.201806480.

(155) Majid, T. N.; Chang, M.; Yeh, P.; Knochel, P. *Svnthesis and Reactivitv of &en-Chain and Cwlic 2-Cvano Zinc and Comer Organometallics*; 1989; Vol. 30.

(156) Hannick, S. M.; Kishi, Y. Improved Procedure for the Blaise Reaction: A Short, Practical Route to the Key Intermediates of the Saxitoxin Synthesis. *Journal of Organic Chemistry* **1983**, *48* (21), 3833–3835. https://doi.org/10.1021/jo00169a053.

(157) Pangborn, A. B.; Giardello, M. A.; Grubbs, R. H.; Rosen, R. K.; Timmers, F. J.; Beckman, M. Safe and Convenient Procedure for Solvent Purification. *Organometallics* **1996**, *15* (5), 1518–1520.

(158) Fulmer, G. R.; Miller, A. J. M.; Sherden, N. H.; Gottlieb, H. E.; Nudelman, A.; Stoltz, B. M.; Bercaw, J. E.; Goldberg, K. I. NMR Chemical Shifts of Trace Impurities: Common Laboratory Solvents, Organics, and Gases in Deuterated Solvents Relevant to the Organometallic Chemist. *Organometallics* **2010**, *29* (9), 2176–2179. https://doi.org/10.1021/om100106e.

(159) Davies, S. G.; Mulvaney, A. W.; Russell, A. J.; Smith, A. D. Parallel Synthesis of Homochiral β-Amino Acids. *Tetrahedron Asymmetry* **2007**, *18* (13), 1554–1566. https://doi.org/10.1016/j.tetasy.2007.06.008.

Appendix

Appendix A: Plasmid structures of both the CBP^{BRD} and BRD4(1) domains

H_6-CREBBP BRD (1081…1197aa) sequence:
MHHHHHHSSGVDLGTENLYFQSMRKKIFKPEELRQALMPTLEALYRQDPESLPFRQP
VDPQLLGIPDYFDIVKNPMDLSTIKRKLDTGQYQEPWQYVDDVWLMFNNAWLYNRKT
SRVYKFCSKLAEVFEQEIDPVMQSLG
Plasmid: CREBBP (addgene #38977)
Vector backbone: pNIC28-Bsa4 (addgene #26103)

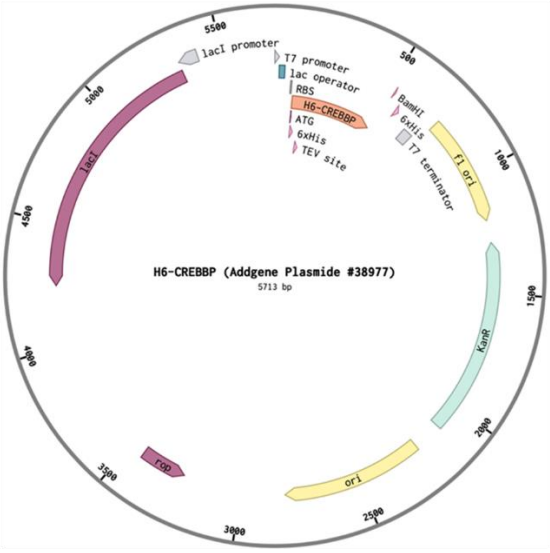

H_6-BRD4(1) (44…168aa) sequence
MHHHHHHSSGVDLGTENLYFQSMNPPPPETSNPNKPKRQTNQLQYLLRVVLKTLWKH
QFAWPFQQPVDAVKLNLPDYYKIIKTPMDMGTIKKRLENNYYWNAQECIQDFNTMFT
NCYIYNKPGDDIVLMAEALEKLFLQKINELPTEE
Plasmid: BRD4(1) (addgene #38942)
Vector backbone: pNIC28-Bsa4 (addgene #26103)

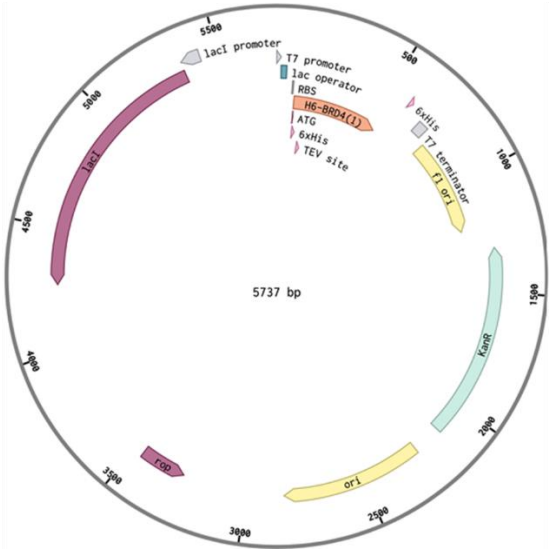

Appendix A: A visual representation of the plasmid cloning and expression vector, pNIC28-Bsa4, which is drawn to scale. The vector contains in-frame hexa-histidine (His6) codons, located directly after the initiation start (ATG), for protein purification by immobilized metal affinity chromatography. The T7promoter is used for transcribing target gene. Protein expression can be initiated by addition of IPTG (isopropyl β-D-1-thiogalactopyranoside), which removes transcriptional repression exerted by the LacI repressor (encoded by the constitutively expressed *lacI* gene). The locations of TEV site (protease cleavage site for removal of the His6 tag) are indicated.

Appendix B: Protein gels and MS data after purification for CBP^{BRD} and BRD4(1)

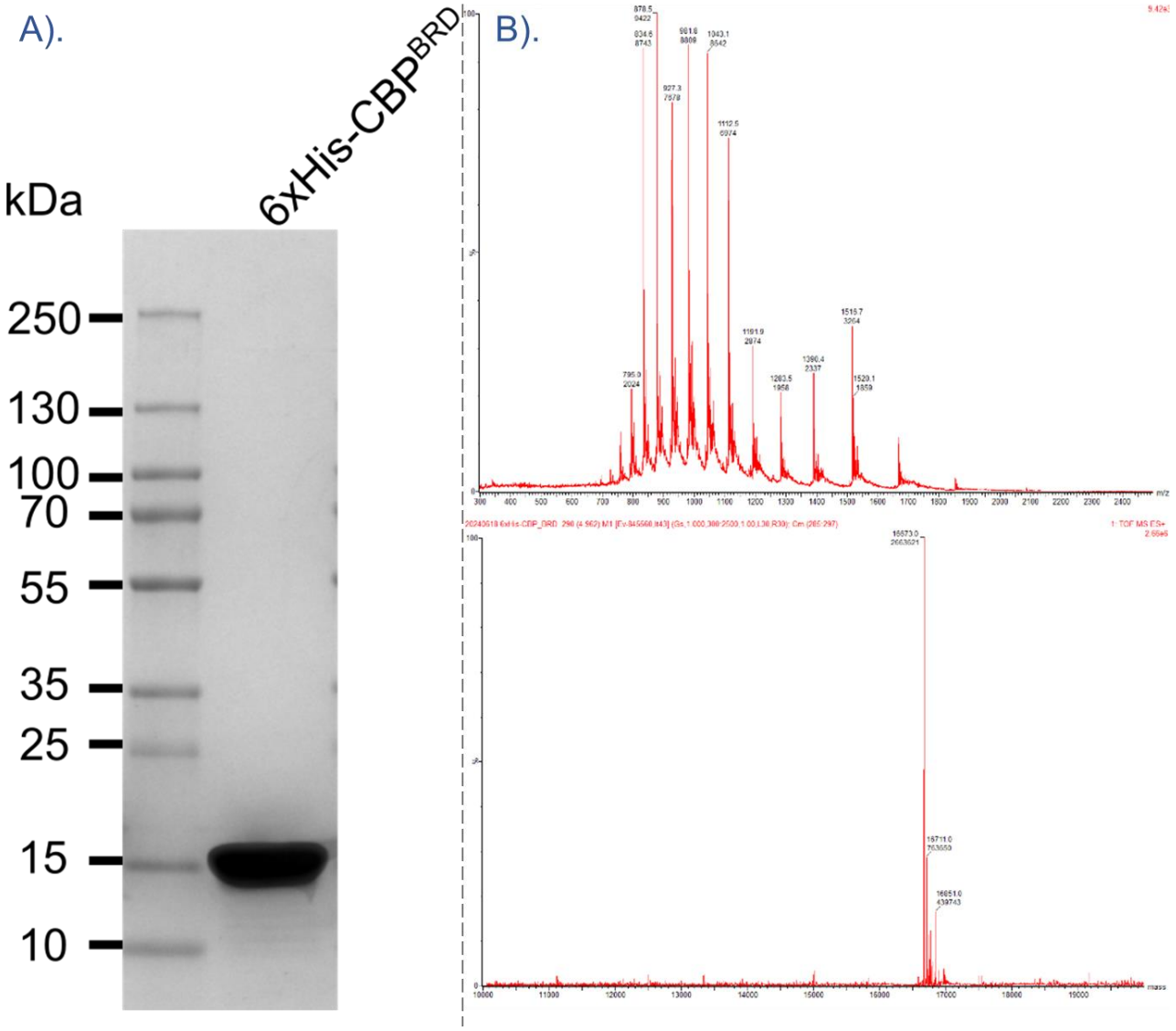

Appendix B Figure 1: Analysis of purified H_6-CBP^{BRD} (1081…1197aa); A). Imaged gel of purified H_6-CBP^{BRD} and page rule prestained protein ladder demonstrating protein mass; B). raw MS data of CBP^{BRD} analysed by LC-MS(TOF) (top) and the deconvoluted MS between 10 kDa and 20 kDA showing the protein mass of 16673 Da.

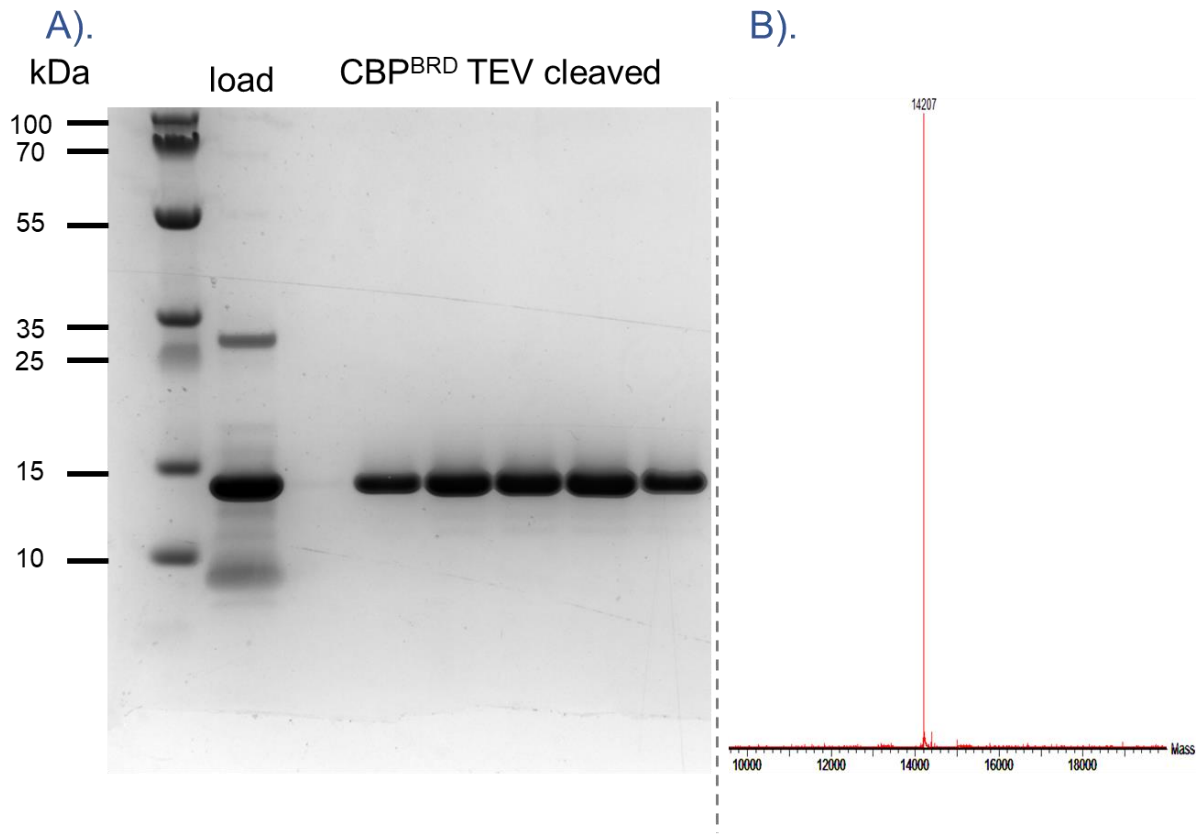

Appendix B Figure 2: Analysis of purified CBP^{BRD} post TEV cleavage; A). Imaged gel of purified CBP^{BRD} and page rule prestained protein ladder demonstrating protein mass; B). deconvoluted MS of CBP^{BRD} purified after TEV site cleavage analysed by LC-MS(TOF), demonstrating the mass of 14207 Da.

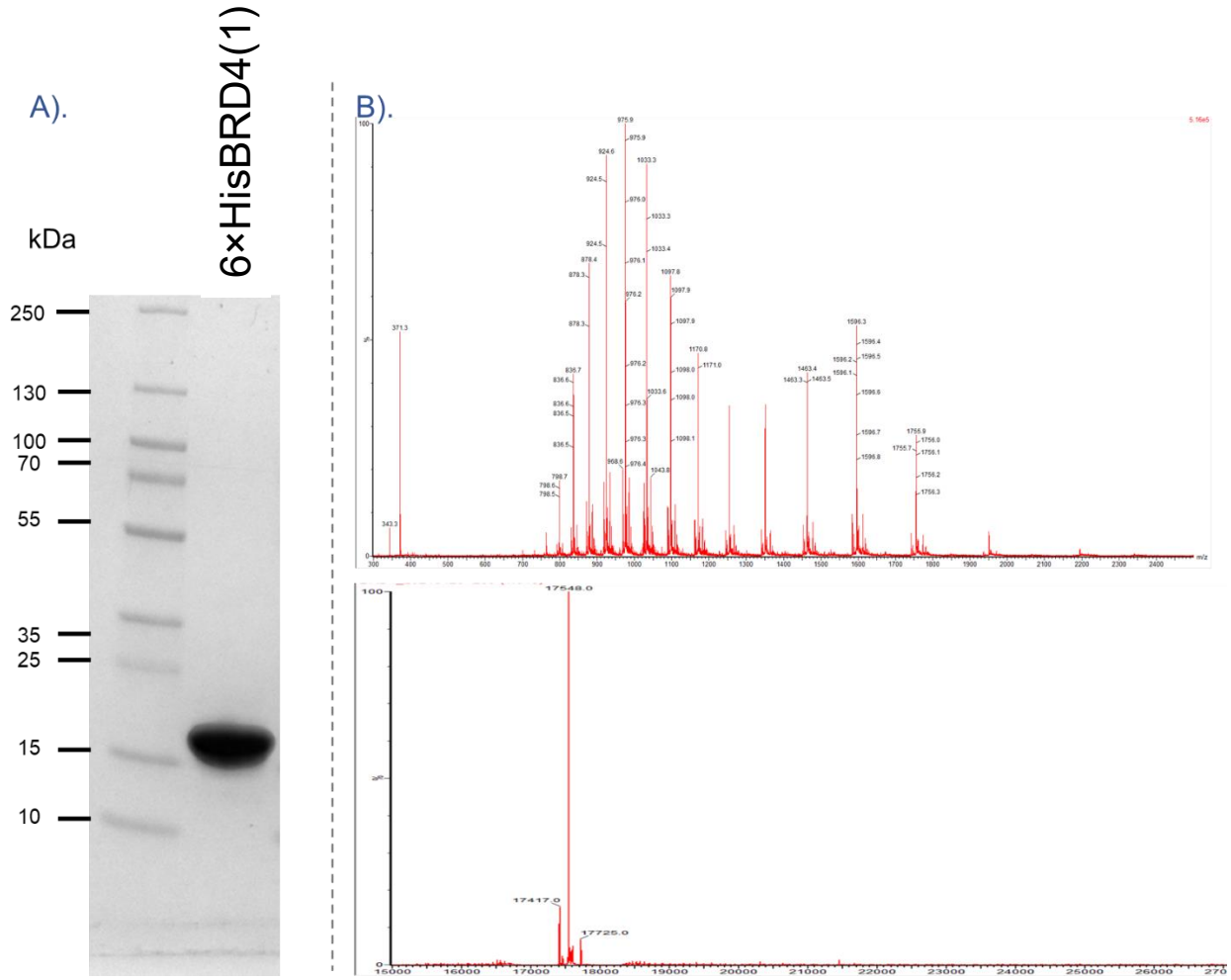

Appendix B Figure 3: Analysis of purified H_6-BRD4(1) (44…168aa) A). Imaged gel of purified H_6-BRD4(1) and page rule prestained protein ladder demonstrating protein mass; B). raw MS data of CBP^{BRD} analysed by LC-MS(TOF) (top) and the deconvoluted MS between 15 kDa and 27 kDA showing the protein mass of 17548 Da.

Appendix C: LC-MS traces from different reaction screens presented throughout this thesis

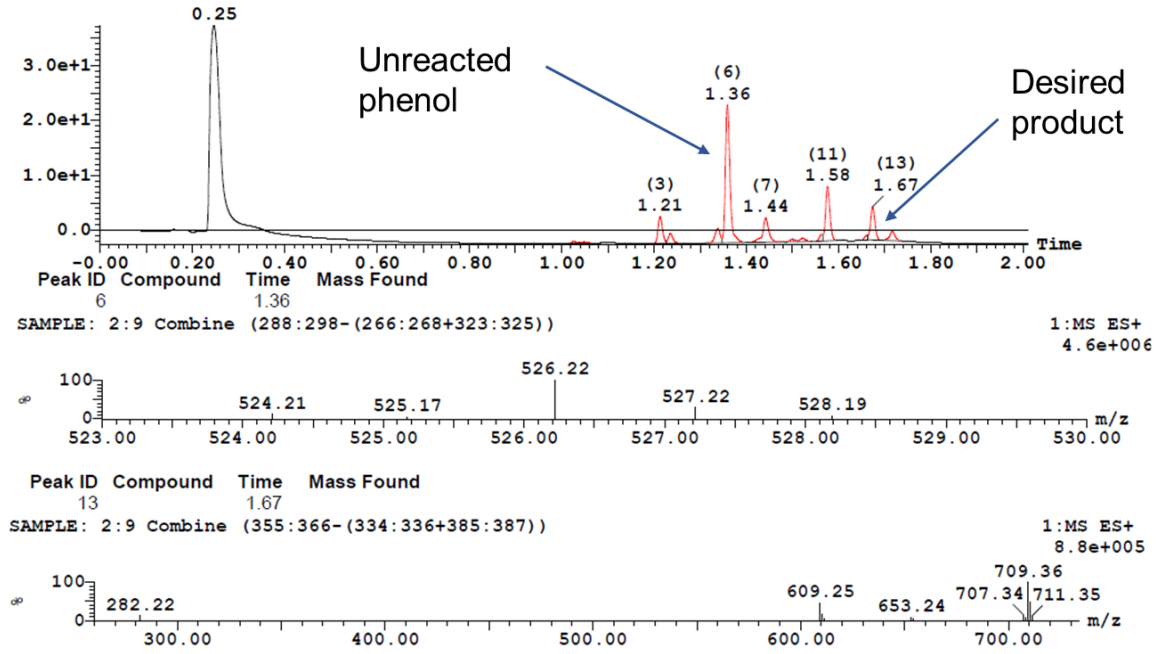

Appendix C Figure 1: reaction condition 1, K_2CO_3, DMF, 85 °C, 18 h, gives a 1 : 0.2 ratio of unreacted phenol with desired product.

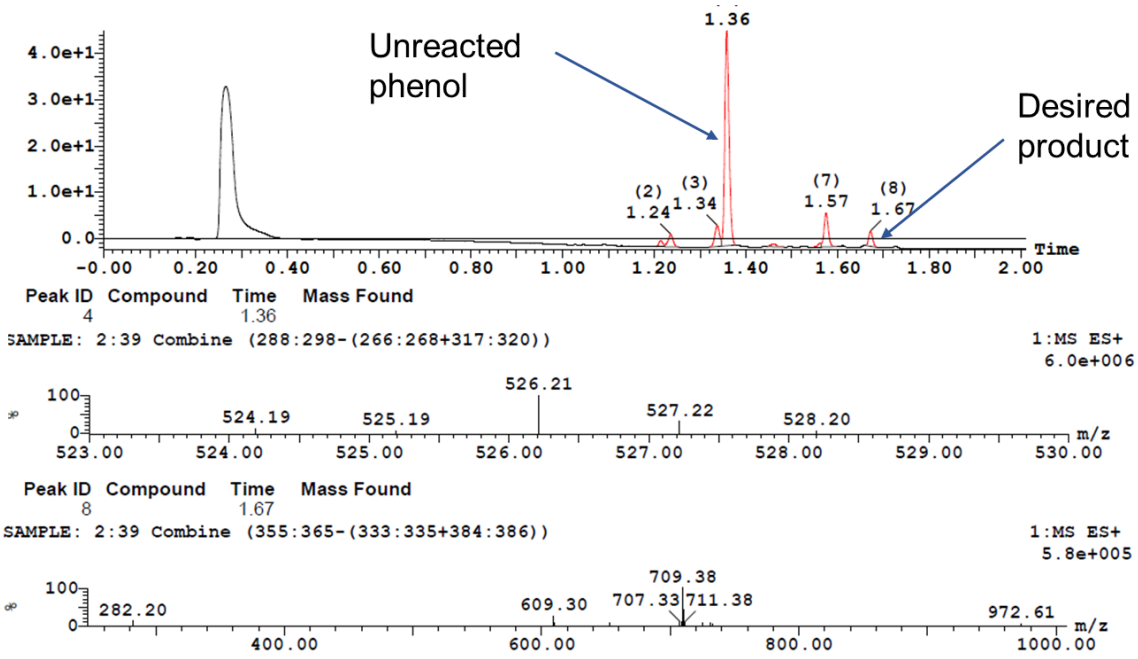

Appendix C Figure 2: reaction condition 2, K_2CO_3, DMF, 100 °C, 18 h, gives a 1 : 0.1 ratio of unreacted phenol with desired product.

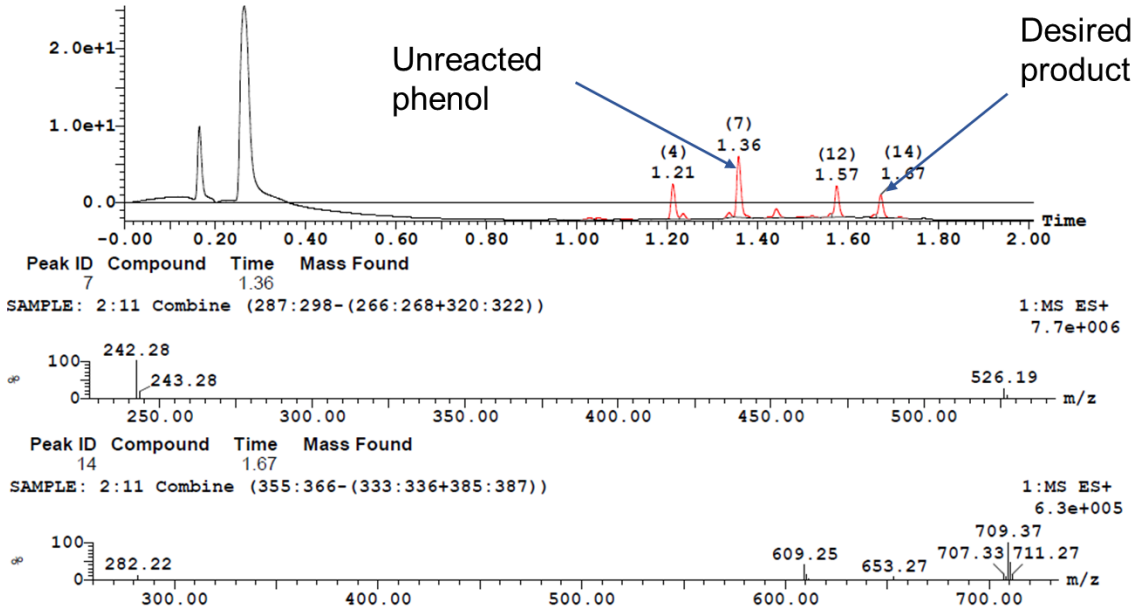

Appendix C Figure 3: reaction condition 3, K_2CO_3, TBAI, DMF, 85 °C, 18 h, gives a 1 : 0.4 ratio of unreacted phenol with desired product.

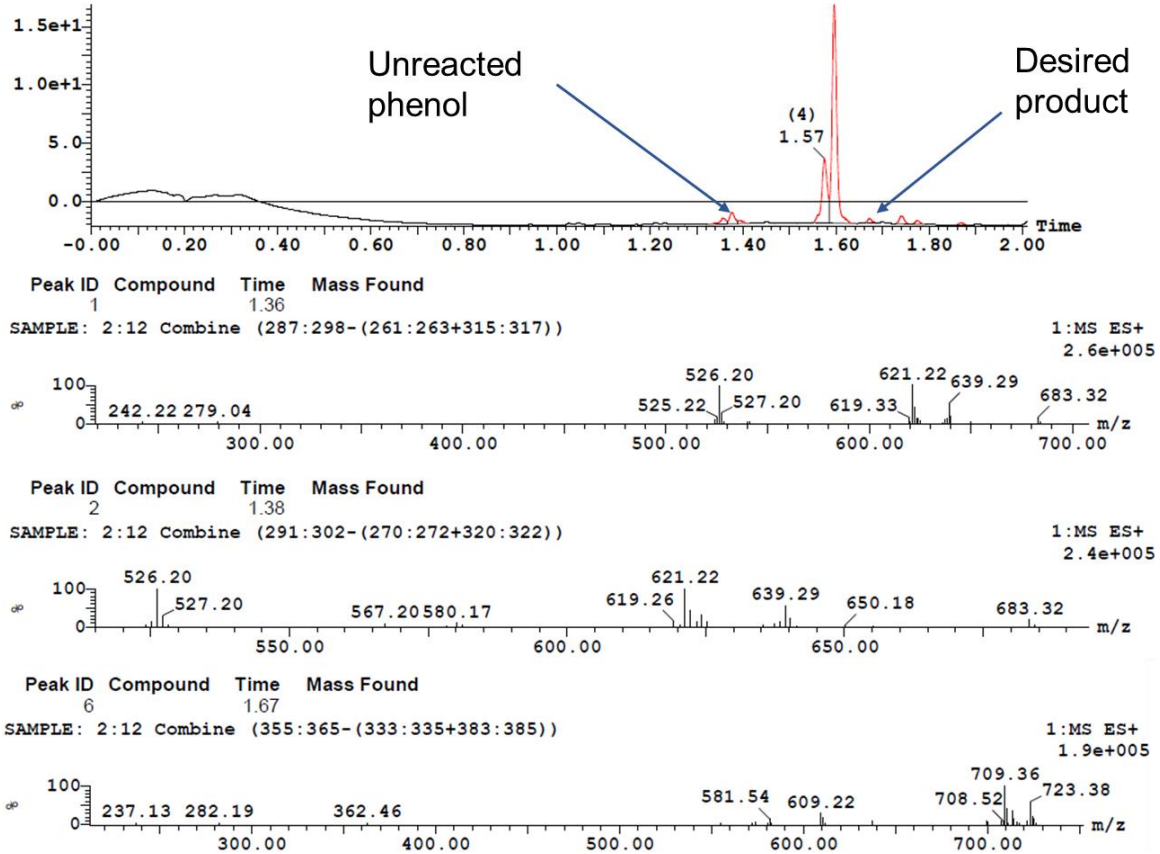

Appendix C Figure 4: reaction condition 4, K_2CO_3, MeCN, 85 °C, 18 h, gives a 1 : 0.2 ratio of unreacted phenol with desired product.

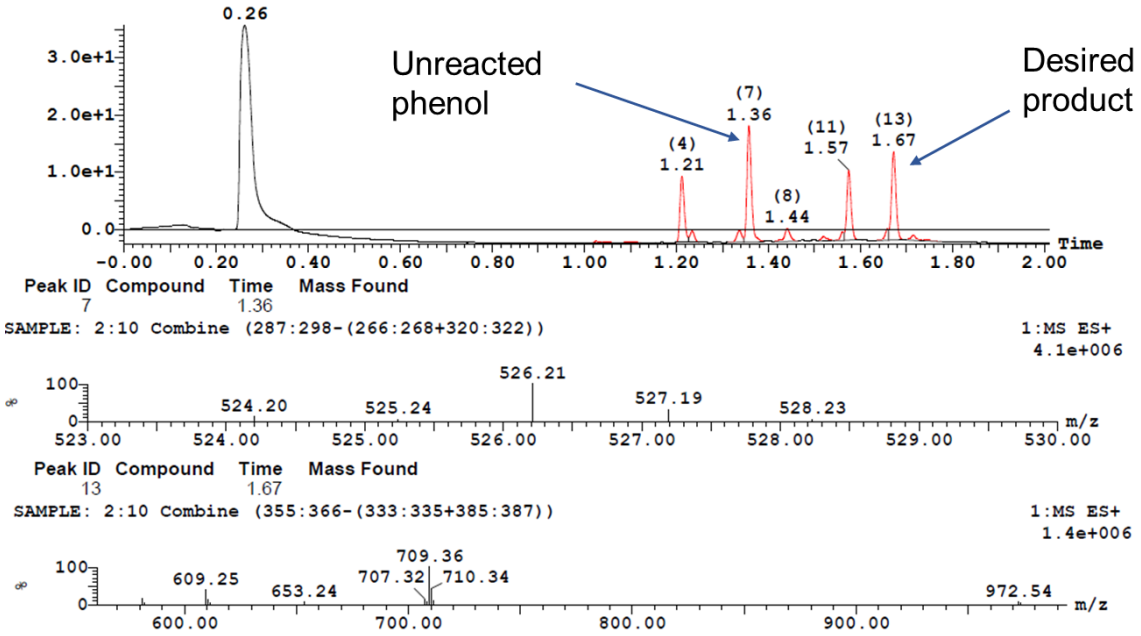

Appendix C Figure 5: reaction conditions 5, Cs_2CO_3, DMF, 85 °C, 18 h, gives a 1 : 0.7 ratio of unreacted phenol with desired product.

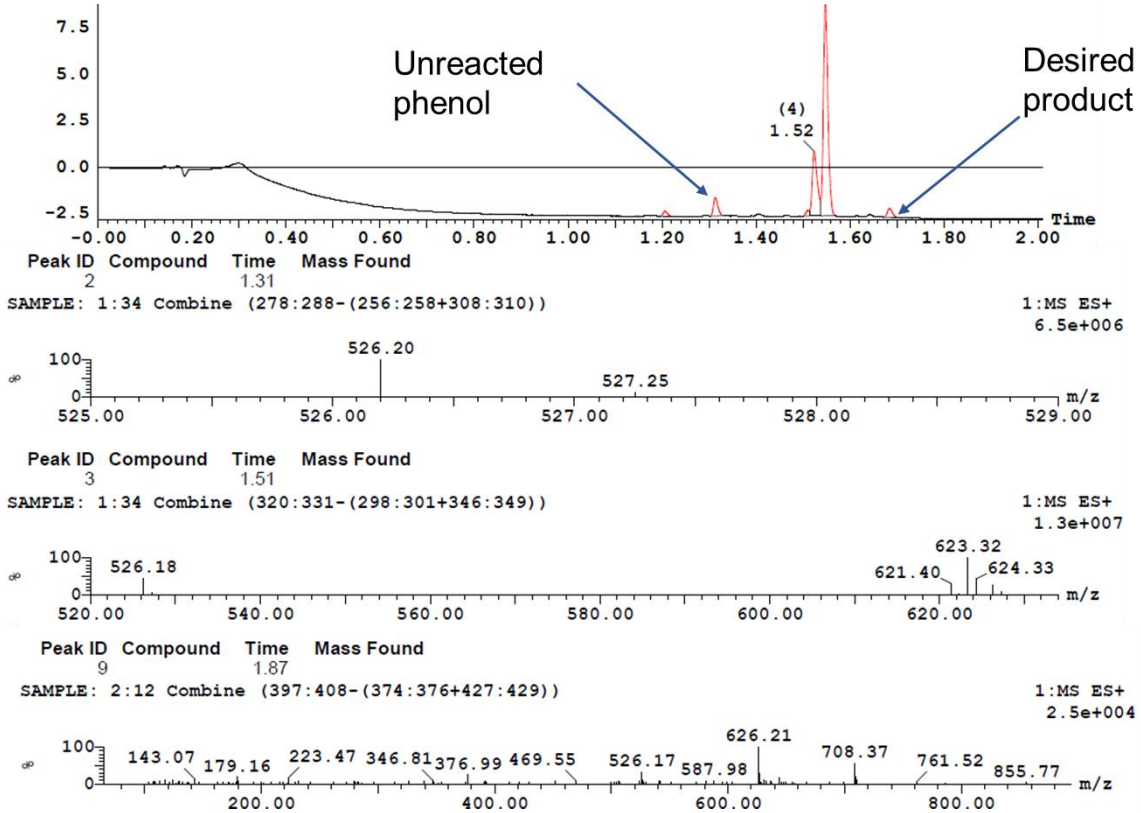

Appendix C Figure 6: reaction conditions 6, Cs_2CO_3, MeCN, 85 °C, 18 h, gives a 1 : 0.2 ratio of unreacted phenol with desired product.

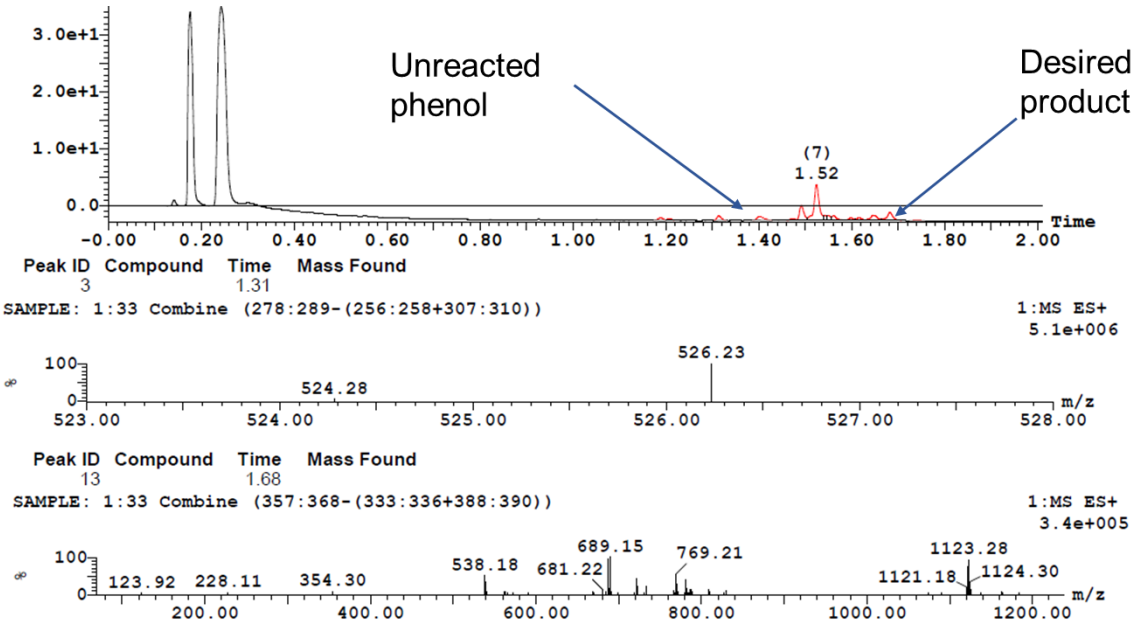

Appendix C Figure 7: reaction conditions 7, K_2CO_3, DMSo/MeCN (1:1), 100 °C, 1 h, μW, gives a 1:0.2 ratio of unreacted phenol with desired product.

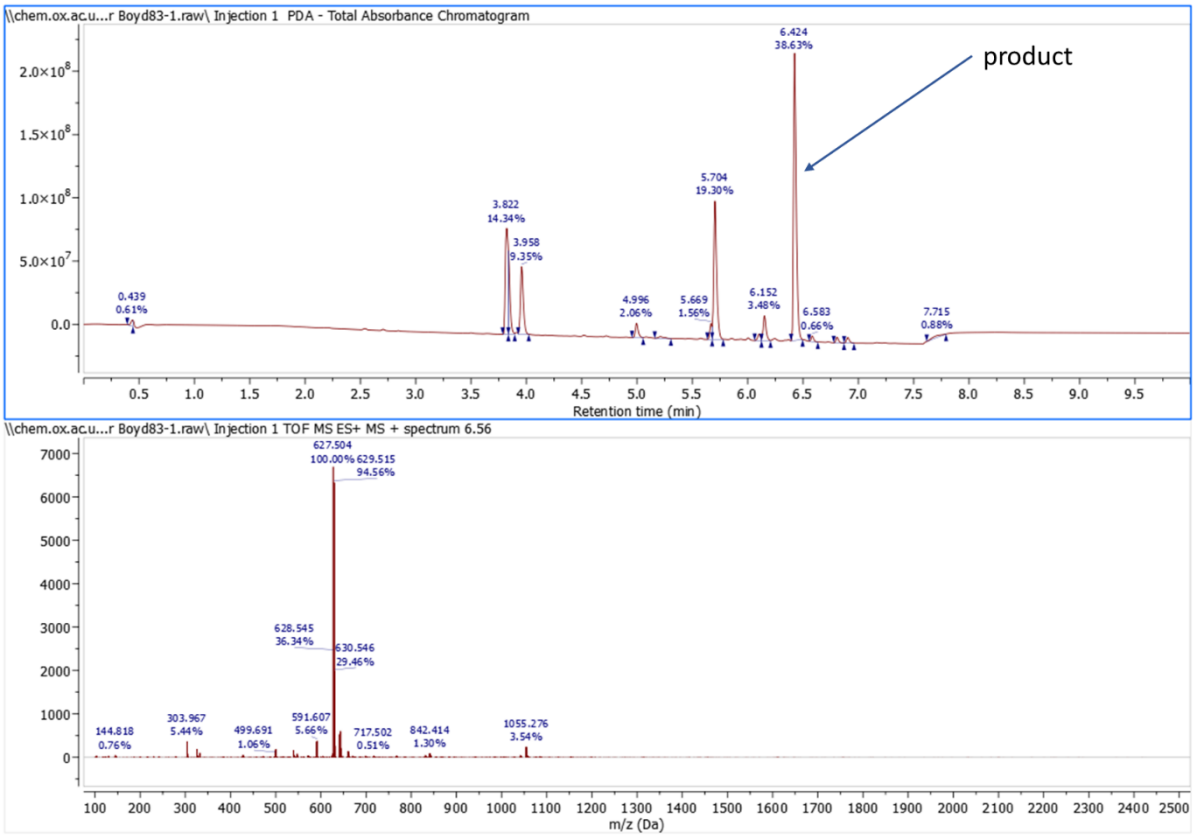

Appendix C Figure 8: LC-MS chromatogram and MS shown for Mitsunobu reaction screen (Chapter 5, Figure XX8) for DIAD, triphenylphosphine in THF, which is the condition carried forward to large scale, with the product peak shown by blue arrow.

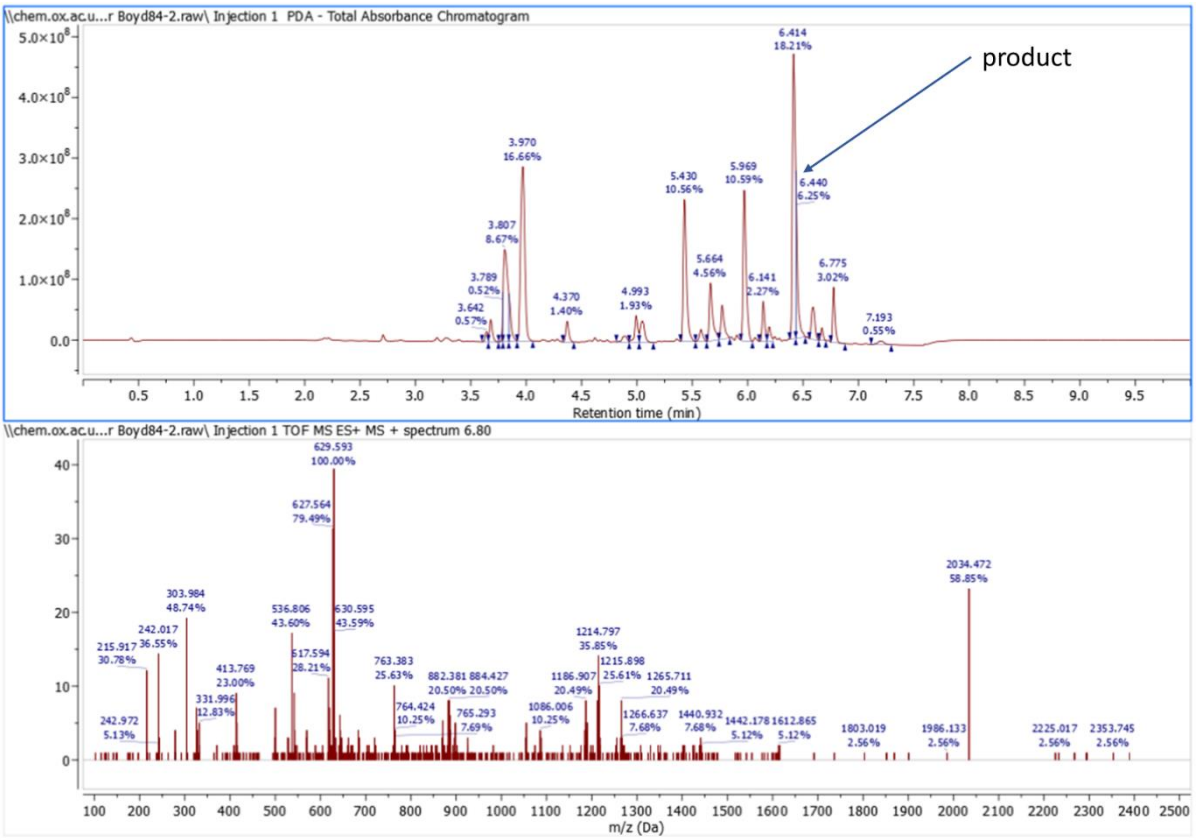

Appendix C Figure 9: LC-MS chromatogram and MS shown for Mitsunobu reaction screen (Chapter 5, Figure XX8) for DEAD, triphenylphosphine in THF, with the product peak shown by blue arrow.

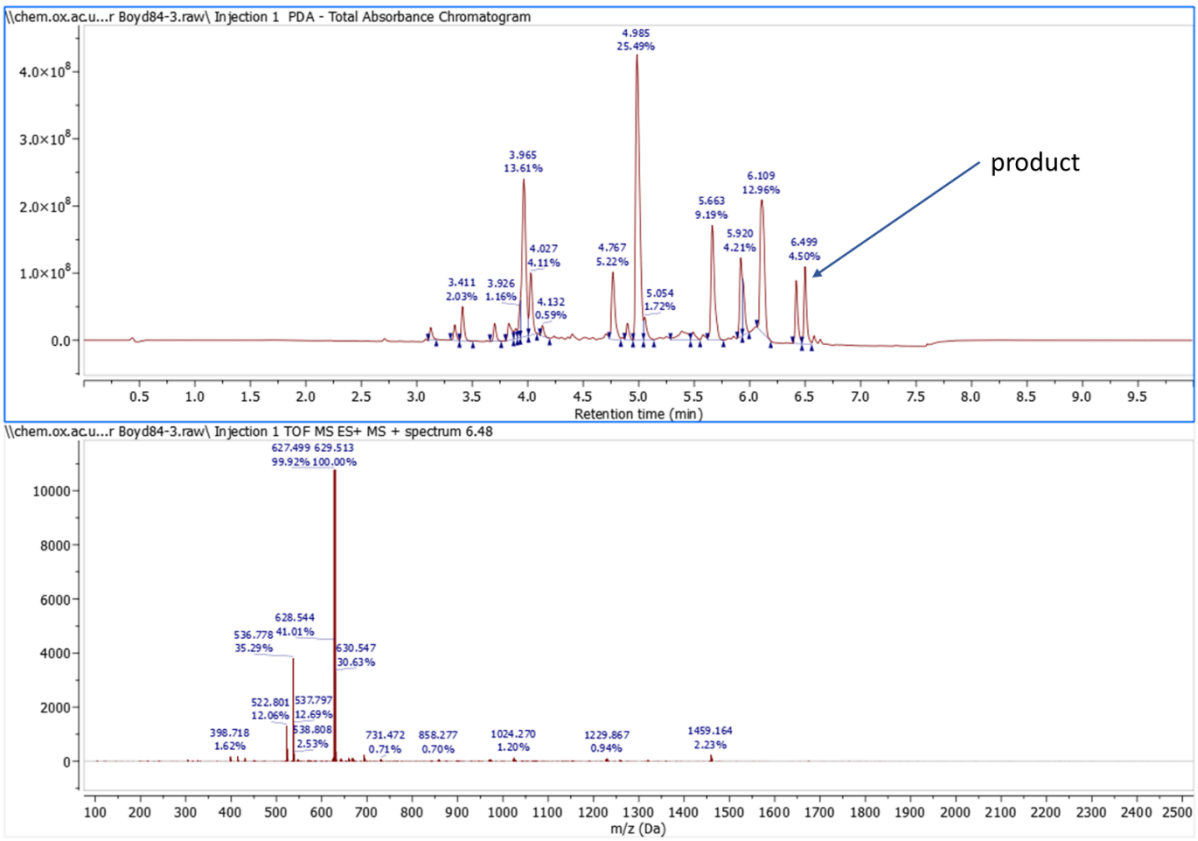

Appendix C figure 10: LC-MS chromatogram and MS shown for Mitsunobu reaction screen (Chapter 5, Figure XX8) for DTBAD, triphenylphosphine in THF, with the product peak shown by blue arrow.

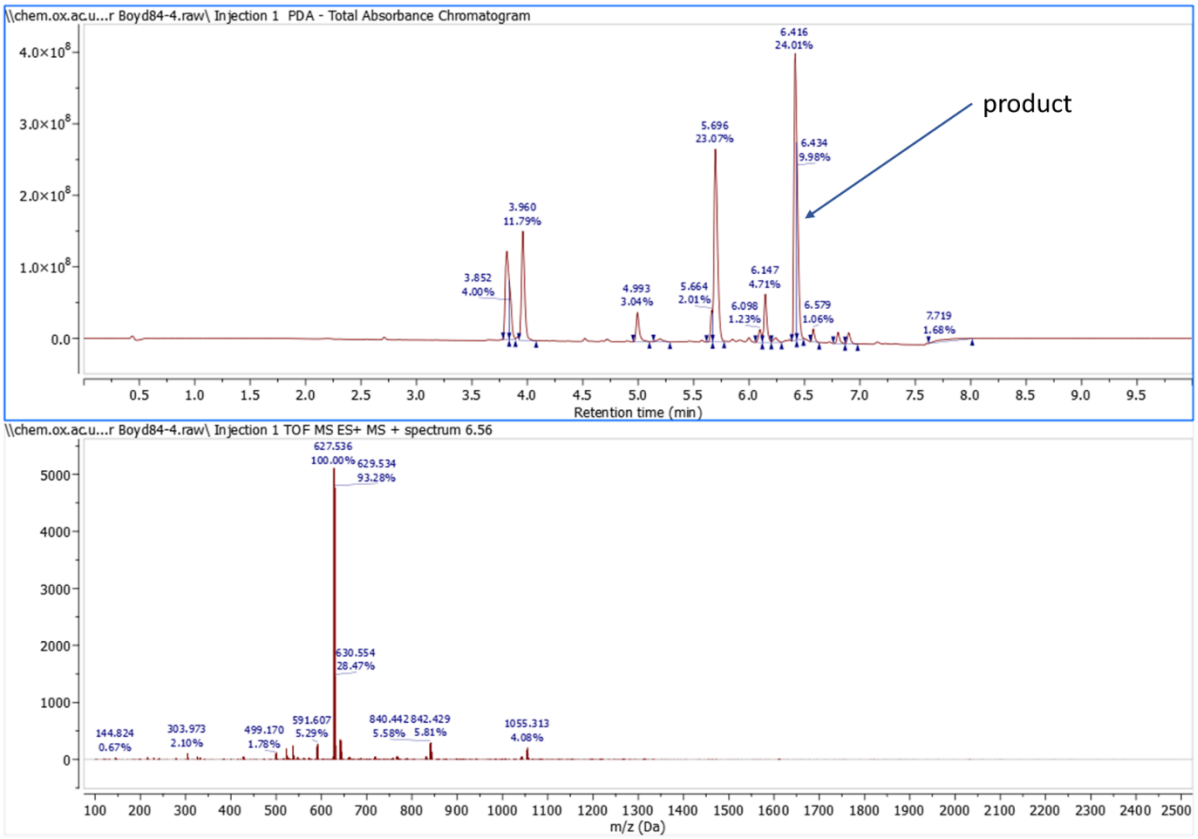

Appendix C Figure 11: LC-MS chromatogram and MS shown for Mitsunobu reaction screen (Chapter 5, Figure XX8) for DIAD, DPPE in THF, with the product peak shown by blue arrow.

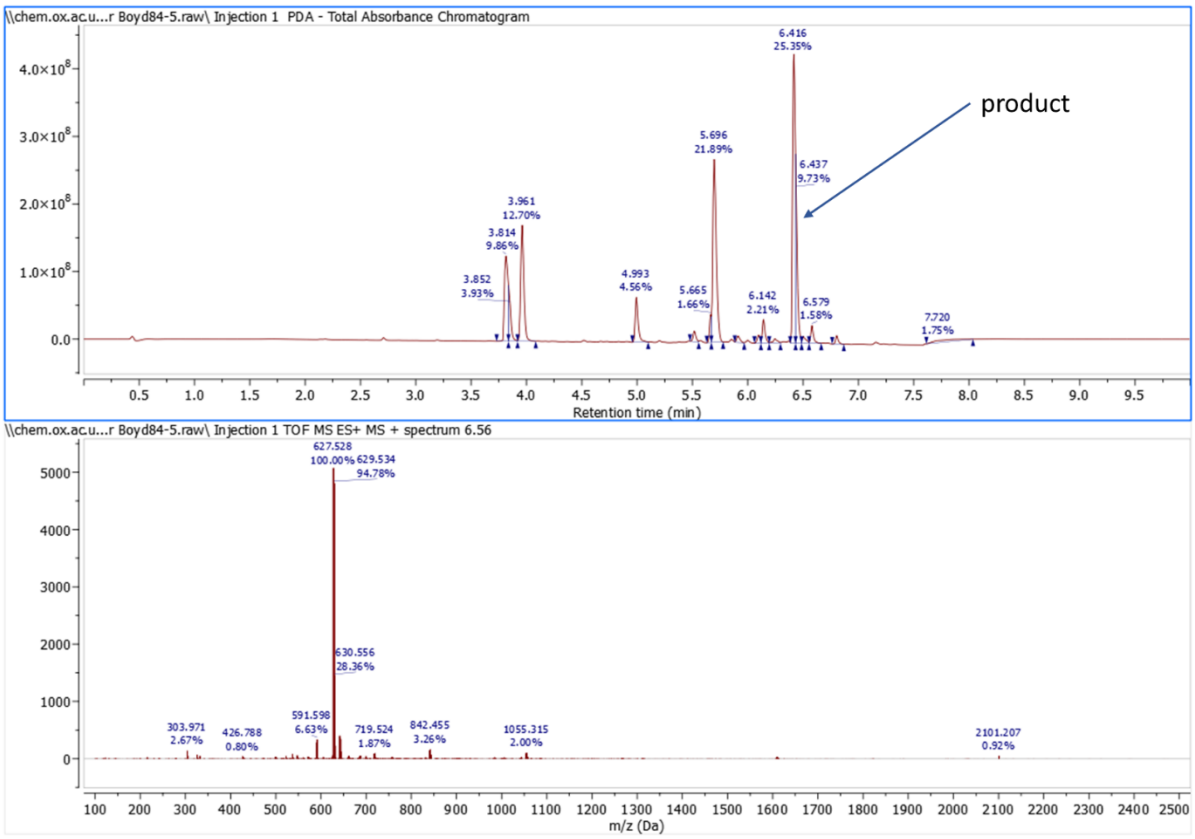

Appendix C Figure 12: LC-MS chromatogram and MS shown for Mitsunobu reaction screen (Chapter 5, Figure XX8) for DIAD, triphenylphosphine in Et_2O, with the product peak shown by blue arrow.

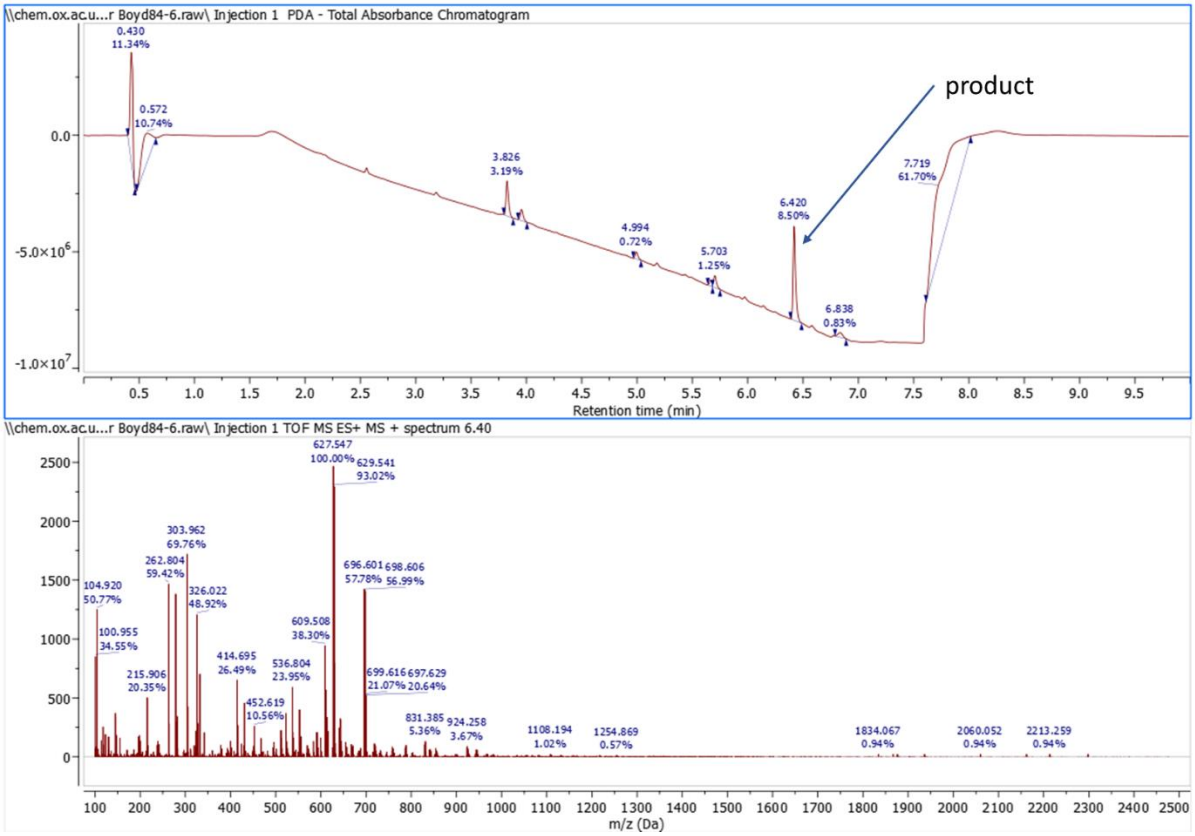

Appendix C Figure 13: LC-MS chromatogram and MS shown for Mitsunobu reaction screen (Chapter 5, Figure XX8) for DIAD, triphenylphosphine in THF/tol (2:3), with the product peak shown by blue arrow.

Appendix D: ITC data for compounds discussed in this thesis

Presented below are the ITC traces (including repeats) for the compounds synthesised in this thesis, including the mean binding affinity (K_d) and stoichiometry (N sites) along with the standard error of each value (SEM) and the number of repeats (n = x). The ITC traces are shown in order of compound numbering.

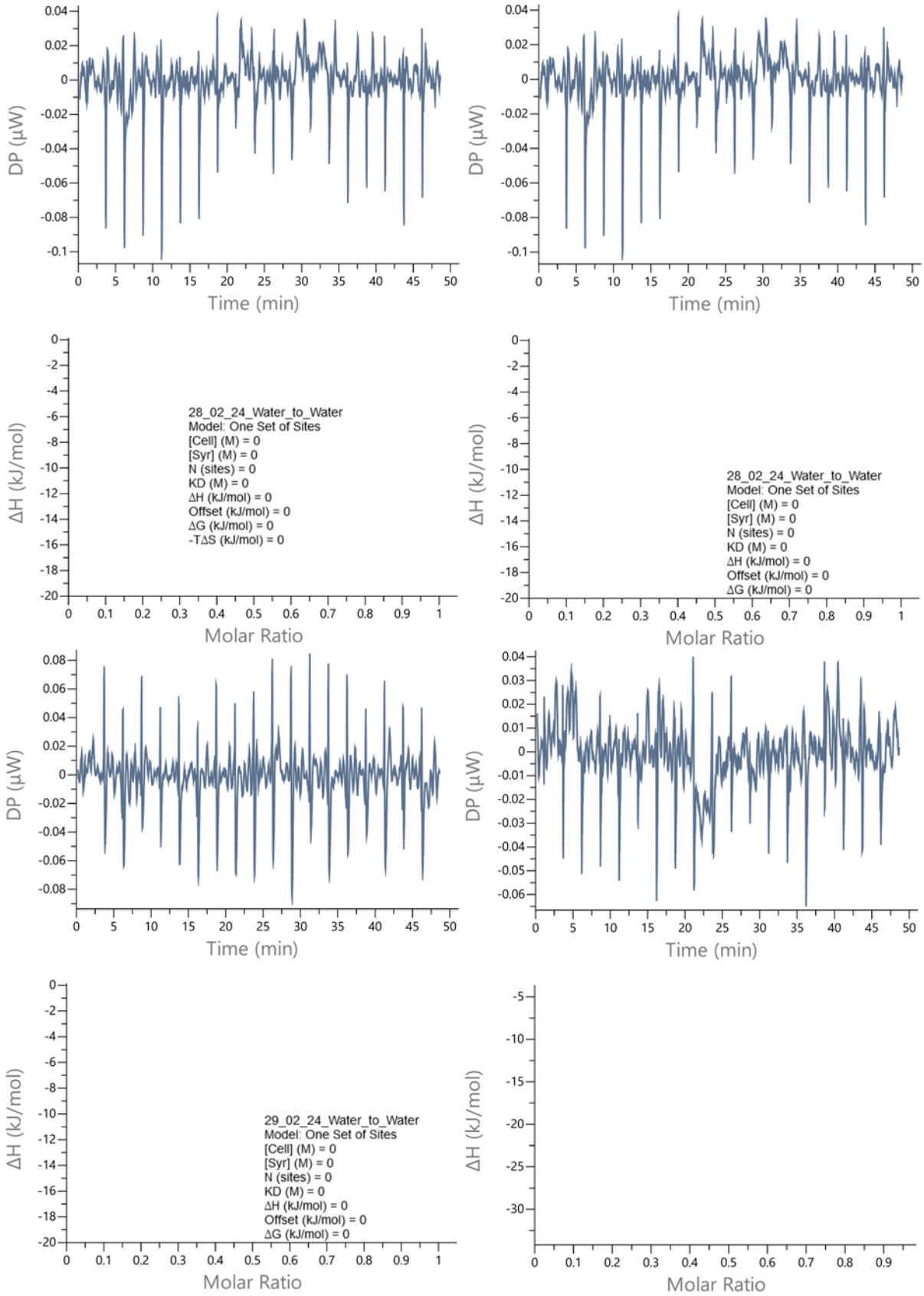

Appendix D, Figure 1: representative examples of water-to-water ITC traces, negative controls.

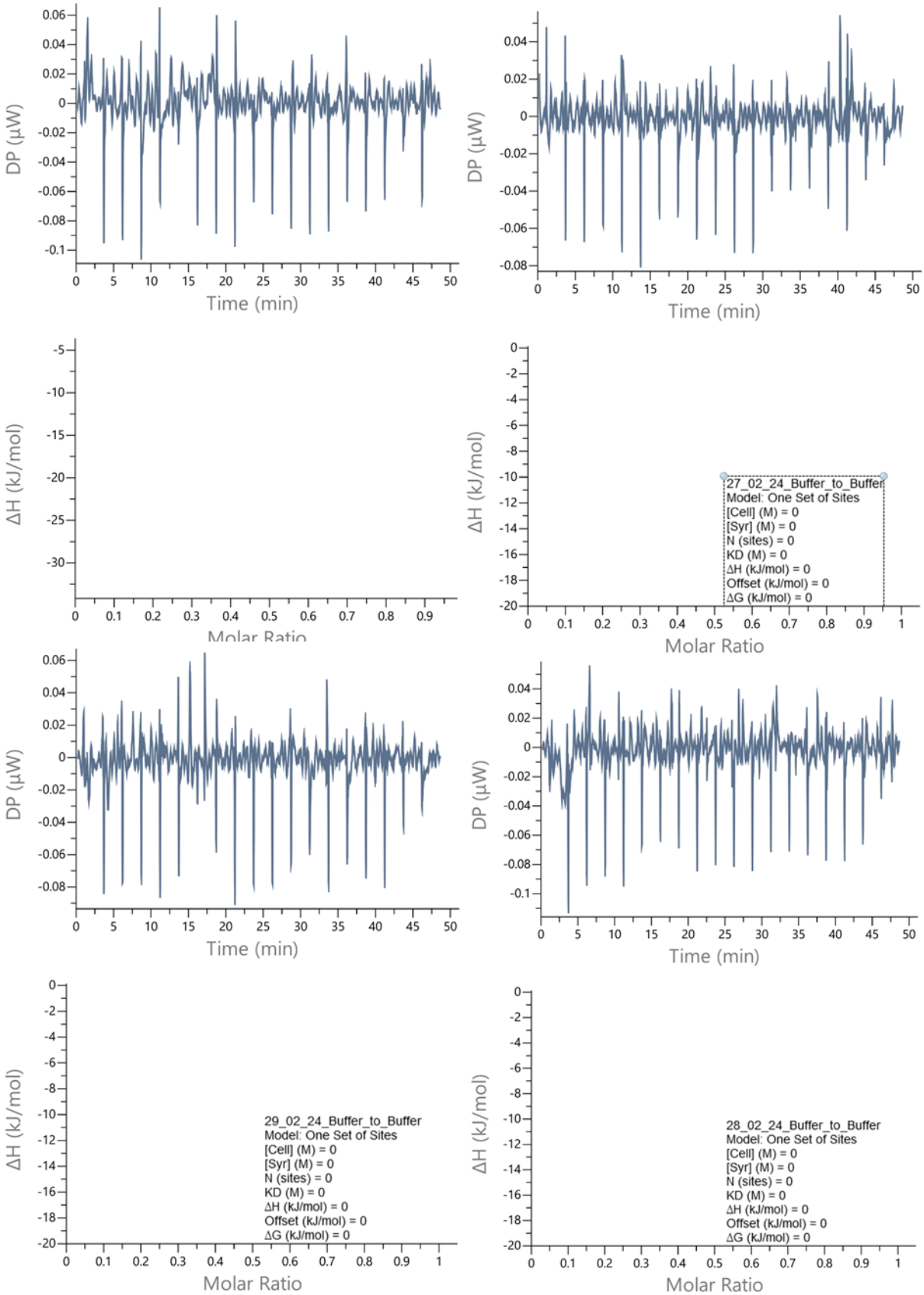

Appendix D, Figure 2: Representative examples of buffer-to-buffer ITC traces, negative controls.

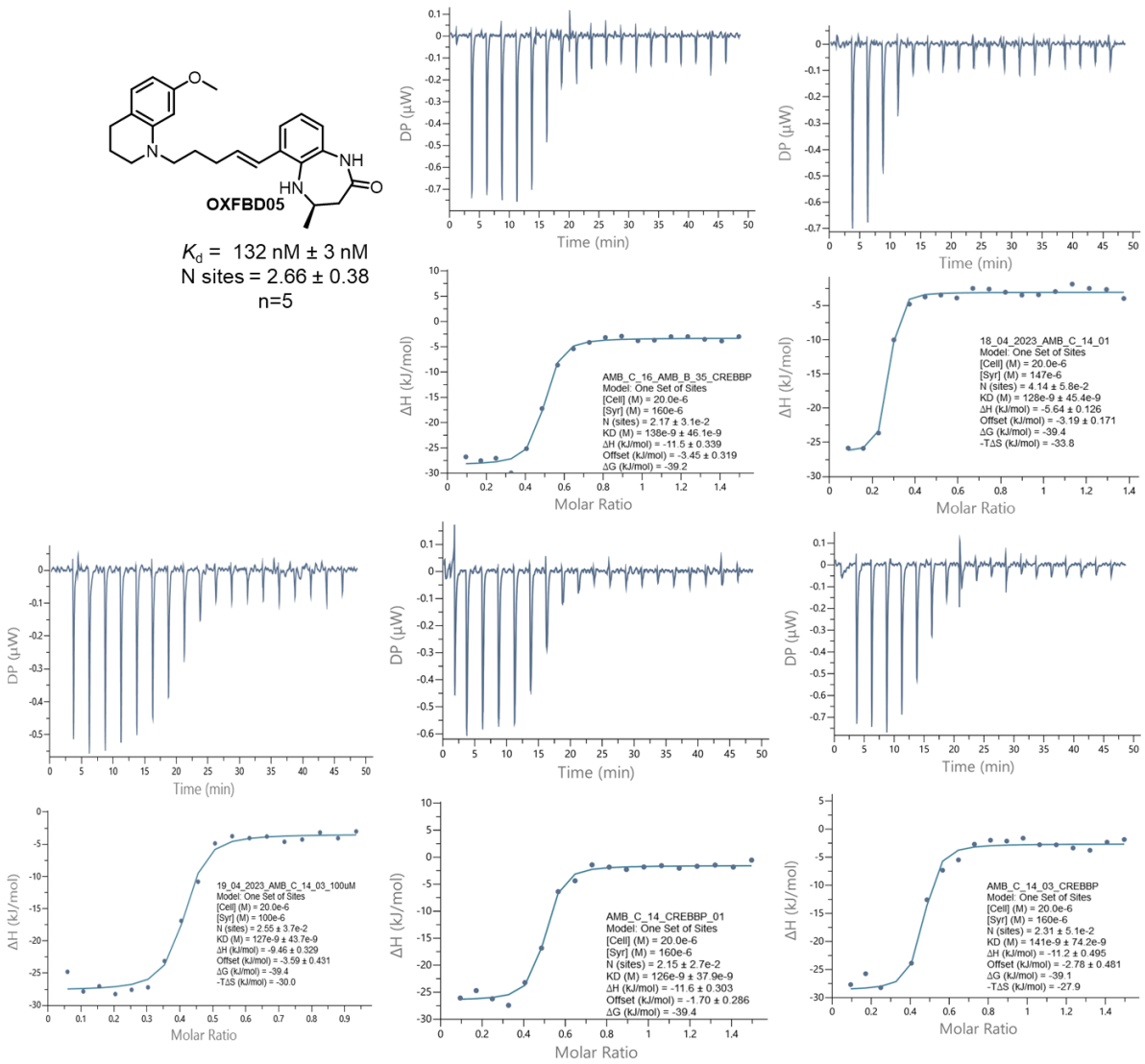

Appendix D, Figure 3: ITC data for ligand **OXFBD05** binding to the CBP^{BRD}.

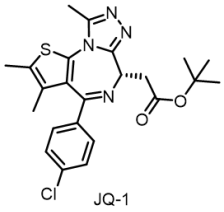

K_d = 52.9 nM ± 0.8 nM
by ITC (n=4)

Appendix D, Figure 4: ITC data for ligand JQ-1 binding to BRD4(1).

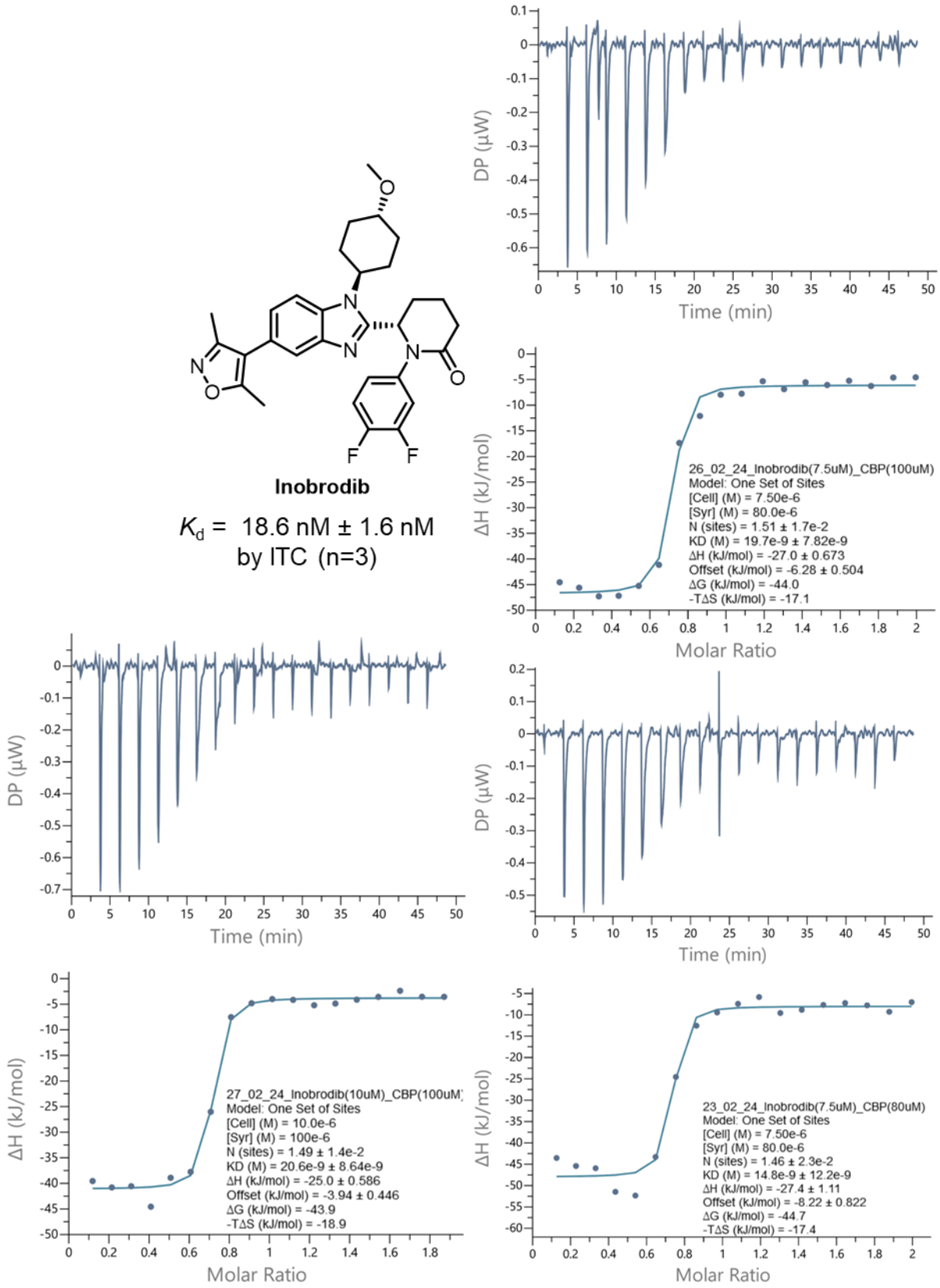

Appendix D, Figure 5: ITC data for Inobrodib binding to the CBP^{BRD}.

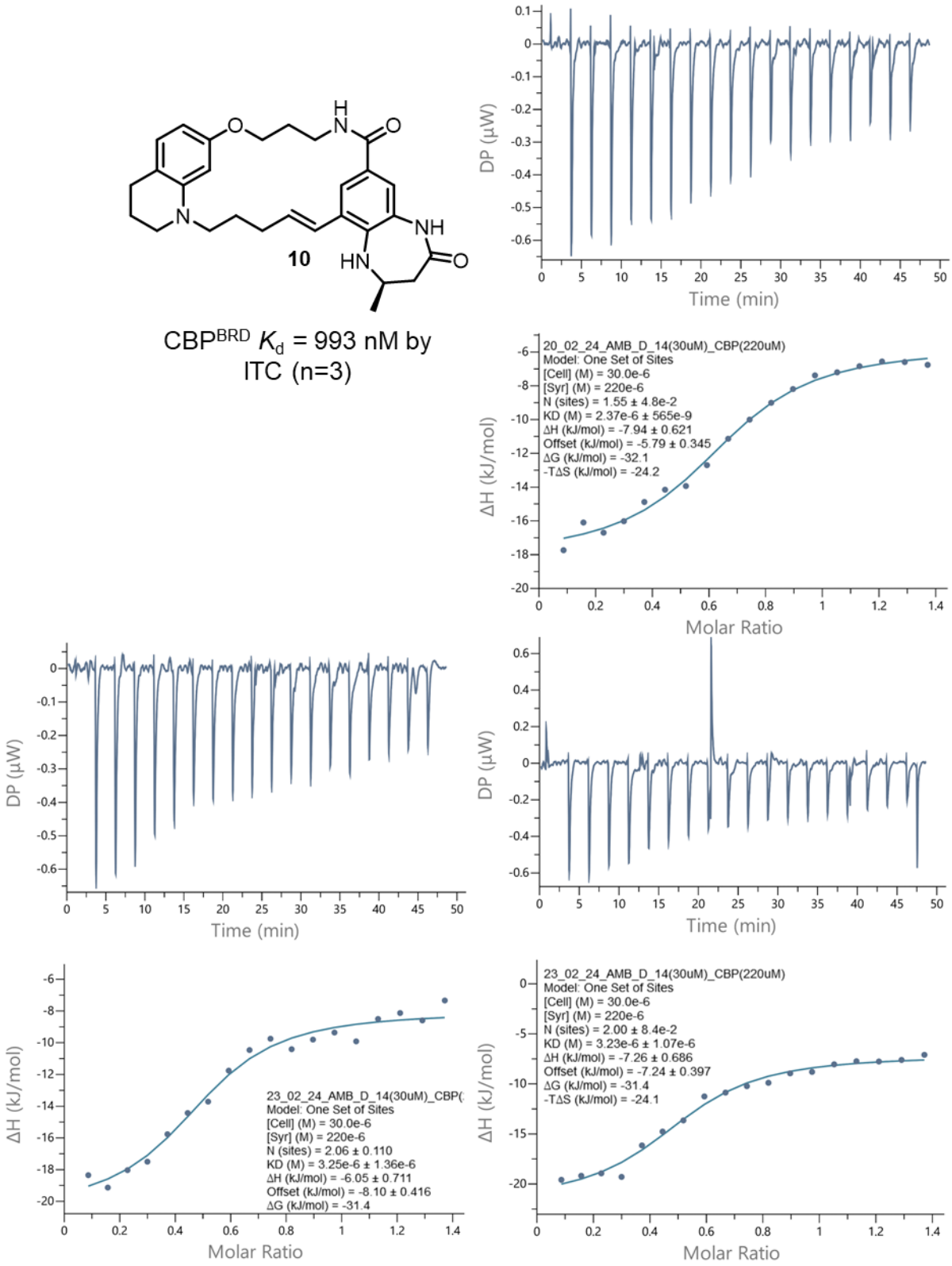

Appendix D, Figure 6: ITC trace for the binding of compound **10** to the CBP^{BRD}.

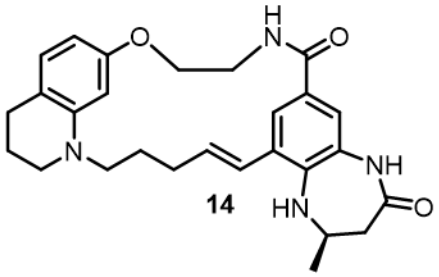

14

CBP^{BRD} K_d = 320 nM by ITC (n=3)

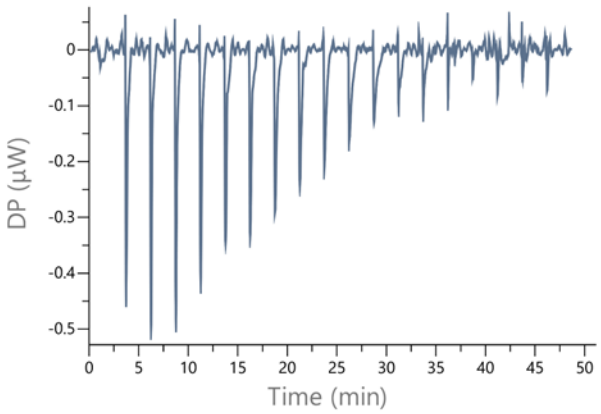

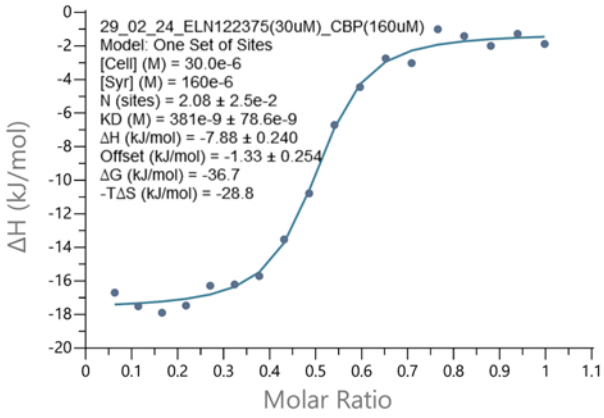

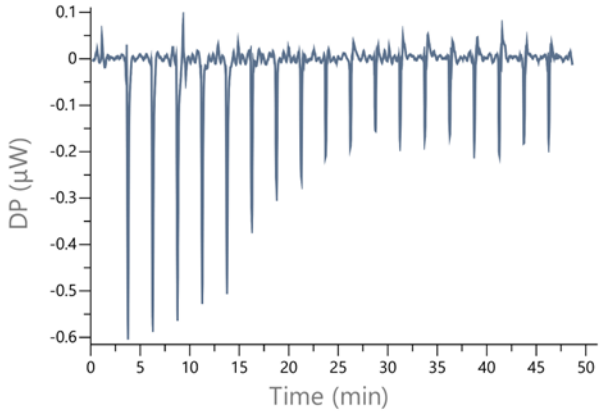

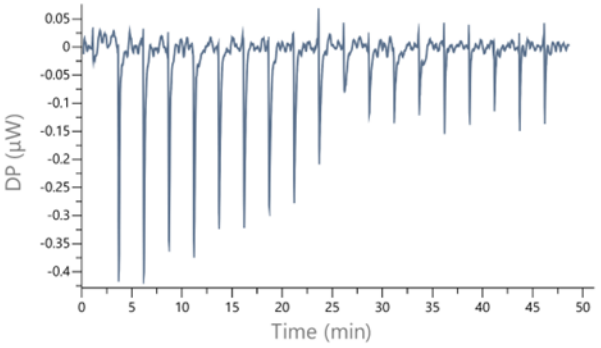

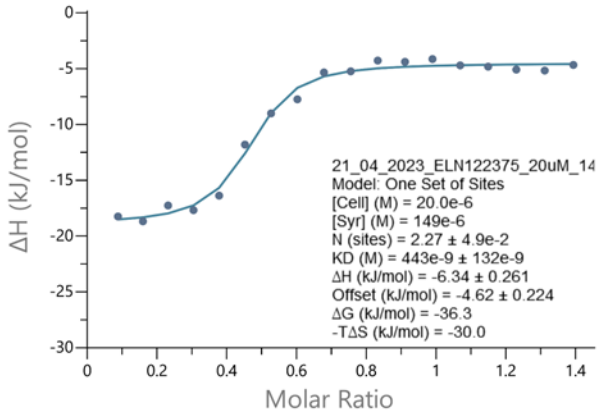

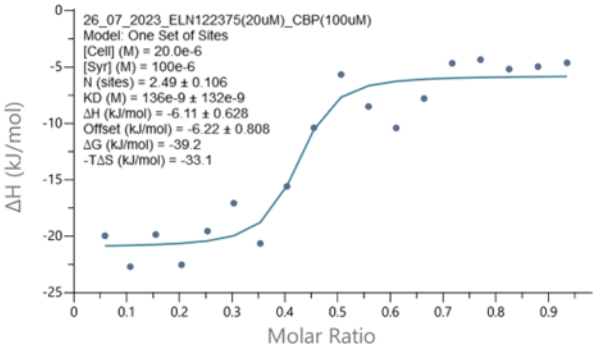

Appendix D, Figure 7: ITC trace for the binding of compound **14** to the CBP^{BRD}.

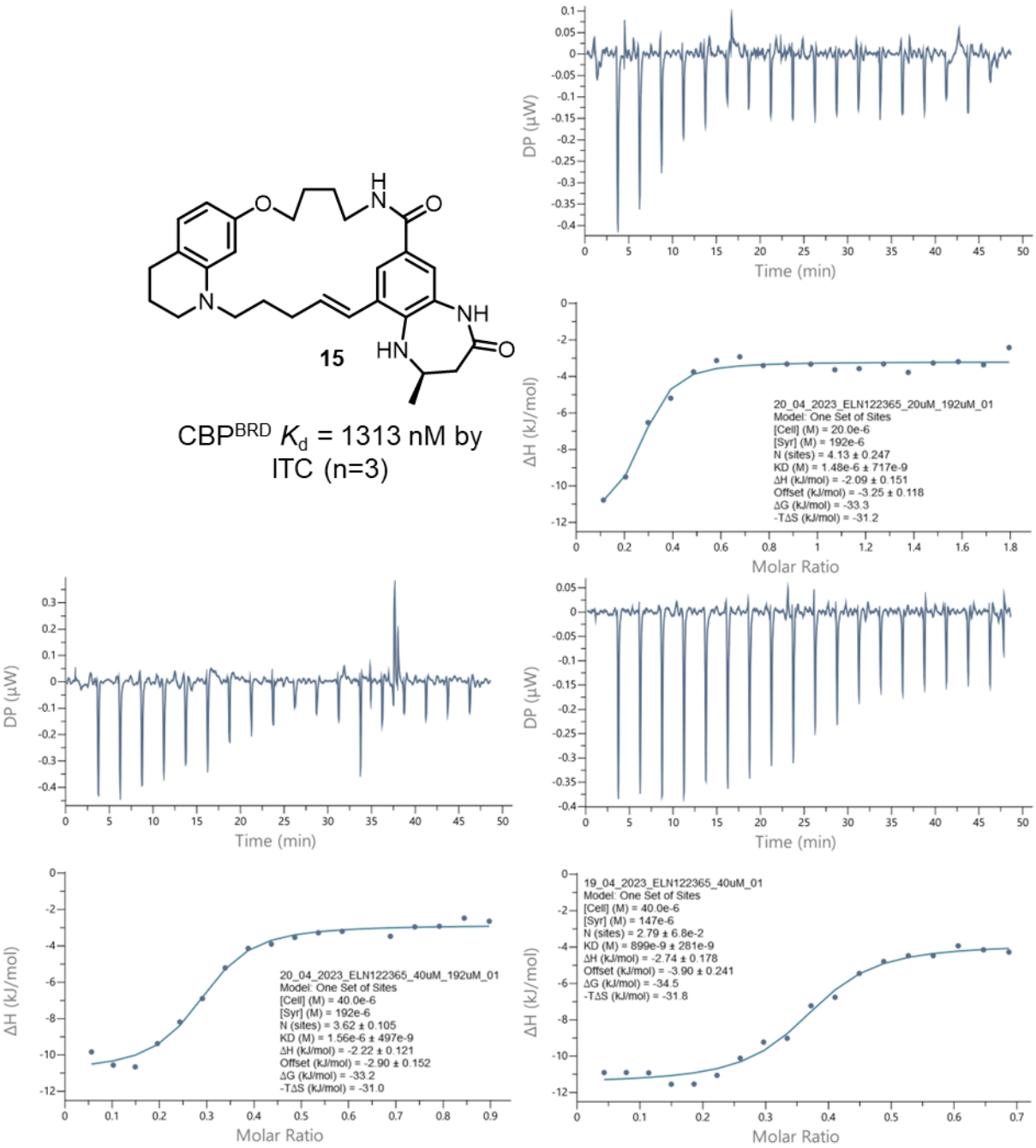

Appendix D, Figure 8: ITC trace for the binding of compound **15** to the CBP^{BRD}.

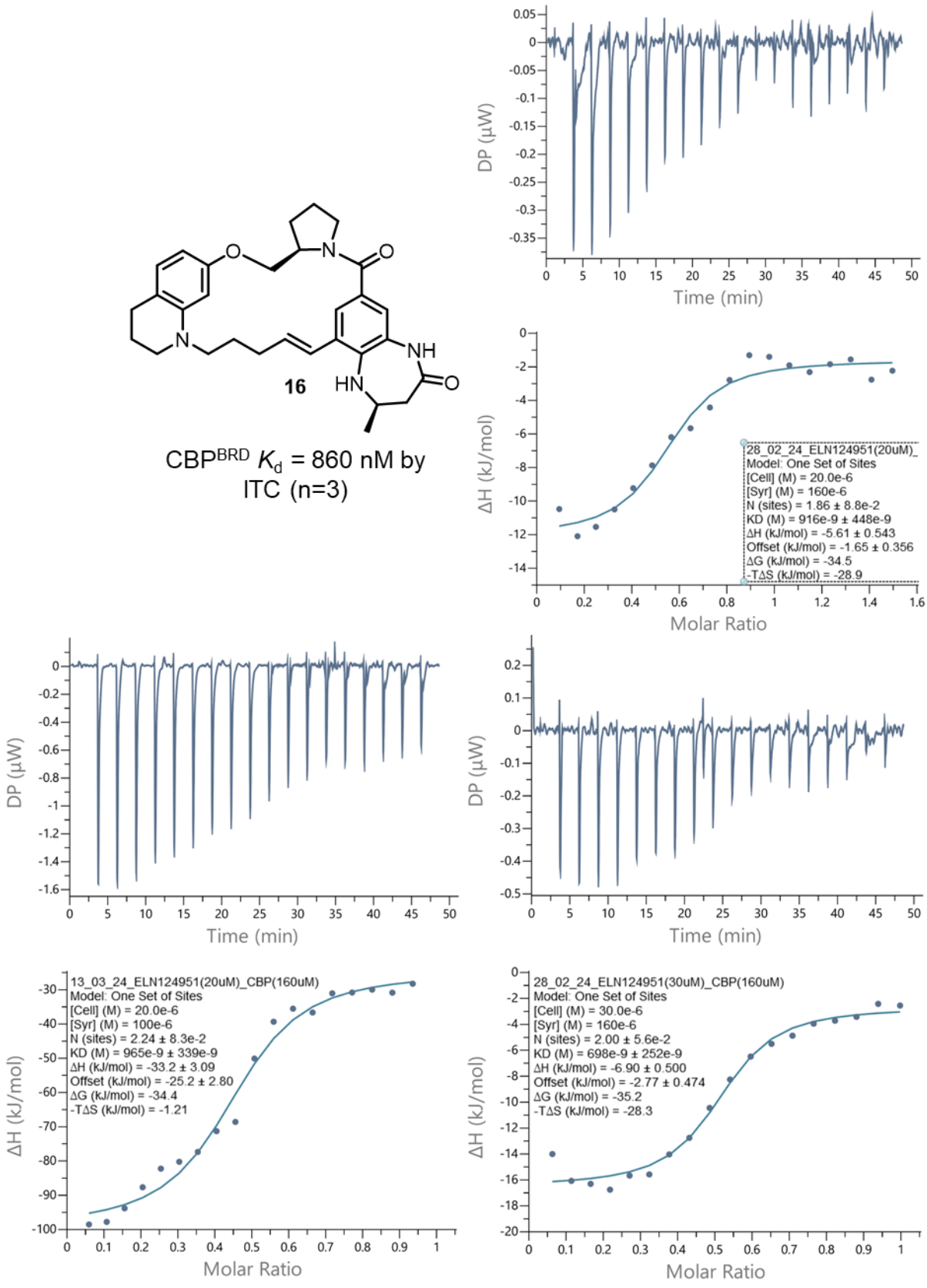

Appendix D, Figure 9: ITC trace for the binding of compound **16** to the CBP^{BRD}.

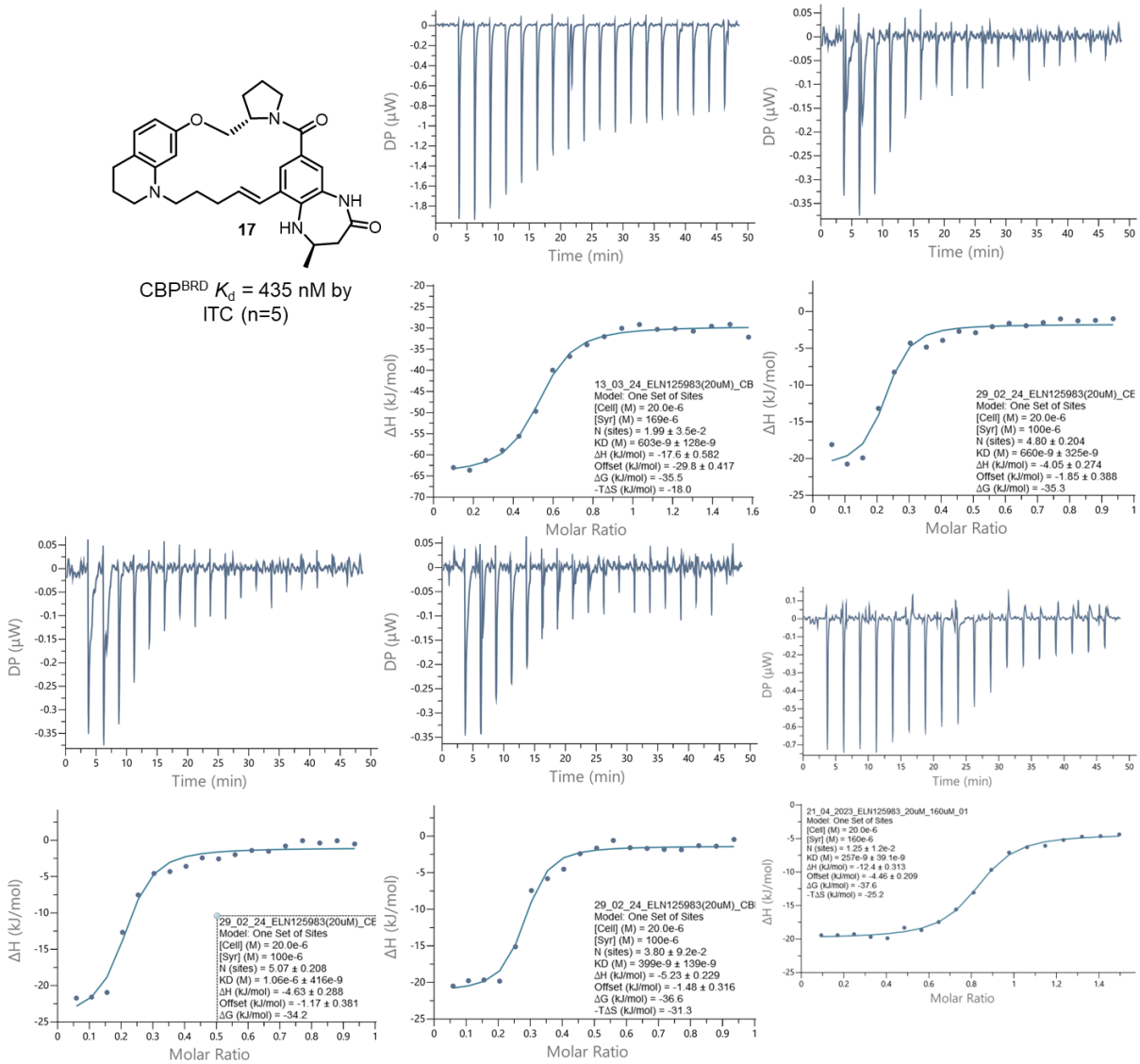

Appendix D, Figure 10: ITC trace for the binding of compound **17** to the CBP^{BRD}.

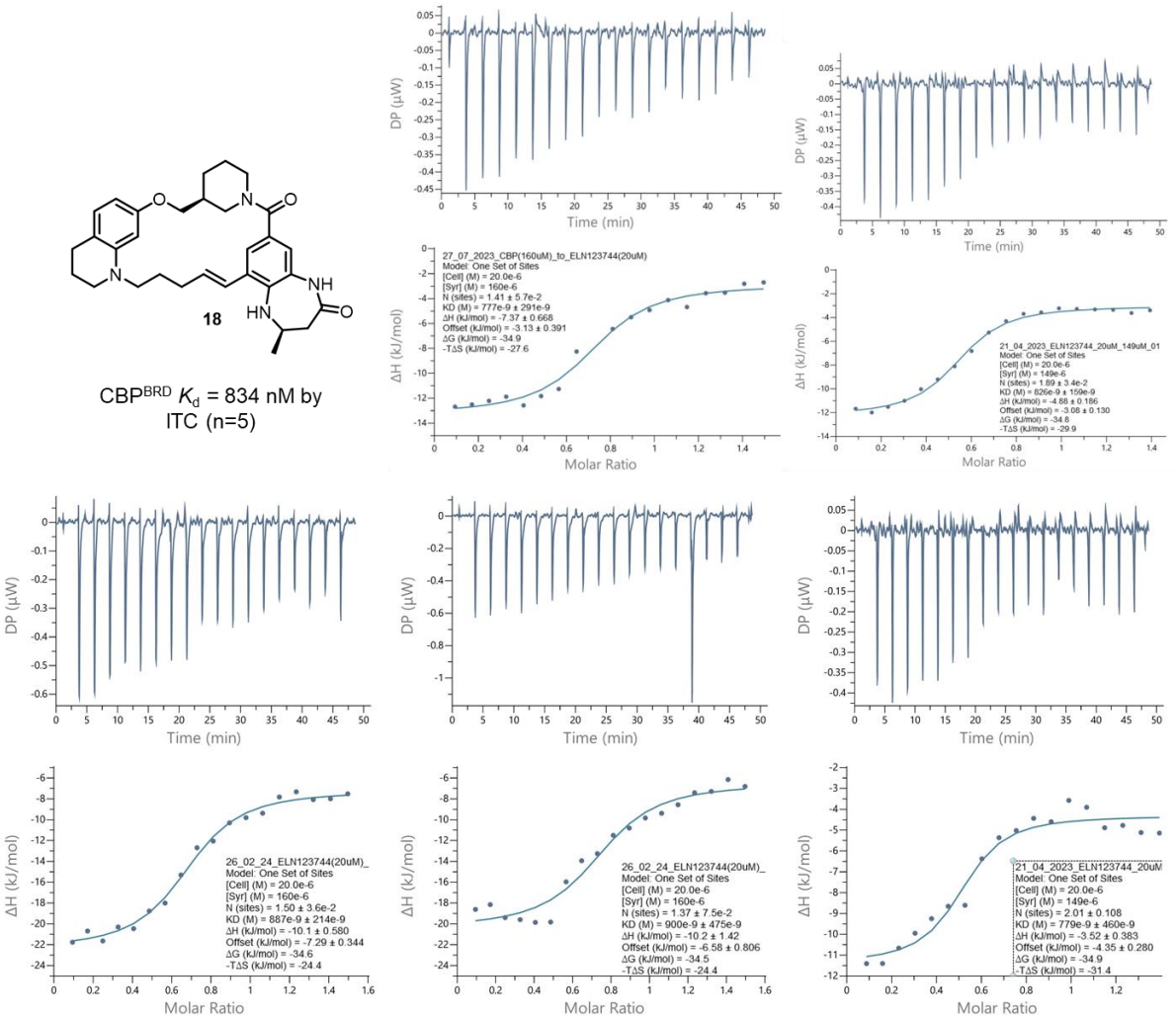

Appendix D, Figure 11: ITC trace for the binding of compound **18** to the CBP^{BRD}.

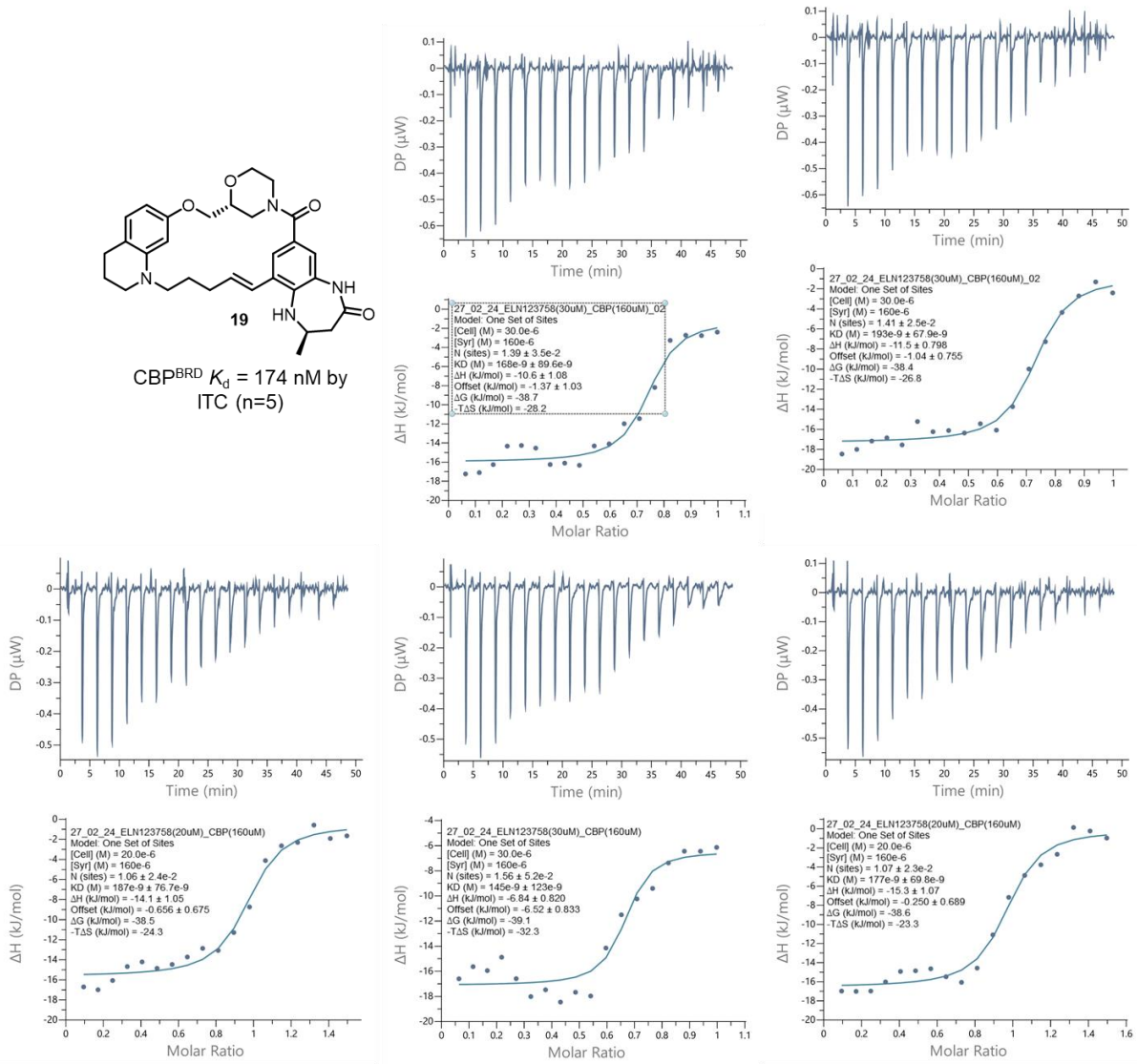

Appendix D, Figure 12: ITC trace for the binding of compound **19** to the CBP^{BRD}.

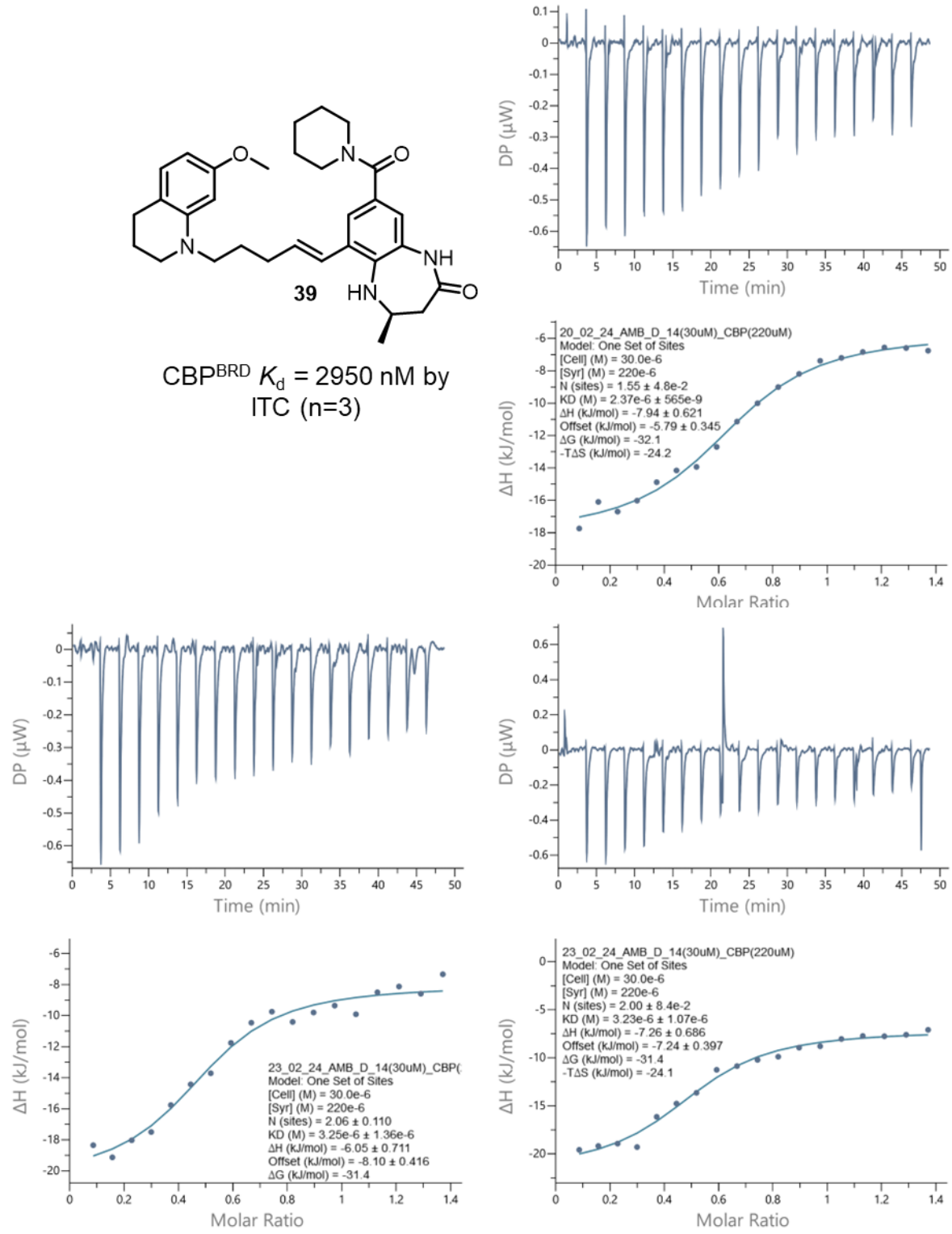

Appendix D, Figure 13: ITC trace for the binding of compound **39** to the CBP^{BRD}.

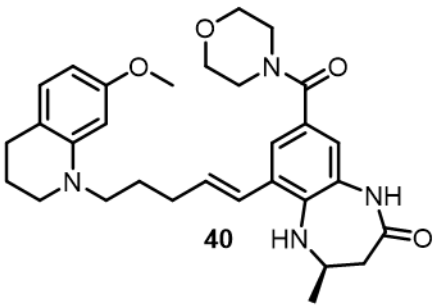

CBP^{BRD} K_d = 816 nM by ITC (n=3)

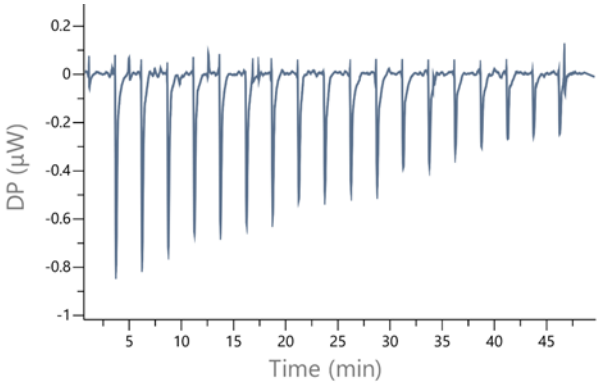

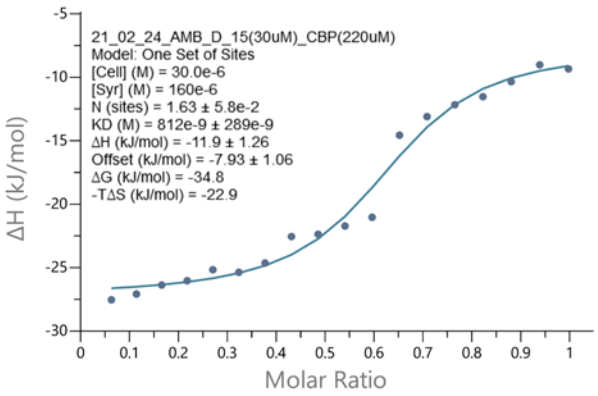

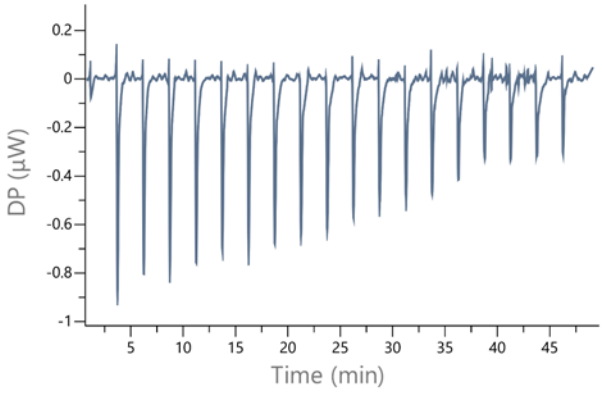

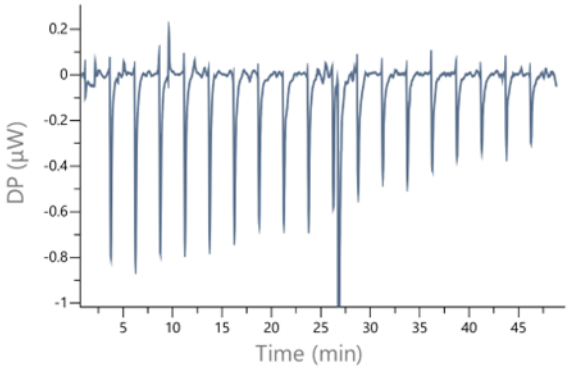

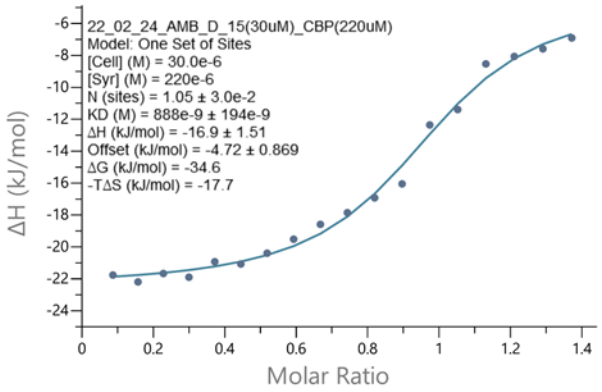

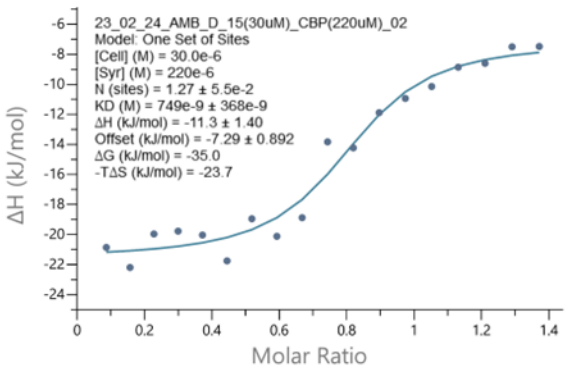

Appendix D, Figure 14: ITC trace for the binding of compound **40** to the CBP^{BRD}.

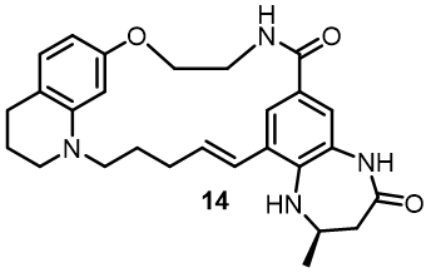

14

BRD4(1) K_d = no binding detected by ITC (n=3)

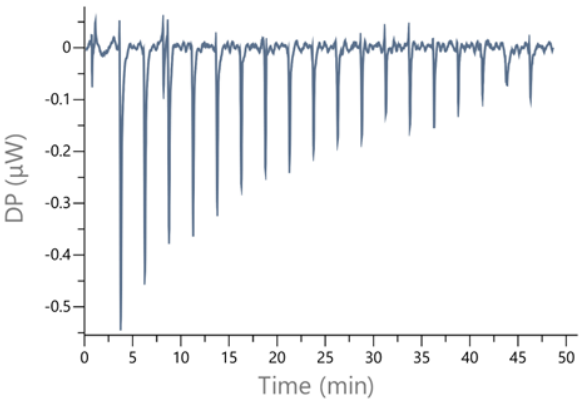

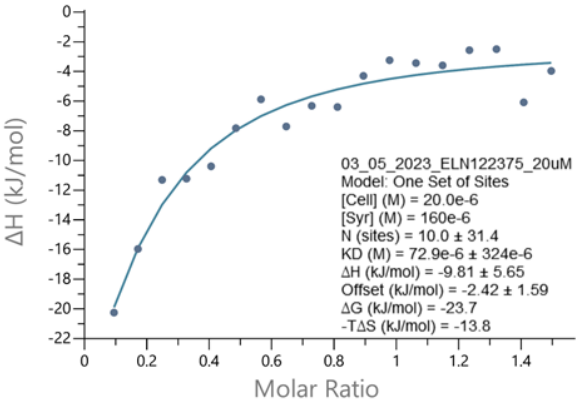

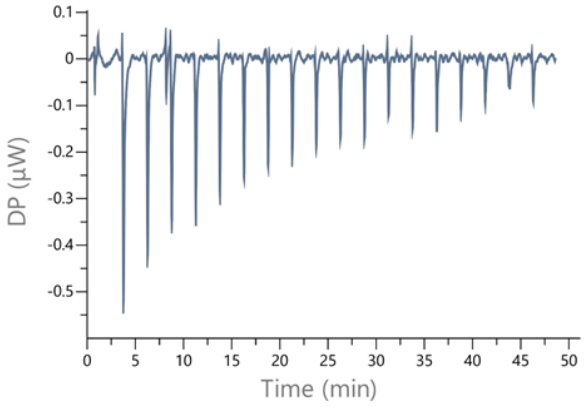

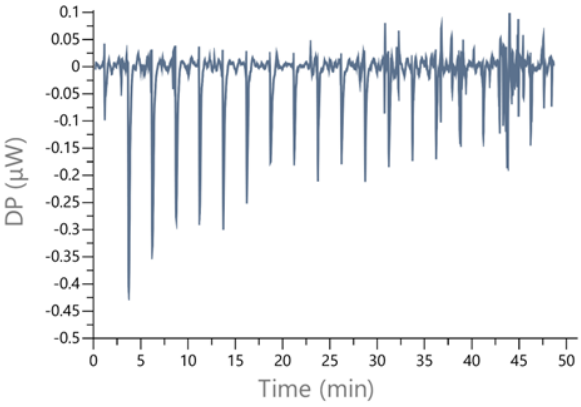

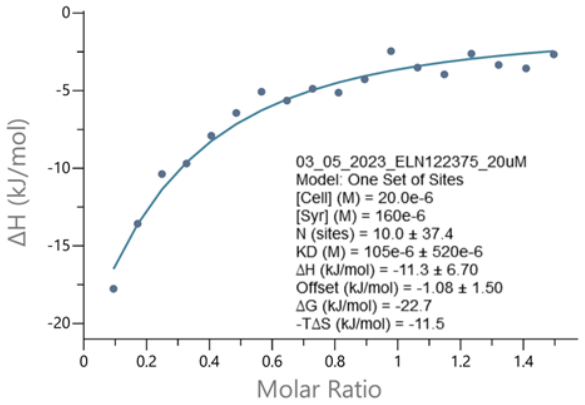

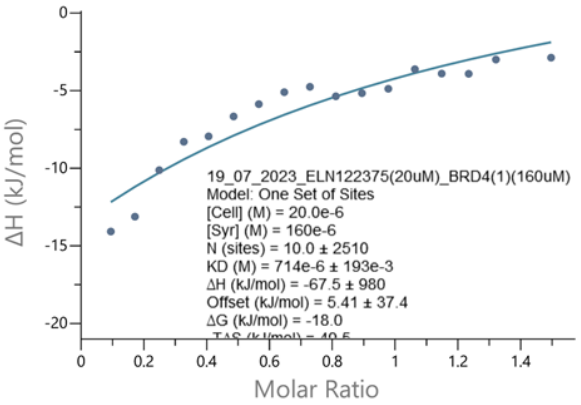

Appendix D, Figure 15: ITC trace for the binding of compound **14** to the BRD4(1).

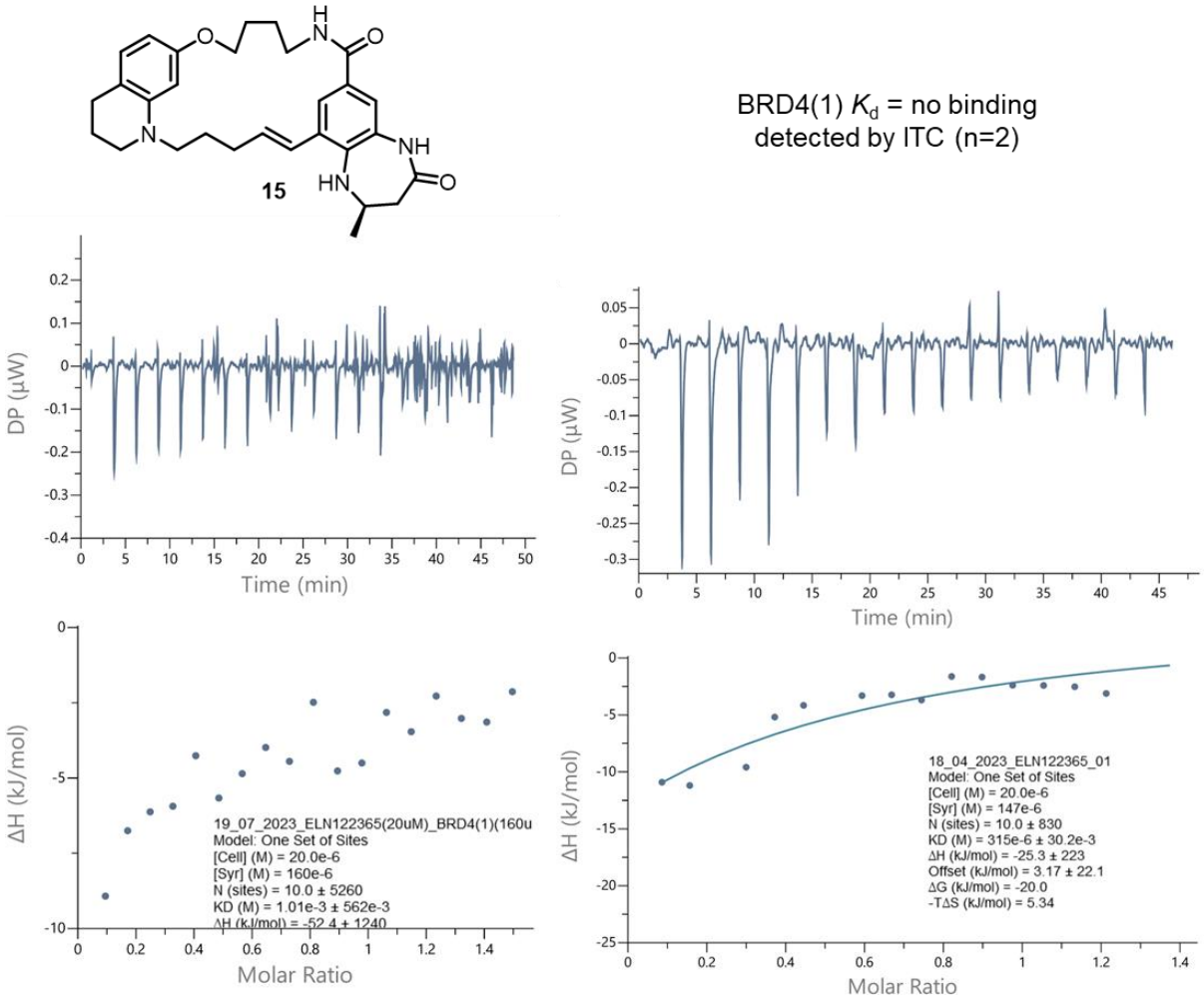

Appendix D, Figure 16: ITC trace for the binding of compound **15** to the BRD4(1).

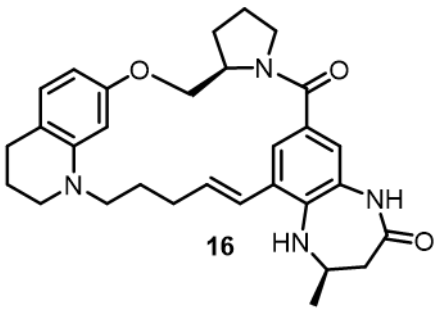

16

BRD4(1) K_d = no binding detected by ITC (n=2)

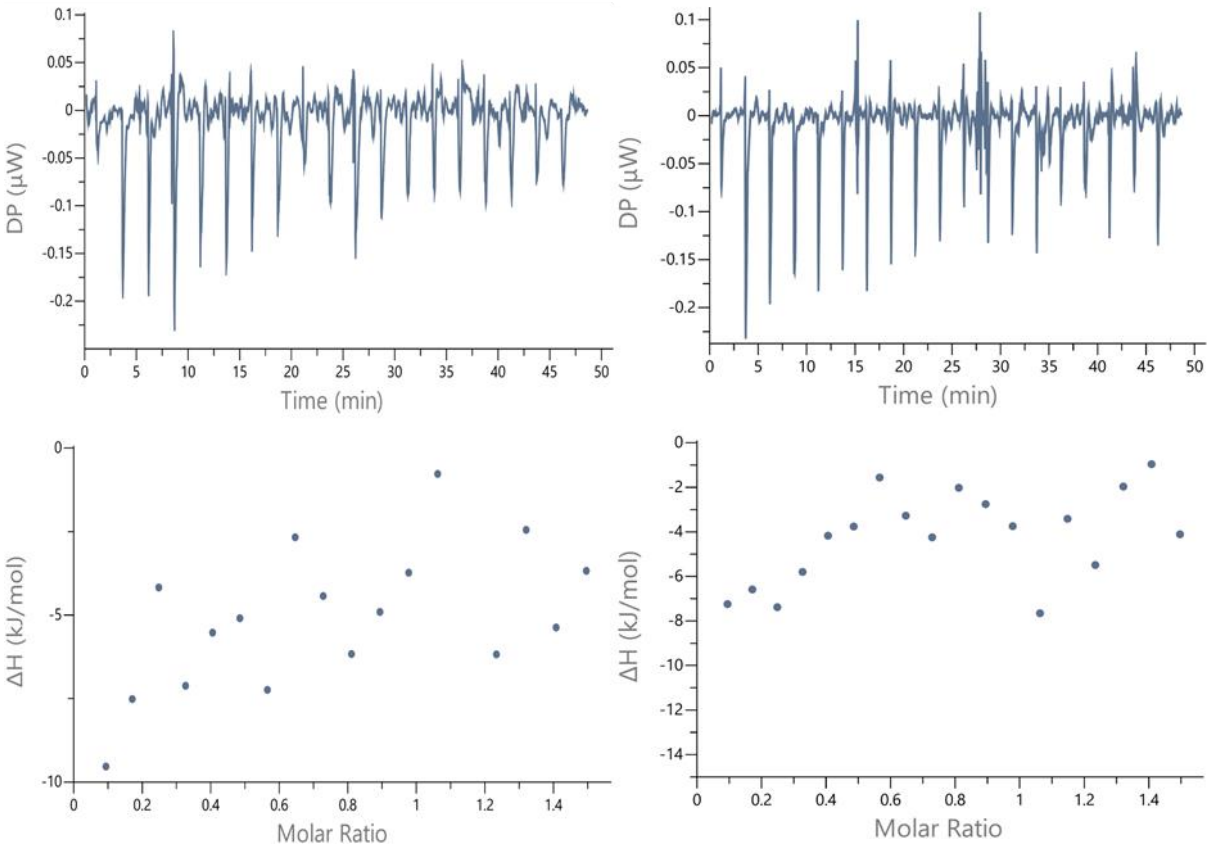

Appendix D, Figure 17: ITC trace for the binding of compound **16** to the BRD4(1).

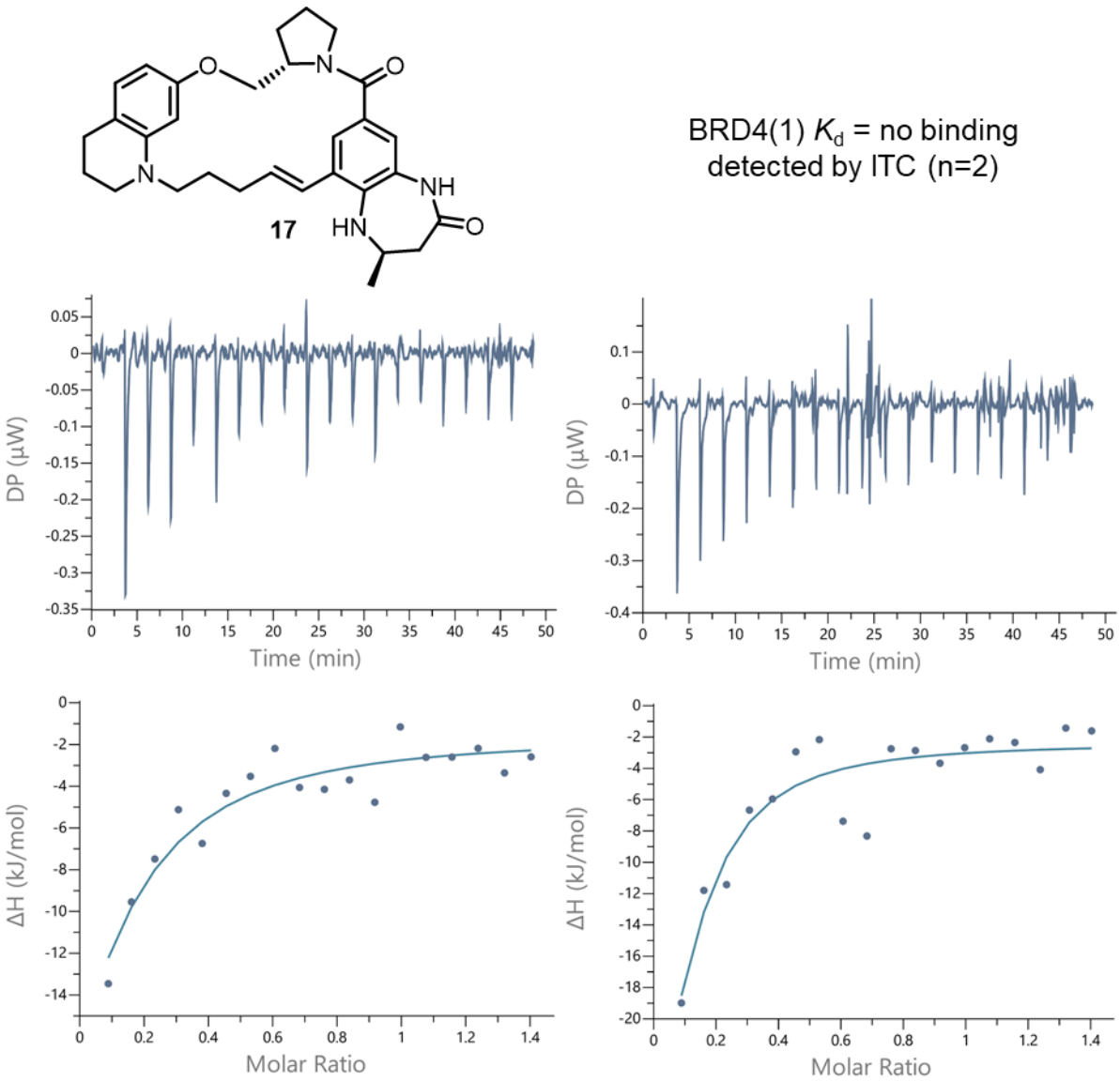

Appendix D, Figure 18: ITC trace for the binding of compound **17** to the BRD4(1).

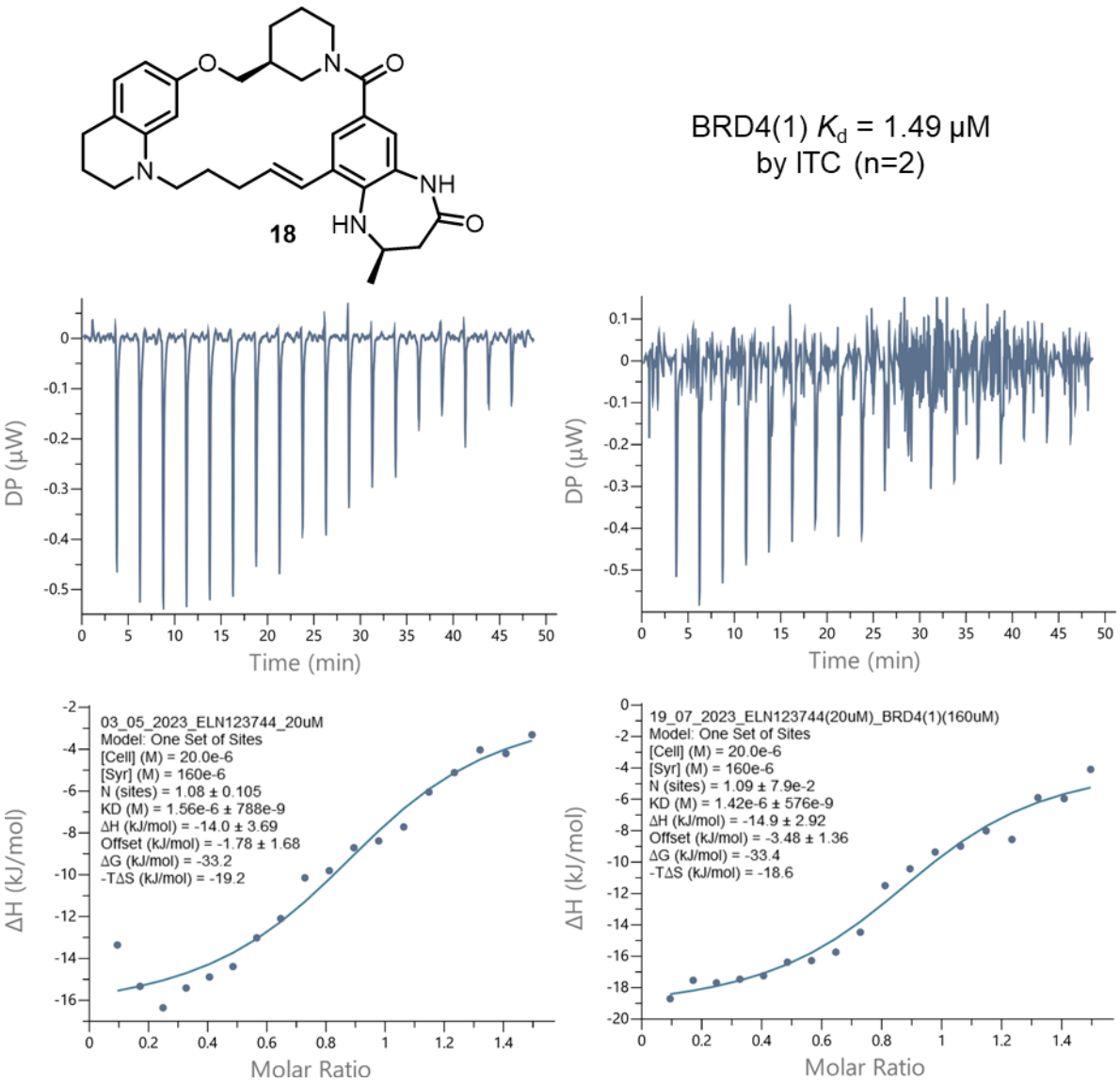

Appendix D, Figure 19: ITC trace for the binding of compound **18** to the BRD4(1).

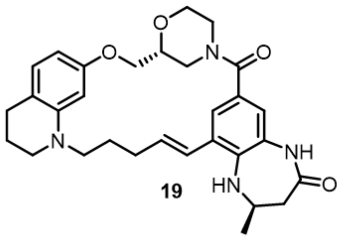

BRD4(1) K_d = no binding detected by ITC (n=5)

Appendix D, Figure 20: ITC trace for the binding of compound **19** to the BRD4(1).

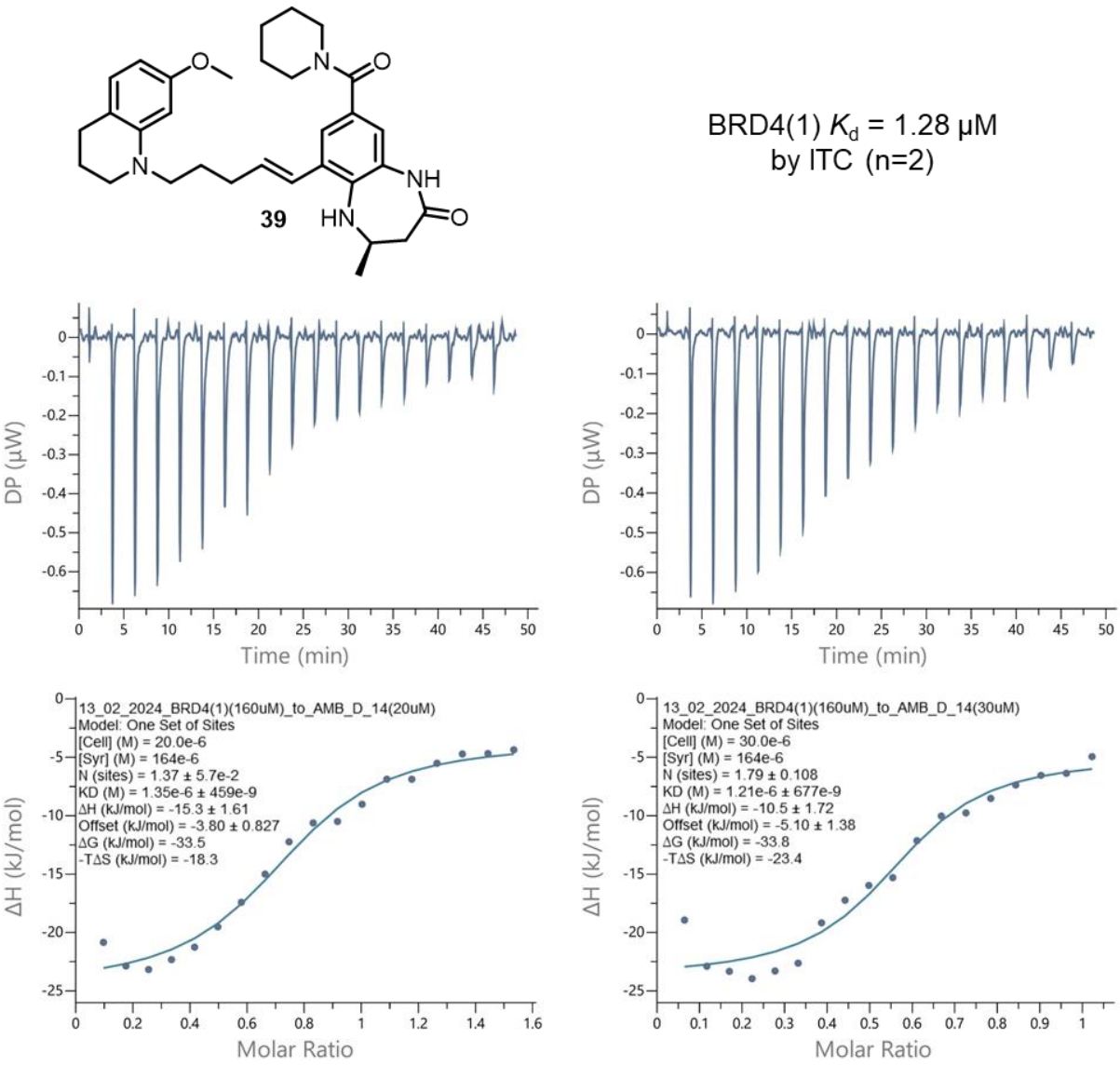

Appendix D, Figure 21: ITC trace for the binding of compound **39** to the BRD4(1).

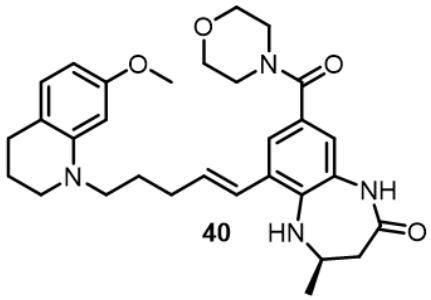

40

BRD4(1) K_d = 0.964 μM
by ITC (n=3)

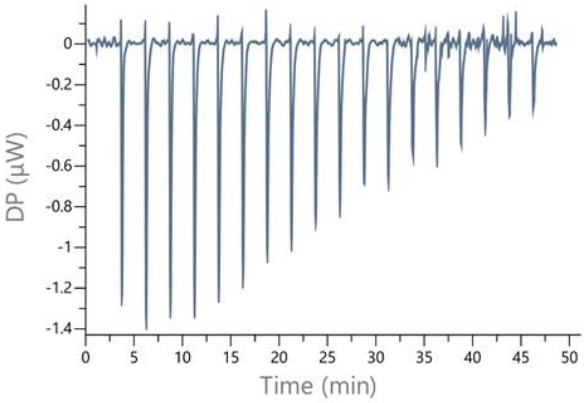

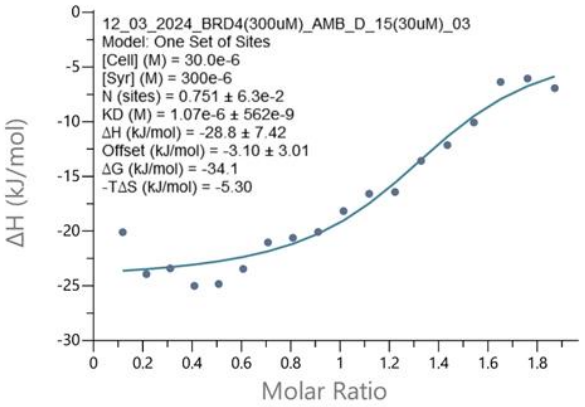

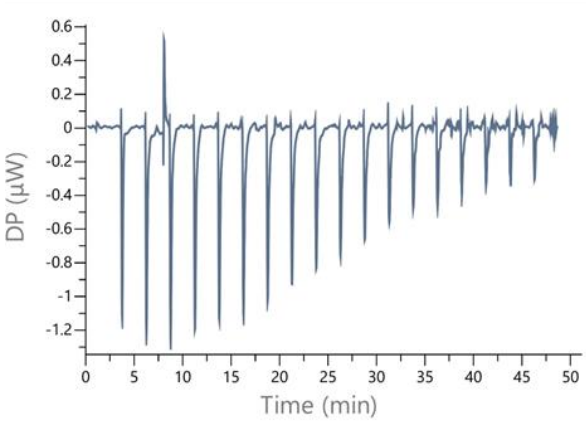

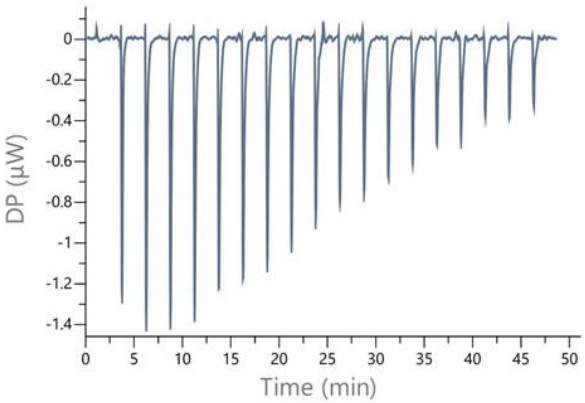

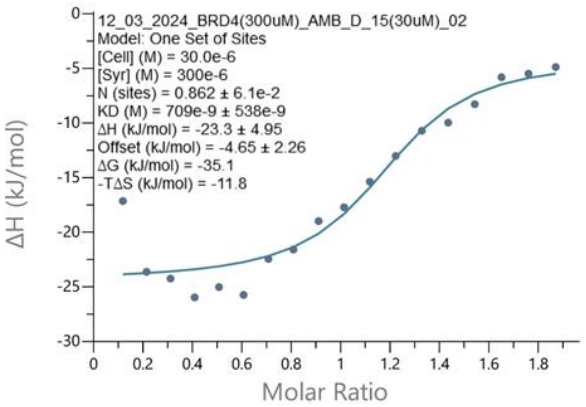

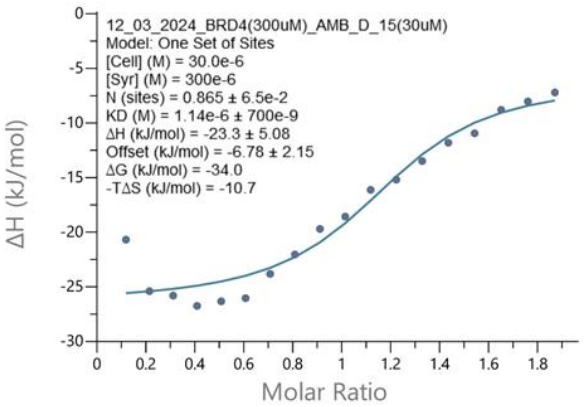

Appendix D, Figure 22: ITC trace for the binding of compound **40** to the BRD4(1).

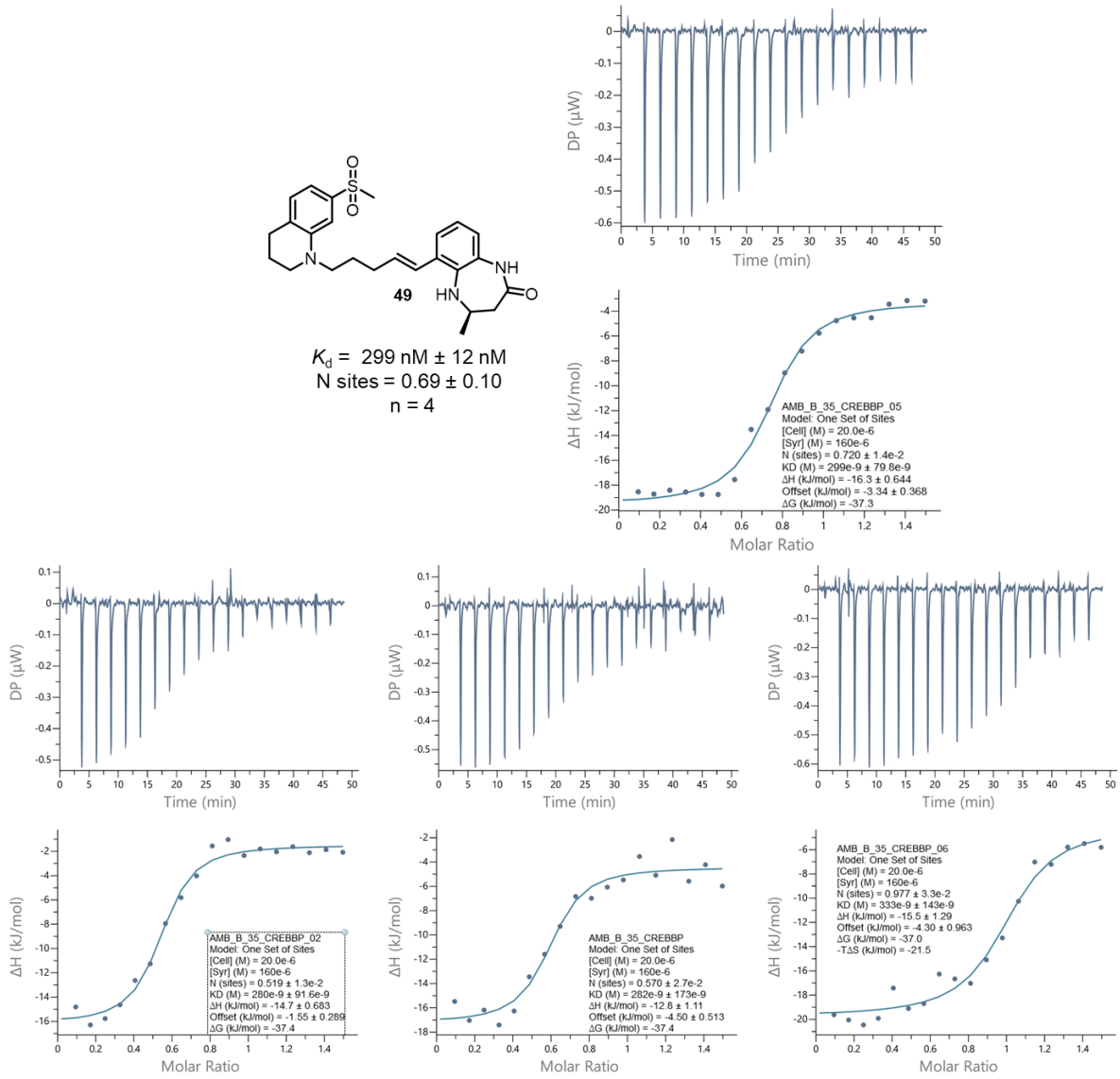

Appendix D, Figure 23: ITC trace for the binding of compound **49** to the CBP^{BRD}.

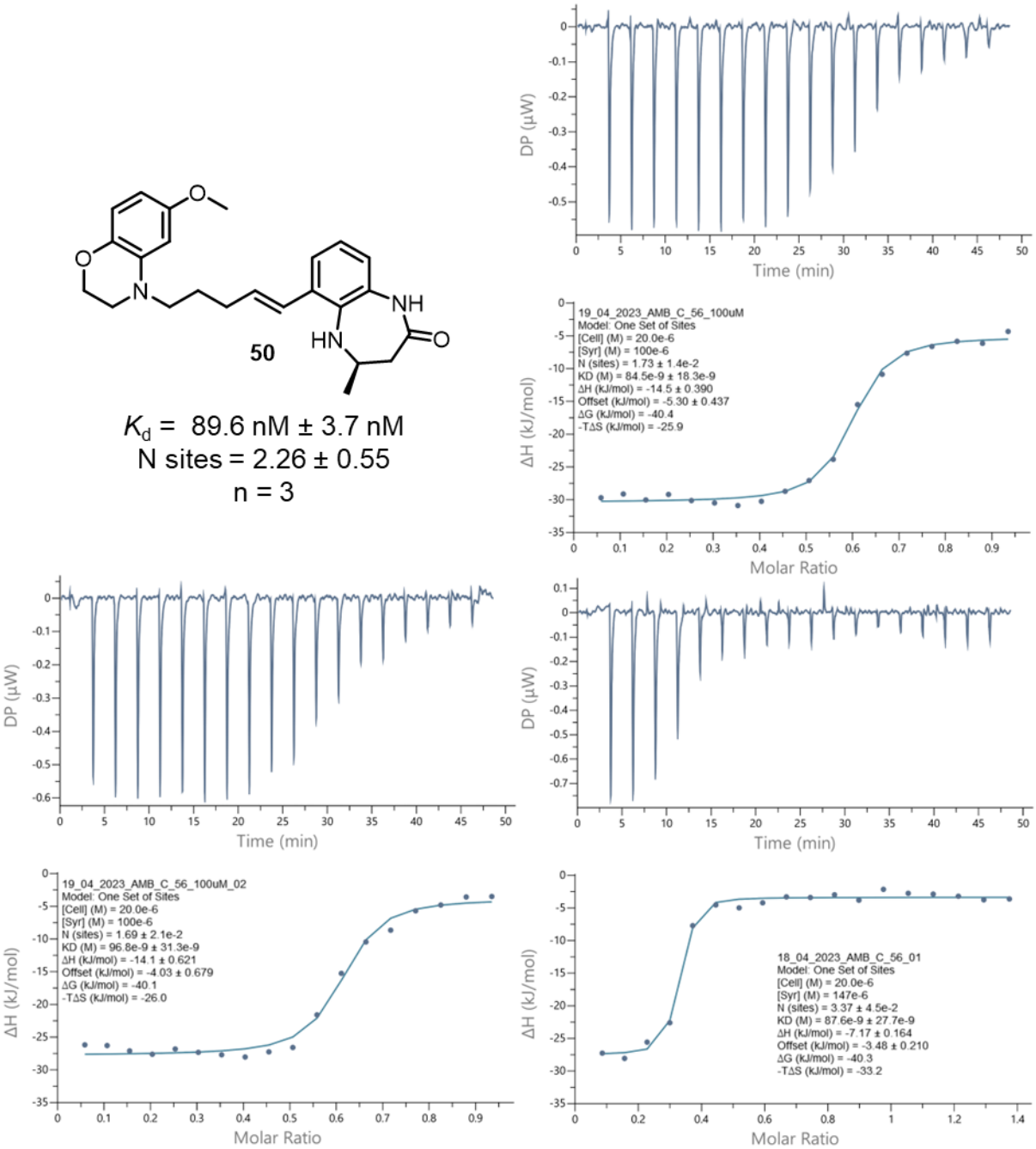

Appendix D, Figure 24: ITC trace for the binding of compound **50** to the CBP^{BRD}.

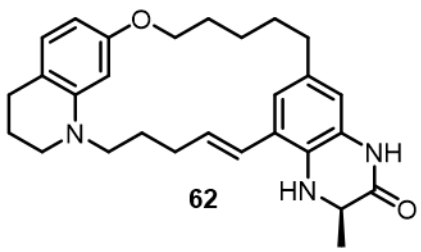

K_d = no binding by ITC
(n=3)

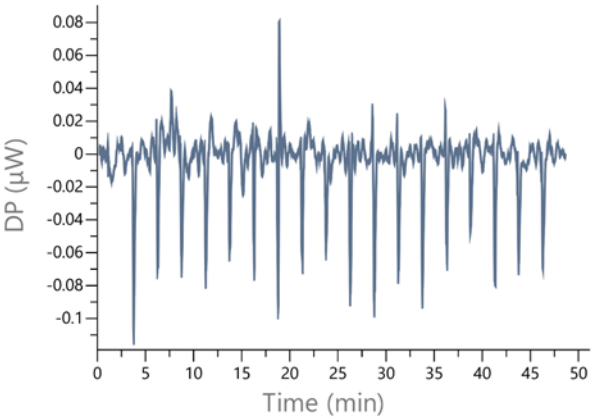

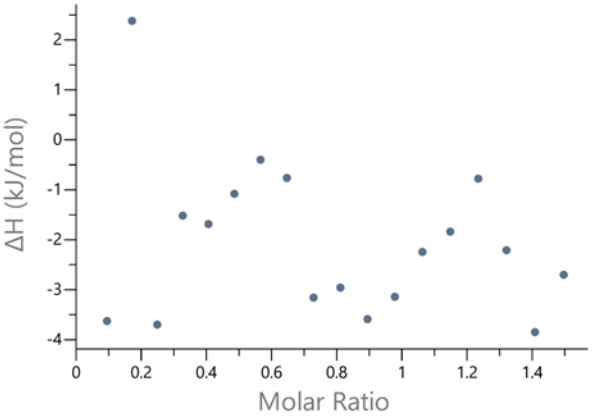

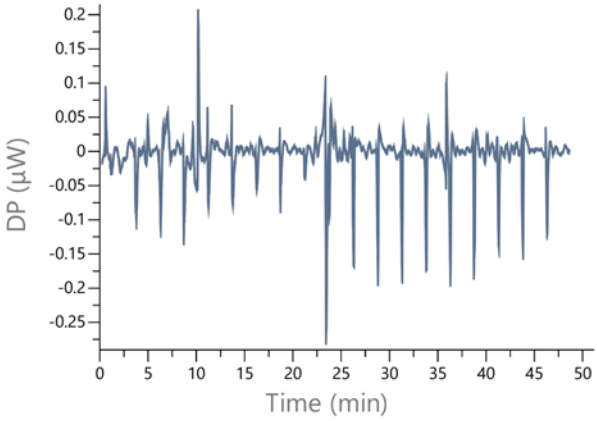

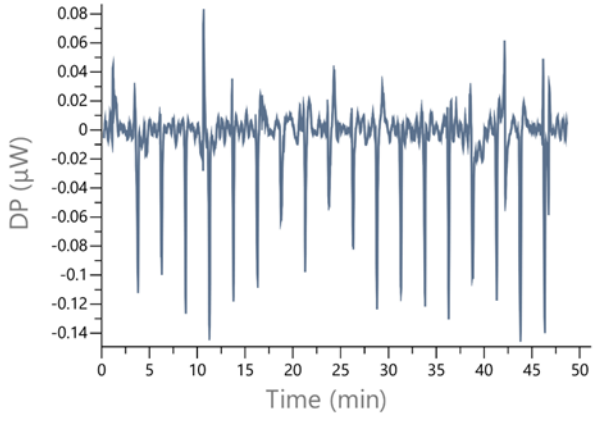

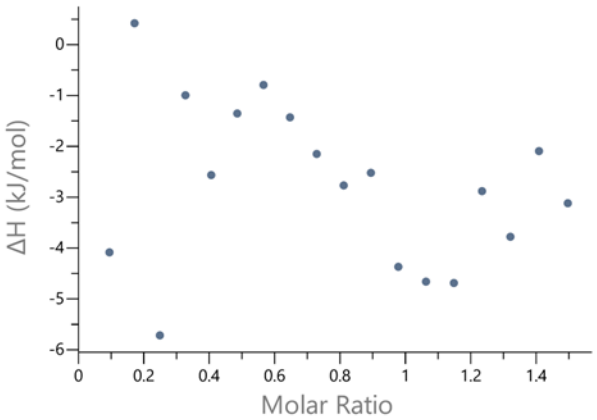

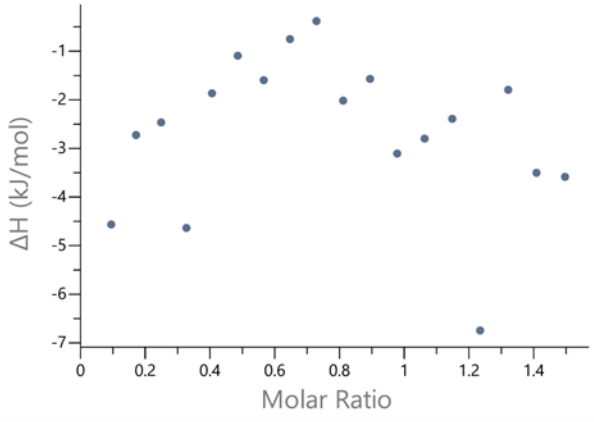

Appendix D, Figure 25: ITC traces for the binding of ligand **62** to the CBP^{BRD}.

Appendix E: Raw BromoKdElect and BromoMax Data and the corresponding compounds

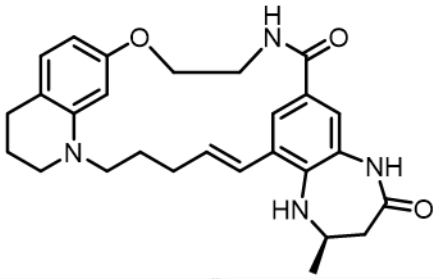

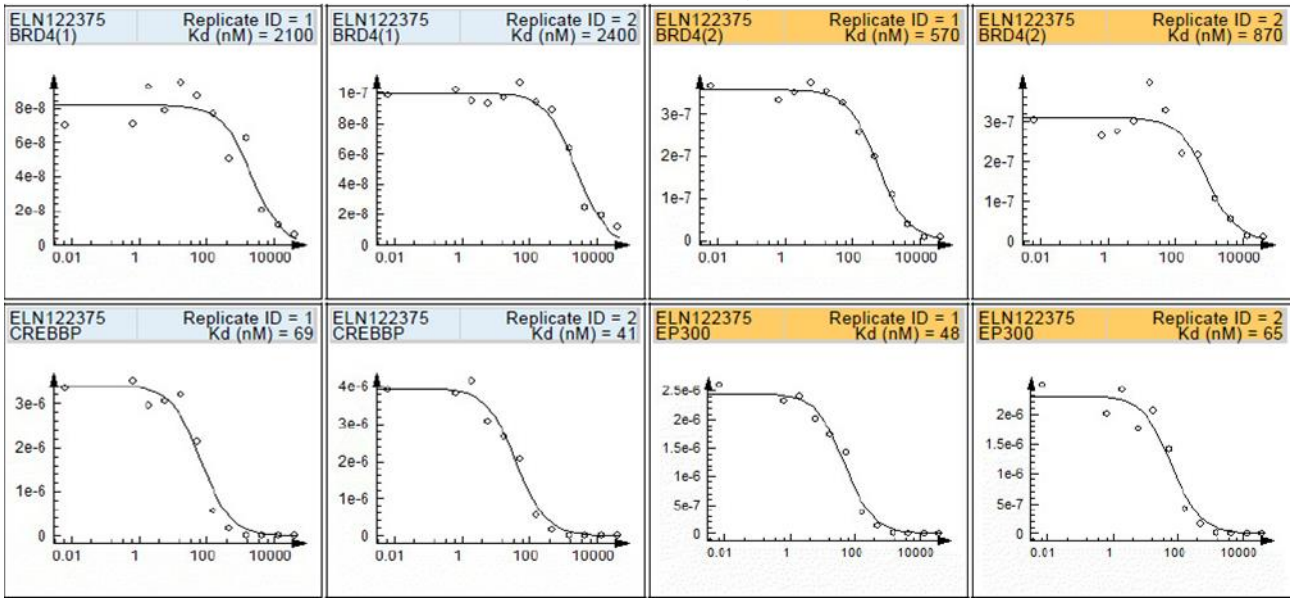

Appendix E Figure 1: BromoKdElect binding curves for CBP^{BRD}, $p300^{BRD}$, BRD4(1) and BRD4(2) for the ligand shown.

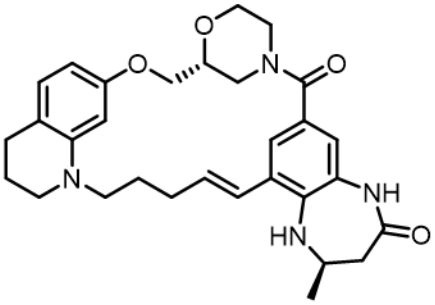

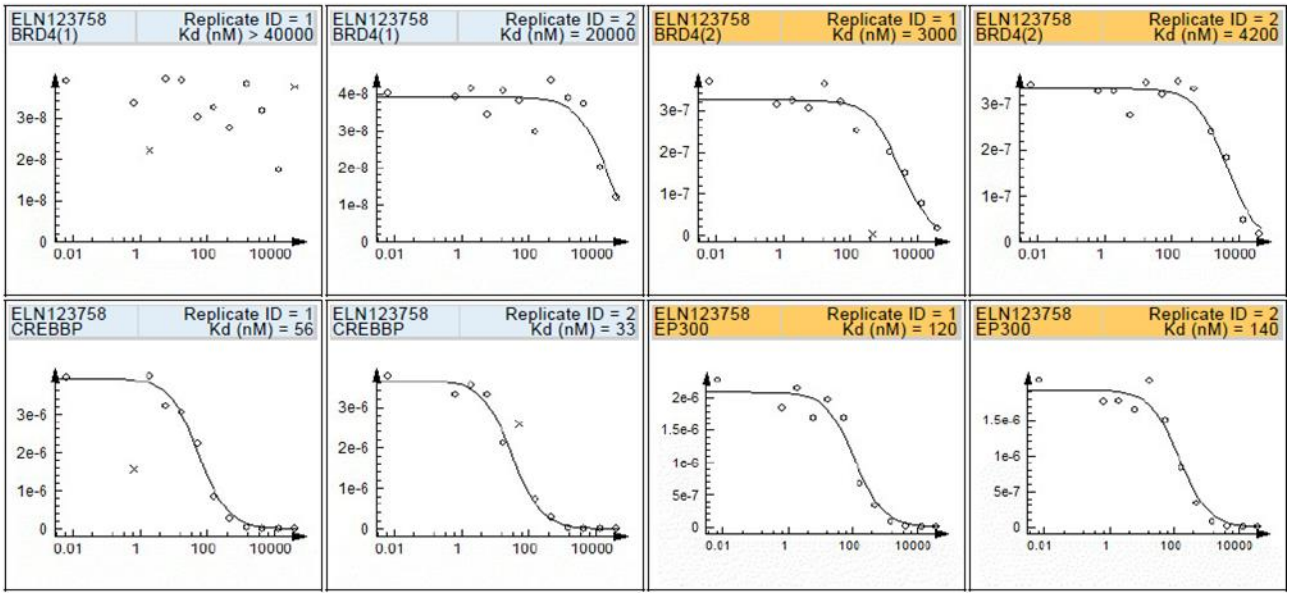

Appendix E Figure 2: BromoKdElect binding curves for CBP^{BRD}, $p300^{BRD}$, BRD4(1) and BRD4(2) for the ligand shown.

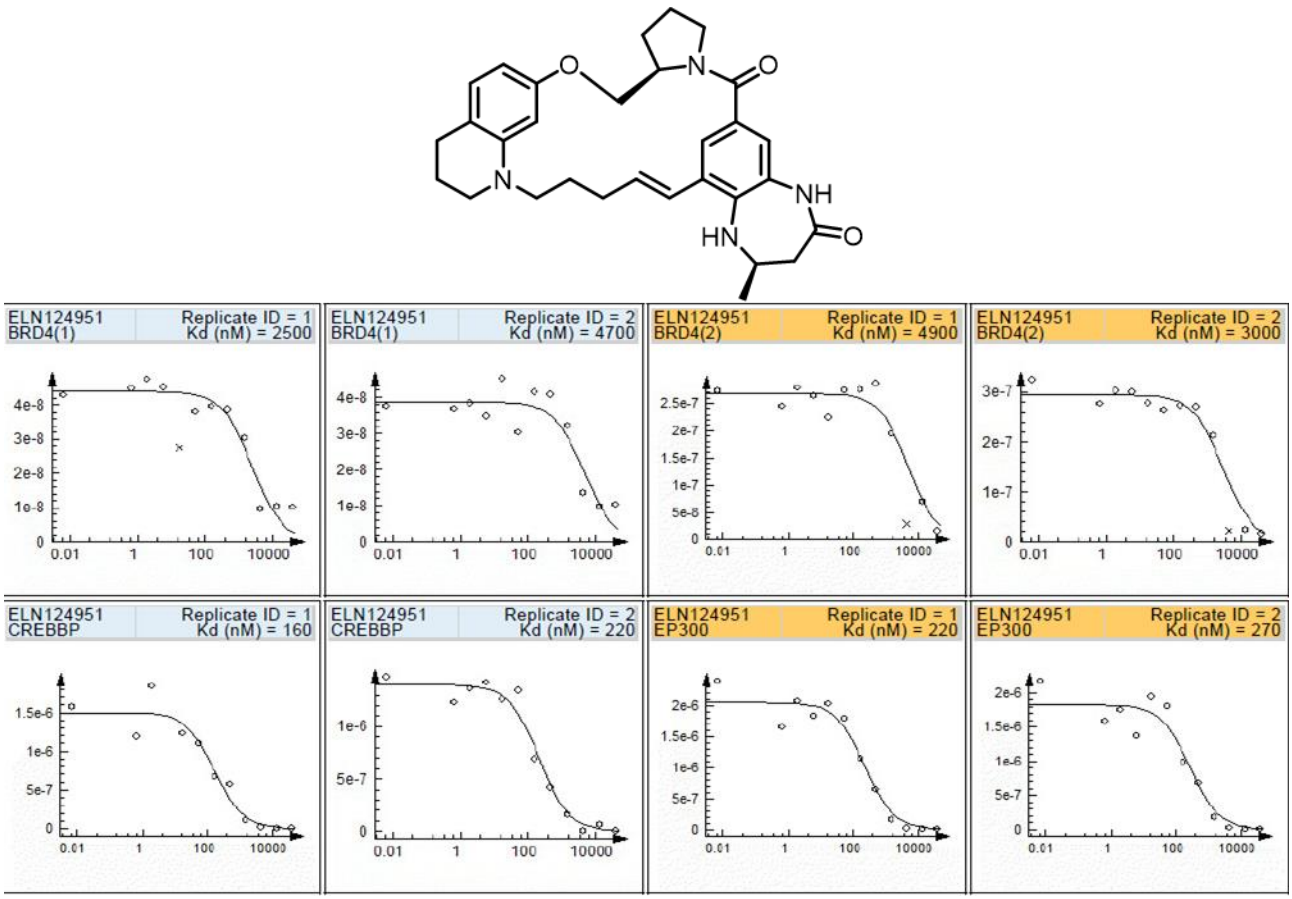

Appendix E Figure 3: BromoKdElect binding curves for CBP^{BRD}, $p300^{BRD}$, BRD4(1) and BRD4(2) for the ligand shown.

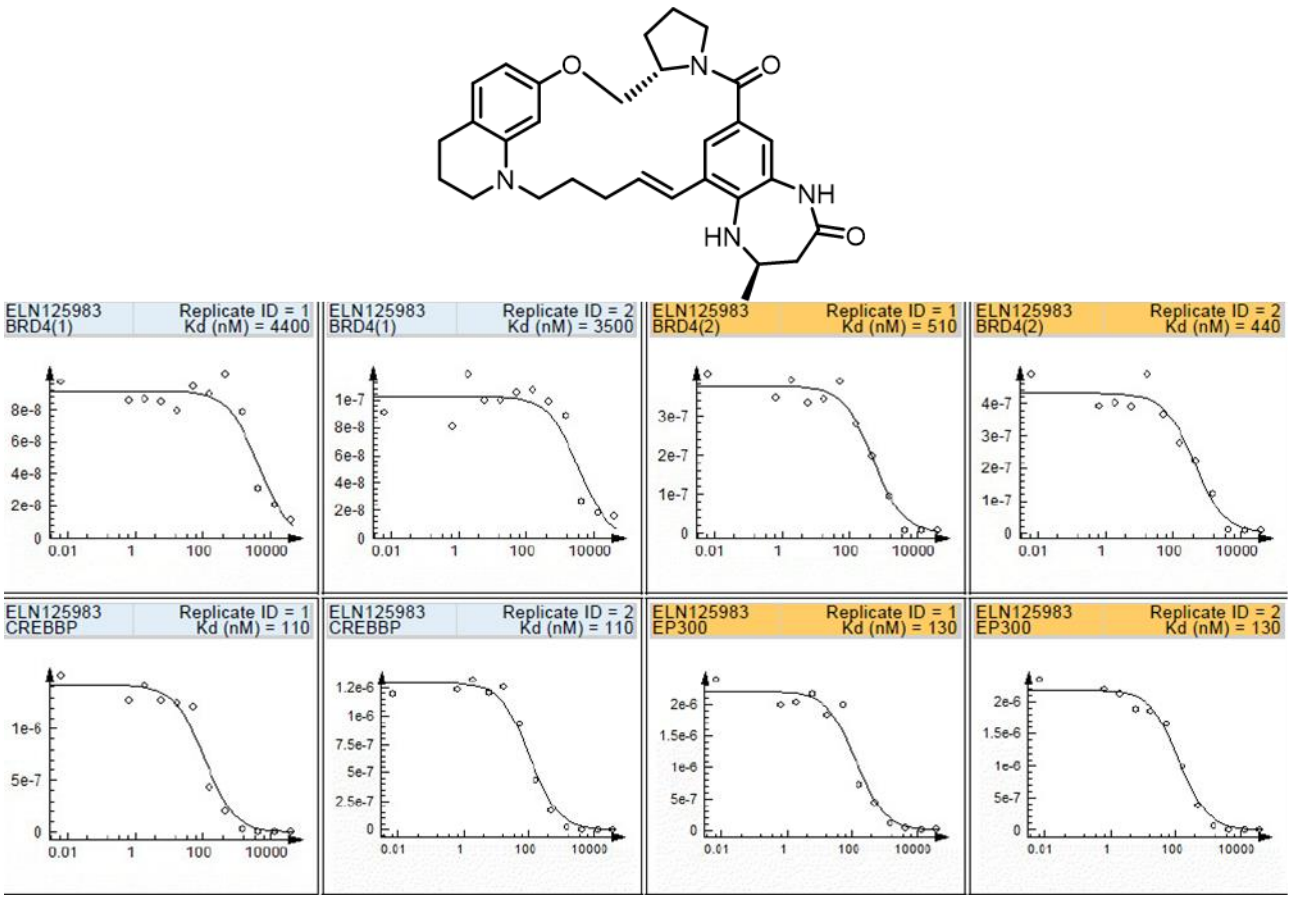

Appendix E Figure 4: BromoKdElect binding curves for CBP^{BRD}, $p300^{BRD}$, BRD4(1) and BRD4(2) for the ligand shown.

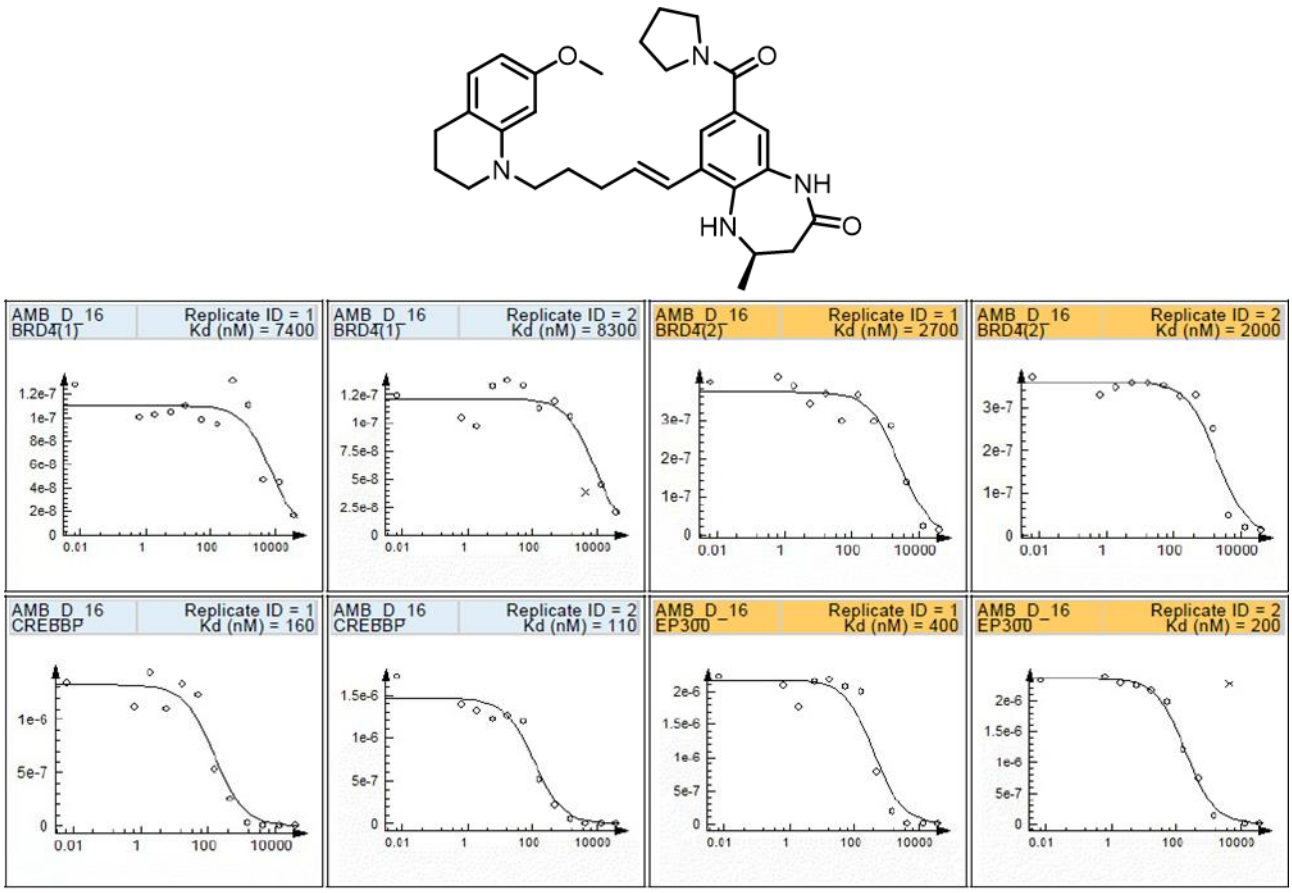

Appendix E Figure 5: BromoKdElect binding curves for CBP^{BRD}, $p300^{BRD}$, BRD4(1) and BRD4(2) for the ligand shown.

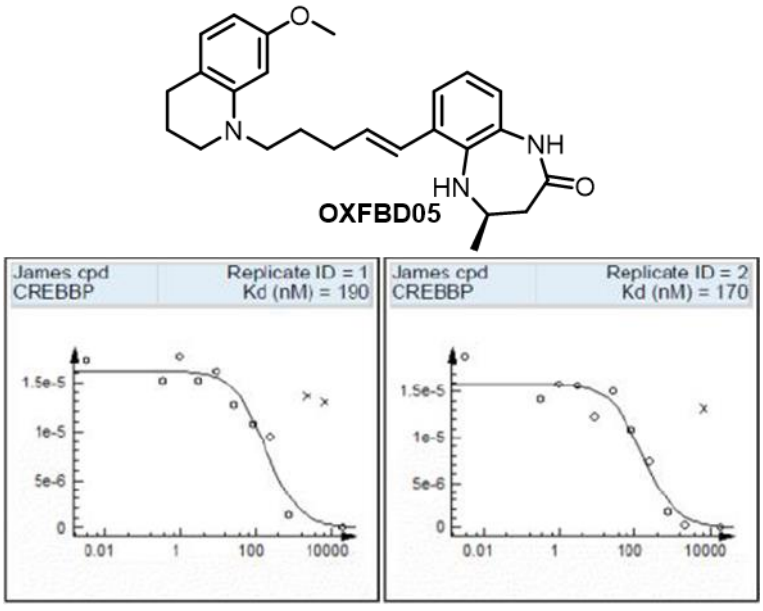

Appendix E Figure 6: BromoKdElect binding curves for CBP^{BRD} for the ligand shown.

Target	ELN123758
Gene Symbol	%Ctrl @ 1000nM
ATAD2A	98
ATAD2B	85
BAZ2A	77
BAZ2B	86
BRD1	100
BRD2(1)	69
BRD2(2)	96
BRD3(1)	97
BRD3(2)	91
BRD4(1)	92
BRD4(2)	88
BRD7	100
BRD9	100
BRDT(1)	96
BRDT(2)	88
BRPF1	85
BRPF3	98
CECR2	100
CREBBP	2.7
EP300	9
FALZ	99
GCN5L2	71
PBRM1(2)	82
PBRM1(5)	100
PCAF	93
SMARCA2	54
SMARCA4	98
TAF1(2)	55
TAF1L(2)	96
TRIM24(PHD,Bromo.)	90
TRIM33(PHD,Bromo.)	87
WDR9(2)	95

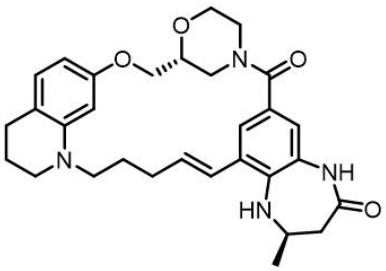

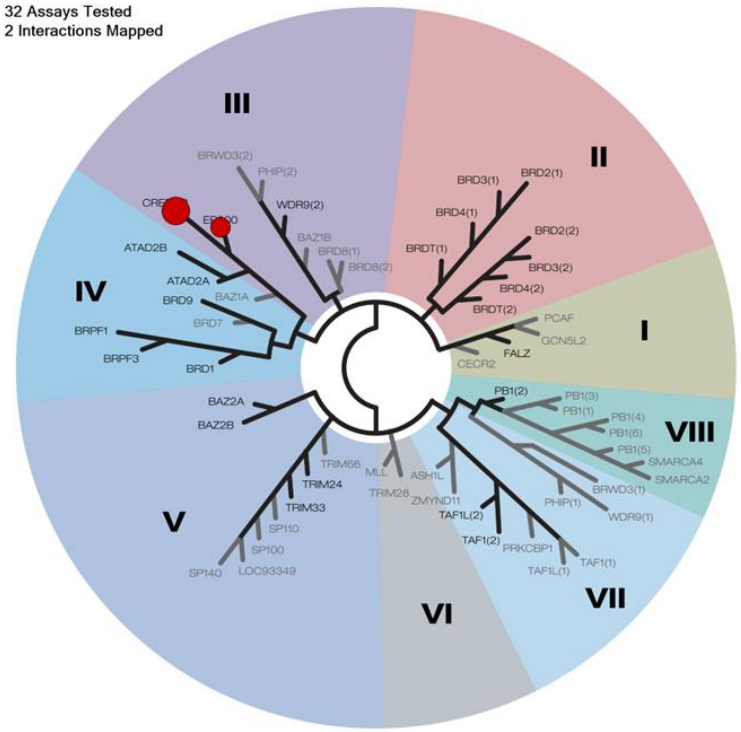

%Ctrl Legend

0≤x<.1	.1≤x<1	1≤x<10	10≤x<35	x≥35

Appendix E figure 7: BromoMax data for the compound **19** at 1 μM shown, binding tested against 32 bromodomain containing protein (green or red dots on the phylogenetic tree), with red dots indicating binding interactions and the sizes of those dots denoting the strength of the interaction (right bottom), the raw data table and the legend are displayed (left hand side) along with the chemical structure (top right).

Target	ELN123758
Gene Symbol	%Ctrl @ 10000nM
ATAD2A	100
ATAD2B	83
BAZ2A	3
BAZ2B	60
BRD1	96
BRD2(1)	56
BRD2(2)	29
BRD3(1)	43
BRD3(2)	16
BRD4(1)	51
BRD4(2)	28
BRD7	48
BRD9	26
BRDT(1)	48
BRDT(2)	39
BRPF1	22
BRPF3	76
CECR2	48
CREBBP	0
EP300	0.1
FALZ	38
GCN5L2	100
PBRM1(2)	97
PBRM1(5)	21
PCAF	100
SMARCA2	3.2
SMARCA4	69
TAF1(2)	2
TAF1L(2)	54
TRIM24(PHD,Bromo.)	36
TRIM33(PHD,Bromo.)	100
WDR9(2)	99

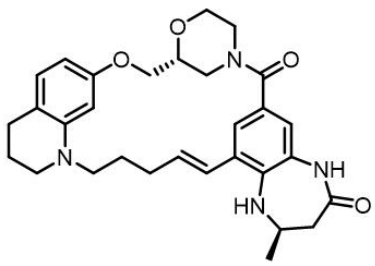

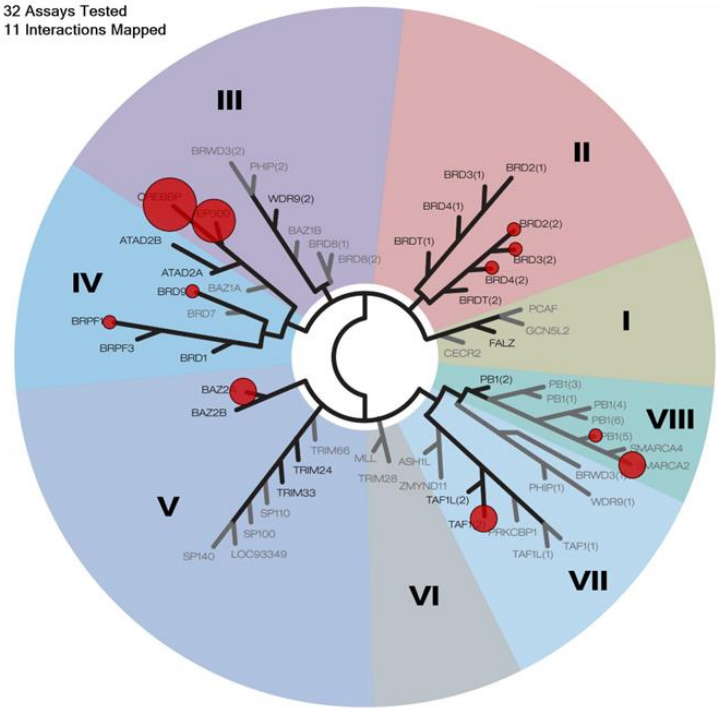

%Ctrl Legend

0≤x<.1	.1≤x<1	1≤x<10	10≤x<35	x≥35

Appendix E figure 8: BromoMax data for the compound **19** at 10 μM shown, binding tested against 32 bromodomain containing protein (green or red dots on the phylogenetic tree), with red dots indicating binding interactions and the sizes of those dots denoting the strength of the interaction (right bottom), the raw data table and the legend are displayed (left hand side) along with the chemical structure (top right).

Appendix F: Supplementary crystal structure figures for the compounds presented in this thesis bound to the CBP^{BRD}

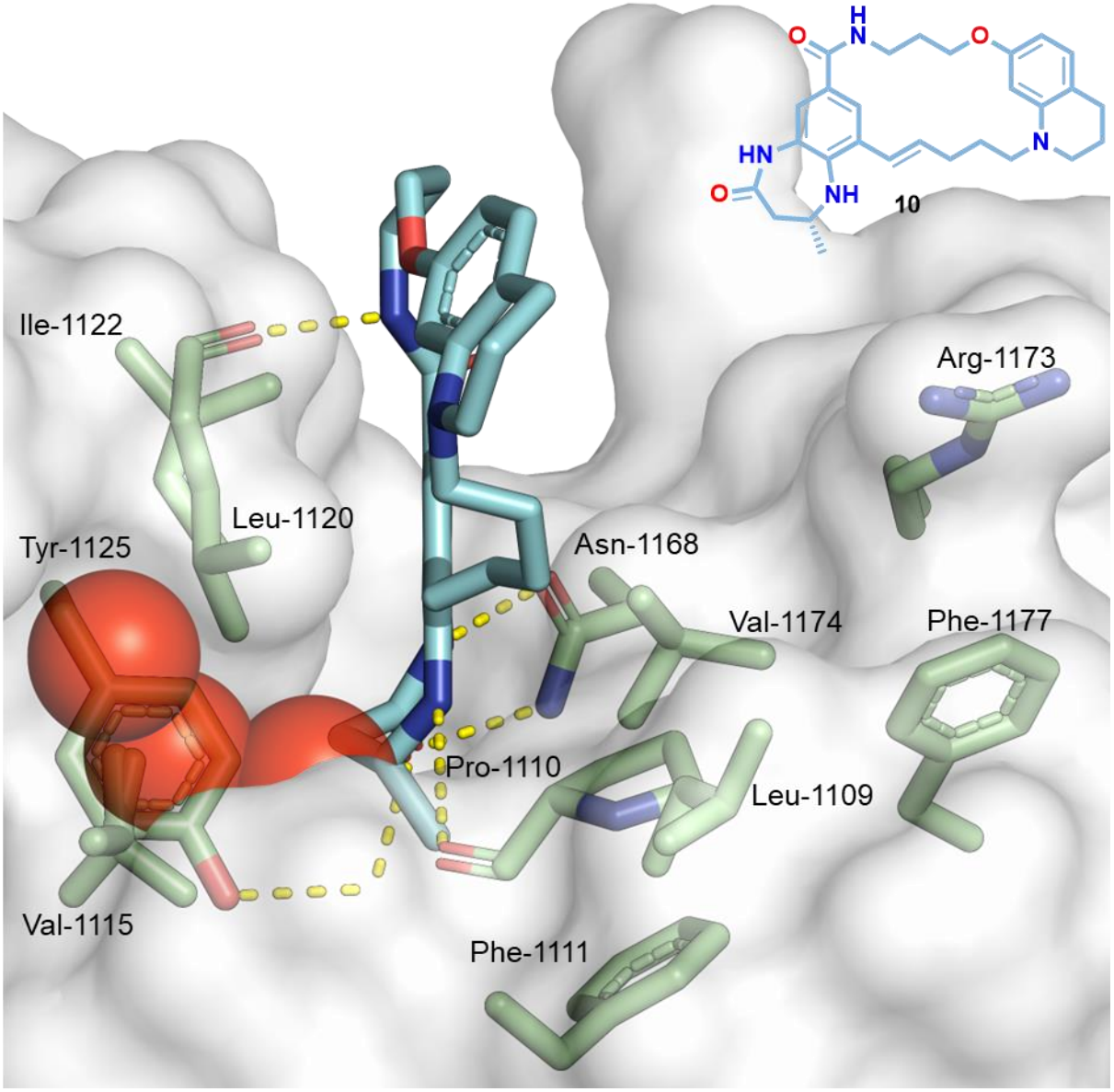

Appendix F, Figure 1: X-ray co-crystal structure of ligand **10** (light blue) in complex with the CBP^{BRD} (PDB: 9GEY) at 1.56 Å resolution, viewed from the side of the binding pocket along the ZA channel with water occupying the channel. All residues which the ligand interacts with are displayed (green) with labels and the backbone amide removed for clarity unless otherwise involved in hydrogen bonding and the hydrogen bonding interactions to the ligand highlighted by the dashed (yellow) lines, and with the chemical structure of **10** shown in the top right.

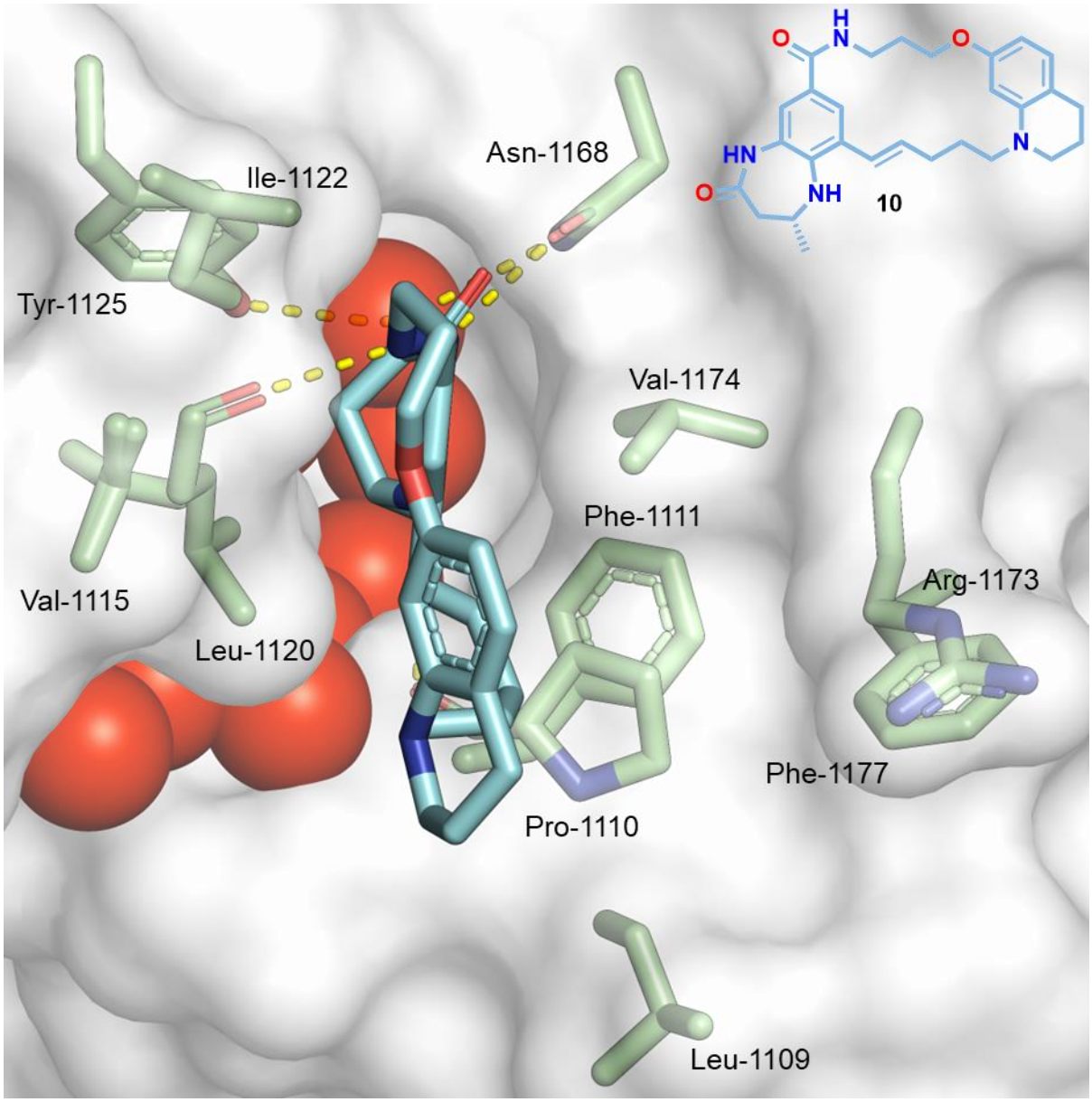

Appendix F, Figure 2: X-ray co-crystal structure of ligand **10** (light blue) in complex with the CBP^{BRD} (PDB: 9GEY) at 1.56 Å resolution, viewed from the top of the binding pocket along the ZA channel with water occupying the channel. All residues which the ligand interacts with are displayed (green) with labels and the backbone amide removed for clarity unless otherwise involved in hydrogen bonding and the hydrogen bonding interactions to the ligand highlighted by the dashed (yellow) lines, and with the chemical structure of **10** shown in the top right.

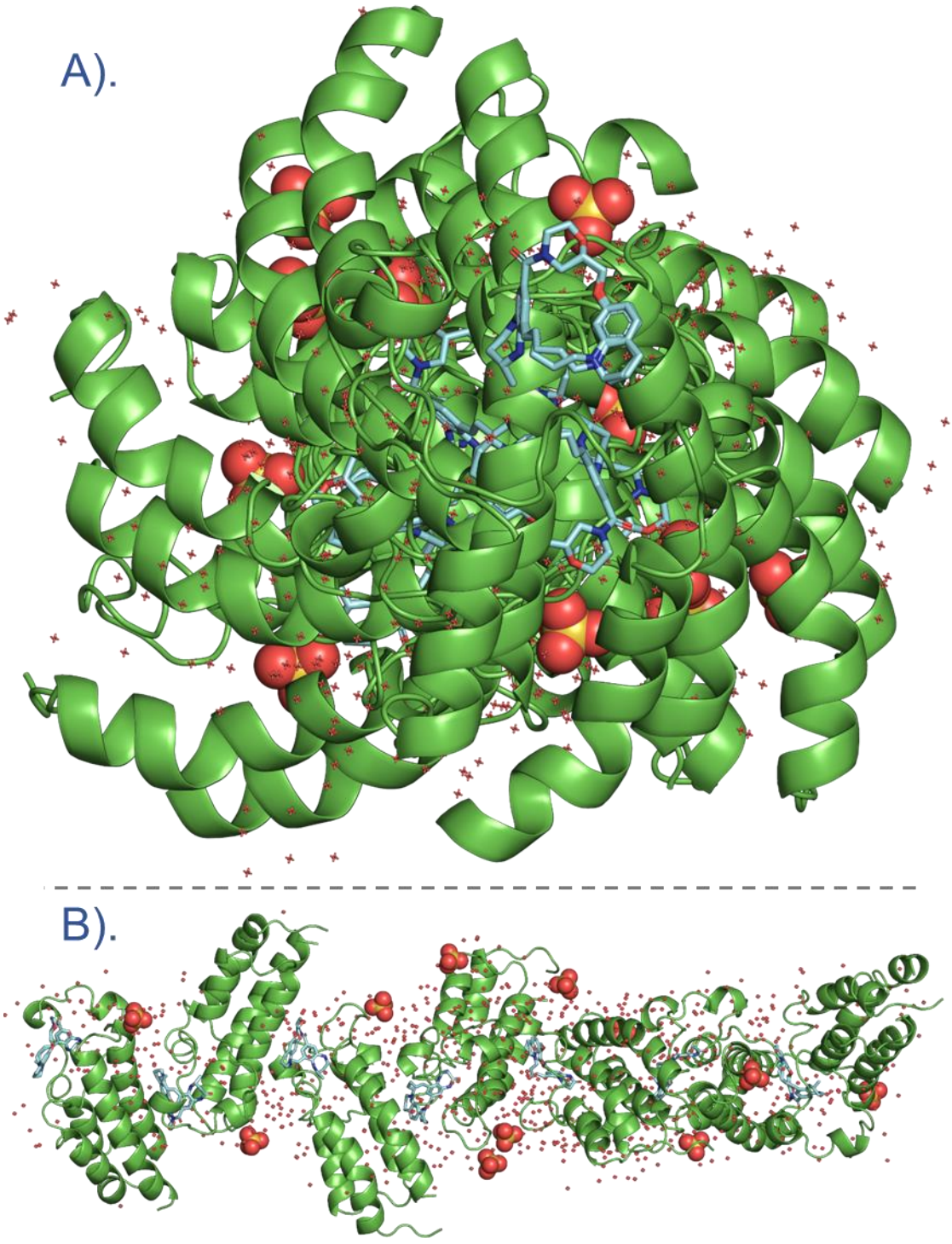

Appendix F Figure 3: Heptameric crystal structure; A). top-down view of the heptamer with the protein units in green, waters molecules in red as crosses, sulphate anions as yellow and macrocycle shown in cyan; B) the same crystal structure but viewed from the side of the heptameric unit.

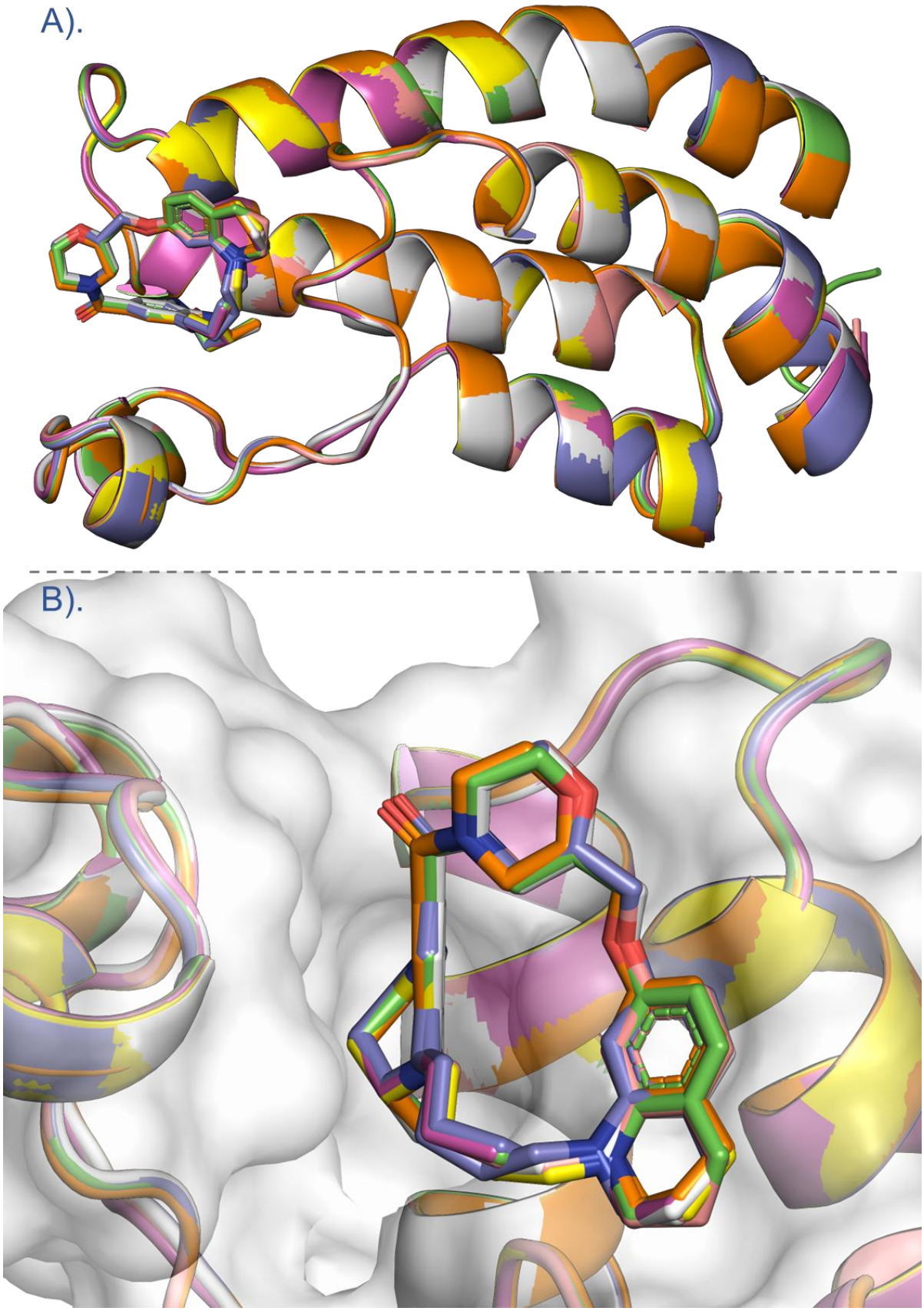

Appendix F Figure 4: Overlay of the seven units within the heptameric structure, proving that it is homo-heptameric, with each unit and its corresponding ligand presented as different colours; A). overlay of the whole bromodomain; B). overlay zoomed into the binding site of the macrocycle, with the surface visible for a single monomer unit.

Appendix G: Full AUC data

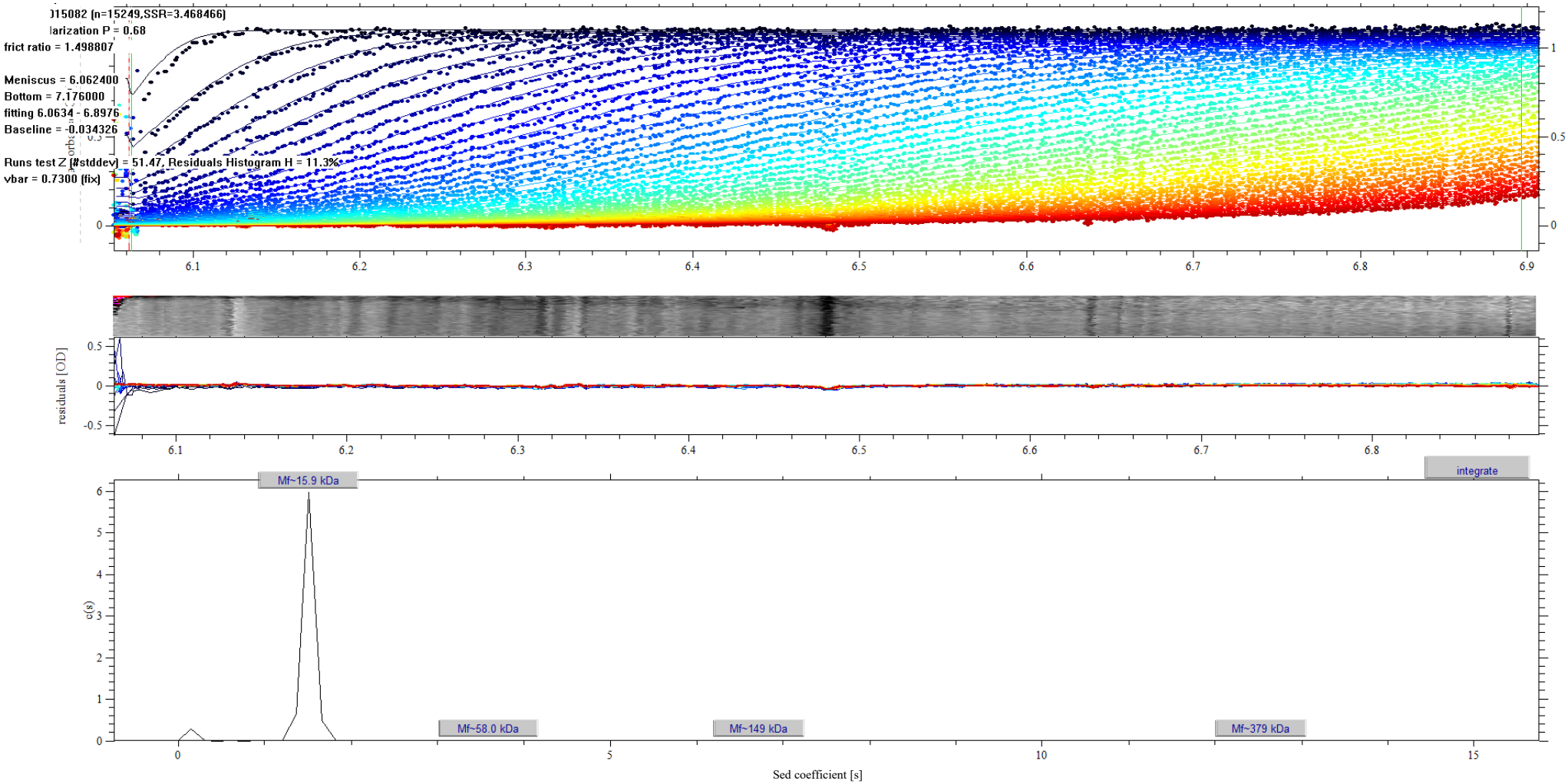

Appendix G Figure 1: AUC data for the CBP^{BRD} only without addition of any ligands.

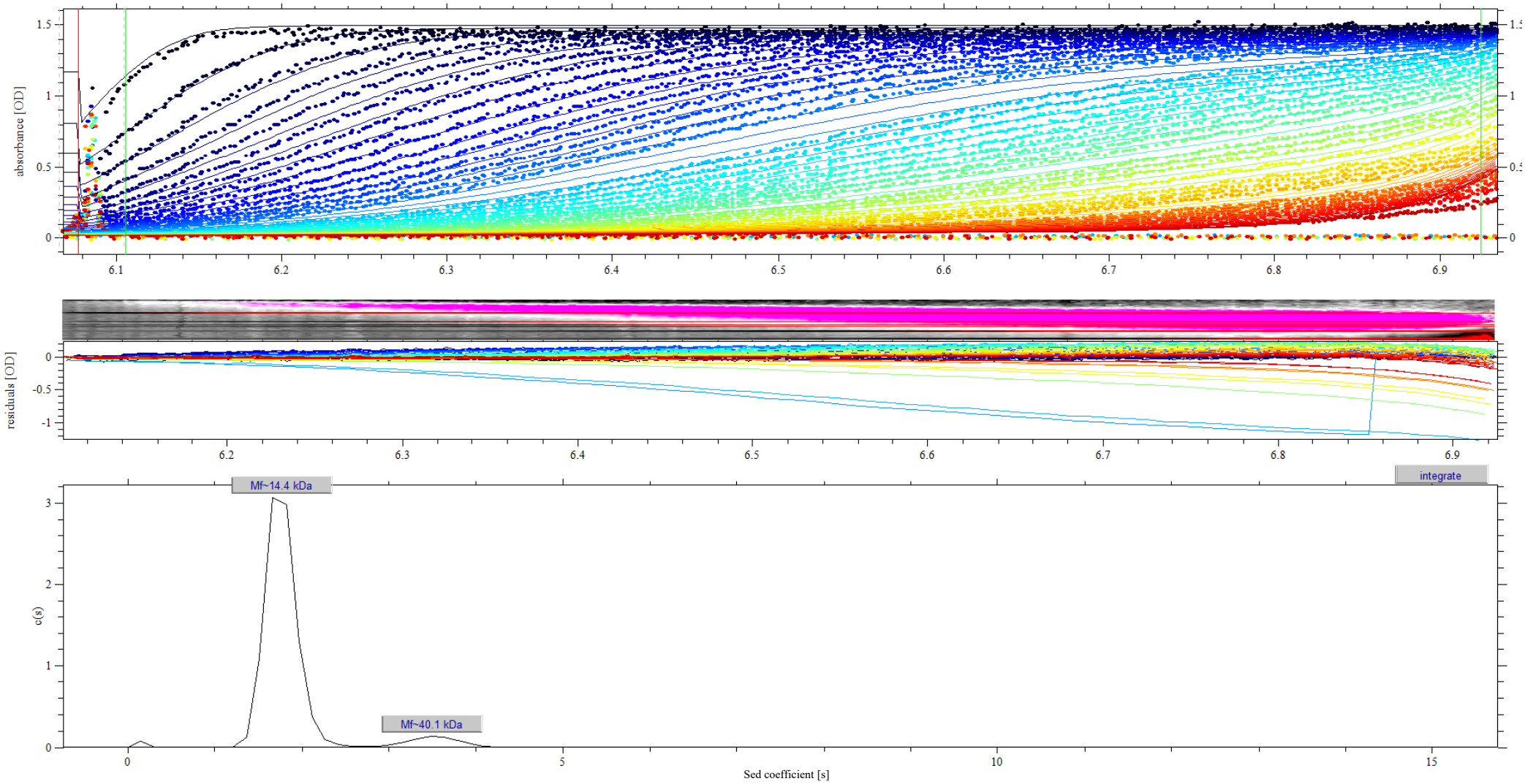

Appendix G Figure 2: AUC data for **19** and the CBP^{BRD} with 20 μM of ligand and 40 μM of protein without ligand **19** added to the reference cell.

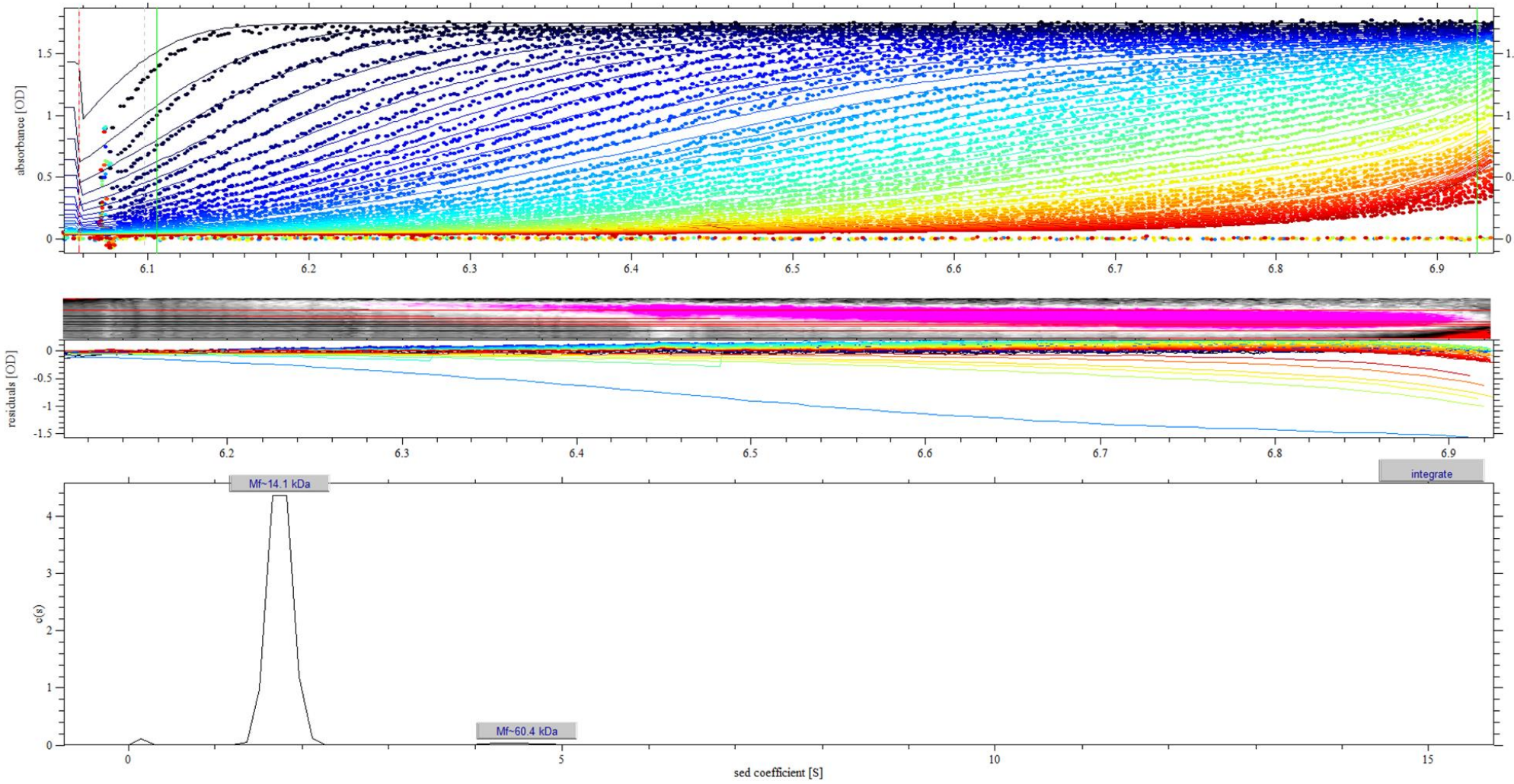

Appendix G Figure 3: AUC data for **19** and the CBP^{BRD} with 40 μM of ligand and 40 μM of protein without ligand **19** added to the reference cell.

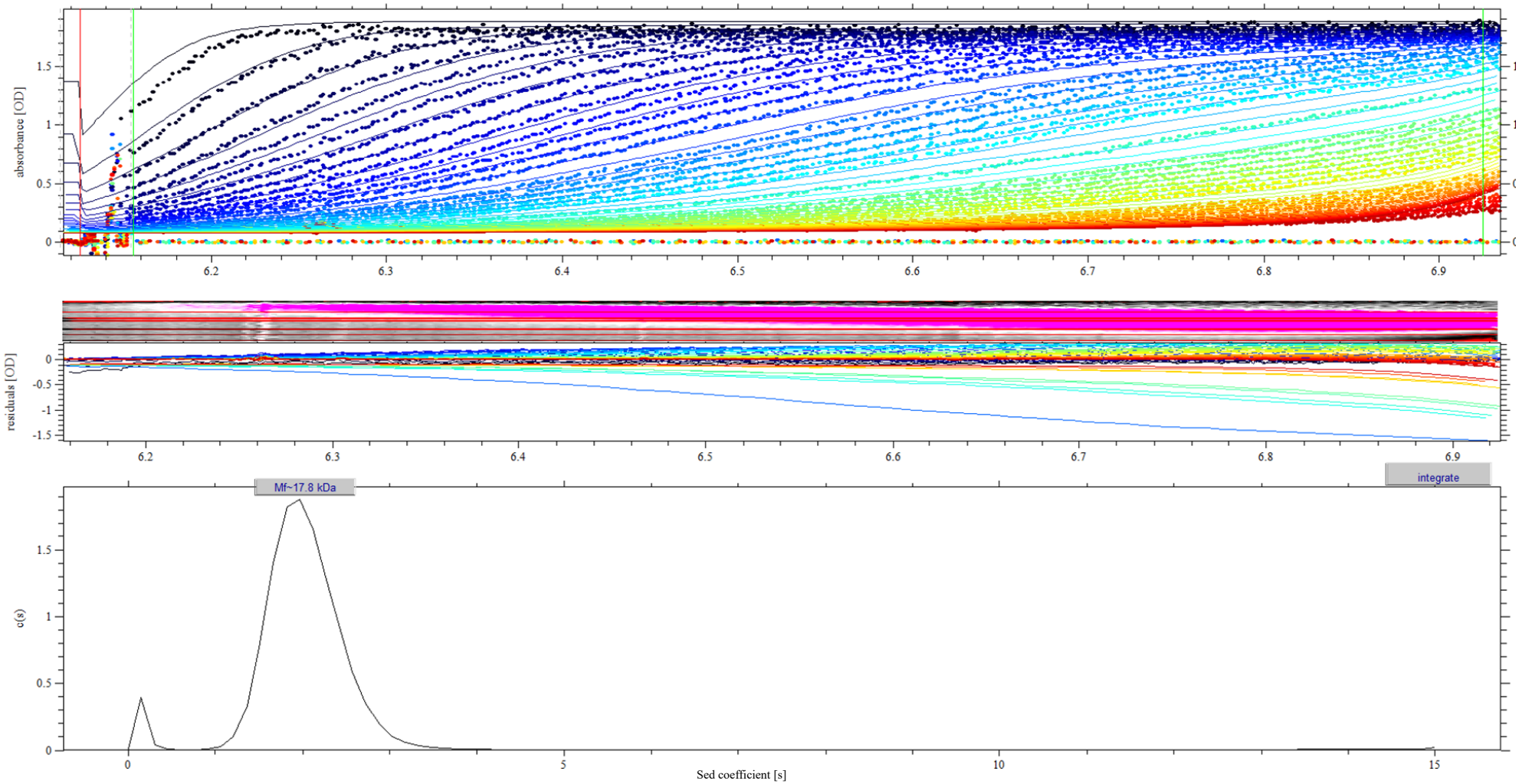

Appendix G Figure 4: AUC data for **19** and the CBP^{BRD} with 60 μM of ligand and 40 μM of protein without ligand **19** added to the reference cell.

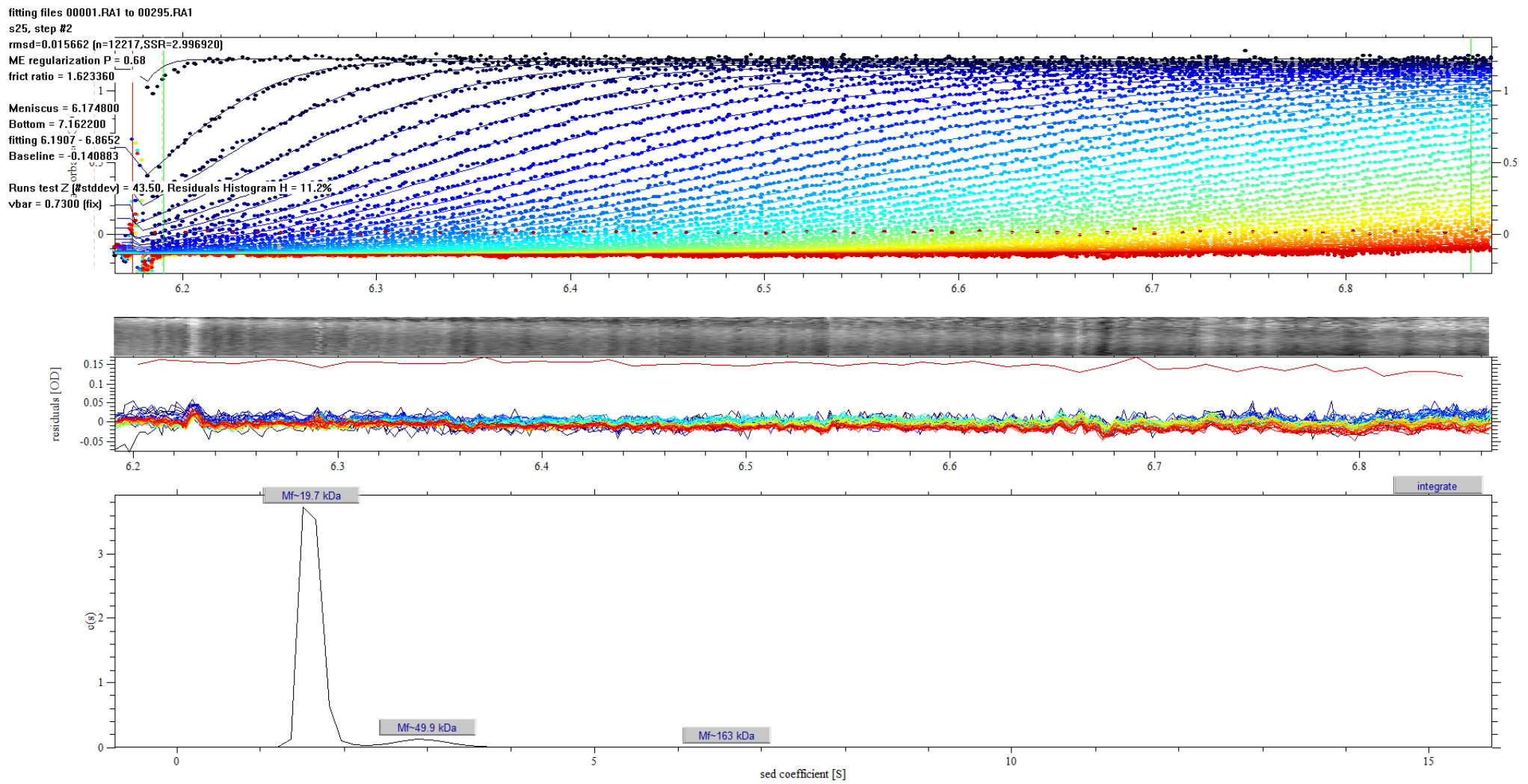

Appendix G Figure 5: AUC data for **19** and the CBP^{BRD} with 20 μM of ligand and 40 μM of protein with ligand **19** added to the reference cell.

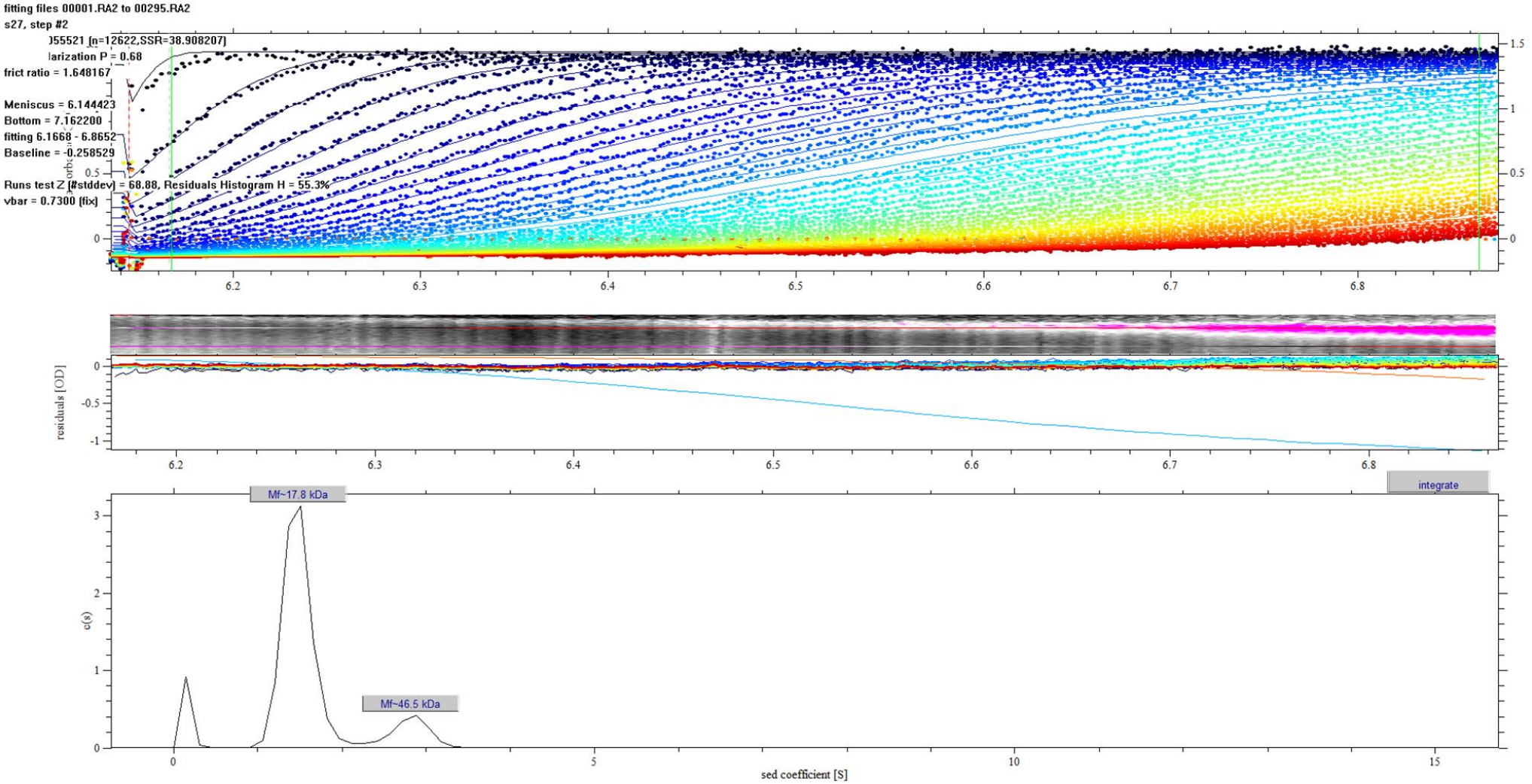

Appendix G Figure 6: AUC data for **19** and the CBP^{BRD} with 40 μM of ligand and 40 μM of protein with ligand **19** added to the reference cell.

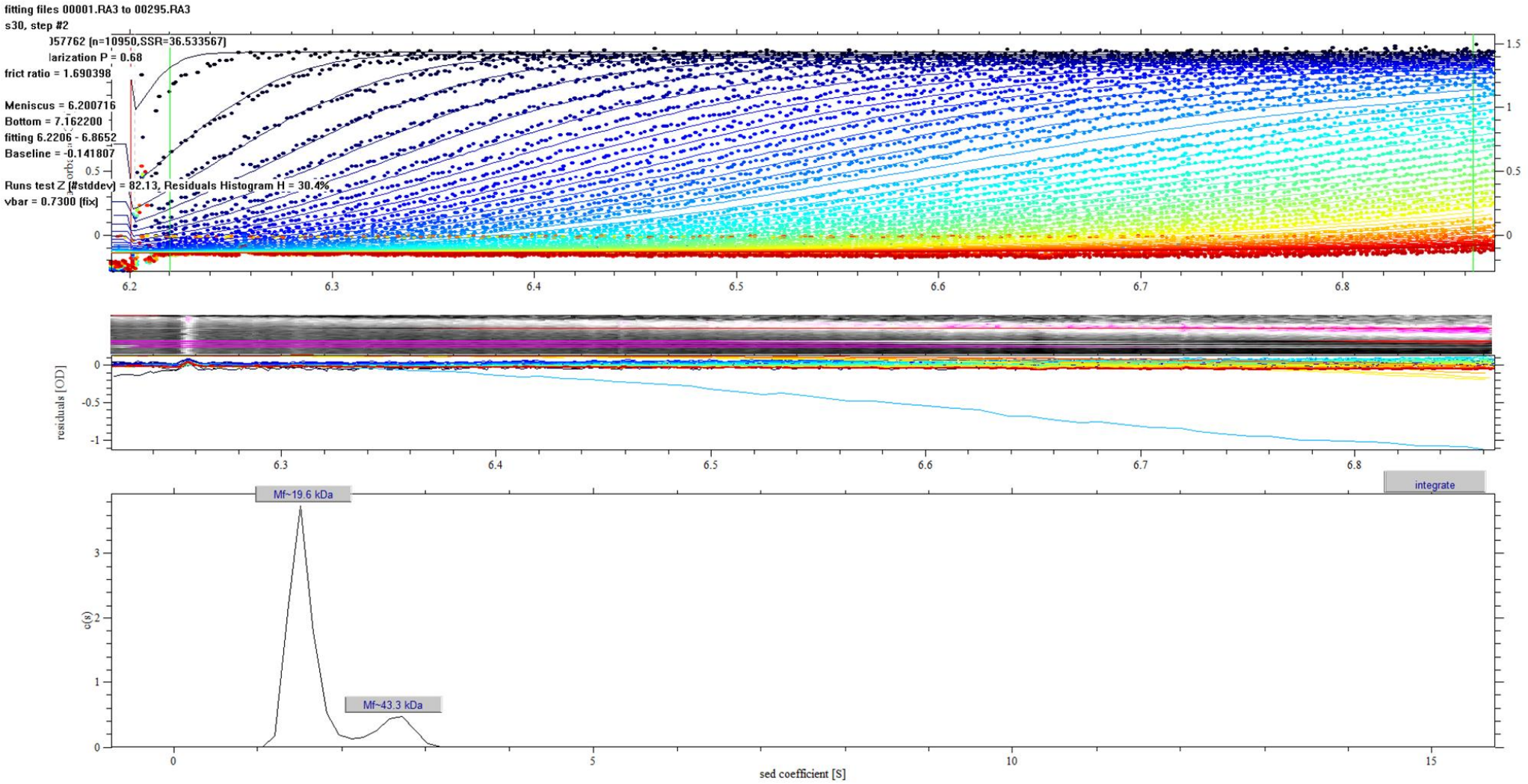

Appendix G Figure 7: AUC data for **19** and the CBP^{BRD} with 60 μM of ligand and 40 μM of protein with ligand **19** added to the reference cell.

Appendix H: Native Protein Mass Spectrometry data

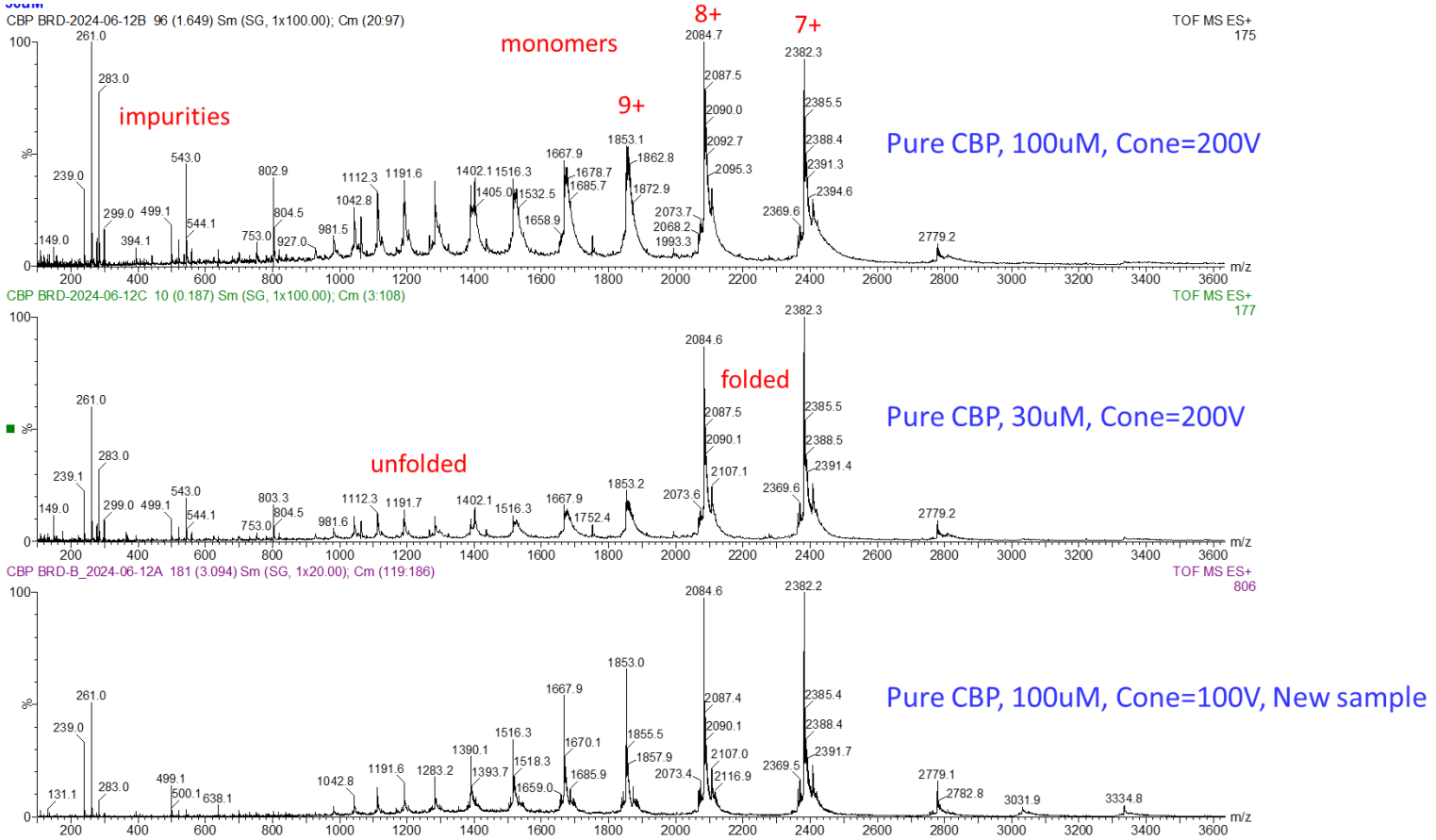

Appendix H, Figure 1: Zoomed in native-MS of the CBP^{BRD} showing different ionisation states with both folded and unfolded BRD at different concentrations and ionisation energies. This demonstrates that the native-MS method can detect the pure CBPBRD with high mass accuracy (molecular weight = 16668.2 ±2.2 Da using this technique) which is close to the mass given using the protein LC-MS method.

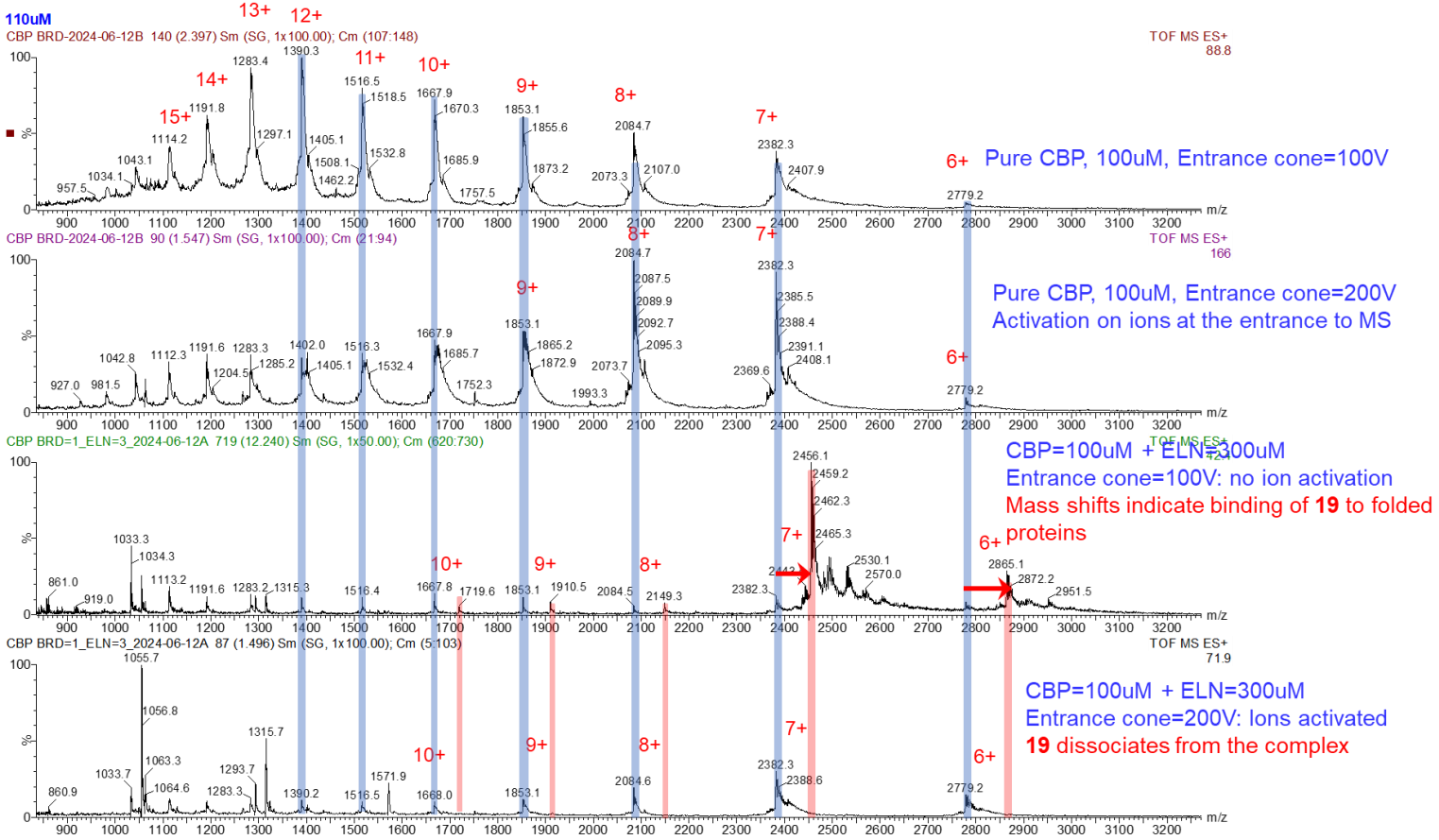

Appendix H, Figure 2: Zoomed in native-MS of the CBP^{BRD} with and without addition of ligand **19**. The addition of the ligand can be seen in the red boxes, causing a mass shift, leaving little unbound CBP^{BRD}, upon increasing the ionisation energy, ligand **19** dissociates from its binding complex. With addition of ligand **19**, the CBP^{BRD} appears stabilised as there are less unfolded protein and partially folded protein present.

Appendix I: HPLC Chromatograms for Biologically evaluated Compounds

Below are the HPLC chromatograms for all biologically evaluated compounds in order of appearance or testing presented in this thesis:

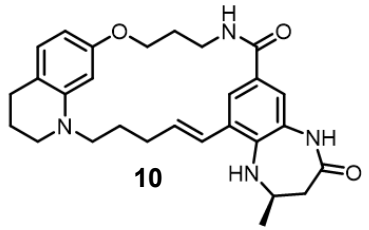

10

Signal 1: DAD1 A, Sig=254,4 Ref=500,100

Peak #	RetTime [min]	Type	Width [min]	Area [mAU*s]	Height [mAU]	Area %
1	9.832	VB R	0.0524	44.94257	10.97737	1.1386
2	10.127	BV R	0.0523	3902.27612	1152.57947	98.8614
Totals :				3947.21869	1163.55684	

Signal 2: DAD1 B, Sig=220,4 Ref=500,100

Peak #	RetTime [min]	Type	Width [min]	Area [mAU*s]	Height [mAU]	Area %
1	9.831	VB	0.0507	35.96590	10.84571	0.7540
2	10.127	BV R	0.0526	4734.14355	1388.27136	99.2460
Totals :				4770.10946	1399.11707	

Signal 3: DAD1 C, Sig=280,4 Ref=500,100

Peak #	RetTime [min]	Type	Width [min]	Area [mAU*s]	Height [mAU]	Area %
1	9.831	VB	0.0579	6.43343	1.67255	0.4711
2	10.127	BV R	0.0523	1359.15454	400.23334	99.5289
Totals :				1365.58798	401.90589	

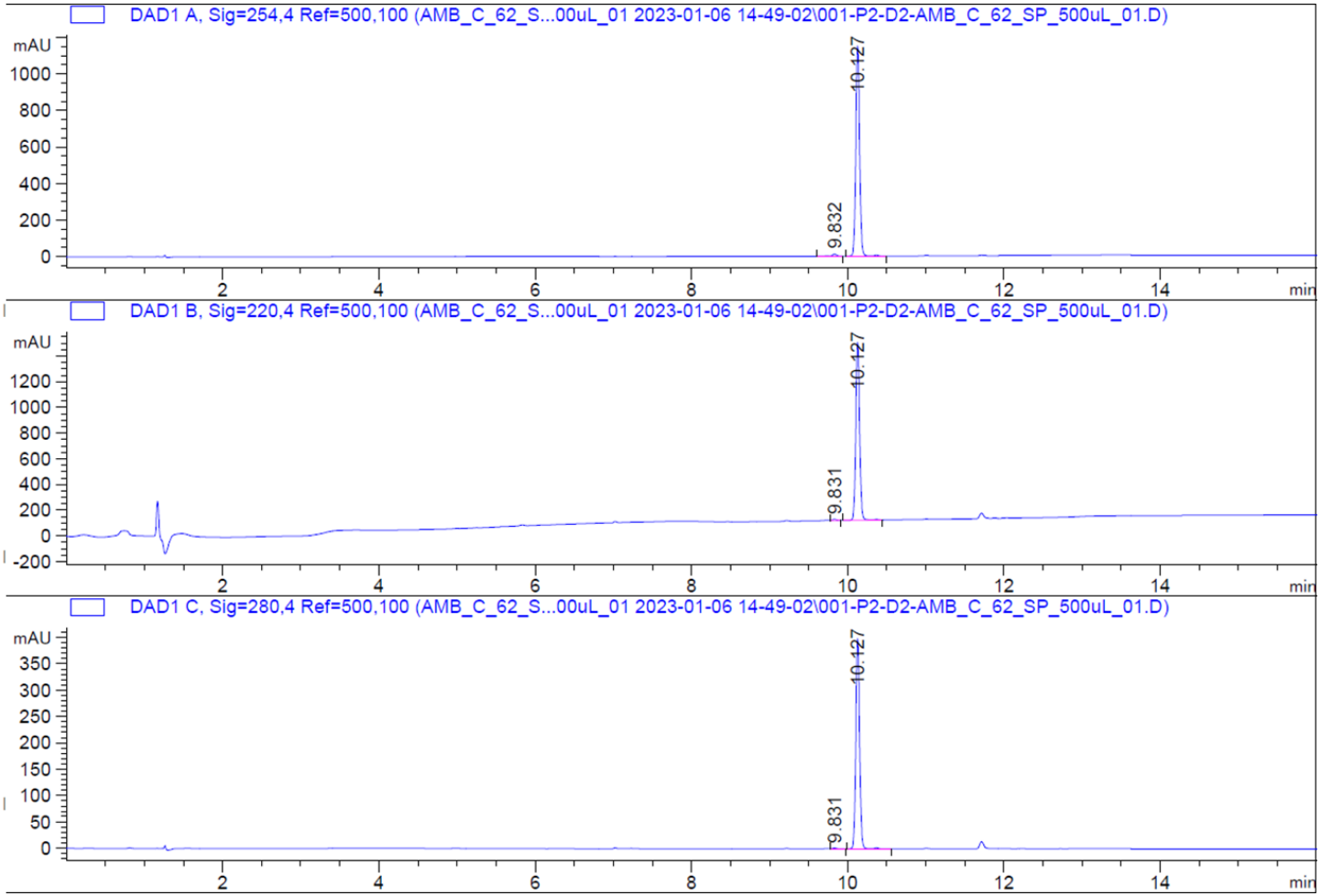

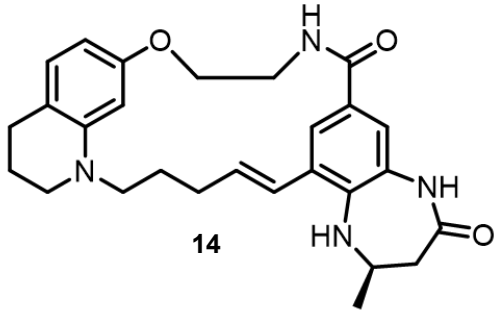

14

Signal 1: DAD1 A, Sig=254,4 Ref=500,100

Peak #	RetTime [min]	Type	Width [min]	Area [mAU*s]	Height [mAU]	Area %
1	5.754	BB	0.0442	39.02588	13.31609	0.3860
2	10.087	BB	0.0750	1.00546e4	2134.45313	99.4566
3	11.004	BB	0.0760	7.30655	1.52214	0.0723
4	12.065	BV	0.1059	8.59854	1.10348	0.0851
Totals :				1.01095e4	2150.39484	

Signal 2: DAD1 B, Sig=220,4 Ref=500,100

Peak #	RetTime [min]	Type	Width [min]	Area [mAU*s]	Height [mAU]	Area %
1	5.755	MM	0.0440	28.43829	10.77239	0.2946
2	10.086	MM	0.0880	9553.19238	1808.65112	98.9515
3	11.281	MM	0.1040	50.92394	8.16021	0.5275
4	11.965	MM	0.1184	21.85952	3.07825	0.2264
Totals :				9654.41413	1830.66198	

Signal 3: DAD1 C, Sig=280,4 Ref=500,100

Peak #	RetTime [min]	Type	Width [min]	Area [mAU*s]	Height [mAU]	Area %
1	5.754	BB	0.0444	9.65834	3.27531	0.2644
2	10.087	BB	0.0747	3642.99609	776.67987	99.7356
Totals :				3652.65443	779.95518	

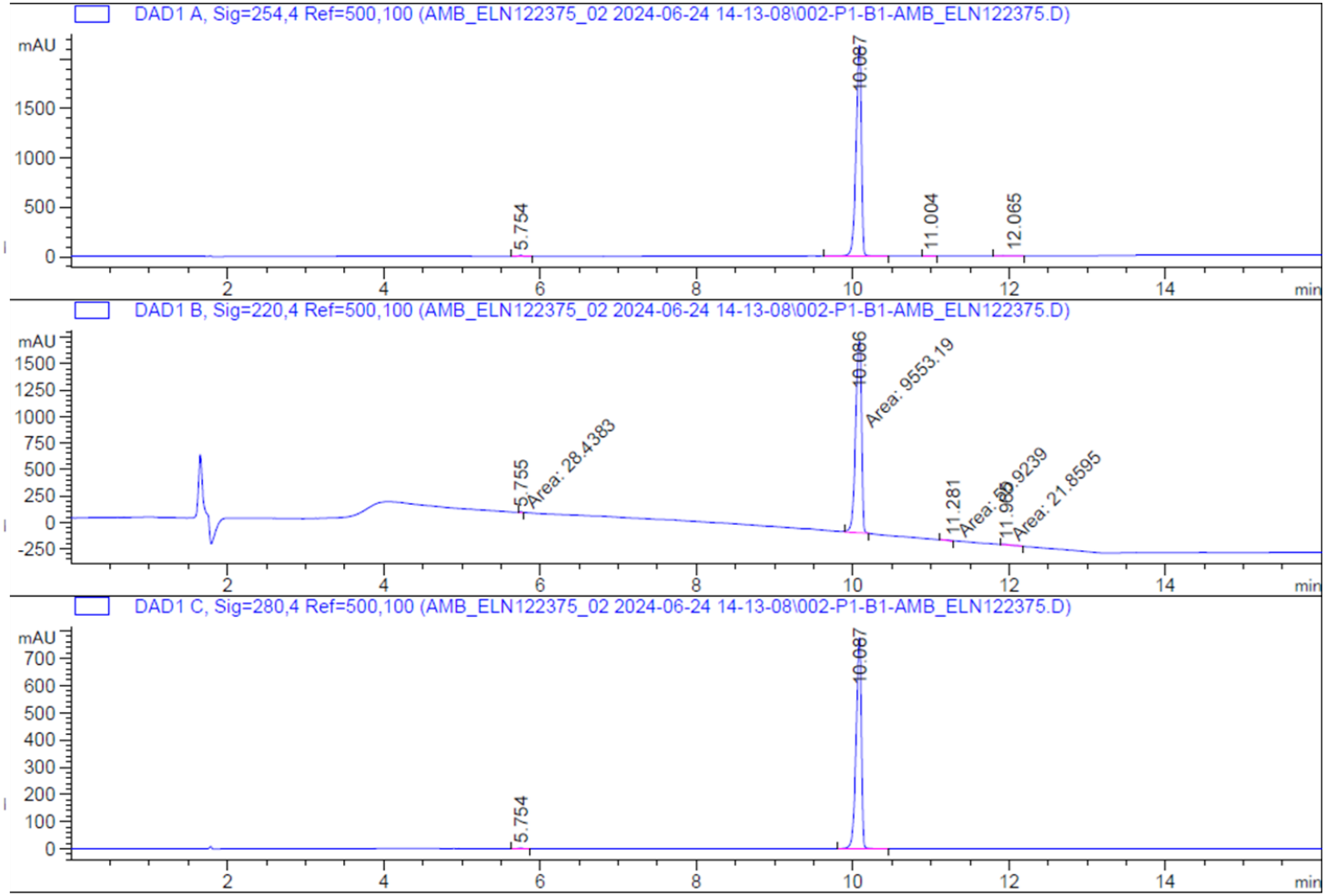

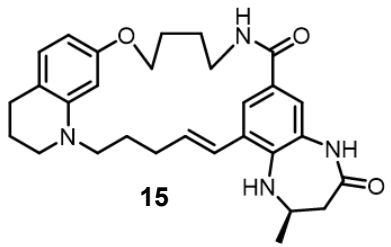

15

Signal 1: DAD1 A, Sig=254,4 Ref=500,100
Signal has been modified after loading from rawdata file!

Peak #	RetTime [min]	Type	Width [min]	Area [mAU*s]	Height [mAU]	Area %
1	6.151	BV	0.0626	40.51285	10.35518	0.8766
2	6.237	VB	0.0365	31.16723	12.73765	0.6744
3	7.043	MM	0.0669	11.58226	2.88426	0.2506
4	8.372	MM	0.0498	10.45135	3.49599	0.2261
5	8.542	MM	0.0524	6.01324	1.91126	0.1301
6	8.761	MM	0.0645	10.22048	2.64236	0.2211
7	10.406	MM	0.0626	23.32967	6.20680	0.5048
8	11.112	BV R	0.0540	4433.74463	1228.36682	95.9321
9	11.241	VV E	0.0644	54.73259	12.19444	1.1842

Totals : 4621.75429 1280.79475

Signal 2: DAD1 B, Sig=220,4 Ref=500,100
Signal has been modified after loading from rawdata file!

Peak #	RetTime [min]	Type	Width [min]	Area [mAU*s]	Height [mAU]	Area %
1	6.237	MM	0.0821	41.11423	8.34420	0.7903
2	8.371	MM	0.0544	22.74654	6.96968	0.4372
3	8.761	MM	0.0464	9.86871	3.54300	0.1897
4	10.405	MM	0.0640	30.76951	8.00914	0.5914
5	10.595	MM	0.0487	8.10464	2.77161	0.1558
6	11.112	MM	0.0609	5059.47852	1384.94604	97.2505
7	11.246	MM	0.0494	30.44224	10.27308	0.5851

Totals : 5202.52439 1424.85675

Signal 3: DAD1 C, Sig=280,4 Ref=500,100
Signal has been modified after loading from rawdata file!

Peak #	RetTime [min]	Type	Width [min]	Area [mAU*s]	Height [mAU]	Area %
1	6.151	BV	0.0640	10.12784	2.57035	0.6019
2	6.237	VB	0.0385	8.33635	3.19393	0.4955
3	8.371	MM	0.0654	6.26252	1.59560	0.3722
4	8.760	MM	0.0869	5.70949	1.09451	0.3393
5	10.406	MM	0.0562	8.05200	2.38973	0.4786
6	11.112	BV R	0.0541	1625.11792	449.89697	96.5850
7	11.241	VV E	0.0649	18.97233	4.18307	1.1276

Totals : 1682.57845 464.92416

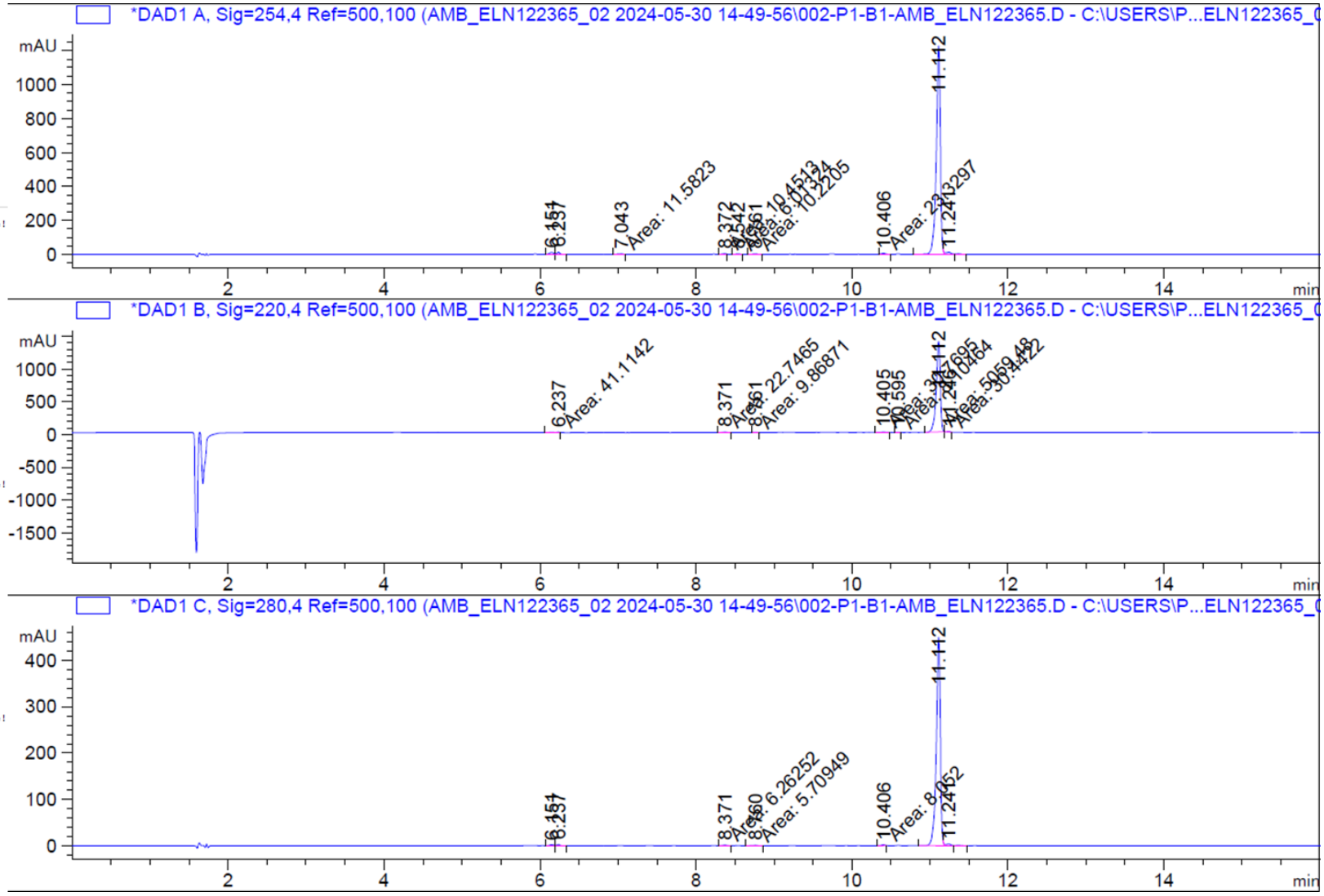

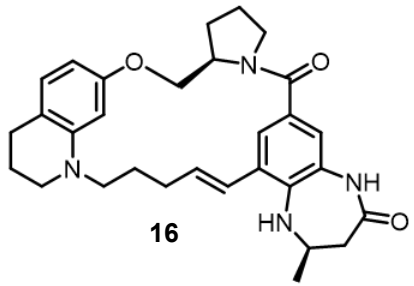

16

Signal 1: DAD1 A, Sig=254,4 Ref=500,100

Peak #	RetTime [min]	Type	Width [min]	Area [mAU*s]	Height [mAU]	Area %
1	6.089	MM	0.0589	171.10876	48.44288	1.6799
2	6.952	MM	0.0464	20.72838	7.44926	0.2035
3	8.290	MM	0.0838	19.52675	3.88225	0.1917
4	8.487	MM	0.0780	27.64810	5.90695	0.2714
5	10.080	MM	0.1127	18.09144	2.67537	0.1776
6	10.735	BV R	0.0563	9742.09473	2565.93970	95.6466
7	10.874	VB E	0.0498	78.77377	24.33406	0.7734
8	11.105	MM	0.0478	53.55987	18.68314	0.5258
9	11.237	MM	0.0490	36.93270	12.55643	0.3626
10	11.448	MM	0.0593	10.07790	2.83314	0.0989
11	11.978	MM	0.0532	6.97001	2.18181	0.0684
Totals :				1.01855e4	2694.88499	

Signal 2: DAD1 B, Sig=220,4 Ref=500,100

Peak #	RetTime [min]	Type	Width [min]	Area [mAU*s]	Height [mAU]	Area %
1	6.089	MM	0.0640	133.86609	34.85189	1.2948
2	10.735	BV R	0.0702	9654.43555	2091.40479	93.3846
3	11.104	MM	0.0479	359.34344	125.05173	3.4758
4	11.237	MM	0.0479	190.71265	66.32446	1.8447
Totals :				1.03384e4	2317.63287	

Signal 3: DAD1 C, Sig=280,4 Ref=500,100

Peak #	RetTime [min]	Type	Width [min]	Area [mAU*s]	Height [mAU]	Area %
1	6.089	MM	0.0699	42.68985	10.17553	1.3328
2	10.735	BV R	0.0556	3085.47925	818.68719	96.3273
3	11.105	MM	0.0468	44.31569	15.76517	1.3835
4	11.237	MM	0.0492	30.63567	10.37379	0.9564
Totals :				3203.12045	855.00168	

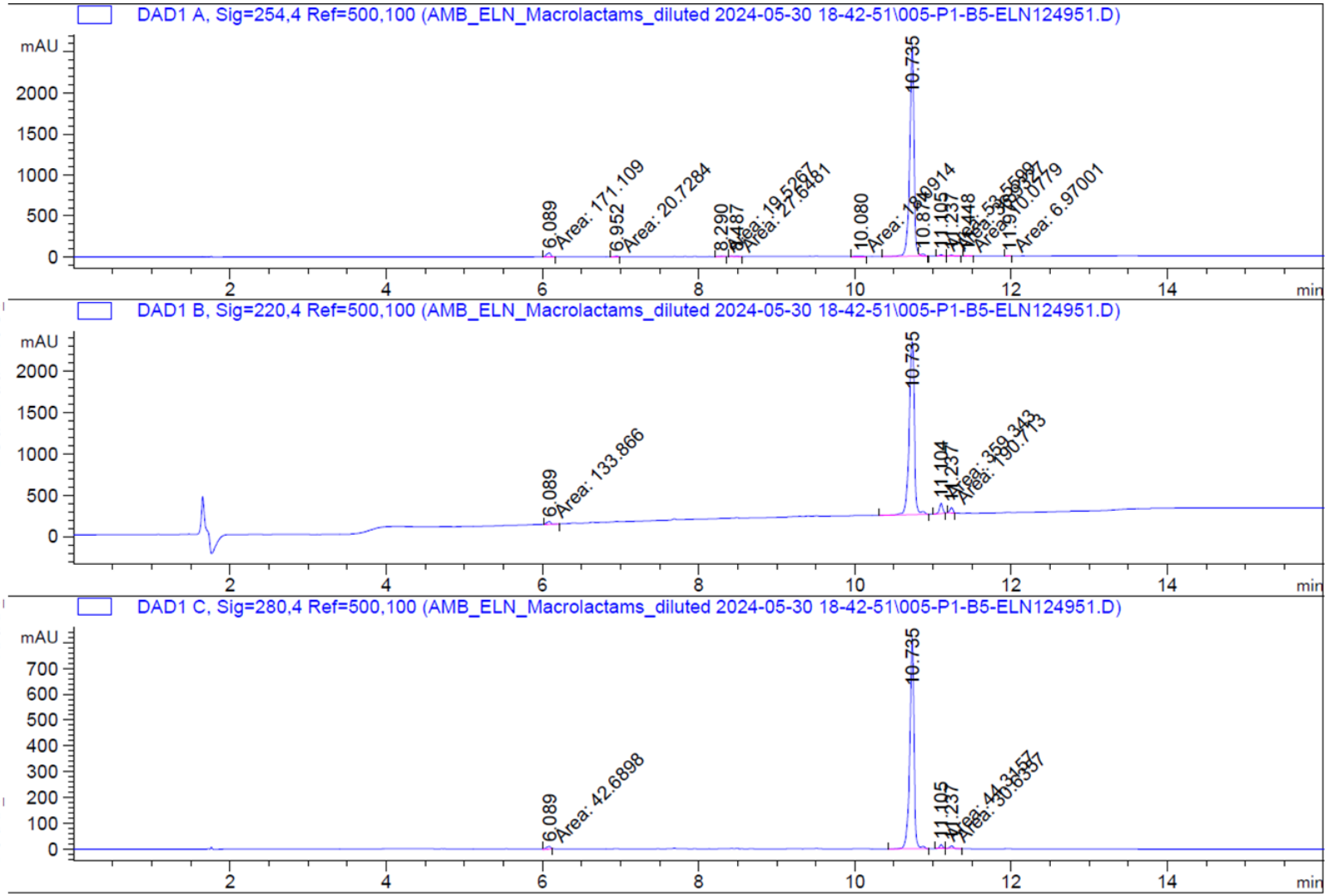

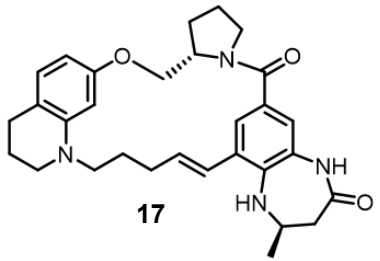

17

Signal 1: DAD1 A, Sig=254,4 Ref=500,100
Signal has been modified after loading from rawdata file

Peak #	RetTime [min]	Type	Width [min]	Area [mAU*s]	Height [mAU]	Area %
1	6.093	VB R	0.0514	200.77266	53.99037	2.4764
2	10.660	BV E	0.0447	176.28867	59.27346	2.1744
3	10.790	VB R	0.0555	7730.28906	2123.46851	95.3491
Totals :				8107.35039	2236.73233	

Signal 2: DAD1 B, Sig=220,4 Ref=500,100
Signal has been modified after loading from rawdata file

Peak #	RetTime [min]	Type	Width [min]	Area [mAU*s]	Height [mAU]	Area %
1	6.093	MM	0.0603	126.25372	34.92287	1.5159
2	10.659	BV E	0.0447	261.08298	87.74912	3.1348
3	10.789	VB R	0.0626	7941.23193	1944.75000	95.3493
Totals :				8328.56863	2067.42199	

Signal 3: DAD1 C, Sig=280,4 Ref=500,100
Signal has been modified after loading from rawdata file

Peak #	RetTime [min]	Type	Width [min]	Area [mAU*s]	Height [mAU]	Area %
1	6.093	MM	0.0540	31.34489	9.68178	1.1728
2	10.659	BV E	0.0506	100.22807	28.80052	3.7500
3	10.790	VV R	0.0543	2541.18628	674.51483	95.0773
Totals :				2672.75924	712.99714	

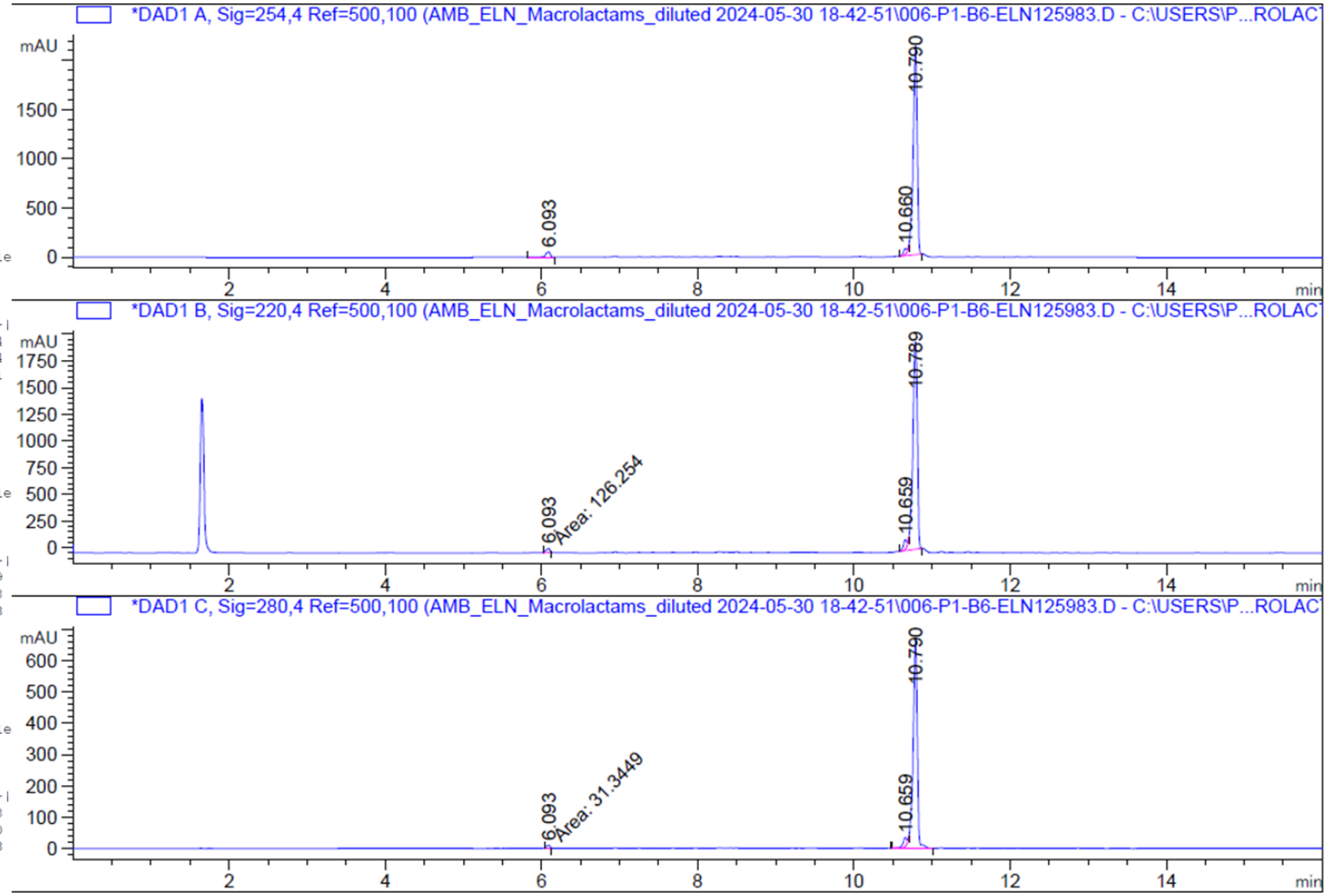

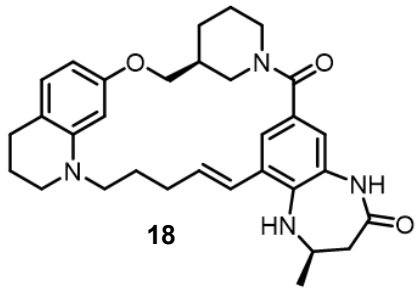

18

Signal 1: DAD1 A, Sig=254,4 Ref=500,100

Peak #	RetTime [min]	Type	Width [min]	Area [mAU*s]	Height [mAU]	Area %
1	6.672	MM	0.0379	26.27095	11.55518	0.4550
2	11.112	MM	0.0538	23.11230	7.16520	0.4003
3	11.282	BV E	0.0523	109.16301	30.83561	1.8906
4	11.449	VV R	0.0575	5541.44531	1452.85608	95.9720
5	11.636	VB E	0.0740	39.46172	7.54686	0.6834
6	13.829	MM	0.0705	34.56674	8.16728	0.5987
Totals :				5774.02003	1518.12620	

Signal 2: DAD1 B, Sig=220,4 Ref=500,100

Peak #	RetTime [min]	Type	Width [min]	Area [mAU*s]	Height [mAU]	Area %
1	6.410	MM	0.0675	26.84168	6.63070	0.4391
2	6.670	MM	0.0706	48.56833	11.47312	0.7944
3	7.688	MM	0.0511	40.44365	13.20228	0.6615
4	11.282	BV E	0.0509	151.50639	44.33384	2.4782
5	11.449	VB R	0.0590	5803.56494	1472.60864	94.9300
6	13.829	MM	0.0710	42.59248	10.00453	0.6967
Totals :				6113.51747	1558.25311	

Signal 3: DAD1 C, Sig=280,4 Ref=500,100

Peak #	RetTime [min]	Type	Width [min]	Area [mAU*s]	Height [mAU]	Area %
1	6.672	MM	0.0444	6.62506	2.48603	0.3299
2	7.688	MM	0.0529	7.28529	2.29322	0.3628
3	11.282	VV E	0.0547	52.85324	14.10260	2.6320
4	11.449	VV R	0.0576	1909.93579	499.97775	95.1125
5	11.636	VB E	0.0817	15.91316	2.74254	0.7925
6	13.829	MM	0.0744	15.46739	3.46286	0.7703
Totals :				2008.07993	525.06501	

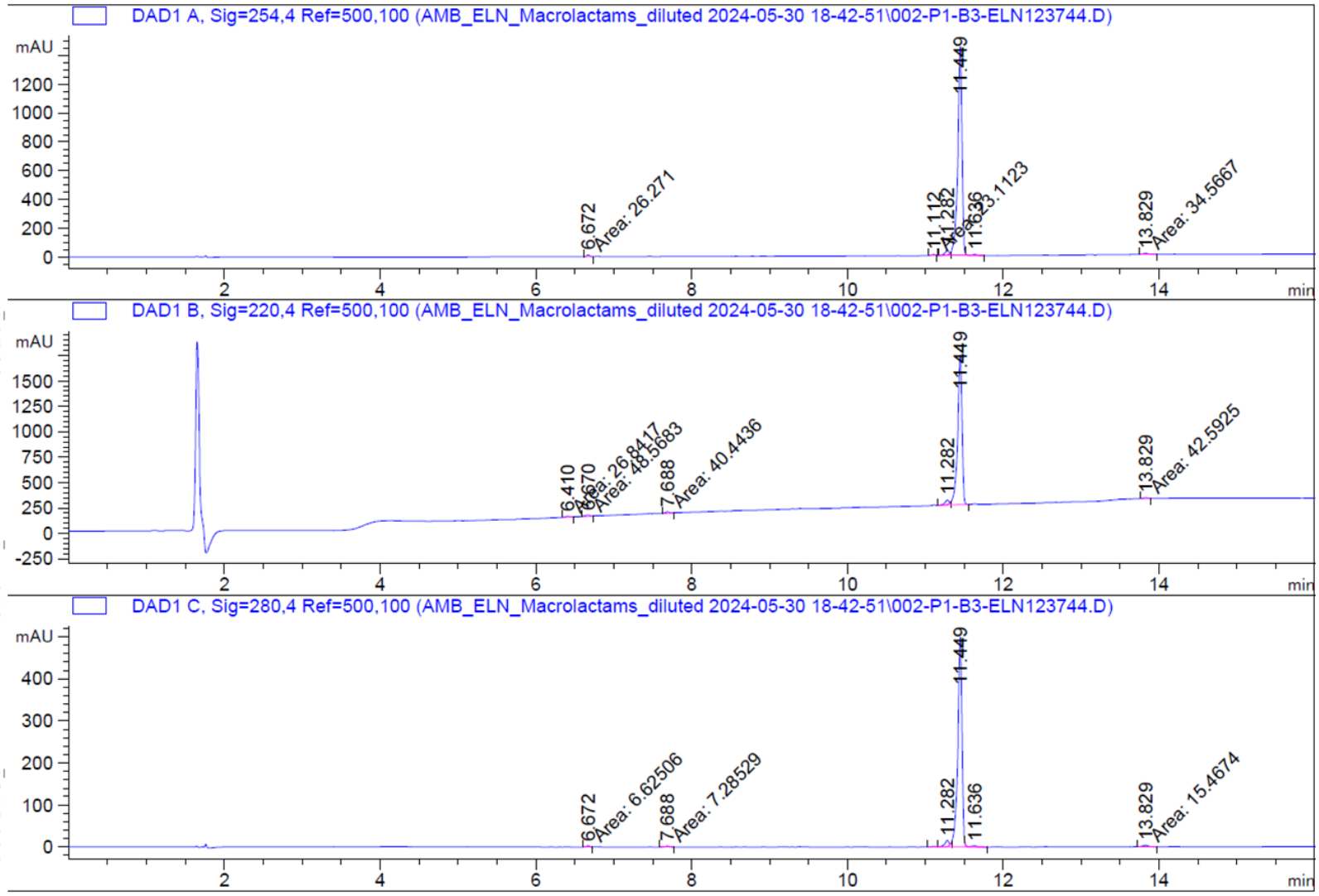

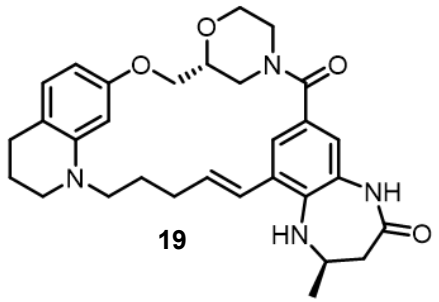

19

Signal 1: DAD1 A, Sig=254,4 Ref=500,100

Peak #	RetTime [min]	Type	Width [min]	Area [mAU*s]	Height [mAU]	Area %
1	6.039	BB	0.0518	13.13255	3.49412	0.3334
2	6.654	BV	0.0453	9.14501	2.93859	0.2322
3	10.459	BV R	0.0534	3892.51318	1095.93823	98.8171
4	10.651	VB E	0.1213	17.61879	1.89851	0.4473
5	10.975	BV	0.0546	6.70084	1.83454	0.1701
Totals :				3939.11037	1106.10401	

Signal 2: DAD1 B, Sig=220,4 Ref=500,100

Peak #	RetTime [min]	Type	Width [min]	Area [mAU*s]	Height [mAU]	Area %
1	6.407	MM	0.0718	40.24092	9.33613	0.9044
2	6.646	MM	0.0454	18.23195	6.68909	0.4098
3	7.689	MM	0.0482	41.75617	14.44187	0.9385
4	8.683	MM	0.0522	12.37817	3.95509	0.2782
5	9.298	MM	0.0448	10.77670	4.01040	0.2422
6	9.391	MM	0.0532	11.79187	3.69757	0.2650
7	10.459	VB R	0.0541	4282.32764	1183.09216	96.2476
8	11.955	MM	0.1226	31.78134	4.32211	0.7143
Totals :				4449.28475	1229.54442	

Signal 3: DAD1 C, Sig=280,4 Ref=500,100

Peak #	RetTime [min]	Type	Width [min]	Area [mAU*s]	Height [mAU]	Area %
1	7.689	BB	0.0442	6.91185	2.35987	0.4422
2	10.460	VB R	0.0523	1556.10791	439.79239	99.5578
Totals :				1563.01976	442.15226	

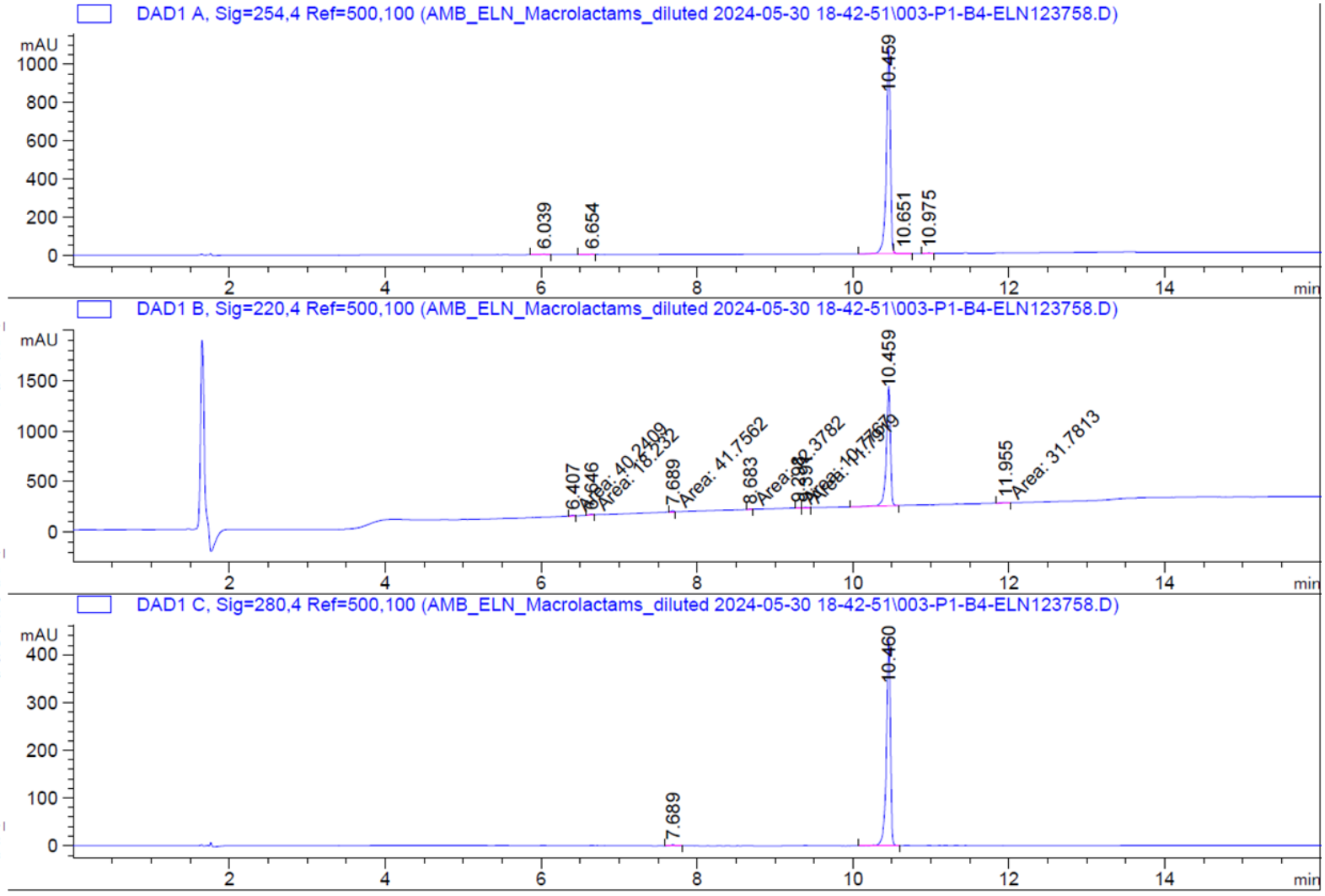

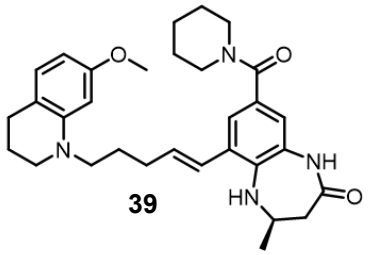

39

Signal 1: DAD1 A, Sig=254,4 Ref=500,100

Peak #	RetTime [min]	Type	Width [min]	Area [mAU*s]	Height [mAU]	Area %
1	7.164	VB R	0.0416	70.57652	22.28534	0.5044
2	7.680	BB	0.0441	18.80732	6.44074	0.1344
3	11.240	BV E	0.0436	88.23196	30.59099	0.6306
4	11.400	VB R	0.0686	1.37664e4	3176.34448	98.3865
5	12.878	BB	0.0633	48.15202	11.38525	0.3441
Totals :				1.39922e4	3247.04680	

Signal 2: DAD1 B, Sig=220,4 Ref=500,100

Peak #	RetTime [min]	Type	Width [min]	Area [mAU*s]	Height [mAU]	Area %
1	7.164	VV R	0.0411	41.35670	15.53870	0.3781
2	10.650	VB	0.0557	14.98356	3.90862	0.1370
3	11.240	BV E	0.0438	131.51845	45.37712	1.2025
4	11.400	VB R	0.0808	1.06960e4	2085.01807	97.7972
5	12.878	VB	0.0661	53.06570	11.65695	0.4852
Totals :				1.09370e4	2161.49945	

Signal 3: DAD1 C, Sig=280,4 Ref=500,100

Peak #	RetTime [min]	Type	Width [min]	Area [mAU*s]	Height [mAU]	Area %
1	11.240	BV E	0.0455	38.40519	12.99076	0.6262
2	11.400	VB R	0.0517	6070.48486	1781.93677	98.9799
3	12.878	VB	0.0614	24.16107	5.82571	0.3939
Totals :				6133.05113	1800.75324	

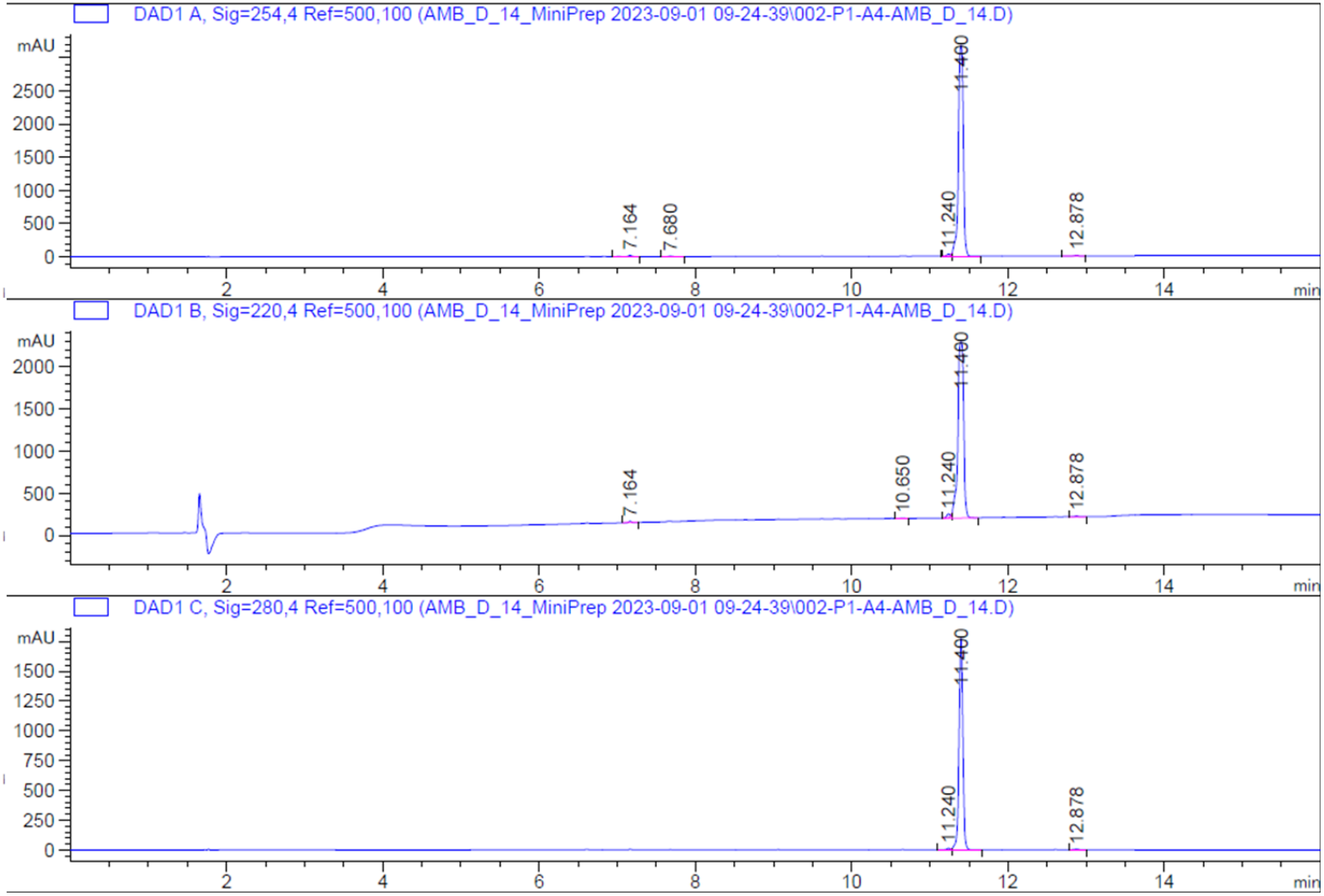

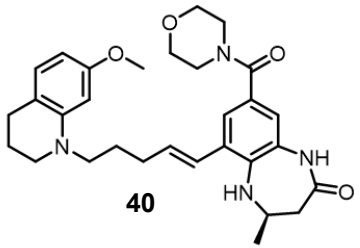

40

Signal 1: DAD1 A, Sig=254,4 Ref=500,100

Peak #	RetTime [min]	Type	Width [min]	Area [mAU*s]	Height [mAU]	Area %
1	10.120	BV E	0.0580	66.57407	16.54153	0.5444
2	10.295	VB R	0.0634	1.21622e4	3056.85913	99.4556
Totals :				1.22288e4	3073.40066	

Signal 2: DAD1 B, Sig=220,4 Ref=500,100

Peak #	RetTime [min]	Type	Width [min]	Area [mAU*s]	Height [mAU]	Area %
1	10.121	BV E	0.0548	81.43195	21.67213	0.8054
2	10.297	VB R	0.0694	1.00294e4	2322.61548	99.1946
Totals :				1.01109e4	2344.28761	

Signal 3: DAD1 C, Sig=280,4 Ref=500,100

Peak #	RetTime [min]	Type	Width [min]	Area [mAU*s]	Height [mAU]	Area %
1	10.119	BV E	0.0545	24.81477	6.65561	0.3930
2	10.295	VB R	0.0462	6289.60840	2087.08667	99.6070
Totals :				6314.42317	2093.74228	

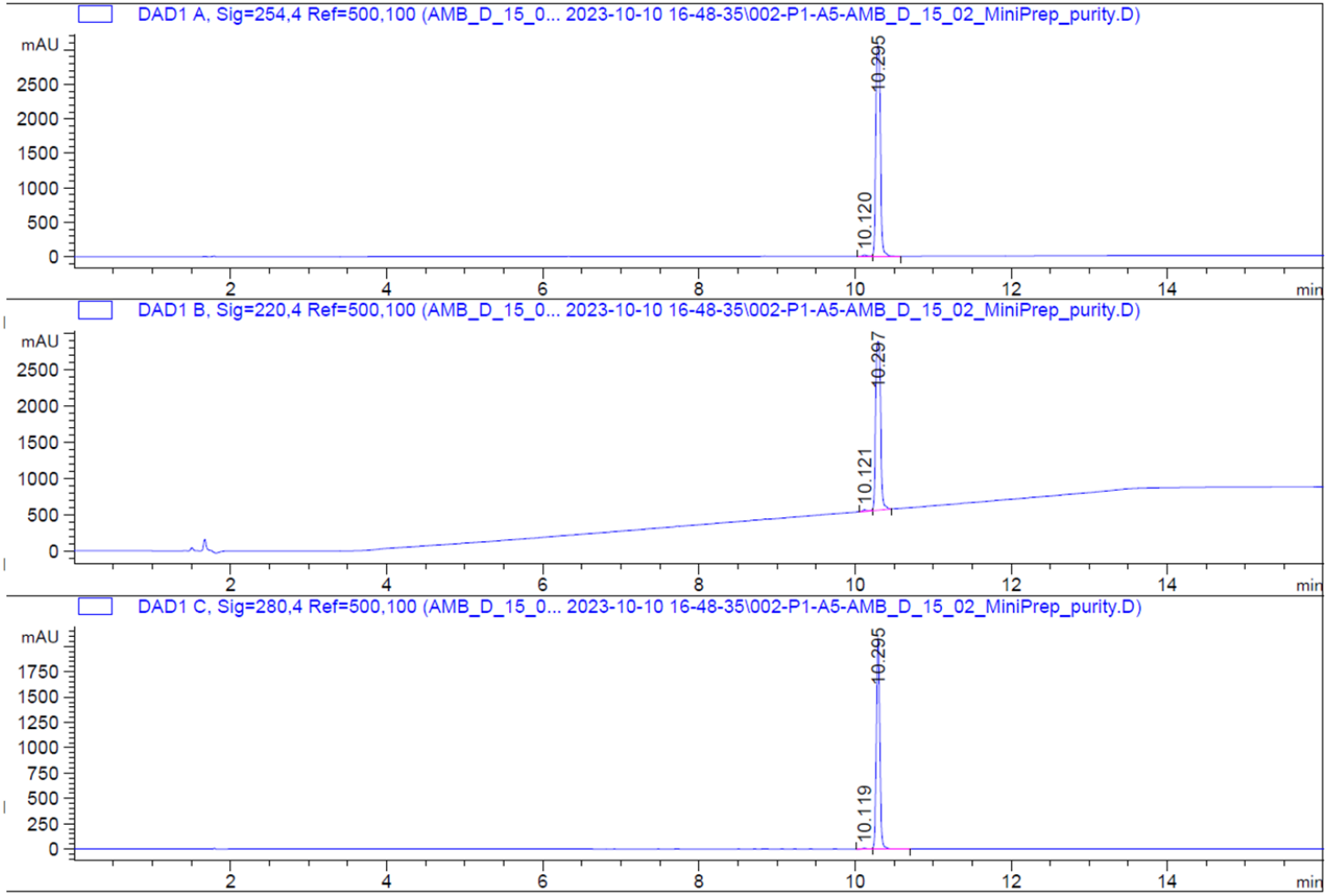

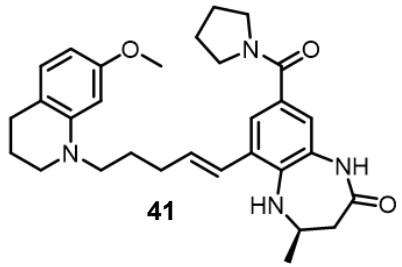

41

Signal 1: DAD1 A, Sig=254,4 Ref=500,100

Peak #	RetTime [min]	Type	Width [min]	Area [mAU*s]	Height [mAU]	Area %
1	10.636	BV E	0.0463	107.02187	35.41579	0.7992
2	10.712	VV E	0.0479	160.96474	52.25437	1.2020
3	10.826	VB R	0.0669	1.31233e4	3193.99121	97.9988
Totals :				1.33913e4	3281.66137	

Signal 2: DAD1 B, Sig=220,4 Ref=500,100

Peak #	RetTime [min]	Type	Width [min]	Area [mAU*s]	Height [mAU]	Area %
1	10.636	BB	0.0411	89.38777	35.80915	0.8141
2	10.712	BV E	0.0390	92.26253	38.45197	0.8403
3	10.827	VB R	0.0706	1.07987e4	2443.74390	98.3457
Totals :				1.09803e4	2518.00501	

Signal 3: DAD1 C, Sig=280,4 Ref=500,100

Peak #	RetTime [min]	Type	Width [min]	Area [mAU*s]	Height [mAU]	Area %
1	10.636	BV E	0.0482	46.52200	15.00690	0.6789
2	10.712	VV E	0.0464	30.78547	10.15508	0.4493
3	10.827	VB R	0.0500	6775.07910	2137.52979	98.8718
Totals :				6852.38658	2162.69177	

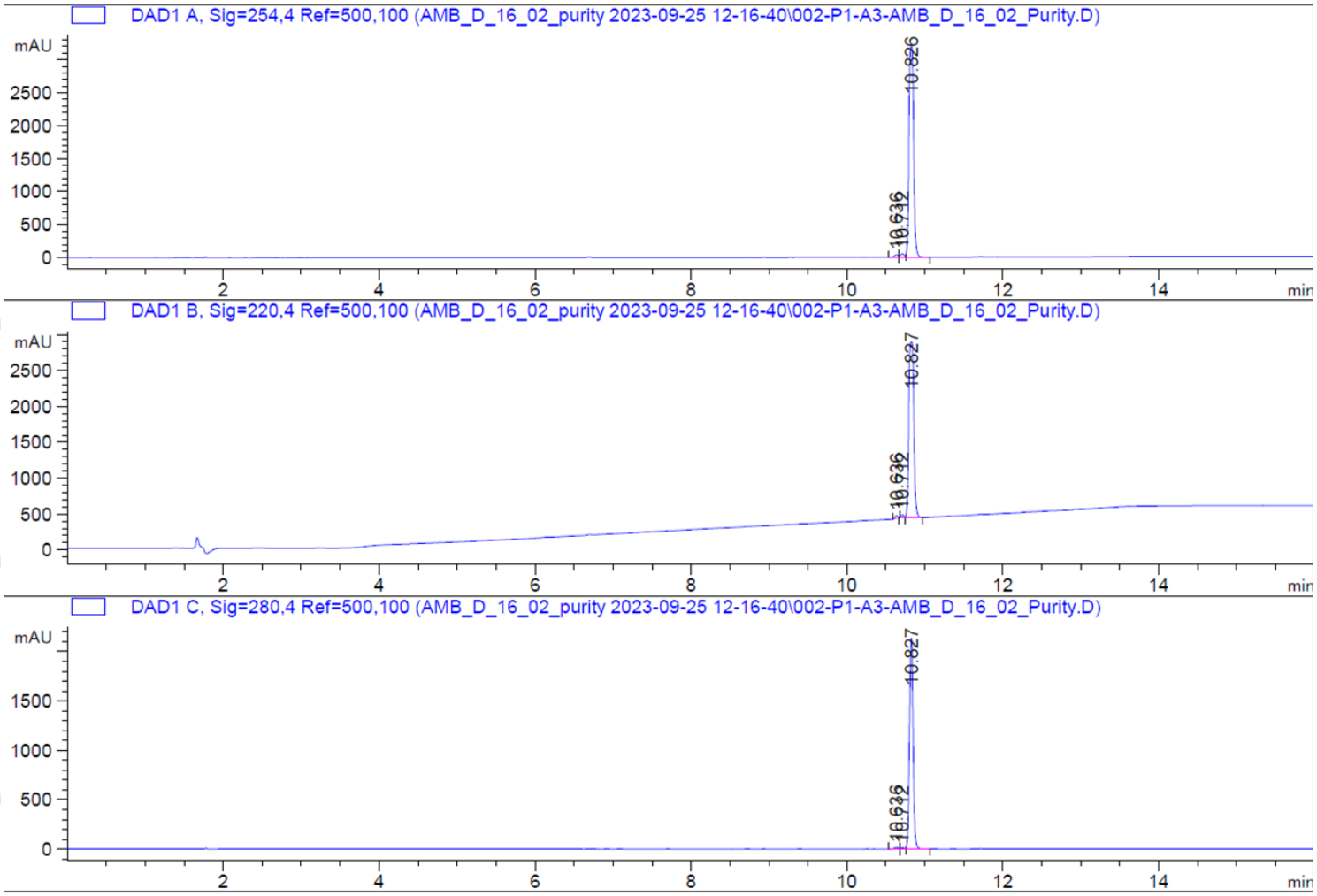

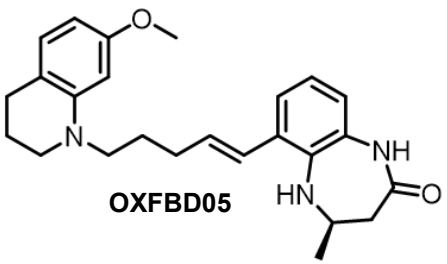

OXFBD05

Signal 1: DAD1 A, Sig=254,4 Ref=500,100

Peak #	RetTime [min]	Type	Width [min]	Area [mAU*s]	Height [mAU]	Area %
1	10.676	VB R	0.0487	6178.94238	1964.18909	100.0000
Totals :				6178.94238	1964.18909	

Signal 2: DAD1 B, Sig=220,4 Ref=500,100

Peak #	RetTime [min]	Type	Width [min]	Area [mAU*s]	Height [mAU]	Area %
1	10.519	BV E	0.0483	12.53897	3.91805	0.1572
2	10.676	VV R	0.0556	7961.96826	2230.60767	99.8428
Totals :				7974.50724	2234.52571	

Signal 3: DAD1 C, Sig=280,4 Ref=500,100

Peak #	RetTime [min]	Type	Width [min]	Area [mAU*s]	Height [mAU]	Area %
1	10.676	VV R	0.0488	2005.32800	636.18054	100.0000
Totals :				2005.32800	636.18054	

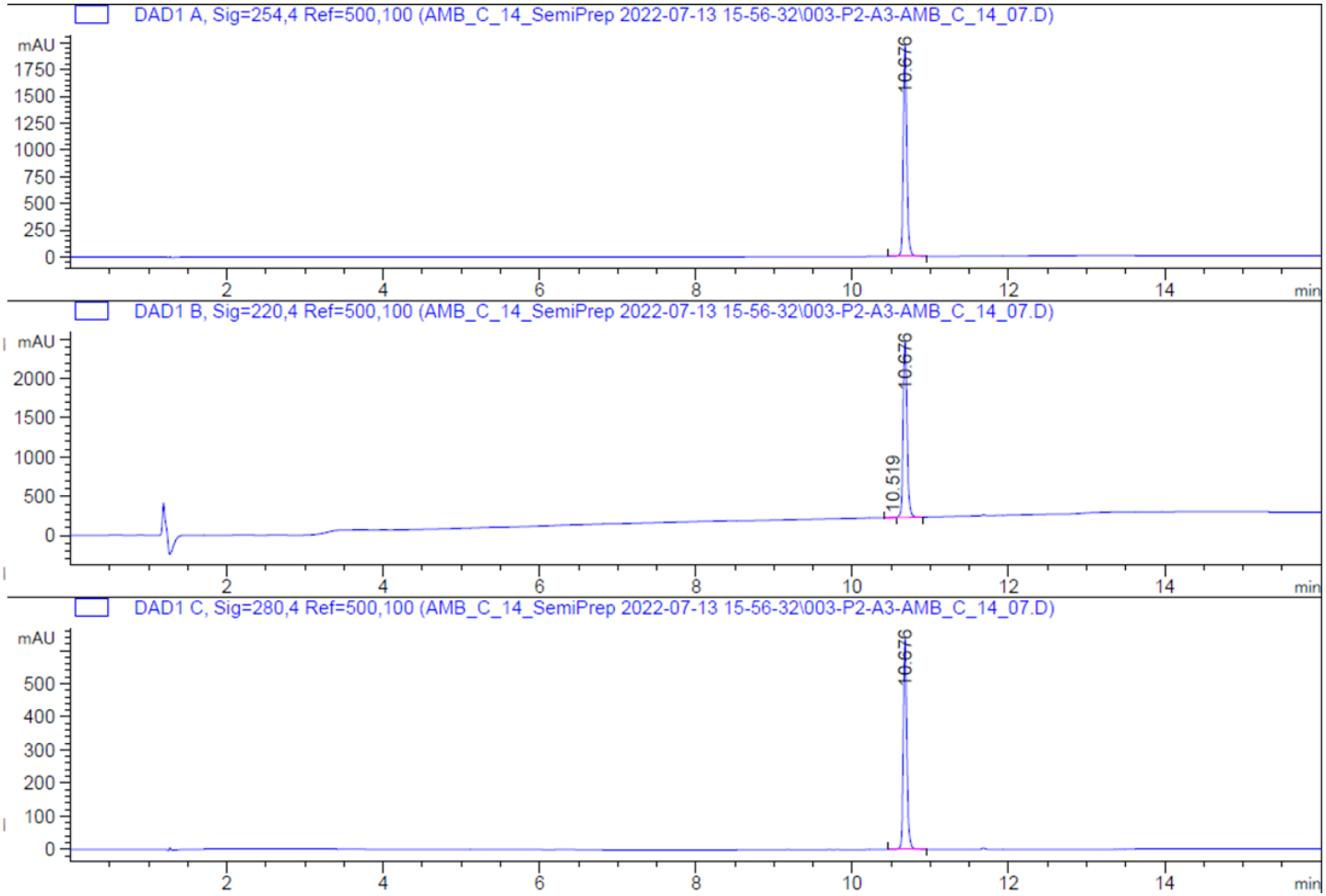

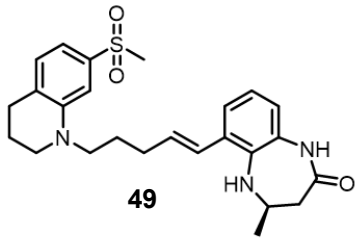

49

Signal 1: DAD1 A, Sig=254,4 Ref=500,100

Peak #	RetTime [min]	Type	Width [min]	Area [mAU*s]	Height [mAU]	Area %
1	8.956	BV E	0.0419	116.20732	41.23539	1.8994
2	9.115	VV R	0.0398	5975.75684	2318.74731	97.6738
3	9.336	BB	0.0429	26.11208	8.97983	0.4268
Totals :				6118.07624	2368.96253	

Signal 2: DAD1 B, Sig=220,4 Ref=500,100

Peak #	RetTime [min]	Type	Width [min]	Area [mAU*s]	Height [mAU]	Area %
1	8.206	BB	0.0376	98.24114	40.14139	1.0598
2	8.956	BV E	0.0409	521.43762	190.45776	5.6249
3	9.115	VV R	0.0496	8520.45898	2663.75513	91.9132
4	9.335	BV R	0.0478	129.97739	36.60950	1.4021
Totals :				9270.11514	2930.96379	

Signal 3: DAD1 C, Sig=280,4 Ref=500,100

Peak #	RetTime [min]	Type	Width [min]	Area [mAU*s]	Height [mAU]	Area %
1	1.105	BB	0.0587	9.88035	2.23055	0.1865
2	1.175	BB	0.0212	8.24444	6.31193	0.1556
3	7.694	BB	0.0392	20.06994	8.00663	0.3788
4	8.766	BB	0.0394	12.76207	4.89196	0.2409
5	8.956	BV E	0.0413	166.29044	60.08946	3.1383
6	9.115	VV R	0.0389	5047.83789	1946.00891	95.2663
7	9.335	BV	0.0392	33.57673	13.42937	0.6337
Totals :				5298.66186	2040.96880	

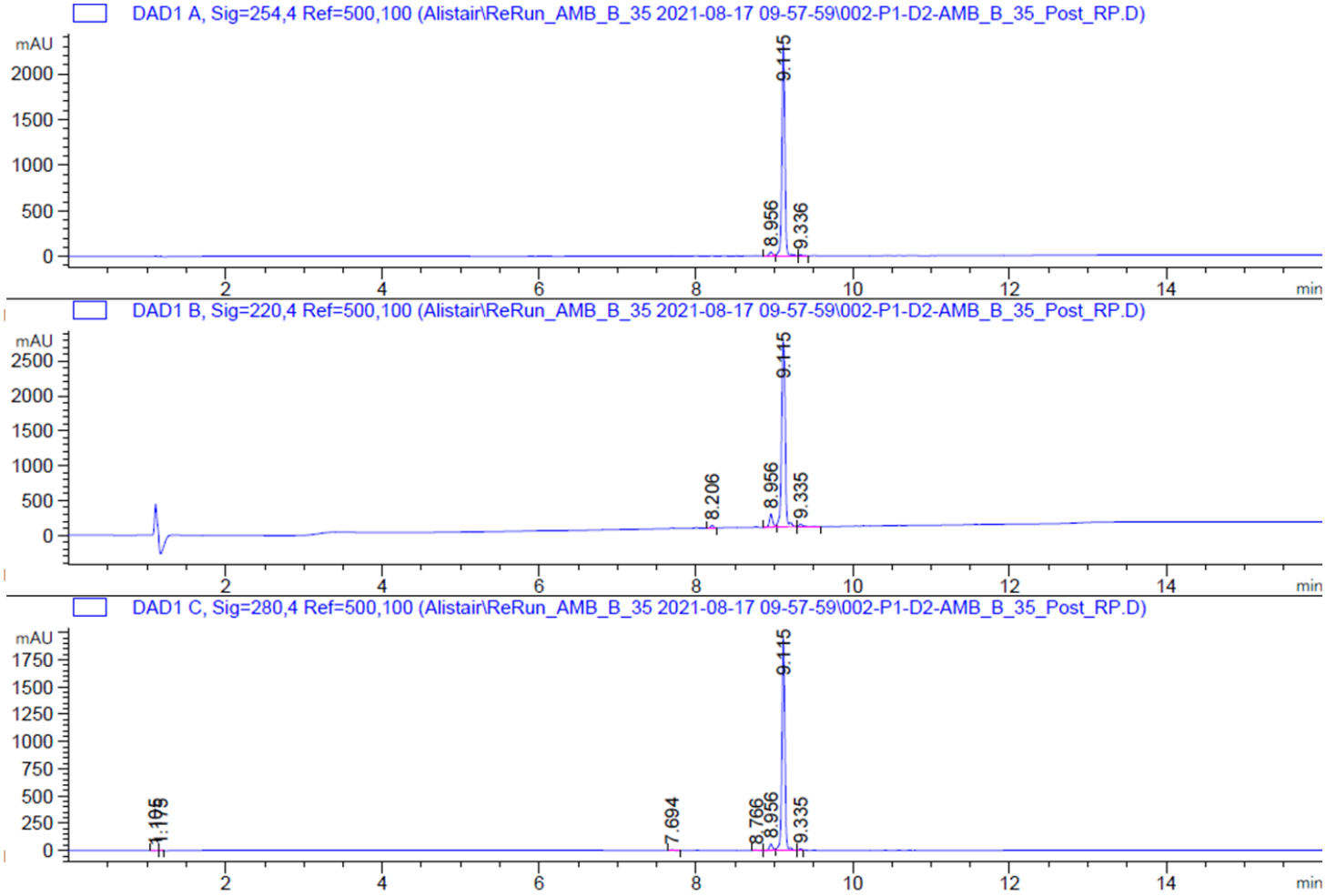

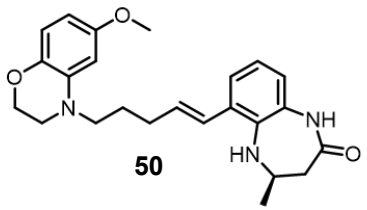

50

Signal 1: DAD1 A, Sig=254,4 Ref=500,100

Peak #	RetTime [min]	Type	Width [min]	Area [mAU*s]	Height [mAU]	Area %
1	9.505	VV E	0.0529	5.56261	1.54928	0.0674
2	9.656	VB R	0.0524	8237.39160	2441.59277	99.8705
3	10.795	MM	0.0988	5.11571	8.62814e-1	0.0620
Totals :				8248.06992	2444.00486	

Signal 2: DAD1 B, Sig=220,4 Ref=500,100

Peak #	RetTime [min]	Type	Width [min]	Area [mAU*s]	Height [mAU]	Area %
1	9.508	BV E	0.0480	13.80539	4.23516	0.1375
2	9.656	VB R	0.0672	1.00020e4	2371.57275	99.6087
3	10.227	MM	0.0637	12.67730	3.31893	0.1263
4	12.020	MM	0.0552	12.80458	3.86859	0.1275
Totals :				1.00413e4	2382.99543	

Signal 3: DAD1 C, Sig=280,4 Ref=500,100

Peak #	RetTime [min]	Type	Width [min]	Area [mAU*s]	Height [mAU]	Area %
1	9.656	VB R	0.0512	2004.07996	596.17499	100.0000
Totals :				2004.07996	596.17499	

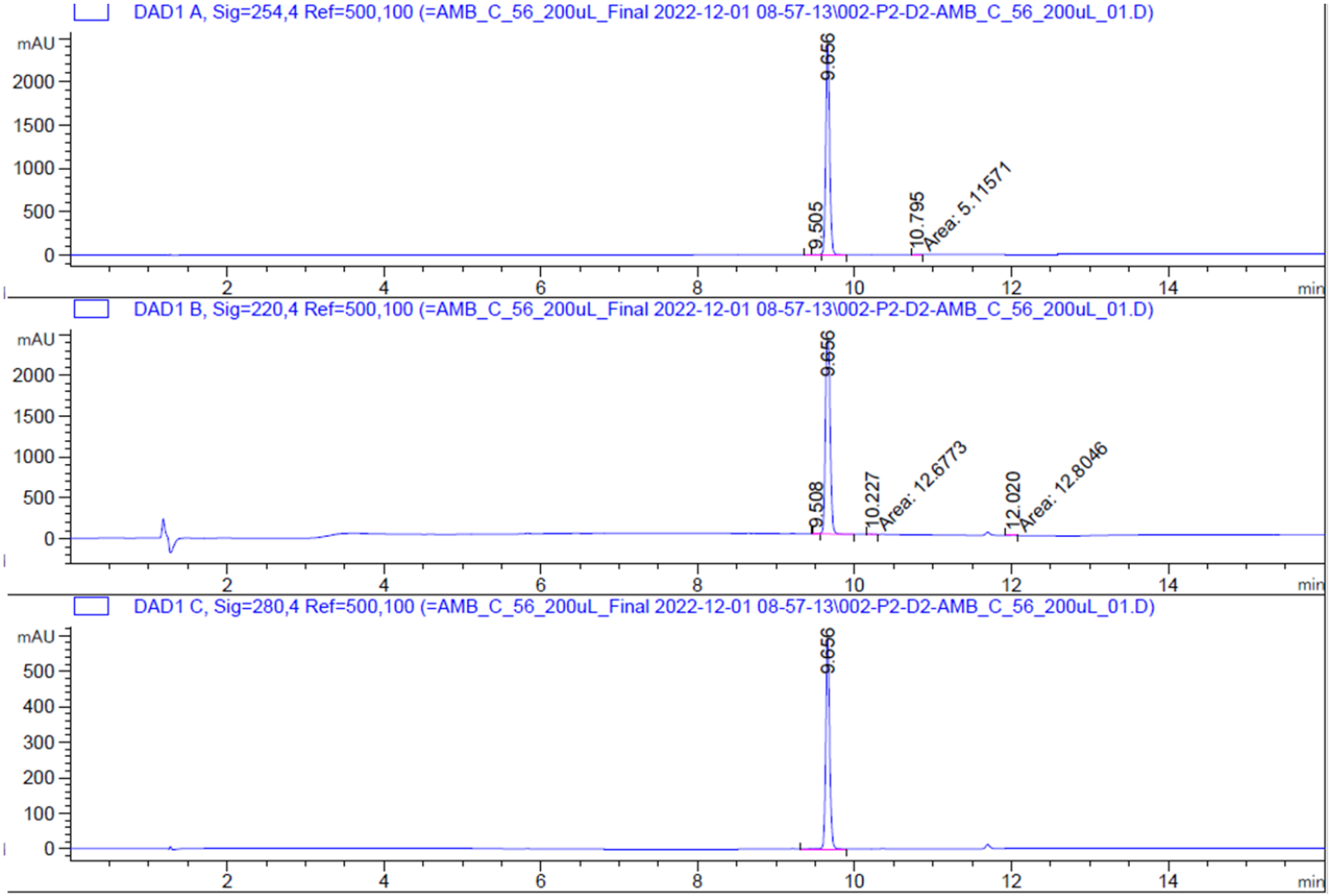

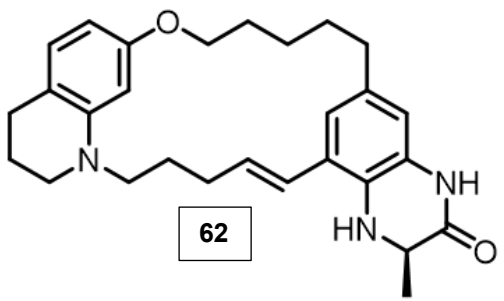

62

Signal 1: DAD1 A, Sig=254,4 Ref=500,100

Peak #	RetTime [min]	Type	Width [min]	Area [mAU*s]	Height [mAU]	Area %
1	12.328	VV R	0.0460	3518.34058	1171.14185	99.4985
2	12.547	VB E	0.0400	5.21119	2.02925	0.1474
3	12.843	BB	0.0453	12.52295	4.26169	0.3541
Totals :				3536.07471	1177.43278	

Signal 2: DAD1 B, Sig=220,4 Ref=500,100

Peak #	RetTime [min]	Type	Width [min]	Area [mAU*s]	Height [mAU]	Area %
1	11.671	BB	0.0450	27.89886	9.57481	0.5798
2	12.328	MM	0.0506	4697.98926	1546.78979	97.6348
3	12.548	MM	0.0853	38.79298	7.57892	0.8062
4	12.845	BV	0.0605	47.11771	11.10714	0.9792
Totals :				4811.79880	1575.05066	

Signal 3: DAD1 C, Sig=280,4 Ref=500,100

Peak #	RetTime [min]	Type	Width [min]	Area [mAU*s]	Height [mAU]	Area %
1	11.670	BB	0.0471	9.72166	3.14235	0.8703
2	12.328	VV R	0.0464	1100.42969	362.62927	98.5083
3	12.843	BB	0.0462	6.94168	2.30133	0.6214
Totals :				1117.09302	368.07296	

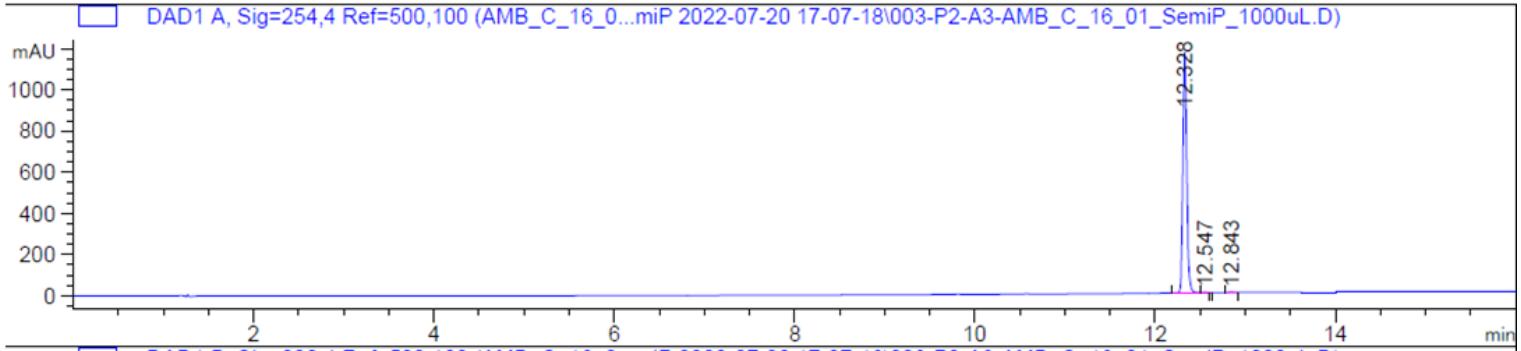

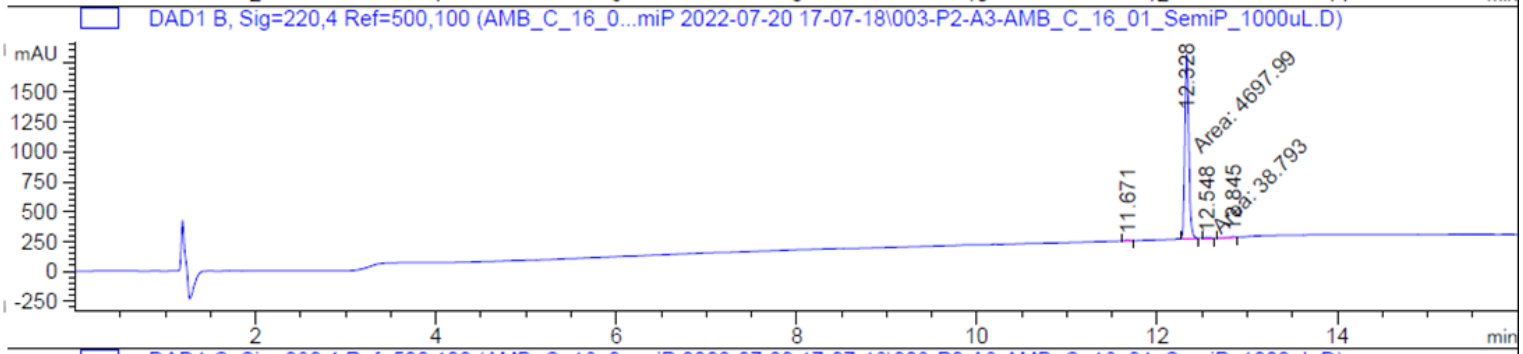

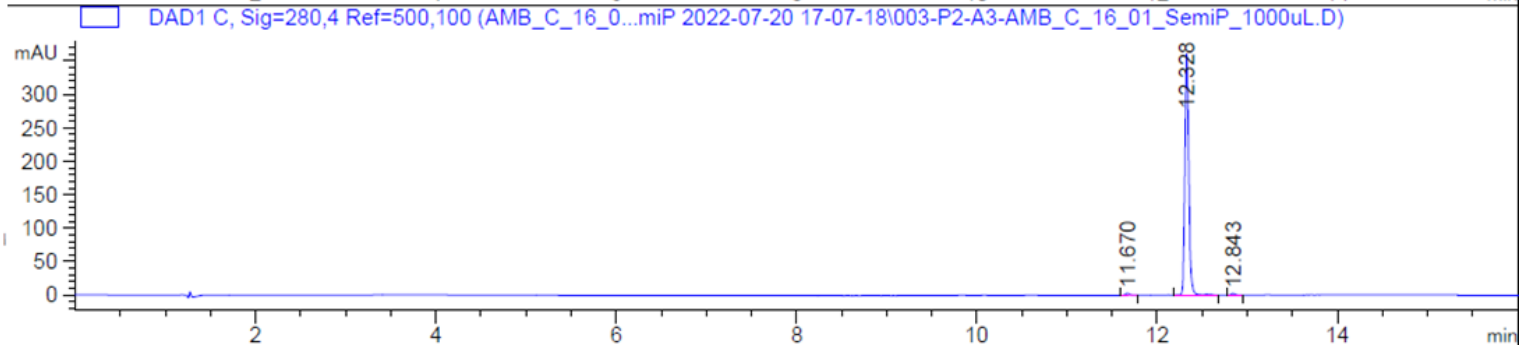

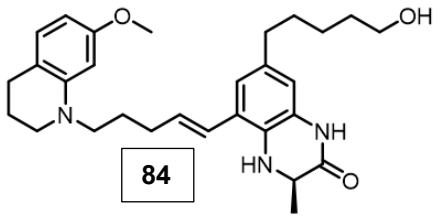

84

Signal 1: DAD1 A, Sig=254,4 Ref=500,100

Peak #	RetTime [min]	Type	Width [min]	Area [mAU*s]	Height [mAU]	Area %
1	10.312	BV E	0.0306	10.32090	5.38986	0.0841
2	10.399	VV R	0.0527	1.21979e4	3678.24438	99.3500
3	10.544	VB E	0.0726	43.84490	8.72366	0.3571
4	10.817	BB	0.0447	25.63556	8.88562	0.2088
Totals :				1.22777e4	3701.24353	

Signal 2: DAD1 B, Sig=220,4 Ref=500,100

Peak #	RetTime [min]	Type	Width [min]	Area [mAU*s]	Height [mAU]	Area %
1	10.251	BV E	0.0321	8.49444	4.28788	0.0767
2	10.316	VV E	0.0348	44.20559	18.55365	0.3994
3	10.400	VB R	0.0652	1.09367e4	2702.82056	98.8102
4	10.555	BB	0.0379	35.55032	14.84464	0.3212
5	10.817	BB	0.0446	43.44479	15.09467	0.3925
Totals :				1.10684e4	2755.60139	

Signal 3: DAD1 C, Sig=280,4 Ref=500,100

Peak #	RetTime [min]	Type	Width [min]	Area [mAU*s]	Height [mAU]	Area %
1	10.252	BV E	0.0377	6.42964	2.61666	0.1224
2	10.312	VV E	0.0364	9.78989	4.02764	0.1864
3	10.399	VV R	0.0426	5195.52832	1860.79565	98.9040
4	10.549	VB E	0.0811	26.98766	4.62555	0.5137
5	10.817	BB	0.0449	14.36452	4.94185	0.2734
Totals :				5253.10002	1877.00736	

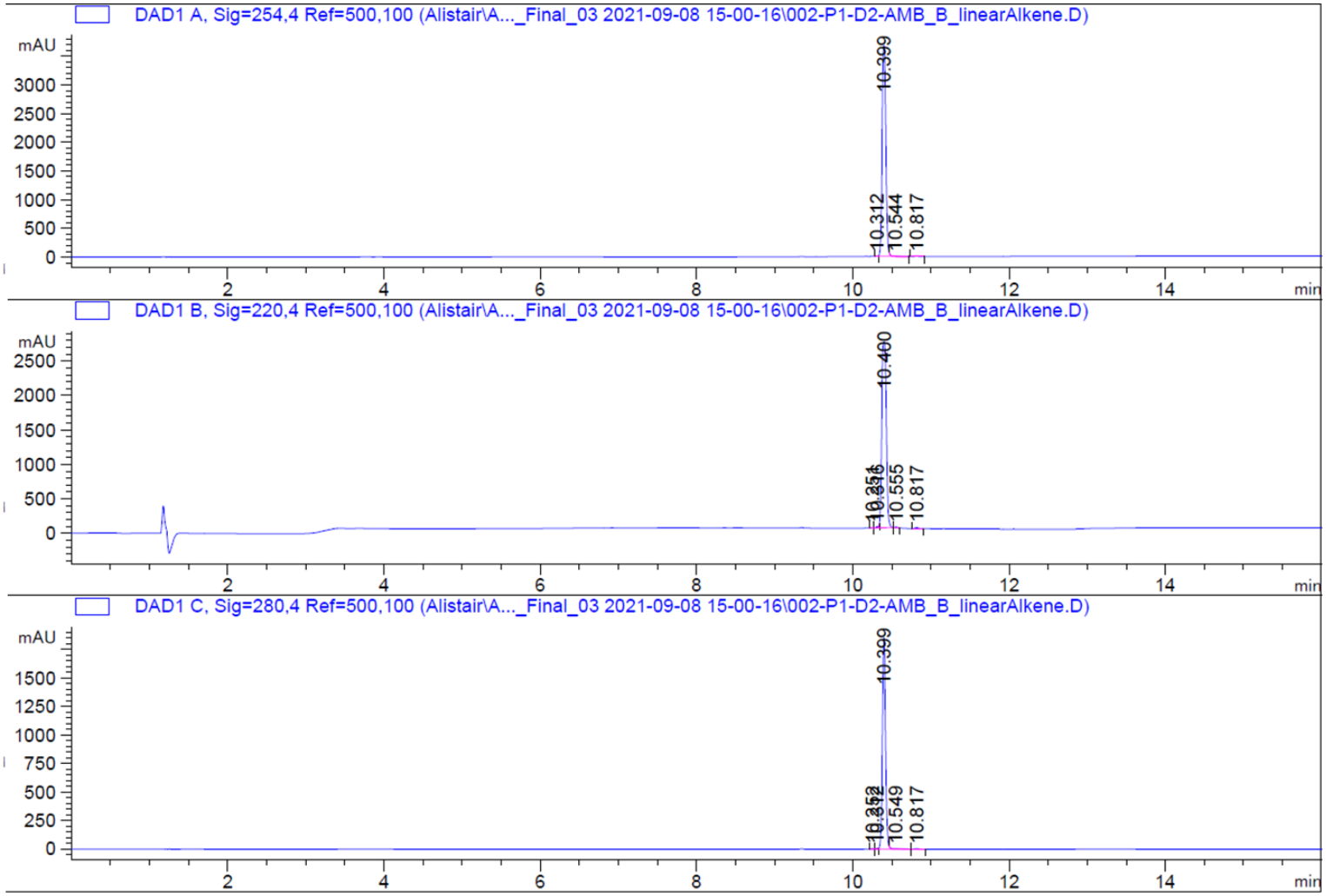

Appendix I: NMR Spectra for Novel Compounds

Below are presented the NMR spectra for all the novel compounds synthesised during this study and any non-novel biologically tested compounds. The spectra for each compound are presented in order of increasing nuclear mass. The spectra are shown in order of compound appearance during the results and discussion chapters presented prior.

^{1}H NMR (*R*,*E*)-2-methyl-1,2,3,9,10,11,12,18,19,21,22,23-dodecahydro-8*H*,17*H*-14,16-(epiethane[1,2]diylidene)-7,26-(metheno)[1,4]diazepino[2,3-*l*]pyrido[2,1-*d*][1]oxa[5,17]diazacycloicosine-4,8(5*H*)-dione

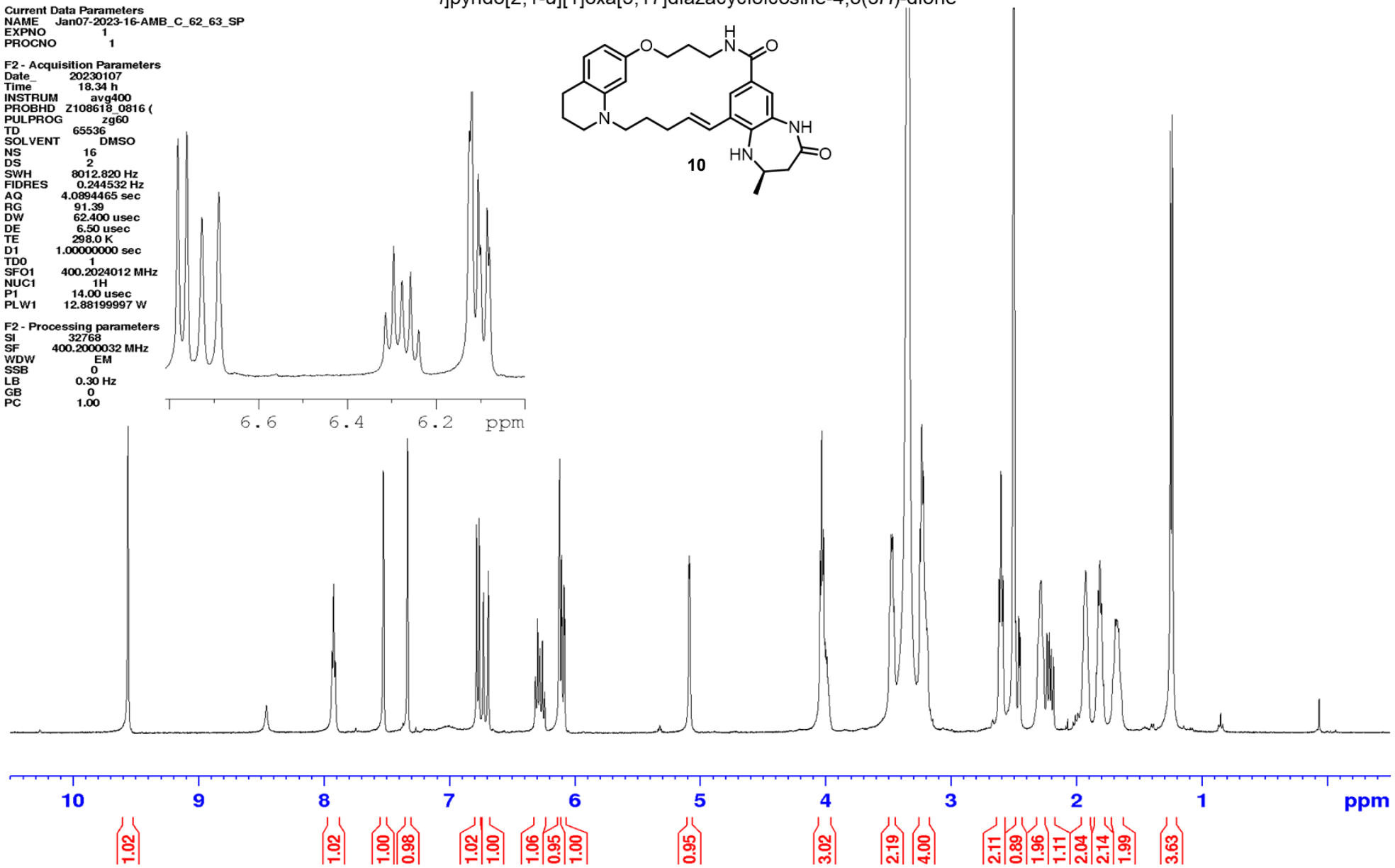

^{1}H NMR benzyl (*R*,*E*)-9-(5-(7-(2-((*tert*-butoxycarbonyl)amino)ethoxy)-3,4-dihydroquinolin-1(2*H*)-yl)pent-1-en-1-yl)-2-methyl-4-oxo-2,3,4,5-tetrahydro-1*H*-benzo[*b*][1,4]diazepine-7-carboxylate

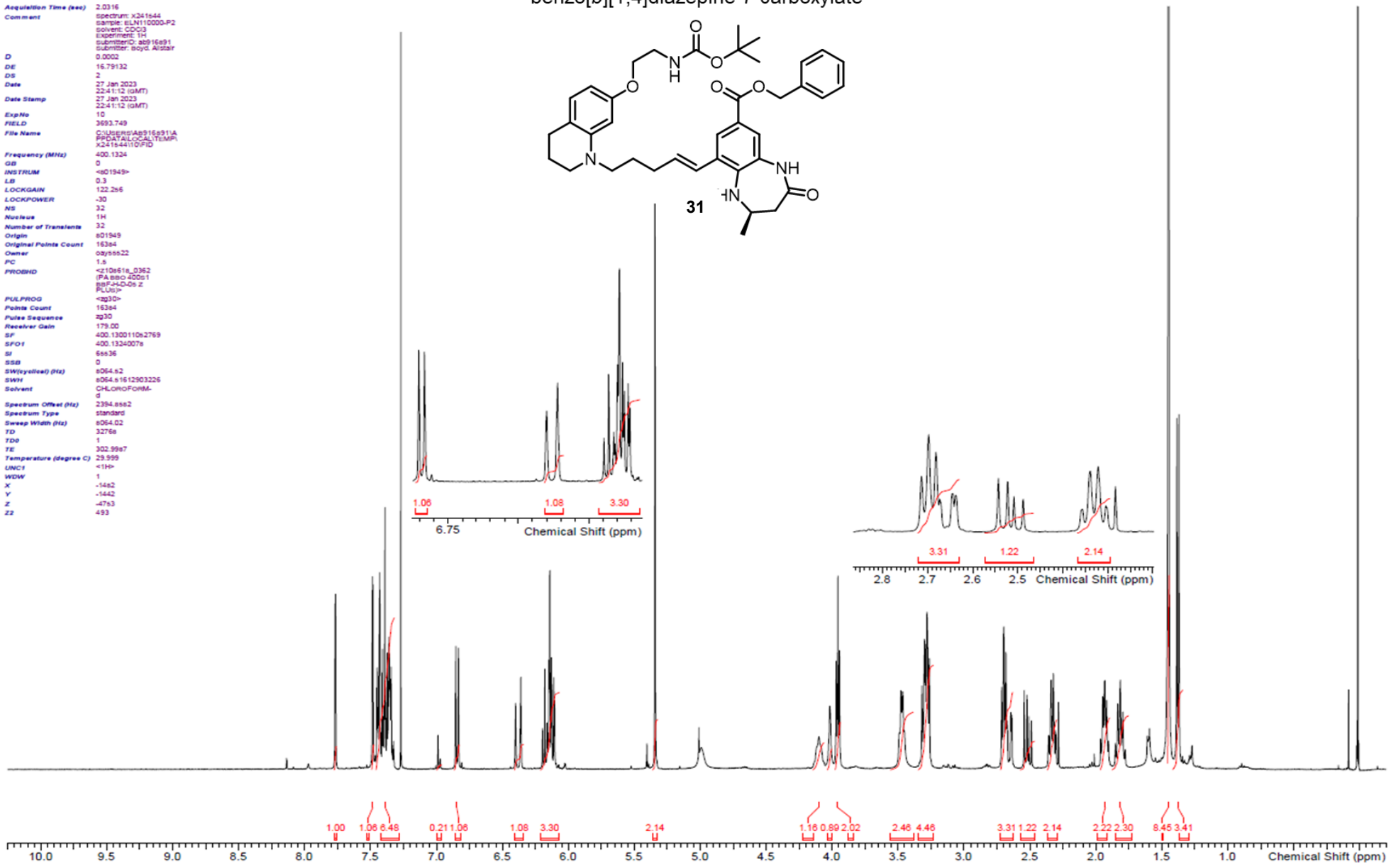

^{13}C NMR benzyl (*R*,*E*)-9-(5-(7-(2-(((*tert*-butoxycarbonyl)amino)ethoxy)-3,4-dihydroquinolin-1(2*H*)-yl)pent-1-en-1-yl)-2-methyl-4-oxo-2,3,4,5-tetrahydro-1*H*-benzo[*b*][1,4]diazepine-7-carboxylate

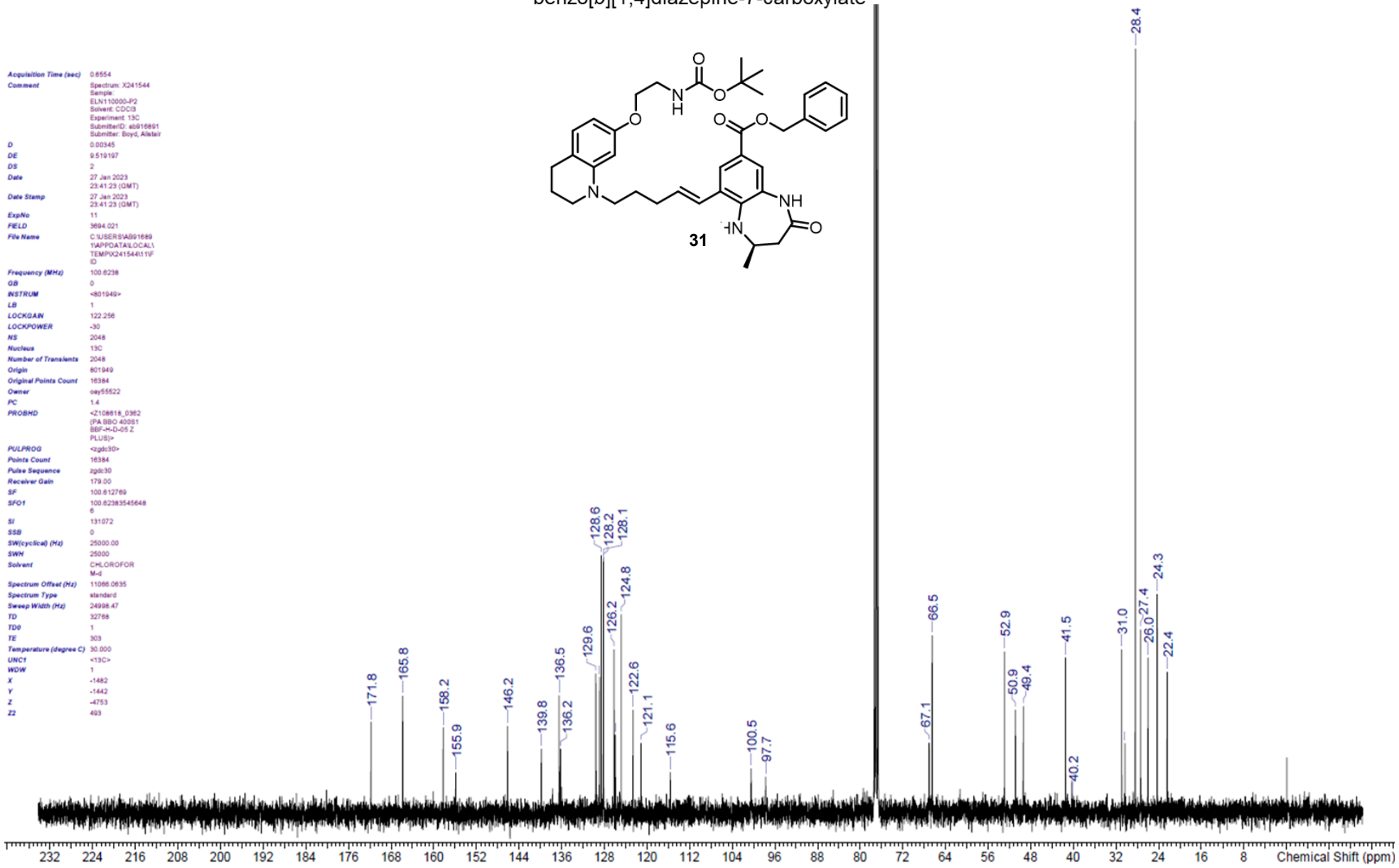

^{1}H NMR benzyl (*R*,*E*)-9-(5-(7-(4-((tert-butoxycarbonyl)amino)butoxy)-3,4-dihydroquinolin-1(2*H*)-yl)pent-1-en-1-yl)-2-methyl-4-oxo-2,3,4,5-tetrahydro-1*H*-benzo[*b*][1,4]diazepine-7-carboxylate

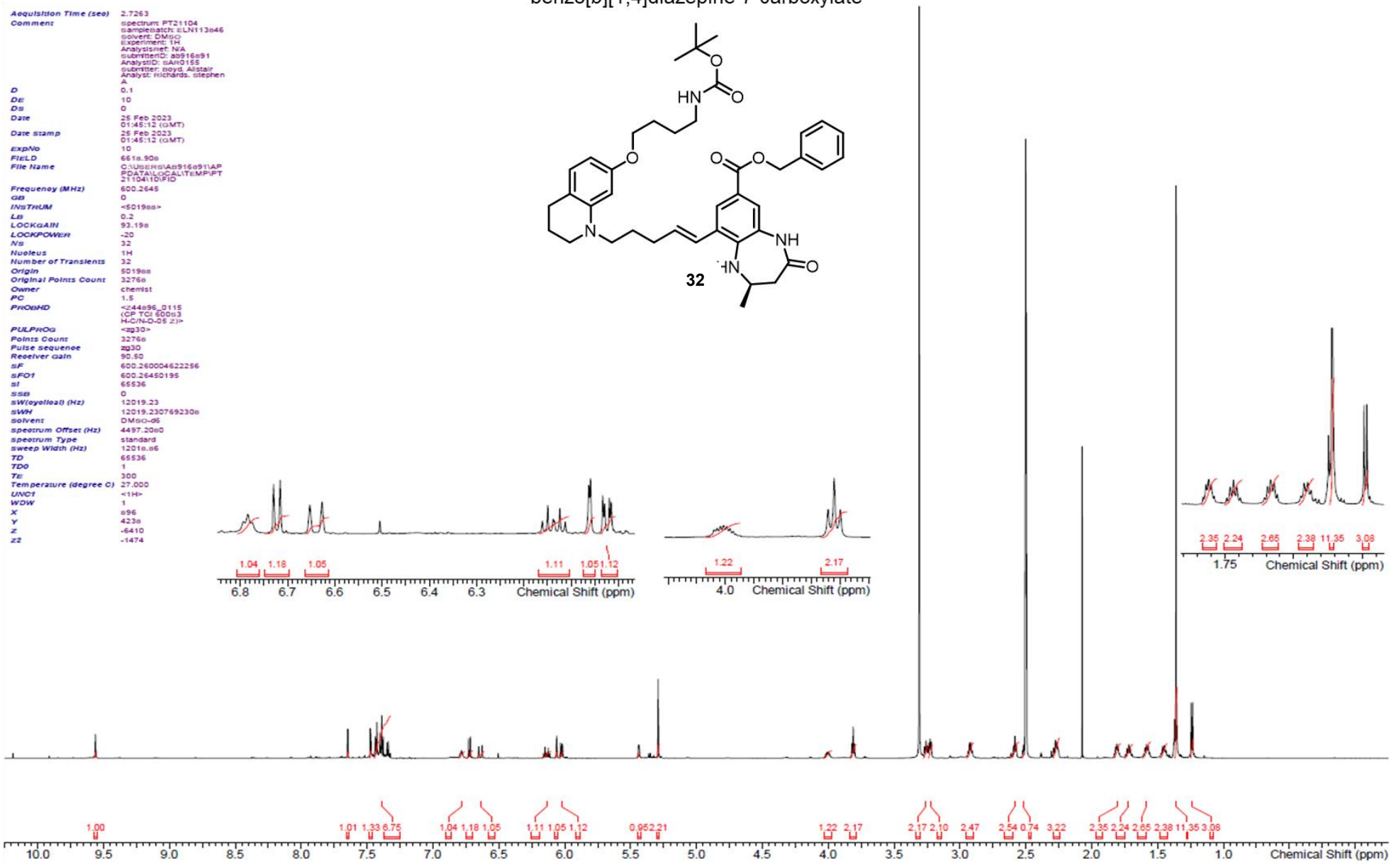

^{1}H NMR benzyl (*R*)-9-((*E*)-5-(7-(((*S*)-1-(tert-butoxycarbonyl)piperidin-3-yl)methoxy)-3,4-dihydroquinolin-1(2*H*)-yl)pent-1-en-1-yl)-2-methyl-4-oxo-2,3,4,5-tetrahydro-1*H*-benzo[*b*][1,4]diazepine-7-carboxylate

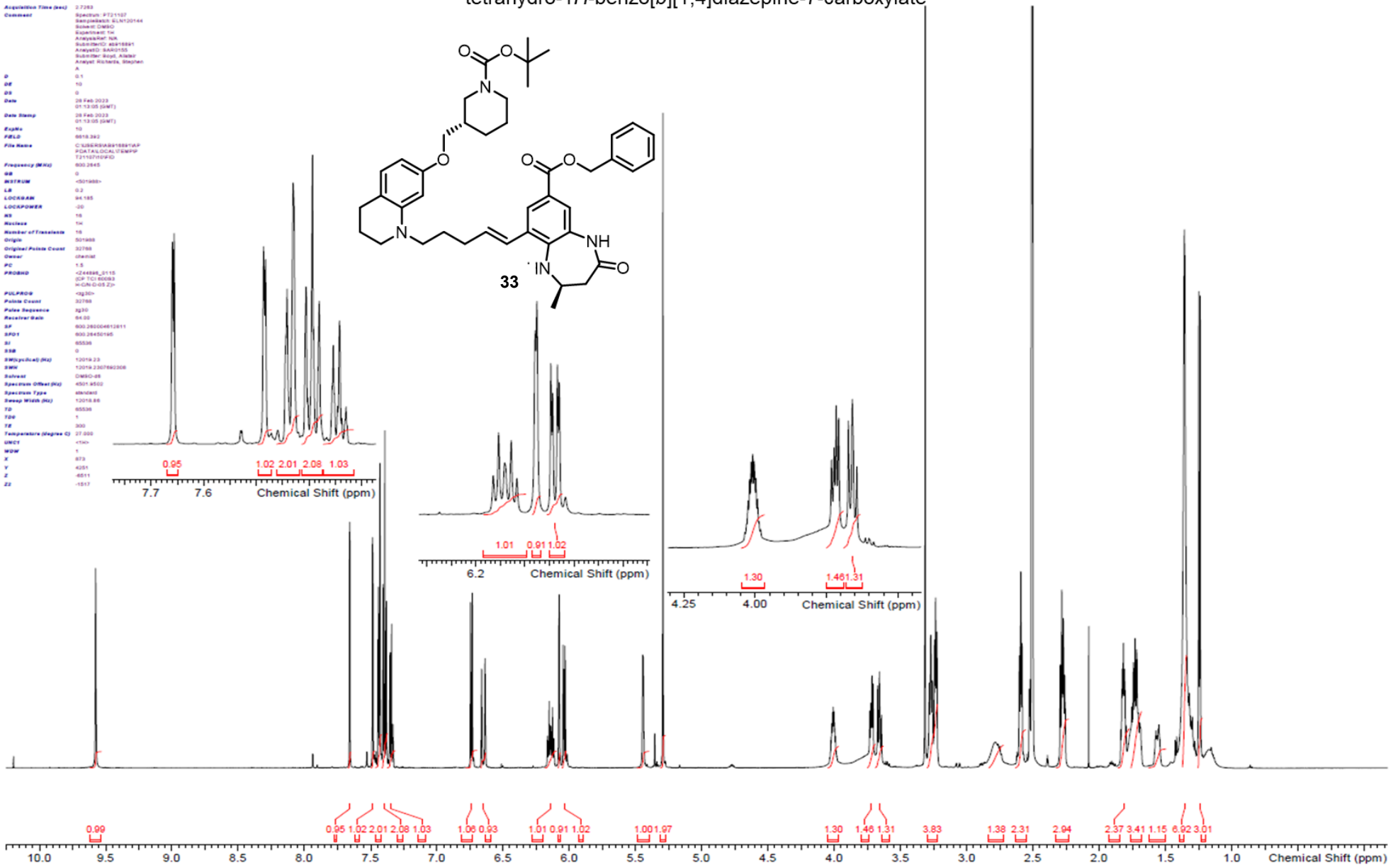

^{13}C NMR benzyl (*R*)-9-((*E*)-5-(7-(((*S*)-1-(tert-butoxycarbonyl)piperidin-3-yl)methoxy)-3,4-dihydroquinolin-1(2*H*)-yl)pent-1-en-1-yl)-2-methyl-4-oxo-2,3,4,5-tetrahydro-1*H*-benzo[*b*][1,4]diazepine-7-carboxylate

Acquisition Time (sec)	1.8088
Comment	Spectrum: PT21107 SampleBatch: ELN120144 Solvent: DMSO Experiment: 13C AnalysisRef: NA SubmitterID: ab916891 AnalystID: SARD155 Submitter: Boyd, Alistair Analyst: Richards, Stephen A
D	0.8
DE	19.22897
DS	2
Date	28 Feb 2023 02:53:24 (GMT)
Date Stamp	28 Feb 2023 02:53:24 (GMT)
ExpNo	12
FIELD	6618.505
File Name	C:\USER\SAB916891\APPDATA\LOCAL\TEMP\PT21107\12\FID
Frequency (MHz)	150.9521
GB	0
INSTRUM	<501988>
LB	1
LOCKGAIN	94.185
LOCKPOWER	-20
NS	2048
Nucleus	13C
Number of Transients	2048
Origin	501988
Original Points Count	65536
Owner	chemist
PC	1.5
PROBHD	<Z44896_0115 (CP TCI 600S3 H-C/N-D-05 Z)>
PULPROG	<zgpg30bo>
Points Count	65536
Pulse Sequence	zgpg30bo
Receiver Gain	256.00
SF	150.935575301097
SFO1	150.952100037
SI	131072
SSB	0
SW(cyclical) (Hz)	36231.88
SWH	36231.884057971
Solvent	DMSO-d6
Spectrum Offset (Hz)	16526.6777
Spectrum Type	standard
Sweep Width (Hz)	36231.33
TD	131072
TD0	1
TE	300
Temperature (degree C)	27.000
UNC1	<13C>
WDW	1
X	873
Y	4251
Z	-6511
Z2	-1517

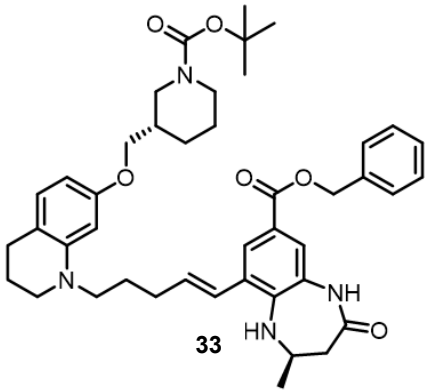

^{1}H NMR benzyl (*R*)-9-((*E*)-5-(7-(((*R*)-1-(*tert*-butoxycarbonyl)pyrrolidin-2-yl)methoxy)-3,4-dihydroquinolin-1(2*H*)-yl)pent-1-en-1-yl)-2-methyl-4-oxo-2,3,4,5-tetrahydro-1*H*-benzo[*b*][1,4]diazepine-7-carboxylate

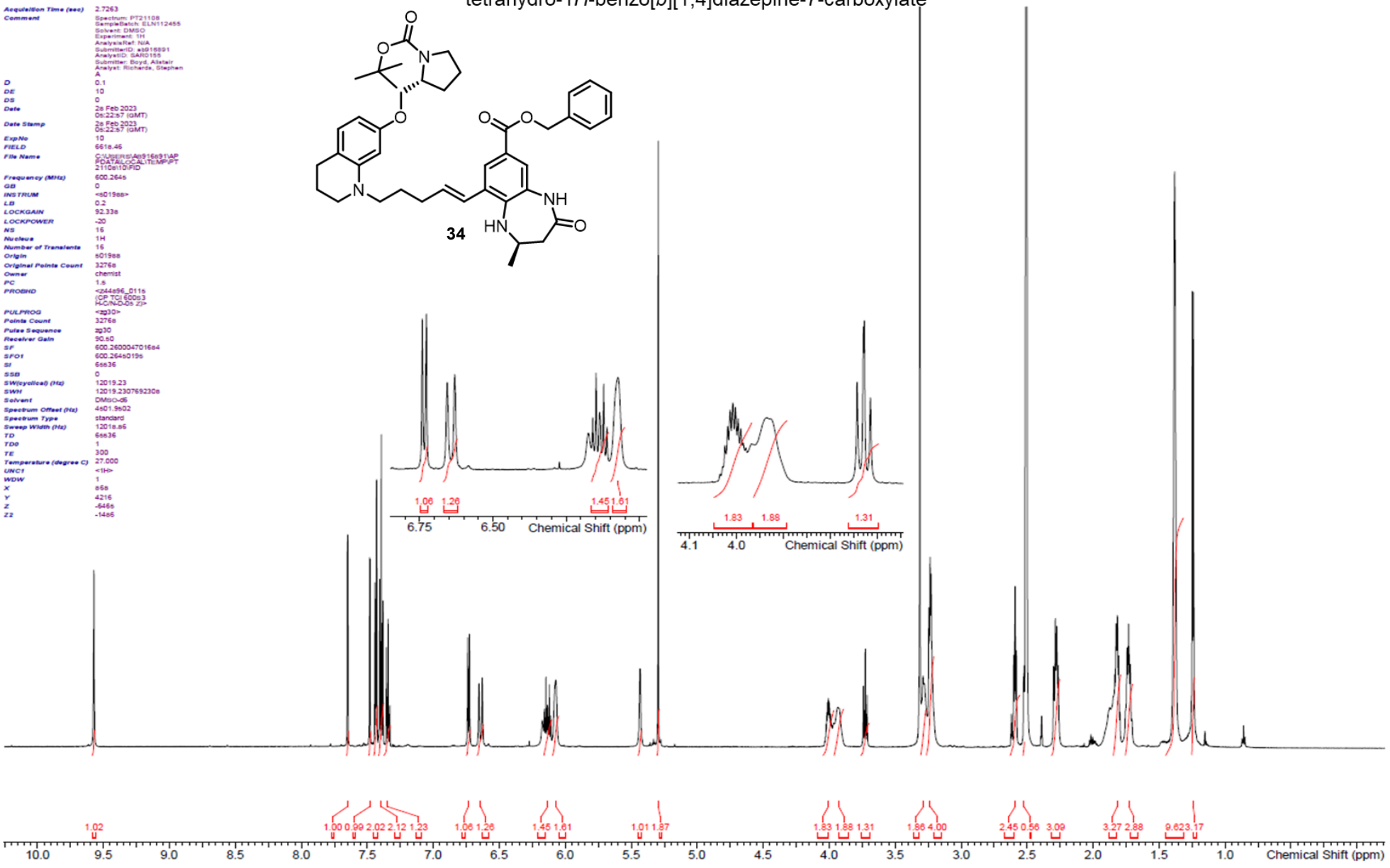

^{13}C NMR benzyl (*R*)-9-((*E*)-5-(7-(((*R*)-1-(*tert*-butoxycarbonyl)pyrrolidin-2-yl)methoxy)-3,4-dihydroquinolin-1(2*H*)-yl)pent-1-en-1-yl)-2-methyl-4-oxo-2,3,4,5-tetrahydro-1*H*-benzo[*b*][1,4]diazepine-7-carboxylate

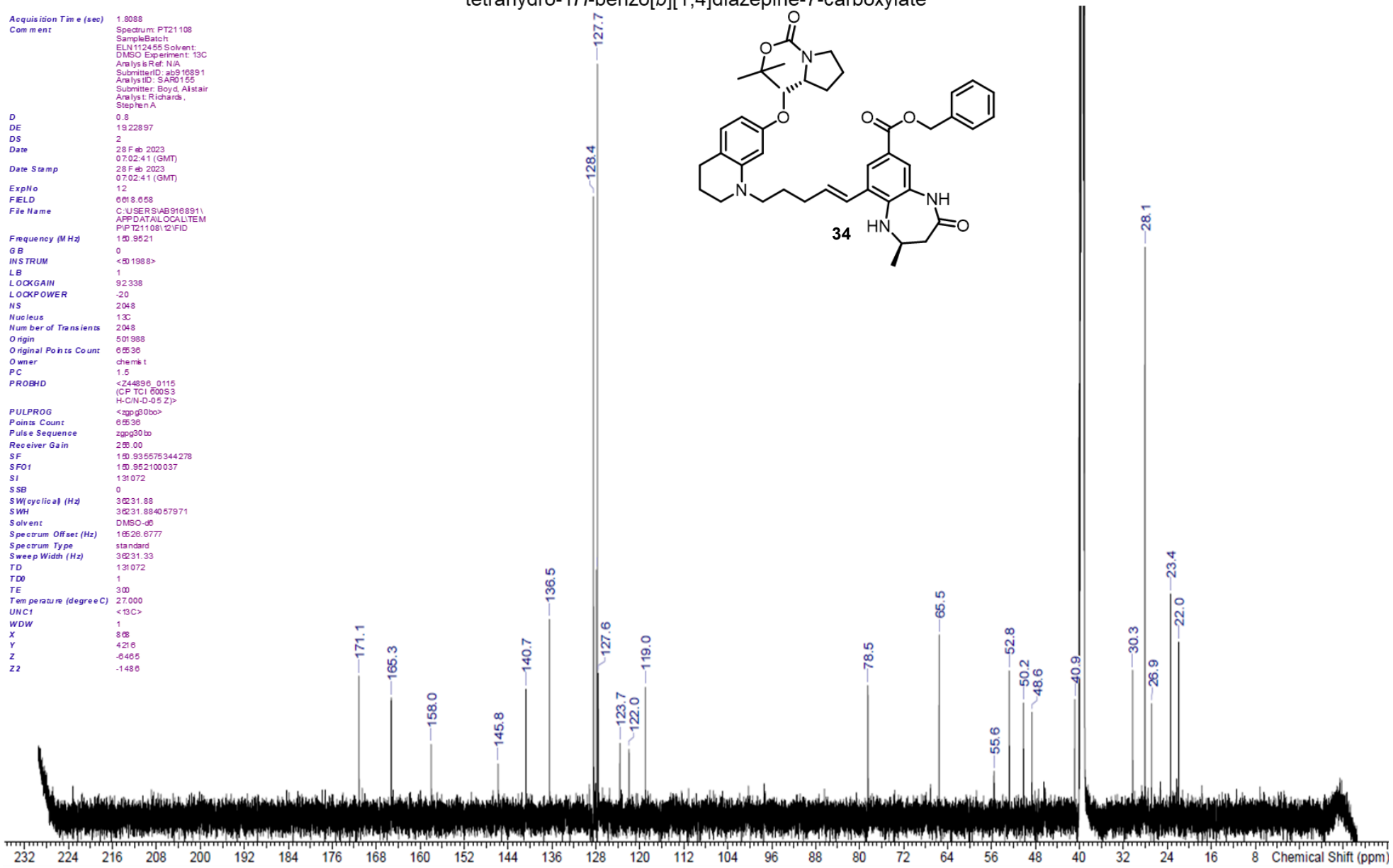

^{1}H NMR benzyl (*R*)-9-((*E*)-5-(7-(((*S*)-1-(*tert*-butoxycarbonyl)pyrrolidin-2-yl)methoxy)-3,4-dihydroquinolin-1(2*H*)-yl)pent-1-en-1-yl)-2-methyl-4-oxo-2,3,4,5-tetrahydro-1*H*-benzo[*b*][1,4]diazepine-7-carboxylate

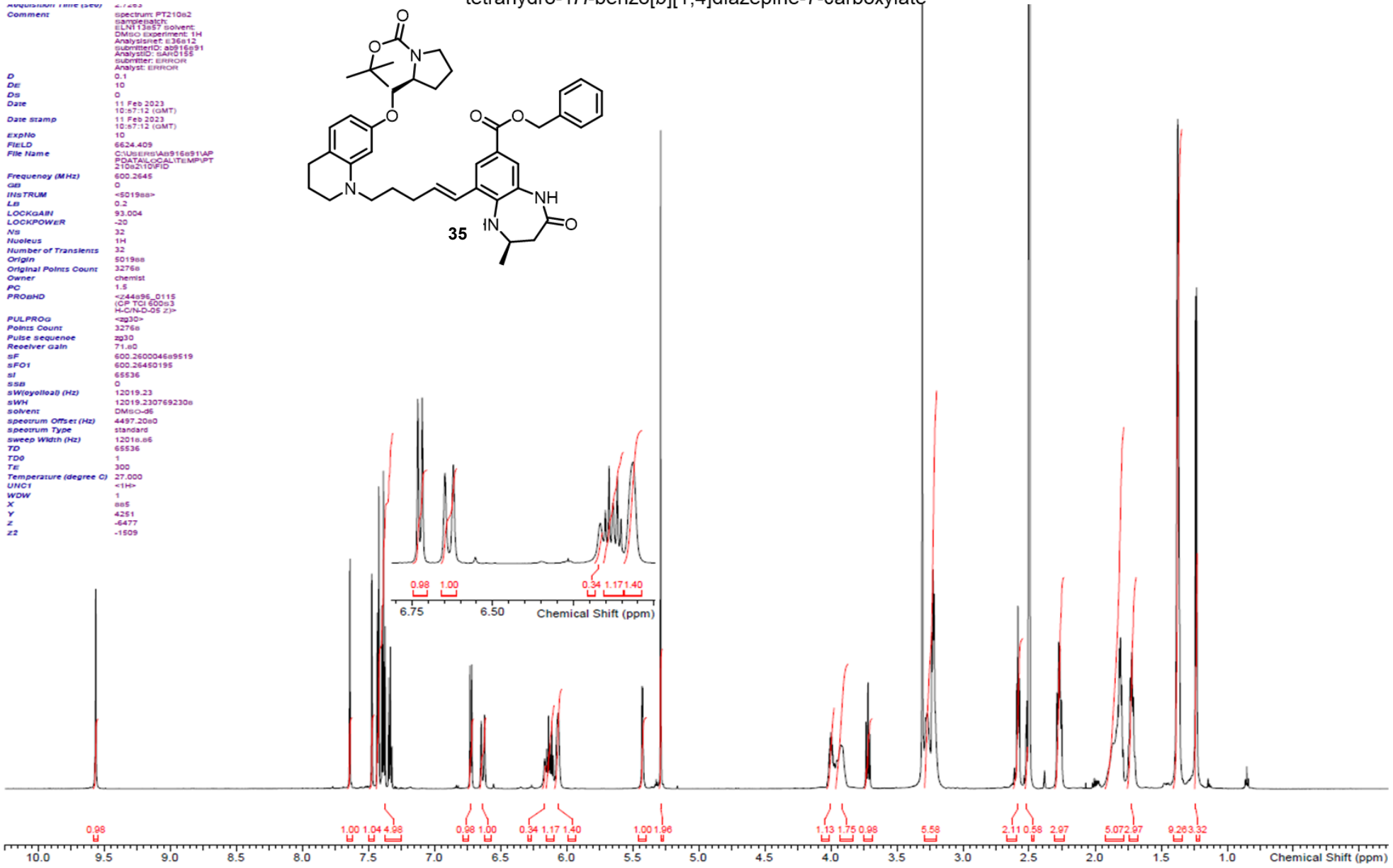

^{13}C NMR benzyl (*R*)-9-((*E*)-5-(7-(((*S*)-1-(*tert*-butoxycarbonyl)pyrrolidin-2-yl)methoxy)-3,4-dihydroquinolin-1(2*H*)-yl)pent-1-en-1-yl)-2-methyl-4-oxo-2,3,4,5-tetrahydro-1*H*-benzo[*b*][1,4]diazepine-7-carboxylate

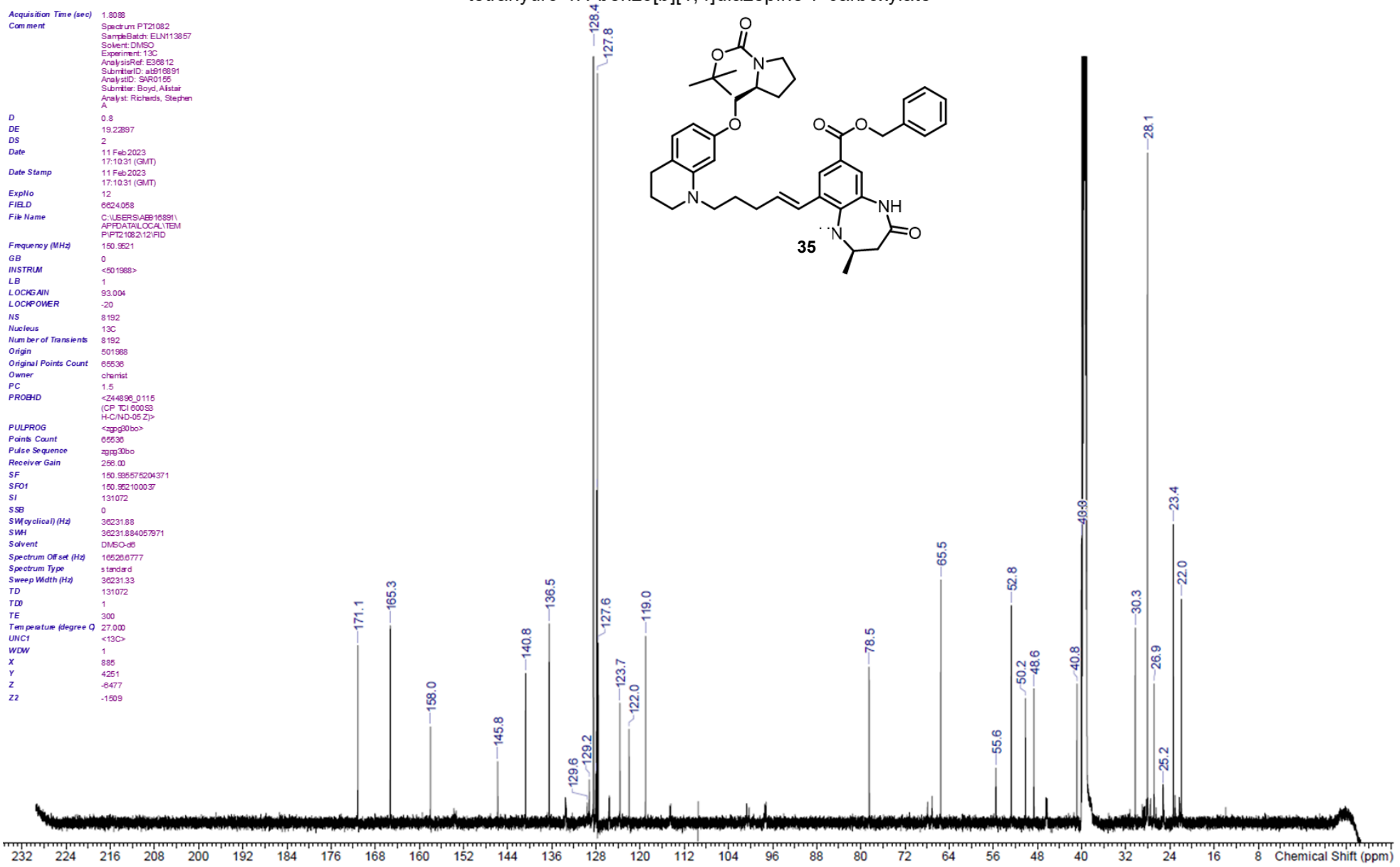

^{1}H NMR *tert*-butyl (*R*)-2-(((1-((*E*)-5-((*R*)-8-((benzyloxy)carbonyl)-4-methyl-2-oxo-2,3,4,5-tetrahydro-1H-benzo[*b*][1,4]diazepin-6-yl)pent-4-en-1-yl)-1,2,3,4-tetrahydroquinolin-7-yl)oxy)methyl)morpholine-4-carboxylate

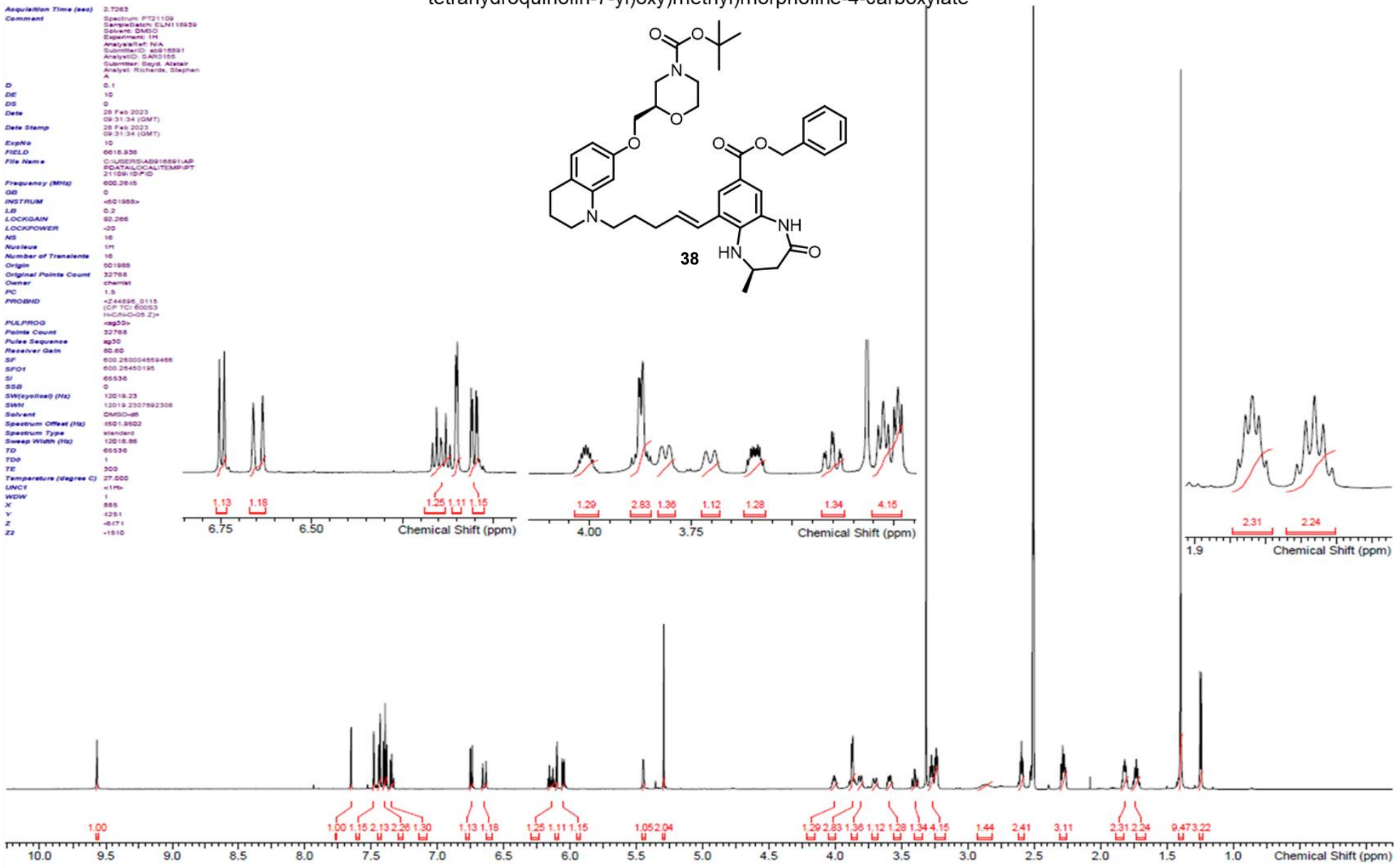

^{13}C NMR *tert*-butyl (*R*)-2-(((1-((*E*)-5-((*R*)-8-((benzyloxy)carbonyl)-4-methyl-2-oxo-2,3,4,5-tetrahydro-1*H*-benzo[*b*][1,4]diazepin-6-yl)pent-4-en-1-yl)-1,2,3,4-tetrahydroquinolin-7-yl)oxy)methyl)morpholine-4-carboxylate

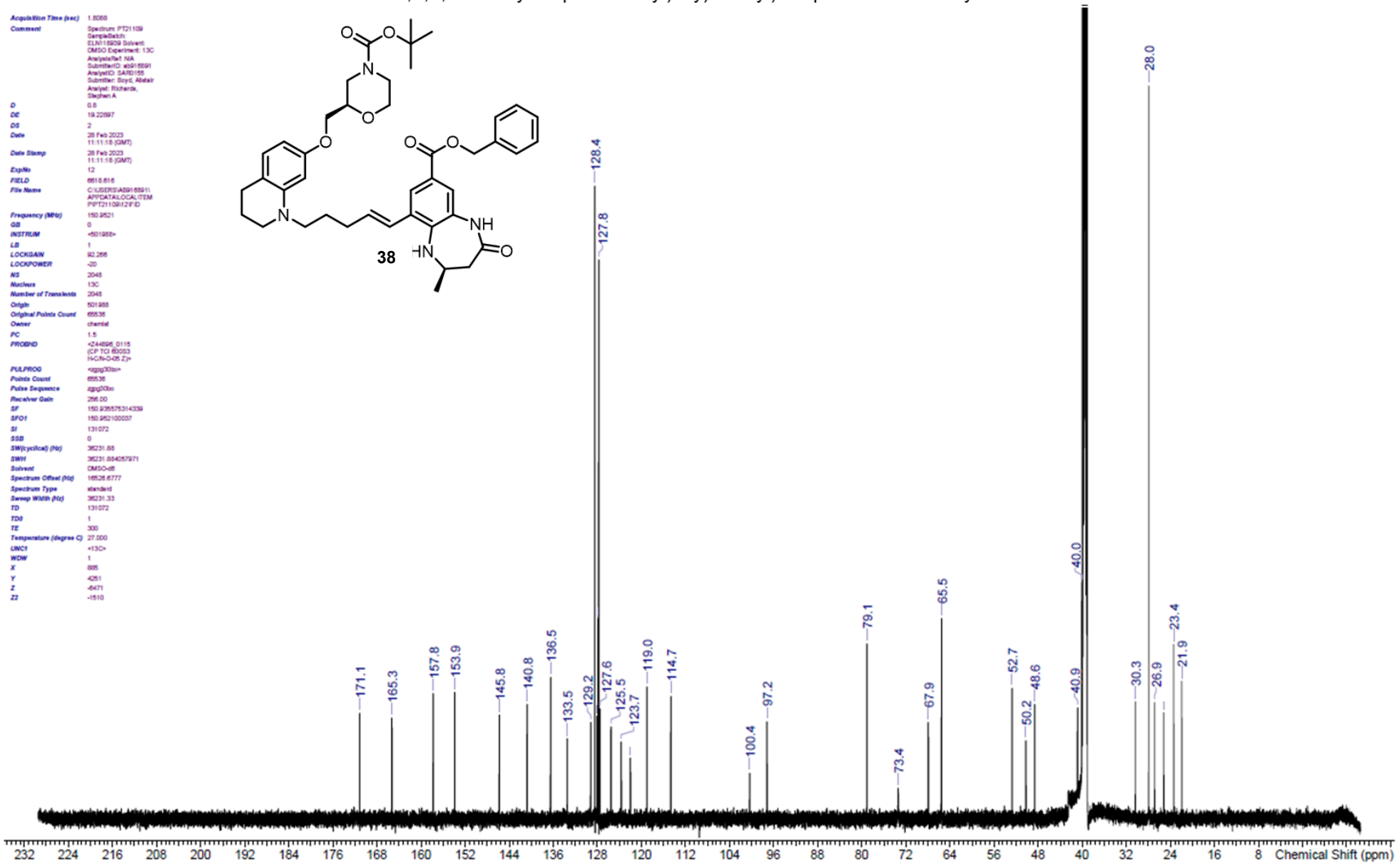

^{1}H NMR (*R*,*E*)-2-methyl-1,2,3,10,11,17,18,20,21,22-decahydro-16*H*-13,15-(epiethane[1,2]diylidene)-7,25-(metheno)[1,4]diazepino[2,3-*h*]pyrido[1,2-*p*][1]oxa[4,16]diazacyclononadecine-4,8(5*H*,9*H*)-dione

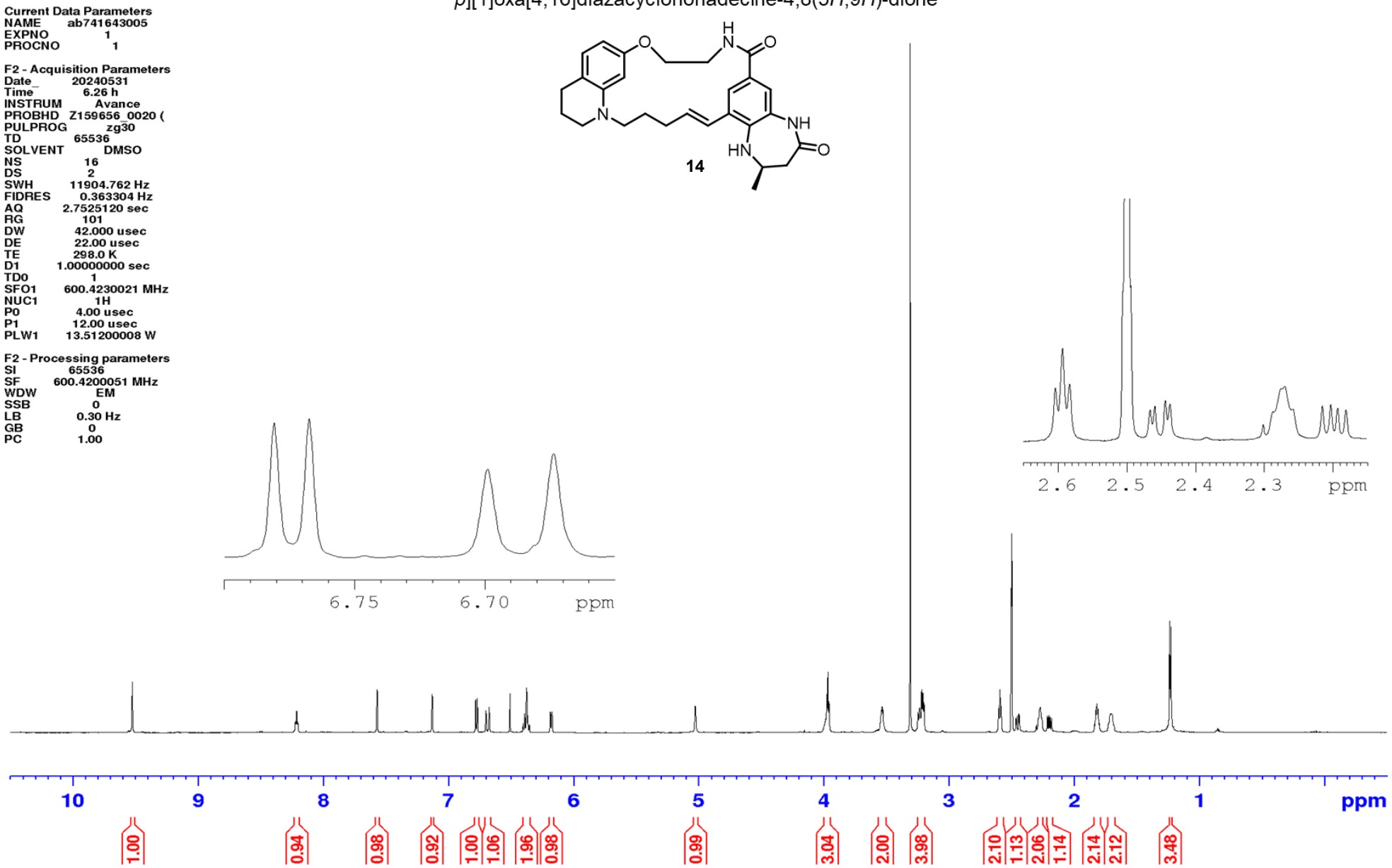

^{1}H NMR (*R*,*E*)-2-methyl-1,2,3,10,11,17,18,20,21,22-decahydro-16*H*-13,15-(epiethane[1,2]diylidene)-7,25-(metheno)[1,4]diazepino[2,3-*h*]pyrido[1,2-*p*][1]oxa[4,16]diazacyclononadecine-4,8(5*H*,9*H*)-dione

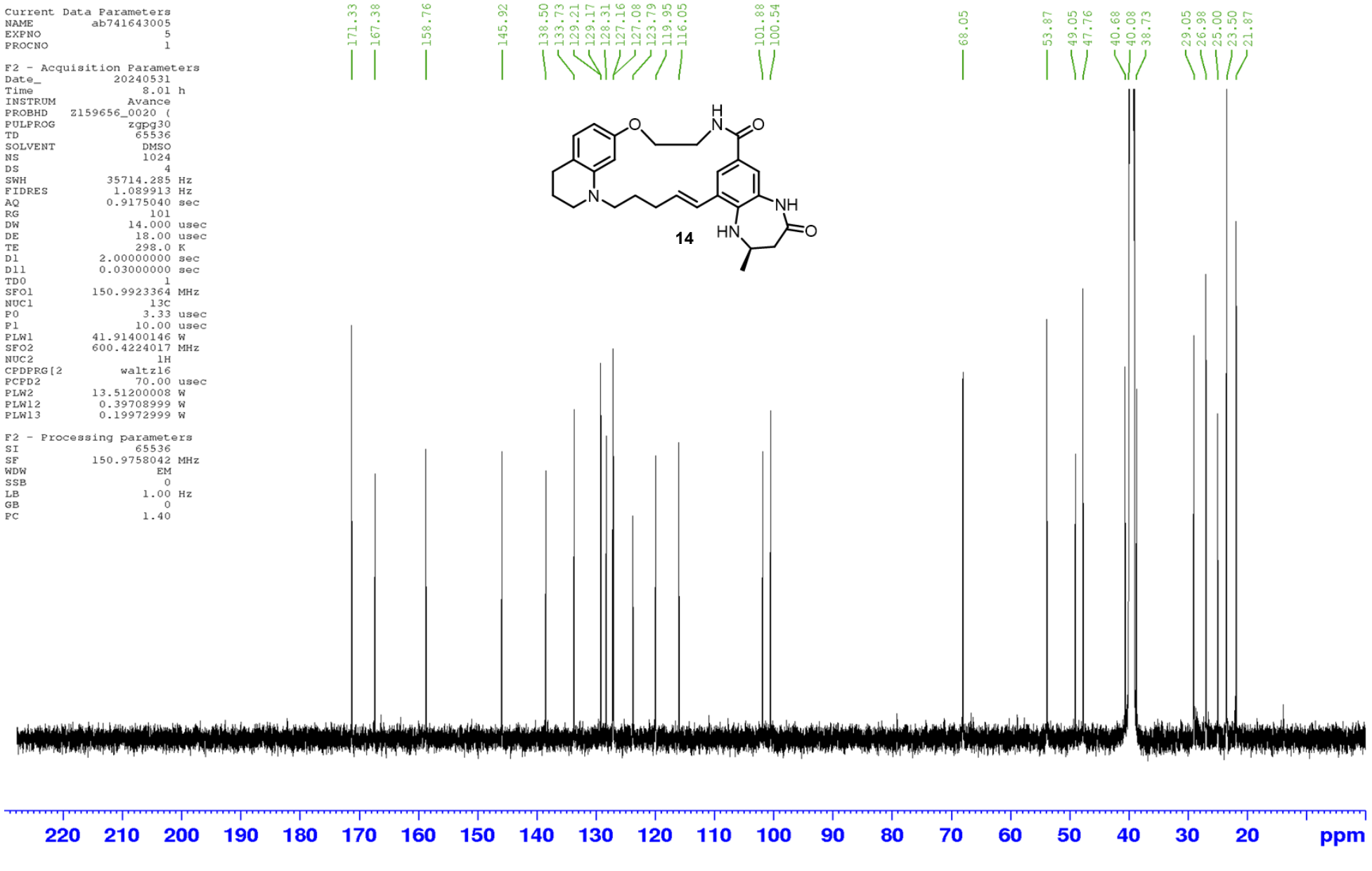

^{1}H NMR (*R*,*E*)-2-methyl-1,2,3,10,11,12,13,19,20,22,23,24-dodecahydro-18*H*-15,17-(epiethane[1,2]diylidene)-7,27-(metheno)[1,4]diazepino[2,3-*l*]pyrido[2,1-*d*][1]oxa[5,17]diazacyclohenicosine-4,8(5*H*,9*H*)-dione

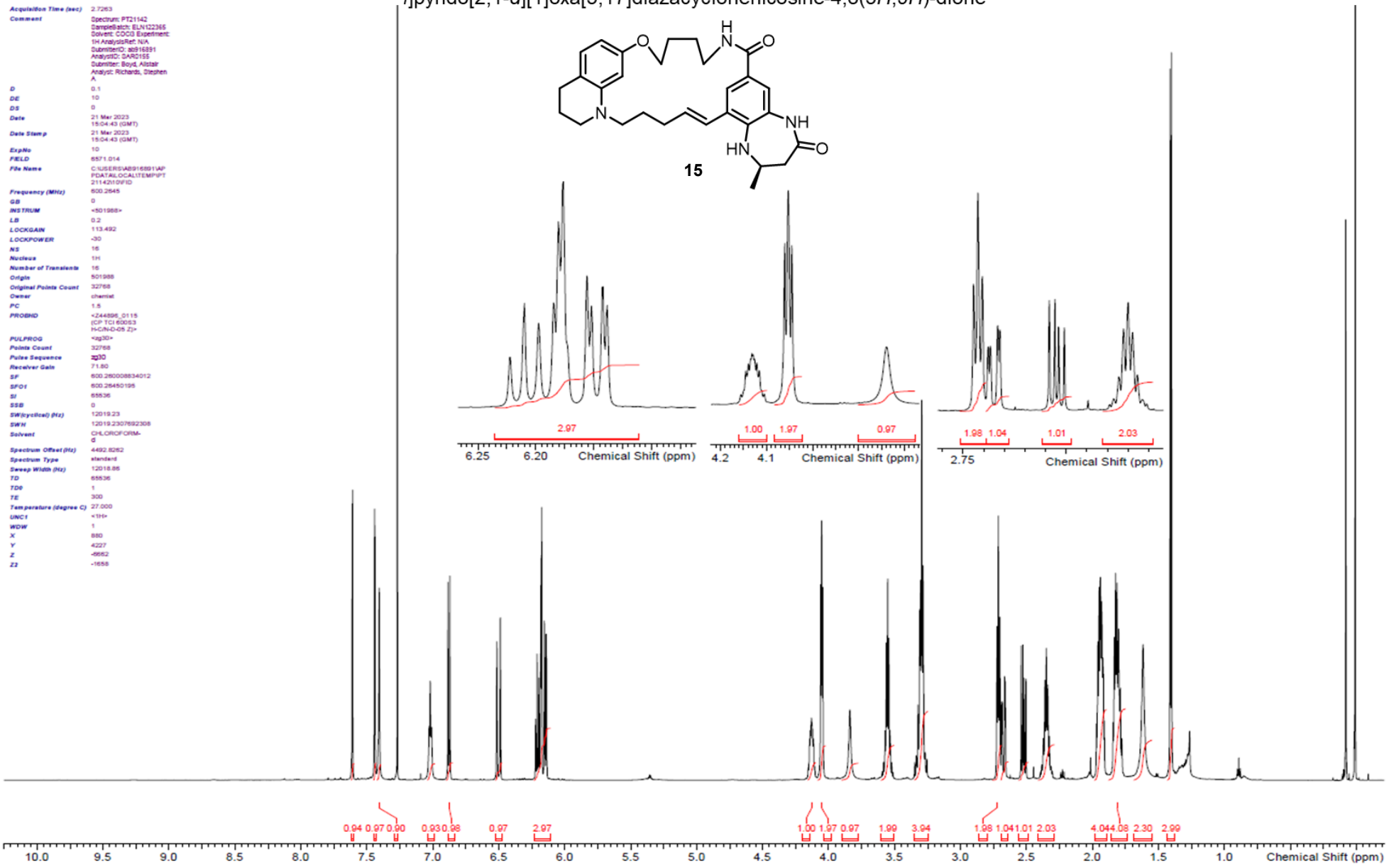

^{13}C NMR (*R*,*E*)-2-methyl-1,2,3,10,11,12,13,19,20,22,23,24-dodecahydro-18*H*-15,17-(epiethane[1,2]diylidene)-7,27-(metheno)[1,4]diazepino[2,3-*l*]pyrido[2,1-*d*][1]oxa[5,17]diazacyclohenicosine-4,8(5*H*,9*H*)-dione

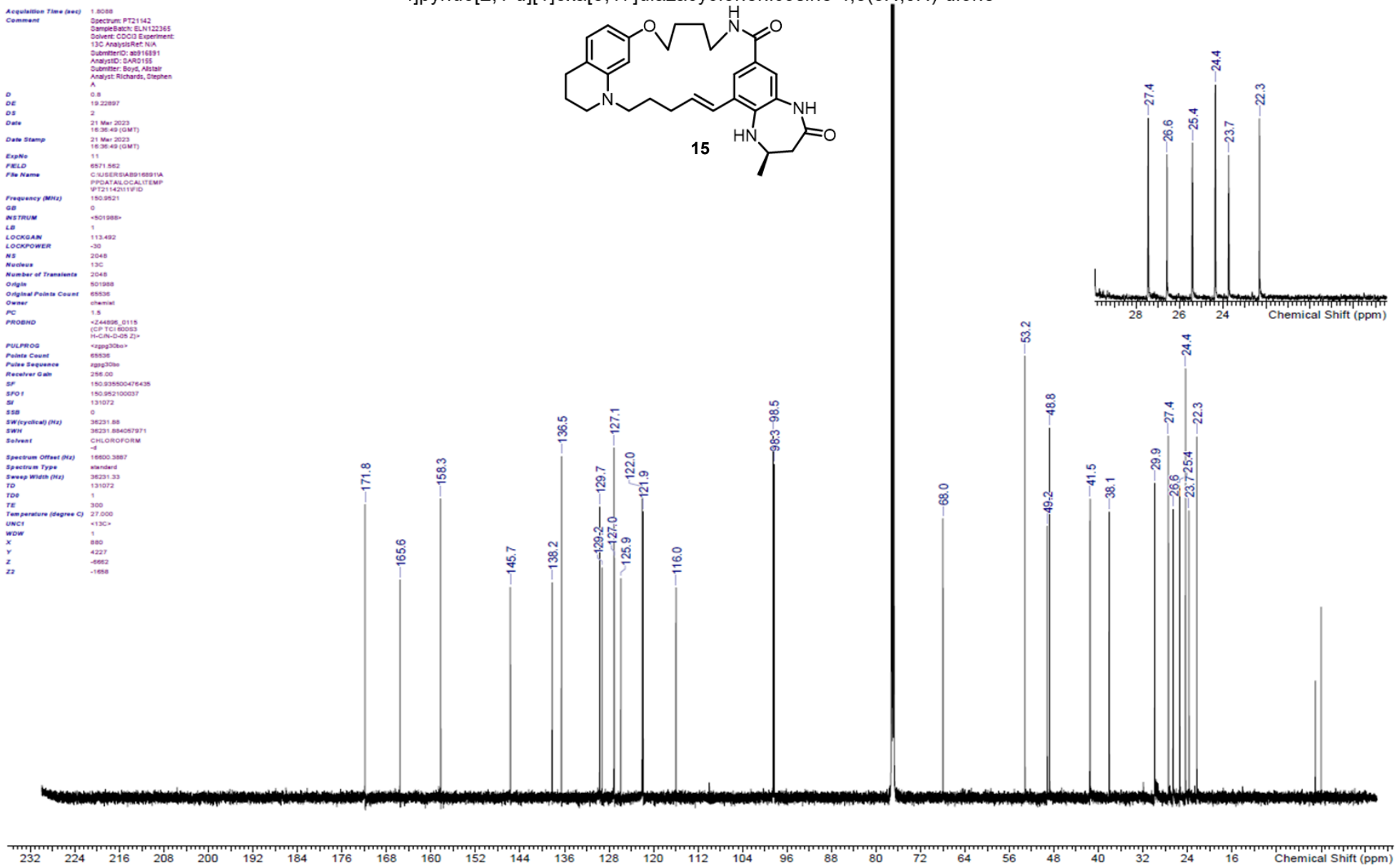

^{1}H NMR (2*R*,12a*R*,*E*)-2-methyl-1,2,3,5,11,12,12a,13,19,20,23,24-dodecahydro-10*H*,18*H*,22*H*-15,17-etheno-7,27-(metheno)[1,4]diazepino[2,3-*h*]pyrido[1,2-*p*]pyrrolo[2,1-*c*][1]oxa[4,16]diazacyclononadecine-4,8-dione

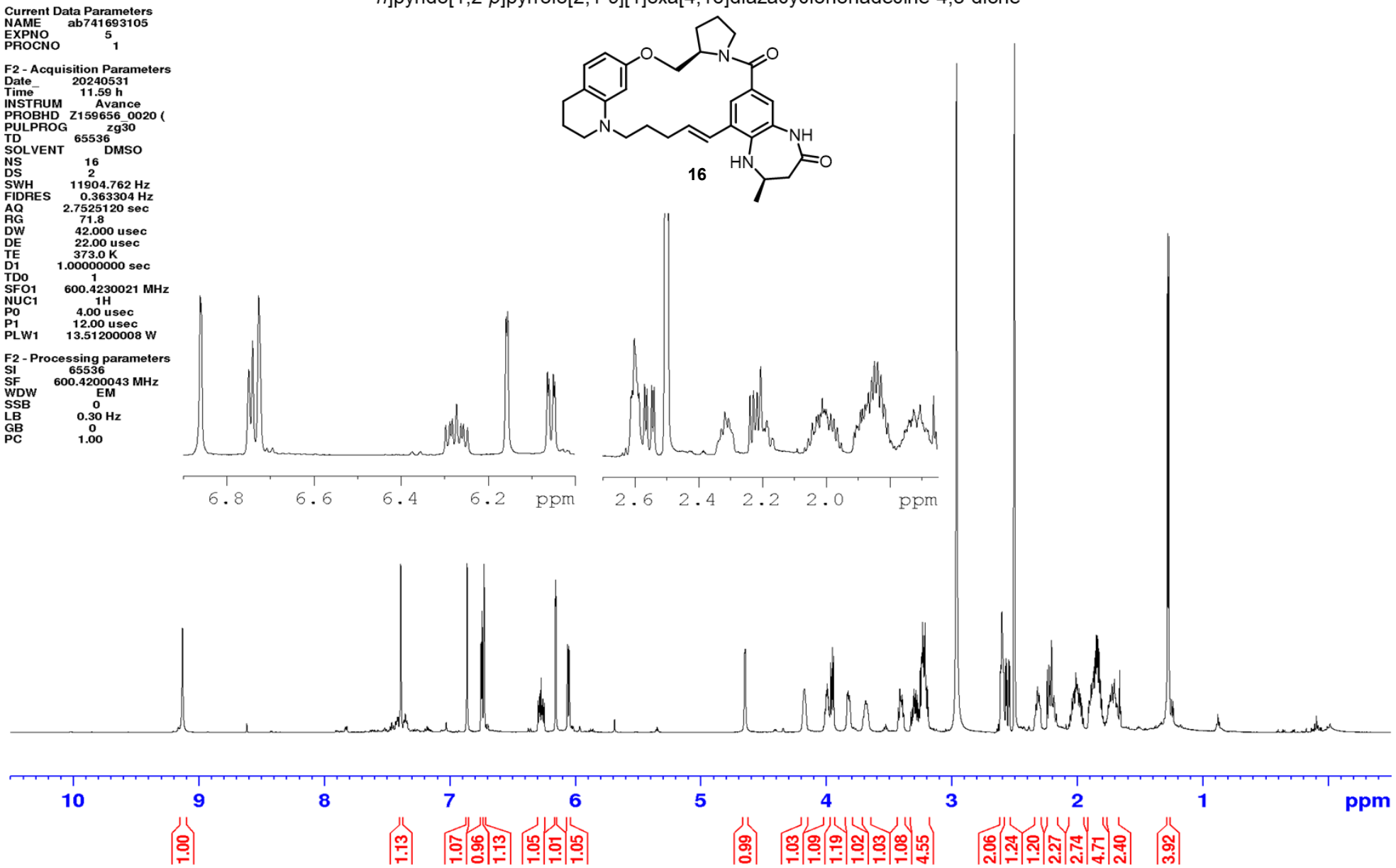

^{13}C NMR (2*R*,12a*R*,*E*)-2-methyl-1,2,3,5,11,12,12a,13,19,20,23,24-dodecahydro-10*H*,18*H*,22*H*-15,17-etheno-7,27-(metheno)[1,4]diazepino[2,3-*h*]pyrido[1,2-*p*]pyrrolo[2,1-*c*][1]oxa[4,16]diazacyclononadecine-4,8-dione

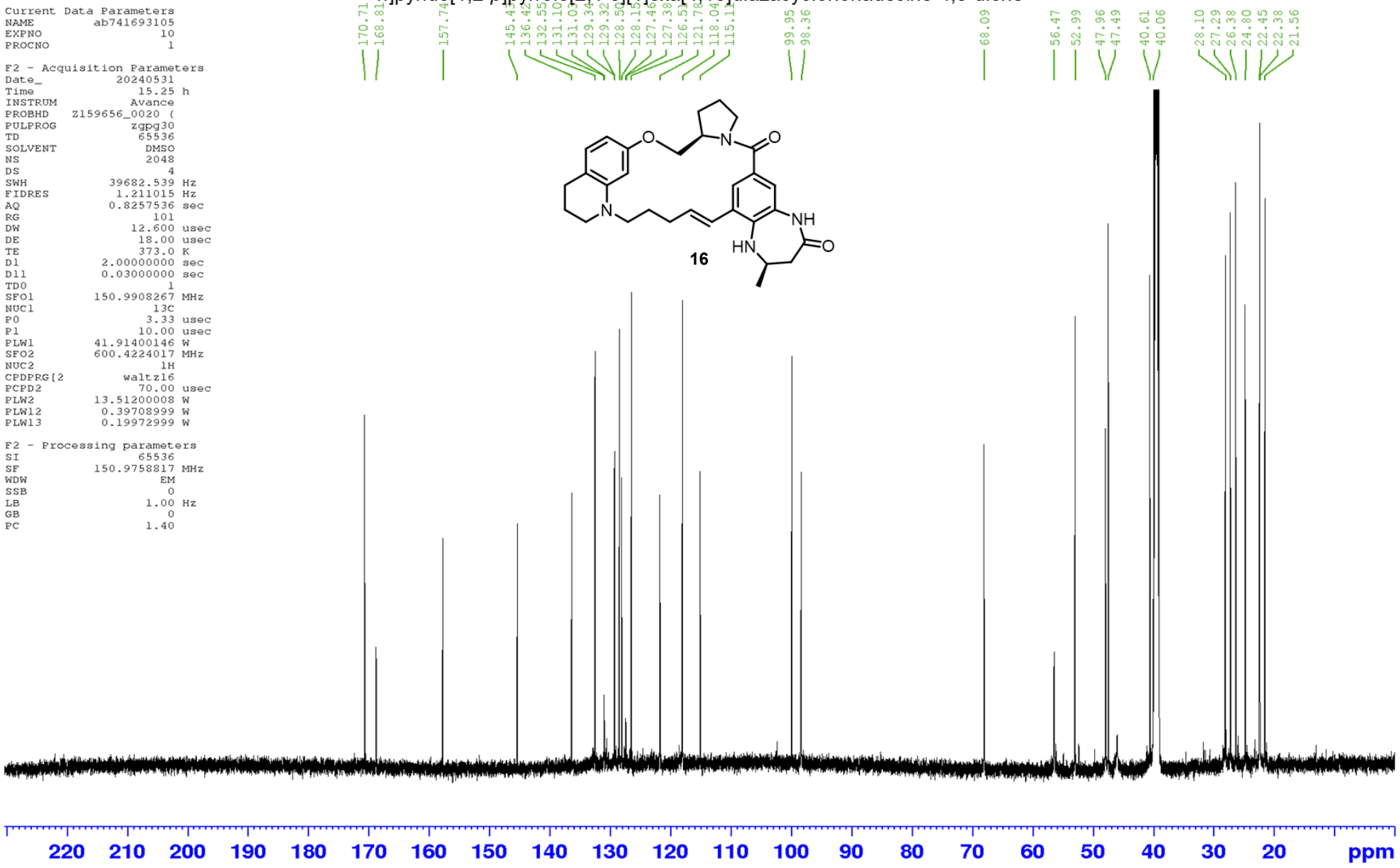

^{1}H NMR (2*R*,12a*S*,*E*)-2-methyl-1,2,3,5,11,12,12a,13,19,20,23,24-dodecahydro-10*H*,18*H*,22*H*-15,17-etheno-7,27-(metheno)[1,4]diazepino[2,3-*h*]pyrido[1,2-*p*]pyrrolo[2,1-*c*][1]oxa[4,16]diazacyclononadecine-4,8-dione

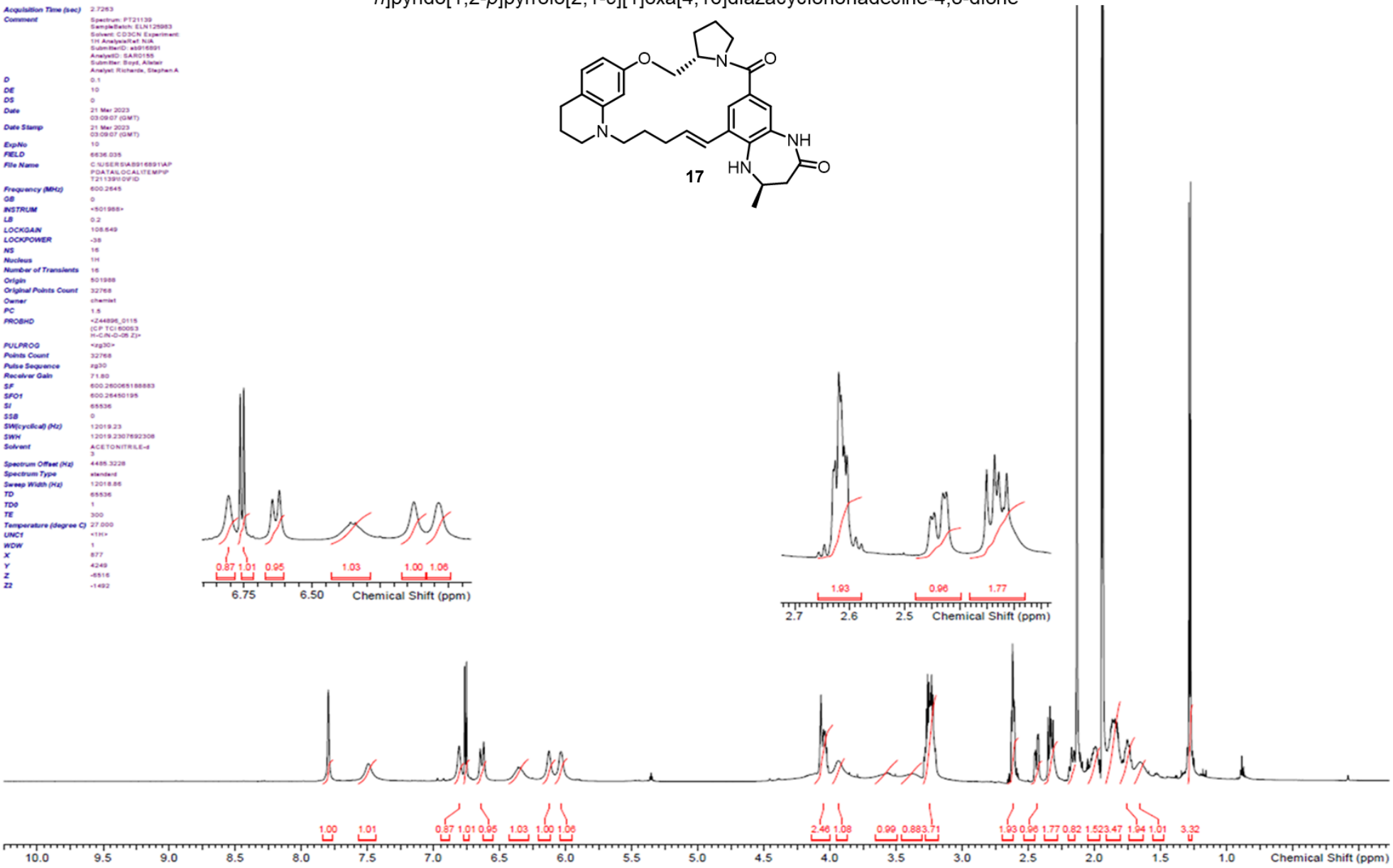

^{13}C NMR (2*R*,12a*S*,*E*)-2-methyl-1,2,3,5,11,12,12a,13,19,20,23,24-dodecahydro-10*H*,18*H*,22*H*-15,17-etheno-7,27-(metheno)[1,4]diazepino[2,3-*h*]pyrido[1,2-*p*]pyrrolo[2,1-*c*][1]oxa[4,16]diazacyclononadecine-4,8-dione

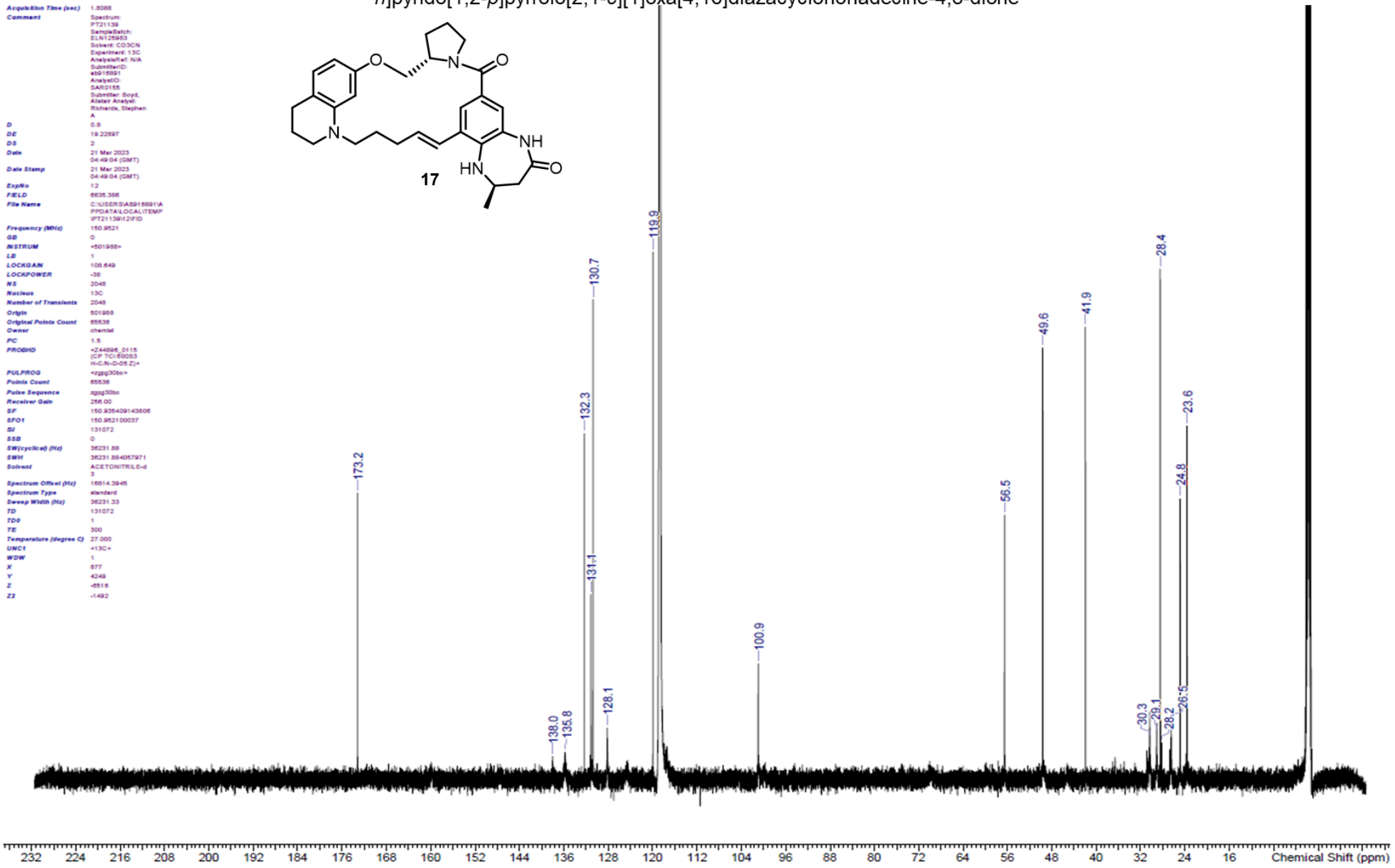

^{1}H NMR (2*R*,9*R*,13*S*,*E*)-2-methyl-1,2,3,11,12,13,14,20,21,23,24,25-dodecahydro-8*H*,10*H*,19*H*-16,18-(epiethane[1,2]diylidene)-9,13-methano-7,28-(metheno)[1,4]diazepino[2,3-*l*]pyrido[2,1-*d*][1]oxa[5,17]diazacyclodocosine-4,8(5*H*)-dione

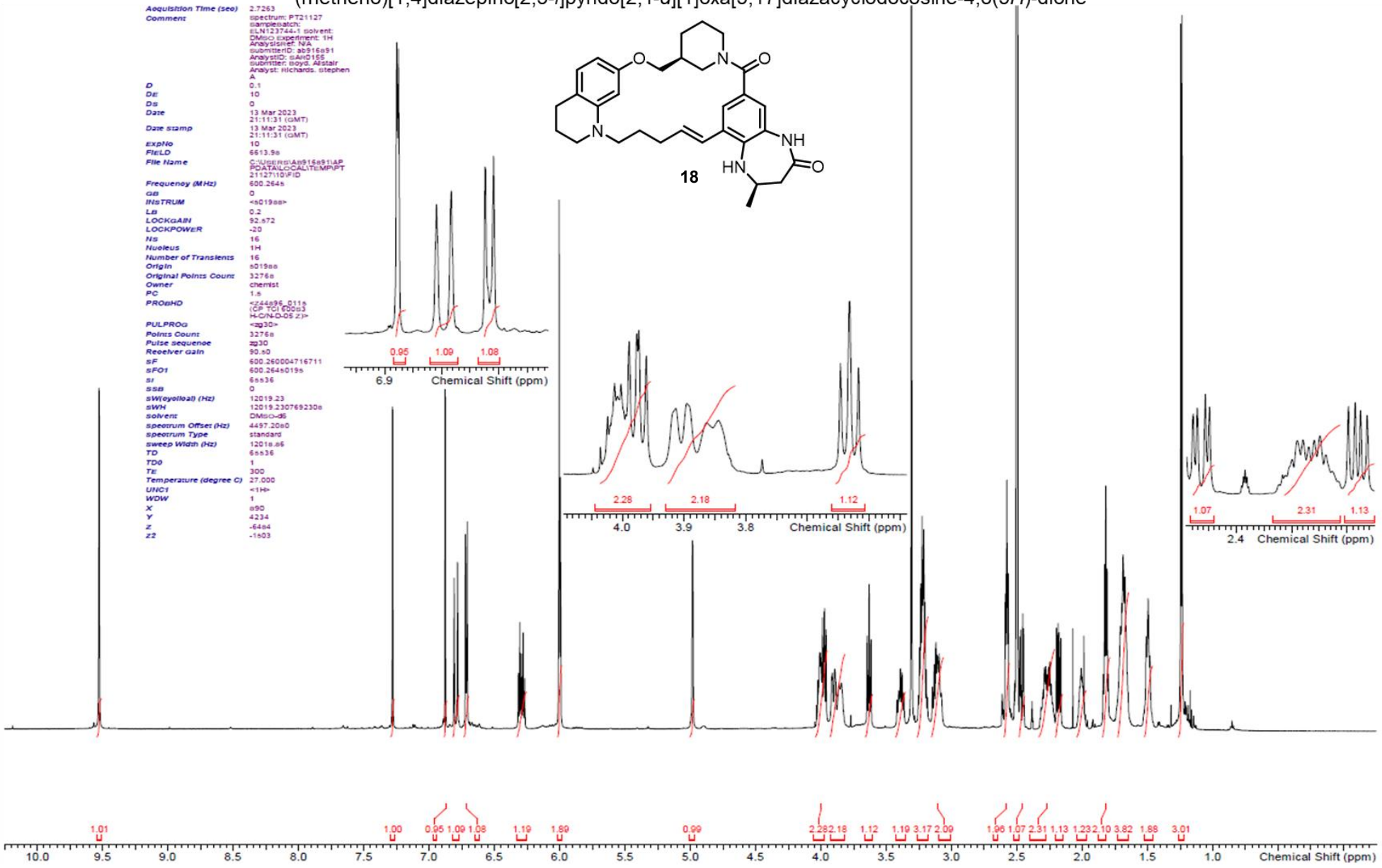

^{13}C NMR (2*R*,9*R*,13*S*,*E*)-2-methyl-1,2,3,11,12,13,14,20,21,23,24,25-dodecahydro-8*H*,10*H*,19*H*-16,18-(epiethane[1,2]diylidene)-9,13-methano-7,28-(metheno)[1,4]diazepino[2,3-*l*]pyrido[2,1-*d*][1]oxa[5,17]diazacyclodocosine-4,8(5*H*)-dione

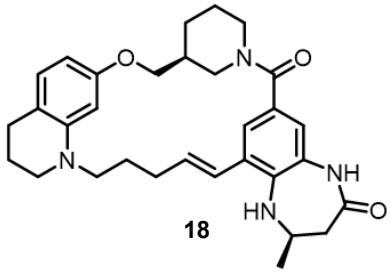

18

^{1}H NMR (2*R*,9*R*,13*R*,*E*)-2-methyl-1,2,3,10,11,13,14,20,21,23,24,25-dodecahydro-8*H*,19*H*-16,18-(epiethane[1,2]diylidene)-9,13-methano-7,28-(metheno)[1,4]diazepino[2,3-*k*]pyrido[1,2-*s*][1,4]dioxa[7,19]diazacyclodocosine-4,8(5*H*)-dione

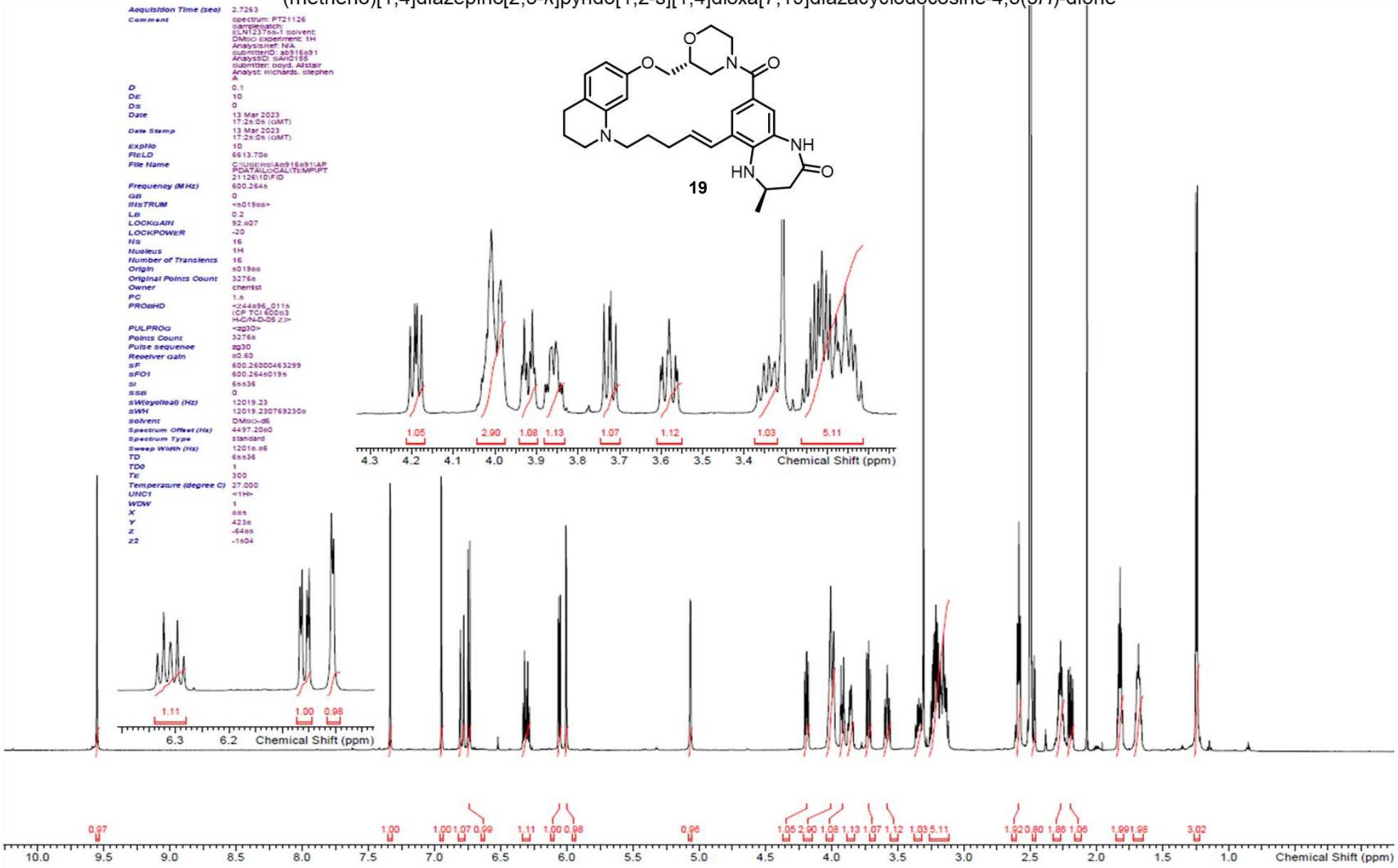

^{13}C NMR (2*R*,9*R*,13*R*,*E*)-2-methyl-1,2,3,10,11,13,14,20,21,23,24,25-dodecahydro-8*H*,19*H*-16,18-(epiethane[1,2]diylidene)-9,13-methano-7,28-(metheno)[1,4]diazepino[2,3-*k*]pyrido[1,2-*s*][1,4]dioxa[7,19]diazacyclodocosine-4,8(5*H*)-dione

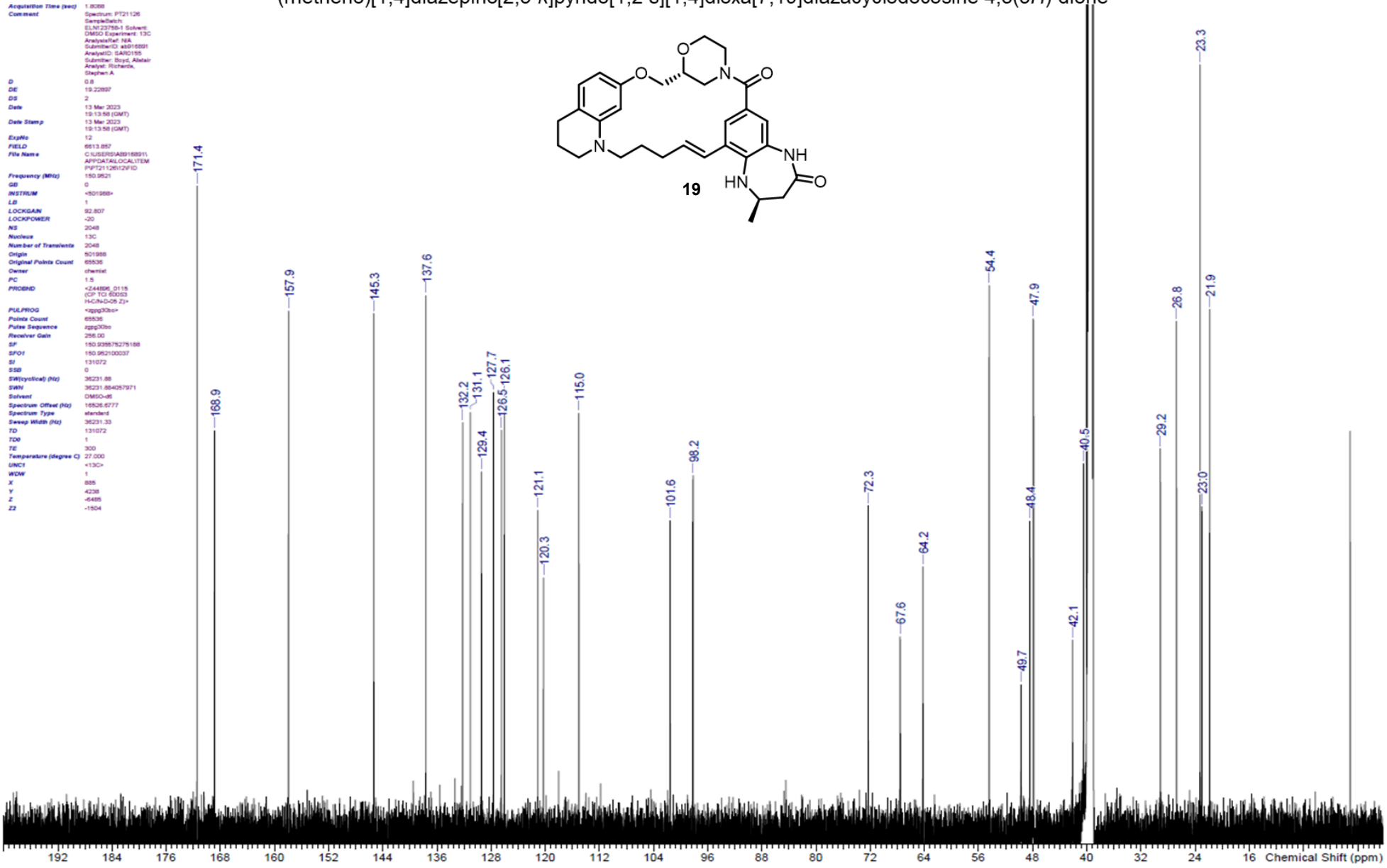

^{1}H NMR (*R*,*E*)-6-(5-(7-methoxy-3,4-dihydroquinolin-1(2*H*)-yl)pent-1-en-1-yl)-4-methyl-8-(piperidine-1-carbonyl)-1,3,4,5-tetrahydro-2*H*-benzo[*b*][1,4]diazepin-2-one

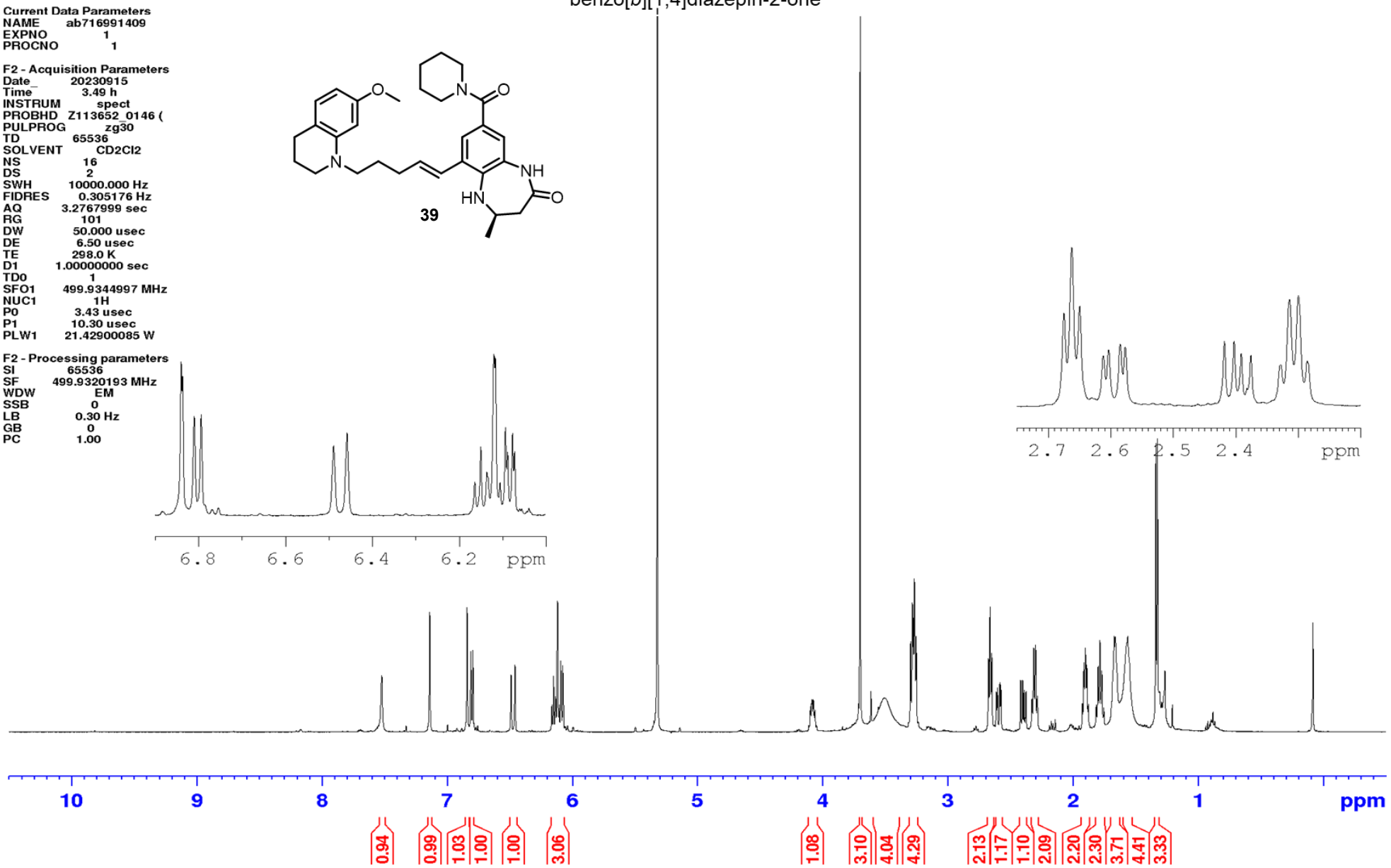

^{13}C NMR (*R*,*E*)-6-(5-(7-methoxy-3,4-dihydroquinolin-1(2*H*)-yl)pent-1-en-1-yl)-4-methyl-8-(piperidine-1-carbonyl)-1,3,4,5-tetrahydro-2*H*-benzo[*b*][1,4]diazepin-2-one

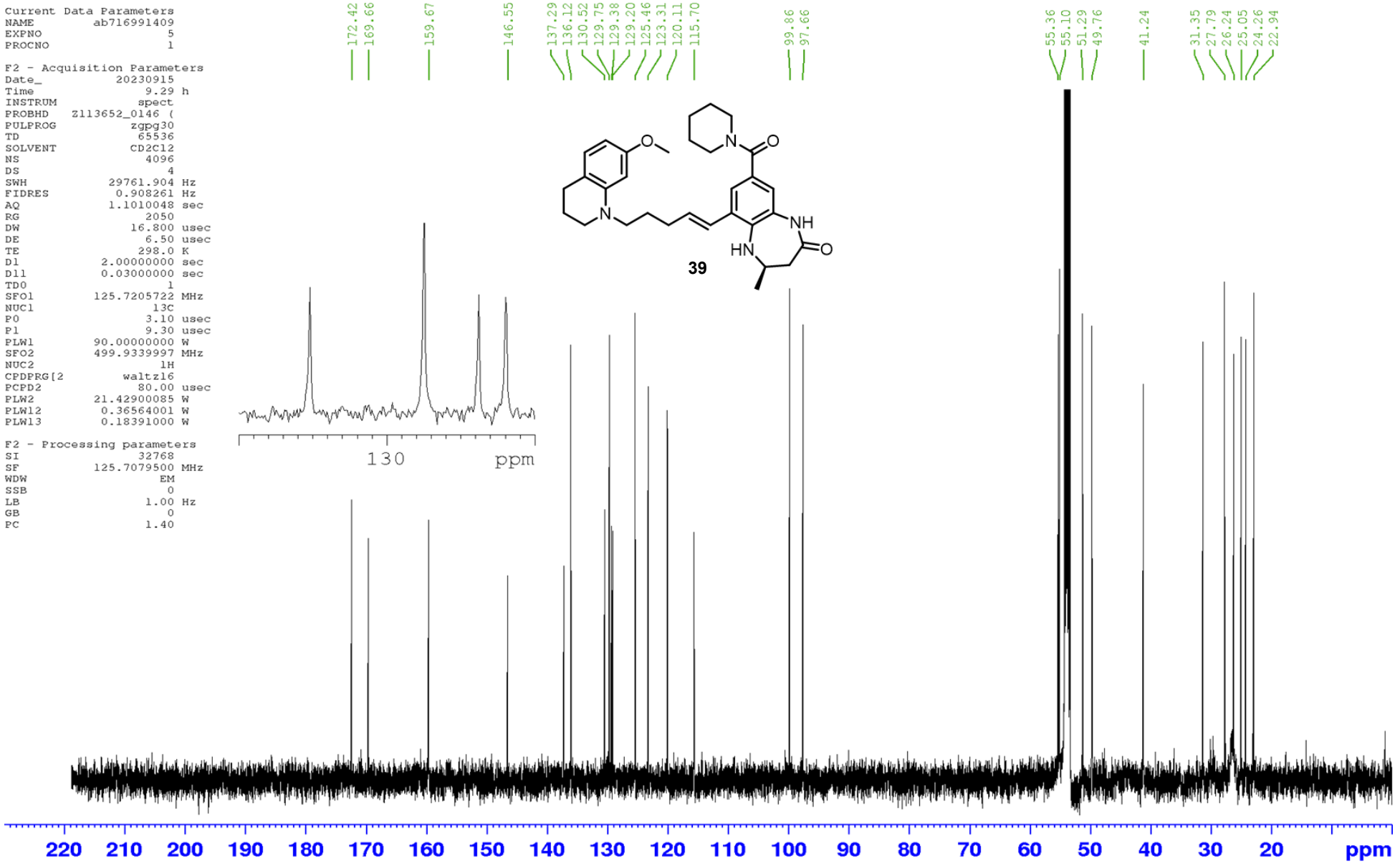

^{1}H NMR (*R*,*E*)-6-(5-(7-methoxy-3,4-dihydroquinolin-1(2*H*)-yl)pent-1-en-1-yl)-4-methyl-8-(morpholine-4-carbonyl)-1,3,4,5-tetrahydro-2*H*-benzo[*b*][1,4]diazepin-2-one

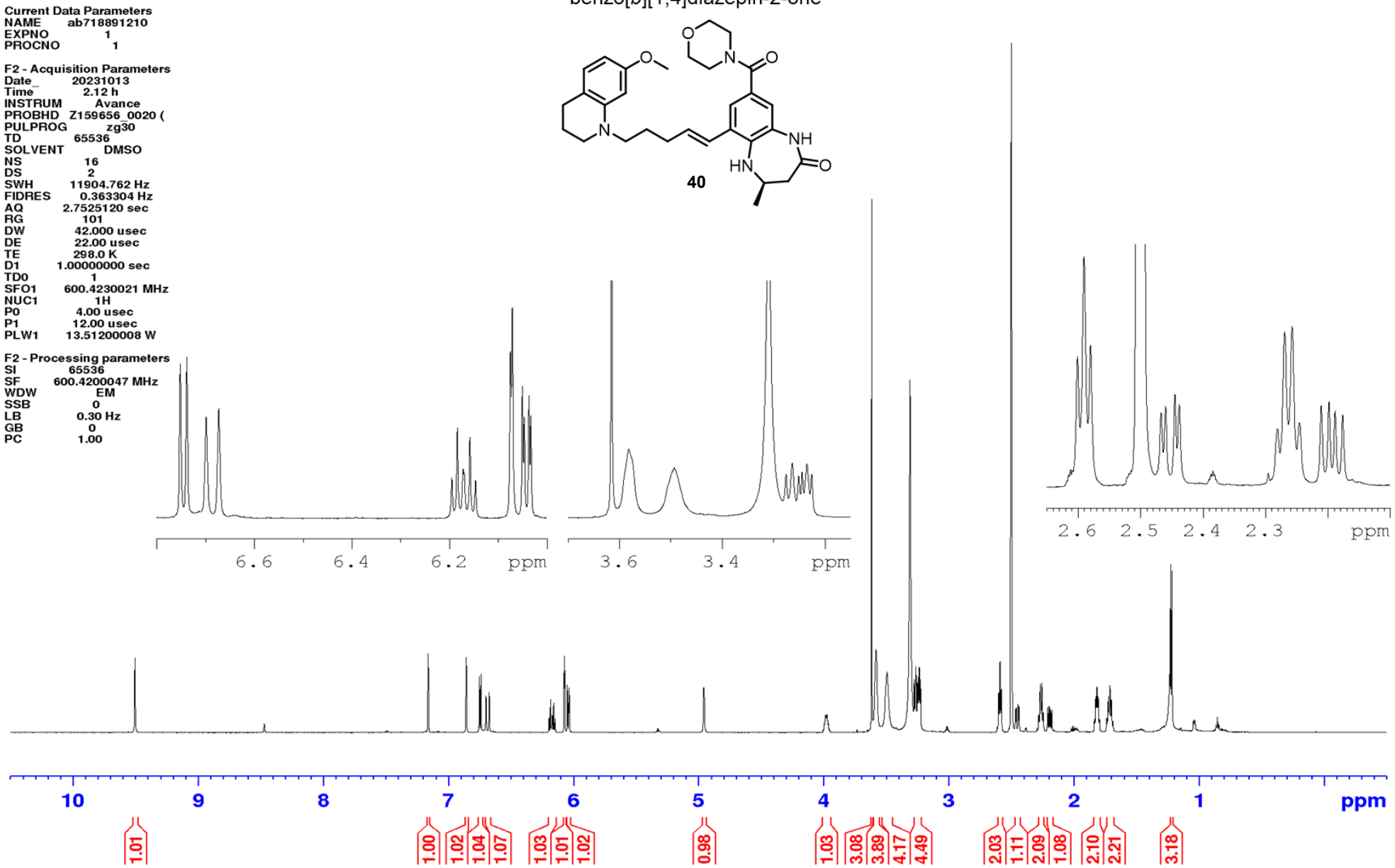

^{13}C NMR (*R*,*E*)-6-(5-(7-methoxy-3,4-dihydroquinolin-1(2*H*)-yl)pent-1-en-1-yl)-4-methyl-8-(morpholine-4-carbonyl)-1,3,4,5-tetrahydro-2*H*-benzo[*b*][1,4]diazepin-2-one

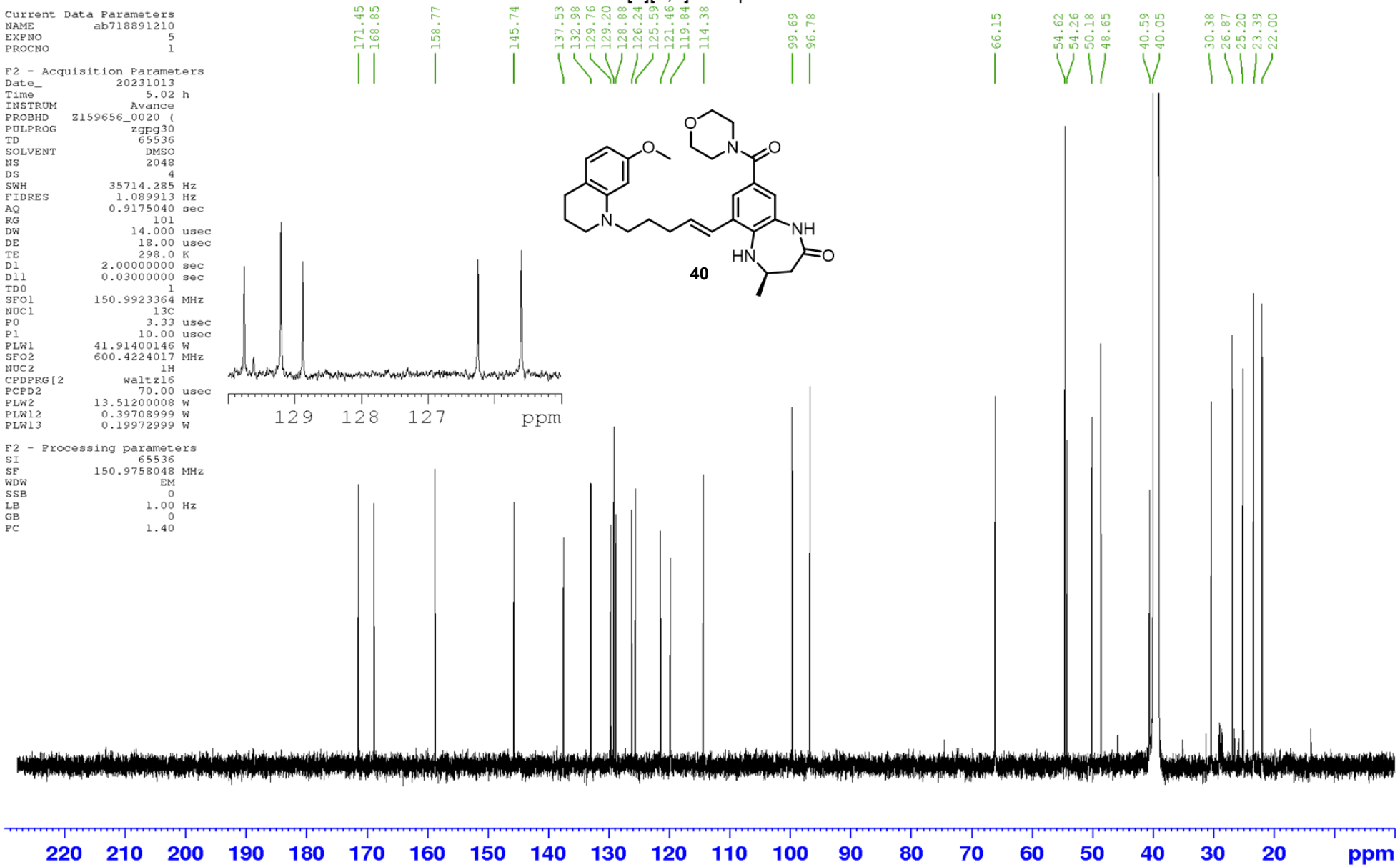

^{1}H NMR (*R*,*E*)-6-(5-(7-methoxy-3,4-dihydroquinolin-1(2*H*)-yl)pent-1-en-1-yl)-4-methyl-8-(pyrrolidine-1-carbonyl)-1,3,4,5-tetrahydro-2*H*-benzo[*b*][1,4]diazepin-2-one

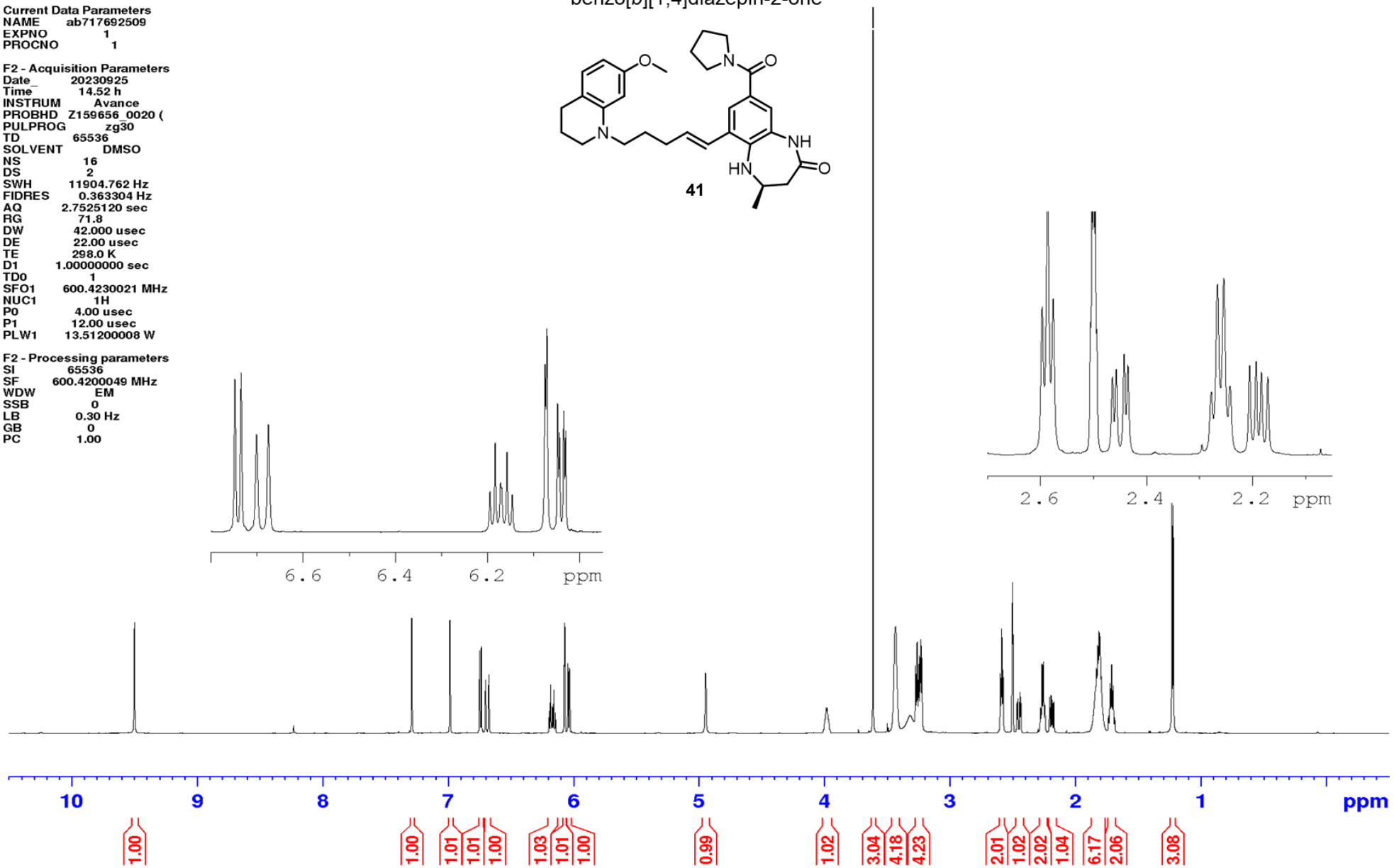

^{13}C NMR (*R*,*E*)-6-(5-(7-methoxy-3,4-dihydroquinolin-1(2*H*)-yl)pent-1-en-1-yl)-4-methyl-8-(pyrrolidine-1-carbonyl)-1,3,4,5-tetrahydro-2*H*-benzo[*b*][1,4]diazepin-2-one

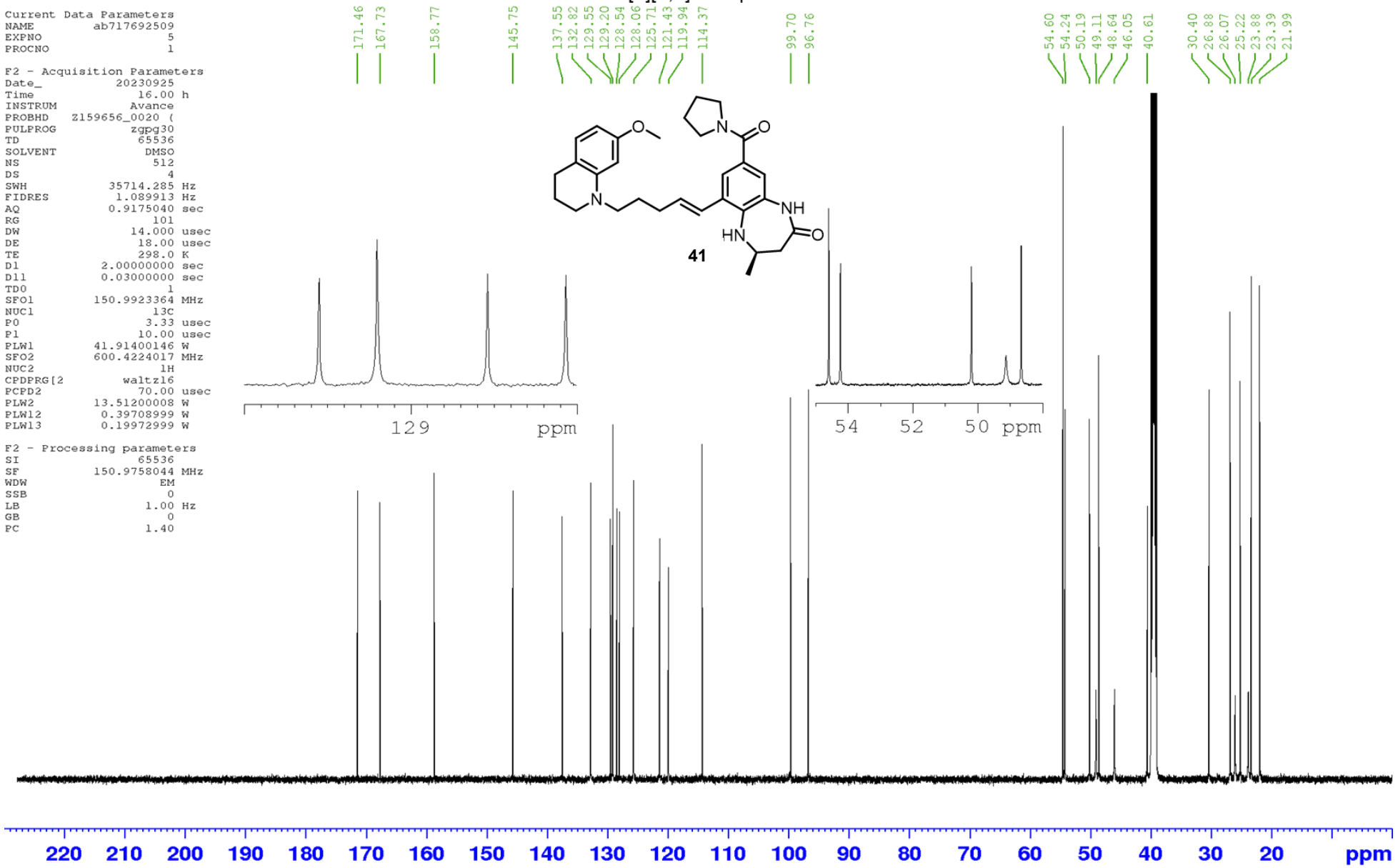

^{1}H NMR (*R*,*E*)-6-(5-(7-methoxy-3,4-dihydroquinolin-1(2*H*)-yl)pent-1-en-1-yl)-4-methyl-1,3,4,5-tetrahydro-2*H*-benzo[*b*][1,4]diazepin-2-one

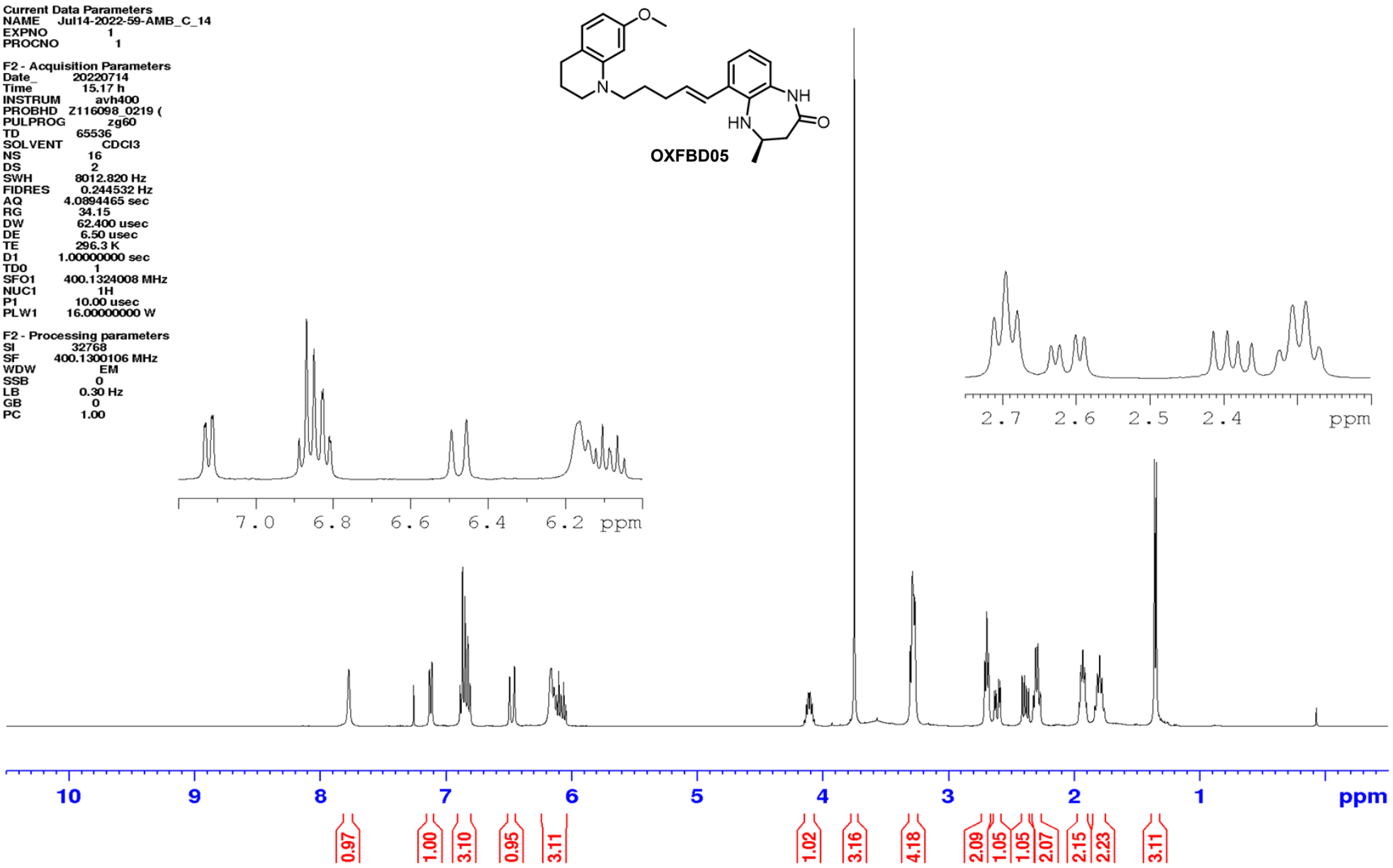

^{1}H NMR 7-(methylsulfonyl)quinoline

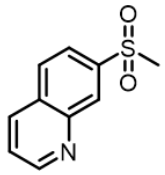

53

Current Data Parameters
NAME ab717852709
EXPNO 1
PROCNO 1

F2 - Acquisition Parameters
Date_ 20230927
Time 20.29 h
INSTRUM Avance
PROBHD Z159656_0020 (
PULPROG zg30
TD 65536
SOLVENT CDCl3
NS 16
DS 2
SWH 11904.762 Hz
FIDRES 0.363304 Hz
AQ 2.7525120 sec
RG 71.8
DW 42.000 usec
DE 22.00 usec
TE 298.0 K
D1 1.00000000 sec
TD0 1
SFO1 600.4230021 MHz
NUC1 1H
P0 4.00 usec
P1 12.00 usec
PLW1 13.51200008 W

F2 - Processing parameters
SI 65536
SF 600.4200137 MHz
WDW EM
SSB 0
LB 0.30 Hz
GB 0
PC 1.00

^{13}C NMR 7-(methylsulfonyl)quinoline

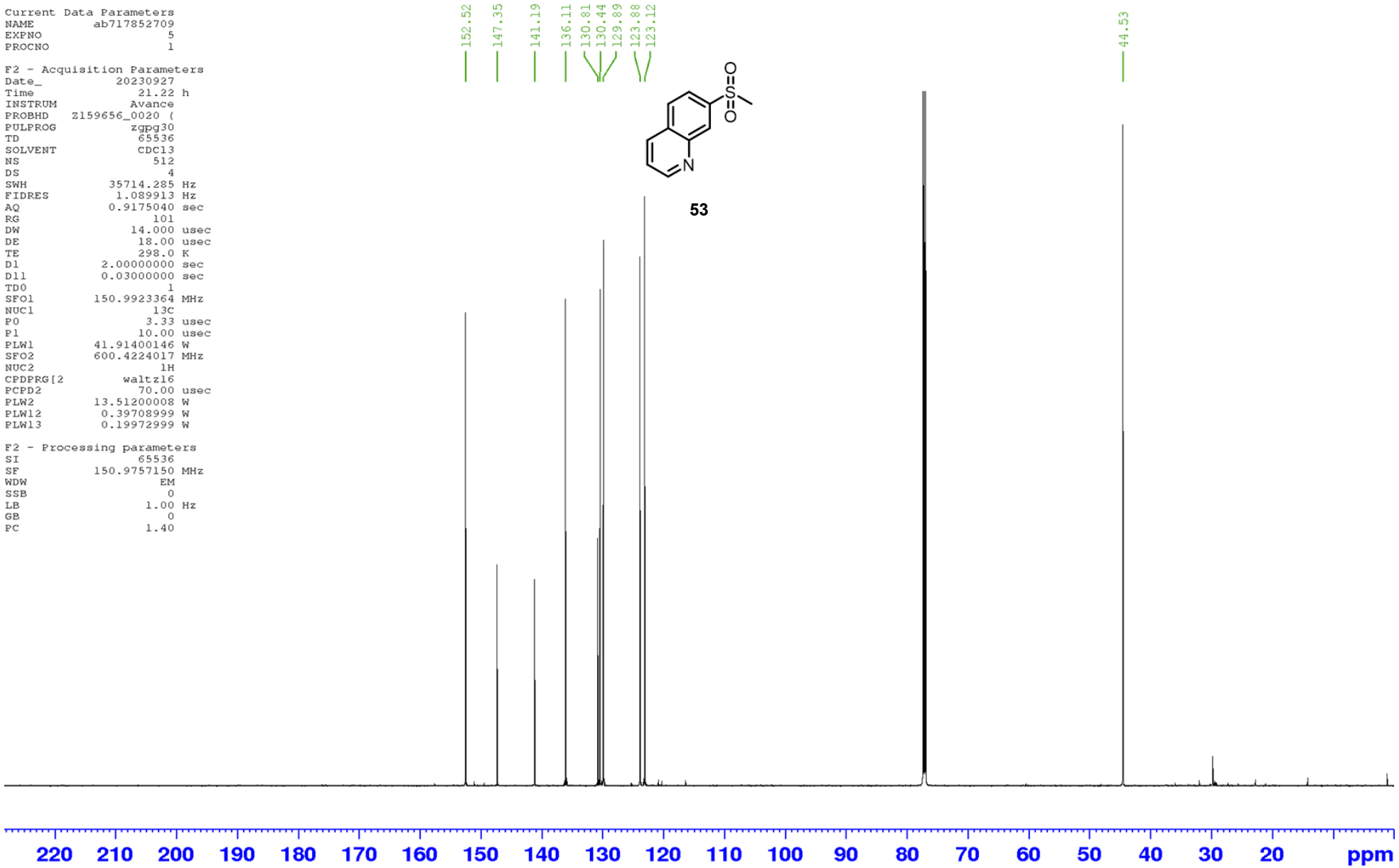

^{1}H 7-(methylsulfonyl)-1,2,3,4-tetrahydroquinoline

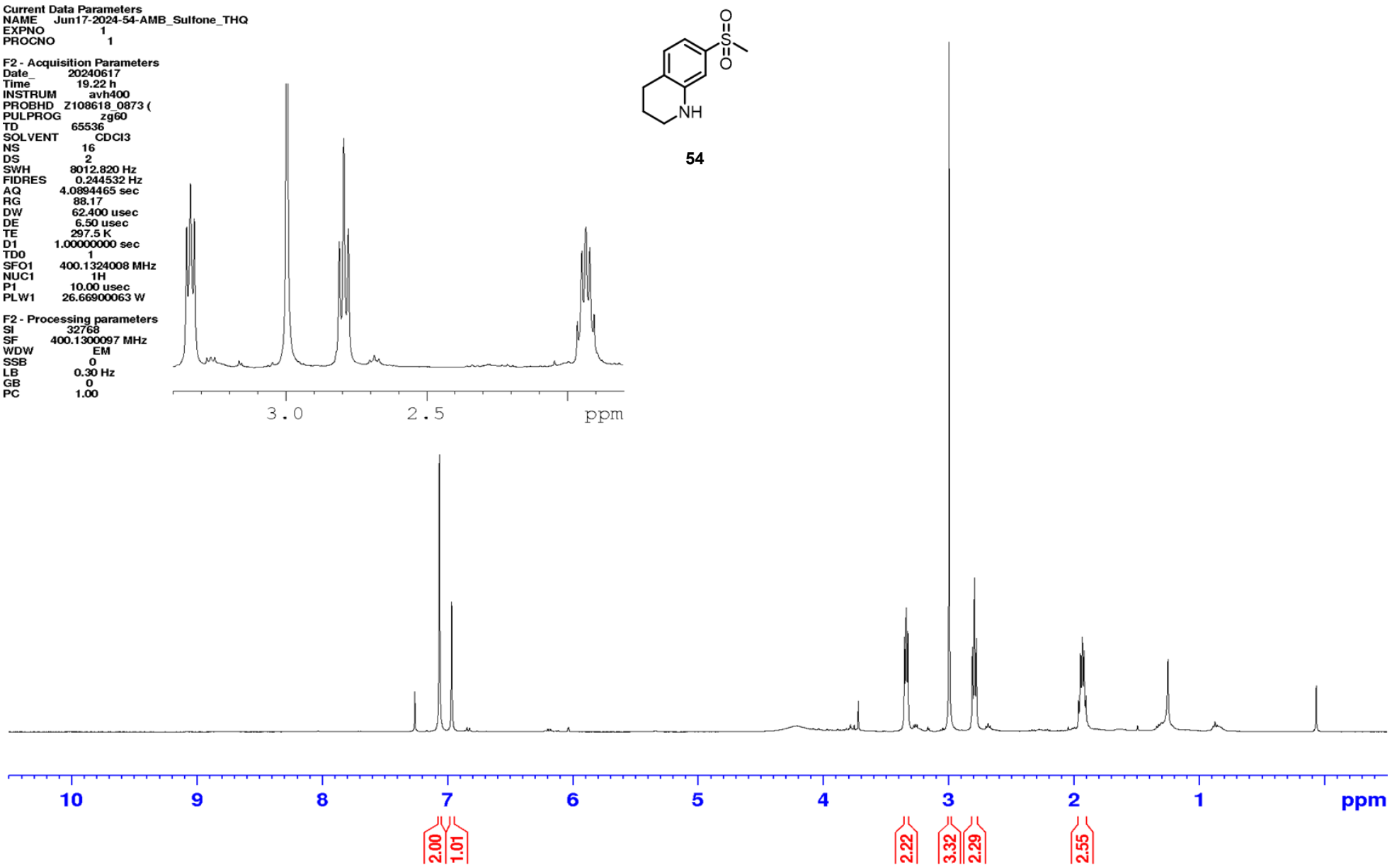

^{13}C 7-(methylsulfonyl)-1,2,3,4-tetrahydroquinoline

```
Current Data Parameters
NAME      Jun17-2024-54-AMB_Sulfone_THQ
EXPNO                  2
PROCNO                 1

F2 - Acquisition Parameters
Date_           20240617
Time              19.47 h
INSTRUM          avh400
PROBHD    Z108618_0873 (
PULPROG          zgpg30
TD                32768
SOLVENT           CDCl3
NS                  512
DS                    4
SWH           26041.666 Hz
FIDRES         1.589457 Hz
AQ            0.6291456 sec
RG               197.18
DW               19.200 usec
DE                6.50 usec
TE                298.5 K
D1           1.00000000 sec
D11          0.03000000 sec
TD0                   1
SFO1        100.6228298 MHz
NUC1                13C
P0                 3.33 usec
P1                10.00 usec
PLW1        49.77399826 W
SFO2        400.1316005 MHz
NUC2                1H
CPDPRG[2        waltz16
PCPD2             90.00 usec
PLW2        26.66900063 W
PLW12        0.32925001 W
PLW13        0.16561000 W

F2 - Processing parameters
SI                32768
SF          100.6127578 MHz
WDW                  EM
SSB                   0
LB                 1.00 Hz
GB                    0
PC                 1.40
```

145.46 138.85 130.27 126.98 114.71 111.79 44.66 41.77 27.32 21.27

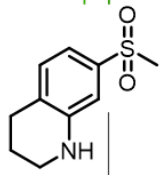

54

220 210 200 190 180 170 160 150 140 130 120 110 100 90 80 70 60 50 40 30 20 ppm

^{1}H NMR 7-(methylsulfonyl)-1-(pent-4-yn-1-yl)-1,2,3,4-tetrahydroquinoline

Current Data Parameters
NAME May12-2021-57-AMB_B_16
EXPNO 1
PROCNO 1

F2 - Acquisition Parameters
Date_ 20210512
Time 17.10 h
INSTRUM avg400
PROBHD Z108618_0816 (
PULPROG zg60
TD 65536
SOLVENT CDCl3
NS 16
DS 2
SWH 8012.820 Hz
FIDRES 0.244532 Hz
AQ 4.0894465 sec
RG 184.19
DW 62.400 usec
DE 6.50 usec
TE 298.1 K
D1 1.00000000 sec
TD0 1
SFO1 400.2024012 MHz
NUC1 1H
P1 14.00 usec
PLW1 14.00000000 W

F2 - Processing parameters
SI 32768
SF 400.2000100 MHz
WDW EM
SSB 0
LB 0.30 Hz
GB 0
PC 1.00

55

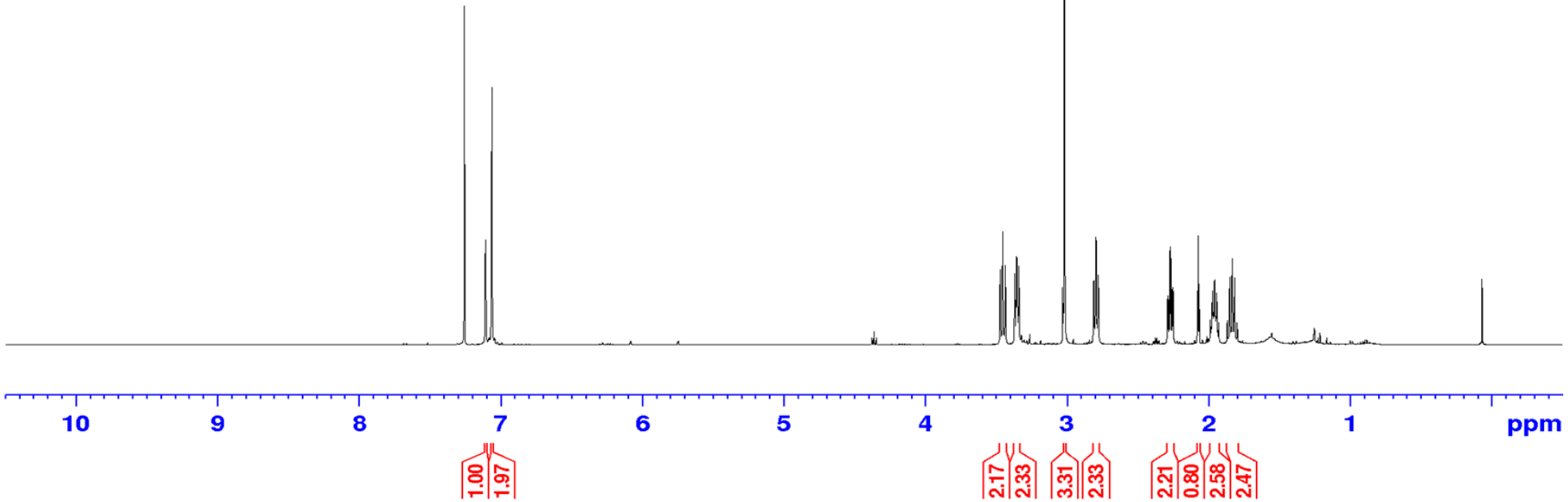

^{13}C NMR 7-(methylsulfonyl)-1-(pent-4-yn-1-yl)-1,2,3,4-tetrahydroquinoline

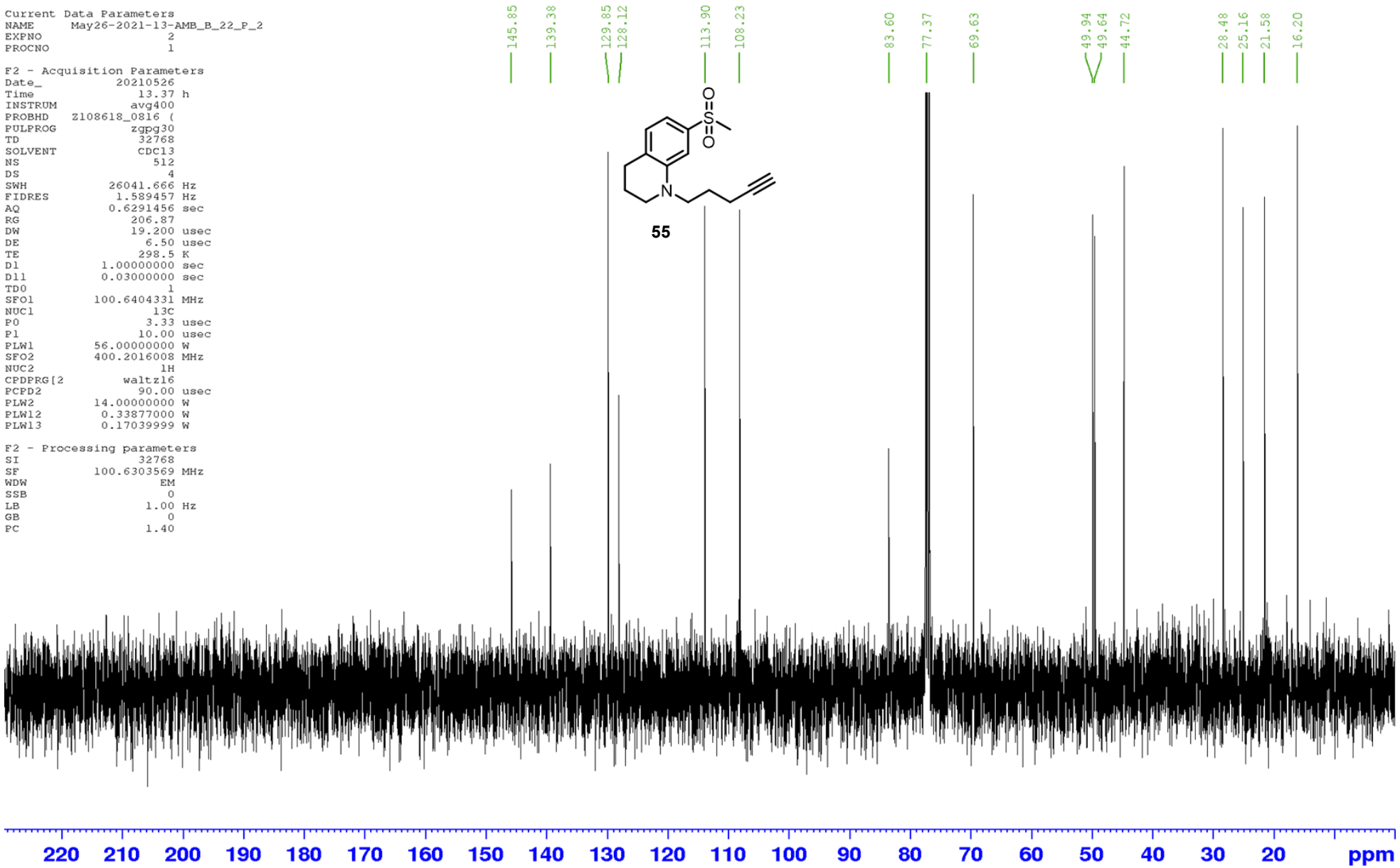

^{1}H NMR (*E*)-7-(methylsulfonyl)-1-(5-(4,4,5,5-tetramethyl-1,3,2-dioxaborolan-2-yl)pent-4-en-1-yl)-1,2,3,4-tetrahydroquinoline

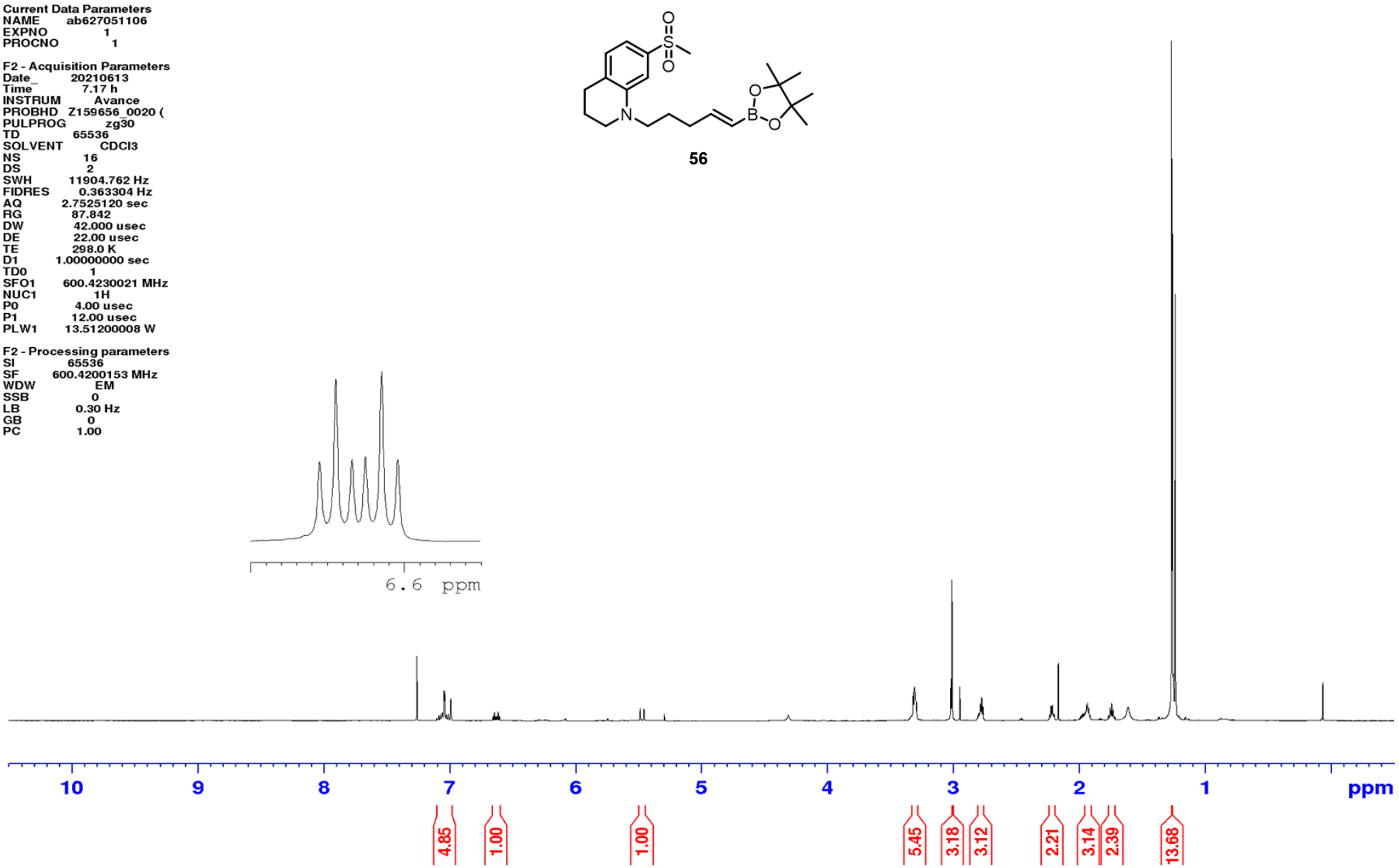

56

^{11}B NMR (*E*)-7-(methylsulfonyl)-1-(5-(4,4,5,5-tetramethyl-1,3,2-dioxaborolan-2-yl)pent-4-en-1-yl)-1,2,3,4-tetrahydroquinoline

```
Current Data Parameters
NAME      AMB_B_25_f7-12
EXPNO                  2
PROCNO                 1

F2 - Acquisition Parameters
Date_           20210628
Time              19.43 h
INSTRUM           Hg400
PROBHD   Z108618_0668 (
PULPROG           zgpg
TD                8192
SOLVENT           CDCl3
NS                 512
DS                   4
SWH           32051.281 Hz
FIDRES         7.825020 Hz
AQ            0.1277952 sec
RG               194.54
DW               15.600 usec
DE                6.50 usec
TE               299.2 K
D1           0.10000000 sec
D11          0.03000000 sec
TD0                  1
SFO1        128.3936485 MHz
NUC1               11B
P1               14.70 usec
PLW1        16.59600067 W
SFO2        400.1716007 MHz
NUC2               1H
CPDPRG[2        waltz16
PCPD2            90.00 usec
PLW2        11.99499989 W
PLW12        0.33318999 W
PLW13        0.16759001 W

F2 - Processing parameters
SI                32768
SF          128.3904388 MHz
WDW                EM
SSB                 0
LB                10.00 Hz
GB                  0
PC                1.40
```

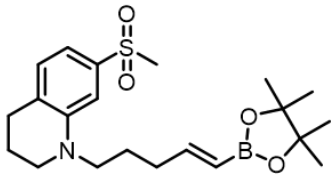

56

^{13}C NMR (*E*)-7-(methylsulfonyl)-1-(5-(4,4,5,5-tetramethyl-1,3,2-dioxaborolan-2-yl)pent-4-en-1-yl)-1,2,3,4-tetrahydroquinoline

```
Current Data Parameters
NAME         ab627051106
EXPNO                  5
PROCNO                 1

F2 - Acquisition Parameters
Date_           20210613
Time                8.51 h
INSTRUM           Avance
PROBHD   Z159656_0020 (
PULPROG          zgpg30
TD                65536
SOLVENT           CDCl3
NS                 1024
DS                    4
SWH           35714.285 Hz
FIDRES         1.089913 Hz
AQ            0.9175040 sec
RG                  101
DW               14.000 usec
DE                18.00 usec
TE                298.0 K
D1           2.00000000 sec
D11          0.03000000 sec
TD0                   1
SFO1        150.9908267 MHz
NUC1                13C
P0                 3.33 usec
P1                10.00 usec
PLW1        41.91400146 W
SFO2        600.4224017 MHz
NUC2                1H
CPDPRG[2         waltz16
PCPD2             80.00 usec
PLW2        13.51200008 W
PLW12        0.30124050 W
PLW13        0.15098180 W

F2 - Processing parameters
SI                 32768
SF          150.9757097 MHz
WDW                   EM
SSB                    0
LB                  1.00 Hz
GB                     0
PC                  1.40
```

153.20 145.93 139.32 129.77 129.36 128.07 114.34 113.70 108.26 108.06 83.32 50.81 49.42 44.73 33.21 28.47 25.02 24.92 24.70 21.53

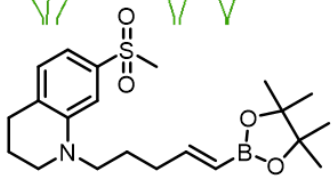

56

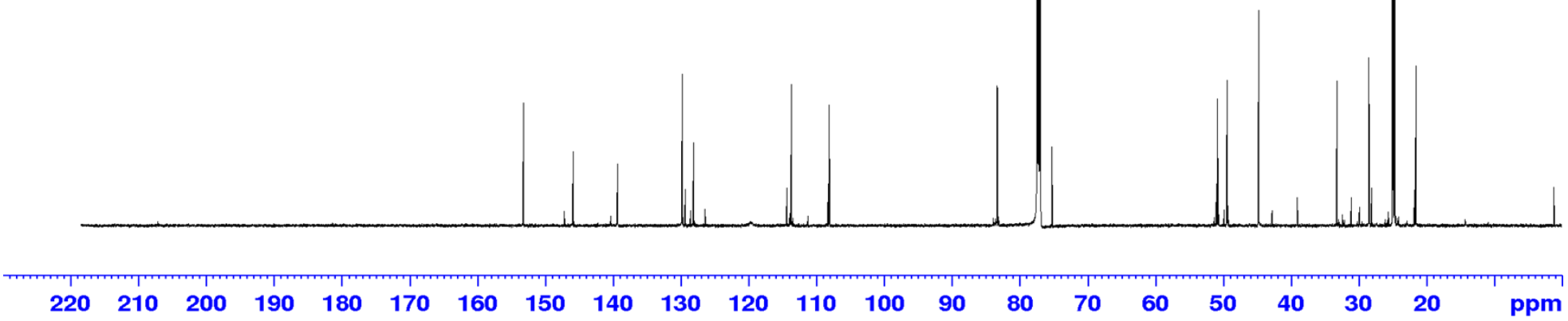

^{1}H NMR (*R*,*E*)-4-methyl-6-(5-(7-(methylsulfonyl)-3,4-dihydroquinolin-1(2*H*)-yl)pent-1-en-1-yl)-1,3,4,5-tetrahydro-2*H*-benzo[*b*][1,4]diazepin-2-one

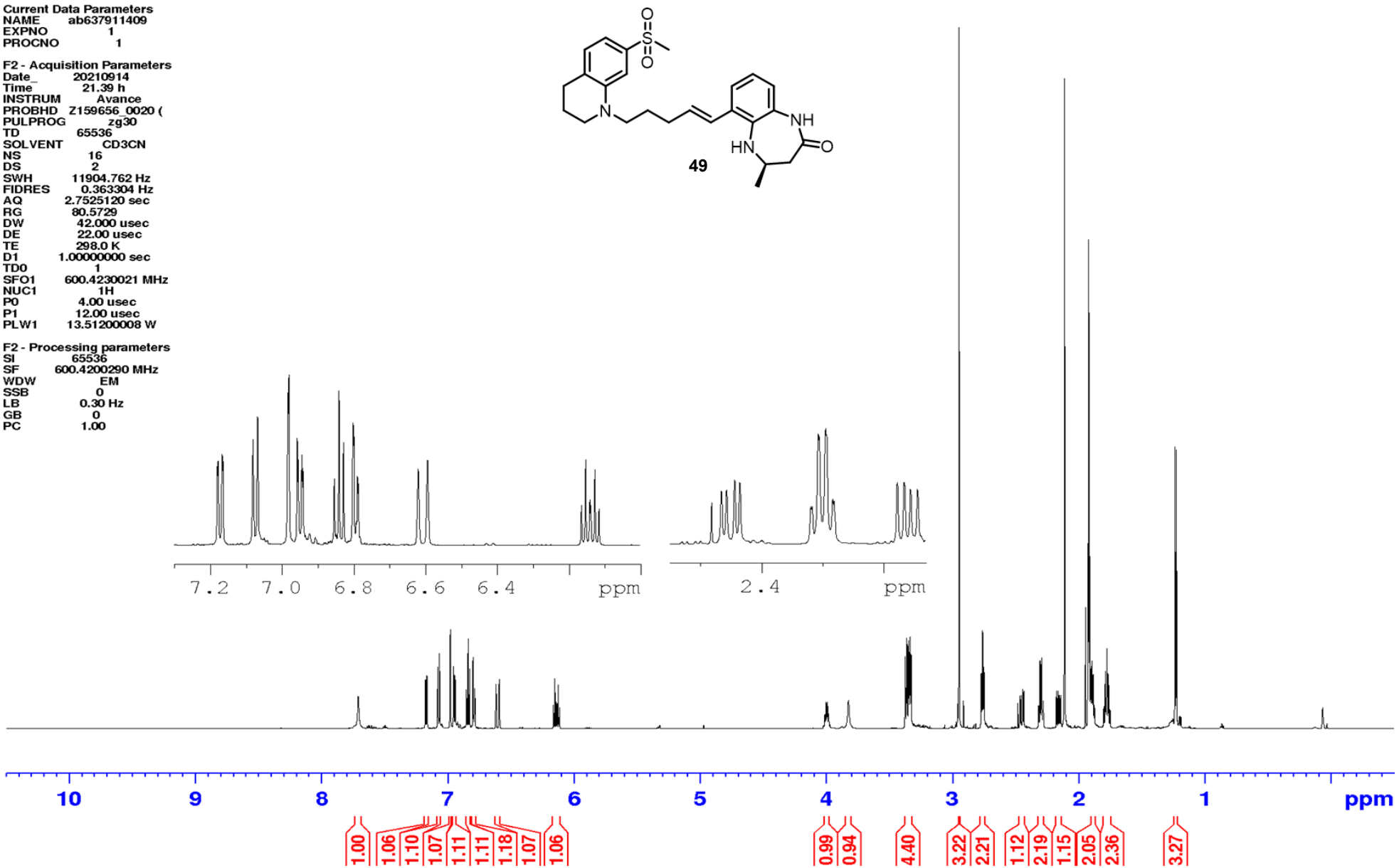

^{13}C NMR (*R*,*E*)-4-methyl-6-(5-(7-(methylsulfonyl)-3,4-dihydroquinolin-1(2*H*)-yl)pent-1-en-1-yl)-1,3,4,5-tetrahydro-2*H*-benzo[*b*][1,4]diazepin-2-one

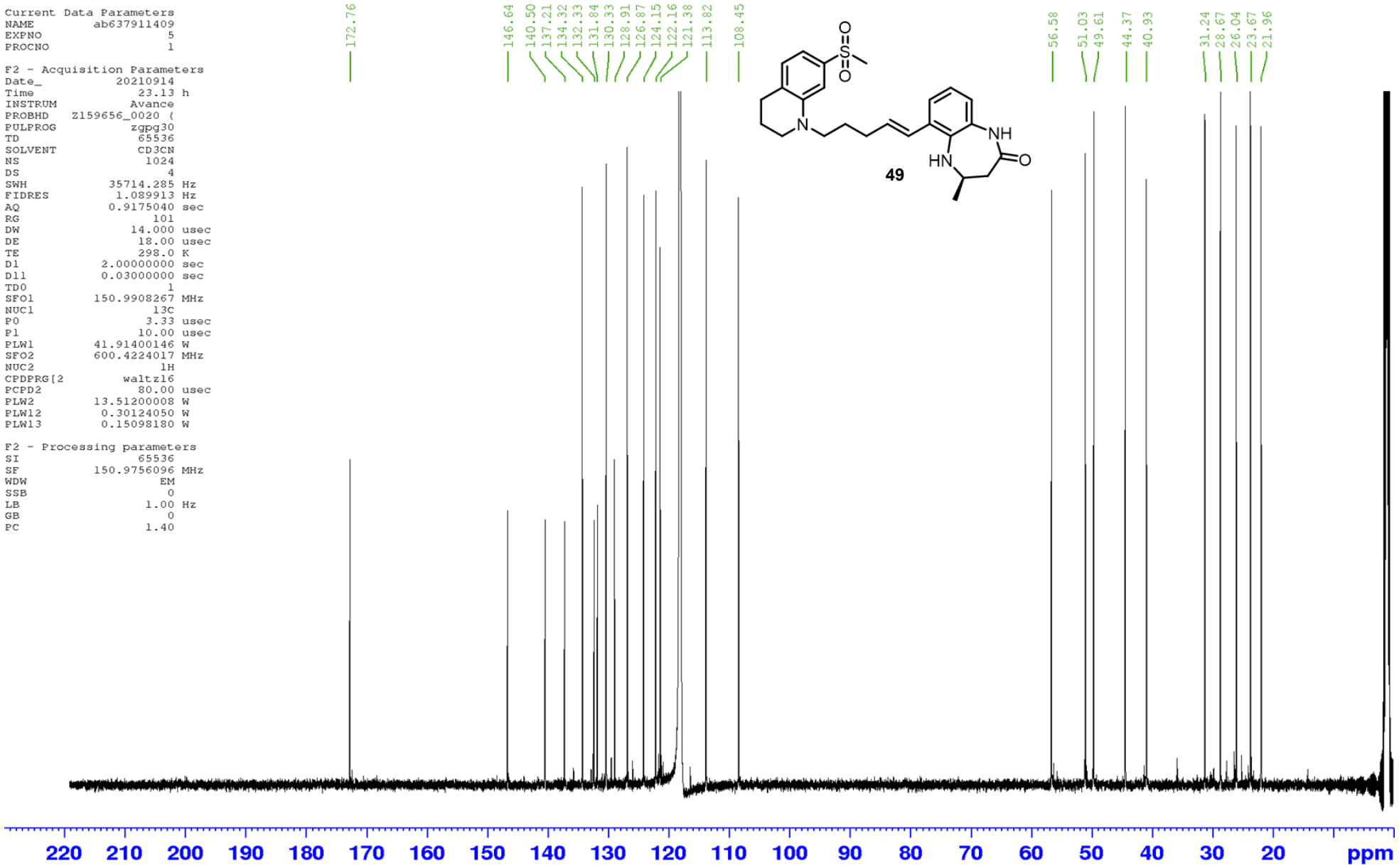


```
Current Data Parameters
NAME         ab637911409
EXPNO                  5
PROCNO                 1

F2 - Acquisition Parameters
Date_           20210914
Time              23.13 h
INSTRUM           Avance
PROBHD   Z159656_0020 (
PULPROG          zgpg30
TD                65536
SOLVENT           CD3CN
NS                 1024
DS                    4
SWH           35714.285 Hz
FIDRES         1.089913 Hz
AQ            0.9175040 sec
RG                  101
DW               14.000 usec
DE               18.00 usec
TE               298.0 K
D1           2.00000000 sec
D11          0.03000000 sec
TD0                   1
SFO1        150.9908267 MHz
NUC1               13C
P0                3.33 usec
P1               10.00 usec
PLW1        41.91400146 W
SFO2        600.4224017 MHz
NUC2               1H
CPDPRG[2        waltz16
PCPD2            80.00 usec
PLW2        13.51200008 W
PLW12        0.30124050 W
PLW13        0.15098180 W

F2 - Processing parameters
SI                65536
SF          150.9756096 MHz
WDW                  EM
SSB                   0
LB                 1.00 Hz
GB                    0
PC                 1.40
```

^{1}H NMR 2-amino-4-methoxyphenol

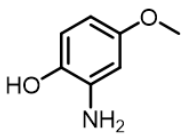

57

Current Data Parameters
NAME Oct19-2022-14-AMB_C_35_02
EXPNO 1
PROCNO 1

F2 - Acquisition Parameters
Date_ 20221019
Time 16.15 h
INSTRUM avf400
PROBHD Z108618_0533 (
PULPROG zg60
TD 65536
SOLVENT DMSO
NS 16
DS 2
SWH 8012.820 Hz
FIDRES 0.244532 Hz
AQ 4.0894465 sec
RG 52.03
DW 62.400 usec
DE 6.50 usec
TE 294.5 K
D1 1.00000000 sec
TD0 1
SFO1 400.2524015 MHz
NUC1 1H
P1 12.50 usec
PLW1 18.00000000 W

F2 - Processing parameters
SI 32768
SF 400.2500033 MHz
WDW EM
SSB 0
LB 0.30 Hz
GB 0
PC 1.00

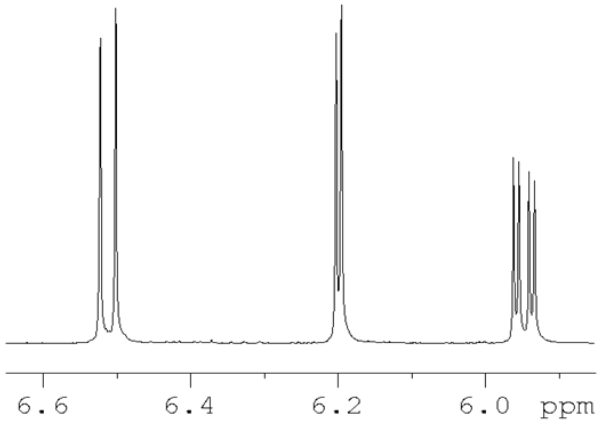

^{1}H NMR 6-methoxy-2*H*-benzo[*b*][1,4]oxazin-3(4*H*)-one

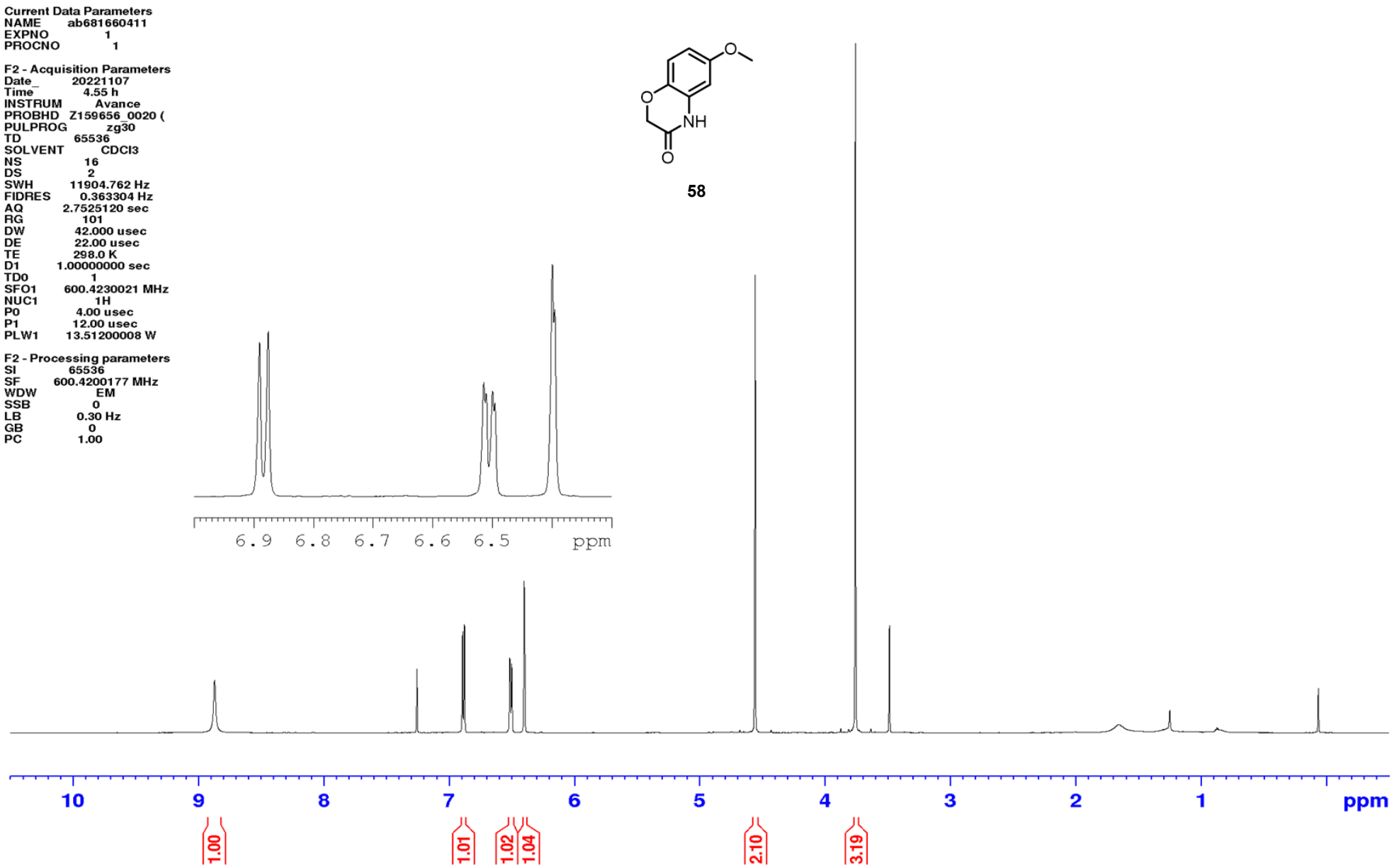

^{13}C NMR 6-methoxy-2*H*-benzo[*b*][1,4]oxazin-3(4*H*)-one

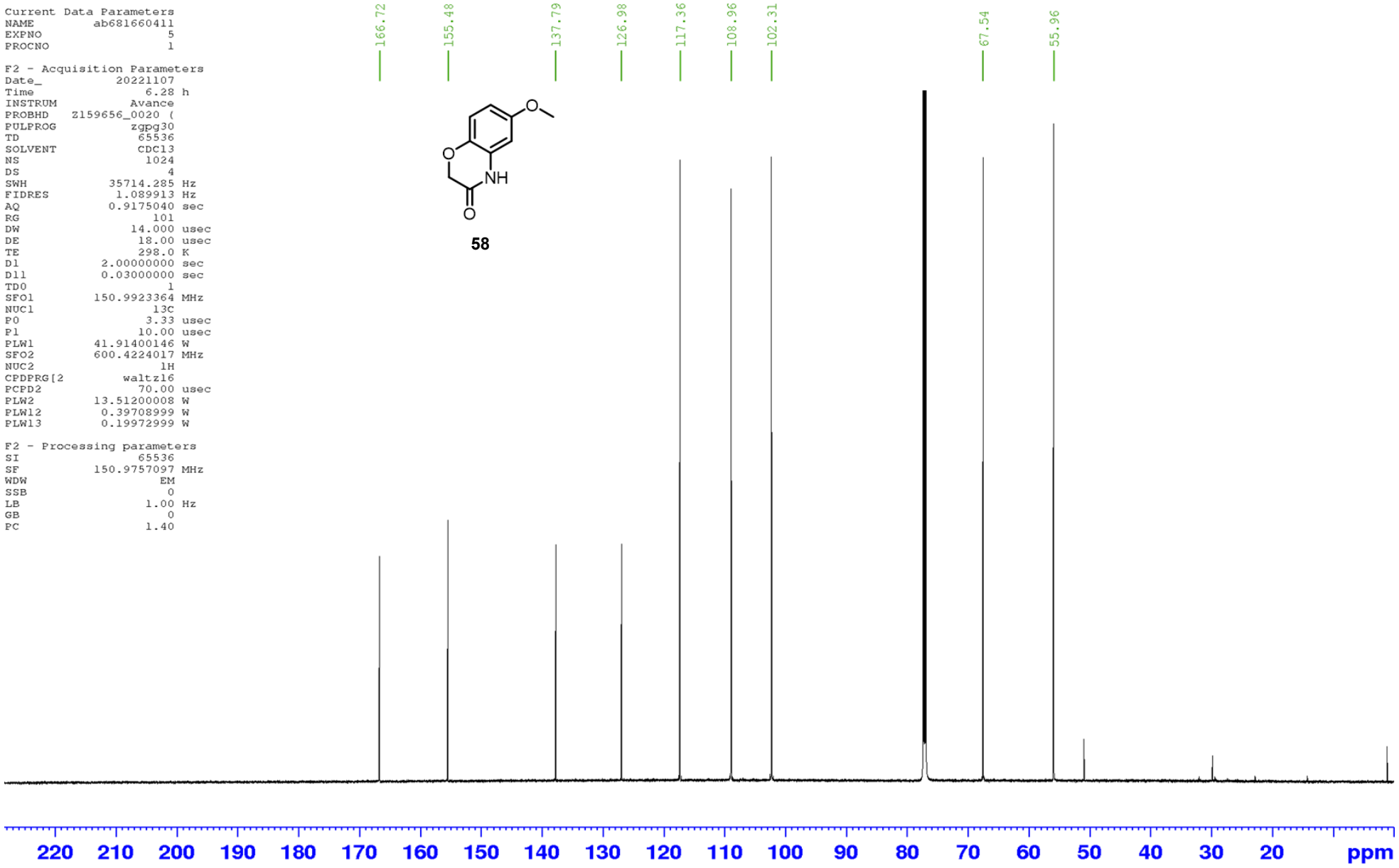

58

^{1}H NMR 6-methoxy-3,4-dihydro-2*H*-benzo[*b*][1,4]oxazine

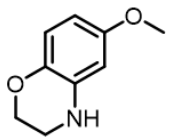

59

Current Data Parameters
NAME ab681670411
EXPNO 1
PROCNO 1

F2 - Acquisition Parameters
Date_ 20221107
Time 6.37 h
INSTRUM Avance
PROBHD Z159656_0020 (
PULPROG zg30
TD 65536
SOLVENT CDCl3
NS 16
DS 2
SWH 11904.762 Hz
FIDRES 0.363304 Hz
AQ 2.7525120 sec
RG 64
DW 42.000 usec
DE 22.00 usec
TE 298.0 K
D1 1.00000000 sec
TD0 1
SFO1 600.4230021 MHz
NUC1 1H
P0 4.00 usec
P1 12.00 usec
PLW1 13.51200008 W

F2 - Processing parameters
SI 65536
SF 600.4200144 MHz
WDW EM
SSB 0
LB 0.30 Hz
GB 0
PC 1.00

^{13}C NMR 6-methoxy-3,4-dihydro-2*H*-benzo[*b*][1,4]oxazine

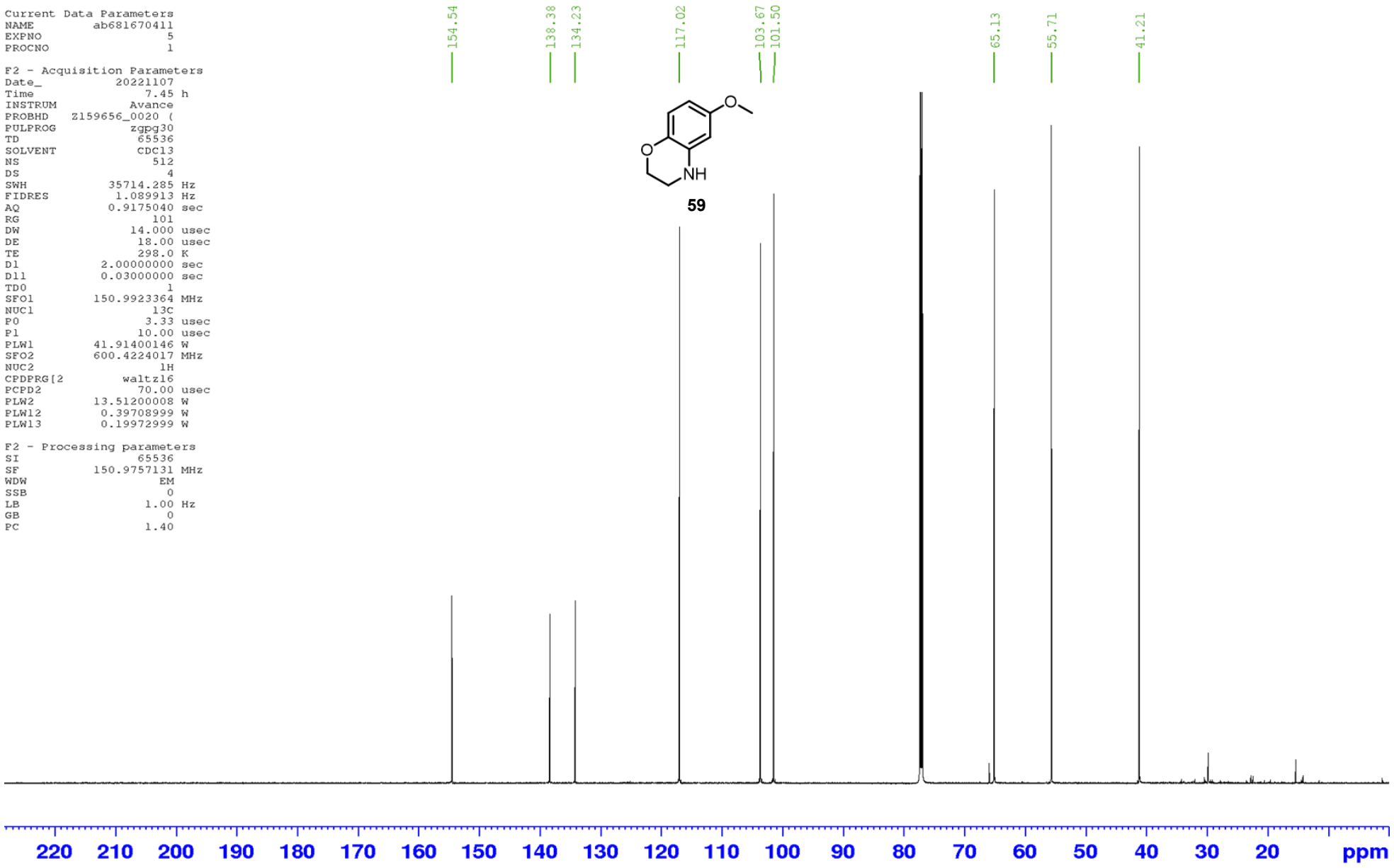


```
Current Data Parameters
NAME         ab681670411
EXPNO                  5
PROCNO                 1

F2 - Acquisition Parameters
Date_           20221107
Time                7.45 h
INSTRUM          Avance
PROBHD   Z159656_0020 (
PULPROG          zgpg30
TD                65536
SOLVENT           CDCl3
NS                  512
DS                    4
SWH           35714.285 Hz
FIDRES         1.089913 Hz
AQ            0.9175040 sec
RG                  101
DW               14.000 usec
DE               18.00 usec
TE               298.0 K
D1            2.00000000 sec
D11           0.03000000 sec
TD0                    1
SFO1        150.9923364 MHz
NUC1                13C
P0                3.33 usec
P1               10.00 usec
PLW1         41.91400146 W
SFO2        600.4224017 MHz
NUC2                1H
CPDPRG[2        waltz16
PCPD2            70.00 usec
PLW2         13.51200008 W
PLW12         0.39708999 W
PLW13         0.19972999 W

F2 - Processing parameters
SI                 65536
SF          150.9757131 MHz
WDW                   EM
SSB                    0
LB                  1.00 Hz
GB                     0
PC                  1.40
```

^{1}H NMR 6-methoxy-4-(pent-4-yn-1-yl)-3,4-dihydro-2*H*-benzo[*b*][1,4]oxazine

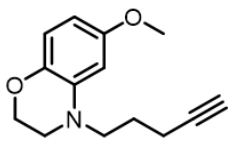

60

Current Data Parameters
NAME ab683331711
EXPNO 1
PROCNO 1

F2 - Acquisition Parameters
Date_ 20221117
Time 18.12 h
INSTRUM Avance
PROBHD Z159656_0020 (
PULPROG zg30
TD 65536
SOLVENT CDCl3
NS 16
DS 2
SWH 11904.762 Hz
FIDRES 0.363304 Hz
AQ 2.7525120 sec
RG 71.8
DW 42.000 usec
DE 22.00 usec
TE 298.0 K
D1 1.00000000 sec
TD0 1
SFO1 600.4230021 MHz
NUC1 1H
P0 4.00 usec
P1 12.00 usec
PLW1 13.51200008 W

F2 - Processing parameters
SI 65536
SF 600.4200146 MHz
WDW EM
SSB 0
LB 0.30 Hz
GB 0
PC 1.00

^{1}H NMR 6-methoxy-4-(pent-4-yn-1-yl)-3,4-dihydro-2*H*-benzo[*b*][1,4]oxazine

```
Current Data Parameters
NAME         ab683331711
EXPNO                  5
PROCNO                 1

F2 - Acquisition Parameters
Date_           20221117
Time              19.00 h
INSTRUM           Avance
PROBHD    Z159656_0020 (
PULPROG           zgpg30
TD                65536
SOLVENT           CDCl3
NS                  512
DS                    4
SWH           35714.285 Hz
FIDRES         1.089913 Hz
AQ            0.9175040 sec
RG                  101
DW               14.000 usec
DE                18.00 usec
TE                298.0 K
D1           2.00000000 sec
D11          0.03000000 sec
TD0                   1
SFO1        150.9923364 MHz
NUC1                13C
P0                 3.33 usec
P1                10.00 usec
PLW1        41.91400146 W
SFO2        600.4224017 MHz
NUC2                1H
CPDPRG[2         waltz16
PCPD2             70.00 usec
PLW2        13.51200008 W
PLW12        0.39708999 W
PLW13        0.19972999 W

F2 - Processing parameters
SI                65536
SF          150.9757095 MHz
WDW                  EM
SSB                   0
LB                 1.00 Hz
GB                    0
PC                 1.40
```

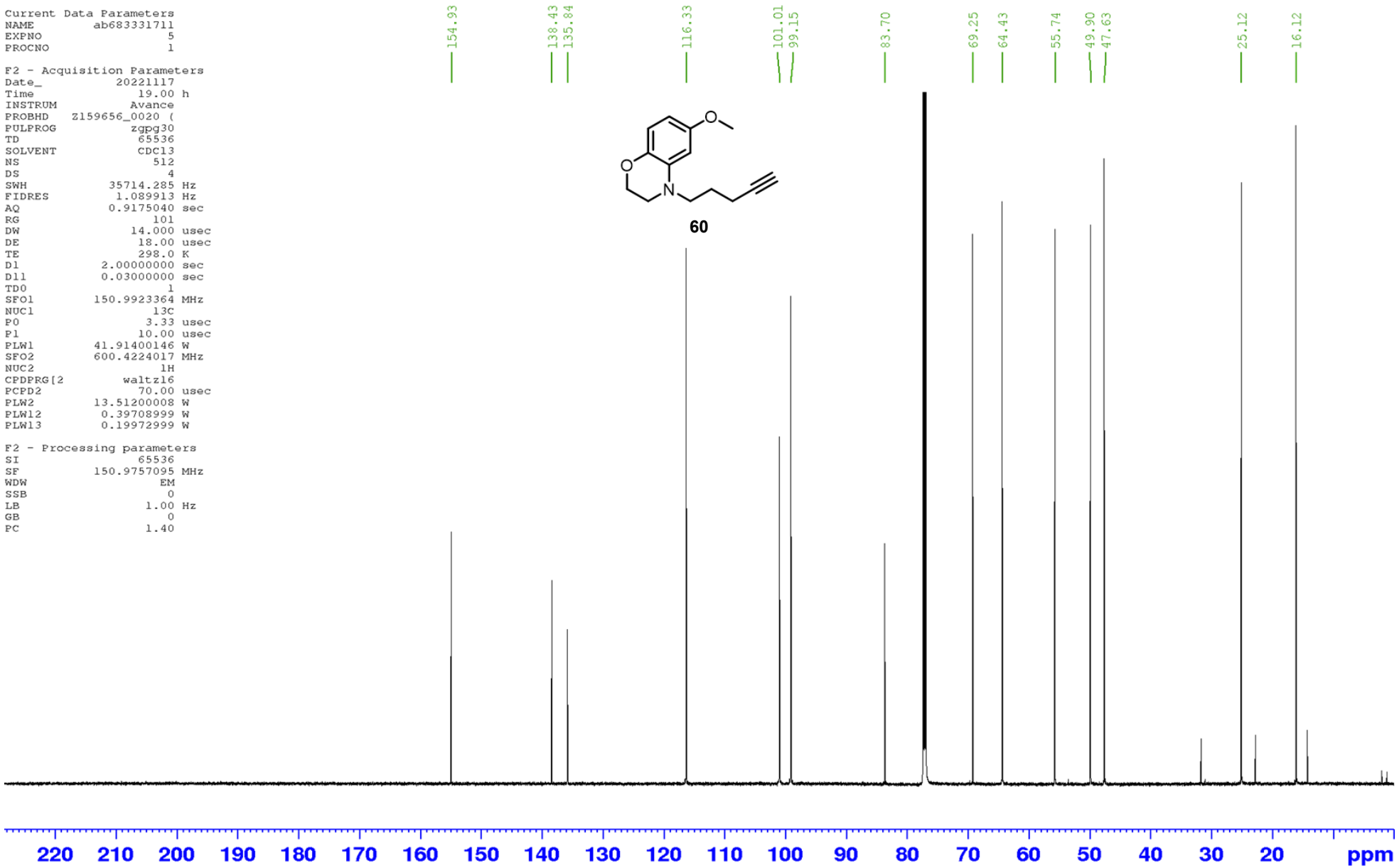

^{1}H NMR (*E*)-6-methoxy-4-(5-(4,4,5,5-tetramethyl-1,3,2-dioxaborolan-2-yl)pent-4-en-1-yl)-3,4-dihydro-2*H*-benzo[*b*][1,4]oxazine

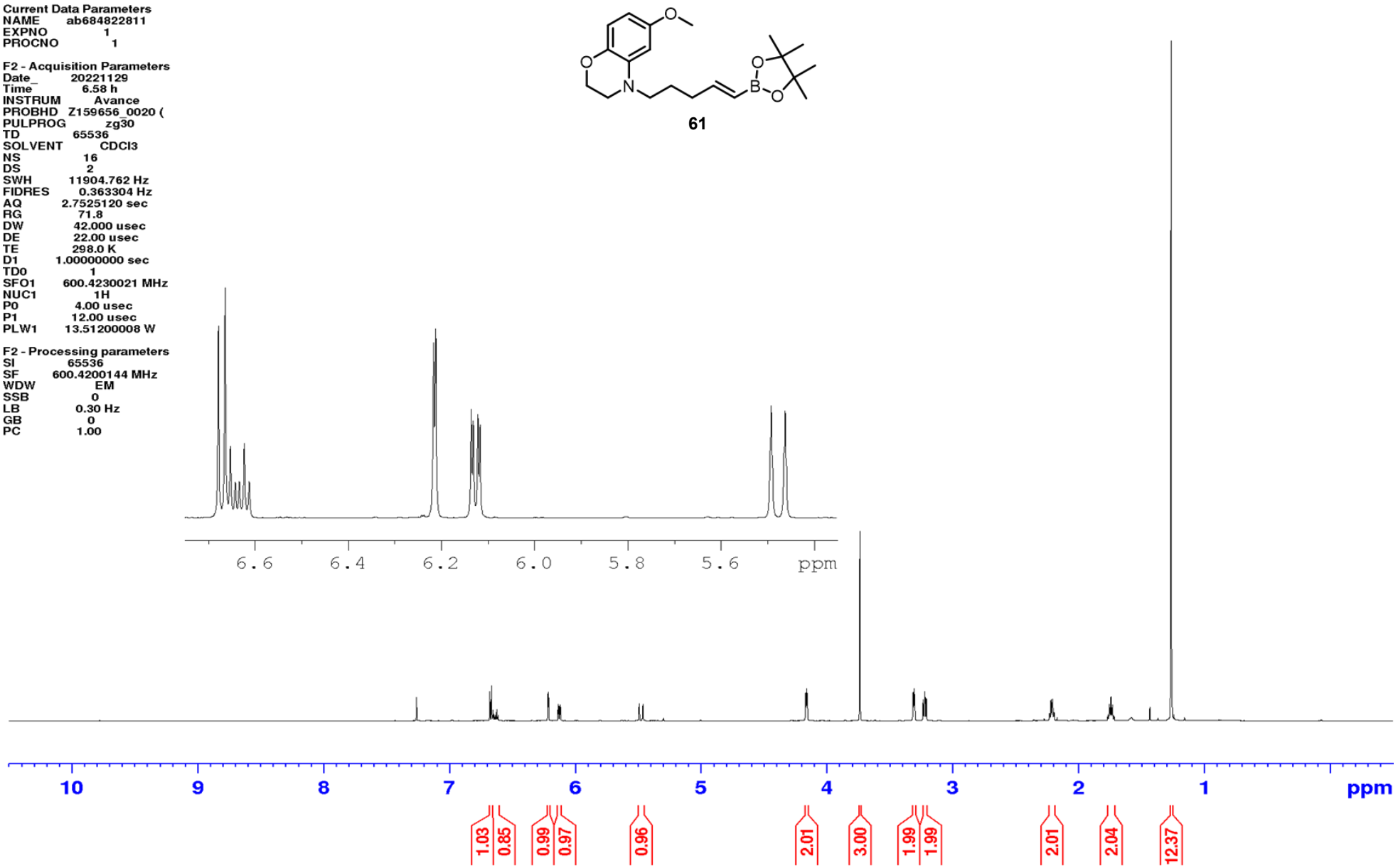

^{11}B NMR (*E*)-6-methoxy-4-(5-(4,4,5,5-tetramethyl-1,3,2-dioxaborolan-2-yl)pent-4-en-1-yl)-3,4-dihydro-2*H*-benzo[*b*][1,4]oxazine

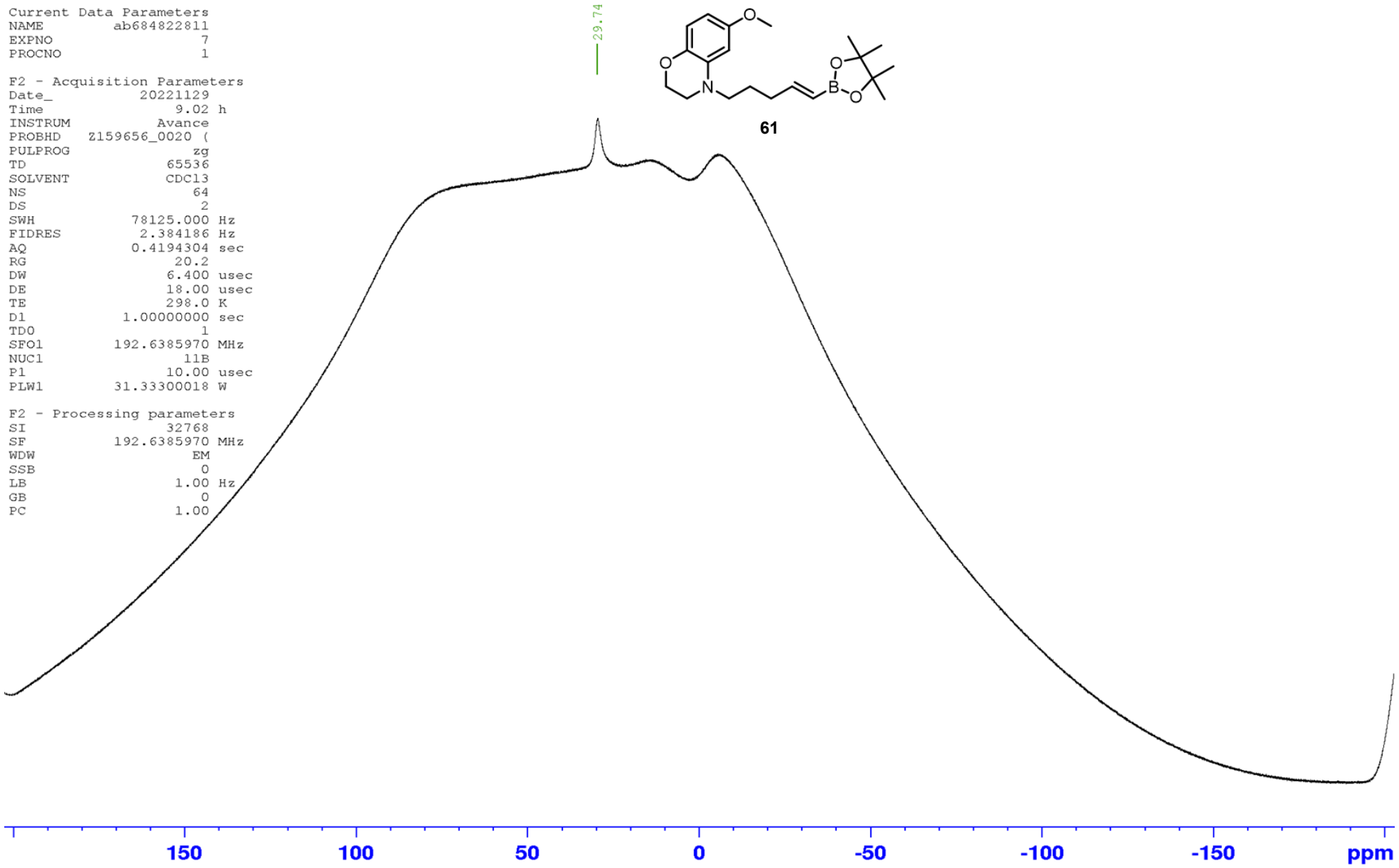

^{13}C NMR (*E*)-6-methoxy-4-(5-(4,4,5,5-tetramethyl-1,3,2-dioxaborolan-2-yl)pent-4-en-1-yl)-3,4-dihydro-2*H*-benzo[*b*][1,4]oxazine

```
Current Data Parameters
NAME         ab684822811
EXPNO                  5
PROCNO                 1

F2 - Acquisition Parameters
Date_           20221129
Time                8.07 h
INSTRUM           Avance
PROBHD   Z159656_0020 (
PULPROG          zgpg30
TD                65536
SOLVENT           CDCl3
NS                  512
DS                    4
SWH           35714.285 Hz
FIDRES         1.089913 Hz
AQ            0.9175040 sec
RG                  101
DW               14.000 usec
DE                18.00 usec
TE                298.0 K
D1           2.00000000 sec
D11          0.03000000 sec
TD0                   1
SFO1        150.9923364 MHz
NUC1                13C
P0                 3.33 usec
P1                10.00 usec
PLW1        41.91400146 W
SFO2        600.4224017 MHz
NUC2                1H
CPDPRG[2         waltz16
PCPD2             70.00 usec
PLW2        13.51200008 W
PLW12        0.39708999 W
PLW13        0.19972999 W

F2 - Processing parameters
SI                65536
SF          150.9757083 MHz
WDW                  EM
SSB                   0
LB                 1.00 Hz
GB                    0
PC                 1.40
```

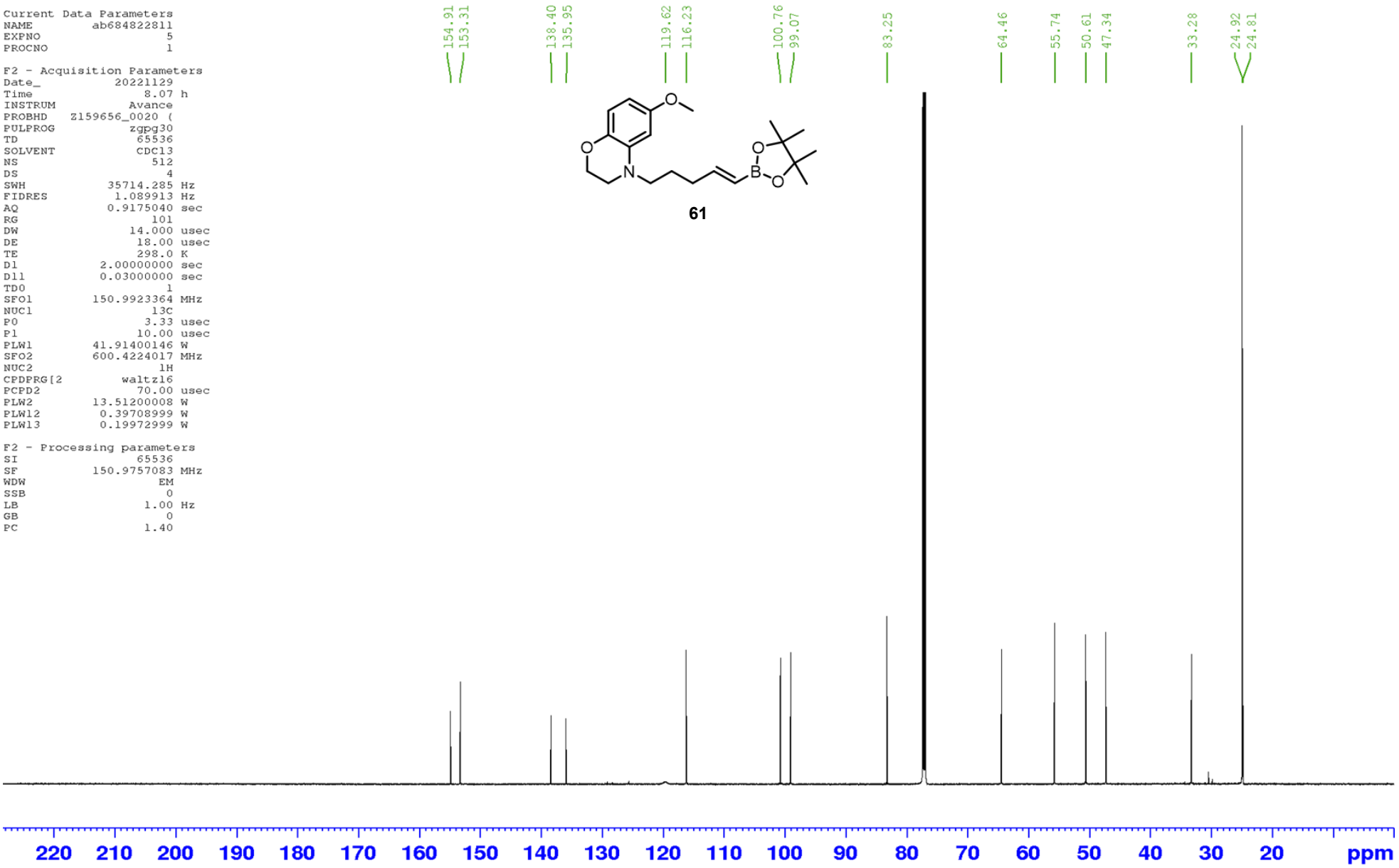

61

^{1}H NMR (*R*,*E*)-6-(5-(6-methoxy-2,3-dihydro-4*H*-benzo[*b*][1,4]oxazin-4-yl)pent-1-en-1-yl)-4-methyl-1,3,4,5-tetrahydro-2*H*-benzo[*b*][1,4]diazepin-2-one

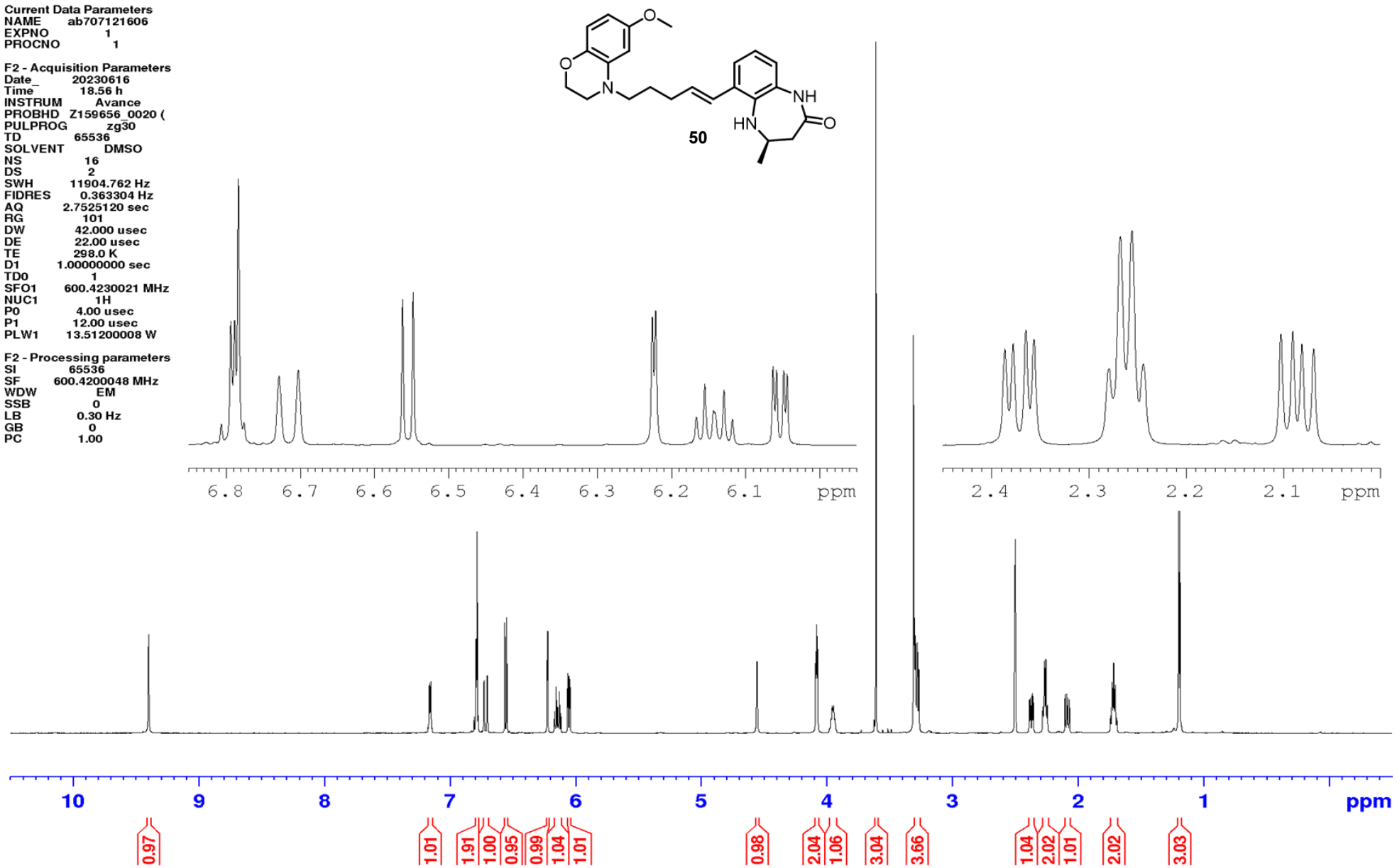

^{13}C NMR (*R*,*E*)-6-(5-(6-methoxy-2,3-dihydro-4*H*-benzo[*b*][1,4]oxazin-4-yl)pent-1-en-1-yl)-4-methyl-1,3,4,5-tetrahydro-2*H*-benzo[*b*][1,4]diazepin-2-one

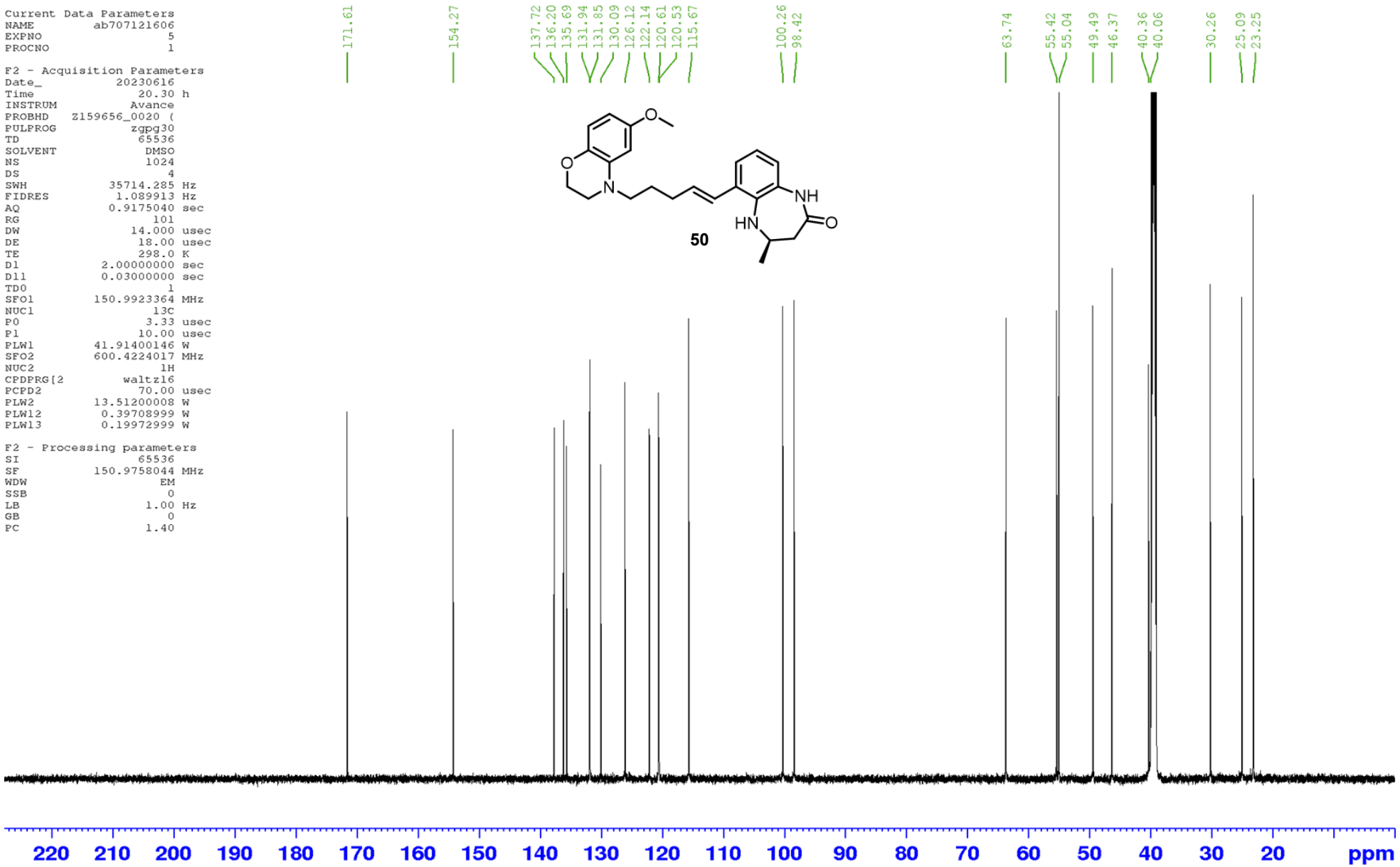

^{1}H NMR methyl (2-bromo-4-iodo-6-nitrophenyl)-*D*-alaninate

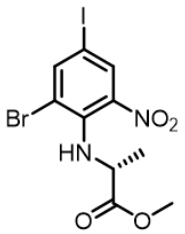

70

```
Current Data Parameters
NAME      Aug10-2020-28-AMB_A_04_Pure
EXPNO              1
PROCNO             1

F2 - Acquisition Parameters
Date_          20200810
Time           16.11 h
INSTRUM          avg400
PROBHD   Z108618_0816 (
PULPROG           zg60
TD             65536
SOLVENT          CDCl3
NS                16
DS                 2
SWH            8012.820 Hz
FIDRES            0.244532 Hz
AQ             4.0894465 sec
RG               147.08
DW               62.400 usec
DE                6.50 usec
TE               301.3 K
D1             1.00000000 sec
TD0                1
SFO1           400.2024012 MHz
NUC1               1H
P1               14.00 usec
PLW1          14.00000000 W

F2 - Processing parameters
SI             32768
SF          400.2000095 MHz
WDW                EM
SSB                0
LB              0.30 Hz
GB                 0
PC              1.00
```

^{13}C NMR methyl (2-bromo-4-iodo-6-nitrophenyl)-*D*-alaninate

```
Current Data Parameters
NAME      Aug10-2020-28-AMB_A_04_Pure
EXPNO                 2
PROCNO                1

F2 - Acquisition Parameters
Date_          20200810
Time              20.17 h
INSTRUM         avq400
PROBHD   Z108618_0816 (
PULPROG         zgpg30
TD              32768
SOLVENT           CDCl3
NS                  512
DS                    4
SWH           26041.666 Hz
FIDRES         1.589457 Hz
AQ            0.6291456 sec
RG               206.87
DW               19.200 usec
DE                6.50 usec
TE               303.6 K
D1           1.00000000 sec
D11          0.03000000 sec
TD0                   1
SFO1        100.6404331 MHz
NUC1                13C
P0                 3.33 usec
P1                10.00 usec
PLW1        56.00000000 W
SFO2        400.2016008 MHz
NUC2                1H
CPDPRG[2        waltz16
PCPD2             90.00 usec
PLW2        14.00000000 W
PLW12        0.33877000 W
PLW13        0.17039999 W

F2 - Processing parameters
SI                32768
SF          100.6303549 MHz
WDW                  EM
SSB                   0
LB                 1.00 Hz
GB                    0
PC                 1.40
```

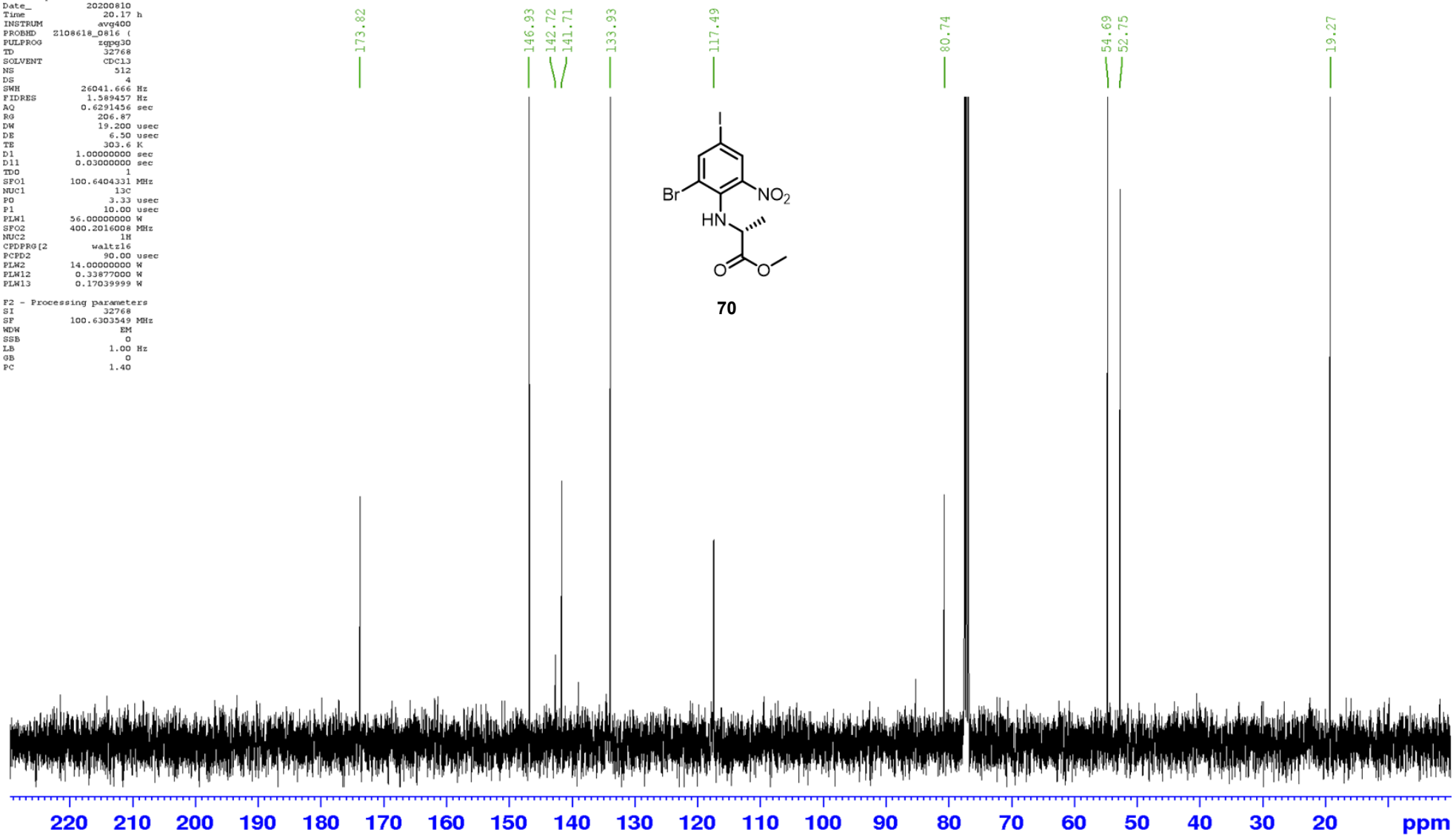

70

^{1}H NMR methyl (2-bromo-4-(5-hydroxypent-1-yn-1-yl)-6-nitrophenyl)-*D*-alaninate

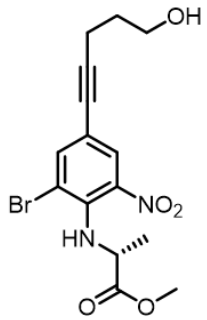

71

```
Current Data Parameters
NAME     Aug21-2020-54-AMB_A_11_Pure
EXPNO            1
PROCNO           1

F2 - Acquisition Parameters
Date_        20200821
Time         15.37 h
INSTRUM      avg400
PROBHD   Z108618_0816 (
PULPROG      zg60
TD           65536
SOLVENT      CDCl3
NS           16
DS           2
SWH          8012.820 Hz
FIDRES       0.244532 Hz
AQ           4.0894465 sec
RG           206.87
DW           62.400 usec
DE           6.50 usec
TE           300.6 K
D1           1.00000000 sec
TD0          1
SFO1         400.2024012 MHz
NUC1         1H
P1           14.00 usec
PLW1         14.00000000 W

F2 - Processing parameters
SI           32768
SF           400.2000096 MHz
WDW          EM
SSB          0
LB           0.30 Hz
GB           0
PC           1.00
```

^{13}C NMR methyl (2-bromo-4-(5-hydroxypent-1-yn-1-yl)-6-nitrophenyl)-*D*-alaninate

```
Current Data Parameters
NAME      Aug17-2020-59-AMB_A_09_1
EXPNO                  2
PROCNO                 1

F2 - Acquisition Parameters
Date_           20200817
Time              23.24 h
INSTRUM           avg400
PROBHD   Z108618_0816 (
PULPROG           zgpg30
TD                32768
SOLVENT           CDCl3
NS                  512
DS                    4
SWH           26041.666 Hz
FIDRES         1.589457 Hz
AQ            0.6291456 sec
RG               206.87
DW               19.200 usec
DE                6.50 usec
TE               300.7 K
D1           1.00000000 sec
D11          0.03000000 sec
TD0                   1
SFO1         100.6404331 MHz
NUC1                13C
P0                 3.33 usec
P1                10.00 usec
PLW1         56.00000000 W
SFO2         400.2016008 MHz
NUC2                1H
CPDPRG[2         waltz16
PCPD2             90.00 usec
PLW2         14.00000000 W
PLW12         0.33877000 W
PLW13         0.17039999 W

F2 - Processing parameters
SI                32768
SF           100.6303593 MHz
WDW                  EM
SSB                   0
LB                 1.00 Hz
GB                    0
PC                 1.40
```

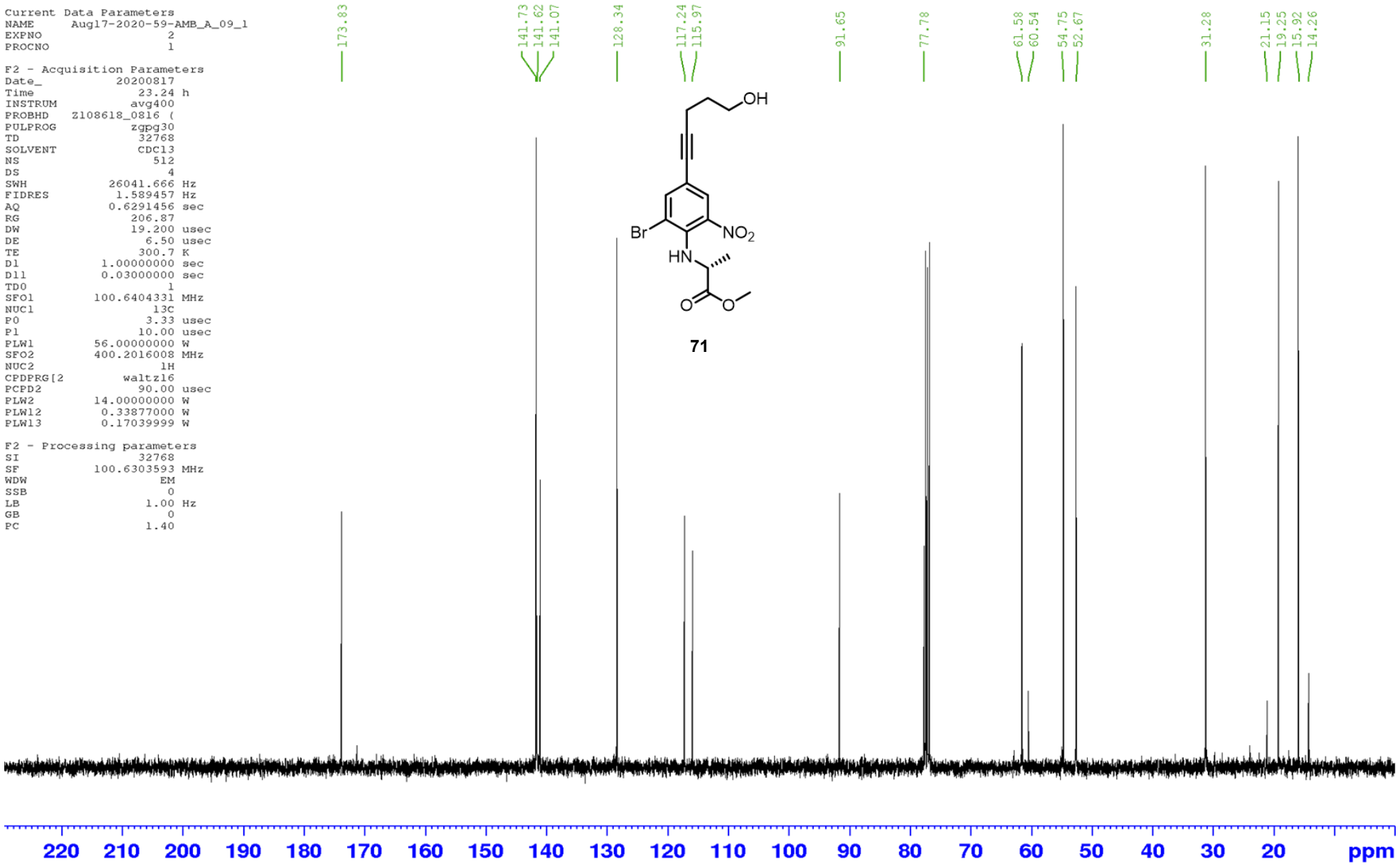

71

^{1}H NMR methyl (2-bromo-4-(5-hydroxypentyl)-6-nitrophenyl)-*D*-alaninate

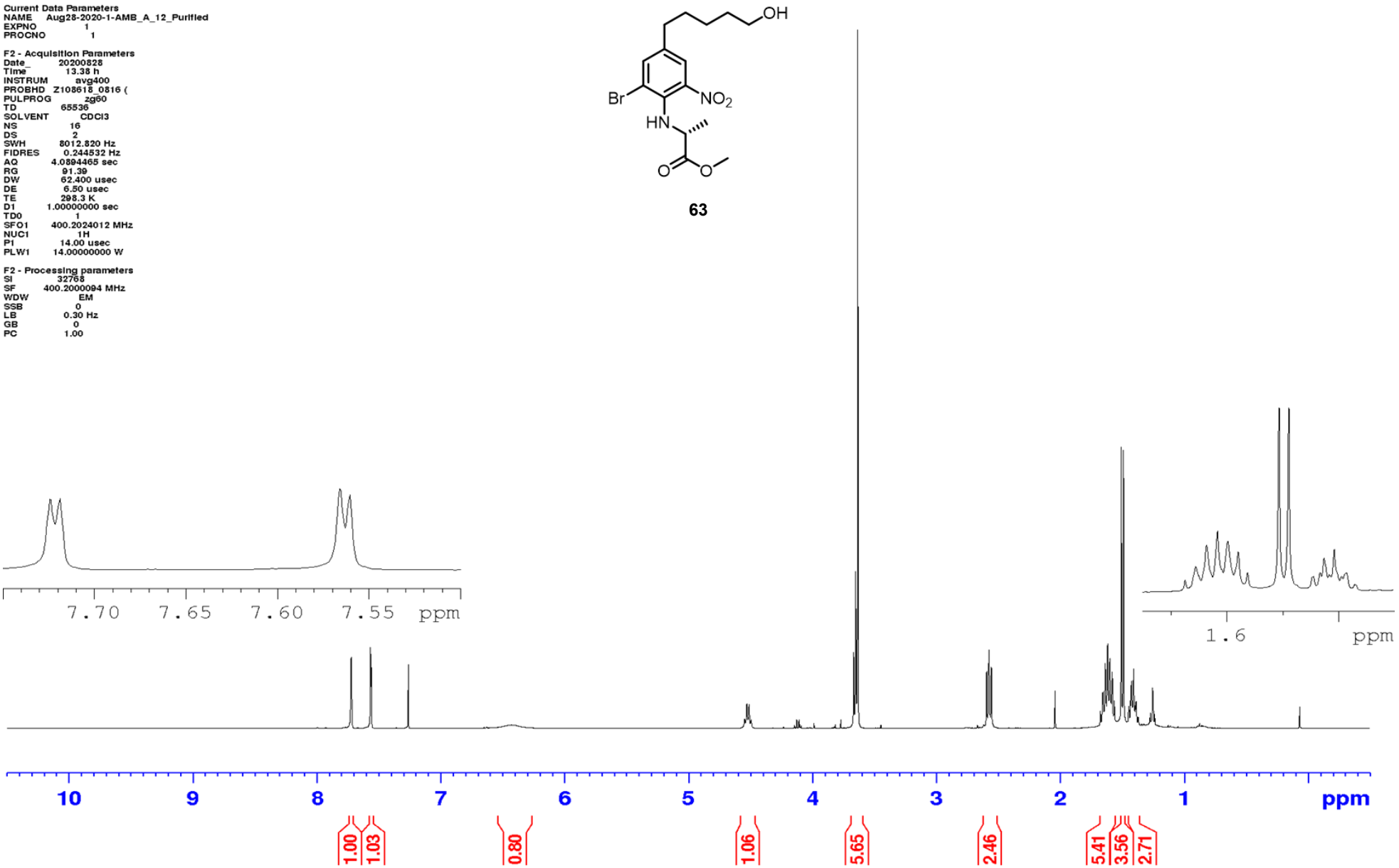

^{1}H NMR methyl (2-bromo-4-(5-hydroxypentyl)-6-nitrophenyl)-*D*-alaninate

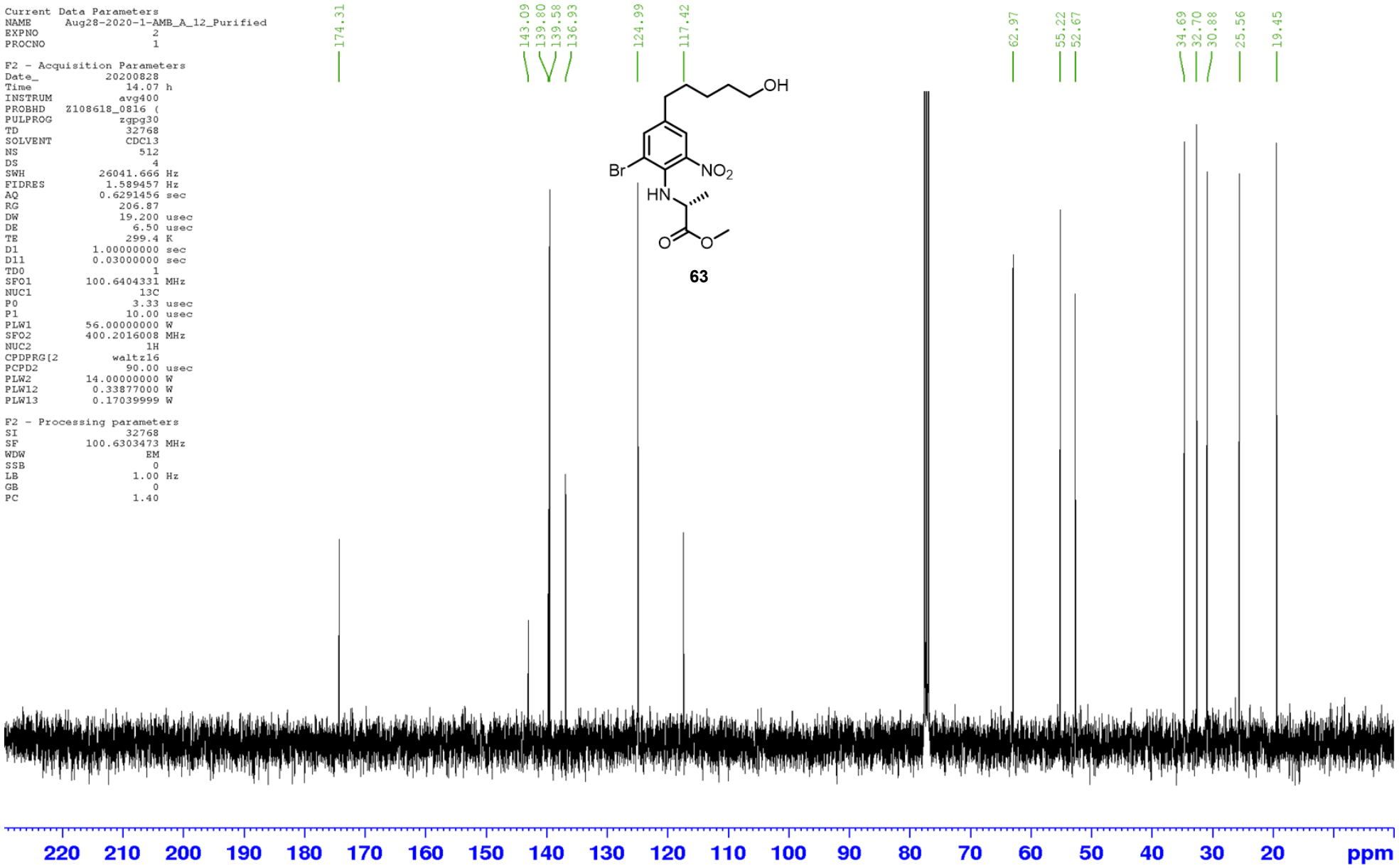

^{1}H NMR *tert*-butyl (2-bromo-4-iodo-6-nitrophenyl)-*D*-alaninate

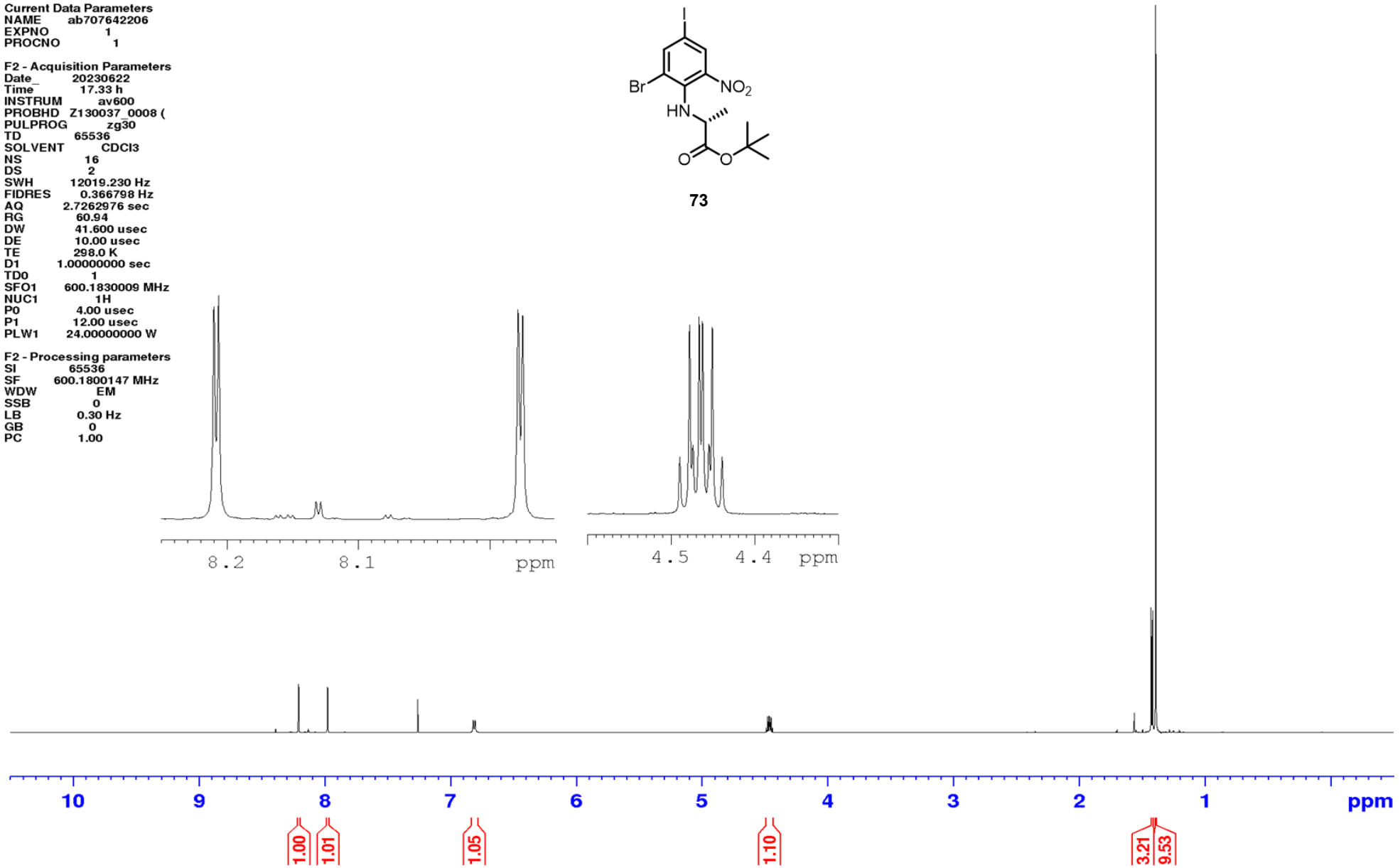

^{13}C NMR *tert*-butyl (2-bromo-4-iodo-6-nitrophenyl)-*D*-alaninate

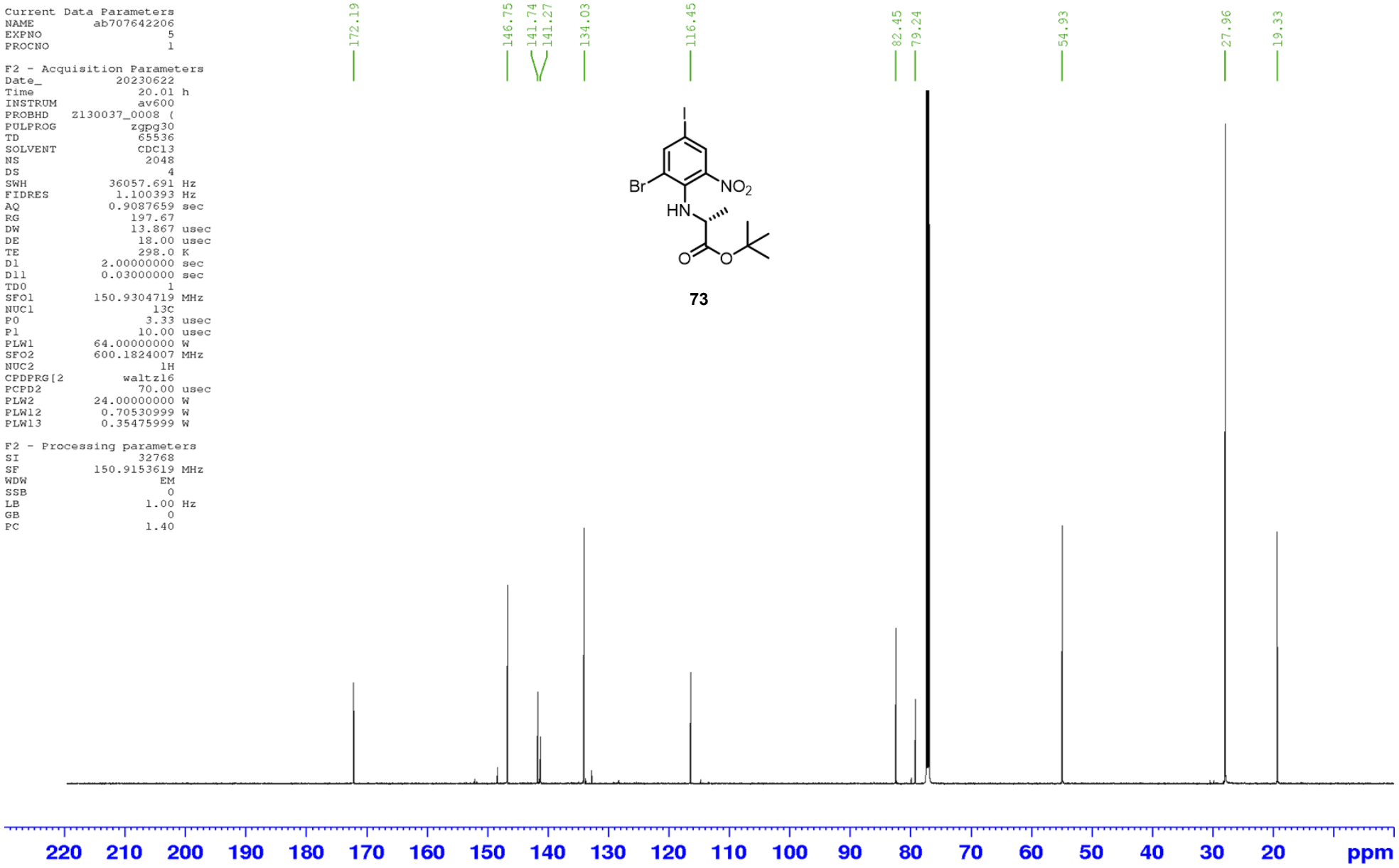

73

^{1}H NMR *tert*-butyl (2-bromo-4-(5-hydroxypent-1-yn-1-yl)-6-nitrophenyl)-*D*-alaninate

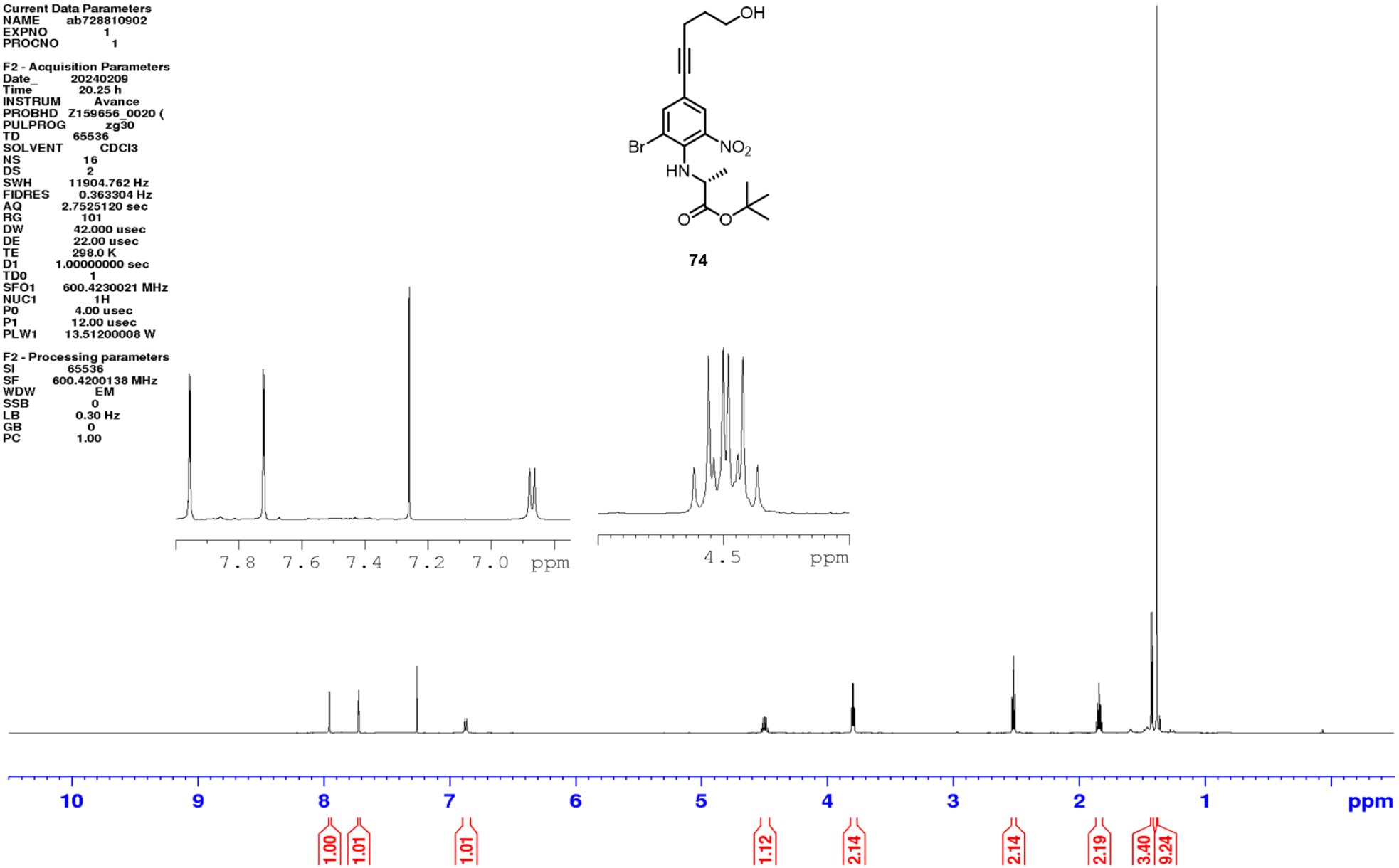

^{13}C NMR *tert*-butyl (2-bromo-4-(5-hydroxypent-1-yn-1-yl)-6-nitrophenyl)-*D*-alaninate

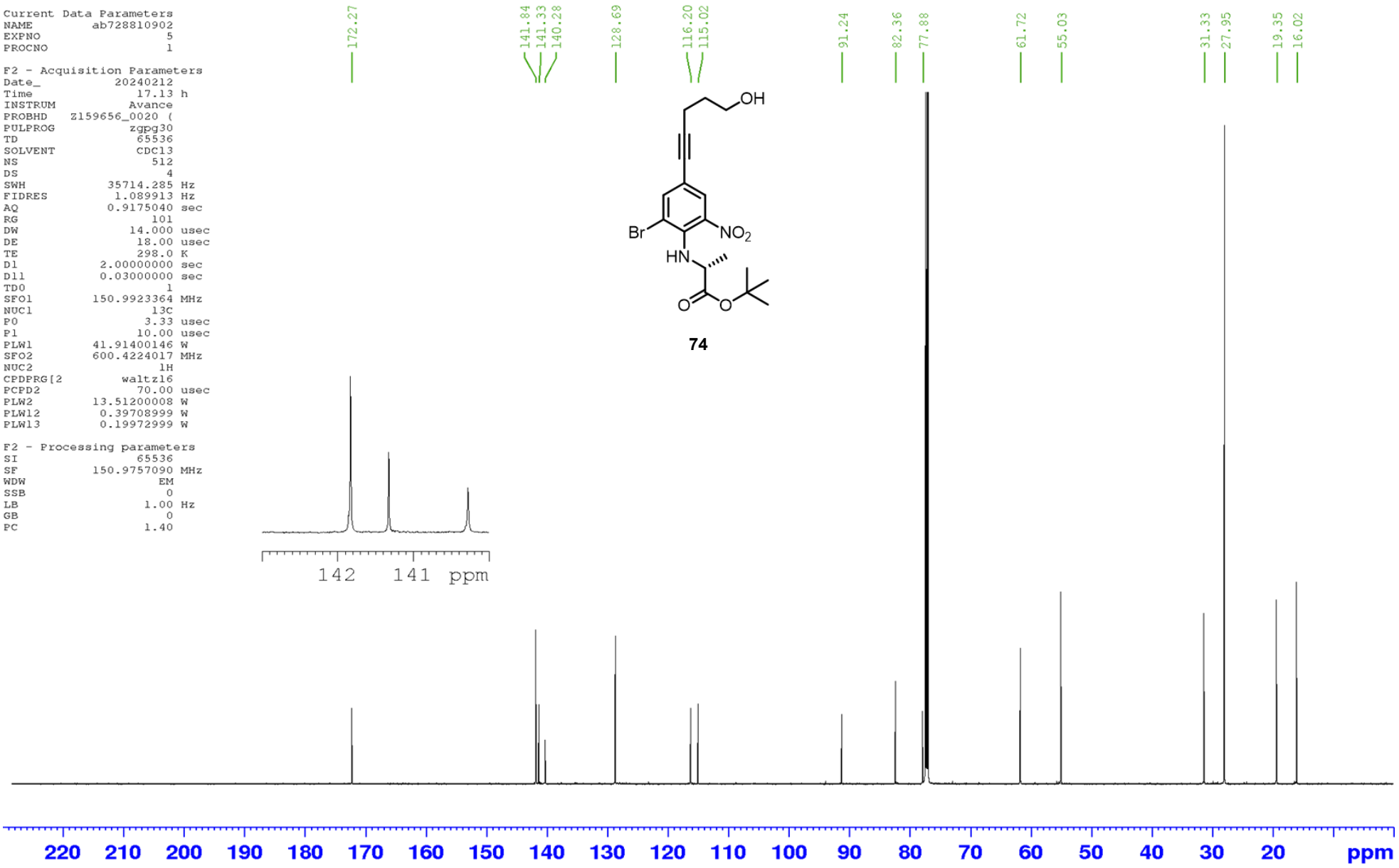

74

^{1}H NMR *tert*-butyl (2-bromo-4-(5-hydroxypentyl)-6-nitrophenyl)-*D*-alaninate

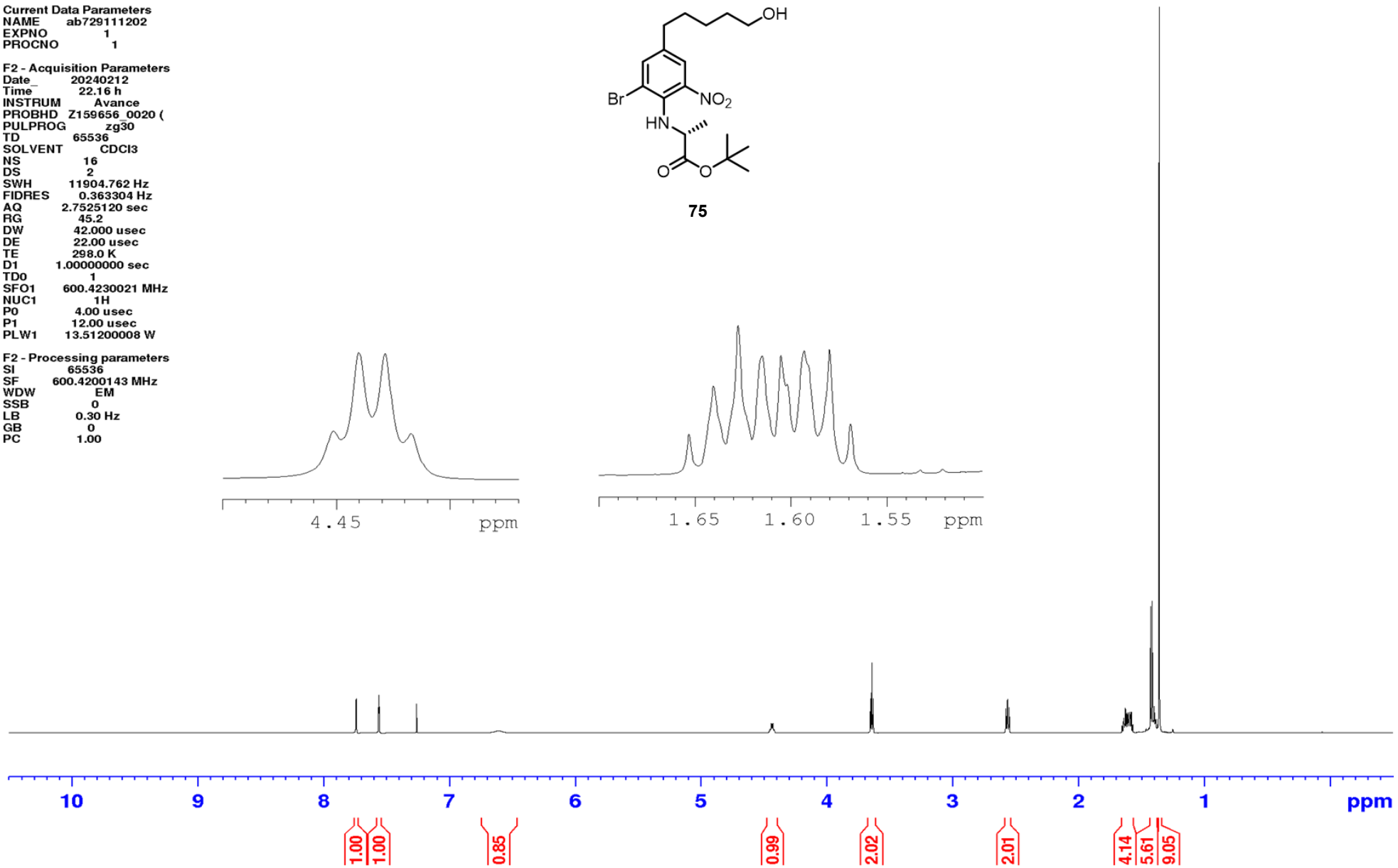

75

^{13}C NMR *tert*-butyl (2-bromo-4-(5-hydroxypentyl)-6-nitrophenyl)-*D*-alaninate

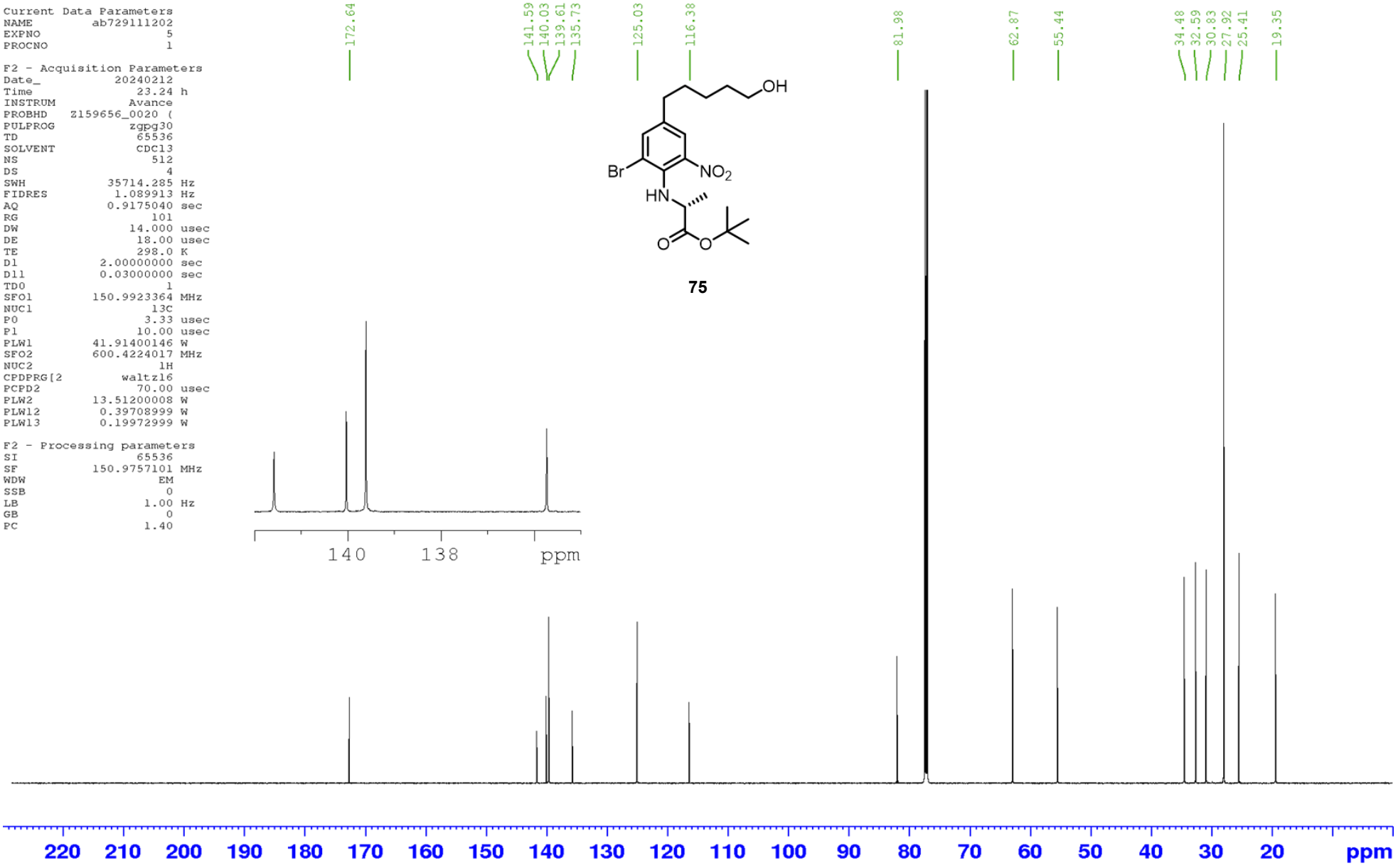

75

^{1}H NMR *tert*-butyl (*E*)-(4-(5-hydroxypentyl)-2-nitro-6-(5-(7-(((triisopropylsilyl)oxy)-3,4-dihydroquinolin-1(2*H*)-yl)pent-1-en-1-yl)phenyl)-*D*-alaninate

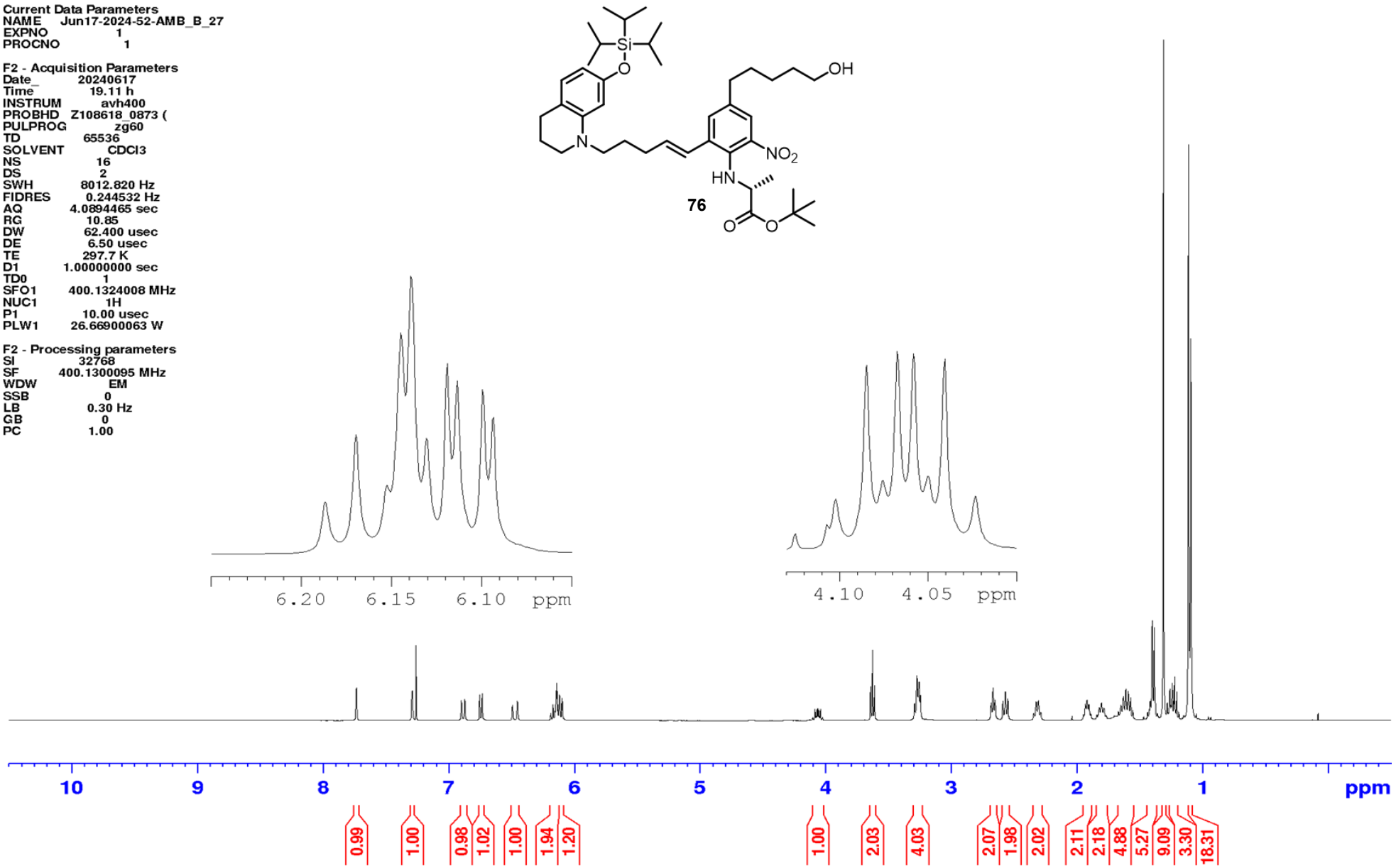

^{13}C NMR *tert*-butyl (*E*)-(4-(5-hydroxypentyl)-2-nitro-6-(5-(7-((triisopropylsilyl)oxy)-3,4-dihydroquinolin-1(2*H*)-yl)pent-1-en-1-yl)phenyl)-D-alaninate

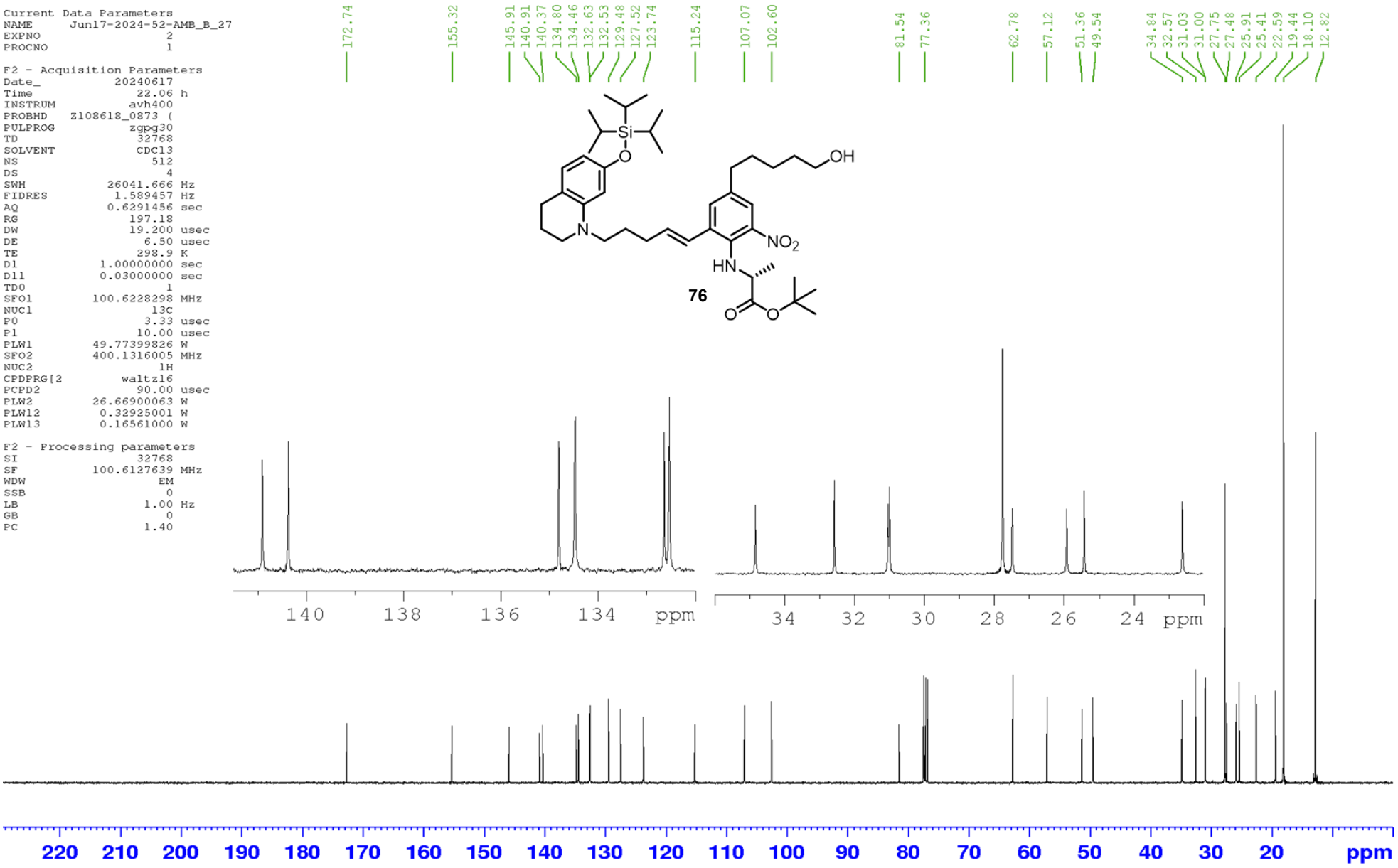

^{1}H NMR (*R*,*E*)-7-(5-hydroxypentyl)-3-methyl-5-(5-(7-((triisopropylsilyl)oxy)-3,4-dihydroquinolin-1(2*H*)-yl)pent-1-en-1-yl)-3,4-dihydroquinoxalin-2(1*H*)-one

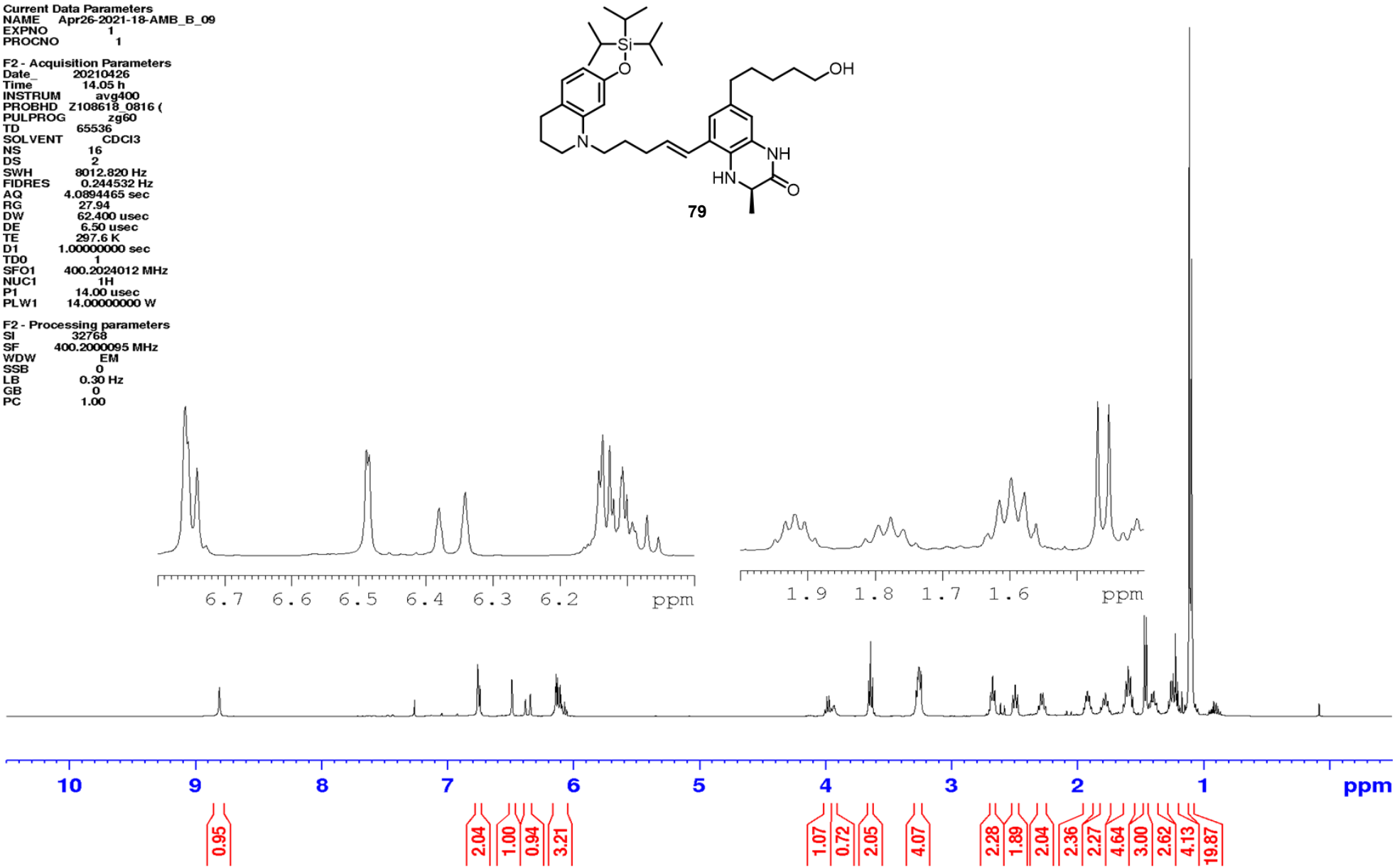

^{13}C NMR (*R*,*E*)-7-(5-hydroxypentyl)-3-methyl-5-(5-(7-((triisopropylsilyl)oxy)-3,4-dihydroquinolin-1(2*H*)-yl)pent-1-en-1-yl)-3,4-dihydroquinoxalin-2(1*H*)-one

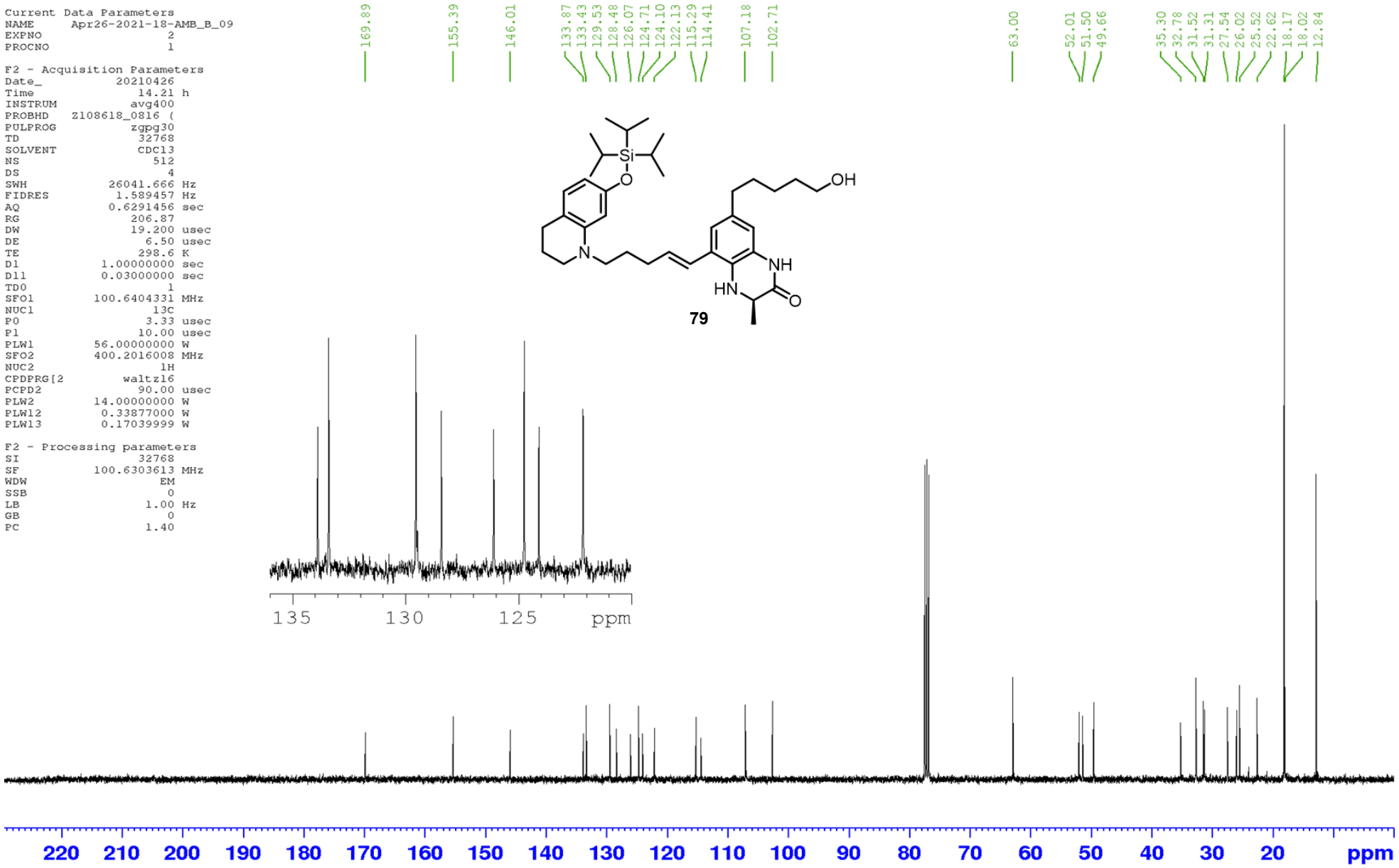

^{1}H NMR 1-(pent-4-yn-1-yl)-1,2,3,4-tetrahydroquinolin-7-ol

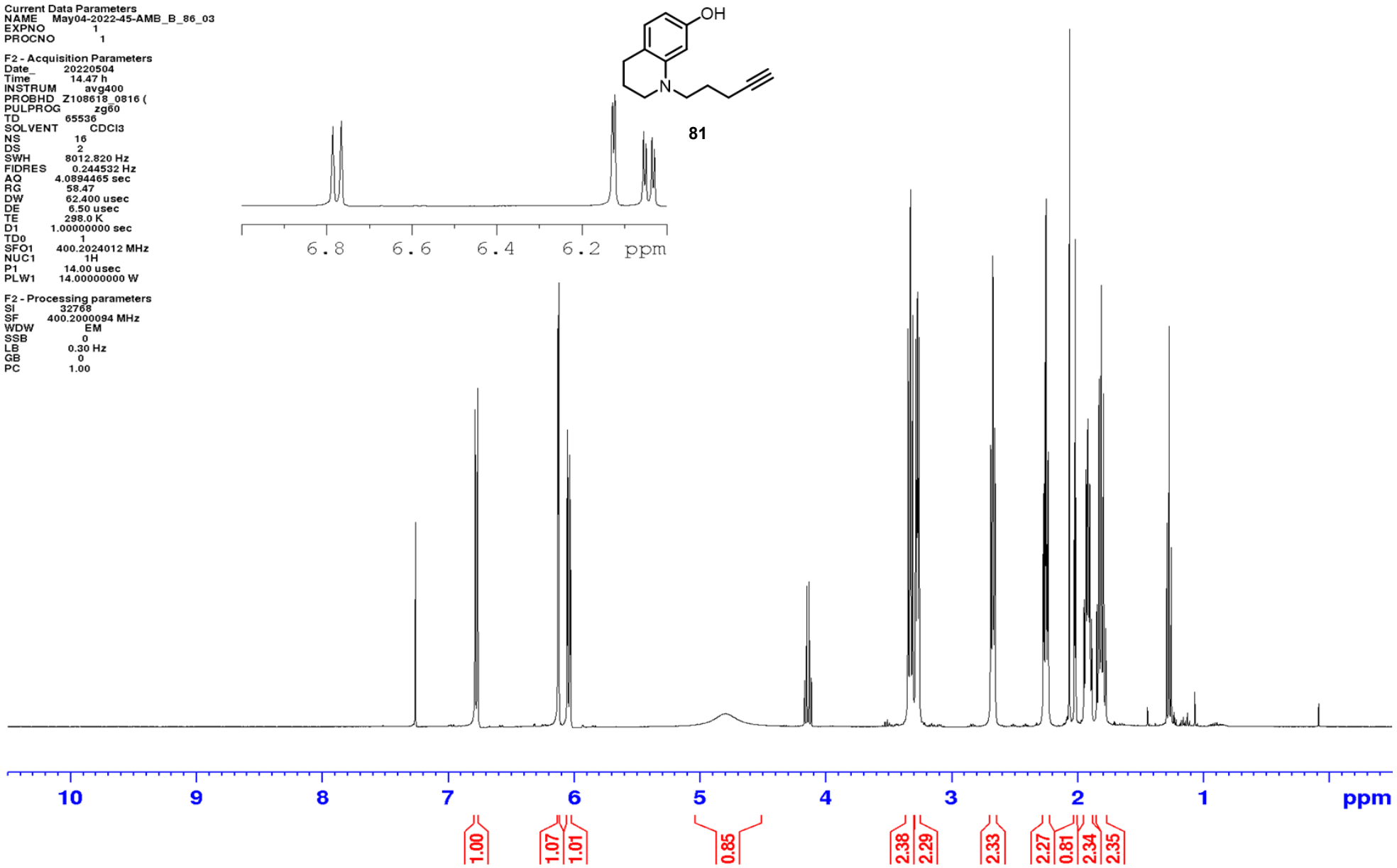

^{1}H NMR *tert*-butyl (2-bromo-6-nitro-4-(5-((1-(pent-4-yn-1-yl)-1,2,3,4-tetrahydroquinolin-7-yl)oxy)pentyl)phenyl)-*D*-alaninate

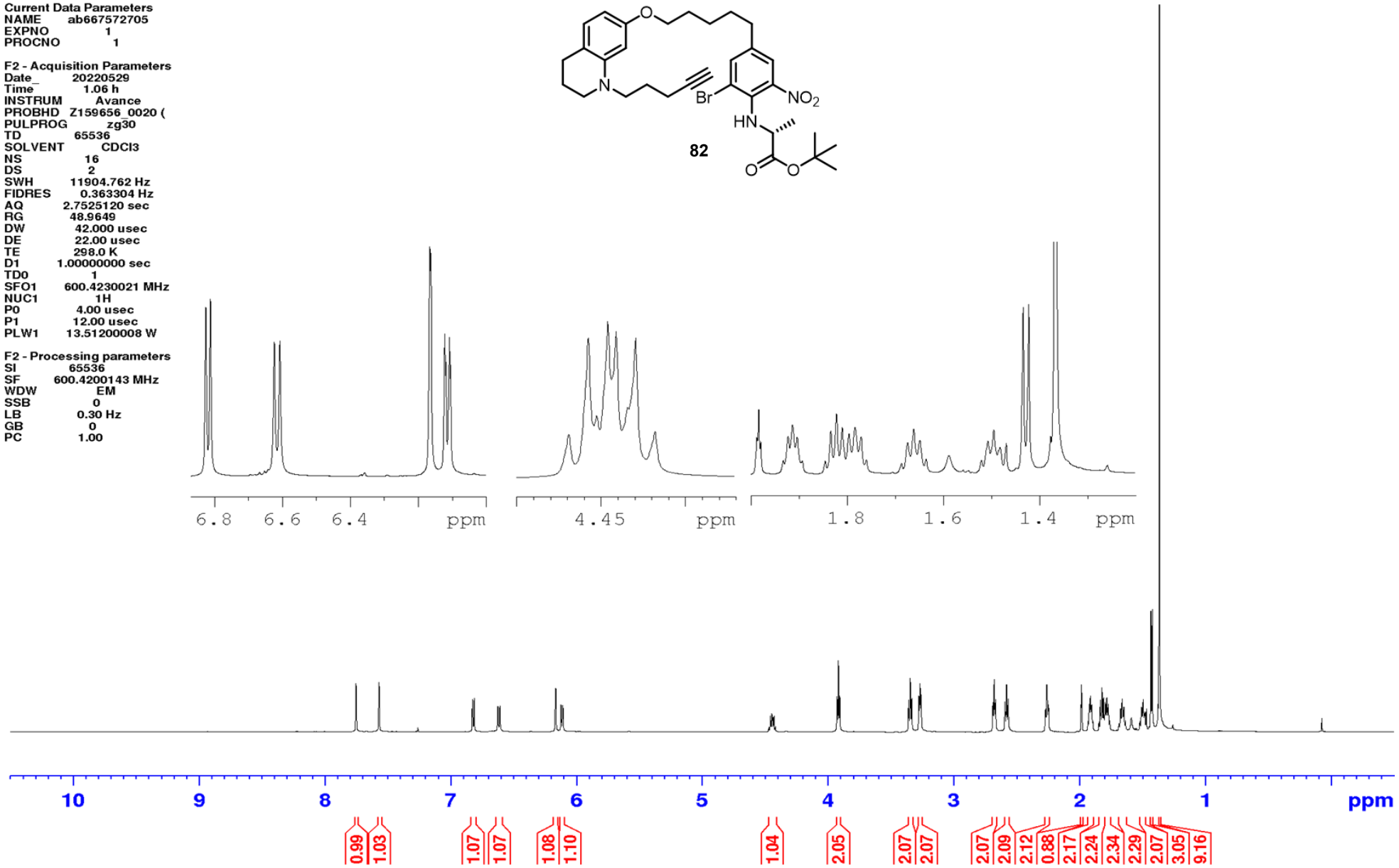

^{13}C NMR *tert*-butyl (2-bromo-6-nitro-4-(5-((1-(pent-4-yn-1-yl)-1,2,3,4-tetrahydroquinolin-7-yl)oxy)pentyl)phenyl)-*D*-alaninate

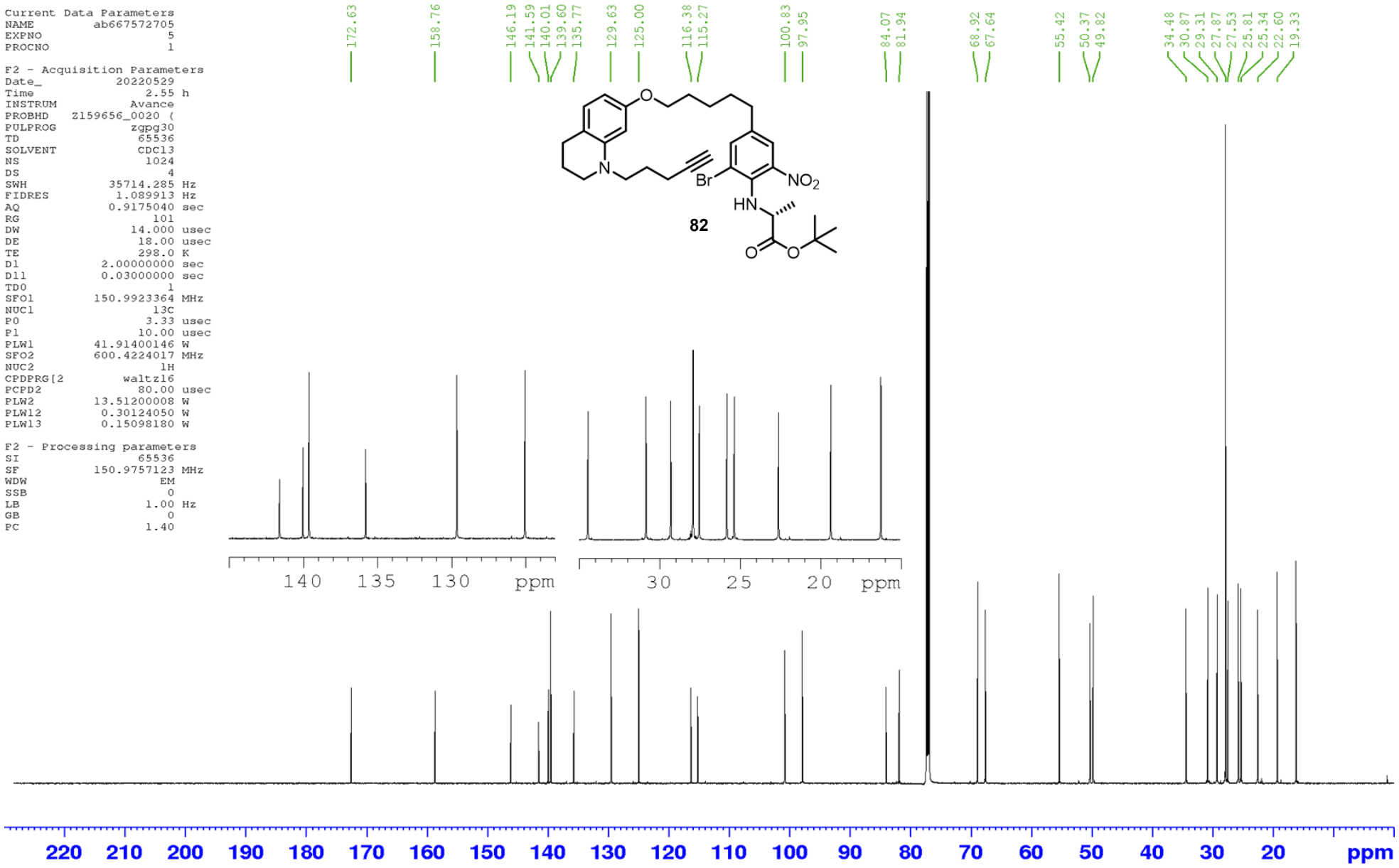

^{1}H NMR *tert*-butyl (*E*)-(2-bromo-6-nitro-4-(5-((1-(5-(4,4,5,5-tetramethyl-1,3,2-dioxaborolan-2-yl)pent-4-en-1-yl)-1,2,3,4-tetrahydroquinolin-7-yl)oxy)pentyl)phenyl)-*D*-alaninate

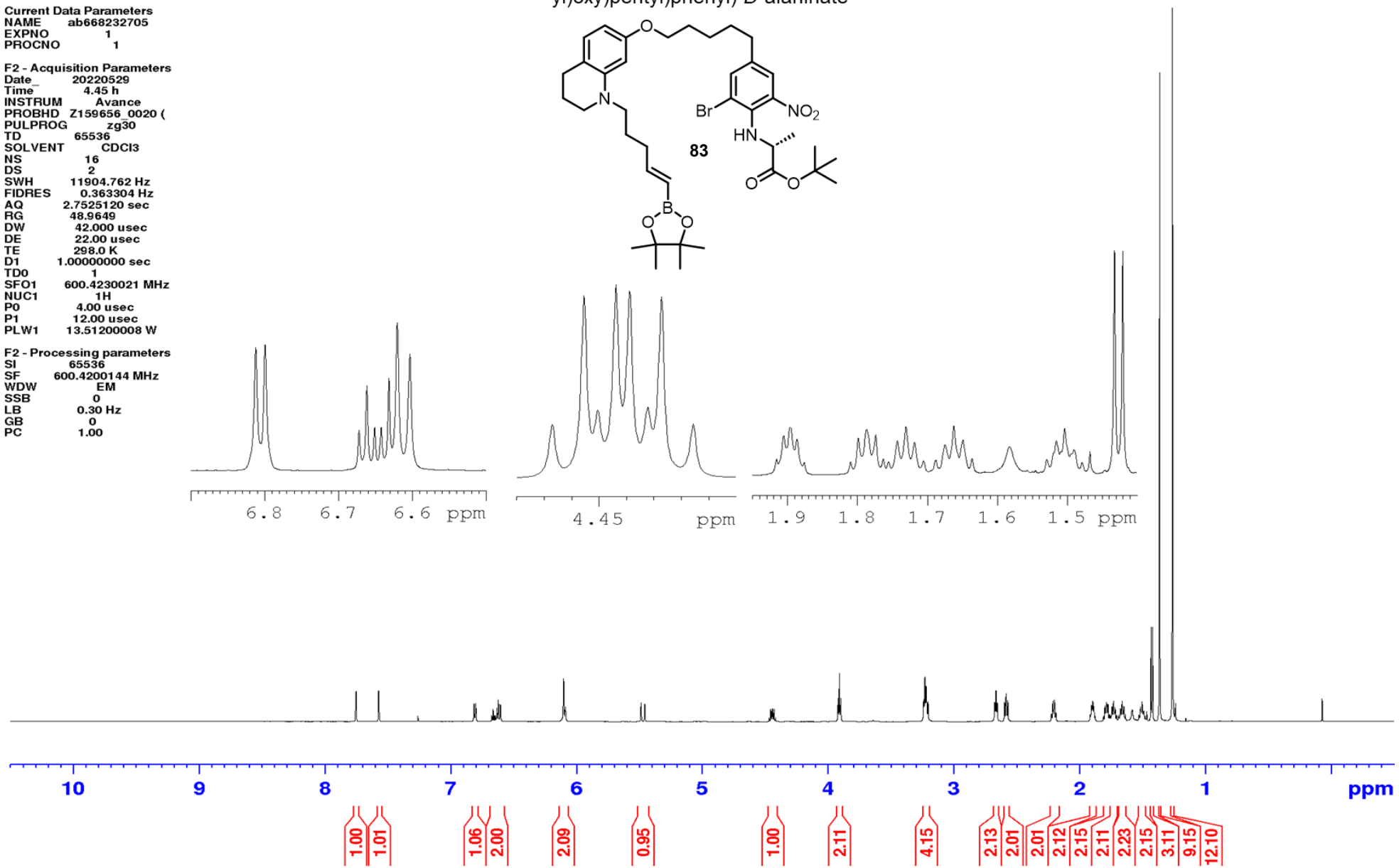

^{11}B NMR *tert*-butyl (*E*)-(2-bromo-6-nitro-4-(5-((1-(5-(4,4,5,5-tetramethyl-1,3,2-dioxaborolan-2-yl)pent-4-en-1-yl)-1,2,3,4-tetrahydroquinolin-7-yl)oxy)pentyl)phenyl)-*D*-alaninate

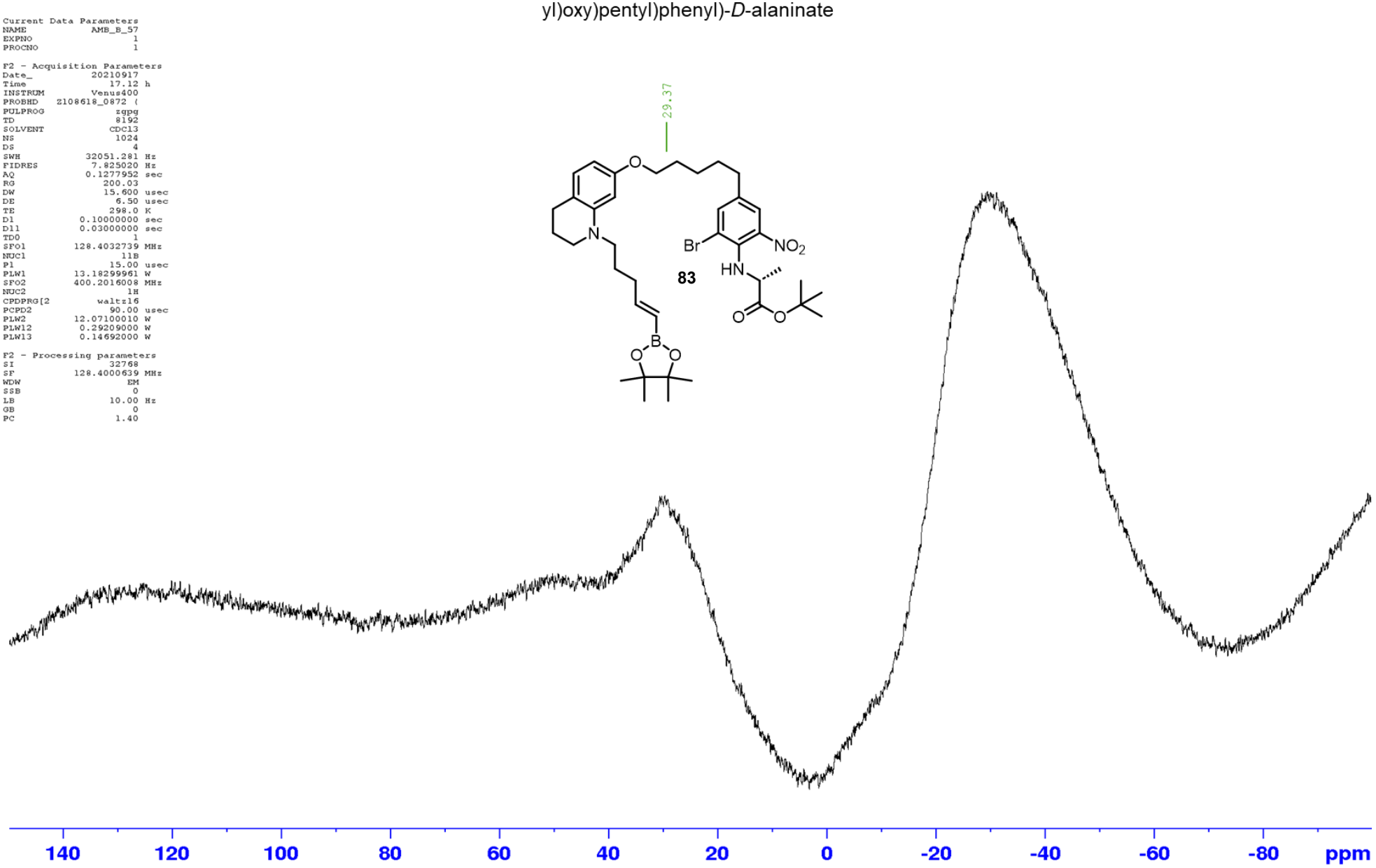

^{13}C NMR *tert*-butyl (*E*)-(2-bromo-6-nitro-4-(5-((1-(5-(4,4,5,5-tetramethyl-1,3,2-dioxaborolan-2-yl)pent-4-en-1-yl)-1,2,3,4-tetrahydroquinolin-7-yl)oxy)pentyl)phenyl)-*D*-alaninate

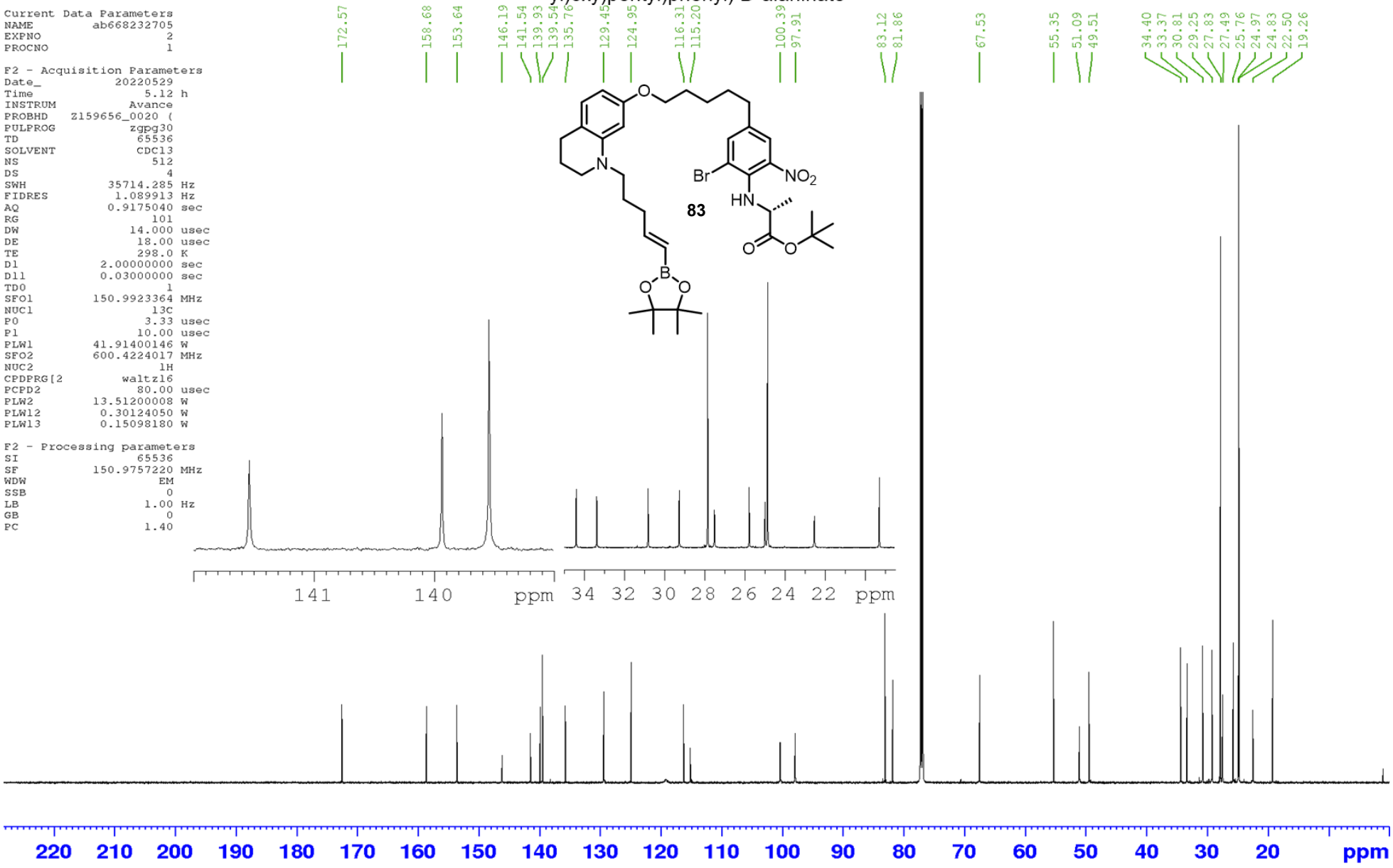

^{1}H NMR *tert*-butyl (*E*)-(7^{5}-nitro-1^{1},1^{2},1^{3},1^{4}-tetrahydro-13-oxa-1(1,7)-quinolina-7(1,3)-benzenacyclotridecaphan-5-en-7^{6}-yl)-*D*-alaninate

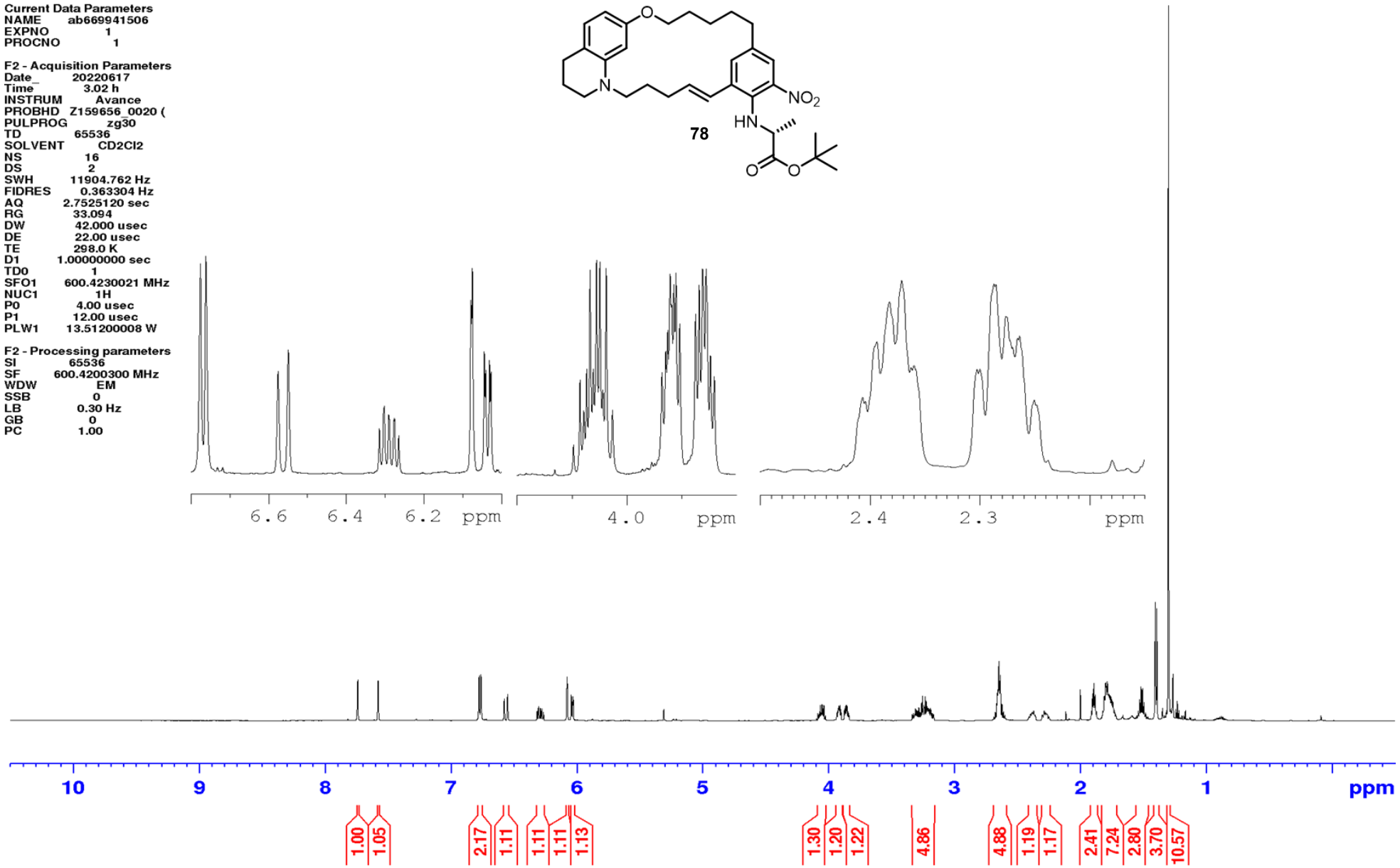

^{13}C NMR *tert*-butyl (*E*)-(7^{5}-nitro-1^{1},1^{2},1^{3},1^{4}-tetrahydro-13-oxa-1(1,7)-quinolina-7(1,3)-benzenacyclotridecaphan-5-en-7^{6}-yl)-*D*-alaninate

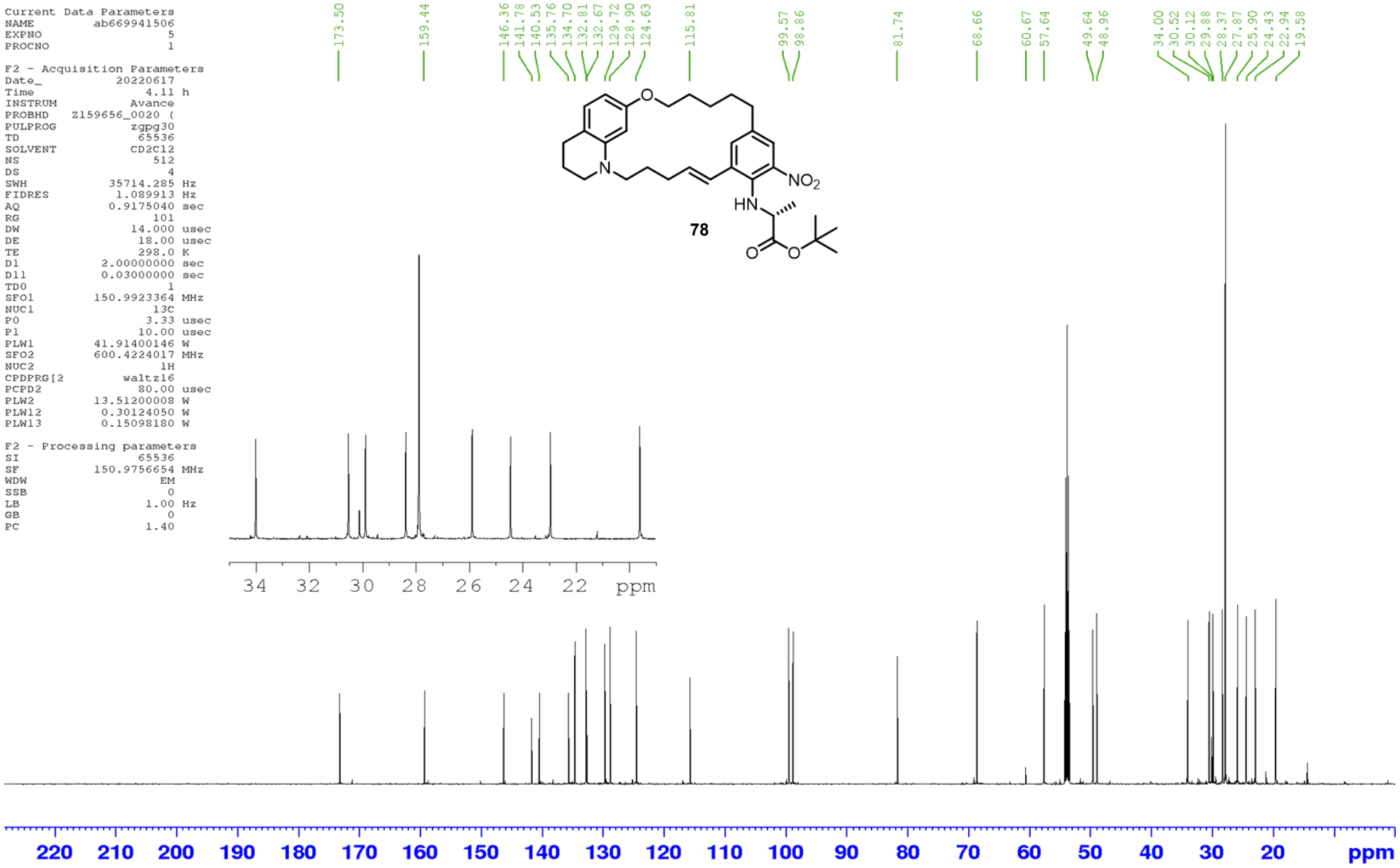

^{1}H NMR (*R*,*E*)-2-methyl-1,7,8,9,10,11,17,18,21,22-decahydro-2*H*,16*H*,20*H*-13,15-(epiethane[1,2]diylidene)-6,25-(metheno)pyrazino[2,3-*l*]pyrido[2,1-*d*][1]oxa[5]azacycloicosin-3(4*H*)-one

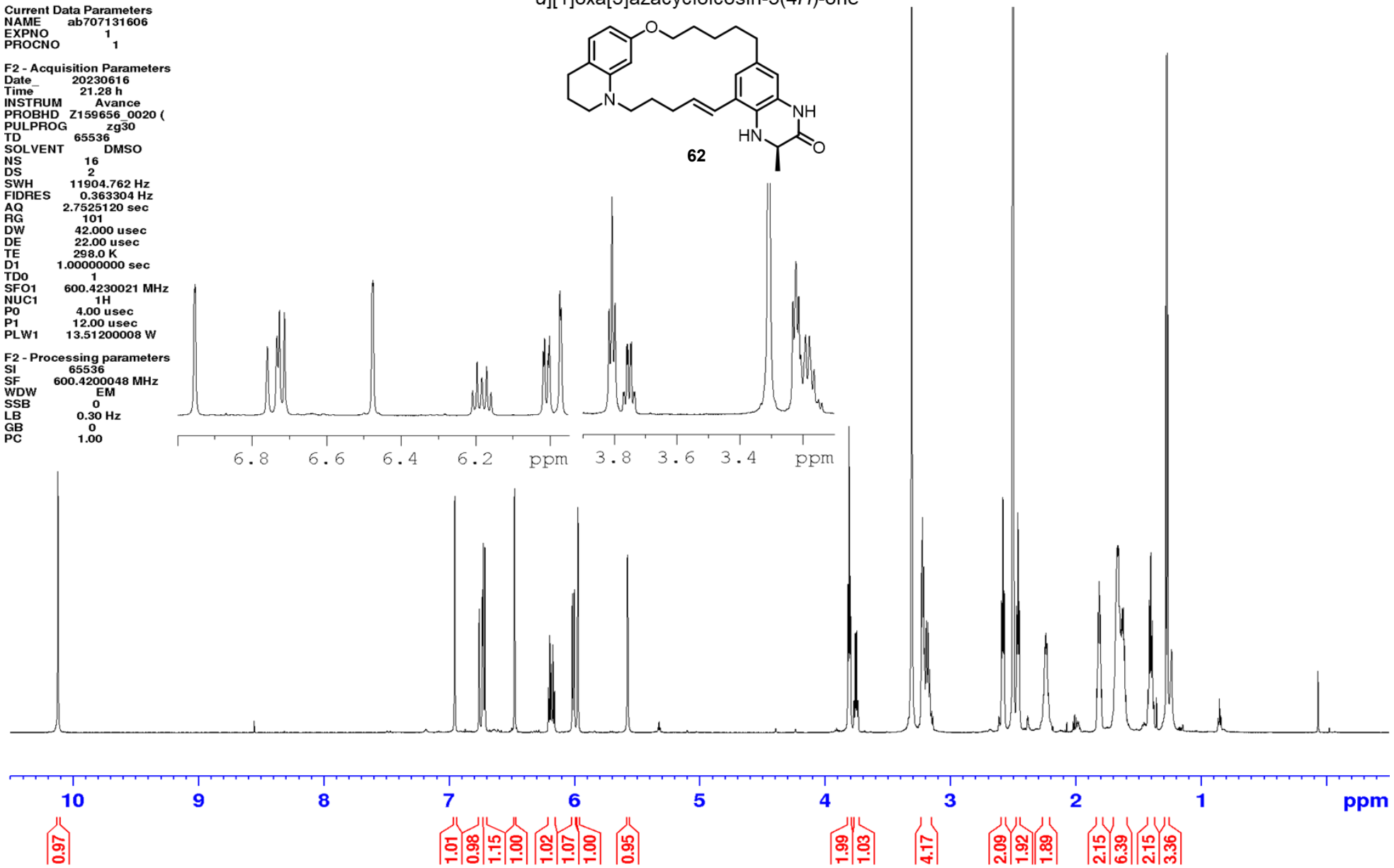

^{13}C NMR (*R*,*E*)-2-methyl-1,7,8,9,10,11,17,18,21,22-decahydro-2*H*,16*H*,20*H*-13,15-(epiethane[1,2]diylidene)-6,25-(metheno)pyrazino[2,3-*l*]pyrido[2,1-*d*][1]oxa[5]azacycloicosin-3(4*H*)-one

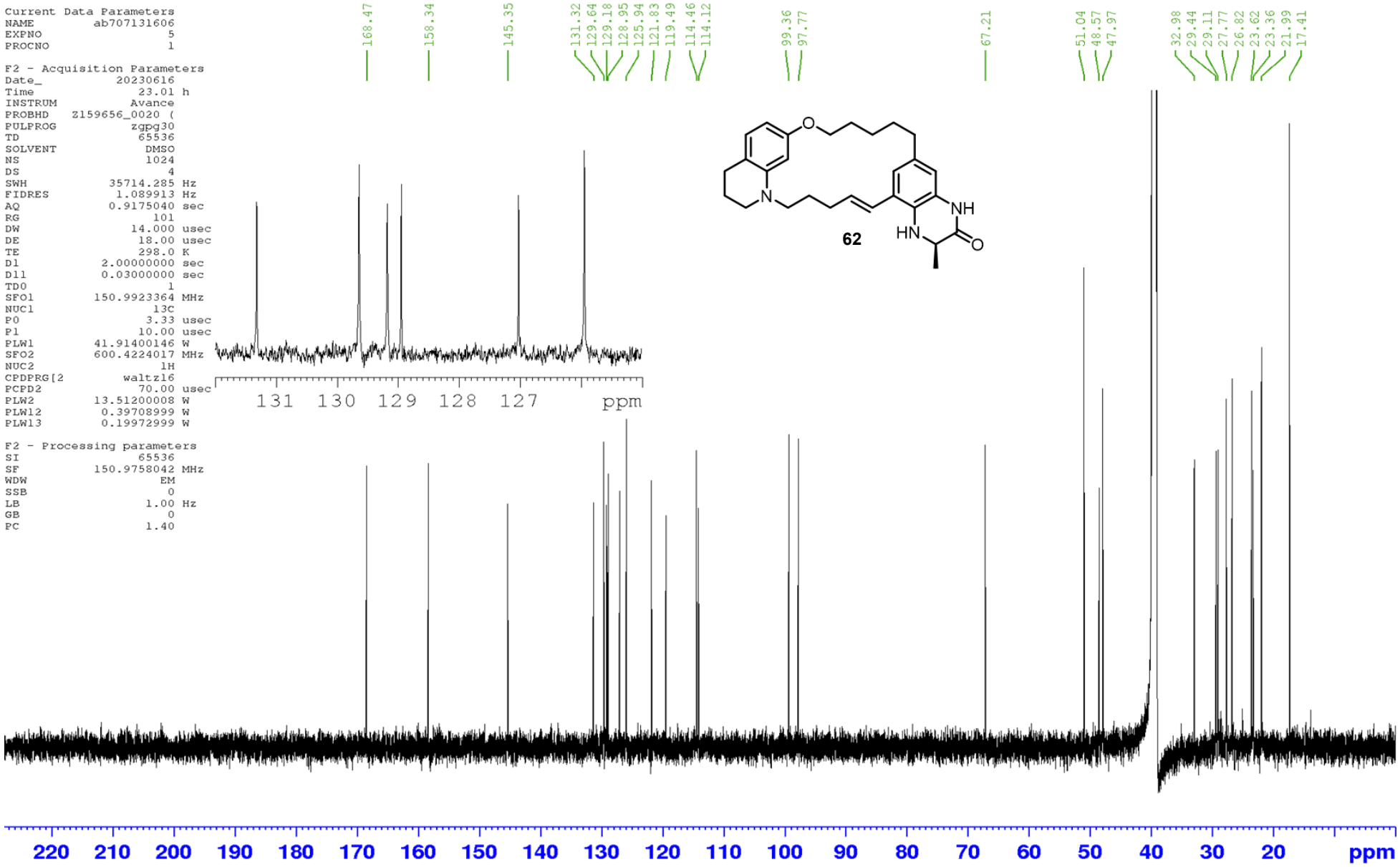

^{1}H NMR *tert*-butyl (*E*)-(4-(5-hydroxypentyl)-2-(5-(7-methoxy-3,4-dihydroquinolin-1(2*H*)-yl)pent-1-en-1-yl)-6-nitrophenyl)-*D*-alaninate

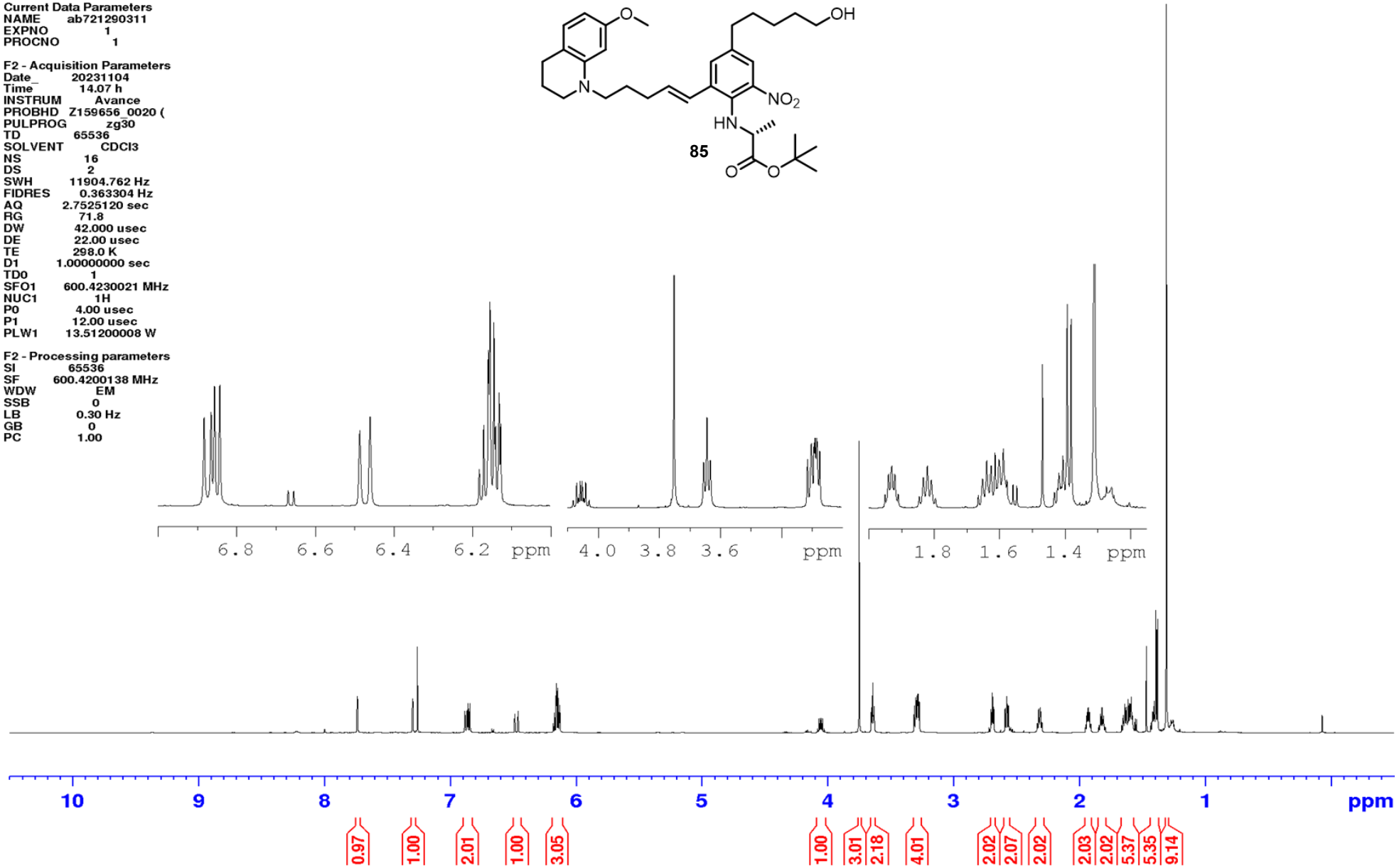

^{13}C NMR *tert*-butyl (*E*)-(4-(5-hydroxypentyl)-2-(5-(7-methoxy-3,4-dihydroquinolin-1(2*H*)-yl)pent-1-en-1-yl)-6-nitrophenyl)-*D*-alaninate

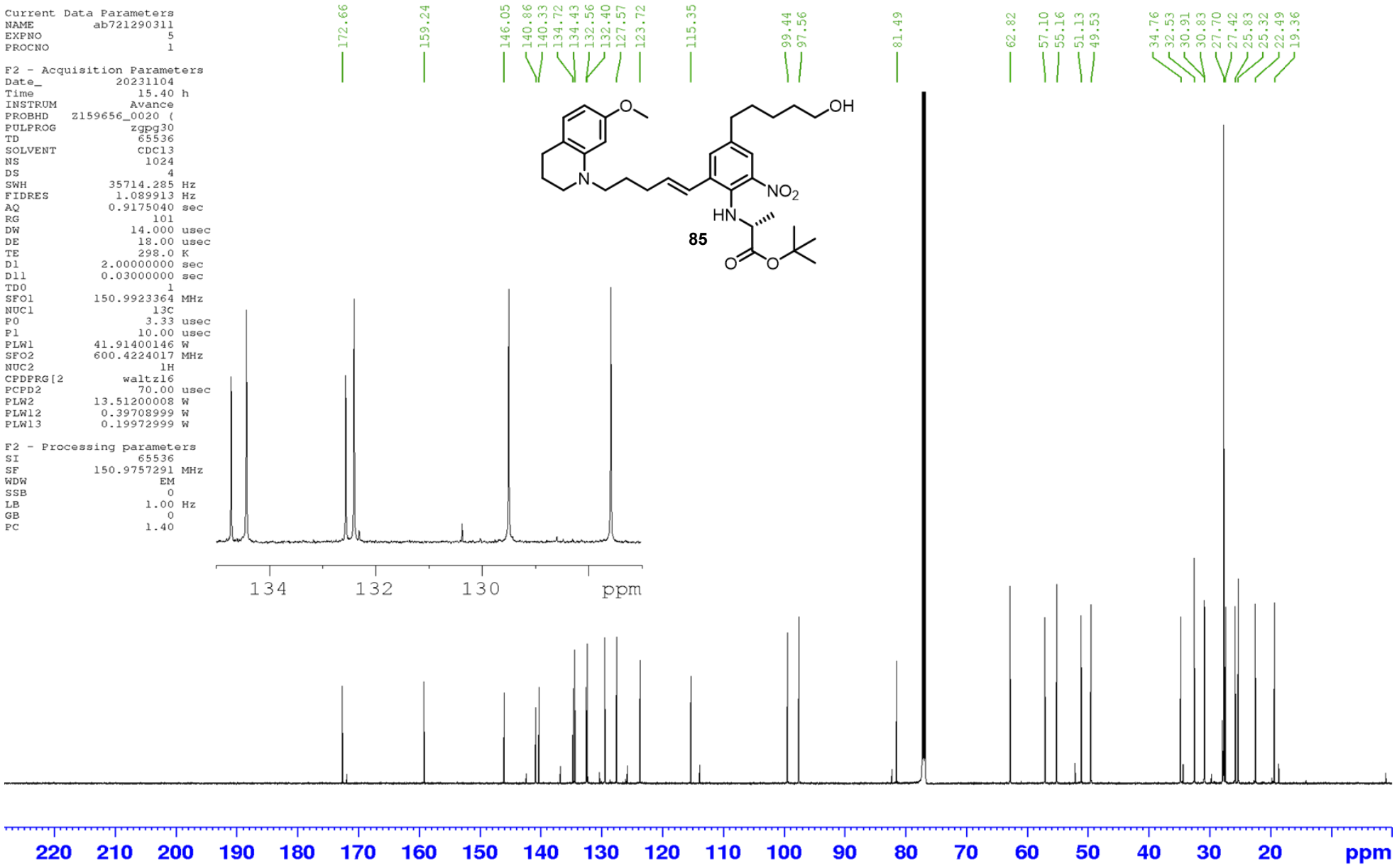

^{1}H NMR (*R*,*E*)-7-(5-hydroxypentyl)-5-(5-(7-methoxy-3,4-dihydroquinolin-1(2*H*)-yl)pent-1-en-1-yl)-3-methyl-3,4-dihydroquinoxalin-2(1*H*)-one

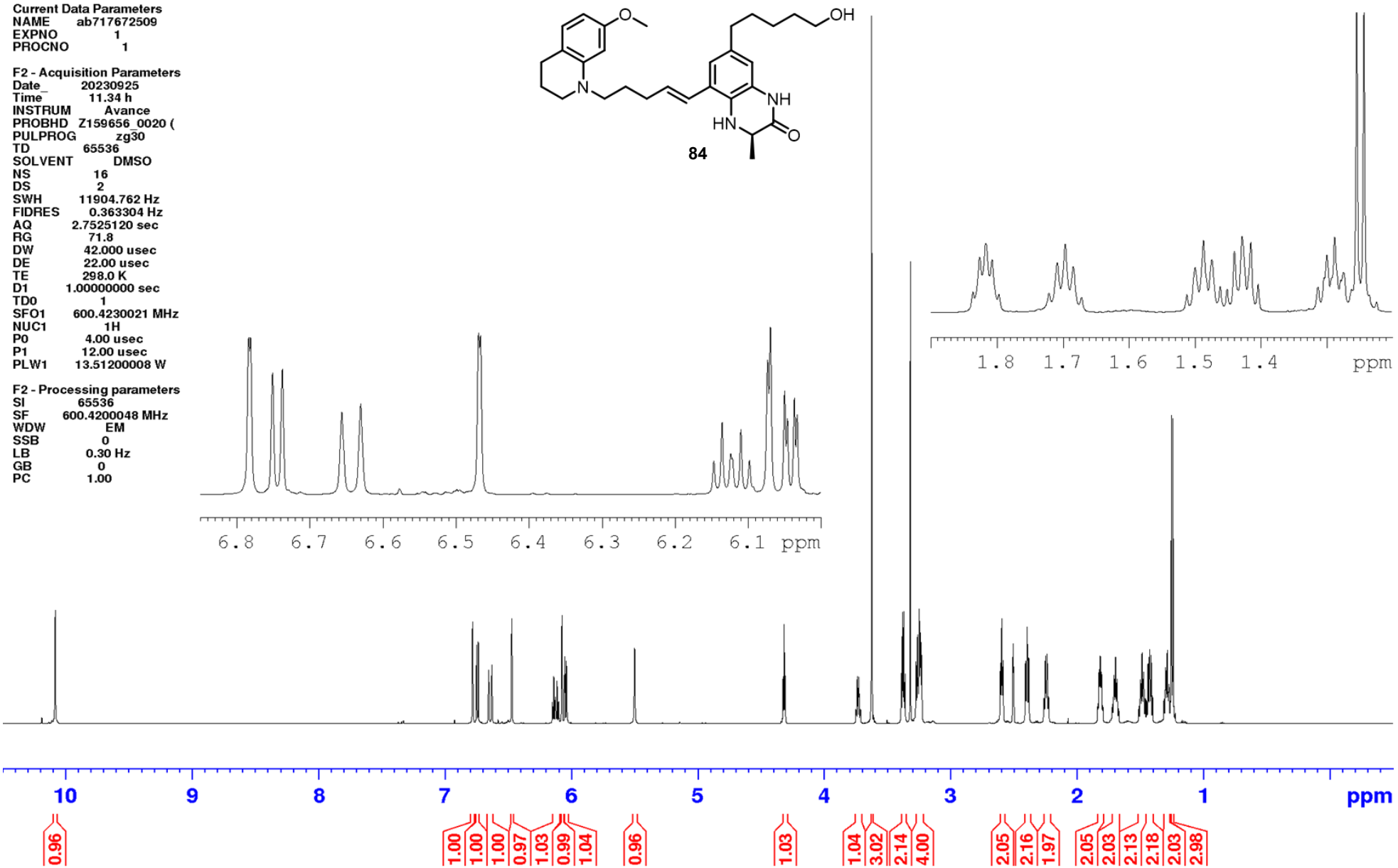

^{13}C NMR (*R*,*E*)-7-(5-hydroxypentyl)-5-(5-(7-methoxy-3,4-dihydroquinolin-1(2*H*)-yl)pent-1-en-1-yl)-3-methyl-3,4-dihydroquinoxalin-2(1*H*)-one